RIGA TECHNICAL UNIVERSITY

Jānis Narbuts

ADAPTIVE BUILDING FACADE SYSTEMS WITH THERMAL ENERGY STORAGE

Doctoral Thesis

RTU Press
Riga 2026

RIGA TECHNICAL UNIVERSITY
Faculty of Natural Sciences and Technology
Institute of Energy Systems and Environment

Jānis Narbuts
Doctoral Student of the Study Programme "Environmental Engineering"

ADAPTIVE BUILDING FACADE SYSTEMS WITH THERMAL ENERGY STORAGE

Doctoral Thesis

Scientific supervisors

Professor Dr. sc. ing.
RUTA VANAGA

Tenured Professor Dr. sc. ing.
ANDRA BLUMBERGA

Riga 2026

Narbuts, J. Adaptive Building Facade Systems with Thermal Energy Storage. Doctoral Thesis. Riga: RTU Press, 2026. 311 p.

Published in accordance with the decision of the Promotion Council "RTU P-19" of 12. March 2026, No. 240.

This Thesis research has been supported by the European Social Fund within the Project No 8.2.2.0/20/I/008 "Strengthening of PhD students and academic personnel of Riga Technical University and BA School of Business and Finance in the strategic fields of specialization" of the Specific Objective 8.2.2 "To Strengthen Academic Staff of Higher Education Institutions in Strategic Specialization Areas" of the Operational Programme "Growth and Employment".

ANNOTATION

The European Union's ambition to achieve climate neutrality by 2050 places increasing pressure on the building sector, which remains one of the largest energy consumers and sources of CO_2 emissions. As the European Green Deal and the revised Energy Performance of Buildings Directive call for higher energy efficiency and deeper renovation, traditional static facade systems are proving insufficient to meet rising climatic variability, growing cooling needs and the demand for more flexible building operation. This context has intensified interest in adaptive facade technologies capable of responding dynamically to changing environmental conditions. Among these solutions, facades integrating phase change materials (PCMs) present significant potential by enabling thermal energy storage, reducing peak loads and stabilising indoor temperatures.

The aim of this Thesis is to develop an adaptive solar facade system that integrates PCMs for thermal energy storage and to evaluate its effectiveness in improving building energy performance under both controlled and real outdoor conditions. The work is grounded in a multidisciplinary framework that spans material science, physics, mechanical engineering and computational modelling.

The Thesis begins with a systematic literature review that examines the state of thermal energy storage technologies, PCM behaviour, insulation innovations and adaptive facade concepts, as well as the experimental and numerical methodologies used globally to analyse dynamic building envelopes.

The research continues with the development of small-scale and full-scale facade prototypes, designed to explore the interaction between concentrated solar input, PCM heat storage, insulation layers and dynamic reflective components. Laboratory experiments establish the thermal properties of two paraffin-based PCMs, while a series of optimisation studies refine the facade configuration to enhance heat-transfer efficiency and reduce losses. A comprehensive year-round outdoor testing study follows, carried out using PASLINK-type test stands that enable detailed evaluation of facade behaviour under real climatic fluctuations. These experiments reveal strong seasonal dynamics: the PCM facade effectively reduces indoor overheating during summer, enhances thermal stability in spring and autumn through controlled charging and discharging and provides improved insulation in winter due to its low steady-state U-value.

Numerical models developed at material and module scale complement the experimental findings. Although the precision of small-scale numerical model is limited, the simulations provide conceptual insight into solar facade performance in different climates and support broader comparative analysis with conventual technology.

The Thesis concludes that PCM-integrated adaptive facades hold strong potential for improving building energy efficiency, particularly when operated with appropriate control strategies and tailored to climatic conditions. The work contributes new knowledge to the design, analysis and optimisation of dynamic facade systems and supports the wider transition toward energy-efficient, climate-responsive buildings.

ANOTĀCIJA

Eiropas Savienības mērķis panākt klimatneitralitāti līdz 2050. gadam rada pieaugošu spiedienu uz ēku sektoru, kas joprojām ir viens no lielākajiem enerģijas patērētājiem un CO_2 emisiju radītājiem. Tā kā Eiropas zaļais kurss un pārskatītā Ēku energoefektivitātes direktīva nosaka augstākas energoefektivitātes prasības un plašākas renovācijas nepieciešamību, tradicionālās statiskās ēku norobežojošās konstrukcijas arvien mazāk spēj nodrošināt komfortu pieaugošas klimata mainības, palielināta dzesēšanas pieprasījuma un elastīgākas ēku darbības apstākļos. Šajā kontekstā pastiprinās interese par adaptīvām fasāžu tehnoloģijām, kas spēj dinamiski reaģēt uz mainīgiem laika apstākļiem. Starp šādiem risinājumiem īpaši izceļas ēku norobežojošās konstrukcijās, kurās iestrādāti fāžu pārejas materiāli (FPM), kas spēj veiksmīgi nodrošināt siltumenerģijas uzkrāšanu fasādē, maksimālās siltuma slodzes samazināšanu un iekštelpu temperatūras uzturēšanu komforta robežās.

Šīs disertācijas mērķis ir izstrādāt adaptīvu saules fasādes sistēmu ar siltumenerģijas uzkrāšanu FPM, un novērtēt tās efektivitāti ēku energoefektivitātes uzlabošanā gan kontrolētos laboratorijas, gan reālos laika apstākļos. Darbs balstās uz starpdisciplināru pieeju, kas ietver materiālzinātni, fiziku, mehāniku un datormodelēšanu.

Disertācijas pētījuma pirmā daļa satur sistemātisku literatūras apskatu, kurā analizētas siltumenerģijas uzkrāšanas tehnoloģijas, FPM uzvedība, inovatīvi ēku izolācijas materiāli un adaptīvo fasāžu koncepcijas, kā arī eksperimentālās un skaitliskās metodes, kuras visplašāk pielieto statisku un dinamisku ēku norobežojošo konstrukciju izpētē.

Pētījums turpinās ar mazizmēra un pilnizmēra fasāžu prototipu izstrādi, lai analizētu koncentrētās saules enerģijas, FPM uzkrātā siltuma, izolācijas slāņu un dinamisko atstarojošo elementu mijiedarbību. Laboratorijas eksperimentos tika noteikti divu uz parafīna bāzes ražotu FPM termālās īpašības, savukārt optimizācijas pētījumos tika pilnveidota fasādes sistēmas ietverošo elementu galvenā konfigurācija, lai būtu iespējams uzlabot siltuma pārnesi un samazināt siltumenerģijas zudumus. Tam sekoja visaptverošs gadu ilgs āra eksperimentu cikls, kas veikts PASLINK tipa testēšanas stendos, ļaujot detalizēti novērtēt saules fasādes sistēmas darbību reālos klimatiskos apstākļos. Eksperimentu rezultāti parāda izteiktu sezonālo dinamiku: FPM fasāde vasarā efektīvi spēj samazināt iekštelpu pārkaršanu, pavasarī un rudenī nodrošināt iekštelpas temperatūras stabilitāti, pateicoties dinamiski kontrolētai uzlādei un izlādei, savukārt ziemā nodrošināt augstvērtīgu siltumizolāciju, pateicoties zemajai stacionārajai U vērtībai.

Eksperimentos iegūtie rezultāti ir papildināti ar diviem simulāciju modeļiem (FPM un mazizmēra testa stenda), kuri tika izstrādāti ANSYS Fluent vidē. Lai gan mazizmēra modeļa precizitāte ir ierobežota vairāku pieņēmumu dēļ, iegūtās simulācijas tomēr sniedz konceptuālu ieskatu fasādes darbībā dažādos klimatiskos apstākļos, kā arī ļauj veikt salīdzinošo analīzi ar statiskajām fasāžu sistēmām.

Disertācijas noslēguma secinājumi apliecina, ka saules adaptīvās FPM fasādes spēj sniegt ievērojamu potenciālu ēku energoefektivitātes uzlabošanā, īpaši tad, ja tās tiek ekspluatētas ar piemērotām vadības stratēģijām un pielāgotas konkrētajiem klimatiskajiem apstākļiem. Darbs sniedz būtisku ieguldījumu dinamisko fasāžu sistēmu projektēšanā, analīzē un optimizācijā, kā arī parāda tehnoloģiskā risinājuma potenciālu ēku sektora dekarbonizācijas virzienā.

TABLE OF CONTENTS

ABBREVIATIONS

ADBE - Adaptive dynamic building envelope
APDC - Active–passive dual-control
BIPV - Building-integrated photovoltaics
BPIE - Buildings Performance Institute Europe
BRP - Building Renovation Passport
CPCM - Composite phase change material
DO - Discrete ordinates
ECPI - Energy-Comfort Performance Index
EED - Energy Efficiency Directive
EPBD - Energy Performance of Buildings Directive
EU - European Union
GDP - Gross domestic product
GHG - Greenhouse gas
GHP - Guarded hot plate
HFM - Heat Flow Meter
HVAC - Heating, ventilation and air conditioning
IPCC - Intergovernmental Panel on Climate Change
LCA - Life cycle assessment
LHTES - Latent heat thermal energy storage
MOEA - Multi-Objective Evolutionary Algorithm
nZEB - Nearly zero-energy buildings
PCC - Phase change composites
PCM - Phase change material
PETG - Polyethylene terephthalate glycol
PMMA - Poly-methyl methacrylate
PV - Photovoltaic
RES - Renewable energy sources
S2S - Surface-to-surface
SAH - Solar air heater
SHB-CAC - Superhydrophobic cellulose aerogel cooler
SMA - Shape memory alloy
SPSWB - Sun-powered smart window blind
SRI - Smart Readiness Indicator
TES - Thermal energy storage
UHI - Urban heat island
UNFCCC - United Nations Framework Convention on Climate Change
XPS - Extruded polystyrene
ZEB - Zero-emission buildings

INTRODUCTION

Topicality

The European Union's long-term vision to reach carbon neutrality by 2050, as defined in the European Green Deal [1], places unprecedented emphasis on accelerating the transition toward technologies that consume less energy and produce fewer CO_2 emissions. This challenge is particularly acute in the building sector, which is responsible for approximately 40% of total energy consumption and 36% of CO_2 emissions in the EU [2]. As a result, amendments to Directive 2010/31/EU on the energy performance of buildings and Directive 2012/27/EU on energy efficiency [3] call for a new generation of buildings - ones capable of delivering significantly better energy performance, integrating renewable energy systems and responding intelligently to environmental conditions. Increasing the role of on-site renewable energy is therefore highlighted as an essential decarbonisation pathway [4].

International climate policy documents - including the Intergovernmental Panel on Climate Change (IPCC) Assessment Reports, UNFCCC protocols and global climate agreements - repeatedly stress that reducing energy demand and improving energy efficiency are among the most effective mitigation measures for limiting global warming [5]. However, despite this recognition, the building sector continues to face major inefficiencies, with a substantial share of potential energy savings still unrealised [6]. Current projections indicate that global energy consumption may increase by 53% over the coming decade, driven by demographic expansion, increasing comfort expectations, digitalisation and urbanization, thereby further intensifying greenhouse gas emissions if no corrective measures are taken [7].

Conventional building designs - largely static in nature - are no longer adequate for meeting climate-neutrality targets. Most building envelopes are constructed using traditional insulation and fixed-performance facade elements, which do not respond dynamically to fluctuating outdoor conditions. Consequently, there is significant untapped potential for stored energy within facade elements to balance indoor thermal comfort during both heating and cooling periods, thereby improving the overall energy efficiency of the building. To address these limitations, a strong shift toward adaptive architectural solutions is emerging. Dynamic and kinetic facade systems, capable of responding to variations in solar radiation, temperature, wind, humidity and light [8], represent a promising direction for next-generation energy-efficient buildings.

In this broader policy and technological context, the EU Green Deal reinforces the need to pair renewable energy sources (RES) with intelligent control and energy management in buildings [1], [4], [9]. Nearly zero-energy buildings (nZEB) and the more recent concept of zero-emission buildings (ZEB), are now central pillars of European decarbonisation strategies. However, their practical implementation remains challenging because the availability of renewable energy rarely aligns with the building's actual energy demand. Unlike fossil-based systems, RES generation fluctuates daily and seasonally, creating periods of surplus production as well as intervals when supply is insufficient. These temporal mismatches make it difficult to ensure stable and efficient building operation, regardless of season. Consequently, innovative

approaches to the building thermal envelope - especially solutions capable of storing and later releasing solar thermal energy - offer a promising pathway to improve the balance between renewable supply and building energy needs.

Aim and objectives

The main goal of this Thesis is to develop an innovative adaptive facade system integrating thermal energy storage through the application of phase change materials (PCMs) and to evaluate its effectiveness in enhancing building energy performance. Achieving this aim requires a comprehensive investigation spanning conceptual development, experimental validation and numerical simulation. To fulfil this goal, the following research objectives have been established:

1) Conduct a systematic literature review covering thermal energy storage (TES) principles, PCM technologies, state-of-the-art insulation materials, adaptive facade concepts and existing experimental and numerical testing methodologies relevant to dynamic building envelopes.
2) In iterative process design and develop experimental prototypes, including a small-scale facade module for controlled laboratory investigations and a full-scale solar facade module integrated into outdoor test stands for real-environment performance evaluation.
3) Plan and execute experiments, ensuring controlled parameter variation, accurate instrumentation and reliable data acquisition under both steady-state laboratory and dynamic outdoor weather conditions.
4) Develop and validate numerical simulation models for the small-scale facade prototypes, enabling detailed heat-transfer analysis, performance prediction and comparative assessment with experimental data.
5) Collect, process and analyse measurement data to quantify the thermal performance, energy efficiency benefits and operational potential of the proposed adaptive facade solution, ultimately assessing its contribution to reducing heating and cooling energy demand.

Hypothesis

The integration of phase change materials into an adaptive facade system will improve building energy efficiency by enabling controlled thermal energy storage and release, thereby reducing indoor temperature fluctuations and lowering heating and cooling demand across varying climatic conditions.

Novelty

The novelty of this research lies in paradigm shift of the building envelope not merely as a passive insulating barrier but as an active solar-thermal energy storage system. While dynamic and adaptive facade concepts have gained attention in recent years, their integration with PCMs

for seasonal and diurnal thermal storage remains underexplored, especially under real weather conditions characteristic of northern European climates.

This work advances the state of the art by:

- Transforming the facade into a solar harvesting and storage unit, capable of absorbing, storing and releasing thermal energy through PCM phase transitions.
- Addressing the critical challenge of renewable energy intermittency by embedding thermal buffering capacity directly into the building envelope.
- Experimentally analysing the performance of PCM-integrated solar facades under dynamic boundary conditions, including outdoor testing under real climatic conditions, thereby providing data that are currently scarce in the literature.
- Evaluating how such systems can reduce heating and cooling loads, thereby increasing on-site renewable energy utilization and contributing to the transition toward zero-emission buildings by lowering operational greenhouse gas emissions.
- Providing new insights into operational regimes, environmental impacts and adaptive potential of PCM-based dynamic envelopes, supporting the design of next-generation high-performance zero emission buildings.

Through this combined experimental and practical approach, the Thesis offers a novel pathway to bridge the gap between renewable energy availability on-site and building energy demand at the building thermal envelope level - something current static building systems cannot achieve.

Practical relevance

The practical relevance of this research lies in its strong alignment with ongoing EU decarbonisation efforts, evolving building performance regulations and emerging architectural trends that emphasize adaptive and energy-responsive design. As EU member states progress toward transforming their building stock into nearly zero-energy or even positive-energy buildings, the demand for facade systems capable of dynamically responding to environmental conditions and significantly reducing energy use becomes increasingly critical. The PCM-integrated solar facade concept investigated in this Thesis directly addresses these needs by offering a multifunctional building envelope capable of harvesting, storing and redistributing solar thermal energy. Such systems have the potential to substantially reduce heating and cooling loads, enabling buildings to meet stringent EPBD requirements while lowering operational costs for occupants. By embedding thermal storage directly into the facade, buildings are able to use a greater share of on-site renewable energy during periods of availability, thereby decreasing reliance on fossil fuels and grid electricity during peak-demand hours. The approach is also highly scalable: it can be implemented in both new construction and deep renovation projects, which is essential for upgrading Europe's aging building stock. Moreover, buildings equipped with facade-integrated thermal storage can function as energy-flexible assets within larger district energy systems, helping to mitigate the intermittency of renewable energy sources and contributing to overall grid stability. This research is particularly relevant for northern European climates, where heating demand is high and traditional solar

technologies often deliver limited benefits; the findings provide climate-specific insights into how dynamic solar-thermal facades can be effectively utilized even under low-sun conditions. In this way, the study advances both scientific understanding and practical deployment of adaptive envelope technologies, offering a viable pathway toward energy-positive, climate-neutral buildings and supporting the long-term objectives of the EU Green Deal.

Approbation of the research results

1. Narbuts, J., Vanaga, R., Freimanis, R., Blumberga, A. Laboratory and outdoor testing of small-scale active solar facade module. Environmental and Climate Technologies 2021, vol. 25, no. 1, pp. 455–466. Available: doi: https://doi.org/10.2478/rtuect-2021-0033
2. Vanaga, R., Narbuts, J., Freimanis, R., Blumberga, A. Laboratory testing of small-scale solar facade module with phase change material and adjustable insulation layer. *Energies.* 2022, 15, 1158. Available: https://doi.org/10.3390/en15031158
3. Narbuts, J., Blumberga, A., Zundāns, Z., Freimanis, R., Bāliņš, R., Vanaga, R. The Effect of Fresnel Lens Focal Point Location on Heat Transfer in Phase Change Material (PCM) Enhanced Dynamic Solar Facade. Environmental and Climate Technologies, 2022, vol. 26, no. 1, pp. 1268–1278. e-ISSN 2255-8837. Available: doi:10.2478/rtuect-2022-0096
4. Vanaga, R., Narbuts, J., Zundāns, Z., Blumberga, A. On-site Testing of Dynamic Facade System with the Solar Energy Storage, *Energy,* 2023, vol. 283, 128257, ISSN 0360-5442. Available: https://doi.org/10.1016/j.energy.2023.128257
5. Vanaga, R., Narbuts, J., Freimanis, R., Zundāns, Z., Blumberga, A. Performance Assessment of Two Different Phase Change Materials for Thermal Energy Storage in Building Envelopes, *Energies*, 2023, vol. 16, no. 13, 5236. Available: https://doi.org/10.3390/en16135236
6. Narbuts, J., Vanaga, R. Revolutionizing the Building Envelope: A Comprehensive Scientific Review of Innovative Technologies for Reduced Emissions. Environmental and Climate Technologies 2023, vol. 27, no. 1, pp. 724–737. Available: https://doi.org/10.2478/rtuect-2023-0053
7. Vanaga, R., Narbuts, J., Zundāns, Z., Gušča, J. Systematic literature review of software tools for modeling heat transfer in phase change materials for building applications. *IOP Conference Series: Earth and Environmental Science*. 2024, 1372 012017. Available: https://doi.org/10.1088/1755-1315/1372/1/012017

Approbation of the research results at scientific conferences

1. Vanaga, R., Narbuts, J., Freimanis, R., Blumberga, A. Laboratory testing of different melting temperature phase change materials under four-season conditions for thermal energy storage in building envelopes. *International Conference on Applied Energy* 2021, Nov. 29 – Dec. 2, 2021, Bangkok, Thailand.

2. Narbuts, J., Blumberga, A., Zundāns, Z., Freimanis, R., Bāliņš, R., Vanaga, R. The effect of Fresnel lens focal point location on heat transfer in phase change material (PCM) enhanced dynamic solar facade. *International Scientific Conference of Environmental and Climate Technologies Conect* 2022, May 11–13, 2022, Riga, Latvia.
3. Narbuts, J., Vanaga, R. Revolutionizing the Building Envelope: Innovative Technologies for Reduced Emissions. *International Scientific Conference of Environmental and Climate Technologies, CONECT* 2023, May 10–12, 2023, Riga, Latvia.
4. Narbuts, J., Vanaga, R., Zundāns, Z. Validating ANSYS Heat Transfer Models with Two Phase Change Materials. *International Scientific Conference of Environmental and Climate Technologies, CONECT* 2024, May 15–17, 2024, in Riga, Latvia.

Other publications

1. Narbuts, J., Vanaga, R. Comparative Study of the Thermal Properties of Nanoparticle-Enhanced Phase Change Materials for Building Envelope Applications. CONECT 2025. International Scientific Conference of Environmental and Climate Technologies, 40. https://doi.org/10.7250/CONECT.2025.017
2. Narbuts, J., Vanaga, R. Nano-Enhanced Phase Change Materials for Building Envelopes: A Systematic Review of Thermal Performance and Applications. Environmental and Climate Technologies 2023, vol. 29, no. 1, pp. 359–389. Available from: https://doi.org/10.2478/rtuect-2025-0025

Structure of the Thesis

The structure of this Doctoral Thesis is grounded in the paradigm shift from conventional to adaptive building envelopes, driven by the necessity to decarbonize the existing and future building stock. This transition is operationalized through three interlinked development cycles (see Fig. 1), which collectively form the methodological and conceptual backbone of the research:

Stage 1: Initial design optimisation of the technological solution and testing of PCM properties for computer simulations. This process leads to a technological concept and a preliminary small-scale prototype. Parallel to this, a numerical simulation model is developed to enhance understanding of heat transfer dynamics and identify energy-efficiency improvements.

Stage 2: Small-scale laboratory and outdoor testing, where the developed prototype undergoes performance evaluation under controlled and real environmental conditions.

Stage 3: Large-scale solar facade module development, where the prototype is transferred into a full-scale operational system for outdoor testing.

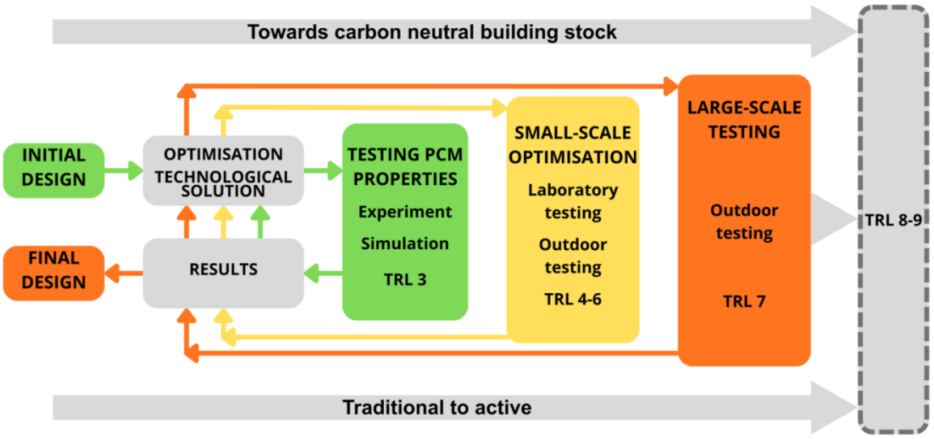

Fig. 1. Structure of the Thesis.

The Doctoral Thesis consists of eight main chapters: (1) Introduction, (2) Literature Review, (3) Methodology, (4) Testing PCM Properties for ANSYS Simulations, (5) Small-scale Optimisation, (6) Large-scale Testing, (7) Discussion and (8) Conclusions.

The Introduction presents the topicality of the research, aim and objectives, hypothesis, novelty, practical relevance and the approbation of results.

The Literature Review provides a comprehensive synthesis of existing knowledge on thermal energy storage systems, PCMs, state-of-the-art insulation materials, adaptive facade systems and the methodologies used for experimental and numerical investigations.

The Methodology chapter outlines the structure and sequence of the experiments, numerical simulations, measurement instrumentation and materials employed in this Thesis.

Chapters 4–6 present the methodological approach combined with the results of each experiment and simulation. These chapters describe the findings obtained from laboratory tests, outdoor measurements and numerical simulations in a logical sequence aligned with the technological development cycles. Together, they demonstrate a clear and traceable progression of the proposed adaptive facade technology from conceptual development to full-scale implementation.

The Discussion chapter critically evaluates the obtained experimental and numerical results, analyses the thermal behaviour and operational performance of the developed adaptive facade system and compares the proposed technology with conventional facade solutions. In addition, this chapter discusses the limitations of the applied methodologies, evaluates the validity of the research hypothesis and assesses the practical applicability and future development potential of PCM-integrated adaptive facades.

The Conclusions chapter summarises the main findings, discusses key insights and outlines future research directions.

Table 1 provides an overview of the scientific publications that form the scientific foundation of the Thesis and support the individual research components.

The AI tool (DeepL) was used to assist in translating and editing text to provide clarity and flow throughout the Thesis.

Table 1

Scientific articles used in Doctoral Thesis

Field	**Title of scientific research article**
Literature review	Revolutionizing the Building Envelope: A Comprehensive Scientific Review of Innovative Technologies for Reduced Emissions
	Systematic literature review of software tools for modelling heat transfer in phase change materials for building applications
Testing PCM properties for ANSYS simulations	Performance Assessment of Two Different Phase Change Materials for Thermal Energy Storage in Building Envelopes
Small-scale optimisation	Laboratory Testing of Small-Scale Solar Facade Module with Phase Change Material and Adjustable Insulation Layer
	Laboratory Testing of Small-Scale Active Solar Facade Module
	The Effect of Fresnel Lens Focal Point Location on Heat Transfer in Phase Change Material (PCM) Enhanced Dynamic Solar Facade
Large-scale testing	On-site testing of dynamic facade system with the solar energy storage

1. LITERATURE REVIEW

1.1. EU building stock policy

The scientific literature consistently identifies anthropogenic greenhouse gas (GHG) emissions as the principal driver of global climate change [10], with the EU responding through a robust policy framework aimed at reducing emissions and improving energy efficiency across all sectors of the economy. The European Green Deal positions climate neutrality by 2050 as the central strategic objective of EU policy [1], acknowledging the well-documented correlation between national energy consumption, CO_2 emissions and GDP per capita [11]. Despite this overarching vision, studies show an uneven contribution from EU Member States, particularly in Eastern Europe, where ageing building stocks and insufficient renovation capacity impede progress toward climate objectives [12].

International assessments highlight the building sector as a major contributor to global energy demand and emissions. According to the Global Buildings Status Report, buildings accounted for 36% of final energy use and 37% of CO_2 emissions in 2021 [13]. Within Europe, expert analyses from the Buildings Performance Institute Europe (BPIE) argue that the decarbonisation of the EU building stock is advancing too slowly to meet the requirements of the Green Deal [14]. Low renovation rates, combined with the prevalence of inefficient envelopes and outdated construction practices, present a substantial barrier to energy savings. Recent literature emphasises that conventional building methods are inadequate for supporting low-carbon transitions and often hinder the integration of renewable energy solutions, particularly in large multifamily buildings typical of the Eastern European region [12], [15].

The EPBD - initially adopted in 2010, amended in 2018 and recast in 2023/2024 - constitutes the central regulatory instrument shaping the EU's building stock transformation. The literature notes that the EPBD mandates increasingly stringent minimum performance requirements, the transition from nZEB to Zero-Emission Buildings (ZEB) and the introduction of Building Renovation Passports (BRPs) to support long-term renovation planning. Studies highlight the EPBD's emphasis on building-level renewable integration and dynamic performance assessment, including the Smart Readiness Indicator (SRI), which evaluates a building's capacity for adaptive and demand-responsive operation. These policy directions support research into adaptive facades, thermal-storage-integrated envelopes and advanced insulation strategies.

The Energy Efficiency Directive (EED) provides broader energy-reduction obligations for Member States and reiterates the "energy efficiency first" principle. Literature on policy implementation consistently identifies building envelopes as one of the most impactful areas for reducing energy demand [16]. Envelope-level improvements are aligned with EED targets and are widely studied as cost-effective measures for supporting EU energy-efficiency goals.

The Renovation Wave Strategy (launched in 2020) strengthens the role of the building sector within the Green Deal framework by targeting doubled renovation rates, improved thermal comfort and widespread adoption of high-performance envelope systems. Recent research emphasises that Green Deal and Renovation Wave policies prioritise innovation,

material efficiency and envelope-integrated renewable technologies [17], underscoring a growing demand for solutions such as aerogel insulation, PCM-enhanced facades and hybrid solar-thermal systems [18], [19]. Studies on facade system obsolescence further argue that traditional curtain-wall configurations no longer meet EU performance expectations, accelerating the need for innovative building-skin technologies [20].

A significant body of literature examines the complementary policy goal of coupling envelope improvements with on-site renewable energy generation. Reducing energy demand through insulation and dynamic facades, followed by compensation of residual loads using renewables, is identified as a synergistic strategy for achieving EU decarbonisation targets [16]. Solar technologies are highlighted for their versatility and high integration potential within building envelopes [21], [22]. Empirical studies report that solar systems can deliver over 30% primary energy savings and cover up to 50% of a building's energy load in optimal conditions [23].

However, renewable intermittency requires effective energy storage. Research consistently points to PCM as a key component in thermal energy storage systems, enabling increased solar-thermal utilisation and reduced reliance on active HVAC systems [24]. These characteristics make PCM-enhanced systems particularly relevant to EU policy objectives concerning smart energy management, peak-load reduction and renewable-energy self-consumption.

The literature widely recognises the building envelope as a primary determinant of operational energy demand and indoor comfort. High-performance insulation materials, such as aerogels, are frequently referenced for their extremely low thermal conductivity and suitability for deep-renovation contexts [25], [18]. The Green Deal's emphasis on research and innovation directly supports the development of such materials, viewing envelope innovation as central to achieving cost-effective emission reductions [17]. Simultaneously, recent studies critique conventional facade systems - particularly standardised curtain walls - as outdated in terms of thermal, solar and comfort performance, reinforcing the relevance of novel facade technologies that support EU decarbonisation pathways [19], [20].

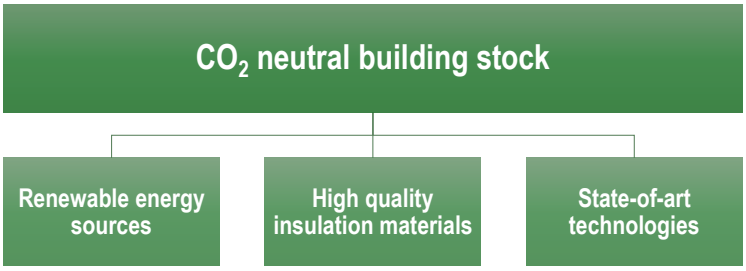

Fig. 1.1. The research directions in this Thesis.

The literature demonstrates a clear alignment between EU building-stock policy and research efforts aimed at reducing energy consumption, improving thermal performance and integrating renewable energy at the building-envelope scale. Key legislative frameworks - most notably the EPBD, EED, the European Green Deal and the Renovation Wave - collectively define a policy environment that encourages the development and implementation of adaptive,

energy-efficient and storage-enhanced building envelopes. The research directions (Fig. 1.1) explored in this Thesis, including exploitation of on-site RES, advanced insulation materials and solar-thermal storage solutions, are therefore directly supported by current EU policy priorities and address recognised gaps in both scientific literature and practical implementation.

1.2. Thermal energy storage

The utilisation of on-site RES is one of the key strategies for achieving a CO_2-neutral building stock. Because the availability of on-site RES - particularly solar energy - is intermittent, energy systems must incorporate appropriate storage technologies to ensure that harvested energy can be used whenever generation is insufficient. TES provides a means to store thermal energy by heating or cooling a storage medium, which can later be discharged for space heating, cooling, or other thermal applications. TES systems can store energy within a PCM through two mechanisms: sensible heat and latent heat [26].

Sensible heat refers to the energy required to raise or lower the temperature of a material, while latent heat is associated with energy absorbed or released during a phase transition, typically at an almost constant temperature [27]. Figure 1.2 illustrates a theoretical latent heat curve during a solid–liquid phase transition.

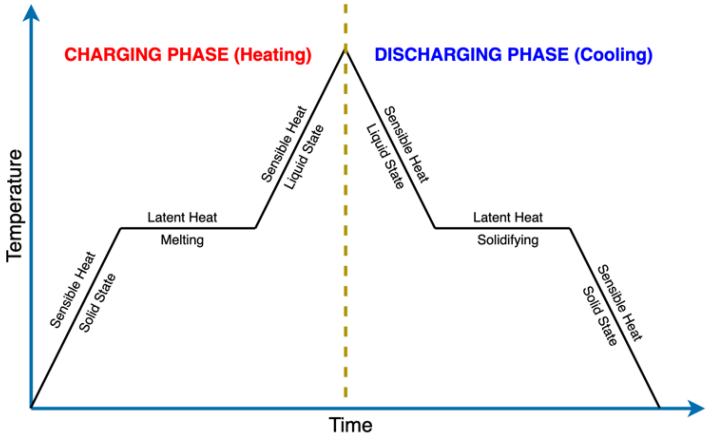

Figure 1.2. Theoretical latent heat curve for solid/liquid phase transition [28].

During the charging phase, heat is supplied to the PCM and stored either as sensible or latent heat, while in the discharging phase, the stored energy is released as the material cools. The integration of TES into energy systems offers multiple advantages: increased overall efficiency and reliability, reduced maintenance and operating costs and significant reductions in atmospheric pollutants such as CO_2 due to decreased energy demand for heating [29]. TES technologies can be either passive or active and they are applied across various domains - including HVAC systems, building envelope components and energy systems integrated into the immediate building surroundings [30].

TES systems are generally classified into sensible, latent and thermochemical storage types, with the first two being particularly suitable for building applications. Sensible heat systems are commercially mature and relatively simple, whereas latent heat thermal energy storage (LHTES) systems offer substantially higher energy storage density per unit volume [31]. LHTES systems are especially relevant for passive or net-zero-energy buildings, as they can be embedded directly into building envelopes that exploit on-site renewable energy - most notably solar-thermal input. A significant advantage of such technology is the reduction of the effective heating-season duration, which is critically important in Northern European climates characterised by prolonged autumn and spring periods.

1.2.1. Phase change materials

PCMs serve as the storage medium in LHTES systems (see Fig. 1.3).

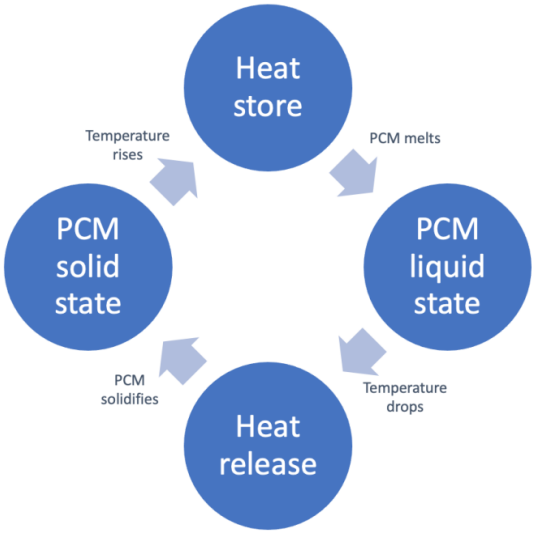

Fig. 1.3. Working cycle of phase change material [32].

Solid–liquid PCMs are the most widely used category in building applications and are typically grouped into organic, inorganic and eutectic PCMs [33]. Organic PCMs (such as paraffins, fatty acids and sugar alcohols) are frequently applied in buildings due to favourable phase change temperature ranges - for example, paraffins exhibit melting points between 10°C and 100°C, making them particularly suitable for envelope integration [34]. Numerous studies have investigated PCM-enhanced building components, including interior boards, masonry units, facade panels and shading devices [35], [36], [37]. Despite active research, PCM-based building products have not yet reached large-scale commercial deployment, indicating considerable potential for further optimisation and technological development. Increasing scientific understanding of PCM behaviour strengthens the foundation for such innovation.

A PCM's melting temperature is a key parameter determining its suitability for specific building applications and performance requirements. This Thesis examines the thermal

behaviour of two PCMs across four climatic seasons - winter, spring, summer and autumn - through laboratory testing under defined boundary conditions.

PCMs differ widely in their thermophysical characteristics. Inorganic PCMs, typically hydrated salts, have high thermal storage density and good thermal conductivity but may suffer from phase segregation, subcooling and corrosive effects on metal containers. Organic PCMs, conversely, exhibit lower thermal conductivity and enthalpy but offer several advantages: minimal or no supercooling, chemical stability, non-corrosiveness and reliable cycling durability. Eutectic PCMs, formed by combining two or more components, may be organic, inorganic, or mixed; they exhibit stable melting points and good latent heat capacity, but more research is required to identify eutectics with long-term phase stability and optimal transition temperatures for building applications [38].

Solid–liquid PCMs such as paraffin waxes remain particularly attractive for building integration owing to their low supercooling, non-toxicity, chemical stability and high latent heat of fusion [39].

1.2.2. Phase change material applications in buildings

A wide range of PCM applications in buildings is currently being investigated and several technologies have already been commercialised for heating, cooling and solar-energy storage systems.

Recent study explores PCM incorporation into bio-based composite materials. For example, research involving hempcrete combined with gypsum and PCM demonstrates that integrating up to 20 wt.% of microencapsulated PCM can increase heat capacity by 70.4%, with only moderate reductions in compressive strength and negligible changes in density or thermal conductivity [40]. Such bio-composites offer promising opportunities for low-carbon construction while improving thermal stability.

Rucevskis et al. [41] evaluate an active TES system using PCM for cooling residential buildings, where standalone PCM units are installed between a concrete slab and interior finish layers and actively regenerated via night cooling. Their findings show indoor air temperature reductions of up to 6.8°C, demonstrating the potential of PCM systems to provide low-energy cooling in residential applications.

Wu et al. [42] investigate a multilayer envelope system combining PCM and bio-based hygroscopic materials such as hemp concrete. Their experiments show significant reductions in temperature and humidity fluctuations (50–60%), peak temperature delays of 70.4% and energy consumption reductions of 15.3%. The placement of PCM on the exterior side yielded the highest storage efficiency and energy participation.

Phase change composites (PCCs) have also been explored as potential high-performance envelope materials. A recent study [43] demonstrates that an n-octadecane/fumed silica PCC exhibits high latent heat storage (155.8 J/g), high crystallisation fraction (96.5%) and suitable melting temperature (26.76°C). In comparative tests, PCC panels substantially outperformed polystyrene insulation by delaying indoor temperature rise and maintaining lower interior temperatures under thermal load.

Similarly, another study [44] investigates shape-stabilised composite PCMs (CPCM) using LA-SA/Al_2O_3/C formulations, demonstrating high latent heat (205.9 kJ/kg), adequate thermal conductivity and good mechanical compatibility with concrete. CPCM-enhanced panels stabilised indoor temperatures, reduced fluctuations and delayed heat transfer, confirming their suitability for building-envelope thermal regulation and energy conservation.

The literature demonstrates that thermal energy storage - particularly latent heat storage using phase change materials - offers significant potential for improving the energy efficiency, thermal stability and renewable-energy utilisation of buildings. PCM-enhanced systems are capable of reducing heating and cooling loads, shifting peak demand and improving indoor comfort, making them highly relevant for nearly zero-energy and climate-resilient buildings. Although a wide range of PCM applications has been explored, from facade-integrated systems to bio-composites and active storage units, further optimisation, validation and large-scale deployment remain necessary. The findings from previous studies highlight clear opportunities for innovation in material composition, system design and integration strategies.

1.3. High quality insulation materials

Achieving a climate-neutral building stock requires substantial improvements in the thermal performance of building envelopes, as mandated by the European Green Deal and supporting EU policy frameworks. High-quality insulation materials play a central role in this transition, particularly in cold and temperate climates where heating demand remains a major contributor to operational energy use. In this context, aerogels have emerged as a leading candidate for next-generation superinsulation, offering an opportunity to significantly reduce heat losses, minimise envelope thickness and enable multifunctional facade solutions aligned with the main aim of this Thesis - to develop an energy-efficient building envelope capable of supporting building-stock decarbonisation.

Aerogels distinguish themselves from conventional insulation materials through a unique combination of ultralow thermal conductivity, low density and compatibility with advanced envelope technologies. Whereas mineral wool, EPS and polyurethane-based insulations typically achieve thermal conductivities in the range of 0.022–0.040 W/m·K, silica aerogels reach values as low as 0.013–0.020 W/m·K [45], [46], placing them firmly in the category of superinsulation. This substantial improvement allows aerogel-based components to achieve equivalent U-values at a fraction of the thickness required by traditional materials, enabling more compact envelope assemblies, improved architectural flexibility and enhanced retrofit suitability for constrained building facades.

The comparison in Table 1.1 highlights the fundamental differences between aerogels and conventional insulation materials across performance categories such as thermal conductivity, density, mechanical behaviour, durability and cost. While aerogels achieve by far the highest insulation performance and offer additional benefits such as transparency or translucency in certain product forms, they remain significantly more expensive - often exceeding the cost of mineral wool by a factor of ten [46]. Nevertheless, life-cycle analyses suggest that aerogels can deliver net environmental benefits in long-term facade applications [47].

Table 1.1

Aerogel vs. traditional insulation materials

Property	Silica aerogel (blankets / granules)	Mineral wool (Rock wool / Glass wool)	EPS (Expanded polystyrene)	PUR / PIR (Polyurethane / Polyisocyanurate)
Thermal conductivity λ (W/m·K)	0.013–0.020	0.030–0.040	0.032–0.038	0.022–0.028
Density (kg/m³)	80–200	20–150	15–30	30–40
Water absorption / moisture sensitivity	Moderate to high (requires hydrophobic treatment)	Low–moderate	Low	Low
Fire behaviour	Non-combustible, high thermal resistance	Non-combustible	Combustible unless treated	Combustible
Durability / ageing	Stable insulation performance; more research needed on hygrothermal ageing	Good long-term durability	Good durability	Good but can degrade with moisture
Mechanical strength	Low; requires composites or reinforcement	Medium–high	Low–medium	Medium
Thickness required to reach U ≈ 0.15 W/m²K	Very thin (≈ 20–30 mm)	120–150 mm	120–150 mm	80–100 mm
Recyclability	Limited; currently low	High	Moderate	Low
Cost (relative)	Very high (≈ ×10 higher than mineral wool)	Low	Very low	Medium
Advantages	Superinsulation, lightweight, translucent options, thin retrofits	Fire-safe, acoustic insulation, low cost	Low cost, easy installation	Very good thermal resistance, thin layers
Limitations	High cost, moisture sensitivity, mechanical fragility	Lower R-value than aerogel	Flammability, lower durability	Flammability, moisture sensitivity

Given these properties, aerogels provide a promising technological pathway for enhancing the thermal efficiency of building envelopes, especially in deep-renovation and high-performance construction contexts. Their integration into facade elements, glazing systems and composite insulation layers provides a potential route to significantly enhance energy efficiency of the building envelopes capable of supporting the transition toward a climate-neutral building stock.

1.3.1. Characteristics of Aerogels

Nanostructured solid materials composed of amorphous silicon dioxide (SiO_2) - commonly referred to as silica aerogels (Fig. 1.4) - are among the most widely researched superinsulation

materials. Silica aerogels typically consist of approximately 96% air and 4% open-pored silica solid, forming an ultralight, nanoporous network with unique thermal and optical properties. They are generally produced by drying silica gels through ambient, supercritical, or freeze-drying processes, depending on the targeted performance characteristics. Owing to their exceptionally low density (80–200 kg/m³) and nanoscale porosity, silica aerogels exhibit thermal conductivities below 0.020 W/m·K, which places them in the category of superinsulating materials [45].

Fig. 1.4. Silica aerogel.

A widely applied variant, known as opaque aerogel blankets, is used to improve the thermal efficiency of opaque building envelopes by significantly reducing conductive heat transfer. These blankets reach thermal conductivities as low as 0.013 W/m·K. However, compared to conventional insulation materials with similar thermal properties, the production cost of opaque aerogels remains more than ten times higher [46]. Despite this drawback, life-cycle assessment (LCA) research by Lolli and Andresen [47] demonstrates that aerogel-based glazing can yield meaningful reductions in GHG emissions when used for deep renovation of existing apartment buildings. Although aerogel manufacturing produces more GHG emissions per kilogram than argon, the overall cradle-to-grave analysis shows a 5–9% reduction in total GHG emissions, illustrating the long-term environmental benefits of aerogel insulation.

The potential of aerogels extends beyond simple thermal insulation. The integration of aerogel technologies - such as the use of lightweight aerogel glass, aerogel granules in translucent glazing systems and aerogel-enhanced solar walls - enables the development of advanced, multifunctional building envelopes. When combined with other smart materials such as electrochromic, thermochromic and photochromic coatings, as well as PCMs, aerogels create opportunities for hybrid facade systems capable of dynamic optical control, thermal storage and improved solar-energy utilisation [45].

1.3.2. Aerogel Insulation Applications in Buildings

Aerogels are widely regarded as one of the most promising insulation solutions for building applications due to their extremely low thermal conductivity, lightweight composition and high solar-spectrum transmittance - an attribute particularly valuable for daylighting and solar-energy facade systems [48]. Recent years have seen a rapid increase in research focused on the

integration of aerogels into facade systems, renders, glazing units and composite insulation materials.

A recent study evaluated a novel aerogel-based insulating external render subjected to large-scale weathering tests [49]. Despite significant water absorption, the thermal conductivity of the aerogel render remained largely unchanged and overall system performance exhibited minimal degradation. The impact of hygrothermal deterioration on monthly heating loads was negligible, indicating strong durability and energy-saving potential over the system's lifetime.

Knowledge gaps concerning the long-term hygrothermal and mechanical performance of aerogel-based coating mortars were examined by Naman, Pär and Angela [50]. Their findings highlight aerogel mortars as promising multifunctional wall finishes capable of delivering thermal performance comparable to traditional insulation materials. However, further research is needed regarding: (1) hygrothermal and mechanical compatibility with other components in multilayer wall systems, (2) performance under severe moisture exposure and freeze–thaw conditions, (3) early-age behaviour and long-term degradation mechanisms.

These studies indicate that aerogel coating mortars have strong potential for increasing energy efficiency while enabling slimmer, lightweight envelope constructions.

Further research by Paulos and Berardi [51] explored the optimisation of window frames using aerogel granules. Using 48 commercially available window-frame configurations, they showed that filling existing cavities with aerogel can reduce frame thermal transmittance by 4–29%, with complete cavity filling yielding reductions of up to 35%. Aluminium frames demonstrated the greatest improvements, achieving U_f-values as low as 0.46 W/m²·K - performance levels typically difficult to achieve without altering frame geometries or emissivity. Their work highlights aerogel's potential to significantly enhance thermal performance in facade systems with high window-to-wall ratios.

In China, a superhydrophobic wastepaper-based aerogel was developed and assessed as a radiative cooling component for building applications [52]. The resulting superhydrophobic cellulose aerogel cooler (SHB-CAC) demonstrated high solar reflectance and long-wave infrared emittance, achieving surface temperatures 8.5°C below ambient under solar irradiation of 800 W/m². Its hydrophobic and self-cleaning properties prevented moisture accumulation and maintained radiative performance under different humidity conditions. The study recommends further optimisation and modular integration of SHB-CAC into building cooling systems, indicating strong potential for passive cooling in hot climates.

The literature review clearly demonstrates that aerogels represent one of the most promising high-performance insulation technologies for next-generation building envelopes. Their ultralow thermal conductivity, lightweight structure and potential for optical transparency make them uniquely suitable for multifunctional facade systems that contribute both to energy efficiency and to the wider decarbonisation goals of the EU building stock. While current cost barriers and knowledge gaps concerning long-term hygrothermal behaviour still limit large-scale deployment, recent advancements in aerogel-based renders, glazing systems and composite materials indicate strong future potential. As building-envelope innovation moves toward superinsulating, thin and adaptive facade assemblies, aerogels provide a viable technological pathway that aligns closely with the overarching aim of this Thesis - advancing

energy-efficient envelope solutions capable of supporting the transition toward a climate-neutral built environment.

1.4. Adaptive building envelopes

A building envelope that incorporates active components - such as mechanical systems, actuators and responsive materials - to regulate indoor environmental parameters (temperature, humidity, ventilation and daylight) is referred to as an active building envelope [53]. Adaptive building envelopes extend this concept by dynamically modifying their physical, optical, or thermal properties in response to changing exterior climatic loads or interior comfort demands [54]. These systems may integrate mechanical shading devices, automated ventilation strategies, smart glazing technologies, dynamic insulation layers, or other responsive components.

The overarching purpose of both active and adaptive envelope systems is to maintain a comfortable indoor environment while maximising overall energy efficiency, thereby reducing operational CO_2 and GHG emissions. As buildings account for a substantial share of global and European energy consumption, adaptive envelope solutions are increasingly recognised as essential components of high-performance, low-carbon architecture.

1.4.1. Smart Windows

Windows typically constitute the least thermally efficient portion of a building envelope, often driving increased cooling loads due to excessive solar gains. To address this challenge, smart windows have been developed to dynamically modulate solar transmittance. However, conventional smart glazing technologies often struggle to respond effectively to the complexities of real outdoor climate conditions and may still allow considerable heat transfer through convection.

A recent study [55] proposes embedding poly(N-isopropylacrylamide) hydrogel - known for its ultrahigh luminous transmittance and strong solar modulation - into a double-glazed unit during matrix formation to create an active–passive dual-control (APDC) smart window. This system can reduce indoor air temperatures by up to 16 °C compared to conventional glazing. When combined with fluid glass, the APDC configuration demonstrates high energy-saving potential and offers significant reductions in carbon emissions. The primary limitation identified is the risk of water evaporation from the hydrogel, which requires mitigation for long-term stability.

A novel sun-powered smart window blind (SPSWB) system has also been developed [56]. It incorporates self-powered sensing, control and actuation based on thin-film photovoltaic cells, which harvest solar energy, regulate voltage and charge a battery with 55% efficiency. Excess heat absorbed by the PV cells is dissipated using a PVdF-HFP porous cooling coating, achieving surface temperature reductions of more than 9%. An Arduino-based controller manages blind orientation, energy harvesting and thermal regulation. Tests confirm that the system generates substantially more power than required for operation, making it a robust and

autonomous solution for smart-building envelope applications. Potential challenges include acceptance by architects due to its visible PV integration.

Another innovative development involves adaptive solar-modulating windows based on PCM and photonic co-doped vanadium dioxide coatings [57]. These windows display vivid, angle-dependent colours similar to tetra fish skin and achieve high visible transmittance, suitable transition temperatures and enhanced solar modulation performance - surpassing the best-reported VO_2 windows. Simulations demonstrate annual energy savings of up to 35.9 kWh/m² for a typical office building in Asia-Pacific climates. This research illustrates the potential for combining thermal, optical and aesthetic functions in smart window technologies, supporting the evolution of next-generation net-zero energy buildings.

1.4.2. Adaptive facade solutions

Adaptive facade systems incorporate material or structural mechanisms that autonomously respond to shifting internal and external environmental conditions, often without complex electronics, thereby improving energy efficiency while reducing reliance on user intervention [58]. By lowering energy demand and associated emissions, such systems contribute directly to broader goals of building-stock decarbonisation and climate neutrality [59].

Three primary design strategies are typically employed in non-conventional adaptive facades [58]:

1) Geometric transformations using basic movement to create three-dimensional modulation.
2) Deployable or foldable structures capable of altering solar exposure or ventilation.
3) Biomimetic mechanisms, inspired by adaptive behaviours observed in nature

Modelling and simulation tools are crucial in the early design stages, enabling evaluation of energy performance, cost implications and operational strategies for different adaptive configurations [60].

A comprehensive annual performance study evaluated adaptive dynamic building envelopes (ADBEs) for retrofitting buildings in Cardiff, Wales and Grevena, Greece [61]. The implemented systems - comprising building-integrated photovoltaics (BIPVs), added insulation layers, mechanical ventilation with heat recovery and solar air heaters (SAHs) - demonstrated significant contributions to building energy supply. In Cardiff, ADBEs provided up to 60% of annual electricity demand and 21.8% of heating loads, with SAHs further contributing 22% to heating and reducing fuel consumption by 12%. In Grevena, BIPV panels met approximately 43% of total electricity demand. These results highlight the substantial potential of integrated adaptive envelope systems for reducing building energy consumption.

Another study assessed the climate responsiveness of a BiPV facade system incorporating PCM at the rear of PV modules [62]. The PCM reduced PV operating temperatures significantly - particularly under peak solar irradiation - thereby enhancing electrical efficiency. Optimal performance occured under outdoor conditions of up to 600 W/m² solar radiation and 26 °C ambient temperature. Beyond these thresholds, the PCM's latent heat capacity was depleted before the end of the diurnal cycle. The study suggests that controlling airflow velocity and

direction in the facade cavity, based on interior demands, could further enhance the BiPV/PCM system's value as an auxiliary HVAC component. Economic feasibility remains a challenge due to initial investment costs.

Koukelli, Prieto and Asut [63] examined the use of shape memory alloys (SMAs) in kinetic solar envelopes in Athens, Greece. Their prototype demonstrated automatic shading behaviour without external energy input, reducing direct urban heat island (UHI) impact by 40% of reflected solar radiation and decreasing cooling loads by 21%. Although the system's effect on overall UHI mitigation was minimal, the study reveals strong potential for SMA-based adaptive systems while emphasising challenges such as feasibility, user control and material ageing.

Finally, a recent case study proposed a performance-evolution framework for multi-functional kinetic facades using Multi-Objective Evolutionary Algorithms (MOEA) [64]. This approach enables designers to identify optimal facade configurations by balancing criteria such as daylighting, energy consumption, cost and form. The framework's integration of ranking methods and Pareto optimisation allows for systematic evaluation of competing objectives. Future research may incorporate soft-computing techniques (e.g., fuzzy logic) to link occupant comfort perceptions with adaptive design parameters, further advancing the field of intelligent facade systems.

In summary, the literature demonstrates that adaptive facade technologies - ranging from smart glazing systems and kinetic shading devices to PCM-integrated BiPV panels - offer significant potential for reducing building energy consumption and enhancing indoor comfort. These systems leverage responsive materials, innovative control strategies and multifunctional design principles to optimise thermal, optical and ventilation performance under varying climatic and operational conditions. Despite notable advances, challenges remain regarding long-term durability, cost-effectiveness, system integration and the development of reliable modelling tools capable of predicting their behaviour across diverse climates and building types. Addressing these gaps is essential for wider adoption and underpins the motivation of this Thesis, which seeks to advance adaptive envelope research through the development and experimental validation of a dynamic, PCM-enhanced solar facade system designed to improve energy efficiency in Northern European conditions.

1.5. Experimental testing methods for adaptive solar envelopes

The design, construction and operational evaluation of buildings involve multiple stages, each governed by specific energy-efficiency requirements. Many traditional building regulations focus predominantly on limiting the U-values of walls and windows while overlooking other critical parameters such as thermal capacity, dynamic behaviour, or solar-energy utilisation. Furthermore, some regulations fail to account for the contribution of passive solar components - such as ventilated facades or green roofs - to the overall energy balance of a building. Consequently, historical efforts by manufacturers and researchers have concentrated primarily on determining U-values through experimental measurements, leading to the development of standards that define test stand configurations, testing procedures and data analysis methods for this purpose [65].

With the introduction of new regulatory frameworks, emphasis has shifted from the thermal transmittance of individual components to requirements governing a building's overall energy consumption. The total energy demand of a building is influenced not only by the thermal quality of envelope components but also by building systems and occupant behaviour. Therefore, much more precise modelling and testing of envelope energy performance is necessary. Relying solely on steady-state U-value measurements under controlled laboratory conditions is insufficient for characterising the behaviour of modern, adaptive, or solar-responsive facade components. To meet contemporary energy targets, both experimental and numerical approaches must account for dynamic thermal behaviour, which has led to the development of diverse testing procedures - some of which have become internationally recognised standards [66].

In addition to analysing individual components, it is essential to assess the energy performance of entire buildings, particularly in the context of renovation. The poor thermal quality of the existing building stock, combined with slow rates of new construction, necessitates large-scale energy retrofits to meet national and European decarbonisation goals. To evaluate the effectiveness of such interventions, energy audits must be performed both before and after renovation. The need to quantify actual energy performance, combined with requirements for building energy certification, has stimulated the development of a wide range of experimental procedures and standards for characterising both component-level and whole-building energy efficiency.

Given the complexity of thermal processes and boundary conditions in building testing, decision-tree methodologies are recommended for selecting the most appropriate testing approach. These methods help practitioners identify relevant procedures or standards based on the specific objectives of a test. High-quality full-scale testing requires appropriate infrastructure, precise instrumentation and reliable monitoring systems to ensure accurate data acquisition. Data analysis approaches vary from simple averaging and regression techniques to advanced dynamic methods based on systems identification [67].

1.5.1. PASLINK testing method

Dynamic testing of building components requires a carefully designed sensor network and a high-precision monitoring system capable of capturing detailed thermal responses under real outdoor conditions. Such data form the basis of subsequent analyses aimed at determining the thermal balance and performance characteristics of the tested element. Although dynamic data analysis has been widely discussed in the literature since the late 1980s [68], information on the design of monitoring systems is less comprehensive.

The PASLINK methodology evolved from the European research project PASSYS, initiated in 1985 to increase confidence in passive solar building technologies and their evaluation procedures [69]. PASSYS focused on the use of test cells - full-scale, highly instrumented experimental chambers - to characterise the energy performance of passive solar building components and to support the development of design tools for building simulation [70]. The main advantage of PASSYS/PASLINK test cells is their ability to provide a controlled

but realistic indoor environment, free from occupancy effects, enabling accurate and repeatable measurements of component behaviour [71].

Initially, PASSYS test procedures focused on steady-state performance assessment. However, it quickly became evident that dynamic testing and analysis were necessary to obtain high-quality performance indicators for building components exposed to real outdoor climatic variations [72]. This resulted in refinements to the original test-cell design to enhance measurement accuracy [73] and these updated facilities became known as PASLINK cells. Over time, the PASLINK network transitioned from a shared-equipment approach to one based on harmonised quality procedures, including standardised calibration, instrumentation, data acquisition and analysis. These developments significantly improved the robustness, comparability and scientific value of PASLINK test results.

Steady-state testing method

From a building designer's perspective, the most important steady-state performance parameters are the UA-value, representing the total thermal transmittance of a component and the gA-value, describing its solar heat gain. These parameters are defined as follows [74]:

- UA (W/K): the heat flow rate under steady-state conditions divided by the temperature difference across the component;
- gA (m²): the heat flow delivered to the interior environment due to incident solar radiation, divided by the irradiance on the component's plane.

A component's thermal storage capacity and dynamic interaction with the indoor environment are particularly important in systems where solar gains contribute to thermal performance. However, experimental determination of these dynamic properties is complex. Passive solar systems appear simple but involve highly nonlinear thermal processes influenced by component geometry, orientation, building mass and interacting heat sources. The purpose of experimental testing is to isolate these factors and characterise both the component's behaviour and its interaction with the building and occupants.

Direct measurement of heat losses or solar gains is not possible due to the simultaneous occurrence of multiple heat-transfer mechanisms - conduction, convection, longwave radiation and shortwave solar radiation. Instead, their effects can be determined indirectly using net heat-flow measurements across the component, which test cells are specifically designed to capture. The heat balance of a PASSLINK test cell under steady-state conditions can be expressed as:

$$Q_{tc} = P_{hc} - (UA)_t \times \Delta T_s, \tag{1.1}$$

where

Q_{tc} – heat loss through test component, W;

P_{hc} – heating or cooling power for testing room, W;

$(UA)_t$ – UA-value of testing room envelope, W/K;

ΔT_s – temperature between inner and outer surfaces of testing room envelope.

Also, the steady-state heat loss can be expressed as:

$$Q_{tc} = (UA)_{tc} \times T_{in\,out} - (gA)_{tc} \times G_{tc}, \tag{1.2}$$

where

$(UA)_{tc}$ – UA value of the testing component, W/K;
$\Delta T_{in\ out}$ – temperature difference between inside and outside, K;
$(gA)_{tc}$ – gA value of the testing component, m^2;
G_{psc} – solar irradiance on the plane of testing component, W/m^2.
The subsequent transformations lead to linear relationships:

$$\frac{Q_{tc}}{T_{in\ out}} = (UA)_{tc} - (gA)_{tc}\frac{G_{tc}}{T_{in\ out}}, \tag{1.3}$$

that enable determination of UA and gA values from measured data. Only two distinct measurement points are theoretically required to derive these parameters.

Theoretical schematic of a PASSLINK test stand is visualised in Figure 1.5.

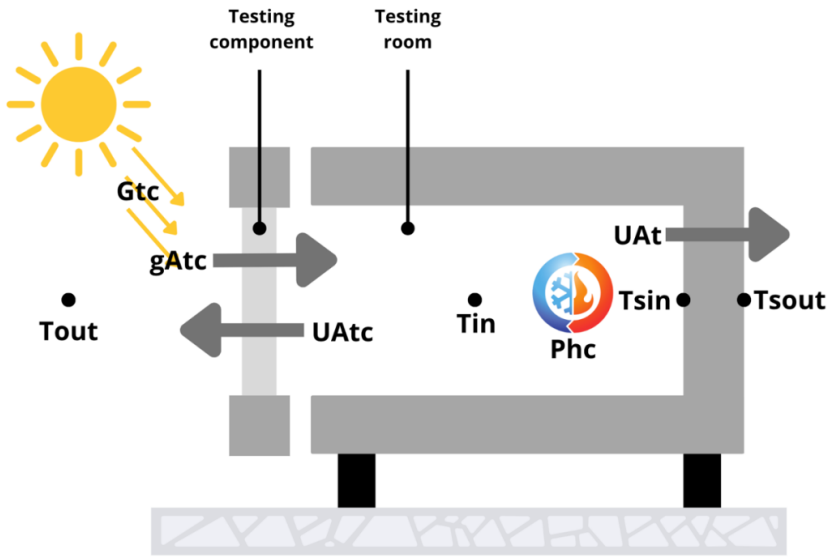

Fig. 1.5. Principle of thermal balance in a PASSLINK test cell.

Dynamic Testing Method

Dynamic characterisation of building components requires high-resolution, high-accuracy data representing temperatures within the component, indoor and outdoor air temperatures, heat fluxes at interior surfaces and solar radiation incident on the component plane. Depending on the component type, additional variables - such as diffuse radiation, longwave exchange, wind speed and direction, relative humidity and precipitation - may also be relevant. The test component must be south-facing and the temperature difference between indoor and outdoor environments should be approximately 20°C to minimise measurement errors. To avoid correlation between the heating/cooling input and outdoor temperature, PRBS or ROLBS excitation signals are required [69].

Accurate heat-flux measurement (>5% precision) is essential. For opaque components in PASLINK cells, direct heat-flux sensors provide reliable data [75]. For semi-transparent elements, heat flux must be derived indirectly through an energy balance of the test cell. This

requires in situ calibration procedures to account for boundary effects, air infiltration and other parasitic influences.

By applying parameter identification techniques, a mathematical model representing the test cell and component can be derived. Model parameters - thermal resistances, capacities and heat flows - govern both dynamic and steady-state behaviour. The model outputs are iteratively adjusted to match measured data until an optimal fit is achieved, typically using specialised optimisation software (Fig. 1.6).

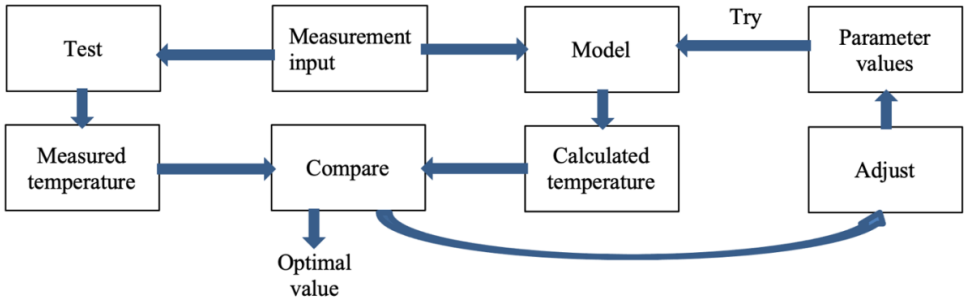

Fig. 1.6. Parameter identification method [74].

An appropriate system-dynamics model must:

- accurately reproduce both steady-state and transient thermal processes;
- separate the thermal behaviour of the test cell from that of the tested component;
- allow linking of identified physical parameters to international standards;
- accommodate certain nonlinearities, such as temperature-dependent thermal resistance or solar transmittance.

When these conditions are satisfied, the resulting model is considered transparent, meaning that all key elements of the thermal balance are clearly represented and physically interpretable.

The PASLINK methodology represents one of the most advanced and reliable experimental frameworks for evaluating the real-world thermal performance of building envelope components. Its combination of full-scale test cells, controlled indoor conditions and exposure to natural outdoor climates enables precise characterisation of both steady-state and dynamic behaviour - capabilities that conventional laboratory methods cannot achieve. By integrating high-resolution monitoring, rigorous calibration procedures and system-identification techniques, PASLINK provides performance indicators that are physically meaningful, reproducible and directly applicable to design and simulation workflows. This makes PASLINK especially valuable for assessing innovative and adaptive facade technologies, including PCM-integrated solar envelopes, where transient effects, solar gains and thermal storage processes play a critical role. Consequently, the PASLINK approach forms a crucial foundation for the experimental validation carried out in this thesis.

1.6. Adaptive envelope computer simulation

The development of adaptive building envelope systems is a complex process that cannot be easily aligned with standardised design workflows. Each prototype typically exhibits unique physical and operational characteristics that limit the applicability of uniform development procedures across different technological cases. To structure and formalise the role of computer simulation within the innovation process, a dedicated seven-step methodology has been established for evaluating the feasibility, performance and potential of novel envelope components (Fig. 1.7) [76]. This methodology serves as a guiding framework that links conceptual development with simulation-based evidence, enabling iterative refinement of prototypes under controlled and representative conditions.

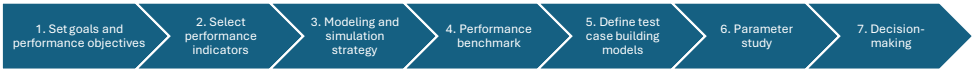

Fig. 1.7. Simulation-based methodology for the research and development of building envelope components.

The first step entails defining the overarching research objective and specifying the operational goals that the innovative component must achieve. Establishing these priorities is essential for identifying the performance dimensions most relevant to the intended application and for delimiting the analytical boundaries of the study, including climatic conditions, building typology and technical constraints. Once the objectives are determined, the second step focuses on identifying suitable performance indicators. These indicators must reflect the component's capacity to influence environmental, economic and user-related outcomes and must be aligned with the criteria defined during the initial planning stage.

The third step involves translating the technological concept into a simulation-ready model. This requires capturing all relevant physical processes - such as heat transfer, solar interactions and material behaviour - and implementing them at an appropriate level of detail to ensure a balance between complexity and numerical accuracy. Empirical measurements play a central role in this stage, as they support parameter identification, model calibration and validation procedures. Because many innovative envelope systems introduce functionalities not yet supported by conventional simulation tools, their modelling may require simplifications, custom algorithms, or rapid virtual prototyping approaches to avoid excessively time-consuming numerical development.

The fourth step consists of evaluating the performance of the prototype in its current state by comparing it with conventional or competing technologies. This comparative analysis typically requires the development of a reference building model that incorporates widely used envelope solutions, enabling the innovative component's advantages and limitations to be assessed in context. This phase often reveals critical weaknesses and improvement opportunities, helping to direct subsequent development.

The fifth step entails defining a set of representative building models for testing. As innovative envelope systems are usually intended for deployment across different building types, the evaluation cannot rely on a single case study. Sensitivity analysis is therefore used to determine which design parameters - whether related to the building or the component - most strongly influence comfort conditions or energy performance. Through this analysis, a structured selection of representative building models is established, ensuring that the prototype is assessed within an appropriately diverse design space.

The sixth step is centred on parameter optimisation and scenario development. Here, the innovative component is systematically integrated into the predefined building models and variations in its physical or operational parameters are analysed to identify the most favourable configurations. Virtual prototyping allows for exploration of specifications that may not yet be practically feasible, while scenario analysis helps to evaluate the robustness of the component under different climatic, operational, or user-related conditions.

Finally, the seventh step focuses on decision-making and iterative refinement. The simulation results are evaluated against the initial objectives and performance requirements defined in Step 1. Based on this evaluation, further improvements to the component are identified and the simulation cycle is repeated as necessary. This process continues until the technological solution meets all required performance criteria and is considered ready for practical implementation. Each iteration of the process represents a new developmental stage, gradually transforming the prototype into a mature and functional system.

1.6.1. Principles for evaluating energy efficiency

A comprehensive evaluation of the effectiveness of an innovative building envelope system requires integrating the component into a complete building model. This approach enables a meaningful comparison with a reference solution - typically a widely used envelope element such as a glazed window - by analysing their respective energy balances over a defined period. When constructing such models, several fundamental considerations must be addressed to ensure analytical consistency and accuracy [77]. First, the heat transfer through all envelope elements must be assessed on an hourly basis across an entire year. The thermal interaction between the building foundation and the surrounding environment must also be represented, as it significantly affects overall heat exchange. In addition, the building's geometric orientation must be considered to account for solar energy gains and all construction materials must be appropriately characterised. Finally, identical boundary conditions - such as indoor temperature and humidity - must be applied to both the innovative and reference cases to ensure comparability. Energy balance and performance assessment may rely either on empirical data measured over at least one full year or on detailed computer simulations carried out using established modelling software.

Building energy consumption analysis typically follows a structured sequence of analytical steps designed to describe thermal behaviour, system operation and economic implications [78]. The process begins with calculating the heating and cooling loads required to maintain a stable indoor temperature as external weather conditions and internal heat sources fluctuate.

This load calculation determines the thermal demand placed on the building and quantifies how much heating or cooling is necessary to maintain comfort conditions given the effects of thermal mass and dynamic gains.

The next step evaluates the energy delivered or extracted by the HVAC system in response to this demand. This analysis accounts for system characteristics, operational strategies and equipment performance, forming the basis for determining the total energy required for conditioning the indoor environment. Subsequently, the primary energy needed to operate the generation systems - such as boilers, chillers, or solar collectors - is assessed, taking into consideration their efficiencies and operational characteristics. This provides insight into the actual fuel and electricity requirements associated with maintaining indoor comfort conditions.

The final step concerns the economic evaluation of the chosen building systems. Costs associated with equipment, installation, operation, maintenance and potential upgrades are compared with alternative investment options. This financial assessment ultimately determines whether the integration of energy-efficient or innovative technological solutions is economically viable relative to conventional approaches.

Simulation tools support all steps of this analytical framework. Depending on the complexity of the research and the specificity of the system under study, analyses may be conducted using a single software environment or by combining several specialised tools capable of representing different physical domains or system interactions.

1.6.2. Simulation tools for adaptive solar envelopes

A wide range of software tools is used to model thermodynamic processes in building envelopes, especially when phase change materials (PCMs) or other dynamic elements are integrated into adaptive solar facades. Among the most widely applied tools are ANSYS, TRNSYS, COMSOL Multiphysics, MATLAB and EnergyPlus. As highlighted in earlier reviews [79], these programs support PCM-enhanced envelope modelling to varying degrees of complexity, ranging from simplified to intermediate and fully sophisticated approaches. Tools such as ANSYS and COMSOL fall into the latter category, offering high-fidelity modelling capabilities for complex geometries, transient heat transfer and phase change processes. All the reviewed tools have been applied in studies assessing PCM behaviour within building envelopes [80].

To determine which of these platforms are most suitable for adaptive solar envelope simulations, a systematic literature review was conducted using bibliometric analysis and detailed examination of modelling practices in PCM research. The initial Web of Science search combined terms related to PCMs and numerical simulation to identify the main domains where PCM behaviour is studied. This broad search yielded 6207 articles and revealed four dominant research themes: building and solar-energy technologies, lithium-ion battery thermal management, heat transfer enhancement (including nano-enhanced PCMs) and molecular dynamics. VOSviewer was used to analyse keyword co-occurrence patterns and visualise these thematic clusters (Fig. 1.8) [81].

A second stage of the review focused specifically on the five heat transfer simulation tools - ANSYS, COMSOL, TRNSYS, MATLAB and EnergyPlus - using keyword combinations such as building, PCM, simulation, numerical analysis and the name of each software. This allowed comparison of how frequently each tool is used and in what research contexts. ANSYS yielded the largest number of publications (613), followed by COMSOL (365), MATLAB (363), TRNSYS (212) and EnergyPlus (173).

ANSYS-related studies commonly combine PCM research with themes such as heat transfer enhancement, building thermal performance and battery thermal management. COMSOL studies similarly address PCM behaviour but show stronger links to finite element methods and coupled multiphysics approaches. TRNSYS is more frequently associated with building-level modelling, thermal comfort, heat pumps and renewable energy integration. MATLAB is used for simplified or control-oriented PCM modelling and for investigations linking building envelopes with photovoltaic or thermal systems. EnergyPlus appears less frequently but is consistently applied to building energy performance assessments and thermal comfort evaluations.

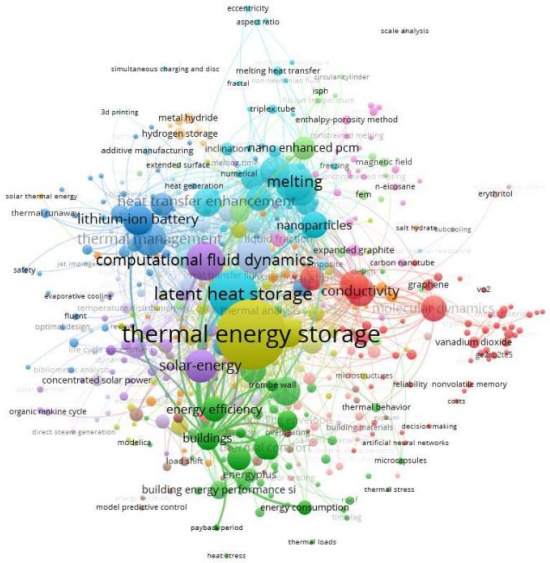

Fig. 1.8. VOSviewer keyword network for PCMs and numerical simulation.

A more focused analysis of ANSYS studies - conducted using a refined Web of Science search for the period 2019–2023 - resulted in 42 relevant publications. These were categorised according to the ANSYS module used, the modelling time scale, the model size, the building element studied and the validation method. Most studies relied on ANSYS Fluent, with only two using ANSYS CFX. A clear pattern was observed regarding modelling time scales: only one study performed a year-long simulation [82], whereas the majority used much shorter periods such as a day [83],[84],[85], a week [86], or up to a month [41],[87],[88],[89],[90],[91].

Many studies used even shorter time steps or did not clearly specify duration. This indicates a notable research gap, as very few studies investigate seasonal or annual PCM performance using ANSYS.

Regarding model scale, most studies employed small-scale element models [41], [80], [84], [85], [86], [87], [88], [89], [90], [91], [92], [93], [94], [95], [96], [97], [98], [99], [100], [101], [102], reflecting early-stage investigations of novel envelope materials or configurations. A smaller portion examined room-scale performance [41], [82], [85], [86], [87], [89], [90], [103], [104], [105], while only isolated cases explored full-building applications. Across these publications, PCM integration was studied in a wide variety of envelope components: walls [106], [107], [108], [109], [110], [111], [112], [113], [114], [115], [116], [117], [118], [119], roofs [120], [121], [122], [115], floors [114], windows [123] and HVAC systems, including ventilation ducts [124], [125], [126], [127], [128], [129], [130], [131] and heat exchangers [132], [133], [134], [135], [136], [137], [138], [139].

Model validation practices were also diverse. Experimental validation was used most frequently, appearing in 20 studies [106], [124], [125], [120], [140], [109], [132], [112], [133], [126], [127], [122], [135], [136], [129], [130], [138], [115], [139], [117]. One study applied analytical validation [113], while four relied on comparisons with results published in other scientific literature [46–49] [120], [131], [114], [116].

Overall, the literature review highlights several important insights for simulation of adaptive solar envelopes. ANSYS Fluent remains the most dominant platform for high-fidelity PCM modelling, especially at small scales where complex phase change dynamics must be resolved. However, the limited number of long-term or whole-building simulations points to an existing research gap, particularly relevant for adaptive solar envelope design where seasonal performance is critical. The review also illustrates the versatility of PCM applications across various envelope components and HVAC subsystems, reinforcing the need for multi-scale and multi-tool simulation approaches in future research.

1.7. Conclusions

The comprehensive literature review presented in the preceding chapters establishes a coherent scientific, technological and policy-based foundation for the development of an adaptive solar facade system integrating phase change materials for thermal energy storage. The analysis has addressed six interrelated domains: EU building-stock policy, thermal energy storage principles, PCM technologies, high-performance insulation materials, adaptive building envelopes and experimental–numerical evaluation methodologies. Together, these domains define both the urgency of building-envelope innovation and the methodological pathway required to realise it.

The review of EU building-stock policy clearly demonstrates that the decarbonisation of the building sector is a central pillar of the European Green Deal and its associated legislative instruments, including the EPBD, the EED and the Renovation Wave Strategy. These frameworks collectively promote the transition toward ZEB, increased renovation rates, integration of on-site RES and the adoption of smart, adaptive building technologies. Since

buildings account for a substantial proportion of final energy consumption and CO_2 emissions in Europe, improvements at the building-envelope level represent one of the most effective strategies for reducing operational energy demand. The policy context therefore directly supports the development of adaptive, energy-efficient and storage-integrated facade systems, confirming the scientific and societal relevance of this Thesis.

The investigation of TES technologies highlights the critical role of storage systems in enabling effective utilisation of intermittent renewable energy sources, particularly solar energy. LHTES, based on PCMs, offers significantly higher energy storage density than sensible heat systems and enables thermal energy to be stored and released at nearly constant temperatures. This characteristic makes PCMs particularly suitable for integration into building envelopes, where they can moderate indoor temperature fluctuations, shift peak loads and enhance solar-energy utilisation. The literature confirms that PCM-enhanced components can reduce heating and cooling demand, improve indoor comfort and support net-zero-energy building objectives. However, despite extensive laboratory research and small-scale applications, large-scale, long-term validation of PCM-integrated facade systems remains limited. This gap underlines the need for systematic experimental and numerical investigation at both component and building scales.

The analysis of PCM categories further clarifies the suitability of different materials for building integration. Solid–liquid PCMs, particularly paraffin-based organic materials, demonstrate favourable thermophysical properties, including appropriate melting-temperature ranges, stable cycling behaviour, low supercooling and chemical stability. Although inorganic and eutectic PCMs offer certain advantages, issues such as phase segregation and long-term stability require further optimisation. These findings support the material-selection strategy adopted in this Thesis, which focuses on PCMs appropriate for Northern European climatic conditions and seasonal performance variability.

High-performance insulation materials represent another essential component of advanced envelope design. The literature review identifies silica aerogels as one of the most promising superinsulation technologies due to their ultralow thermal conductivity, lightweight nanoporous structure and potential for integration into multifunctional facade systems. Aerogels enable significant reductions in envelope thickness while maintaining high thermal resistance, making them particularly suitable for deep renovation and space-constrained applications. Although current cost levels and long-term hygrothermal durability require further research, life-cycle assessments indicate meaningful reductions in greenhouse gas emissions when aerogel-based systems are implemented. Their compatibility with PCM layers and adaptive facade concepts further reinforces the feasibility of hybrid envelope solutions combining insulation, thermal storage and solar management functions.

The review of adaptive building envelope technologies demonstrates a paradigm shift from static envelope components toward responsive, multifunctional systems capable of dynamically regulating thermal and solar performance. Smart glazing, kinetic shading devices, BiPV and PCM-enhanced facade systems illustrate the broad spectrum of adaptive solutions currently under development. Experimental and simulation-based studies show measurable reductions in cooling loads, improved photovoltaic efficiency and significant annual energy savings.

Nevertheless, challenges remain regarding durability, cost-effectiveness, modelling reliability and system integration. These limitations highlight the importance of robust validation methodologies capable of capturing both steady-state and transient thermal behaviour under real climatic conditions.

In this context, the review of experimental testing methods confirms that traditional steady-state U-value measurements are insufficient for characterising adaptive and solar-responsive facade systems. Dynamic performance evaluation requires high-resolution monitoring of temperatures, heat fluxes and solar radiation under realistic outdoor conditions. The PASLINK methodology, evolved from the PASSYS project, provides a comprehensive experimental framework based on full-scale, highly instrumented test cells. By combining controlled indoor environments with exposure to natural climatic variations, PASLINK enables accurate determination of both steady-state and dynamic performance parameters. Its integration with system-identification techniques allows derivation of physically interpretable thermal resistances, capacities and solar-gain indicators. This methodology is particularly suitable for evaluating PCM-integrated adaptive solar envelopes and therefore forms a central component of the experimental strategy adopted in this Thesis.

Complementing experimental validation, computer simulation plays a fundamental role in the development and optimisation of innovative envelope systems. The seven-step simulation methodology identified in the literature provides a structured approach for linking conceptual design, performance indicators, modelling, benchmarking, optimisation and iterative refinement. High-fidelity numerical tools such as ANSYS Fluent, COMSOL, TRNSYS, MATLAB and EnergyPlus enable analysis of transient heat transfer, phase-change behaviour and whole-building energy performance. However, bibliometric analysis reveals that most PCM-related simulations are conducted at small scales and over short time periods, with relatively few studies addressing seasonal or annual performance at the building level. This gap is particularly relevant for adaptive solar envelopes intended to operate under highly variable Northern European climates. Consequently, the integration of multi-scale modelling by combining detailed CFD analysis with long-term building energy simulations represents a key methodological advancement pursued in this research.

In conclusion, the literature review confirms that building-envelope innovation is central to achieving EU climate-neutrality objectives and that PCM-integrated adaptive solar facades represent a promising pathway toward enhanced energy efficiency and renewable-energy utilisation. At the same time, significant gaps persist in long-term validation, multi-scale modelling and full-system integration. By combining material science, full-scale experimental testing and advanced numerical simulation within a structured methodological framework, this Thesis addresses these gaps and advances the development of adaptive, storage-enhanced solar envelope systems tailored to Northern European conditions.

2. METHODOLOGY

The methodological framework of this research is based on a systematic, multi-stage investigation of a dynamic solar facade system incorporating thermal energy storage using phase change materials. To evaluate the feasibility, performance and adaptability of the facade concept, the methodology integrates 3 stages (Fig. 2.1):

1) Testing PCM properties for ANSYS simulations: material-level experimental and numerical characterisation of PCM behaviour under controlled thermal loading.
2) Small-scale optimisation: component-level testing of small-scale facade modules using PASLINK-type laboratory and outdoor setups with simulated and real solar loads.
3) Large-scale outdoor testing: System-level outdoor comparative testing of full-scale facade module in relevant climatic conditions.

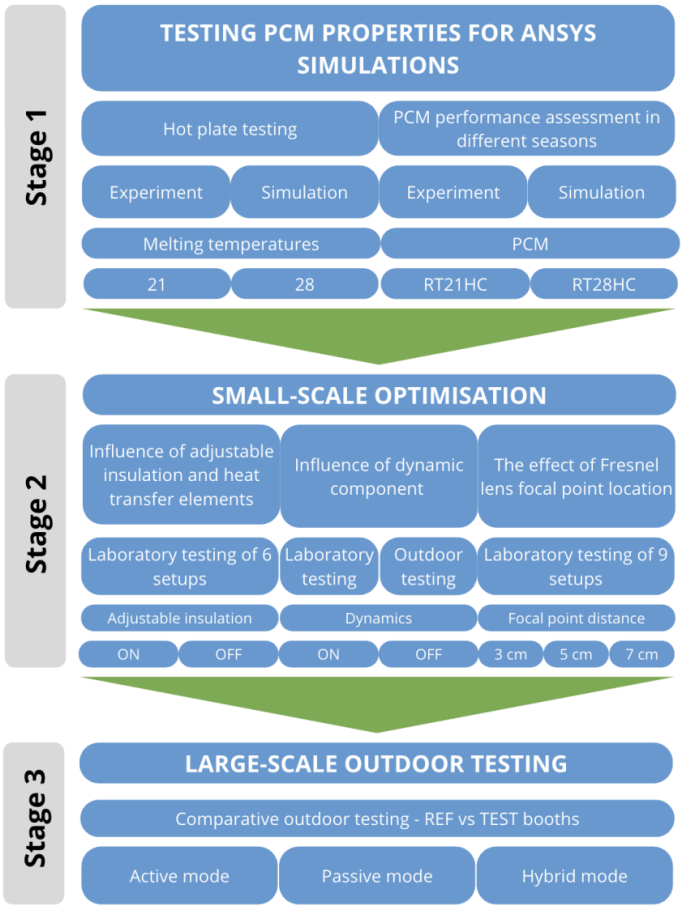

Fig. 2.1. Research methodology.

Together, these stages form an iterative design, testing and validation workflow that supports the development of the technology from conceptual design toward demonstration in

relevant environmental conditions. The following chapter presents the methodological choices, experimental setups, data acquisition systems, analytical tools and simulation approaches used throughout the research.

2.1. Research design and methodological rationale

A quantitative methodological approach was selected because the research required precise and reproducible evaluation of several key thermal parameters, including heat-flux dynamics, PCM charging and discharging behaviour, facade module performance under transient outdoor and simulated weather conditions, indoor temperature responses and associated impacts on heating and cooling energy consumption. All experimental investigations generated high-resolution, time-dependent datasets containing temperatures, heat fluxes, solar irradiance measurements and energy-consumption data. These datasets enabled robust statistical analysis, accurate parameter identification and reliable calibration and validation of the numerical models developed later in the study.

PASLINK-type testing plays an essential role within this methodology because the behaviour of PCM-based dynamic facades cannot be adequately assessed using steady-state analysis. PCMs exhibit hysteresis, rate-dependent phase transitions and varying storage efficiencies depending on the interaction between indoor-outdoor temperature gradients and solar input. PASLINK setups enable controlled indoor boundary conditions while allowing fully dynamic external exposure, thus creating a measurement environment that captures the transient nature of PCM behaviour. The PASLINK approach also supports long-duration monitoring, which is crucial for analysing multi-day charging and discharging cycles, diurnal patterns and seasonal effects that influence the operational viability of PCM-integrated facade systems.

The experimental study (Table 2.1) comprised seven physical experiments and two numerical simulation studies. These included PCM hot-plate tests, seasonal simulations of PCM behaviour using small-scale PASLINK setups, laboratory and outdoor assessments of dynamic optical components, optimisation of Fresnel-lens focal-point positioning and large-scale facade evaluation using PASLINK outdoor test booths. Numerical simulations complemented these tests by modelling PCM phase-transition processes, solar-concentration effects and heat transfer under various climatic conditions.

Table 2.1

Overview of the experimental study

Stage	Denotation	Experiment / Simulation	Type	Data obtained	Aim
1	**E1** – HP 21/28	Hot-plate experiment	Small-scale laboratory experiment	Temperatures, heat fluxes	Comparison of melting temp.: 21°C vs 28°C
	E2 – PCM 21/28	Experiment: PCM performance	Small-scale comparative PASLINK	Temperatures, solar irradiance	PCM performance evaluation: RT21HC vs RT28HC

		assessment in different seasons	laboratory experiment		
	S1 – HP 21/28	Hot-plate simulation	Small-scale simulation	Temperatures, melting/solidification	Calibration of the PCM model for S2
	S2 – PCM 21/28	Simulation: PCM performance in different climate zones	Small-scale simulation	Temperatures, melting/solidification	PCM performance evaluation: RT21HC vs RT28HC
2	**E3** – ADJ ON/OFF	Experiment: Influence of adjustable insulation layer	Small-scale comparative PASLINK laboratory experiment	Temperatures, heat fluxes	Evaluation of adjustable insulation: ON/OFF
	E4 – DYN-LAB ON/OFF	Experiment: Influence of dynamic component	Small-scale comparative laboratory experiment	Temperatures, heat fluxes	Evaluation of dynamic component: ON/OFF
	E5 – DYN-OUT ON/OFF	Experiment: Influence of dynamic component (outdoor)	Small-scale comparative outdoor experiment	Temperatures, heat fluxes, solar irradiance	Evaluation of dynamic component: ON/OFF
	E6 – FP-LAB 3/5/7	Experiment: Fresnel lens focal-point optimization	Small-scale comparative laboratory experiment	Temperatures, solar irradiance	Identification of focal-point distance: 3/5/7 cm
3	**E7** – TEST A/P/H	Experiment: On-site testing of dynamic facade system with solar-energy storage	Large-scale comparative outdoor experiment	Temperatures, heat fluxes, solar irradiance, energy consumption	Evaluation of performance: Active/Passive/Hybrid mode

2.2. Measurement instrumentation

A comprehensive set of measurement instruments was deployed across all laboratory, small-scale and large-scale outdoor experiments to ensure accurate, high-resolution monitoring of thermal behaviour, solar gains, PCM phase-transition dynamics and energy use. Table 2.2 summarises the complete list of equipment used throughout the experimental study, including thermocouples, pyranometers, heat-flux sensors, solar simulators, data-acquisition systems and energy-consumption meters. The table also lists relevant metrological properties such as accuracy and uncertainty, which are essential for evaluating data quality and performing uncertainty analysis.

Table 2.2

Measurement equipment used across experiments

Equipment Type	Model / Type	Measured Variable	Measurement Range	Accuracy / Uncertainty	Relevant experiment
Thermocouple	Type T thermocouple	Temperature, °C	−270 to 1260 °C	±2.2 °C or ±0.75%	E1 to E7

Pyranometer	Kipp & Zonen CMP3	Solar irradiance, W/m²	Spectral range 300–2800 nm	Sensitivity 10–32 µV/Wm²; Temp. dep. <4%; Max. 2000 W/m²	E2 to E7
Heat Flow Plate	ALMEMO FQAD19T	Heat flux, W/m²	Heat flux: +/- 260 kW/m²	Heat flux uncertainty ±5% at 23°C	E1
Heat Flux / Temperature Sensor	Hukseflux FHF04	Heat flux and temperature, W/m² and °C	Heat flux: +/- 10 kW/m²; Temp.: -70 to 120 °C	Heat flux uncertainty ±5% (k=2); Temp uncertainty 2% of value	E7
Heat Flux Sensor	FluxTeq PHFS-01e	Heat flux and temperature, W/m² and °C	Heat flux: +/- 150 kW/m²; Temp.: -50 to 120 °C	Heat flux uncertainty ±5% (k=2); Temp. uncertainty 2% of value	E3 to E5
Solar Simulator – Halogen Lamp	GE SUPER CP60 EXC VNS 230V 1000 W, G16d 3200K	Solar radiation (simulation)	0-1000 W/m²	-	E2 to E6
Solar Lamp Dimmer	UNI BAR, Elation Professional	Modulation of lamp irradiance	0-1000 W/m²	-	E2 to E6
Energy analyzer	CARLO GAVAZZI EM111	Energy consumption	-	-	E7
Multipurpose Data Logger	Campbell Scientific CR1000	Data acquisition (temp., heat flux, irradiance)	-	Sampling period 1 min	E1 to E7
Multiplexer	Campbell AM16/32	Channel expansion for sensors	-	Sampling period 1 min	E1 to E7
Controller	WAGO PFC200	Data acquisition (temp., heat flux, irradiance, energy consumption)	-	Sampling period 1 min	E7

The instrumentation strategy integrates temperature, heat flux, solar irradiance and power consumption measurements into a unified data-logging platform controlled primarily by multipurpose dataloggers. Thermocouples were installed within the PCM at multiple depths, on module surfaces, in air cavities, behind the Fresnel lens and at various locations inside the PASLINK booths. Pyranometers were used to monitor vertical solar irradiance on the facade plane during outdoor tests and to calibrate irradiance levels inside the climate chamber during laboratory solar-simulation tests. Heat-flux sensors were deployed in different locations depending on the experiment, most often on interior module surfaces or on the interior surfaces of PASLINK booths to quantify inward heat flow. During laboratory solar-simulation tests, halogen-based solar simulators provided irradiance levels between 440 and 1000 W/m², adjusted via dimming controllers. All sensor signals were recorded by Campbell Scientific dataloggers (CR1000 series), AM16/32 multiplexer units and WAGO controller (PFC200), providing sampling intervals of approximately one minute.

2.3. Materials and equipment

This research employed a combination of controlled laboratory infrastructure, custom-built test stands and multiple generations of facade module prototypes to experimentally evaluate the thermal performance of PCM-enhanced dynamic solar facades. The materials and equipment

described in this section represent the physical components of the facade modules themselves, as well as the environmental systems used to impose well-defined and repeatable boundary conditions. The aim is therefore to describe the structural materials, phase-change media, solar-concentration elements, insulation components and experimental test stands that formed the basis of all investigations.

Two commercially available paraffin-based PCMs (RT21HC and RT28HC) were used throughout the research. Manufacturer-provided material properties of both PCMs are listed in Table 2.3 and 2.4.

Table 2.3

RT21HC properties

Parameter	Value	Unit
RT21HC		
Melting area	20-23	°C
Congealing area	21-19	°C
Heat storage capacity ±7.5%	190	kJ/kg
Specific heat capacity	2	kJ/kgK
Density solid at 15°	0.88	kg/l
Density liquid at 25°	0.77	kg/l
Heat conductivity (both phases)	0.2	W/mK
Volume expansion	14	%
Flash point	140	°C
Max operation temperature	45	°C

Table 2.4

RT28HC properties

Parameter	Value	Unit
RT28HC		
Melting area	27-29	°C
Congealing area	29-27	°C
Heat storage capacity ±7.5%	250	kJ/kg
Specific heat capacity	2	kJ/kgK
Density solid at 15°	0.88	kg/l
Density liquid at 25°	0.77	kg/l
Heat conductivity (both phases)	0.2	W/mK
Volume expansion	12.5	%
Flash point	165	°C
Max operation temperature	50	°C

These were selected because their melting temperatures align with indoor thermal-comfort ranges and are highly suitable for facade-integrated latent heat storage applications. RT21HC has a melting temperature of approximately 21 °C and is characterised by a high latent heat capacity and a narrow phase-transition range, enabling effective thermal buffering during diurnal charging-discharging cycles. RT28HC, with a melting temperature of around 28 °C,

was used to assess the impact of higher transition temperatures under both cold-season and warm-season outdoor conditions.

Both PCMs were encapsulated in rectangular glass containers whose external dimensions varied between experiments; however, the internal geometry remained constant within each experiment to ensure comparability. In several module generations, copper plates or rods were incorporated into the PCM containers to enhance internal heat transfer and reduce thermal stratification during the phase-transition process.

Multiple insulation strategies were tested. Silica aerogel insulation was used extensively as a high-performance, translucent, low-density insulating layer. Aerogel was applied fully, partially, or within dynamic components such as reflective blades or cone-shaped optical elements. Air gaps (flat and conical) were used to manipulate convective heat transfer and influence the solar-concentration pathway. Cone-shaped air gaps with PMMA or Fresnel lenses on the exterior were key features in experiments investigating the influence of cone geometry and focal-point position on PCM charging efficiency. Additionally, an adjustable insulation layer was applied during nighttime discharging in certain laboratory experiments to reduce heat losses without hindering daytime charging.

Optical components played a central role in the dynamic facade modules. PMMA covers acted as transparent protective layers in non-concentrating configurations, allowing unaltered solar radiation to reach the PCM while providing mechanical stability. Fresnel lenses, also made from PMMA, were used in concentrating configurations to intensify solar radiation on the PCM container and significantly increase charging temperatures. Their positioning relative to the PCM surface was varied to identify optimal focal-point alignment.

All laboratory experiments were conducted using manually constructed testing stands within controlled environmental chambers capable of reproducing both steady-state and dynamic seasonal conditions. Outdoor experiments were carried out on the rooftop of Riga Technical University (Riga, Latvia), on custom-built stands directly facing South. The methodological approach, test-stand design, specific experimental procedures and results for each investigation are described in detail in the following chapters.

3. TESTING PCM PROPERTIES FOR ANSYS SIMULATIONS

Based on the methodological framework outlined in chapter 2, in this chapter the evolution of the experiments and simulations for the material-level testing of PCM behaviour are presented. Two experiments (E1 and E2) and two numerical simulations (S1 and S2) were conducted as part of this initial research stage. The obtained results are compiled and discussed in relation to the subsequent development phases of the study, ensuring a coherent progression from material testing to system-level design.

3.1. Comparison of two PCMs with melting temperatures 21 °C and 28 °C using hot plate experiment (E1 – HP 21/28)

3.1.1. Hot plate testing methods

Recent studies [141], [142], [143] indicate that two principal laboratory methods are used to characterise PCM-based building-envelope components: the Guarded Hot Plate (GHP) and the Heat Flux Meter (HFM) techniques. Both approaches are fundamental for assessing the thermal performance of envelope materials containing PCMs. Following the procedures defined in ISO 8302:1991 and ISO 8301:1991, these methods provide accurate and standardised measurements of effective thermal conductivity under steady-state conditions. They are particularly useful for analysing the complex thermal behaviour of PCMs near the phase-transition region, where apparent conductivity varies significantly. One of the key benefits of hot-plate-type methods is their ability to quantify the effective thermal conductivity of PCM-enhanced materials, which is a critical parameter for evaluating their insulation performance and latent-heat storage capability.

Based on the relevant standards, Table 3.1 presents a comparison of the two methods, highlighting the key differences between the Heat Flow Meter (HFM) and Guarded Hot Plate (GHP) techniques, specifically in the context of testing PCM-integrated building-envelope materials.

Table 3.1

Comparison between GHP and HFM methods

Feature	**Heat Flow Meter (HFM)**	**Guarded Hot Plate (GHP)**
Standardization	ISO 8301, ASTM C518	ISO 8302, ASTM C177
Measurement Principle	Indirect method based on heat flux sensors and temperature difference	Direct method based on electrical power input and steady-state temperature gradient
SI Traceability	Secondary method – relies on calibration with reference materials	Primary method – directly traceable to SI units (W, m, K)
Accuracy	Good (±2-3%) when calibrated correctly; depends on reference material quality	Very high (±1-2%) due to absolute method

Speed	Faster in steady-state or dynamic mode (especially for thin or low-density samples)	Slower due to long time to reach thermal equilibrium (3+ hours)
Dynamic Testing Capability	Supports transient and sinusoidal response analysis; can determine thermal effusivity and dynamic conductivity	Not suitable for dynamic (non-steady-state) testing
Ease of Use	Simpler setup, easier automation, suitable for routine lab and QC use	Requires more complex setup, stable lab environment, careful control of boundary conditions
Adaptability to Moist or Hygroscopic Materials	Supports moisture-coupled tests (e.g., moist insulation or hygroscopic PCMs)	Limited use; typically used under dry, controlled conditions
Suitability for PCM Phase Change Behaviour	Good for capturing phase change effects in dynamic or step-response tests; useful in building-scale applications	Excellent for determining effective conductivity across phase change range in steady-state conditions
Sample Size and Shape Flexibility	Can accommodate large or irregular shapes; typically one-sided measurement	Requires two identical or symmetrical samples (double-sided configuration), although single-sided variants exist
Best Use Case	Routine testing, product development, dynamic PCM behaviour studies	High-precision thermal characterization, material certification, model validation

3.1.2. Experimental design (E1 – HP 21/28)

Based on the comparison between both methods (GHP and HFM), it was concluded that HFM method is the most suitable for PCM testing in this particular experiment.

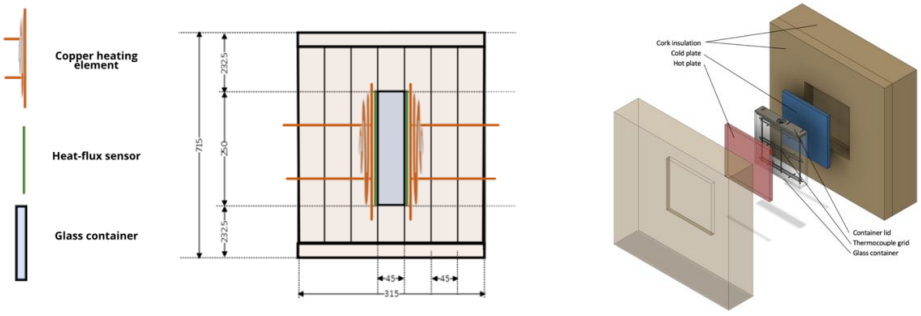

(a) (b)

Fig. 3.1. Experimental stand for the hot plate test: a) cross-section of the apparatus and b) schematic of the component layout.

The hot plate experimental design is based on information provided by standards ISO 8302 and ASTM C177, both of which provide detailed guidelines for apparatus design, sample conditioning and measurement procedures. These standards ensure consistency and

reproducibility of results across laboratories and countries, which is crucial for building certification and scientific comparison. Experimental hot plate stand is presented in Figure 3.1.

The hot plate stand comprises four main components: 1) a glass container filled with PCM; 2) heating and cooling plates fabricated from copper; 3) measurement instrumentation, including two heat flux sensors mounted on the front and rear surfaces of the glass container and thermocouples inserted into the PCM; 4) cork insulation surrounding the setup to minimize the influence of ambient conditions. To achieve the required temperature conditions on the hot and cold plates, water is circulated through embedded copper tubing. Detailed technical specifications of the components used in the hot plate testing setup are presented in Table 3.2.

Table 3.2

Component specifications for hot plate testing setup

Material	Parameter	Value	Unit
Cork insulation boards	thickness	50	mm
	heat conductivity	0.045	W/mK
	density	>230	kg/m^3
	tensile strength	>400	kPa
Copper plate	width	250	mm
	length	250	mm
	thickness	2	mm
	heat conductivity	398	W/mK
Copper pipe	diameter	12	mm
	thickness	1	mm
	heat conductivity	398	W/mK
Copper shavings (around the copper pipe)	heat conductivity	398	W/mK
	Silicone pipe		
	diameter	12	mm
	thickness	2	mm
	heat conductivity	0.17	W/mK
Insulation of pipes	thickness	10	mm
	heat conductivity	0.051	W/mK
Glass container	Dimensions	250 × 250 × 56	mm
	Thickness	4	mm
Water tank with water heater *Huber Microprocessor Control MPC*	-	-	-
Self-priming diaphragm pump 3L/min 12V DC	-	-	-
Three-way valves, valves	-	-	-

The copper heating element, functioning as the “hot plate,” was constructed from two 250 × 250 mm copper plates (1 mm thickness) and an 8 mm outer diameter copper tube, with copper shavings added to enhance thermal contact. The copper tube was bent into a serpentine arc and soldered onto one of the plates to maximize the heat exchange surface area. Copper shavings were inserted between the tube loops to further improve heat distribution. Nine T-type

thermocouples were affixed diagonally across the surface of the copper plate facing the test specimen, spaced evenly and secured using aluminium adhesive tape. To ensure good thermal contact, thermal paste (thermal conductivity: 0.78 W/m·K) was applied over the thermocouples before attaching the second copper plate on top, completing the heating assembly (see Fig. 3.2).

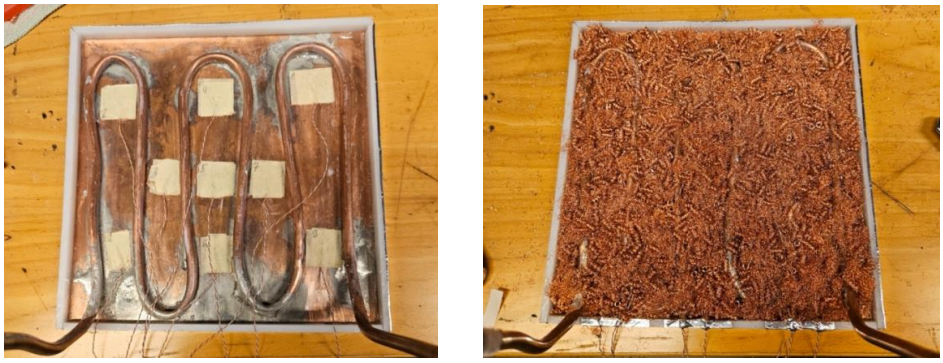

Fig. 3.2. Design of the hot/cold plate for the apparatus.

The PCM container was assembled from 4 mm thick glass sheets bonded using ultraviolet (UV) adhesive, ensuring a clean and durable seal. The container lid and integrated thermocouple holder were fabricated using a 3D printer, specifically designed to maintain precise thermocouple positioning throughout all phases of the experiment. A total of 27 T-type thermocouples were strategically distributed within the container to monitor temperature variations across the entire PCM volume. These sensors were positioned at various depths and heights to capture spatial temperature gradients during thermal cycling (see Fig. 3.3). The external dimensions of the container are 250 × 250 × 56 mm, corresponding to an approximate internal volume of 2.8 litres.

Two separate water tanks were used in the experiment – for heating and cooling both plates. A Huber electric thermal bath provided a stable temperature of maximum 28 °C for the heating circuit, using distilled water as the heat transfer fluid. For the cooling phase, a custom-made 50 L water tank was employed, in which the water temperature should be able to maintain as low as 2 °C. This cooling tank was placed inside a climate chamber to ensure stable thermal conditions throughout the test. A EuroPump 12 water pump, with a rated flow capacity of 12.5 L/min, was used to circulate water through the heating and cooling circuits. During the heating phase, the pump transferred hot water from the heating bath to the copper "hot plate" and back to the tank. In the cooling phase, the pump was redirected to circulate cold water from the chilled tank to the "cold plate" and return it to the reservoir. To minimize thermal losses, all connecting pipes between the tanks, pump and copper tubing in the plates were thermally insulated.

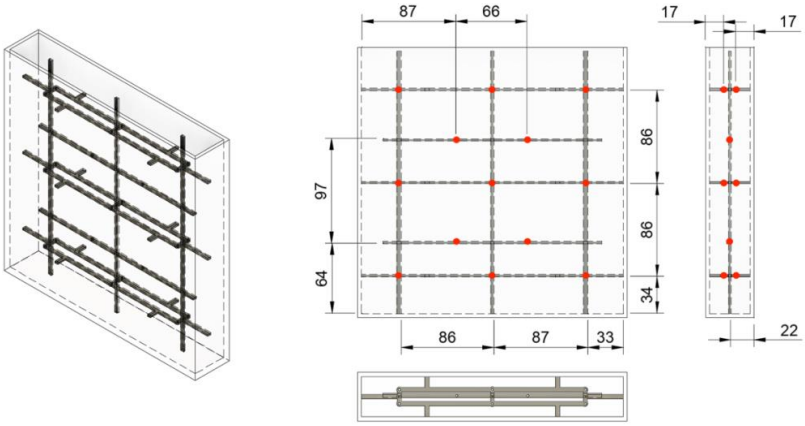

Fig. 3.3. Glass container and a holder for thermocouples. Red dots represent the location of thermocouples.

The test setup was instrumented with thermocouples connected to a data logger for temperature data acquisition (see Fig. 3.4 b). A total of 40 thermocouples were deployed: 22 sensors were embedded within the PCM inside the glass container and 18 sensors were positioned between the two copper plates to monitor the plate temperatures. Heat flux measurements were obtained using two *Ahlborn* 250 × 250 mm heat flux sensors, mounted on either side of the test sample (see Fig. 3.4 a). The heat flux data were recorded using an Ahlborn *Almemo 8590-9* data logger and exported at 10-second intervals via the *AMR WinControl* software to *Microsoft Excel* for further analysis.

(a) (b)

Fig. 3.4. Experimental setup: a) heat-flux sensor; b) hot-plate apparatus.

3.1.3. The principle of HFM method

The HFM method is a steady-state technique used to measure the thermal conductivity (λ) or thermal resistance (R-value) of building materials, including those enhanced with PCMs. It is widely used in research, quality control and materials testing due to its speed, ease of use and standardized protocols (ISO 8301, ASTM C518).

The HFM method is based on Fourier's law of heat conduction, which relates the heat flux (q) through a material to its thermal conductivity and temperature gradient:

$$q = -\lambda \frac{dx}{dt} \tag{3.1}$$

where q - heat flux, W/m2;

λ - thermal conductivity, W/(m·K).

The key idea is to apply a known temperature difference (ΔT) across a sample of known thickness (L) and measure the resulting heat flux (q) using built-in heat flux sensors (Fig. 3.5).

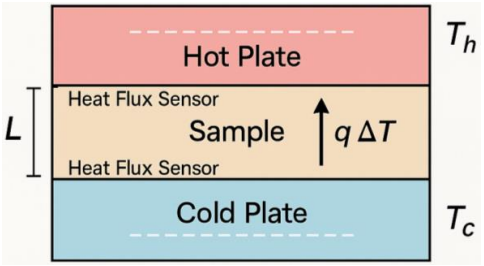

Fig. 3.5. The principle of HFM method.

The HFM method includes several steps:

1) Sample placement. A single flat specimen is sandwiched between two parallel plates - a hot plate and a cold plate. The plates are equipped with precision heat flux transducers (typically thermopile-based) and temperature sensors.
2) Temperature control. The plates are actively heated or cooled to create a controlled and uniform temperature difference (ΔT) across the sample. Common temperature ranges: 10–40 °C, adjustable depending on material type (important for PCM transition zones).
3) Steady-state conditions: the system is allowed to reach a steady thermal state where the temperature gradient across the sample remains constant. This usually takes 0.5 to several hours depending on material thickness and thermal diffusivity.
4) Heat flux measurement: the heat flow sensors embedded in the plates measure the heat flux (q) passing through the sample. This is often calibrated with certified reference materials.
5) Thermal conductivity calculation: once steady state is achieved, the instrument calculates the thermal conductivity (λ) using the formula:

$$\lambda = \frac{q \cdot L}{\Delta T}, \tag{3.2.}$$

where: λ - thermal conductivity, W/(m·K);

q - measured heat flux, W/m^2;

L - sample thickness, m;

ΔT - temperature difference between plates, K.

3.1.4. Experiment plan (E1 – HP 21/28)

The primary aim of this experiment is to characterise the thermal properties and behaviour of the PCMs. In this research, the hot-plate experiment serves two key objectives: (1) to experimentally determine the thermal conductivity of each PCM throughout its phase transition cycle using the HFM method, as recent studies [144] indicate that conductivity varies with temperature; and (2) to record temperature and heat-flux measurements during the charging and discharging periods, corresponding to the phases of thermal energy storage and release.

The data obtained from these measurements are subsequently used to develop and validate the numerical models employed in later stages of the study. Two PCMs (RT21HC and RT28HC) with differing thermophysical characteristics were examined using the hot plate apparatus.

The experiment was carried out over 12 rounds. In the first four rounds, steady-state (ST) tests were performed to determine the thermal conductivity of the PCMs within their melting and solidification temperature range. For these tests, the temperatures of the hot and cold plates were adjusted such that the mean plate temperature remained close to the PCM's phase-transition point.

Rounds 5–12 consisted of dynamic (DN) tests, which were divided into two distinct stages: a heating phase and a cooling phase. During each round, both plates in the apparatus operated simultaneously either as heaters or coolers, depending on the boundary conditions required for the specific test sequence. Before the start of every round, the system was brought to appropriate initial conditions to ensure consistency and repeatability across all measurements.

Each round continued until the heat flux measured on both surfaces reached a stable value, or until the predefined target temperature ("END" temperature) was achieved. A detailed overview of all experimental rounds, together with the corresponding hot-plate settings, is provided in Table 3.3.

Table 3.3

Settings for the hot-plate test

Round	Specimen	Experiment type	Hot plate temperature during the experiment, T_{HP} [°C]	Cold plate temperature during the experiment, T_{CP} [°C]	Specimen initial temperature, T_I [°C]	END temp
1	RT21HC	ST	28	9	20	-
2		ST	28	9	23	-
3	RT28HC	ST	36	16	25	-
4		ST	36	16	35	-
5	RT21HC	DN - Heating	25	25	17	25
6		DN - Cooling	17	17	25	17
7		DN - Cooling	2	2	25	17
8		DN - Heating	45	45	17	25

9	RT28HC	DN - Heating	31	31	25	31
10		DN - Cooling	25	25	31	25
11		DN - Cooling	2	2	31	25
12		DN - Heating	60	60	25	31

3.1.5. Calibration of hot-plate apparatus

HFM systems are classified as secondary measurement methods, which require calibration using reference materials with known thermal conductivity. In accordance with this principle, the hot plate apparatus was calibrated using two well-characterized materials: extruded polystyrene (XPS) with a thermal conductivity (λ) of 0.034 W/m·K and fibrolith with λ = 0.066 W/m·K.

Calibration was performed following the procedural steps of the HFM method. Initially, the XPS sample was placed in the test stand of the hot plate apparatus. Heat flow sensors (plates) were positioned on both sides of the specimen to ensure uniform contact. The temperature of the hot plate was set to 30 °C, while the cold plate was maintained at 10 °C, establishing a 20 °C temperature gradient across the sample. The experiment continued until a steady-state condition was reached, indicated by stable heat flux readings on both sides of the specimen. The same calibration procedure was subsequently applied to the fibrolith sample. The recorded temperature profiles and corresponding heat flux data are presented in Figure 3.6.

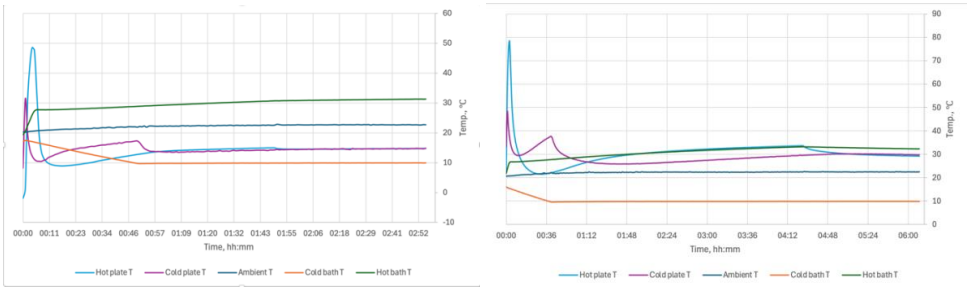

(a) (b)

Fig. 3.6. Temperature graphs: a) XPS sample; b) fibrolith sample.

Based on results, it can be observed that the heat flux on both sides stabilizes relatively quickly, reaching 14.66 W/m² for the XPS sample and 29.83 W/m² for the fibrolith sample. The thermal conductivity (λ) was calculated using Equation (3.2). The resulting values – 0.034 W/m·K for XPS and 0.066 W/m·K for fibrolith - align precisely with the reference values provided in the material datasheets. This confirms that the heat flux apparatus is properly calibrated and operates in accordance with standard measurement protocols.

Table 3.4

Calculations of the lambda value

	Fibrolith				XPS		
T1	9.96	°C		T1	9.93	°C	
T2	32.60	°C		T2	31.23	°C	
ΔT	22.64	°C		ΔT	21.30	°C	
L	0.05	m		L	0.05	m	
A	0.0625	m^2	Surface area	A	0.0625	m^2	Surface area
Heat flow	29.83	W/m^2	On surface area	Heat flow	14.66	W/m^2	On surface area
q	1.864508			q	0.91625		
ʎ	**0.066**	W/mk	Datasheet value	ʎ	**0.034**	W/mk	Datasheet value
ʎ	**0.066**	W/mk	Calculated value	ʎ	**0.034**	W/mk	Calculated value

3.1.6. Steady-state experiment for the precise determination of PCM thermal conductivity (E1 – HP 21/28)

A 12-round experiment was carried out according to the settings specified in Table 3.3. The first four rounds were conducted under steady-state conditions to determine the thermal conductivity (λ) of the PCM. The calculated results for these steady-state measurements are summarised in Table 3.5.

Table 3.5

Experimentally measured values and calculated thermal conductivity

Round	PCM	Stabilization time, h	q - measured heat flux, W/m^2	Hot plate temp., T_{HP} [°C]	Cold plate temp., T_{CP} [°C]	L - sample thickness, m	λ - thermal cond., W/(m·K)
1	RT21HC	15	82.12	28.27	9.68	0.056	0.25
2		22	91.46	29.57	9.67	0.056	0.26
3	RT28HC	10	94.5	34.74	17.69	0.056	0.31
4		53	89.80	34.90	17.71	0.056	0.29

The stabilisation time required to reach steady-state conditions varied depending on the PCM type and its initial temperature at the start of each test. For RT21HC, achieving stable heat-flux readings on both plates required approximately 15-22 hours, whereas RT28HC exhibited a wider stabilisation range, from 10 up to 53 hours. Since the calculated thermal conductivity values showed only minor variations between repeated rounds, the mean value of the two calculations for each PCM was selected for use in subsequent simulation models. The resulting representative conductivity values are 0.255 W/(m·K) for RT21HC and 0.3 W/(m·K) for RT28HC.

3.1.7. Dynamic experiment for assessing PCM thermal behaviour (E1 – HP 21/28)

From rounds 5 to 12, dynamic experiments were carried out using the hot plate apparatus. The measurement data collected during these rounds have been compiled into a series of graphs that illustrate the thermal behaviour of the PCM system throughout both the charging and discharging cycles. These graphs present the average PCM temperature (PCM T), the temperatures of both hot plate surfaces (Plate 1 T and Plate 2 T), the temperatures of the corresponding heating and cooling water baths (Bath 1 T and Bath 2 T), the ambient laboratory temperature (Ambient T) and the heat-flux values recorded on both sides of the specimen (Plate 1 HF and Plate 2 HF).

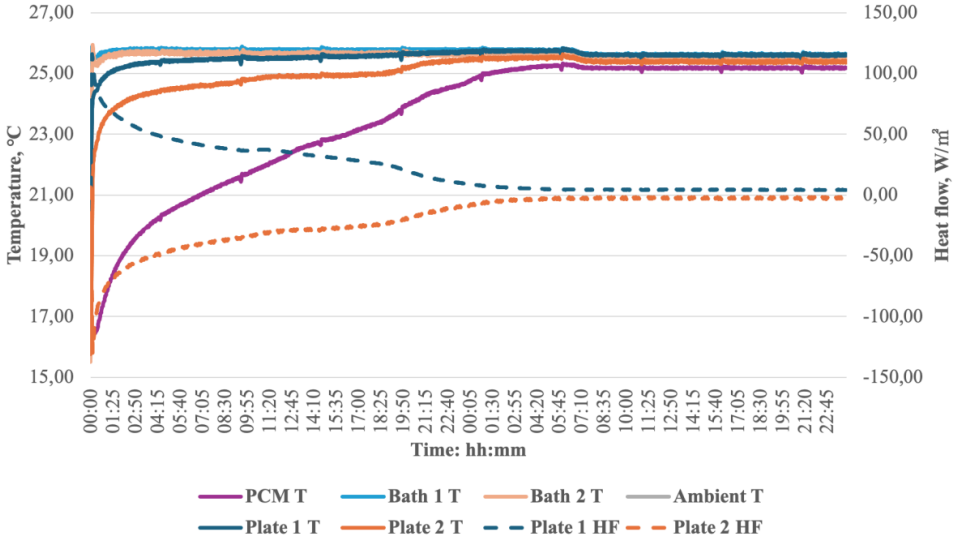

Fig. 3.7. Results from round 5: RT21HC heating.

The results from the fifth round (Figure 3.7) show that at the beginning of the experiment the temperatures of the two heating plates differ noticeably. This initial temperature offset is likely caused by transient thermal response effects and slight variations in heat transfer rates as the system begins to operate. As the test progresses, the system gradually approaches thermal equilibrium and the temperatures of both plates begin to converge. This convergence signifies that heat distribution across the specimen becomes more uniform and that stable thermal contact has been established. Both the heat-flux measurements on the plates and the average PCM temperature begin to stabilise after approximately 31 hours. At this point, the PCM has completed its phase transition cycle and the system reaches a steady thermal state. The relatively long stabilisation period reflects the characteristic thermal inertia of phase-change materials: during melting or solidification, additional energy is absorbed or released without a proportional change in temperature, resulting in delayed thermal stabilisation.

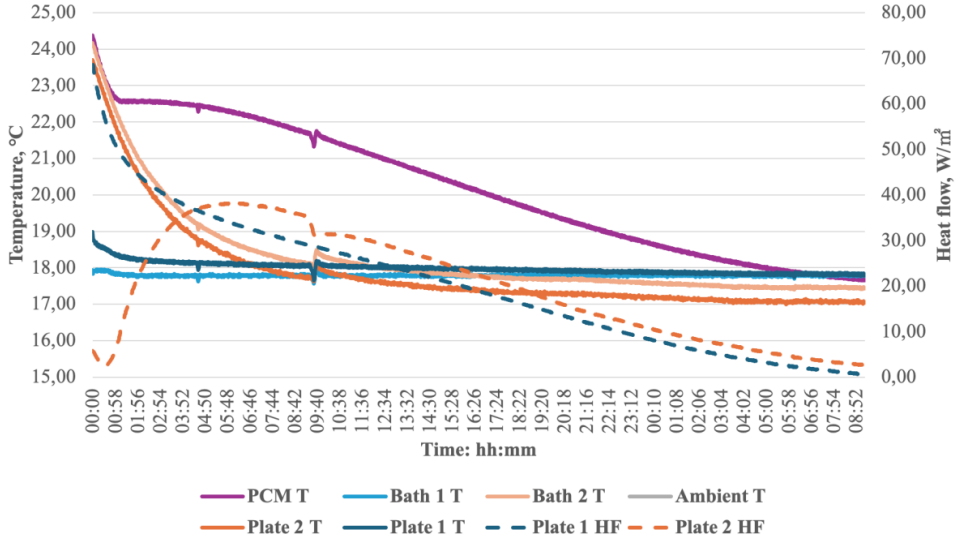

Fig. 3.8. Results from round 6: RT21HC cooling.

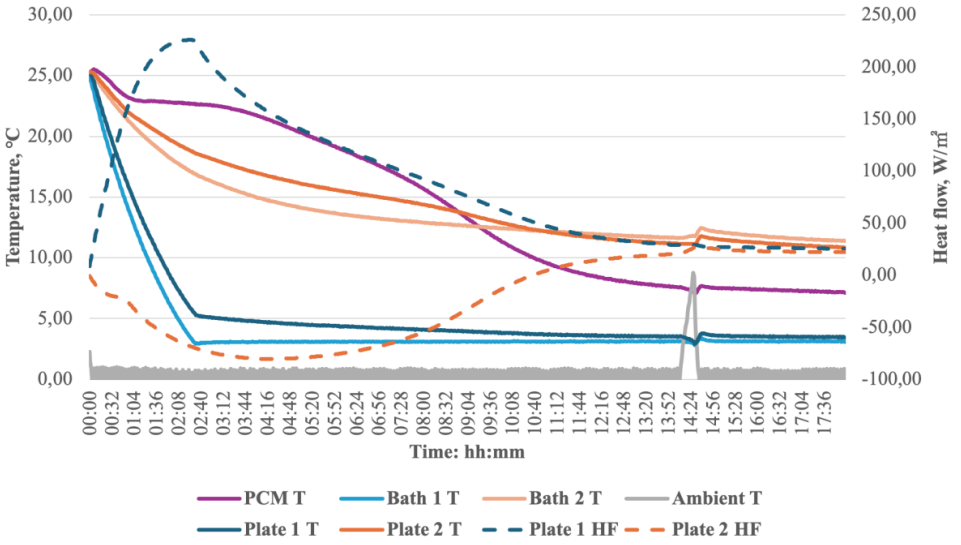

Fig. 3.9. Results from round 7: RT21HC cooling.

In the sixth round (Figure 3.8), the results indicate that Plate 1 maintained stable and effective cooling performance, as reflected by its nearly constant temperature throughout the entire experiment. In contrast, Plate 2 did not provide sufficient cooling: its temperature decreased gradually over time, revealing a slower and less efficient heat extraction process. This thermal imbalance is further confirmed by the heat-flux measurements, which show a clear discrepancy between the two surfaces. The pronounced difference in heat-flux values highlights

the asymmetrical thermal conditions within the specimen and confirms the reduced cooling efficiency on Plate 2.

The cooling issue observed for Plate 2 persists in the seventh experimental round (Figure 3.9), where a temperature difference of nearly 10 °C between the two plates remains for a substantial portion of the test. This sustained thermal imbalance leads to uneven heat distribution across the specimen. Although both temperature and heat-flux values eventually converge after approximately 15 hours - indicating that the system ultimately reaches thermal equilibrium - the prolonged deviation during the early stages is problematic. Such non-uniform boundary conditions can affect the accuracy of measurements obtained during the critical phase-change period, when precise thermal gradients are essential for correctly capturing latent heat effects and determining the material's thermal behaviour. Consequently, the initial instability may introduce uncertainties in the interpretation of the PCM's true thermal response.

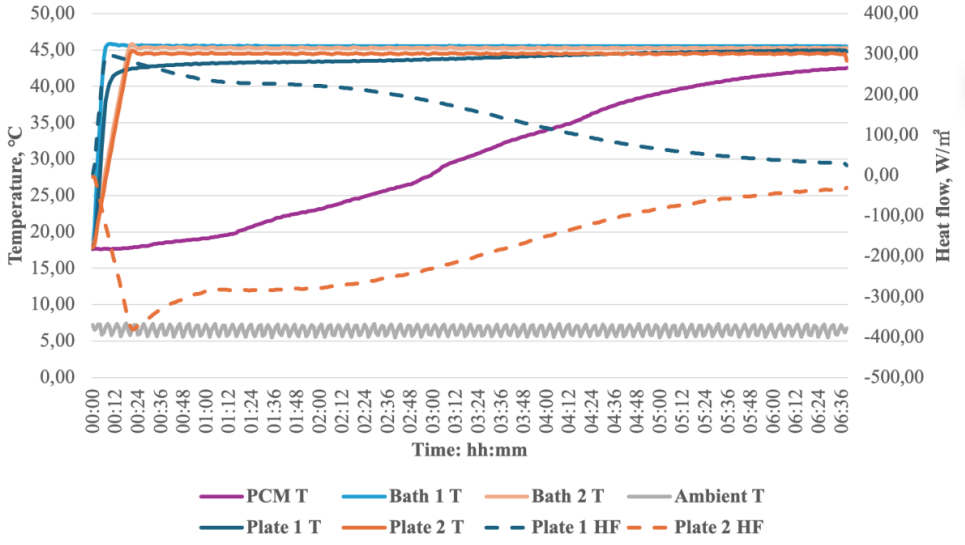

Fig. 3.10. Results from round 8: RT21HC heating.

When the apparatus operates in heating mode at elevated temperatures, as in the eighth round of testing (Figure 3.10), the circulating water successfully reaches the required setpoint temperature to heat both plates. Nevertheless, small temperature deviations between the two hot plates persist, accompanied by corresponding differences in heat flux on the specimen surfaces. These variations indicate minor inconsistencies in thermal delivery or imperfect thermal contact. The experiment was concluded once the average PCM temperature surpassed the predefined "END" temperature threshold, ensuring that the test remained within the intended thermal limits.

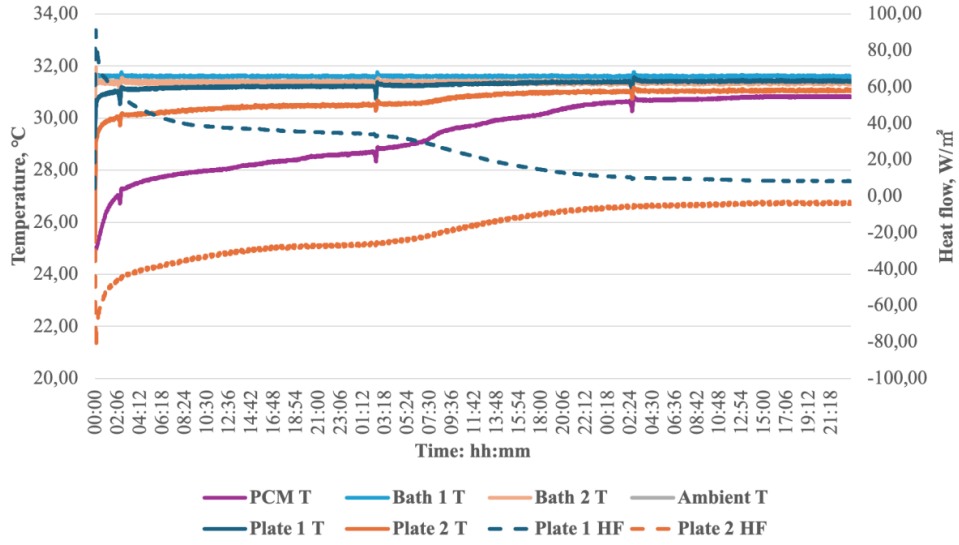

Fig. 3.11. Results from round 9: RT28HC heating.

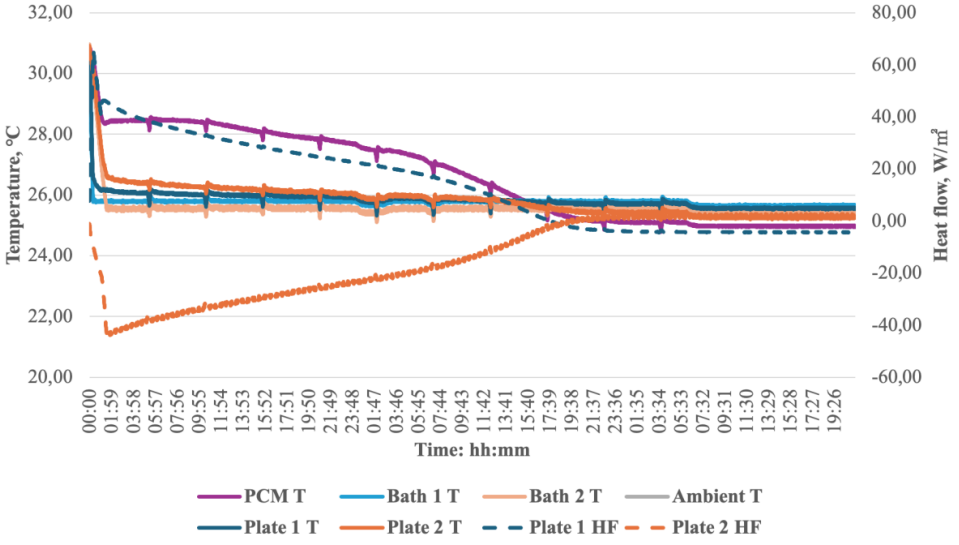

Fig. 3.12. Results from round 10: RT28HC cooling.

Beginning with round 9, the experiments were carried out using the second PCM, RT28HC. The results of the heating round, during which RT28HC was raised to a target temperature of 31 °C, are shown in Figure 3.11. The overall behaviour is similar to that observed in round 5 with RT21HC; however, in this case the temperature difference between the two plates is slightly more pronounced. The heat-flux profiles follow the same trend as the temperature curves, reflecting how the thermal imbalance between the plates influences heat transfer through the specimen. This behaviour is closely linked to the thermal characteristics of

RT28HC, which include a lower phase-change temperature range and a comparatively high latent heat capacity. These properties contribute to slower thermal response during the melting phase, as the material absorbs a substantial amount of heat with only minimal changes in temperature. As a result, even relatively small differences in plate temperature can generate asymmetric heat flow, particularly in the early stages of the phase transition. The observed discrepancies further underline the sensitivity of RT28HC to boundary conditions and highlight the importance of maintaining stable and well-balanced thermal inputs throughout the testing process.

The cooling phase of RT28HC in round 10 (Figure 3.12) exhibits the most stable thermal behaviour of all experimental rounds. Throughout the test, the temperature of the cooling plate remains closely aligned with that of the water bath, indicating strong thermal coupling and consistently efficient cooling performance. This stability is further supported by the heat-flux measurements, which remain nearly identical on both sides of the specimen. Such uniformity confirms that heat is being extracted evenly and that the boundary conditions are well balanced, providing a highly reliable cooling cycle for evaluating the PCM's thermal response.

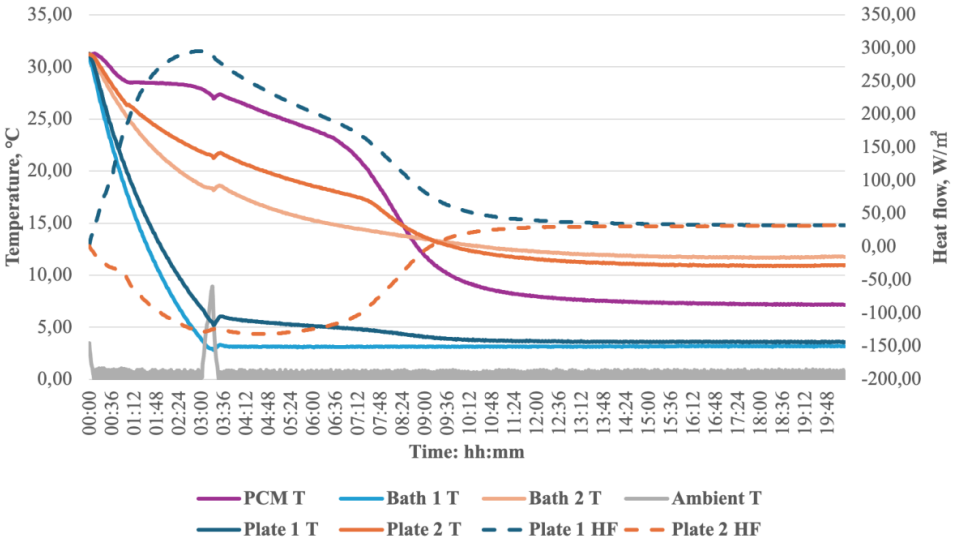

Fig. 3.13. Results from round 11: RT28HC cooling.

Figure 3.13 presents the cooling round of RT28HC, in which the PCM was intended to be cooled to a low target temperature of 2 °C. However, the recurring issue of insufficient cooling on Plate 2 once again prevents the system from reaching this setpoint, despite Plate 1 successfully attaining the required 2 °C. As a consequence of this persistent thermal imbalance, the PCM does not achieve the intended minimum temperature. Instead, after approximately 12 hours, its temperature stabilises at an intermediate level, settling between the temperatures of the two plates. This behaviour reflects the unequal cooling boundary conditions and their direct influence on the PCM's thermal response during the solidification phase.

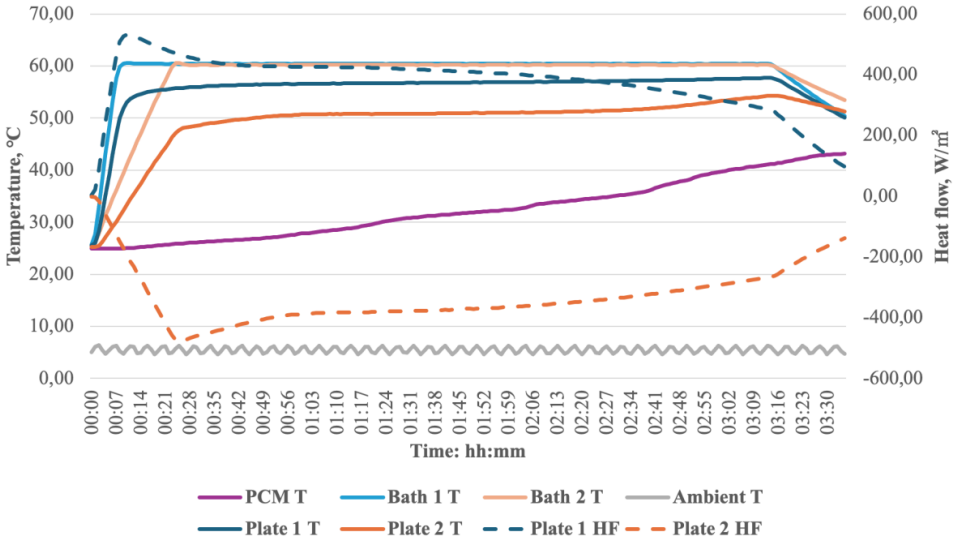

Fig. 3.14. Results from round 12: RT28HC heating.

The results of the twelfth and final round are shown in Figure 3.14. Both the temperature and heat-flux profiles display trends similar to those recorded in round 9, demonstrating consistent thermal behaviour of the PCM under comparable heating conditions. The experiment was concluded after 3 hours and 30 minutes, once the average PCM temperature reached 45 °C, which corresponds to the predefined upper temperature limit for this test.

3.1.8. Conclusions and insights (E1 – HP 21/28)

The experimental investigation of two PCMs using a hot plate apparatus across twelve rounds provided comprehensive insights into their thermal characteristics and behaviour under controlled heating and cooling cycles. The main conclusions from this stage of the research are as follows:

1) Initial verification tests with reference materials - XPS and fibrolith - confirmed the accuracy and reliability of the hot plate apparatus. The experimentally obtained thermal conductivity values were consistent with datasheet values, thereby validating the calibration procedure and compliance with standardised measurement protocols.
2) The HFM method enabled experimental determination of the effective thermal conductivity of RT21HC and RT28HC throughout their phase transition cycles (melting and solidification). These experimentally derived λ-values serve as essential input parameters for subsequent numerical modelling of PCM behaviour.
3) RT21HC exhibited relatively stable thermal response during both heating and cooling stages. Nevertheless, moderate asymmetry in plate temperatures and corresponding heat fluxes was observed in several rounds, primarily due to insufficient cooling

performance on Plate 2. Thermal and heat-flux stabilisation typically occurred after 15-31 hours, reflecting the expected lag associated with latent heat absorption and release.

4) RT28HC demonstrated comparable heat absorption dynamics but showed slightly greater sensitivity to boundary-condition variations. Round 10 produced the most stable thermal environment of the entire testing, with nearly identical plate temperatures and heat-flux profiles - underscoring the value of well-balanced thermal boundaries for accurate PCM characterisation.
5) A recurring limitation across multiple rounds was the inadequate cooling of Plate 2, which hindered the system from reaching the desired setpoint temperatures (e.g., 2 °C) during cooling cycles. This imbalance resulted in non-uniform thermal fields and incomplete PCM solidification, affecting the precision of phase-transition evaluation.
6) The findings highlight the critical importance of precise temperature control and symmetric boundary conditions in PCM testing. Even small discrepancies in plate temperatures produced measurable deviations in heat flux and extended stabilisation periods, potentially influencing the accuracy of extracted thermal properties.
7) Despite the noted operational constraints, the hot plate apparatus proved to be an effective tool for assessing PCM thermal behaviour for building-envelope applications. It enabled detailed observation of melting/solidification processes, heat-flux evolution and stabilisation times under controlled thermal gradients.
8) The extensive dataset generated over the twelve experimental rounds provides a robust foundation for developing and validating numerical models capable of simulating PCM-enhanced systems under dynamic thermal loads.

3.2. Assessment of two PCMs with melting temperatures of 21 °C and 28 °C under steady-state and dynamic laboratory conditions across different seasons (E2 – PCM 21/28)

3.2.1. Method and materials (E2 – PCM 21/28)

The main goal of this experiment was to evaluate the performance of each PCM in various seasons. Comparative testing was performed using custom-made experimental stand based on the PASLINK testing method. The design of experimental stands incorporates various materials, including extruded polystyrene (XPS) for insulation, plywood for external construction, glass for containers, polyethylene terephthalate glycol for container covers and two PCMs (RT21HC and RT28HC) for experimental study. The properties and characteristics of the materials used in the design of the test stands are summarized in Table 3.6.

Table 3.6

Material properties and characteristics

Material	Properties	Characteristics
Plywood	Thickness: 15 mm	$\lambda = 0.13$ W/mK SHGC = 0.28

XPS	Thickness: 50 mm	λ = 0.037 W/mK
Glass	Thickness: 4 mm	λ = 1.2 W/mK SHGC = 0.8
PETG	Thickness: 2 mm	λ = 0.2 W/mK

3.2.2. Experimental design (E2 – PCM 21/28)

This experiment was focused on the use of latent heat thermal energy storage, where a PCM is the main component responsible for thermal energy transfer through the building envelope. Choosing the optimal PCM can significantly reduce heating and cooling loads, particularly during periods when solar radiation is available. Various factors must be considered when selecting the PCM for specific applications, including the optimal volume, layer thickness and melting temperature range, as outlined by Guo and Zhang [145].

The system aims to provide an efficient energy balance for the entire building while maintaining a comfortable indoor environment for occupants, with room temperatures ranging from 16 °C to 26 °C throughout all seasons. To compare the thermal behaviour of two different PCMs under different climatic conditions simulating different seasons of the year, two comparative experiments - steady-state and dynamic - were conducted in laboratory testing. While RT21HC has a lower melting temperature closer to the average indoor temperature, RT28HC has a higher latent heat storage capacity. The experimental setup was designed to replicate a small-scale PASLINK-type test cell, with two test stands prepared for the comparative study - one for RT21HC and the other for RT28HC. The plywood box was lined with 50 mm insulation (XPS) to simulate the “indoor” space and the PCM container was built into one of the walls of each test box (see Figure 3.15).

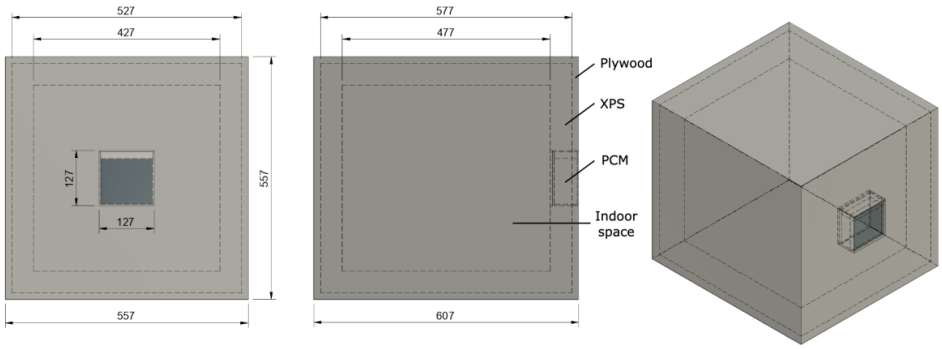

Fig. 3.15. Test box. Small-scale PASSLINK-type test cell.

To monitor the experimental setup, a set of thermocouples was placed as shown in Figure 3.16.

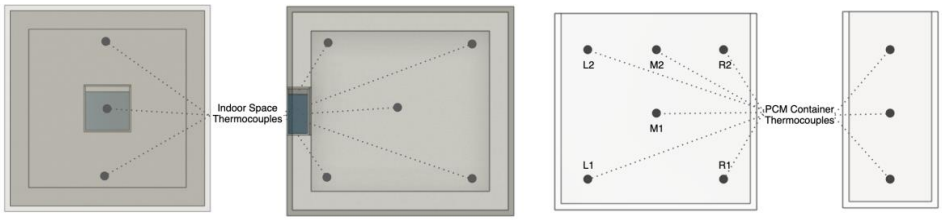

Fig. 3.16. Thermocouples in small-scale PASLINK-type testing boxes (left) and PCM container (right).

A total of eleven thermocouples were installed for each test box - six placed in the PCM container at different heights to observe temperature changes in different layers of the PCMs and five thermocouples located in the indoor space of the test box at different heights. The thermocouples are labelled based on their location inside the PCM container, with letters L, M and R indicating their location on the x-axis (L-left, M-middle and R-right) and numbers indicating their location on the y-axis (1-lower and 2-upper). This set of thermocouples allows for a comparison of changes in PCM temperature and indoor space temperature between the two setups under defined conditions. The test stands were positioned adjacent to each other inside the climatic test chamber *Tera Science TEMI 2500*, as illustrated in Figure 3.17.

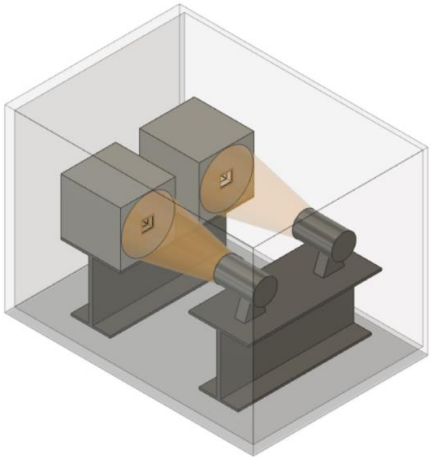

Fig. 3.17. Experimental setup in the climate chamber.

Solar energy consists of radiant light and heat from the Sun [146]. To simulate solar radiation for the test setups, halogen lamps were used since they emit both heat and light with colour characteristics similar to that of the Sun [147]. Specifically, two halogen lamps combined with dimmer were positioned along the longitudinal axes of each test box. A heating/cooling unit was utilized to maintain the desired temperature within the climatic chamber. The experimental setup is designed as a miniature version of a “structure”, comprising a test box with a thermal enclosure and indoor area. This setup is exposed to climate-induced stresses such as heating and cooling, which are created by the predetermined conditions in the

climate chamber. Temperature changes in both the indoor space and the PCM of the thermal enclosure are recorded using measuring equipment.

3.2.3. Experiment plan (E2 – PCM 21/28)

The test conditions were designed to simulate the four seasons: spring, summer, autumn and winter. For the steady-state experiment, three identical 24 h cycles were repeated for each season. The conditions for each season are determined by the following factors:

- The experiment begins with the outdoor temperature as the initial state. Both the solar wall module setups and the climate chamber are cooled to the same initial state before the start of the experiment.
- During both the heating and cooling phases, the outdoor temperature is kept constant, set to the average temperature of a typical day in that season.

The duration of daylight and the intensity of solar radiation are also taken into consideration. To determine the average values of key parameters - such as daylight duration, solar irradiance and outdoor temperature - for a representative day in each season, data from the local meteorological station spanning a five-year period were compiled and analysed.

The complete testing cycle lasts for 72 h and all the experimental conditions are summarized in Table 3.7.

Table 3.7

Conditions for the steady-state experiment

Season	Condition	Value
Spring	Daylight (solar simulation) duration	12 h
	Irradiance intensity	690 W/m^2
	Outdoor temperature	7 °C
Summer	Daylight (solar simulation) duration	12 h
	Irradiance intensity	750 W/m^2
	Outdoor temperature	19 °C
Autumn	Daylight (solar simulation) duration	10 h
	Irradiance intensity	440 W/m^2
	Outdoor temperature	10 °C
Winter	Daylight (solar simulation) duration	9 h
	Irradiance intensity	230 W/m^2
	Outdoor temperature	0 °C

Conditions for the dynamic experiment were kept the same as in the first experiment, except for the solar irradiance intensity. To simulate dynamic environmental conditions, the solar simulator was turned on and off every 30 min during all the season test rounds that occurred during daylight hours.

3.2.4. Steady-state testing (E2 – PCM 21/28)

Figure 3.18a presents a comparison of the average PCM temperatures under autumn testing conditions, showing three-day temperature profiles for both the PCM and indoor air. The RT28HC PCM reaches a higher peak temperature during the charging phase. Its temperature

plateau above 23 °C, followed by a sharp decline once the solar simulation is switched off, indicates partial melting of RT28HC. In contrast, RT21HC maintains lower temperatures during charging but exhibits higher temperatures during the discharging phase. Unlike RT28HC, the temperature of RT21HC decreases more gradually after the heat source is removed. This behaviour suggests that RT21HC remains partially melted for a longer period, with a larger melted fraction contributing to a smoother and more progressive temperature decline throughout the cycle. By the end of each 24-hour cycle, the average PCM temperature in both cases returns to the initial outdoor temperature.

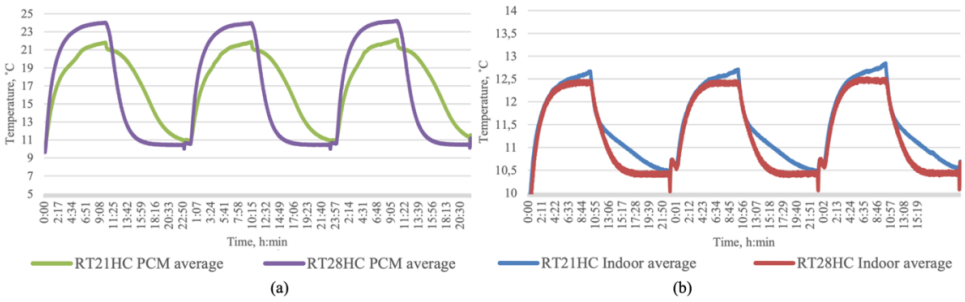

Fig. 3.18. Steady-state test results. Autumn. PCM average (a) and indoor air (b) temperatures.

Due to its latent heat storage characteristics, the RT21HC module achieves a higher indoor air temperature than the RT28HC module, despite the higher peak PCM temperatures observed in RT28HC during charging. Overall, RT21HC outperforms RT28HC in two key aspects: it produces a greater indoor temperature rise and cools down more slowly (Fig. 3.18b). In both modules, the indoor temperature returns to its initial value at the end of each day.

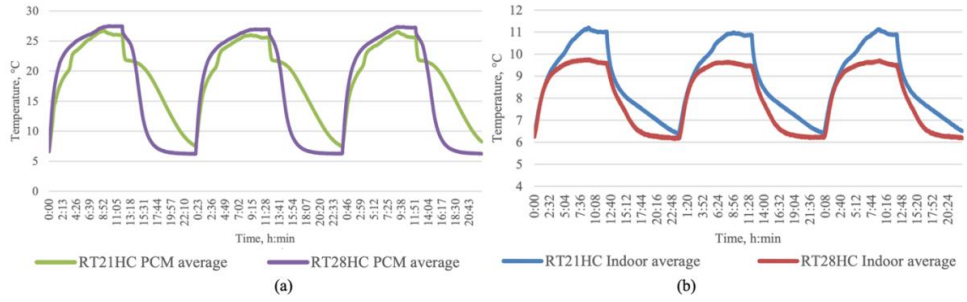

Fig. 3.19. Steady-state test results. Spring. PCM average (a) and indoor air (b) temperatures.

Fig. 3.19a presents the comparison of average PCM temperatures under spring testing conditions. In this setup, solar irradiance is higher than in autumn, whereas the “outdoor” temperature (i.e., climate chamber air temperature) is lower. This combination intensifies the temperature rise during the charging phase, leading to partial melting in both PCMs. As in previous tests, RT28HC reaches a higher peak average temperature. The temperature-decrease plateau occurs in both materials; however, in RT28HC it appears at a higher temperature level (approximately 25 °C) compared to RT21HC (around 21 °C). The plateau of RT28HC is more

inclined, indicating a smaller melted fraction of the material. A distinct plateau above 23 °C followed by a sharp temperature drop during the discharging phase further confirms that RT28HC undergoes only partial melting.

During the charging phase and early discharging phase, the temperature of RT21HC remains lower than that of RT28HC; however, in the final seven hours of the 24-hour cycle, RT21HC maintains a higher temperature. The immediate temperature drop observed after the solar simulator is switched off indicates that neither PCM achieves full melting, although the melted fraction in RT21HC is likely larger. As a result, RT21HC exhibits a slower cooling rate due to its different solidification dynamics.

When comparing these results to the autumn tests, the temperature curves of both materials during the charging phase are more closely aligned - the maximum temperature difference between RT21HC and RT28HC is smaller under spring conditions. Although the PCMs reach higher average temperatures in spring, the lower ambient temperature limits the rise of indoor air temperatures in the test boxes.

Despite the higher PCM peak temperature observed in RT28HC, the indoor temperature inside the RT21HC test box is consistently higher (Fig. 3.19b). This outcome reflects the larger melted fraction of RT21HC, which enables greater latent heat storage and subsequently more effective heat release to the indoor space. Overall, the maximum indoor air temperature in the RT21HC test box is approximately 1.5 °C higher than that in the RT28HC test box.

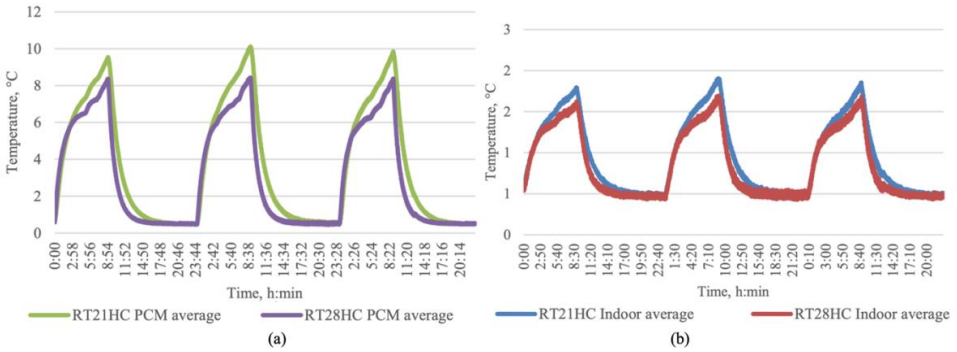

Fig. 3.20. Steady-state test results. Winter. PCM average (a) and indoor air (b) temperatures.

Figure 3.20 presents the results under winter conditions. The data show that the average PCM temperature in RT21HC rises higher than in RT28HC and the indoor air temperature in the RT21HC test stand also reaches a higher peak. Compared to the spring and autumn scenarios, the temperature differences between the two PCMs - and consequently between the indoor temperatures - are smaller. Both temperature curves follow a similar pattern because neither RT21HC nor RT28HC reaches its melting temperature under the defined winter conditions. As a result, no distinct temperature plateaus associated with melting or solidification are observed during either the charging or discharging phases.

In the summer testing round, the behaviour of both PCMs differs noticeably from the patterns observed in previous seasons (Fig. 3.21). Under the defined summer conditions,

RT28HC exhibits a distinctly longer plateau during the solidification phase compared with all other testing periods. This extended plateau indicates prolonged latent heat release as the PCM transitions back toward the solid state. In contrast, the average temperature of RT21HC briefly drops to its solidification temperature immediately after the solar radiation is switched off and then remains at this level throughout the night. This behaviour suggests that RT21HC does not fully solidify by the end of the cycle, implying that a portion of the material remains in a partially melted state.

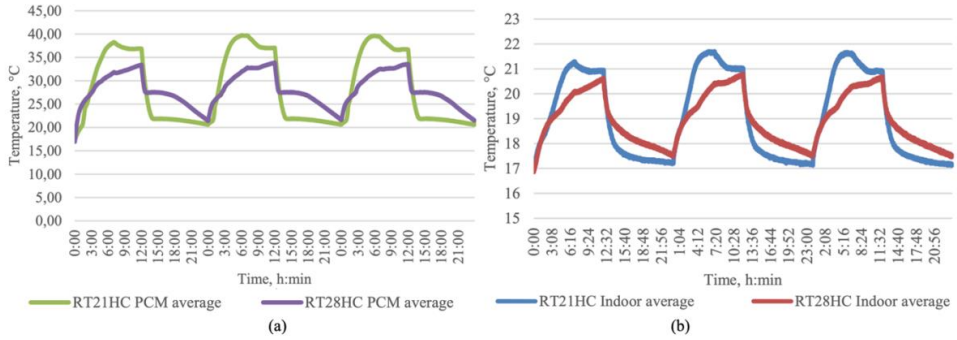

Fig. 3.21. Steady-state test results. Summer. PCM average (a) and indoor air (b) temperatures.

When comparing indoor air temperatures in the two test boxes during the summer cycle, a reversal of the seasonal trend can be observed. During the charging phase, the RT21HC module reaches higher indoor temperatures than the RT28HC module. However, during the discharge phase, the RT28HC module maintains higher indoor temperatures. This shift reflects the differing thermal storage and release patterns of the PCMs at elevated summer temperatures, particularly the prolonged solidification process of RT28HC and the incomplete return to the solid state in RT21HC.

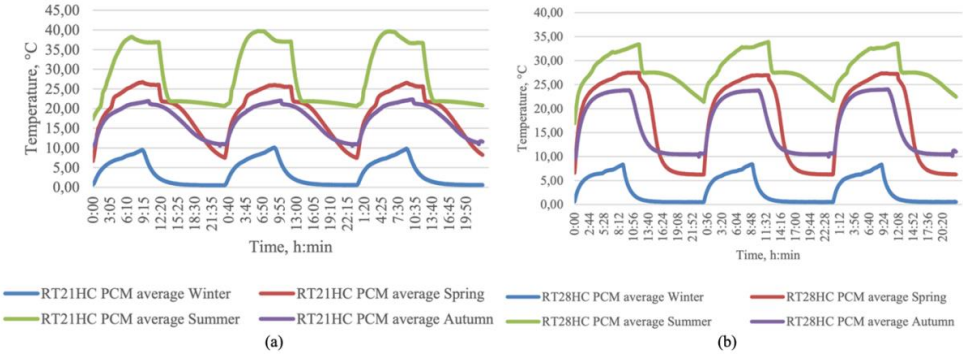

Fig. 3.22. Steady-state test results. Comparison of all seasons. RT21HC (a) and RT28HC (b) average temperatures.

Figure 3.22 presents the average temperatures of RT21HC and RT28HC across all four tested seasons. These graphs enable a direct comparison of the charging and discharging behaviour of both PCMs under varying climatic conditions.

Full and partial melting behaviour across different PCM layers is presented in Figure 3.23. For RT21HC (Fig. 3.23a), it is evident that the upper layers (L1, M1 and R1) reach full melting, whereas the lower layer undergoes only partial melting. This behaviour is characterised by a sharp temperature drop immediately after the solar simulator is switched off, followed by a distinct temperature plateau. Such a pattern indicates that once the PCM in a given layer has fully melted, it continues to absorb sensible heat, which is then rapidly released when the solar input is removed.

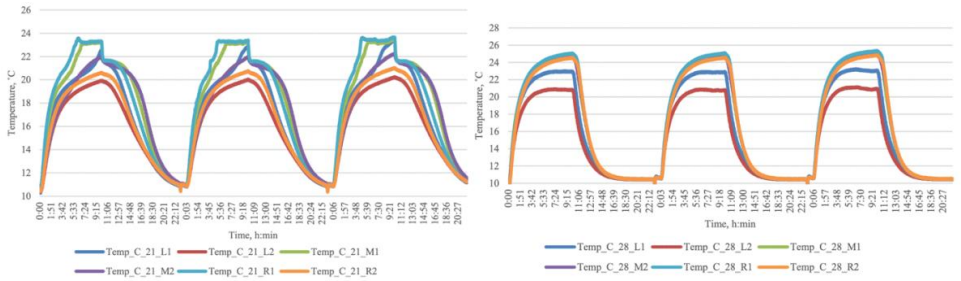

Fig. 3.23. Steady-state test results. Autumn. Comparison of temperatures in different layers: RT21HC (a) and RT28HC (b).

In contrast, RT28HC exhibits no comparable pattern (Fig. 3.23b). Under the same autumn conditions, none of the layers in the RT28HC sample reach the melting temperature and thus no melting plateau is formed. After the solar simulator is switched off, all layers show similar cooling rates, reflecting a more uniform thermal response without pronounced phase-change behaviour. Similar layer-dependent differences between RT21HC and RT28HC are observed across the remaining seasons as well.

3.2.5. Dynamic testing (E2 – PCM 21/28)

The dynamic experiment involved applying the planned testing conditions with alternating periods of simulated solar radiation being switched on and off. Although each seasonal configuration was tested over a total period of 72 h, the temperature curves showed no substantial day-to-day variation. Therefore, the evaluation of dynamic performance is based on a representative 24-hour cycle. Figure 3.24a illustrates the average temperature curves of both PCMs under spring testing conditions.

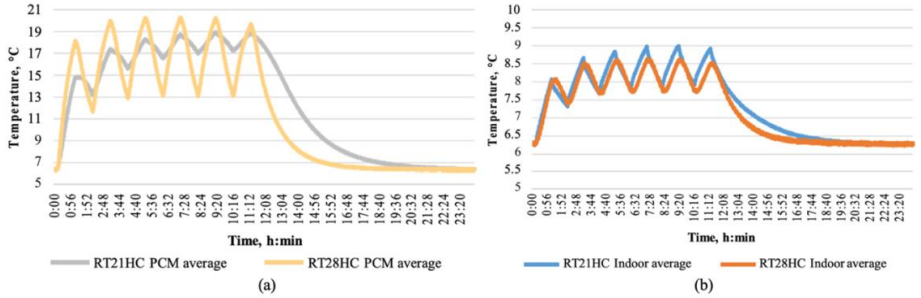

Fig. 3.24. Dynamic test results. Spring. PCM average (a) and indoor air (b) temperatures.

In contrast, RT28HC exhibits higher temperature peaks during the daylight charging period but undergoes a significantly steeper temperature drop once the solar simulator is turned off, as the PCM transitions primarily through sensible heat rather than latent heat storage. The indoor air temperature in the RT21HC test box is consistently higher than in the RT28HC case, with a notably gentler decline during the discharging phase (see Figure 3.24b).

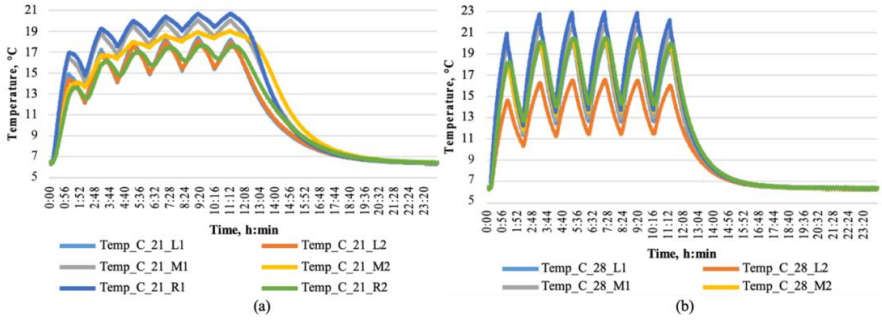

Fig. 3.25. Dynamic test results. Spring. Comparison of temperatures in different layers: RT21HC (a) and RT28HC (b).

Figure 3.25 presents the temperature evolution in different PCM layers during spring testing. All layers in RT21HC reach the melting phase, enabling latent heat storage throughout the charge cycle. By contrast, none of the RT28HC layers reach their melting point and their temperatures fluctuate solely within the sensible heat range during the charging period.

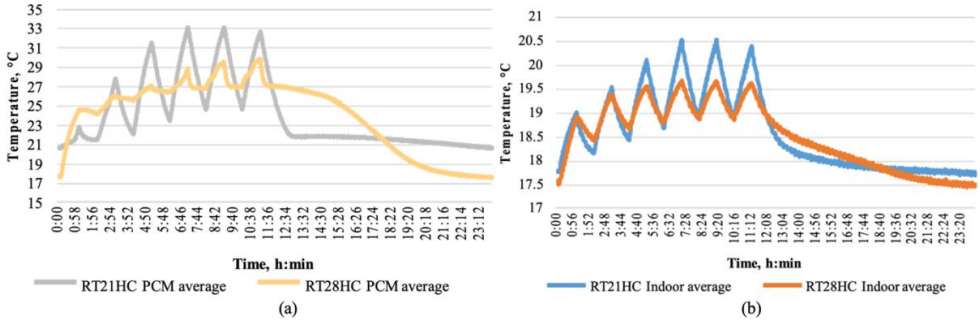

Fig. 3.26. Dynamic test results. Summer. PCM average (a) and indoor air (b) temperatures.

Similar behaviour is observed in the autumn setup. In the summer setup, however, both PCMs reach average temperatures at or above their melting points, producing a more gradual temperature rise (see Figure 3.26a). Although the RT21HC test box again demonstrates the highest indoor air temperatures, the peaks remain below 21 °C (see Figure 3.26b).

Layer-specific temperatures of RT21HC under summer conditions (Figure 3.27a) show that all PCM layers exceed the melting temperature, with complete melting occurring from approximately 02:00 onwards, resulting in sensible heat storage during the remainder of the cycle. In the case of RT28HC (Figure 3.27b), all layers except one point in the upper layer (L2) reach the melting temperature, indicating partial liquefaction and partial latent heat utilisation. Nevertheless, by the end of the 24-hour cycle, RT21HC maintains temperatures 2–3 °C higher than RT28HC, depending on the measurement layer.

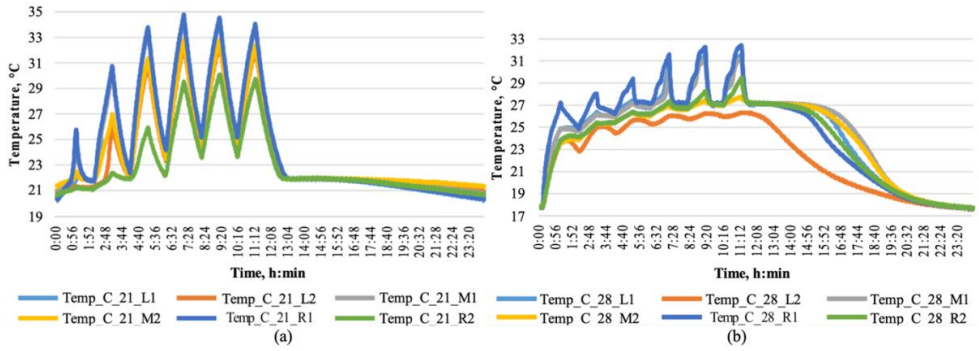

Fig. 3.27. Dynamic test results. Summer. Comparison of temperatures in different layers: RT21HC (a) and RT28HC (b).

3.2.6. Conclusions and insights (E2 – PCM 21/28)

Figure 3.28 presents a comparison of the maximum average temperatures reached by both PCMs, as well as the corresponding indoor air temperatures, under steady-state and dynamic testing conditions. Although the overall temperature trends are similar across the two experimental modes, the absolute values recorded in the steady-state tests are higher, primarily due to the absence of irradiance interruptions during these runs.

Across autumn, winter and spring conditions, RT28HC consistently achieves higher peak PCM temperatures. However, despite these higher PCM temperature peaks, RT21HC systematically results in higher indoor air temperatures in all seasons and in both experimental modes. This indicates that RT21HC is more effective in storing thermal energy within the PCM layer and subsequently releasing it into the interior environment, thus providing superior thermal performance.

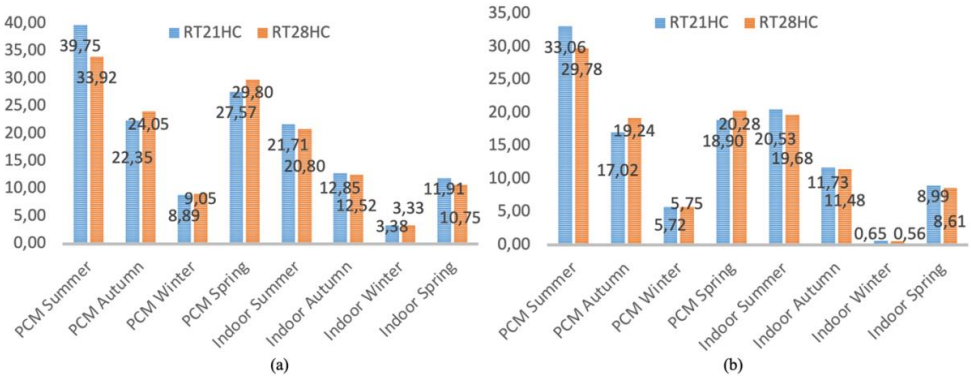

Fig. 3.28. Comparison between the highest temperatures reached by RT21HC and RT28HC in (a) steady-state test and (b) dynamic test.

Further analysis reveals that RT21HC maintains higher indoor temperatures with a noticeably gentler decline during the discharging phase, demonstrating a more stable release of stored heat. In contrast, RT28HC exhibits higher temperature peaks during the charging phase but undergoes a sharper temperature drop once the solar simulator is switched off. This behaviour reflects a predominance of sensible rather than latent heat storage in RT28HC under the tested conditions.

Layer-specific temperature measurements confirm these observations: in the majority of cases, all layers of RT21HC enter the melting range and participate in latent heat storage, whereas none of the RT28HC layers reach the melting point during comparable conditions, showing only oscillations between minimum and maximum temperatures during the charging cycle.

In the summer setup, both PCMs reach the melting point, yet the temperature evolution remains characteristic: RT21HC shows a more gradual temperature rise and retains higher temperatures during the night, while RT28HC exhibits sharper fluctuations due to partial melting and sensible heat dominance.

Overall, the experimental results demonstrate that, under the tested climate conditions, RT21HC provides more efficient thermal energy storage and a more favourable thermal contribution to indoor temperatures compared to RT28HC, particularly in transitional seasons where partial melting plays a key role in performance.

3.3. Modelling in ANSYS Fluent

To complement experimental investigations and enhance the understanding PCM performance under thermal loading, numerical modelling has become an essential tool for simulating transient heat transfer processes. Among various computational platforms, ANSYS Fluent is widely recognized for its robust capabilities in modelling conduction, convection and phase change phenomena with high spatial and temporal resolution. When selecting a computational platform for heat transfer modelling, ANSYS Fluent stands out due to its

comprehensive physics capabilities, built-in models for phase change and high degree of flexibility in defining boundary conditions and material properties.

In the context of this research, Fluent is employed to simulate the heating and cooling cycles performed in a hot plate apparatus, enabling direct comparison between measured and simulated temperature and heat flux data. The modelling is based on the transient heat conduction equation, which governs energy transport within the solid domain:

$$\rho c_P \frac{\delta T}{\delta t} = \nabla \cdot (k \nabla T) + Q, \tag{3.3}$$

where:

ρ – density, kg/m³);

c_P – specific heat capacity, J/kg·K;

T – temperature, K;

k – thermal conductivity, W/m·K;

Q – internal heat generation, W/m³.

To simulate phase change behaviour, the enthalpy-porosity method is applied - an approach built into ANSYS Fluent for modelling latent heat effects in melting and solidification process [148], [149]. In this method, the PCM is treated as a porous medium within the mushy zone and the total enthalpy is defined as the sum of sensible and latent heat. This enables accurate modelling of thermal inertia and the nonlinear response of PCMs near their melting range. A 2D or 3D computational domain can be developed to represent the experimental setup, including boundary conditions such as fixed plate temperatures, convective losses and thermal contact resistance. The material properties of the PCMs (e.g., thermal conductivity, density, latent heat, phase change temperature range) are defined according to datasheet values and validated against experimental calibration data [150]. The transient simulation results, including temperature evolution and heat flux, then can be compared to experimental measurements obtained in the hot plate tests. This comparison enables validation of the model and refinement of parameters, supporting the broader objective of using numerical tools for performance prediction and optimization of PCM-enhanced building components [151].

Before developing and implementing a numerical model for PCMs, screening of existing literature is conducted, that is meant to provide a clear understanding of the current state of the art in PCM modelling, including commonly used simulation techniques, validated approaches and practical limitations. The main goal is to identify best practices, such as appropriate use of the enthalpy-porosity method, selection of solver settings and relevant boundary conditions for building-integrated applications by analysing peer-reviewed studies that use ANSYS Fluent for PCM simulations. This screening also is useful to avoid redundant efforts by learning from previously developed models and reveals gaps or inconsistencies in the literature that the new model can address and ensures that the numerical model to be developed aligns with real-world experimental setups, making it suitable for validation against empirical data. In this work, the screening also guides the definition of input parameters and modelling assumptions that are consistent with the materials, geometry and test conditions used in the hot plate experiments, ultimately improving the reliability and applicability of the simulation results.

To compile a robust list of studies using ANSYS Fluent for simulating PCMs in building envelope applications, a two-stage search strategy was employed. First, articles were identified through a targeted search on the Web of Science (WoS) platform. The search used combinations of relevant keywords such as “ANSYS Fluent”, “phase change material”, “building envelope”, “PCM simulation” and “thermal energy storage”. Papers were prioritized based on citation frequency, publication quality and relevance to building-scale applications, particularly those involving PCM integration in walls, facades and roofs. Only original research articles were selected, excluding reviews and purely theoretical work. In the second stage, additional recent papers (from 2020–2024) were identified through complementary searches in Scopus, ScienceDirect and MDPI, ensuring the inclusion of the latest developments. Each article was manually screened to confirm its focus on building envelope applications, the use of ANSYS Fluent as the primary simulation platform and the inclusion of numerical details such as solver settings and phase change modelling approaches.

Table 3.8

Screened publications on numerical modelling of PCMs in building applications using ANSYS Fluent

No.	Full Title	Year	Application Context	ANSYS Fluent Role	Highlights	Simulation Type and Solver
1	CFD modelling for phase change materials integrated in energy-efficient building envelopes [152]	2023	PCM in ventilated facade cavities	Fluent model validated with experiments	Simulated heat buffering in macro-encapsulated PCM facades	2D transient; enthalpy-porosity method; solar radiation source; laminar model; mesh ~15,000 cells
2	Optimization of a solar air heater with phase change materials: Experimental and numerical study [153]	2021	Roof-integrated PCM air heater	Fluent modelled airflow and heat storage	Identified optimal air velocity range for efficiency	3D transient; standard k-epsilon model; user-defined functions (UDFs) for PCM properties
3	CFD simulation of a solar collector integrated with PCM thermal storage [154]	2022	PCM in solar roof collector	Transient Fluent simulation	Demonstrated PCM effectiveness under solar loads	2D axisymmetric; transient simulation; enthalpy-porosity method; pressure-based solver
4	Numerical study on melting process of phase change material in thermal energy storage [155]	2020	PCM in thermal storage enclosure	Fluent enthalpy-porosity model	Captured melting front and heat transfer behaviour	2D transient; enthalpy-porosity model; pressure-based solver; SIMPLE scheme
5	Numerical investigation on the phase change process of PCM in an energy-efficient wall [156]	2019	PCM inside wall layers	Fluent simulation of latent heat exchange	Analysed dynamic thermal response under loads	2D transient; laminar flow; enthalpy-porosity method; pressure-based solver
6	Numerical study on the performance of a glazed photovoltaic thermal	2021	PV-PCM hybrid facade	3D transient Fluent model	Explored impact of PCM fraction and environment temperature	3D unsteady; sliding mesh; enthalpy-porosity model;

	system integrated with PCM [157]					segregated solver in Fluent
7	Improvement of heat transfer within phase change materials using V-shaped fins in triangular enclosures[158]	2022	Finned enclosure for PCM	Fluent enthalpy-porosity model	Enhanced melting rate with V-fins	2D transient; realizable k-epsilon model; coupled heat and airflow; buoyancy effects included
8	Thermal performance of multifunctional facade panel containing PCM [159]	2023	PCM foam facade panel	Fluent numerical model	Validated with hotbox experiment results	2D transient; laminar flow; enthalpy-porosity method; adaptive time stepping
9	Coupled EnergyPlus–CFD analysis of PCM for thermal simulation of built environment [89]	2020	PCM in roofs and walls	Fluent + EnergyPlus co-simulation	Simulated real-time thermal performance	3D co-simulation; Fluent used for CFD zone; EnergyPlus for full building envelope modelling
10	Optimization study on thermal performance of a novel dynamic phase change material wall [160]	2024	Movable PCM–insulation layers in external walls	ANSYS Fluent transient CFD; enthalpy-porosity model; mesh sensitivity test included	Identified optimal PCM positioning by climate zones (Harbin, Tianjin, etc.)	3D transient CFD; enthalpy-porosity model; pressure-based solver; adaptive mesh refinement
11	Thermal Performance of Multifunctional Facade Solution Containing PCM [161]	2023	Multilayer facade with foam-embedded PCM	Fluent model calibrated with hotbox; transient solver; standard k-epsilon turbulence model	Simulation–experiment match ($R^2 = 0.9674$); strong decrement factor reduction observed	3D transient Fluent model; standard k-epsilon model; pressure-based solver with energy equation
12	Numerical study on the performance of a glazed photovoltaic thermal system integrated with PCM (GPVT/PCM) [157]	2021	PV-T facade with PCM storage	Fluent 18.2; transient simulation; SIMPLE algorithm; radiation model active	Analysed PCM fraction and ambient temperature on thermal output and exergy	Fluent 18.2; transient simulation; SIMPLE algorithm; DO radiation model; UDF for PCM properties
13	Simulation Study on Dynamic Thermal Performance of a New Ventilated Roof with Form-Stable PCM [162]	2020	Ventilated roof with form-stable PCM	3D transient Fluent simulation; buoyancy-driven ventilation; enthalpy-porosity model	Demonstrated cooling effect via night ventilation and PCM melting delay	3D transient; buoyancy-driven ventilation; enthalpy-porosity method; Boussinesq approximation

A screening of 13 studies reveals several consistent modelling practices (see Table 3.8). Most prominently, the enthalpy-porosity method was employed across all studies that simulated phase transitions. This approach is integrated into ANSYS Fluent and models the melting and solidification process by treating the phase change region as a porous medium, incorporating latent heat directly into the energy equation. For example, Zhang et al. [152] the enthalpy-porosity model were using to simulate melting and solidification under dynamic thermal boundary conditions.

All 13 studies conducted transient simulations, recognizing the time-dependent nature of phase change processes in real building scenarios such as diurnal temperature cycles, solar

irradiation and HVAC cycling. The pressure-based solver was used consistently, suitable for low-speed, incompressible internal flows typical in building applications. This was evident in study by Zhang et al. [160], where unsteady conditions were critical to capturing heat storage and release over time.

Regarding radiation modelling, only a few studies accounted for solar or radiative heat transfer, typically using simplified models such as the discrete ordinates (DO) radiation model. However, none of the 14 studies applied the surface-to-surface (S2S) radiation model, which is more suitable for enclosure-type radiative exchange. For example, Shekata et al. [154] included solar radiation using the DO model, but did not simulate surface-to-surface radiation interactions.

Model validation and experimental coupling varied among the studies. Several papers compared simulation outputs with lab-scale experimental results, such as temperature profiles or heat fluxes. For instance, Moradi et al. [153] provided a full coupling between simulation and experimental data to ensure the model's predictive accuracy. Similarly, Brzezinski et al. [161] used a hotbox test to validate Fluent simulation results, achieving strong alignment.

Natural convection within the molten PCM was considered in many simulations by solving the momentum equations, often with Boussinesq approximation for buoyancy effects. Mesh resolution and time step sensitivity were sometimes mentioned, though detailed grid independence tests were only included in a few cases.

The analysis shows a close distribution of simulation type: 7 studies used 2D models and 6 studies employed 3D models. This reflects a balance between computational efficiency (2D) and geometric realism (3D) in PCM modelling.

3.3.1. Numerical model validation

Validating numerical PCM models in ANSYS Fluent requires meticulous comparison between simulated results and experimental data to confirm model accuracy and reliability. Commonly, researchers [163], [164], [165], [166], [167], [168], [169], [170], [171], [172], [173] use lab-scale physical tests, such as hot-box or solar chamber experiments, that measure temperature evolution and heat flux under controlled boundary conditions. Corresponding Fluent simulations are then designed to replicate those conditions, using the enthalpy-porosity method to model phase change, with transient, pressure-based solvers configured to match the experimental setup (e.g., surface temperatures, solar irradiance) in both time and space. Model outputs such as average PCM temperature, melt fraction, or heat flux profiles are directly compared with experimental observations. Calibration of material properties (e.g., thermal conductivity, specific heat, latent heat) and solver parameters is performed to minimize discrepancies. Validated models are those where simulation responses closely align with measured data over the full melting and solidification cycle.

Another benchmark validation approach involves the melting of PCM in symmetric enclosures with detailed temperature and phase front tracking, like the Vogel & Bauer benchmark experiment [173], where high-resolution temporal and spatial data enable rigorous validation of simulated phase interface evolution.

The validation process can be divided in 3 main steps [160], [174], [175]:

1) Experimental data comparison. Key observable outputs, such as time-series of PCM temperature, melt fraction and surface heat flux, are extracted from both simulation and experimental measurements. These data sets are compared using statistical metrics - Root Mean Square Error (RMSE) and Relative RMSE.
2) Calibration and sensitivity analysis. Simulation parameters such as PCM thermal conductivity, specific heat, latent heat and the mushy zone constant (Amushy) are calibrated to minimize error.
3) Evaluation of validation results. Successful validation is claimed when:

1. simulated temperature and heat flux curves closely track experiments over both melting and solidification phases;
2. error metrics remain within acceptable limits (e.g. RMS error < 5–10%, $R^2 \geq 0.95$);
3. phase interface movement and melt fraction evolution match visual or measured data (sometimes through image-based liquid fraction analysis)

The equation to calculate the RMSE is:

$$RMSE = \sqrt{\frac{1}{n}\sum_{i=1}^{n}(T_{sim,i} - T_{exp,i})^2}, \tag{3.4}$$

where: $T_{sim,i}$ – simulated value at time step i (e.g., from ANSYS Fluent);

$T_{exp,i}$ – corresponding experimental value at time step i;

n – total number of time steps or data points.

RMSE gives the average magnitude of the difference between simulation and experiment. It is expressed in the same units as the variable being compared (e.g., °C for temperature). A lower RMSE indicates better agreement between simulated and experimental results.

The Relative RMSE expresses RMSE as a percentage of the observed data range or average, allowing normalized comparison across different datasets.

$$RRMSE = \frac{RMSE}{\overline{T_{exp}}} \times 100, \tag{3.5}$$

where: $\overline{T_{exp}}$ – mean of the experimental values.

This gives a unitless percentage error. RRMSE values below 10% are often considered very good in thermal system validation, while 10–20% is acceptable depending on experimental noise. For example, Kasaeian et al. [176] reported an RRMSE of 5.4% for the comparison between experimental and numerical temperature profiles in a solar air heater containing PCMs.

The R^2 value quantifies how well the variation in the experimental data is captured by the simulation model. It ranges from 0 to 1, where 1 indicates perfect correlation.

$$R^2 = 1 - \frac{\sum_{i=1}^{n}(T_{exp,i} - T_{sim,i})^2}{\sum_{i=1}^{n}(T_{exp,i} - \overline{T_{exp}})^2}, \tag{3.6}$$

$R^2 \approx 1$: Strong agreement and accurate simulation of trends. $R^2 < 0.9$: Indicates potential mismatches or poor trend reproduction. In study by Amaral et al. [159] an R^2 value of 0.9674 was obtained when comparing experimental and simulated heat flux in a multifunctional facade panel, confirming high model reliability.

These validation workflows ensure that Fluent PCM models are not only theoretically sound but also empirically grounded, improving confidence in using them for building envelope performance prediction.

3.3.2. Hot plate model (S1 – HP 21/28)

To accurately design a simulation model in ANSYS Fluent, it is crucial to first understand the underlying physical phenomena involved. Based on insights from the literature screening, a two-dimensional (2D) simulation approach was selected to balance computational efficiency with sufficient physical detail.

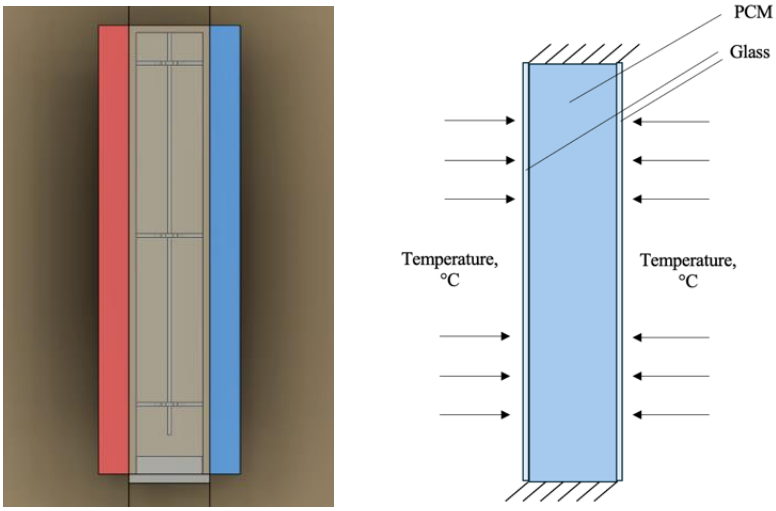

Fig. 3.29. Cross-section of actual test stand (left) and schematic of temperature model (right).

The model replicates the cross-sectional geometry of the experimental setup, capturing key thermal interactions and boundary conditions. A schematic representation of the simulation domain is provided in Figure 3.29. As illustrated in the figure, the simulation model consists of two distinct regions: the phase change material (PCM), represented as a fluid domain and the surrounding glass enclosure, treated as a solid. Boundary conditions are defined to replicate the experimental setup: constant temperatures are applied to the left and right boundaries, corresponding to the hot and cold plates used in testing. The top and bottom surfaces are excluded from the numerical calculations, as they are thermally insulated from the ambient environment and have a negligible influence on the heat transfer through the specimen.

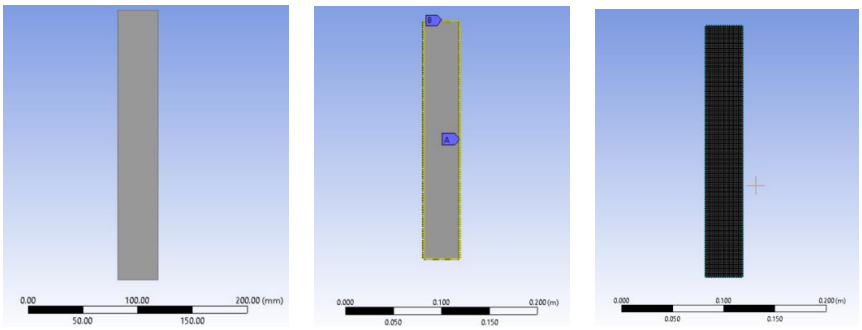

(a) (b) (c)

Fig. 3.30. Sketch in DesignModeler (a), edge-sizing (b) and mesh (c).

The geometry of the simulation model, along with its dimensions, was constructed in ANSYS *DesignModeler* (Fig. 3.30). Within this environment, named selections were defined to represent key boundary and domain regions: plate-1 and plate-2 correspond to the heating and cooling surfaces, top_bottom designates the insulated top and bottom boundaries and PCM defines the region occupied by the phase change material specimen. Meshing was performed using the Face Meshing and Edge Sizing tools, with 100 divisions along the vertical edges and 30 divisions along the horizontal edges to ensure adequate spatial resolution. The resulting mesh comprises 9386 nodes and 9102 elements in total.

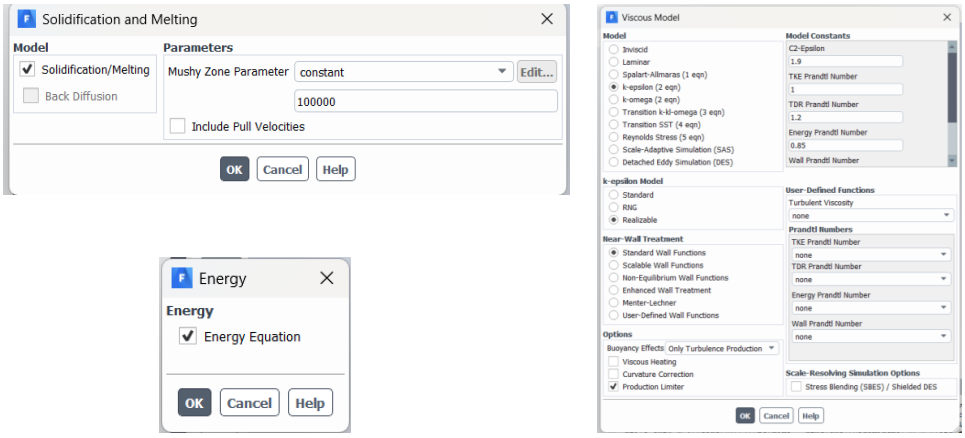

Fig. 3.31. ANSYS Fluent energy models used in hot plate simulation.

The 2D geometry is then imported into ANSYS Fluent, where the general simulation settings are configured as follows: the solver type is set to Pressure-Based, the velocity formulation is defined as Absolute and the time formulation is specified as Transient to capture the unsteady heat transfer behaviour during phase change. The 2D space is set to Planar and gravity is enabled with a value of - 9.81 m/s² applied along the Y-axis to account for buoyancy effects in the liquid phase of the PCM. The next step involves activating the relevant physical models in ANSYS Fluent to accurately capture the heat transfer and phase change processes.

For this simulation, the Energy, Viscous and Solidification and Melting models are enabled. These models allow the solver to account for heat conduction, natural convection within the liquid PCM and latent heat effects during phase transition. The specific configuration settings for each model are presented in Figure 3.31.

It is essential to define the thermophysical properties of each material used in the simulation - specifically, the phase change material (PCM) and the glass enclosure. These properties include thermal conductivity, specific heat capacity, density and, for the PCM, latent heat and phase transition temperature range. All values were assigned based on data provided in the corresponding material datasheets. Notably, the melting and solidification temperature ranges vary depending on the PCM type: for RT21HC, the phase change occurs between 19 °C and 21 °C, whereas for RT28HC, the transition range is between 27 °C and 29 °C. The complete set of material properties used in the simulation is listed in Table 3.9.

Table 3.9

Thermophysical properties of materials used in the simulation model (Glass, RT28HC and RT21HC)

Property	**Glass**	**PCM (RT28HC)**	**PCM (RT21HC)**
Material Type	Solid	Fluid	Fluid
Density [kg/m³]	2500 (constant)	800 (Boussinesq)	770 (Boussinesq)
Specific Heat Capacity [J/kg·K]	780	2000	2000
Thermal Conductivity [W/m·K]	0.8	0.21	0.2
Viscosity [kg/m·s]	–	0.00181	0.0016
Thermal Expansion Coefficient [1/K]	–	0.00012	0.00012
Melting Heat [J/kg]	–	250 000	210 000
Solidus Temperature [°C]	–	27	19
Liquidus Temperature [°C]	–	29	21

The boundary conditions (see Fig. 3.32) in the simulation are defined based on the specific settings listed in Table 3.3. The lateral sides of the specimen, where heating or cooling is applied, are modelled as glass walls with a thickness of 0.04 meters. To replicate the experimental conditions, a thermal boundary condition is used to maintain a constant temperature on these surfaces throughout the entire simulation period.

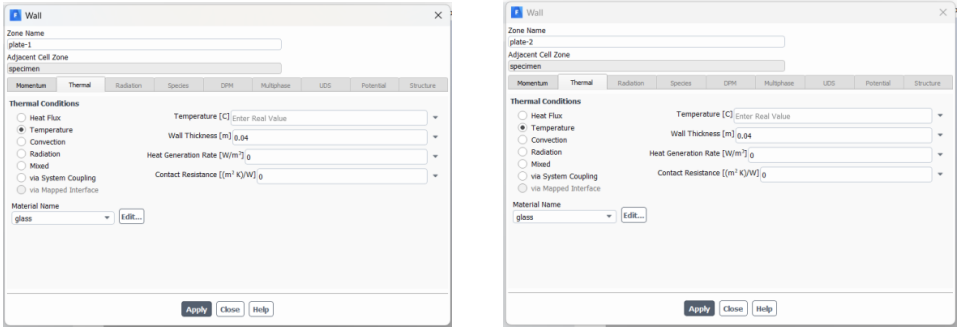

Fig. 3.32. Boundary conditions for the heating and cooling sides.

To ensure an accurate comparison between simulated and experimental results, the placement of measurement nodes must be precisely aligned with the experimental sensor locations. In addition to capturing the average temperature of the PCM domain, two additional monitoring points (PCM CH T and PCM CL T) are introduced in the simulation to record temperatures at the lower and upper sections of the PCM, positioned centrally within the container. The location of these nodes is illustrated in Figure 3.33.

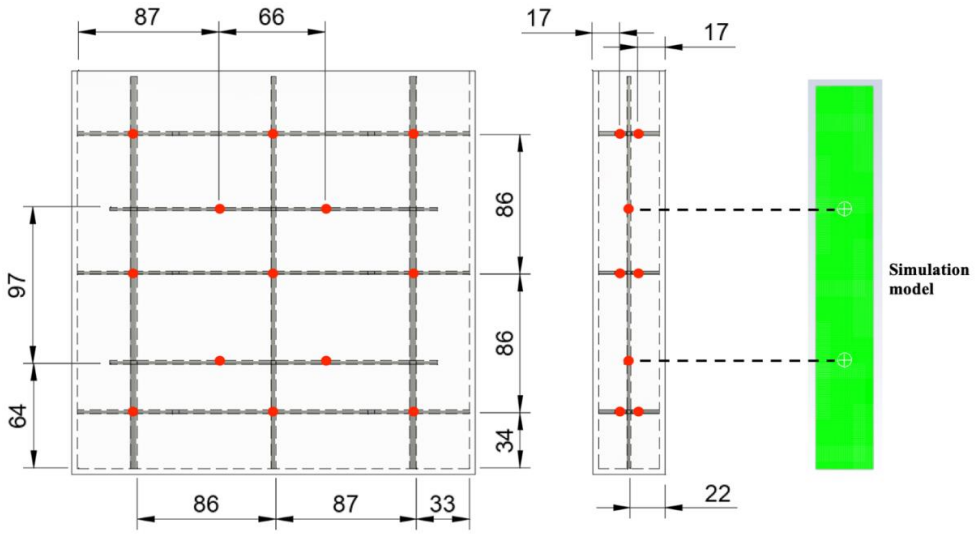

Fig. 3.33. Alignment of temperature nodes matching the actual experimental setup.

To accurately simulate the transient heat transfer and phase change behaviour of the PCM, a robust combination of solution methods and time-stepping parameters was employed in ANSYS Fluent (Fig. 3.34).

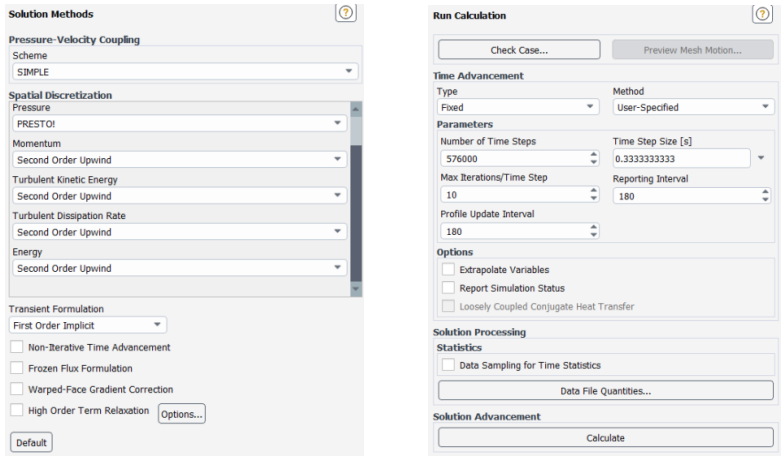

Fig. 3.34. Solution methods and calculation settings for hot plate simulation.

The simulation uses the SIMPLE (Semi-Implicit Method for Pressure Linked Equations) algorithm for pressure-velocity coupling, which is suitable for incompressible, steady or mildly unsteady flows. Pressure interpolation is handled using the PRESTO! (Pressure Staggering Option) scheme, which is recommended for flows involving body forces such as gravity - a critical aspect when modelling buoyancy-driven convection in liquid PCM [177]. For spatial discretization, second-order upwind schemes are applied across all key equations to ensure higher accuracy:

- Momentum – Second Order Upwind;
- Turbulent Kinetic Energy – Second Order Upwind;
- Turbulent Dissipation Rate – Second Order Upwind;
- Energy – Second Order Upwind.

The transient formulation is set to First Order Implicit, which offers greater numerical stability for long-duration, time-dependent simulations, such as those involving PCM melting and solidification. A fixed time-step approach is used with a time step size of 0.3333 seconds. The maximum number of iterations per time step is limited to 10, ensuring convergence within reasonable computational effort.

3.3.3. Simulation results (S1 – HP 21/28)

Eight rounds (5-12) of hot plate experiments were replicated through numerical simulations using ANSYS Fluent 2021 R1 (version 21.1), executed on a Windows 11 system equipped with an Intel i7 2.7 GHz processor and 32 GB RAM. The temperature boundary conditions for each simulation round were set to match those used in the experimental tests, as detailed in Table 3.3. From each simulation, key thermal data, including the average PCM temperature and the temperatures recorded at two central nodes (located in the upper and lower sections of the specimen), were extracted and analysed. These results were compiled into comparative graphs to enable direct comparison with experimental measurements. The designation and description of each curve used in the graphical representations are provided in Table 3.10.

Table 3.10

Curve designations and descriptions of thermal data presented in simulation S1 and experimental graphs

Designation	Description
PCM T	Average temperature in PCM experimentally measured
PCM T SIM	Average temperature in PCM simulated
PCM CH T	Average temperature measured from 2 central sensors in PCM upper section
PCM CL T	Average temperature measured from 2 central sensors in PCM lower section
PCM CH T SIM	Simulated temperature in upper section of PCM
PCM CL T SIM	Simulated temperature in lower section of PCM
Plate 1 T	Temperature on heating/cooling plate 1 experimentally measured
Plate 2 T	Temperature on heating/cooling plate 2 experimentally measured

Figure 3.35 represents the comparison of experimentally measured and simulated results from the fifth round – RT21HC heating from 17 to 25 degrees. It can be observed that the simulated average temperature of the PCM increases significantly faster than the experimentally measured values. In the simulation, the PCM reaches its melting point in approximately 10 minutes, whereas in the experiment, the same temperature is achieved only after about 3 hours. Similarly, the simulated temperatures at the central sections of the PCM also reach the phase-change threshold earlier than their experimental counterparts. This indicates an overall faster phase-change process in the numerical model. Despite these differences in thermal response time, both simulated and experimental average PCM temperatures eventually stabilize at approximately 25 °C after 24 hours, demonstrating reasonable long-term agreement. The discrepancies in early-stage heating can likely be attributed to non-ideal experimental conditions, particularly the temperature variation between the two heating plates. In practice, it was not possible to maintain a perfectly constant temperature of 25 °C on both plates simultaneously. Additionally, one plate consistently reached the target temperature more slowly, causing a delay in the onset of phase change in the physical specimen.

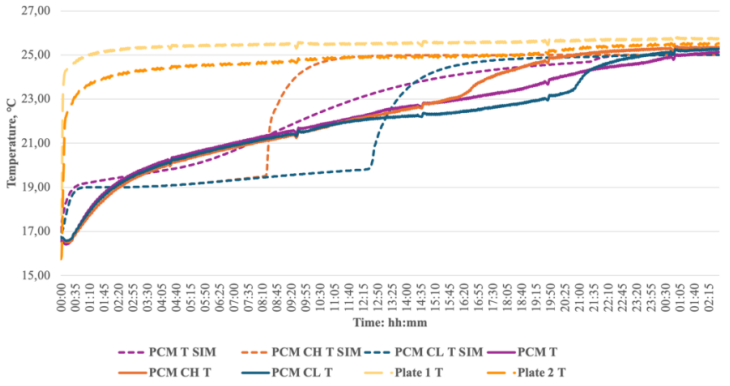

Fig. 3.35. Results from round 5 (simulation vs experiment): RT21HC heating.

The results from the sixth round are presented in Figure 3.36. Similar trends in temperature behaviour are observed as in the ninth round: the initial impact of the applied cooling is significantly more pronounced in the simulation than in the experiment. The PCM temperature in the simulation drops more rapidly and abruptly, indicating a faster thermal response under idealized conditions. In the experimental setup, both plates encounter challenges in reaching the intended cooling temperature of 17 °C, which affects the thermal behaviour of the PCM. As a result, the experimentally measured PCM temperatures remain consistently higher than those predicted by the simulation throughout the entire test cycle. These deviations highlight the influence of imperfect boundary conditions and thermal inertia in the physical system.

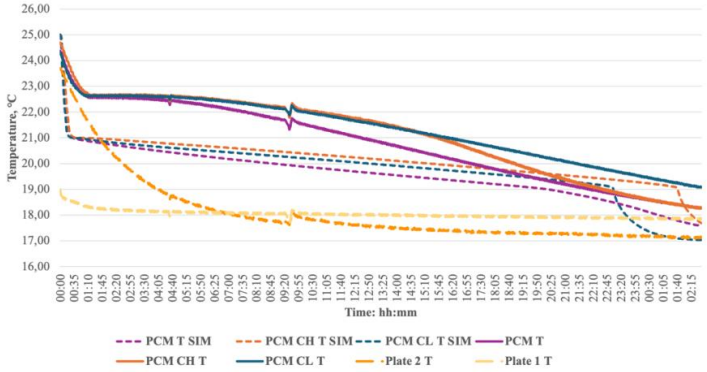

Fig. 3.36. Results from round 6 (simulation vs experiment): RT21HC cooling.

In round 7 (Fig. 3.37), where intensive cooling was tested, the plates in the experimental setup were intended to maintain a constant surface temperature of 2 °C on both sides of the PCM container. However, the system was unable to achieve and sustain these conditions, resulting in a significant deviation from the simulated data. This discrepancy led to substantially different PCM temperature profiles between the experimental and numerical results, particularly during the initial cooling phase.

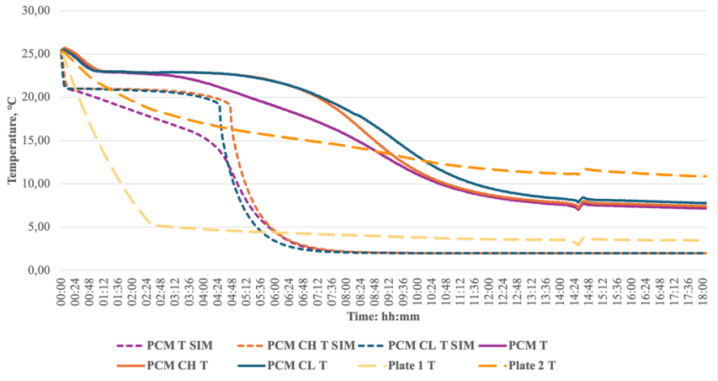

Fig. 3.37. Results from round 7 (simulation vs experiment): RT21HC cooling.

Round 8 (Fig. 3.38) involved testing under intensive heating conditions, with the target plate temperature set to 45 °C. While the heating plates in the experimental setup were able to eventually reach the required temperature, a delay of approximately 15 minutes was observed before achieving stable conditions. The temperature profiles of the simulated and experimental results exhibit similar overall trends, but the phase-change transition is noticeably delayed in the experiment. In the simulation, the PCM average temperature reaches 45 °C in approximately 5 hours, whereas in the experiment, it takes over 7 hours to attain the same temperature. This difference underscores the impact of real-world thermal inertia and imperfect boundary conditions on phase-change dynamics.

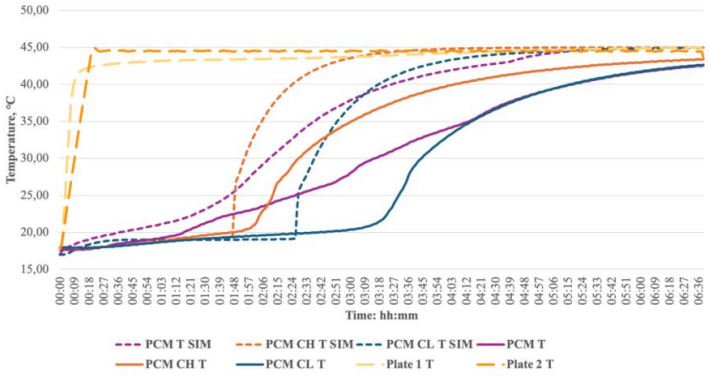

Fig. 3.38. Results from round 8 (simulation vs experiment): RT21HC heating.

Round 9 (Fig. 3.39) marks the beginning of experimental testing with RT28HC as the PCM. The results exhibit similar trends in the alignment of temperature curves compared to the heating scenario with RT21HC in Round 5. The overall thermal response, including the progression of PCM temperature and phase-change behaviour, follows a comparable pattern, indicating consistent performance of the simulation approach across different PCM materials.

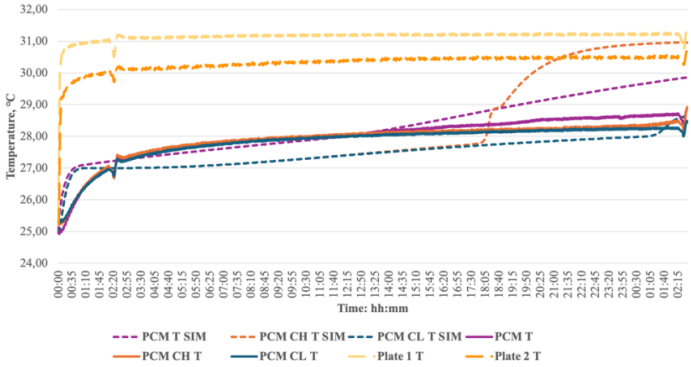

Fig. 3.39. Results from round 9 (simulation vs experiment): RT28HC heating.

In the cooling round with RT28HC (Round 10), the simulated PCM temperatures reach the onset of phase change slightly earlier than the experimental results (Fig. 3.40). However, the experimentally measured temperature curves descend to lower values, reaching approximately 28.5 °C before entering the phase-change plateau. This suggests that the actual solidification onset may occur below the nominal melting point of 29 °C, indicating a degree of thermal hysteresis in the material. Interestingly, in this round, the temperatures in the lower and upper sections of the PCM reach the phase-change region more quickly in the experimental setup than in the simulation, despite a gradual decrease in plate temperatures, which only stabilize at around 26 °C within the first two hours. These observations highlight the complex thermal dynamics of RT28HC during cooling, particularly in real-world conditions, where transient gradients and delayed plate cooling influence material behaviour.

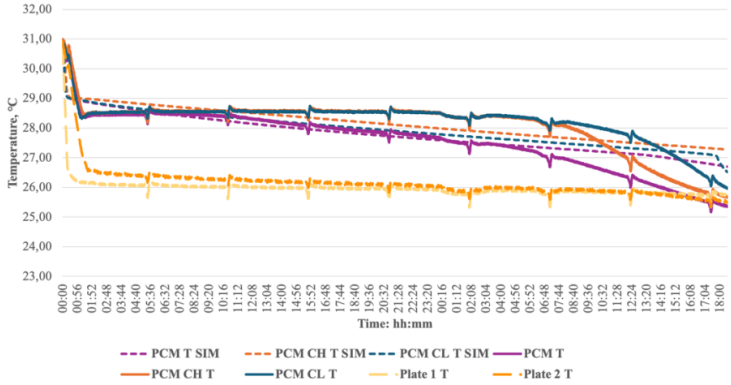

Fig. 3.40. Results from round 10 (simulation vs experiment): RT28HC cooling.

Round 11 (Fig. 3.41) involved intensive cooling of RT28HC, aiming to reduce the PCM temperature to as low as 2 °C. However, the experimental setup once again faced challenges in achieving such low temperatures on the cooling plates, resulting in a significant deviation from the intended boundary conditions.

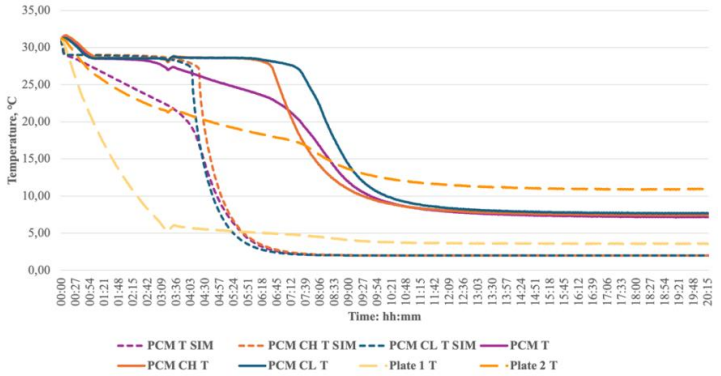

Fig. 3.41. Results from round 11 (simulation vs experiment): RT28HC cooling.

Although the overall trends of the temperature curves from both the simulation and experiment show similar behaviour, the results are not directly comparable due to the substantial temperature differences on the cooling surfaces. This discrepancy limits the ability to accurately validate the numerical model under extreme cooling conditions.

In the final round (Round 12) of RT28HC testing (Fig. 3.42), which involved intensive heating, the plates encountered limitations in reaching the target temperatures. After approximately 3 hours, the maximum temperatures achieved were 55 °C and 57 °C, falling short of the desired setpoints. This limitation resulted in a delayed phase-change initiation in the experimental setup and a lower average PCM temperature compared to the simulation.

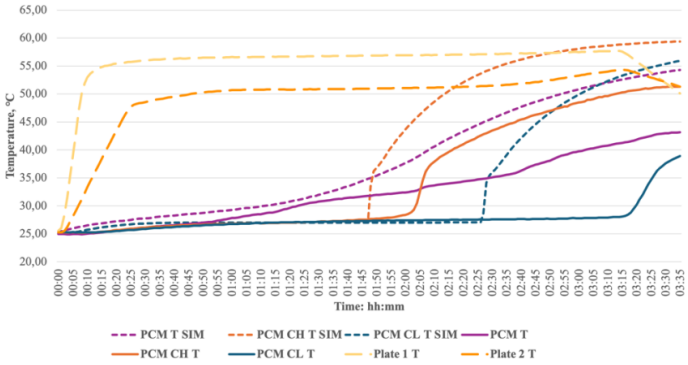

Fig. 3.42. Results from round 12 (simulation vs experiment): RT28HC heating.

3.3.4. Validation of simulation model (S1 – HP 21/28)

The validation of the simulated results was carried out using the methodology and equations outlined in Chapter 3.3.1 (Equations 3.4, 3.5 and 3.6). The key statistical indicators - Root Mean Square Error or RMSE, Relative RMSE or RRMSE and the coefficient of determination R^2 - were calculated to quantitatively assess the agreement between the simulated and experimental data. A summary of these validation metrics for all eight test rounds is presented in Table 3.11.

Table 3.11

Statistical validation metrics for simulated vs. experimental PCM temperature results across all rounds

Round No.	Specimen	Experiment type	Temperature range [°C]	RMSE	RRMSE	R^2
5	RT21HC	Heating	17 - 25	0.75	3%	0.87
6		Cooling	25 - 17	1.34	6%	0.18
7		Cooling	25 - 2	8.54	59%	-0.80
8		Heating	17 - 45	5.70	19%	0.57
9	RT28HC	Heating	25 - 31	0.54	2%	0.37
10		Cooling	31 - 25	0.51	2%	0.73
11		Cooling	31 - 2	7.18	47%	-0.12
12		Heating	25 - 60	7.01	22%	-0.57

The comparison of simulated and experimental PCM average temperature curves reveals varying levels of alignment depending on the PCM type and thermal scenario (heating or cooling). In general, the simulation accuracy is higher during moderate temperature transitions, while it decreases during intensive phase change processes, particularly under extreme cooling conditions.

For RT21HC, the best alignment is observed during the heating phase between 17-25 °C, where the RMSE is 0.75 °C, RRMSE is only 3% and the R^2 value of 0.87 indicates strong correlation between simulated and experimental curves. In contrast, during deep cooling from

25-2 °C, the RMSE increases significantly to 8.54 °C, RRMSE reaches 59% and R^2 drops to -0.80, indicating a poor match and even a reversed trend in the data. This misalignment can likely be attributed to the experimental setup's difficulty in maintaining consistent low temperatures, affecting the cooling plate performance and delaying the phase change.

For RT28HC, the best results are also seen in moderate conditions, particularly during the cooling phase from 31-25 °C, with a low RMSE of 0.51 °C, RRMSE of 2% and R^2 of 0.73. This shows a very good agreement. However, during intensive heating from 25-60 °C, accuracy deteriorates, with RMSE increasing to 7.01 °C, RRMSE to 22% and R^2 falling to -0.57, again indicating poor trend alignment.

Overall, the simulated curves show high accuracy when the boundary conditions in the experiments are stable and the temperature range is within or near the PCM phase change region without extreme gradients. Significant deviations appear in tests involving rapid or deep thermal transitions, largely due to delays and limitations in experimental plate heating/cooling. The results emphasize the importance of accurate boundary condition replication and calibration when validating numerical models against experimental data.

3.3.5. Conclusions and insights (S1 – HP 21/28)

The ANSYS Fluent model developed in simulation S1 successfully reproduced the overall thermal behaviour of both PCMs (RT21HC and RT28HC) under controlled hot-plate conditions and was validated against eight experimental rounds. The comparison revealed that the numerical model performs with high accuracy when boundary conditions are stable and moderate - particularly during low-intensity heating and cooling in both materials. Under these conditions, the RMSE and RRMSE values remain low and the correlation between simulated and measured temperatures is strong (e.g., $R^2 = 0.87$ for RT21HC heating). In contrast, significant discrepancies arise during extreme thermal transitions (cooling to 2 °C or heating above 45 °C), where experimental plate temperatures could not consistently reach or maintain the prescribed setpoints. These boundary inconsistencies delay or suppress phase transitions in the physical PCM and lead to systematic deviations in the simulation, which responds ideally and therefore predicts faster melting or solidification. Despite these limitations, the long-term thermal trends and equilibrium temperatures between simulation and experiment show good agreement, demonstrating that the calibrated material properties and numerical approach provide a physically reliable representation of PCM behaviour.

Simulation S1 establishes a validated modelling framework that captures the dominant heat transfer mechanisms and phase-change dynamics, while also identifying the sensitivity of PCM behaviour to imperfect boundary control. These insights directly inform the transition to simulation S2, in which the small-scale PCM test-box model is developed to evaluate RT21HC and RT28HC under real climatic boundary conditions. Because S2 involves spatially distributed solar gains, diurnal temperature cycles and climate-dependent charging/discharging behaviour, the validated S1 material parameters and heat-transfer settings provide a robust foundation. The observed differences between simulated and experimental phase-change rates in S1 motivate the inclusion of climate-specific transient boundary conditions in S2, enabling

a more accurate comparison of the two PCMs across representative weather profiles and seasons.

3.3.6. Small-scale PCM test box model (S2 – PCM 21/28)

The small-scale PCM test box model was developed based on the configuration (Fig. 3.17), dimensions (Fig. 3.15) and experimental conditions (Table 3.7) established in laboratory experiment E2. As the geometry of the test box is symmetric, a 2D modelling approach was selected to reduce computational load while maintaining accuracy. The schematic representation of the simulation model is shown in Figure 3.43.

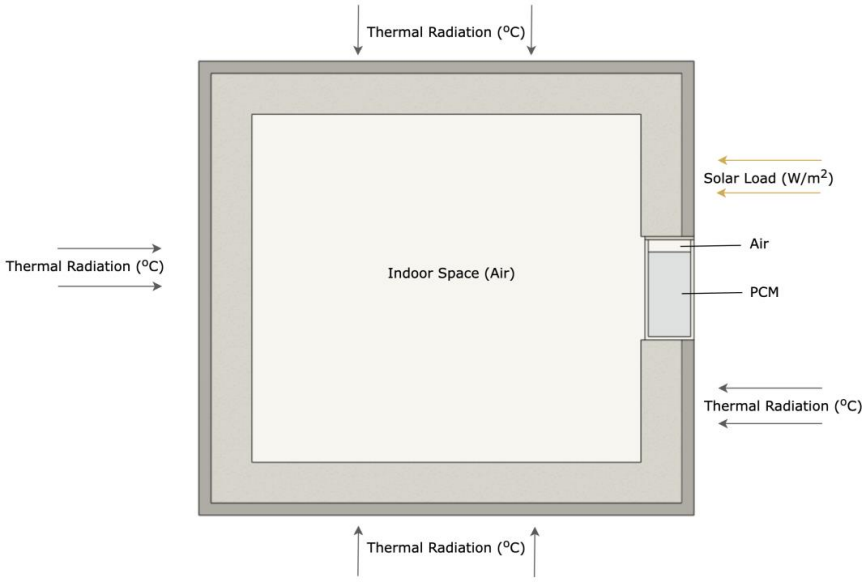

Fig. 3.43. Schematic of the 2D small-scale test box simulation model.

The outer walls, insulation layer and indoor cavity were modelled to replicate the physical test stand used in experiment E2. To ensure realistic behaviour, the model also incorporates an air gap (necessary for PCM expansion during melting) and a plastic cover corresponding to the glass container used in the laboratory setup.

The boundary conditions follow those of the physical experiment: thermal radiation is applied to all exterior surfaces, while direct solar load is applied exclusively to the front wall. The general simulation settings, numerical methods and control parameters were kept consistent with those used in simulation S1. However, in this model an additional Radiation model (Rosseland approximation) was activated to simulate the transport of solar irradiance through the system. The solar heat gain on the front plywood and glass surfaces was defined using surface-specific solar heat gain coefficients: 0.5 for plywood and 0.85 for glass. The solar heat gain was calculated as:

$$SHG = SHGC \times SI \tag{3.7}$$

where: SHG – solar heat gain, W/m^2;

SHGC – solar heat gain coefficient, %;

SI – the value of direct solar irradiation, W/m^2.

Material properties for all components were assigned according to Table 3.6. The simulation outputs included the volume-averaged indoor air temperature and the PCM temperature, both evaluated over the full 24-hour cycle.

After validating the simulation model, it was subsequently applied to assess system performance under real weather conditions. The Solar Ray Tracing function was used to determine the incident solar energy on each surface of the model. Hourly solar irradiance values for a full 24-hour cycle were introduced through a piecewise-linear function constructed from measured solar radiation data. Thermal radiation loads on the model surfaces were defined using hourly outdoor temperature profiles, ensuring that the boundary conditions accurately reflected real climatic variation throughout the simulation period.

3.3.7. Validation of simulation model (S2 – PCM 21/28)

To ensure that the numerical model reliably reflects the real behaviour of the system under varying thermal conditions - including solar irradiance and ambient temperature fluctuations - a validation experiment was performed. In this laboratory test, both experimental setups were heated until the PCM was fully melted, after which the system was allowed to cool down naturally to the ambient temperature. The experimentally measured and simulated temperature responses are presented in Figure 3.44.

Since the physical experiment was conducted inside a climate chamber operating with active air circulation, the numerical model incorporated an inlet air velocity of approximately 0.5 m/s, replicating the real airflow conditions responsible for PCM cooling.

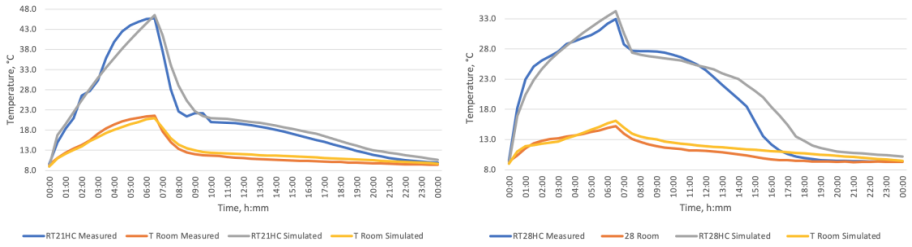

(a) (b)

Fig. 3.44. Comparison between simulated and experimentally collected data of (a) RT21HC and (b) RT28HC PCMs.

The corresponding statistical error metrics (RMSE, RRMSE and R^2) are listed in Table 3.12. The results indicate very good agreement between the simulated and experimentally obtained temperature curves, confirming that the numerical model accurately reproduces both the melting and cooling phases of the PCM.

Table 3.12

Statistical validation metrics for setups with PCMs – RT21HC and RT28HC

Metric	RT21HC	RT28HC
Room RMSE	0.84	0.87
PCM RMSE	2.11	2.37
Room RRMSE	7%	8%
PCM RRMSE	10%	12%
Room R^2	0.95	0.77
PCM R^2	0.96	0.92

3.3.8. Performance assessment in different climate zones (S2 – PCM 21/28)

To evaluate the performance of both PCMs under contrasting climatic conditions, weather data from two European cities - Helsinki (Finland) and Seville (Spain) - were acquired from the National Solar Radiation Database. Hourly average values of direct solar radiation and outside temperature for the past three years were used to define the boundary conditions for the simulations. Seasonal inputs were generated for spring, summer, autumn and winter.

The simulations were run under the assumptions that:

- global horizontal irradiance represents the solar load,
- sky conditions are clear (to ensure comparability),
- only the front facade is solar-exposed,
- wind direction and speed are neglected.

A total of ten simulations were performed: six for Helsinki (spring, summer and autumn for both PCMs) and four for Seville (spring and winter). Simulations for extreme conditions - Helsinki winter and Seville summer - were omitted because laboratory evidence indicated that neither PCM provides performance advantages under excessively cold or excessively hot conditions.

The climate in Helsinki during spring and autumn is comparable and mild, with the exception of slightly higher outdoor temperatures in autumn. Figure 3.45 represents simulation results from the spring test in Helsinki.

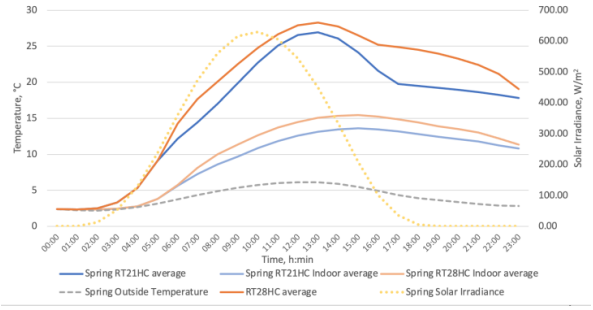

Fig. 3.45. Average temperature in the PCMs and room. Simulation results: Helsinki-spring.

From the Helsinki-spring graphs, it is evident that both RT21HC and RT28HC undergo partial melting, absorbing solar heat effectively. RT28HC reaches slightly higher temperatures during the charging period; however, both PCMs end the cycle at nearly identical temperatures. Given that the ambient temperature does not exceed 6 °C, all thermal gains originate exclusively from solar radiation.

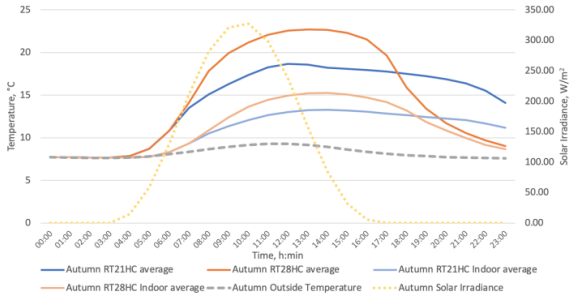

Fig. 3.46. Average temperature in the PCMs and room. Simulation results: Helsinki-autumn.

Figure 3.46 displays the outcomes of the Helsinki autumn simulation. RT28HC achieves a significantly higher peak temperature - approximately 6 °C above RT21HC. Yet by the end of the cycle, RT28HC cools 6 °C below RT21HC. Since RT28HC does not reach its melting point in these conditions, the absorbed heat is quickly lost. RT21HC, on the other hand, stores a part of the absorbed energy in latent form, maintaining higher indoor temperatures during the discharge phase.

Compared to other European cities, especially those in Southern Europe, Helsinki experiences cooler and more moderate summers. Throughout the months of June, July and August, the average high temperature in Helsinki typically falls between 18 °C to 22 °C, while the average low temperature ranges from 10 °C to 14 °C. Figure 3.47 illustrates the temperature graphs of the summer season in Helsinki. As solar radiation intensifies, both PCMs melt during the daytime. However, the higher melting temperature of RT28HC prevents excessive indoor overheating. RT28HC exhibits smoother, more stable temperature curves across the full 24-hour cycle, resulting in improved indoor comfort.

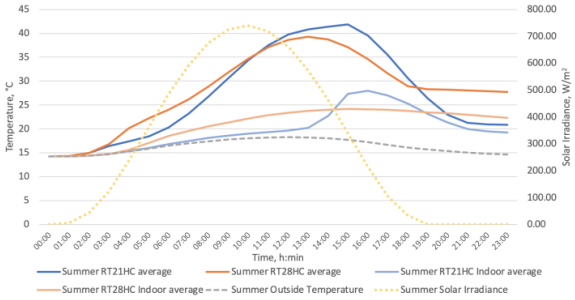

Fig. 3.47. Average temperature in the PCMs and room. Simulation results: Helsinki-summer.

Compared to Northern Europe, Southern Europe, exemplified by Seville, receives a higher amount of sunlight throughout the year in all seasons. Seville experiences an average of 129 sunny days annually and the solar intensity is higher than in other European cities. In spring, the solar irradiance value can surpass 900 W/m^2, which raises concerns about the possibility of overheating. However, the nighttime temperatures are still relatively low, not exceeding 12 °C, which may require additional heating.

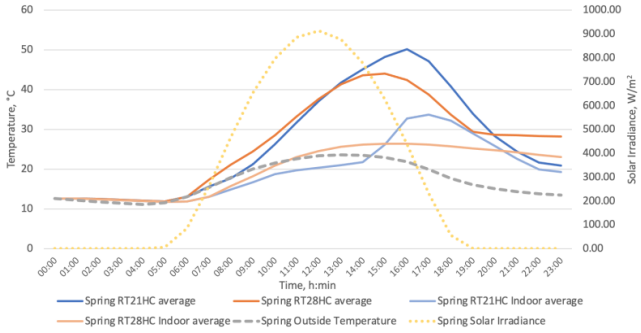

Fig. 3.48. Average temperature in the PCMs and room. Simulation results: Seville-spring.

The simulation results of Seville in spring are depicted in Figure 3.48. In Seville's intense spring conditions, RT21HC overheats, driving indoor temperatures close to 35 °C. RT28HC, however, effectively prevents overheating while still providing nighttime comfort without additional heating, thanks to its higher latent heat storage capacity.

Seville has a milder winter compared to many other European cities due to its southern location and Mediterranean climate. The average temperature in Seville during the winter months (December to February) ranges from 8 °C to 18 °C, which is considerably warmer than many other European cities during the same period. Yet, additional heating is necessary for most of the time. The average PCM temperatures in the Seville - winter numerical simulation are illustrated in Figure 3.49.

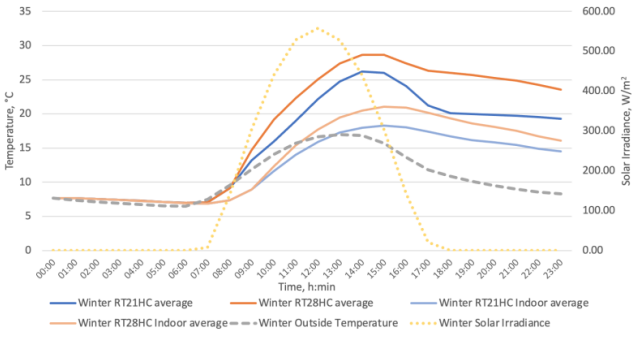

Fig. 3.49. Average temperature in the PCMs and room. Simulation results: Seville-winter.

During winter, both PCMs melt fully and store latent heat. Their thermal behaviours are similar, although RT28HC achieves a slightly higher maximum indoor temperature (≈21 °C), offering marginally improved comfort during the coldest hours.

Figure 3.50 represents the comparison of the highest liquid fraction reached in the PCMs in every simulation. RT21HC fully melts in Helsinki–summer and Seville–spring, highlighting a clear risk of overheating in high-radiation climates. RT28HC, with its higher phase-change temperature and greater latent storage capacity, provides more stable behaviour across all tested climates.

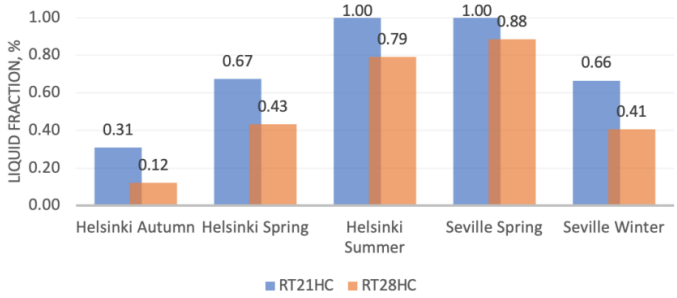

Fig. 3.50. Comparison of the highest reached melted fraction of the PCMs in all simulations.

3.3.9. Conclusions and insights (S2 – PCM 21/28)

The S2 small-scale PCM test box simulation demonstrates that PCM performance is strongly dependent on climate zone, seasonal temperature profiles and solar irradiance intensity. Across all simulated climates, RT28HC consistently provides more stable thermal behaviour than RT21HC due to its higher melting temperature and greater latent heat capacity. In mild and moderate climates (Helsinki spring/autumn), both PCMs partially melt, but RT21HC retains heat more effectively during the discharge phase. In high-irradiance climates (Seville spring), RT21HC overheats, whereas RT28HC maintains indoor temperatures within the comfort range. Under winter conditions in Seville, both PCMs demonstrate similar storage capacity, though RT28HC performs slightly better. In Helsinki summer, both PCMs melt, but RT28HC suppresses overheating more efficiently.

These findings confirm that RT21HC is better suited for colder northern climates where the risk of overheating is minimal, whereas RT28HC provides superior performance in warmer or high-irradiance regions. Nonetheless, the limited internal volume of the small-scale test box remains a major constraint for fully evaluating the behaviour of a building envelope under real operating conditions.

4. SMALL-SCALE OPTIMISATION

In this chapter, the evolution of component-level testing of small-scale facade modules, conducted using PASLINK-type laboratory setups and outdoor experimental stands, have been presented. Experimental results have been analysed to support the development of the large-scale facade module. Four experiments (E3–E6) were carried out within this stage of the research, each focusing on different components and their configurations. These tests enabled the evaluation and optimisation of the solar facade module's performance, with the aim of improving its thermal response and overall energy efficiency.

4.1. Influence of adjustable insulation and heat-transfer elements - air gap, aerogel, heat-transfer enhancer and Fresnel lens (E3 – ADJ ON/OFF)

To maximise the utilisation of incident solar energy within the PCM, the building envelope must incorporate appropriate heat-transfer enhancement elements. Given that on-site solar irradiance under real climatic conditions is inherently intermittent, the system must be capable of absorbing as much thermal energy as possible during periods of solar availability and retaining this energy within the PCM for extended durations. These operational modes correspond to the charging and discharging cycles of the PCM, respectively. To support detailed investigation of these processes, a dedicated experimental test stand was designed and constructed for the present research. This facility enables controlled evaluation of multiple heat-transfer elements integrated within the facade assembly, including silica aerogel, air gaps, PMMA glazing, copper lattice structure, a Fresnel lens and an adjustable outer insulation layer. The test stand allows systematic assessment of how each configuration influences heat-transfer efficiency during the charging phase and storage performance during the discharging phase, thereby providing empirical evidence for optimising PCM-based facade design.

4.1.1. Experimental design (E3 – ADJ ON/OFF)

The aim of this experiment was to evaluate the influence of selected heat-transfer elements during the PCM charging phase, as well as the performance of an adjustable external insulation layer during the discharging phase. In the discharging mode, a 5 cm thick external insulation layer was added to the solar facade module to reduce thermal losses without compromising charging efficiency (Fig. 4.1).

In total, six experimental configurations were developed, each incorporating a different combination of heat-transfer elements, as illustrated in Figure 4.2. The influence of the adjustable external insulation layer was evaluated for all six configurations to ensure a consistent assessment of its effect across the full range of heat-transfer enhancement strategies.

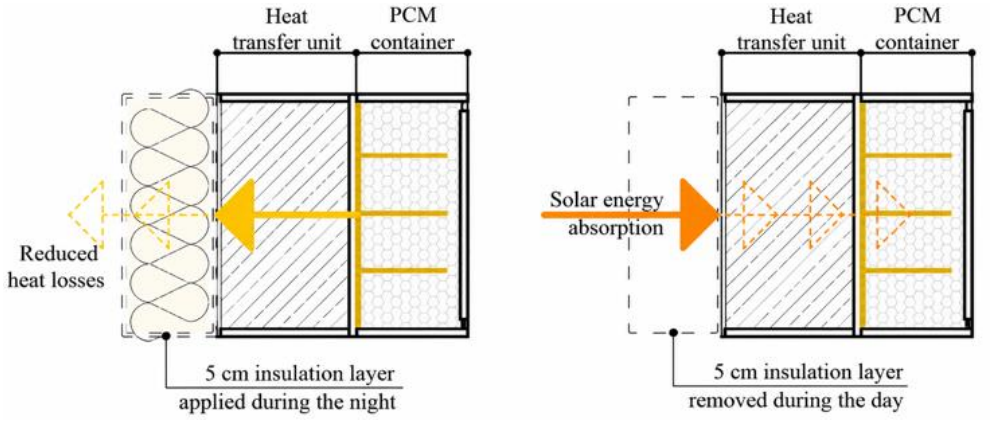

Fig. 4.1. Charging phase with no insulation layer (a), discharging phase with insulation layer (b).

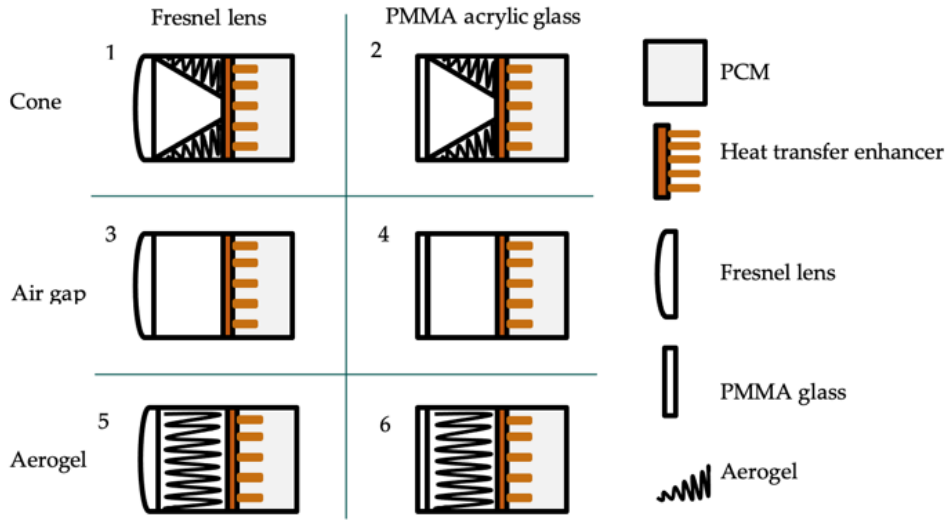

Fig. 4.2. Schematic representation of six solar facade variations.

The experimental setup represents a small-scale adaptation of the PASLINK testing approach. The test box (0.6 × 0.6 × 0.55 m) replicates the thermal behaviour of a building envelope, including walls, floor, roof and a small unconditioned interior space. The structure is constructed from 18 mm plywood and internally lined with 200 mm of thermal insulation (λ = 0.037 W/mK). The insulation thickness was selected to achieve a U-value consistent with the requirements specified in Latvian construction standards. The developed facade module is integrated into one of the box walls, as shown in Figure 4.3.

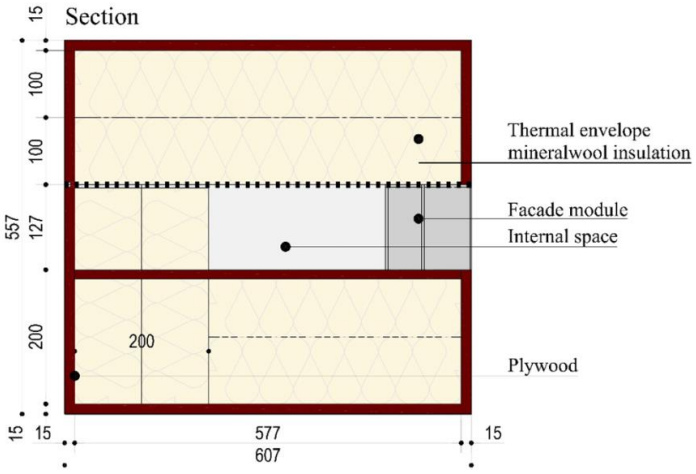

Fig. 4.3. Small-scale PASLINK type test box.

For monitoring purposes, the experimental setup is equipped with a set of thermocouples and heat-flux sensors (Fig. 4.4). Five thermocouples (T1–T5) are used in total: three (T1–T3) are embedded within the PCM container at different vertical positions to capture temperature variations across the PCM layers; one thermocouple (T4) measures the air temperature inside the climate chamber; and one (T5) is installed in the "indoor space" of the test box. This configuration enables direct comparison of PCM temperature evolution and the resulting indoor-space temperature response across all experimental configurations under controlled conditions.

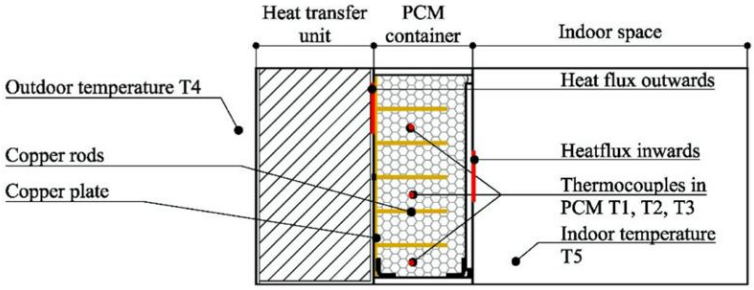

Fig. 4.4. Measuring equipment location in small-scale solar facade module.

Two heat-flux sensors are installed on the inner and outer surfaces of the PCM container. The inner sensor (facing the "indoor space") records the heat exchange between the PCM and the test-box interior, while the outer sensor (facing the heat-transfer unit) quantifies heat flows between the PCM and the external environment.

The entire test box is placed inside a climate chamber (Fig. 4.5.), where a dedicated heating/cooling unit maintains the prescribed boundary conditions required for the experimental investigations.

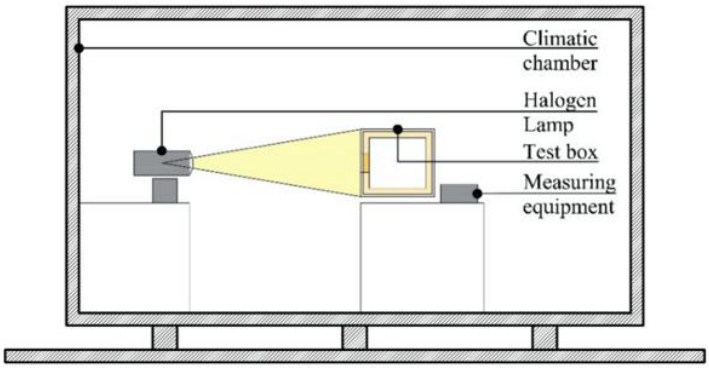

Fig. 4.5. Experimental setup in climate chamber.

4.1.2. Experiment plan (E3 – ADJ ON/OFF)

Six variations of the designed solar facade module were tested under controlled laboratory conditions, as presented in Figure 4.2. The PCM container constitutes the core of the facade module and remained unchanged throughout all experiments. The PCM used in all configurations was paraffin RT21HC. The differences among the six setups were introduced exclusively in the heat-transfer unit, which employed different configurations: an unventilated air gap, a silica-aerogel filling and a cone-shaped unventilated air gap embedded within the aerogel layer.

To investigate the complete energy charging–discharging cycle, a controlled sequence of heating and cooling conditions was applied:

1) Initial state (10 °C). Prior to each experiment, all facade module configurations and the climate chamber were cooled to 10 °C. This temperature reflects typical outdoor conditions during spring and autumn in Northern Europe - periods during which space heating is required and during which on-site solar energy has significant potential to offset heating demand.
2) Heating phase. The climate chamber temperature was increased to 15 °C and a halogen lamp equipped with a dimmer was used to simulate solar radiation. Solar irradiance was set to 1000 W/m² in accordance with international testing standards. The charging phase lasted 7 h 39 min.
3) Cooling phase. After the heating period, the lamp was switched off and the chamber temperature was reduced again to 10 °C. The discharging phase continued for 40 h 21 min.

The total duration of each complete test cycle was 48 hours. For each of the six configurations, two test rounds were conducted - one with and one without an additional 5 cm external insulation layer mounted on the outer surface of the solar facade module. In total, 12 unique test configurations were evaluated (S-setup; 1, 2, 3… corresponding to each variation), as summarised in Table 4.1.

Table 4.1

Experiment plan with twelve setup variations

Outer layer / Heat transfer unit variations	Cone (unventilated air gap + aerogel)	Unventilated air gap	Aerogel filling
Fresnel Lens	S1 – W/O	S3 – W/O	S5 – W/O
PMMA	S2 – W/O	S4 – W/O	S6 – W/O
Fresnel Lens + adjustable insulation	S1 – W	S3 – W	S5 – W
PMMA + adjustable insulation	S2 – W	S4 – W	S6 – W

W-with, W/O without adjustable insulation

Characteristics of materials used in modules and PASLINK test cell is summarized in Table 4.2.

Table 4.2

Components of the small scale PASLINK test cell

Component	Characteristics
PCM RT21HC	See Table 2.3
PCM glass container	Dimensions: 127 × 127 × 60 mm
Plastic box	Material: Polyethylene terephthalate glycol (PETG)
Cone	Material: Polyethylene terephthalate glycol (PETG)
Glass	Dimensions: 129 × 129 × 4 mm
Poly (methyl methacrylate) PMMA glass	Dimensions: 127 × 127 × 1.5 mm
Fresnel lens	Dimensions: 127 × 127 × 1.5 mm Focal length: 71.12 mm
Aerogel	LUMIRA translucent aerogel LA1000
Plywood	15 mm λ = 0.13 W/mK
Mineral wool	200 mm λ = 0.037 W/mK
Adjustable layer XPS insulation	50 mm λ = 0.037 W/mK

4.1.3. Comparison of PCM temperatures throughout all setups (E3 – ADJ ON/OFF)

Figures 4.6, 4.7, 4.8 and 4.9 present the average PCM and "indoor" temperatures for all six experimental configurations. A summary of the fixed average PCM temperature (Tavg) and indoor temperature (Tin) after 24 h and 48 h - both with and without the adjustable insulation layer - is provided in Table 3.6. Comparable values are highlighted using the same colour.

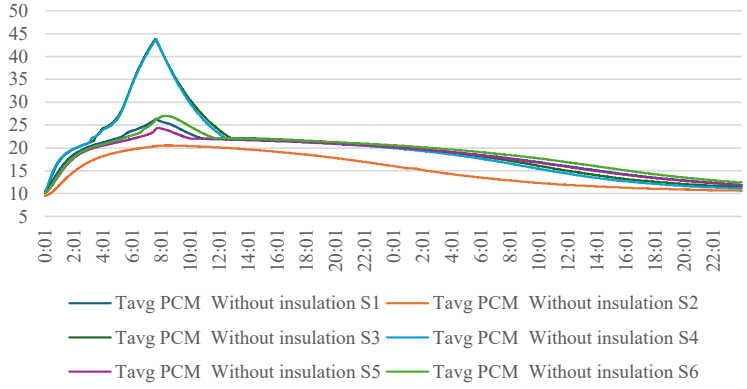

Fig. 4.6. Average PCM temperature in six setups without insulation during the discharging phase.

After 24 h, the PCM in most setups (except Setup 2) is partially solidified, with Tavg distributed within a narrow temperature band of 0.4 °C (without insulation) and 0.7 °C (with insulation). After 48 h, the range widens to 1.0 °C for the non-insulated setups but becomes narrower when the insulation layer is applied. This indicates that the additional night-time insulation improves performance particularly for setups with initially higher heat losses.

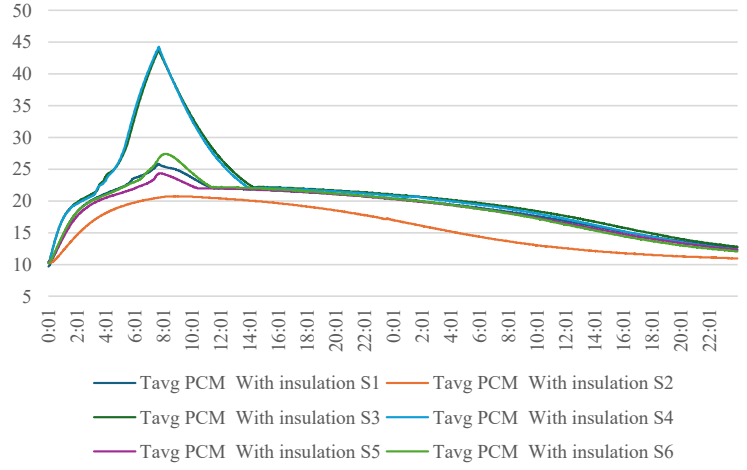

Fig. 4.7. Average PCM temperature in six setups with insulation during the discharging phase.

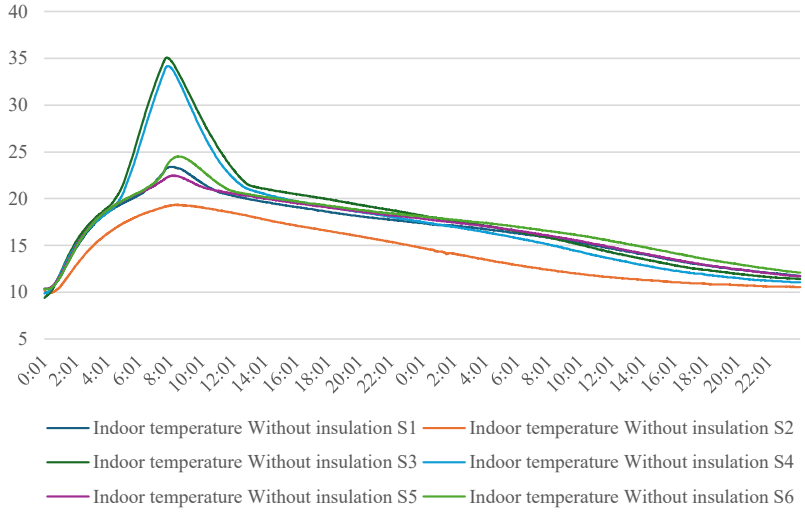

Fig. 4.8. “Indoor” temperature in six setups without insulation during the discharging phase.

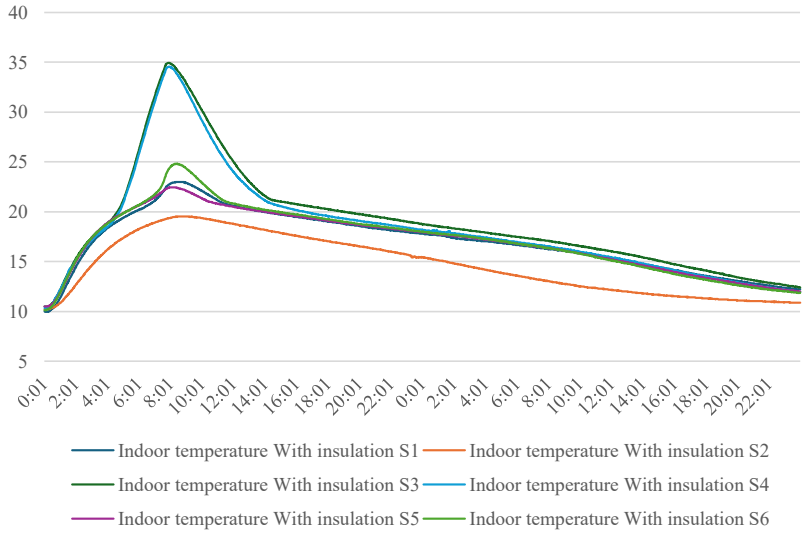

Fig. 4.9. “Indoor” temperature in six setups with insulation during the discharging phase.

A similar trend is observed for the “indoor” temperature. After 24 h, temperature variability is smaller in the setups without the insulation layer, but after 48 h, the spread becomes larger. In contrast, setups with the additional insulation converge to nearly identical indoor temperatures after 48 h. This confirms the equalising effect of the adjustable insulation layer.

Table 4.3

Highest and lowest average PCM temperature in solar facade module

	Without adjustable insulation layer T_{avg}		With adjustable insulation layer T_{avg}		Without adjustable insulation layer T_{Indoor}		With adjustable insulation layer T_{indoor}		T_{avg}	T_{in}	T_{avg}	T_{in}	
Type	t, °C 24h	t, °C 48h	t, °C 24h	t, °C 48h	t, °C 24h	t, °C 48h	t, °C 24h	t, °C 48h	Max Δt, °C	Max Δt, °C	Δt, °C 48h	Δt, °C 48h	Time delay, min
Setup 1 Fresnel lens, cone, aerogel	20.1	11.8	20.4	12.6	17.4	11.7	17.8	12.2	**0.98**	**0.78**	**0.77**	**0.49**	**30**
Setup 2 PMMA, cone, aerogel	16.0	106	17.0	10.9	14.7	10.5	15.5	10.9	**1.07**	**0.93**	**0.32**	**0.32**	**-**
Setup 3 PMMA and air	20.0	11.1	20.8	12.3	17.5	11.0	18.2	12.2	**3.02**	**2.13**	**1.20**	**0.91**	**90**
Setup 4 Fresnel lens and air	20.2	11.5	21.0	12.7	18.2	11.4	18.8	12.2	**2.82**	**1.98**	**1.29**	**1.00**	**95**
Setup 5 Fresnel lens and aerogel	20.2	11.9	20.3	12.3	17.9	11.7	18.0	12.2	**0.73**	**0.51**	**0.41**	**0.28**	**15**
Setup 6 PMMA glass and aerogel	20.4	12.1	20.6	12.4	18.0	11.9	18.1	12.1	**0.58**	**0.44**	**0.33**	**0.21**	**30**

In Table 4.3, the grey-shaded cells summarise the temperature differences (ΔT) for each module between the insulated and non-insulated configurations. ΔT is compared for both the average PCM temperature and the indoor temperature and additionally, the maximum ΔT occurring between 24 h and 48 h is documented. The largest ΔT values occur in Setups 3 and 4, which include an air-gap layer in front of the PCM container. These setups also exhibit the longest time delay before entering the solidification phase. This indicates that the adjustable insulation layer has the greatest influence when the air gap is present, significantly reducing heat loss during the discharging process.

The largest ΔT values in Setups 3 and 4 demonstrate that these configurations benefit most from the adjustable insulation layer. The time delay between comparable insulated and non-insulated cases is also the longest in these setups.

Table 4.4 provides the ranking of all setups across each evaluation criterion. Performance rankings differ across checkpoints. Setup 2 consistently performs the worst. When ranking based on performance at 48 h with adjustable insulation, four setups share 1st place, demonstrating that the adjustable insulation serves as a levelling mechanism - its influence is minor in already well-insulated setups but substantial in poorly insulated ones. This finding is consistent with the larger ΔT values observed in Setups 3 and 4.

Because solar facade systems may be installed in different climates, cardinal orientations and functional contexts, the optimal setup choice can vary. For example, Setups 3 and 4 exhibit the fastest melting rate and the highest peak temperatures; therefore, they may be best suited for locations with short solar exposure periods, where rapid phase change is advantageous. Conversely, in locations with prolonged solar exposure, other setups - or combinations of setups

- may be more suitable to prevent excessive sensible heat accumulation that could raise indoor temperatures above comfort levels.

Table 4.4

Ranking of setups in defined points of reference

	Without adjustable insulation layer		With adjustable insulation layer		Without adjustable insulation layer		With adjustable insulation layer		T_{avg}	T_{in}	T_{avg}	T_{in}	
	T_{avg}		T_{avg}		T_{Indoor}		T_{indoor}						
	t, °C 24h	t, °C 48h	t, °C 24h	t, °C 48h	t, °C 24h	t, °C 48h	t, °C 24h	t, °C 48h	Max Δt, °C	Max Δt, °C	Δt, °C 48h	Δt, °C 48h	Time delay, min
Setup 1 Fresnel lens, cone, aerogel	3	3	4	2	5	2	5	1	**4**	**4**	**3**	**3**	**3**
Setup 2 PMMA glass and aerogel	5	6	6	5	6	5	6	3	**3**	**3**	**5**	**4**	-
Setup 3 Fresnel lens and aerogel	2	4	1	1	1	3	1	1	**2**	**2**	**1**	**1**	**1**
Setup 4 Fresnel lens and air	4	5	2	4	4	4	2	1	**1**	**1**	**2**	**2**	**2**
Setup 5 PMMA and air	2	2	5	4	2	2	4	1	**5**	**5**	**4**	**5**	**4**
Setup 6 PMMA, cone, aerogel	1	1	3	3	3	1	3	2	**6**	**6**	**5**	**6**	**3**

Ranking: 1 – best performance; 6 – worst performance

4.1.4. Conclusions and insights (E3 – ADJ ON/OFF)

Applying the adjustable insulation layer resulted in increased average temperatures in both the PCM and the "indoor space" across all setups. However, the most significant impact was observed in modules featuring an air-gap layer, where the additional insulation most effectively reduced heat loss during the discharging phase. These modules demonstrated superior performance compared to more heavily insulated configurations, as their temperature curves converged more closely after solidification, indicating slower heat dissipation and improved thermal retention.

Overall, when considering the complete thermal cycle (charging and discharging), modules containing an air-gap layer gained and released more energy than the other configurations. In contrast, modules equipped with higher levels of fixed insulation demonstrated advantages primarily in latent heat storage, showing more stable temperature plateaus during phase transition.

It is important to note that the relatively small size of the test stand contributed to elevated PCM and indoor temperatures in all configurations. For this reason, the following stage of the research focuses on scaling the system to a larger format and validating its behaviour under realistic environmental conditions.

The comparative evaluation - based on multiple reference points such as indoor temperature and average PCM temperature at 24 and 48 hours, with and without the adjustable insulation - confirmed that the choice of configuration should depend on the intended functional objective of the solar facade. For instance, setups with an air-gap layer demonstrated the fastest melting rate and highest temperatures under the tested conditions, making them suitable for locations with short periods of solar exposure. Conversely, more insulated setups may be better suited for orientations with high solar loads, where controlling excessive sensible heat gains becomes important.

These insights directly inform the next steps of the research. In experiments E4 and E5, attention shifts to evaluating the influence of the dynamic component - both in laboratory conditions and in outdoor testing. The findings from the present experiment highlight the thermal sensitivities and energy-storage dynamics of different PCM-insulation configurations, which are essential for interpreting the behaviour of the dynamic facade module. As the system transitions from passive PCM-insulation optimisation (this experiment) to active solar-tracking and outdoor operation (E4–E5), the identified thermal patterns, phase-change characteristics and system sensitivities provide a foundational reference for assessing how dynamic sunlight concentration, blade motion and real-weather loads further enhance or alter the PCM performance.

4.2. Influence of dynamic component (E4 – DYN-LAB ON/OFF and E5 – DYN-LAB ON/OFF)

4.2.1. Experimental design (E4 – DYN-LAB ON/OFF)

The small-scale solar facade module developed for this experiment represents the next step in the ongoing design and optimisation process. Its architecture builds on the insights gained from the previous experimental stage described in chapter 4.1, where several material options and heat-transfer enhancement concepts were comparatively evaluated. Components and materials that demonstrated favourable performance in the earlier tests were selected and adapted for inclusion in this subsequent developmental version of the facade module.

A detailed overview of the components integrated into this iteration of the module design is provided in Table 4.5.

Table 4.5

Components of the small-scale facade module

Component	Characteristics
PCM RT21HC	See Table 2.6
PCM glass container	Dimensions: 127 × 127 × 60 mm
Plastic box	Material: Polyethylene terephthalate glycol (PETG)
Cone	Material: Acrylonitrile styrene acrylate (ASA) white
Glass	Dimensions: 129 × 129 × 4 mm
Poly(methyl methacrylate)	Dimensions: 127 × 127 × 2 mm

(PMMA) glass	
Fresnel lens	Dimensions: 127 × 127 × 1,5 mm Focal length: 71,12 mm
Aerogel 1	LUMIRA translucent aerogel LA1000
Aerogel 2	ENERSENS Kwark GS
Aerogel 3	Thermal Wrap 8mm blanket

In this experimental design, several heat-transfer elements were incorporated, including silica aerogel, unventilated air gaps, PMMA glazing and a Fresnel lens. Three types of aerogel were used for thermal insulation and optical enhancement:

1) Aerogel 1 is a high-performance insulation material composed of modified synthetic amorphous silica gel. Its particle size ranges from 0.7 to 4 mm and it provides more than 90% light transmission per centimetre, making it suitable for translucent solar-thermal applications.
2) Aerogel 2 was selected due to its superior thermal conductivity (0.018–0.022 W/mK) and fine particle size (10–1250 μm), which improves packing density and reduces convective losses.
3) Aerogel 3 (thermal wrap) was used as internal filling for the rotating blades due to its flexible, easily formable structure.

The main advancement compared with the previous study is the integration of a dynamic component consisting of rotating blades. This component serves two primary functions:

- light concentration, directing incident solar radiation toward the heat-transfer element to increase energy input to the PCM;
- thermal insulation, as the blade interiors are filled with aerogel to reduce heat losses from the module during the discharging phase (adjusted insulation).

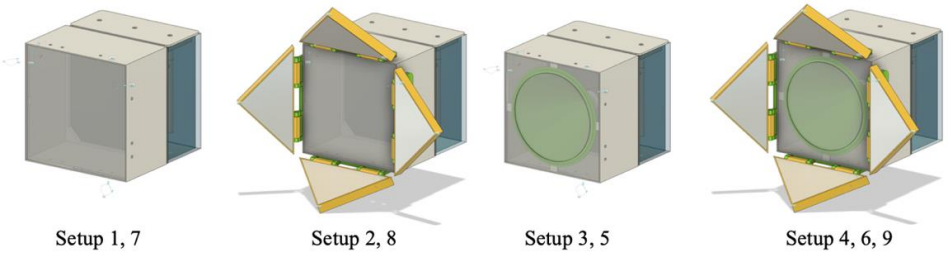

Fig. 4.10. Drawings of solar facade module in different setups.

To identify the optimal combination of materials and geometric parameters, the module was tested in several configurations. Across all setups, the PCM, glass container and the supporting glass and plastic box components remained unchanged throughout the first experimental phase. Based on the performance of each configuration, incremental adjustments were introduced - for example, modifying the aerogel filling volume and adjusting the cone diameter - to improve heat transfer, optical concentration and overall PCM charging efficiency. The components used

in all configurations are listed in Table 4.6 and schematic drawings of the setups are shown in Figure 4.10.

Table 4.6

Components in all of the setups

Setup	1	2	3	4	5	6	7	8	9
Phase-change material (PCM)	+	+	+	+	+	+	+	+	+
PCM glass container	+	+	+	+	+	+	+	+	+
Glass	+	+	+	+	+	+	+	+	+
Plastic box	+	+	+	+	+	+	+	+	+
Hinges		+		+		+		+	+
Aerogel 1 (1006,69 cm^3)	+	+							
Aerogel 1 (768,47 cm^3)					+	+	+	+	
Aerogel 1 (763,62 cm^3)			+	+					
Aerogel 2 (683,80 cm^3)									+
Aerogel 3		+		+		+		+	+
Cone (diameter 1,5 cm)			+	+					
Cone (diameter 2,4 cm)					+	+			
Cone (diameter 4 cm)									+
Fresnel lens			+	+	+	+			+
Blades with reflector and aerogel filling		+		+		+		+	+

The aerogel filling for Setups 1 and 2 was selected according to the focal length requirements determined for Setups 3-6, while Setups 7 and 8 used aerogel volumes equivalent to those in Setups 3 and 4. To enhance heat transmission to the PCM, the cone diameter was increased from 1.5 cm to 2.4 cm in Setups 5 and 6.

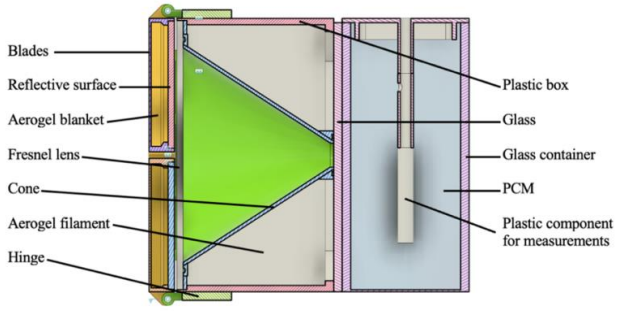

Fig. 4.11. Cross-section of a solar facade module with dynamic component.

Figure 4.11 presents a cross-section of the solar facade module with the dynamic component. The module is composed of three main subsystems:

1) the dynamic component (rotating blades with hinges);
2) the heat-transfer assembly (Fresnel lens, cone and plastic enclosure);
3) the thermal storage unit (PCM container).

The plastic measurement box ensures accurate placement of thermocouples to measure PCM temperatures at different points within the container. The PCM glass container was fabricated from five layers of 4 mm glass bonded with silicone sealant. This sealed glass unit encloses the aerogel layer in the heat-transfer assembly and enables easy repositioning of components across setups.

The plastic box, hinges and rotating blades were manufactured using an Original Prusa I3 MK3S+ 3D printer. Material selection was based on the expected thermal and mechanical loads. PETG was used for the hinges and plastic box due to its high impact strength, durability and service temperature range of 51–64 °C - suitable because these components are not directly exposed to concentrated solar radiation. The blades and cones were printed using ASA, which provides high thermal resistance (up to 105 °C) and dimensional stability under elevated temperatures. The cone, glass pane and Fresnel lens were fixed using transparent adhesive.

The blade interior incorporates a stepped shelf geometry that supports the aerogel blanket on one side while creating space for the reflective surface on the other. PMMA mirror material was selected as the reflective element due to its durability, low weight and optical properties; its density is roughly half that of glass and it can be easily cut into triangular sections to match the blade geometry. The aerogel blanket (thermal wrap) was used as the filling due to its excellent insulation performance, with an operating temperature range from –200 °C to +125 °C and thermal conductivity of approximately 23 $mW \cdot m^{-1} \cdot K^{-1}$ at room temperature.

To reduce heat losses during periods when the ambient temperature is lower than the PCM temperature, rubber sealing was added around the dynamic component's air gaps, ensuring improved airtightness and insulation performance.

4.2.2. Experiment plan (E4 – DYN-LAB ON/OFF)

The primary objective of the component-level laboratory testing is to identify the most efficient and suitable solar facade module configuration for subsequent outdoor experimentation, with specific emphasis on PCM temperature evolution and heat-flow performance. This experiment was designed as a comparative study, enabling direct evaluation of the thermal behaviour of multiple module setups under identical and strictly controlled indoor conditions. All configurations were subjected to the same heating and cooling cycles to ensure comparability and eliminate boundary-condition bias. A detailed overview of the experimental conditions applied in this stage is provided in Table 4.7.

Table 4.7

Conditions of the experiment

Condition	Value
Heating	7 hours
Cooling	17 hours
Irradiance	1000 W/m^2
Temperature of PCM	16 °C
Cooling temperature	2 °C
Cooling humidity	30 %

The total duration of each test was 24 hours. The 7-hour heating phase was selected to represent typical spring and autumn conditions in a temperate climate, during which average daily solar irradiance can reach approximately 1000 W/m². The initial PCM temperature was set to 16 °C to ensure that the material remained fully solid prior to the onset of heating, as its melting process begins at approximately 20 °C. During the cooling phase, the temperature was reduced to 2 °C to simulate night-time outdoor conditions.

Artificial irradiance during the heating phase was supplied by a halogen lamp, with the intensity manually adjusted using a dimmer to maintain the desired irradiance level. During the cooling phase, the test module was placed inside an environmental test chamber, where the required temperature and humidity were controlled. Before each experiment, the PCM component was pre-cooled to 16 °C to ensure a consistent solid-state starting condition for all tests.

In configurations equipped with the dynamic component (Setups 2, 4, 6, 8 and 9), the reflective blades were positioned to focus incident light toward the centre of the module during the heating phase. During the cooling phase, the blades were closed and secured with screws at the hinge points to minimise heat losses to the surroundings.

During the tests, all measurements were recorded using a data logger equipped with a multiplexer to accommodate the large number of sensors. A pyranometer was used to monitor the incident solar irradiance, while thermocouples were employed to measure the temperature distribution within the PCM. Heat-flux sensors were installed to capture both heat-flow rates and corresponding surface temperatures.

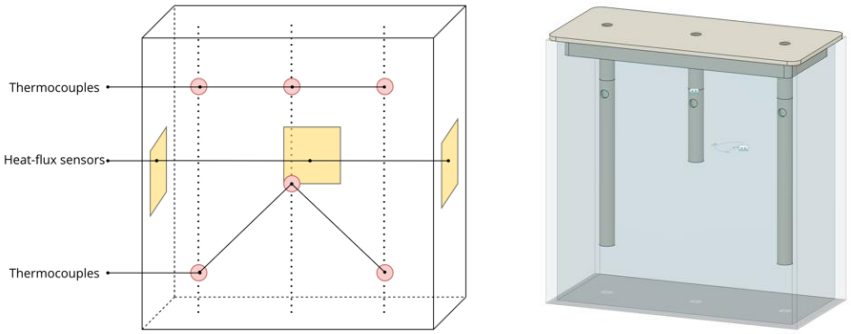

Fig. 4.12. Location of measuring sensors in PCM container.

Temperature measurements within the PCM were taken at six locations to characterise the vertical and horizontal temperature gradients during both charging and discharging (Fig. 4.12). Additional measurements included ambient room temperature, outdoor (chamber) temperature and the temperature inside the cones for the relevant setups. Heat-flux measurements for the cooling cycle were obtained by mounting a heat-flux sensor either on the Fresnel lens or on the PMMA glazing, depending on the configuration being tested.

4.2.3. Laboratory testing results (E4 – DYN-LAB ON/OFF)

To determine which solar facade module configuration offers the highest efficiency in terms of solar energy absorption and thermal conservation, a total of nine setups (see Table 4.6) were experimentally evaluated under controlled laboratory conditions.

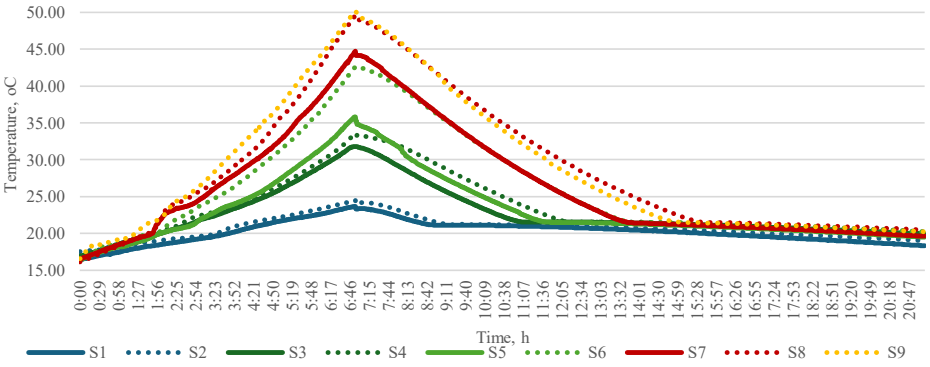

Fig. 4.13. Average temperature comparison in PCM between setups.

Figure 4.13 presents the comparison of average PCM temperatures across all nine experimental configurations. The first series of tests was carried out using Setups 1 and 2, where the aerogel layer thickness was matched to the focal length of the Fresnel lens. The temperature measurements showed that, in both configurations, full phase change occurred only in the upper PCM layer, while the lower layer did not reach temperatures high enough for complete melting. In Setup 2, reflective blades were added to enhance solar concentration on the module; however, the thermal behaviour remained largely similar to Setup 1, with no full melting across all PCM layers. The peak average PCM temperature in Setup 2 was only 1 °C higher than in Setup 1.

To accelerate heat transfer to the PCM during the charging phase, a cone and Fresnel lens were introduced in Setups 3 and 4. A thermocouple was placed inside the cone to monitor the air-gap temperature between the lens and PCM container. The recorded cone temperatures were 69 °C in Setup 3 and 75.6 °C in Setup 4, with Setup 4 yielding approximately 1.5 °C higher peak PCM temperatures than Setup 3. Temperature measurements confirmed that complete melting of all PCM layers was achieved in both Setups 3 and 4. Due to the higher temperatures reached in Setup 4, the heat-release (solidification) period was noticeably longer. Overall, Setup 4 demonstrated the strongest performance among the first four configurations, delivering higher PCM temperatures and an extended solidification period.

Despite full melting, the maximum temperature in the lower PCM layers in Setups 3 and 4 did not exceed 28.5 °C. Meanwhile, the high cone temperatures recorded in both setups indicated unused potential for transferring additional heat into the PCM. To improve heat delivery, the cone diameter at the PCM container was increased from 1.5 cm to 2.4 cm in Setups 5 and 6. The temperature profiles show that phase change in the lower PCM layers occurred

significantly faster - approximately at 5:30 h - in Setup 6 compared to prior setups. Peak PCM temperatures increased to 40.6 °C in Setup 5 and 46.4 °C in Setup 6, demonstrating the benefits of the enlarged cone geometry.

In Setups 1 and 2, incomplete melting in the lower PCM layers was likely caused by excessive aerogel thickness. Therefore, in Setups 7 and 8, the aerogel layer was reduced by the volume corresponding to the cone dimensions used in Setups 5 and 6. This modification had a dramatic effect on performance: peak average PCM temperature rose from 23.7 °C in Setup 1 to 49.5 °C in Setup 8. In Setup 8, the onset of melting in the lower PCM layers occurred at approximately 4:40 h and the solidification period became the longest among all previous configurations. Significant differences were also observed between Setups 7 and 8, demonstrating the strong positive contribution of adding reflective blades.

Comparing Setup 6 and Setup 8 further highlights the influence of system components. Setup 6, which incorporated the cone, underperformed Setup 8 in both maximum average PCM temperature (42.6 °C versus 49.5 °C) and solidification duration (7 h versus 8.5 h). Nonetheless, the extremely high temperatures achieved inside the cone - reaching up to 79 °C - suggest considerable potential for transferring additional thermal energy into the PCM.

Taking into account all the observations described above, Setup 9 was developed. This configuration combined an increased cone diameter of 4 cm with a new aerogel material (Aerogel 3) offering superior thermal properties. The intention behind Setup 9 was to maximize both heat gain and thermal storage, building upon the strengths identified in earlier configurations.

Using the technical specifications provided by the PCM manufacturer, it was possible to calculate the amount of thermal energy stored and released by the material throughout the complete testing cycle. The calculations followed the standard equations for sensible (Eq. 4.1) and latent (Eq. 4.2) heat storage during heating, phase transition and cooling:

$$Q_{sensible} = m \times c \times \Delta T \tag{4.1}$$

where m – mass, kg;

c – specific heat capacity, $J \times kg^{-1} \times K^{-1}$;

ΔT – change of temperature, ^{o}C.

$$Q_{latent} = m \times L \tag{4.2}$$

where L – specific latent heat, $kJ \times kg^{-1}$.

The PCM mass was measured prior to all experiments and remained constant across all setups at 0.521 kg. The specific heat capacity of the material is 2 $kJ \cdot kg^{-1} \cdot K^{-1}$. Partial enthalpy distribution data, required for calculating latent heat contribution during melting and solidification, were obtained from the material datasheet. Table 4.8 summarises the corresponding latent heat values between 13 °C and 28 °C, representing the active enthalpy range relevant to the performed experiments.

Table 4.8

Stored and released energy in partial PCM enthalpy [178]

Temperature, °C	l melting, kJ/kg	l solidification, kJ/kg	Q melting, kJ	Q solidification, kJ
13	6	5	12	10
14	5	5	10	10
15	5	6	10	12
16	8	7	16	14
17	7	10	14	20
18	10	13	20	26
19	15	24	30	48
20	26	47	52	94
21	42	58	84	116
22	40	3	80	6
23	24	2	48	4
24	2	3	4	6
25	2	3	4	6
26	2	3	4	6
27	3	3	6	6
28	2	3	4	6

Figure 4.14 presents the calculated stored and released thermal energy for each experimental configuration. The results clearly show progressive optimisation of energy performance across the setups: stored energy increases consistently, while released energy (during night-time cooling) is reduced as the component design improves. This demonstrates the effectiveness of systematic adjustments to the optical elements, insulation layers and heat-transfer pathways.

The primary aim of the laboratory testing was to identify the most efficient facade module configuration for subsequent outdoor evaluation. When comparing Setups 8 and 9, their overall energy balance appears nearly identical. However, Setup 9 exhibits superior adaptability under variable environmental conditions - an essential requirement for real outdoor applications. For this reason, Setup 9 was selected as the final configuration for further experimental investigation.

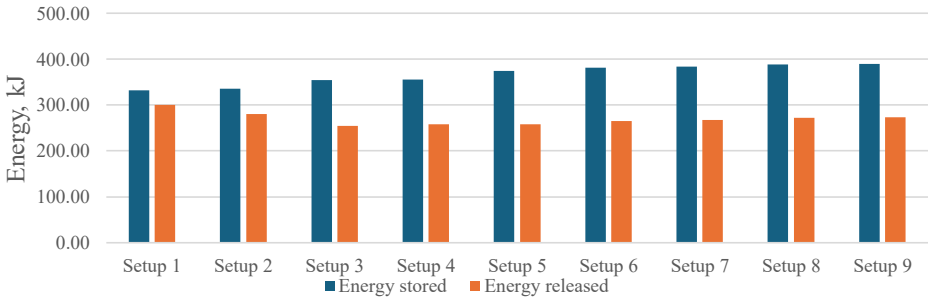

Fig. 4.14. Comparison of stored and released heat energy in PCM between different setups.

4.2.4. Design of the control system for dynamic component

The primary function of the dynamic component is to concentrate incident solar radiation onto the facade module, which is installed on the south-facing side of the building to maximise solar exposure. Using reflective blades, sunlight is directed through the transparent aerogel layer and the Fresnel lens, focusing the rays onto the PCM element where the thermal energy is stored. This stored energy can later be released indoors, contributing to space heating.

The operating principle of the dynamic system is straightforward: four reflective blades track the solar position during the day and continuously redirect sunlight onto the centre of the lens. When solar radiation decreases below a defined threshold - such as during sunset or overcast conditions - the blades return to their closed position to insulate the module and minimise heat losses from the PCM. The blades reopen automatically once sufficient irradiance is detected. Two operational constraints must be observed:

1) The blades must not open when solar irradiance is below the predetermined minimum value;
2) The blades must remain closed during night-time.

Based on these functional requirements, a control algorithm for the dynamic component was developed. The operational principle is illustrated in Figure 4.15.

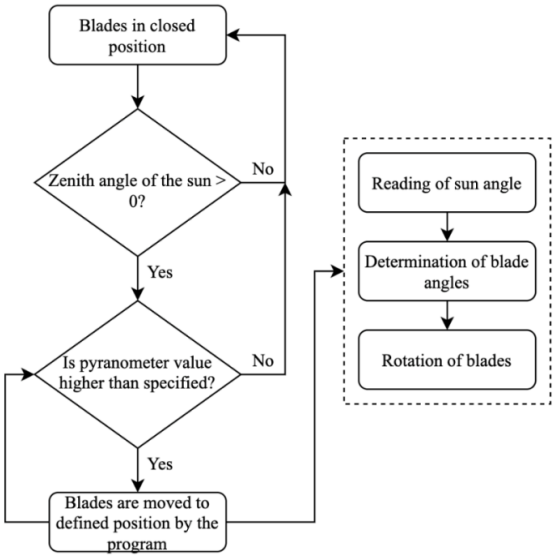

Fig. 4.15. The control algorithm principle for the dynamic component

4.2.5. Calculations for blade positioning

The rotation angles of the reflective blades can be calculated directly from the solar position angles - solar zenith (or altitude) and azimuth. These angles can be determined for any location and time of year using standard solar-position algorithms [179]. Once the sun angles are known, the blade orientation can be derived using basic trigonometric principles.

Figure 4.16 illustrates the operational concept: the blades redirect incoming solar rays toward the focal point of the facade module following the law of reflection, which states that "the angle of incidence equals the angle of reflection" [180].

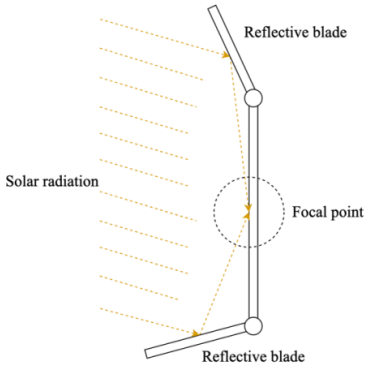

Fig. 4.16. Principle of the solar radiation reflection into facade module.

For control purposes, the four blades can be categorised according to the planes describing the sun's movement:

- the upper and lower blades compensate for solar altitude (zenith plane);
- the eastern and western blades respond primarily to solar azimuth.

The solar altitude angle varies between 0° and 90° depending on geographical location, while the relevant azimuth angle for a south-facing facade spans approximately 90° to 270°. All blades are defined with a rotation range from 0° (fully closed) to 180° (fully open). Based on these principles, blade motion can be expressed using geometric relationships. The complete cycle can be divided into three characteristic cases:

- case (a): lower and eastern blades operate within 90-180° (Fig. 4.17 a);
- case (b): upper and western blades operate within 90-180° (Fig. 4.17 b);
- case (c): all blades operate within 0-90° (Fig. 4.17 c).

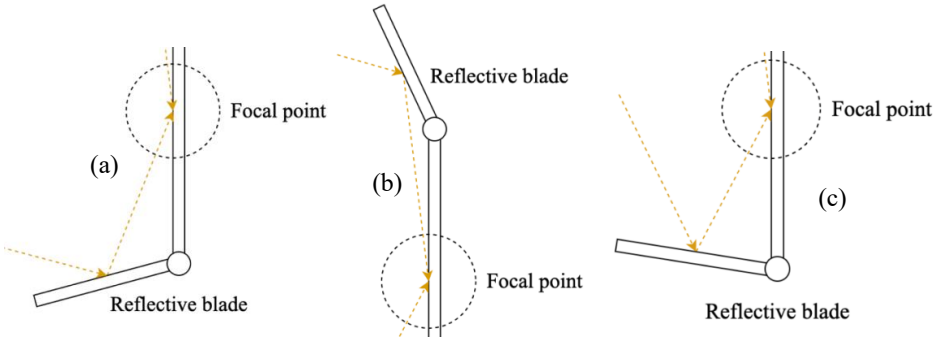

Fig. 4.17. Three different situations of blade position.

Case (a): If triangle geometry is used to describe case (a) - with γ representing the blade angle and α the solar angle (α + δ = 90°) - two sides of the triangle can be set to *a* and *2a* (Fig. 4.18). In triangle a_1–b_1–a, the sides a_1 and b_1 are equal due to the law of reflection. Therefore:

$$\beta = \alpha + \gamma \text{ and } \theta = 180^o - \alpha - \gamma \quad (4.3)$$

For triangle b-b1-2a:

$$\delta = 90 - \alpha,\ \zeta = 180 - (180 - \alpha - \gamma) = \alpha + \gamma \text{ and } \varepsilon = 180 - (90 - \alpha + \alpha + \gamma) = 90 - \gamma \quad (4.4)$$

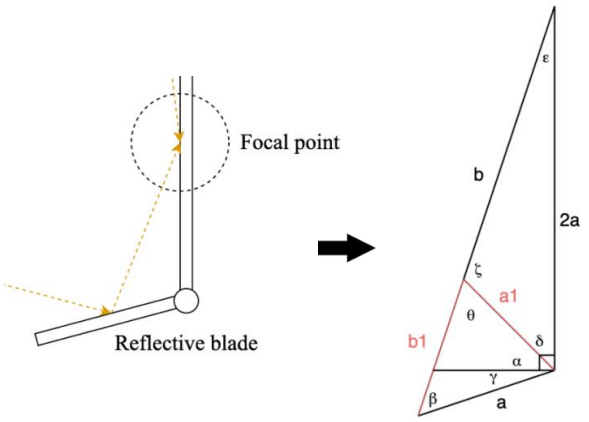

Fig. 4.18. Trigonometric representation of Case (a).

Applying the sine law to triangle b–b_1–2a:

$$b1 / \sin(90 - \gamma) = 2a / \sin(\alpha + \gamma) \quad | \quad \sin(90-\gamma) = \cos(\gamma)$$

$$b1 = 2a \times \cos(\gamma) / \sin(\alpha + \gamma) \quad (4.5)$$

Applying the sine law to triangle a–a_1–b_1:

$$b1 / \sin(\alpha + \gamma) = a / \sin(180 - 2\alpha - 2\gamma) \quad | \quad \sin(180 - 2(\alpha + \gamma)) = - \sin2(\alpha + \gamma)$$

$$b1 = a \times \sin(\alpha + \gamma) / \sin2(\alpha + \gamma) =$$

$$a \times \sin(\alpha + \gamma) / 2 \times \sin(\alpha + \gamma) \times \cos(\alpha + \gamma) = a / \cos(\alpha + \gamma) \quad (4.6)$$

Equating the two expressions for b_1:

$$2a \times \cos(\gamma) / \sin(\alpha + \gamma) = a / \cos(\alpha + \gamma) \quad | \quad /a$$

$$2\cos(\gamma) = \sin(\alpha + \gamma) / \cos(\alpha + \gamma)$$

$$2\cos(\gamma) = \tan(\alpha + \gamma) \quad (4.7)$$

$$\gamma = \arccos(\tan(\alpha + \gamma) / 2)$$

The resulting equation contains two variables, γ and α and can be solved numerically. For the lower blade, the solar angle equals α and the blade angle is γ + 90°. For the western blade, the solar angle becomes α − 180° and the blade angle remains γ + 90°.

Case (b) follows similar logic, with modified angular relationships. (Fig. 4.19).

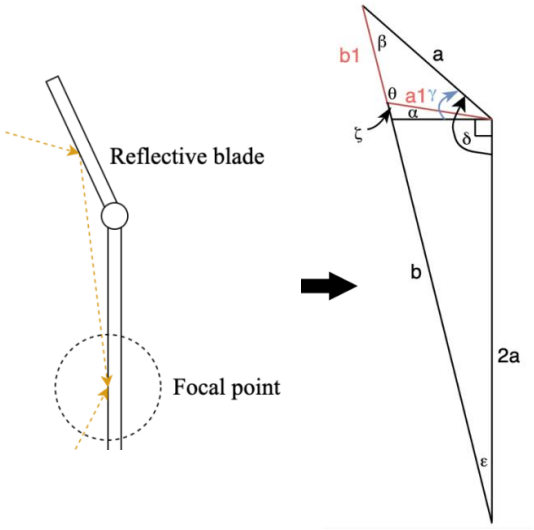

Fig. 4.19. The corresponding trigonometric representation of case (b).

In triangle a-a1-b1:

$$\beta = \gamma - \alpha \text{ and } \theta = 180o + 2\alpha - 2\gamma \tag{4.8}$$

And in triangle a-2a-b-b1:

$$\delta = 90^o + \gamma \text{ and } \varepsilon = 180^o - (\gamma - \alpha) - (90^o + \gamma) = 90^o - \gamma + \alpha - \gamma = 90^o - 2\gamma + \alpha \tag{4.9}$$

Applying the sine law:

$$\begin{aligned} a / \sin(90^o - 2\gamma + \alpha) &= 2a / \sin(\gamma - \alpha) \mid \quad :a \\ \sin(\gamma - \alpha) &= 2 \times \sin(90^o - 2\gamma + \alpha) \mid \quad \sin(90^o - x) = \cos x \\ \sin(\gamma - \alpha) &= 2 \times \cos(2\gamma - \alpha) \\ \gamma &= \arcsin(2 \times \cos(2\gamma - \alpha)) + \alpha \end{aligned} \tag{4.10}$$

This equation again depends on γ and α and is solved numerically.

The trigonometric representation of Case (c) is shown in Figure 4.20. In triangle b1-a1-c:

$$\lambda = \mu = \alpha - \gamma \text{ and } \theta = 180o - (2\alpha - 2\gamma) = 180o - 2\alpha + 2\gamma \tag{4.11}$$

In triangle a1-b-2a:

$$\begin{aligned} \zeta &= 180^o - (180^o - 2\alpha + 2\gamma) = 2\alpha - 2\gamma \; ; \; \delta = 90^o - \alpha \\ \varepsilon &= 180^o - (90^o - \alpha) - (2\alpha - 2\gamma) = 90^o - \alpha + 2\gamma \end{aligned} \tag{4.12}$$

In triangle a-c-c1:

$$\eta = 180^o - (\alpha - \gamma) = 180^o - \alpha + \gamma \text{ and } \beta = 180^o - (180^o - \alpha + \gamma) - \gamma = \alpha - 2\gamma \tag{4.13}$$

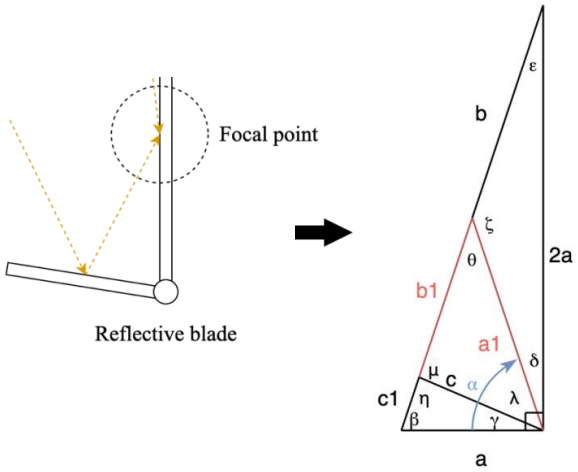

Fig. 4.20. Blade angle interpretation in case (c).

Applying the sine law in triangle 2a-b-b1-c:

$$a / \sin(90^o - \alpha + 2\gamma) = 2a / \sin(\alpha - \gamma) \quad | \ :a$$
$$\sin(\alpha - \gamma) = 2 \times \sin(90^o - \alpha + 2\gamma) \quad | \ \sin(90^o - x) = \cos x \qquad (4.14)$$
$$\sin(\alpha - \gamma) = 2 \times \cos(\alpha - 2\gamma)$$
$$\gamma = \alpha - \arcsin(2 \times \cos(\alpha - 2\gamma))$$

Blade-angle interpretation for Case (c):

- lower blade: sun angle = α, blade angle = 90° − γ.
- upper blade: sun angle = 90° − α, blade angle = 90° − γ.
- eastern blade: sun angle = α − 180°, blade angle = 90° − γ.
- western blade: blade angle = α − 180°.

For each date and location used in the experimental study, all blade angles were computed numerically using the *Microsoft Excel Solver*, integrating the derived trigonometric equations into the solver routine to obtain γ for each solar position.

4.2.6. Development of the control system for outdoor testing

For the outdoor experiment, a dynamic component equipped with a control system was implemented to orient the blades according to the calculated solar angles. Blade movement was achieved using four motors - one for each blade - allowing precise tracking throughout the day. A dedicated program code was developed to execute the control algorithm described in Figure 4.15, ensuring that each blade adjusted its position in real time based on solar altitude and azimuth. The mechanical components required for the dynamic control system are summarised in Table 4.9.

Table 4.9

Mechanical components for the dynamic control

Component	Characteristics
Servo motor SG90 × 4	Voltage: 4,8 – 6 V
Arduino Mega microcontroller	Operating voltage: 5V Flash memory: 128 KB
Operational amplifier	
3D printed protection box × 4	Material: PETG
Rotational axes × 4	Material: Steel

The control code is structured around four data arrays that store the predefined blade angles for each 6-minute interval, along with the corresponding solar irradiance values measured by the pyranometer. Because the pyranometer outputs voltage signals, a conversion algorithm was implemented to translate these voltage readings into irradiance values expressed in W/m². An "IF" conditional routine then evaluates whether the measured solar irradiance exceeds the specified threshold. When this condition is met, a signal is sent to the motors to position the blades at the calculated angles; otherwise, all blades return to their default closed position. To prevent mechanical interference during closing, a short delay is introduced between the movement of the upper and lower blades. At each time step, the processed irradiance value is stored in the designated array for later analysis.

Servo SG90 motors were selected due to their simple control interface, rapid response and inherent positional feedback. Mechanical wedges were added to reinforce the blade hinge axes, ensuring stable operation during rotation. To protect the microcontroller from electrical disturbances, a noise-filtering circuit consisting of two capacitors was integrated into the power supply to mitigate voltage spikes.

4.2.7. Outdoor testing (E5 – DYN-LAB ON/OFF)

For the outdoor experiment, the highest-performing solar facade module identified during the laboratory experiments was examined in a comparative study to evaluate the effectiveness of the dynamic component under real climatic conditions. A 24-hour outdoor test was conducted using a fully operational small-scale solar facade module incorporating the dynamic element. The design was based on the best-performing indoor configuration (Setup 9).

Two test stands were constructed for this purpose - Setup 10, which included the dynamic component (rotating blades) and Setup 11, which excluded it. Both setups were installed on the roof of Riga Technical University and oriented towards the south to ensure optimal exposure to solar radiation. A photograph of the test stands is presented in Figure 4.21. The tests were performed on 12 May, under predominantly sunny weather conditions.

Fig. 4.21. Outdoor testing stands. Setup 10 to the right and Setup 11 to the left.

The recorded results are presented in Figures 4.22 and 4.23.

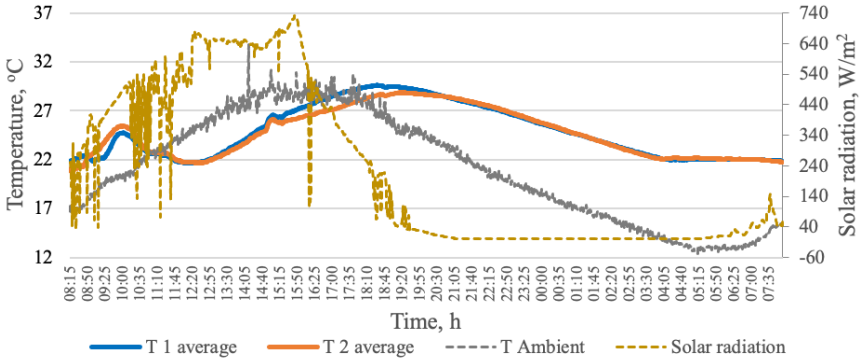

Fig. 4.22. Solar irradiance, ambient and average PCM temperatures is Setups 10 (blue line) and 11 (orange line).

During the experiment, solar irradiance fluctuated throughout the day, reaching a peak of approximately 700 W/m². Ambient air temperature was relatively high for the season, ranging between 20 °C and 30 °C. The PCM temperatures in both setups followed a similar trend overall, but notable differences emerged at specific times. The most pronounced temperature deviations occurred between 14:00 and 19:00, where the cone temperature in Setup 10 exceeded that in Setup 11 by up to 4 °C, while surface temperature differences reached approximately 1 °C at peak moments.

In the morning hours (09:00-11:00), Setup 11 showed slightly higher PCM temperatures; however, in the late afternoon and evening - when the solar azimuth angle shifted toward the west - the advantage of the dynamic component became evident. From approximately 15:00 until 20:00, Setup 10 consistently outperformed Setup 11 in terms of heat absorption. During the discharging phase, the average PCM temperatures of both setups converged again as the stored heat gradually dissipated.

A comparison of PCM surface temperatures further confirms that Setup 10, equipped with rotating blades, delivered superior performance for most of the testing period. The cone

temperatures were also consistently higher in Setup 10, attributable to two mechanisms: (1) the ability of the reflective blades to direct solar radiation into the lens during the day and (2) the additional insulating effect of the cone during nighttime cooling. As shown in Figure 4.23, the heat flux profiles of Setup 10 exhibit fewer sharp peaks and a smoother trend, indicating more stable and sustained heat transfer into the PCM. This suggests that the dynamic component enhances the efficiency of solar energy capture by moderating fluctuations and improving the overall thermal response of the module.

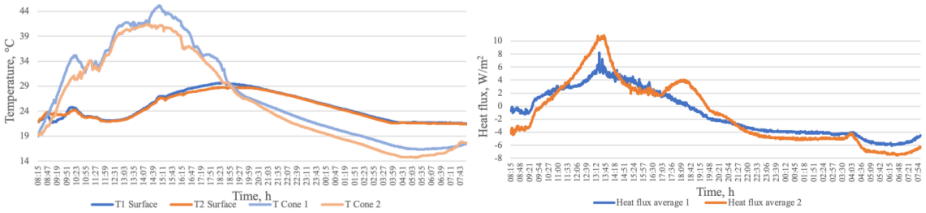

Fig. 4.23. Average PCM surface and cone temperatures (left) and heat fluxes (right) in Setups 10 (blue) and 11 (orange).

4.2.8. Conclusions and insights (E4 – DYN-LAB ON/OFF and E5 – DYN-LAB ON/OFF)

The combined results of the laboratory investigation (E4) and the outdoor testing (E5) demonstrate a consistent and measurable advantage of the dynamic component - comprising reflective blades with an aerogel-filled structure - within the proposed solar facade module. Under controlled laboratory conditions, the dynamic component significantly enhanced thermal energy absorption during the PCM charging phase and improved heat retention in the discharging phase. This improvement was especially evident in setups where the cone, aerogel layer and adjustable insulation were optimised to facilitate heat transfer from the Fresnel lens to the PCM.

Introducing the Fresnel lens further increased the concentration and intensity of solar gains, producing a more dynamic thermal response in the PCM. The combined action of the reflective blades and the Fresnel lens reduced thermal losses, accelerated PCM melting in upper and lower layers and extended the duration of effective thermal discharge. The laboratory results confirm that both geometrical configuration and component interaction play a crucial role in determining the overall thermal efficiency of the solar facade module.

Outdoor experiments reinforced these findings under real climatic conditions. Even with fluctuating solar irradiance, variable solar angles and intermittent cloud cover, the facade module equipped with the dynamic component (Setup 10) outperformed the static version (Setup 11). The dynamic configuration achieved higher PCM temperatures, smoother heat-flux profiles and more effective heat storage during late-day conditions when the sun's azimuth angle shifted westward - highlighting the operational benefit of blade actuation. The improved performance during the discharging period further confirmed that strategic concentration and insulation elements reduce the rate of heat loss and extend the usable storage period.

Together, the results of E4 and E5 demonstrate that the performance of the facade module is highly sensitive to how effectively the optical and thermal components - reflective blades, cone, aerogel insulation and Fresnel lens - work together to direct and retain solar energy. While the positive influence of the Fresnel lens was clearly observed, the experiments also indicated that its effectiveness depends strongly on the precise location of the focal point relative to the aerogel layer, cone geometry and PCM container. These insights provided the foundation for the next stage of development - Experiment E6 - in which the focal point position of the Fresnel lens is systematically evaluated.

4.3. Effect of focal point distance and cone diameter on heat transfer within the small-scale facade module (E6 – FP-LAB 3/5/7)

The final component-level laboratory experiment, conducted to complete the development of the small-scale module intended for integration into a full-scale facade system, focused on determining the optimal focal-point position and cone diameter. The custom-designed small-scale solar facade module constructed for this purpose comprises several key elements (see Fig. 4.24): a dynamic component with movable reflective blades filled with aerogel insulation; a Fresnel lens; a concentrating cone; a semi-transparent aerogel insulation layer; a PCM container; and a transparent glass shell enclosing the aerogel layer.

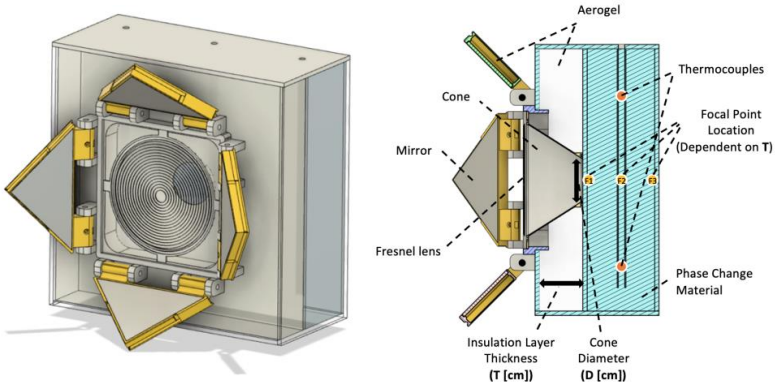

Fig. 4.24. Design of the small-scale solar facade module and its cross-section.

Within this assembly, the dynamic component plays a critical role by governing the amount of solar radiation concentrated onto the facade module. The Fresnel lens serves as an energy-enhancement element, intensifying irradiance delivered to the PCM storage. Findings from the previous experiment (E4) demonstrated that both the aerogel-layer thickness and cone diameter exert a direct influence on PCM temperature evolution. These parameters control the heat-transfer pathway between the indoor and outdoor environments: the cone diameter defines the air-gap volume between the Fresnel lens and the PCM container, whereas the aerogel insulation layer determines the focal-point position of the Fresnel lens and provides thermal protection around the cone.

Based on these considerations, dedicated experimental stands were developed to systematically examine how cone diameter and focal-point location affect heat transfer within the small-scale solar facade module.

4.3.1. Experimental design (E6 – FP-LAB 3/5/7)

For the experimental stands, the small-scale solar facade modules were enclosed within an extruded polystyrene (XPS) insulation layer and a plywood casing to minimise thermal losses and ensure stable storage conditions for the accumulated heat (see Fig. 4.25).

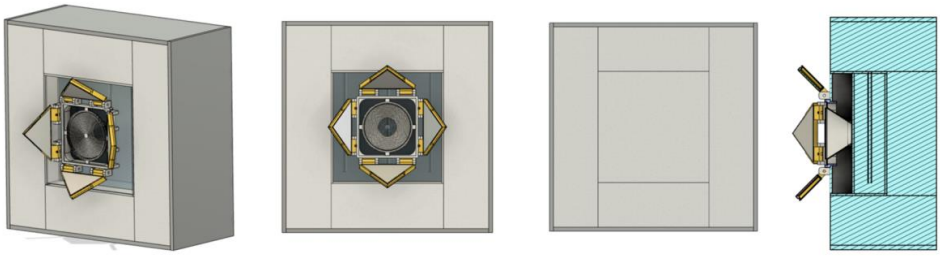

Fig. 4.25. Experimental stand of small-scale solar facade module.

The material characteristics of the components used in the test stands are summarised in Table 4.10.

Table 4.10

Components of the small-scale solar facade module

Component	**Charesteristics**
PCM RT21HC	See Table 2.6
PCM glass container	Dimensions: 242 × 242 × 62 mm Thickness: 4 mm
Plywood	Thickness: 9 mm λ = 0.13 W/mK
XPS	100 mm λ = 0.037 W/mK

Temperature evolution inside the PCM container was recorded using five thermocouples placed at predefined locations (Fig. 4.26.b). The labels L, M and R denote positions along the x-axis (left, middle, right), while the numbers 1 and 2 correspond to lower and upper positions along the y-axis.

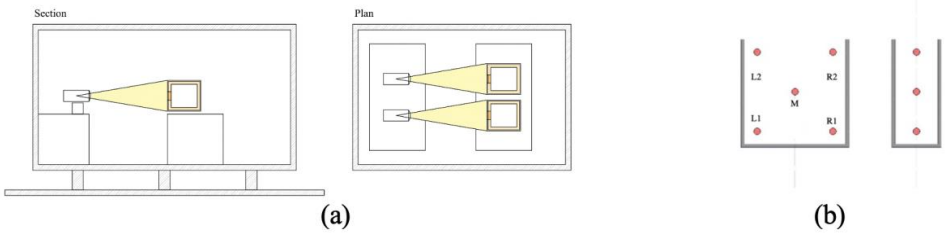

Fig. 4.26. Experimental setup in the climate chamber (a) and temperature measurement spots inside the PCM container (b).

4.3.2. Experiment plan (E6 – FP-LAB 3/5/7)

A total of nine experimental stands were tested under controlled indoor conditions. Each stand differed in two key parameters: the location of the Fresnel lens focal point and the diameter of the cone. Three focal-point positions were defined, corresponding to the inner surface of the PCM container, the outer surface and the mid-plane of the PCM layer. Cone diameters were varied between 2 and 4 cm. The combinations of these parameters used in the nine test setups are shown in Table 4.11.

Table 4.11

Variations of the Experimental Settings in Test Setups

Insulation layer thickness **T [cm]** / Cone diameter **D [cm]**	3	5	7
2	Setup F1 D2	Setup F2 D2	Setup F3 D2
3	Setup F1 D3	Setup F2 D3	Setup F3 D3
4	Setup F1 D4	Setup F2 D4	Setup F3 D4

All test stands were examined in the climate chamber under identical boundary conditions. Two setups were tested simultaneously using two halogen lamps to simulate solar irradiance. The experimental variations - cone diameters of 2, 3 and 4 cm (D2, D3, D4) and focal-point locations F1, F2 and F3 (see Fig. 4.24) - enabled systematic evaluation of the effects on solar heat transfer into the PCM.

The operating conditions for all experimental setups are summarised in Table 4.12. Autumn and spring climatic conditions offer the greatest potential for the proposed solar facade system to reduce energy demand for supplementary heating provided by conventional fuel-based systems. In the northern European climate zone, these two seasons exhibit similar average temperatures and comparable levels of solar radiation. Accordingly, parameters such as solar irradiance, ambient temperature and daylight duration were defined to reflect a typical autumn/spring day in Riga (Latvia). These values were determined through an analysis of long-term meteorological data obtained from the local weather station (see Fig. 4.27).

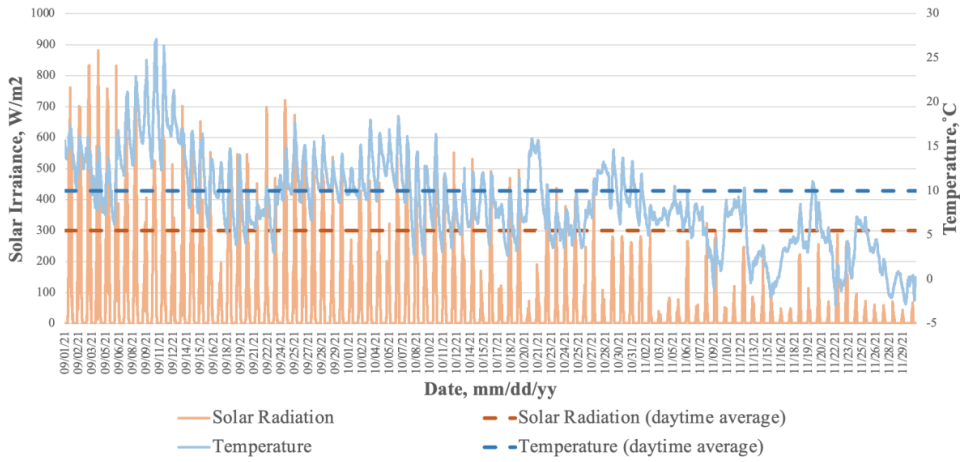

Fig. 4.27. Data from metrological station of the Riga Technical University from September to December 2021.

The experiments were performed by exposing the test module to simulated solar radiation for a duration of 8 hours, followed by an 8-hour cooling period at an ambient temperature of 10 °C. During the simulated daylight period, the blades of the dynamic component were positioned such that the light from the lamps was concentrated precisely on the centre of the Fresnel lens. During the night-time cooling phase, the blades were placed in the closed position, ensuring that the accumulated heat remained insulated within the PCM container.

Table 4.12

Conditions of the Test Setups

Condition	Value
Daylight duration (solar simulation is active)	8 h
Night-time period (solar simulation is inactive)	8 h
Irradiance (solar simulator) intensity	300 W/m^2
Outdoor (ambient) temperature	10 °C

4.3.3. Laboratory testing results (E6 – FP-LAB 3/5/7)

To complete the development of the small-scale facade module, the final component-level laboratory experiment (E6) was carried out to evaluate the effect of the Fresnel lens focal point location. The experiment was performed according to the setups listed in Table 4.11 and under the conditions specified in Table 4.12.

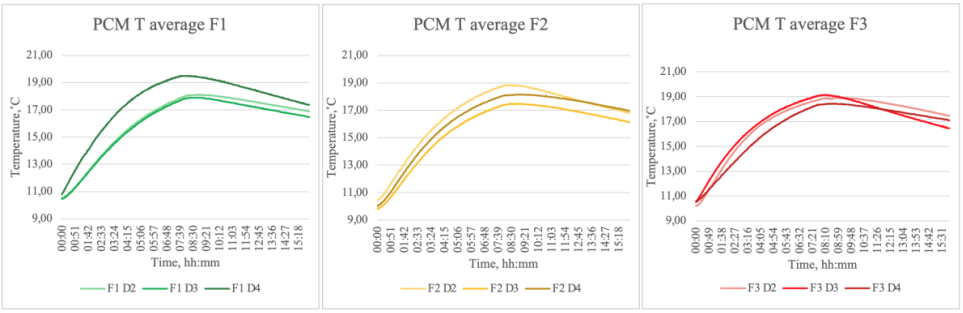

(a) (b) (c)

Fig. 4.28. Average PCM temperatures in all setups grouped by focal point location: (a) F1, (b) F2, (c) F3.

Nine test rounds were conducted and the resulting average temperatures in the PCM container for all setups - grouped by focal point location and cone diameter - are presented in Figure 4.28 and Figure 4.29.

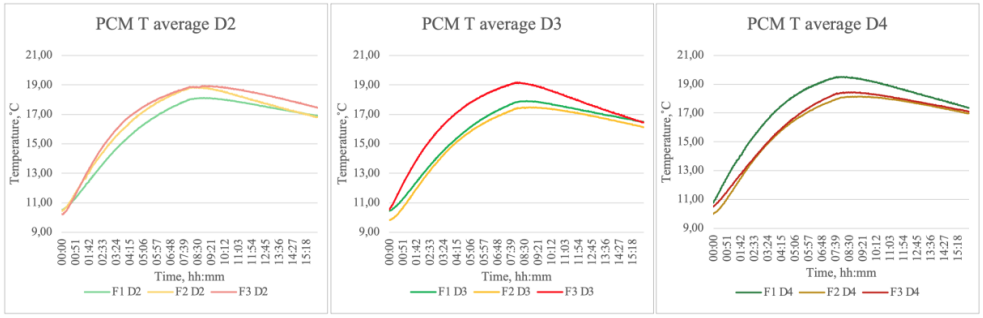

(a) (b) (c)

Fig. 4.29. Average PCM temperatures in all setups grouped by cone diameter: (a) D2, (b) D3, (c) D4.

In the setups with focal point location F1, the highest average PCM temperature is achieved with the widest cone diameter (D4). However, when the focal point is positioned deeper inside the PCM container, higher PCM temperatures are obtained with cone diameters D3 and D2. The graphs corresponding to setups F2 D2 and F3 D3 show a steeper night-time temperature decline than other setups with the same focal point location. A similar behaviour can be observed in the diagrams in Figure 4.29, where steeper night-time cooling appears as the cone diameter increases.

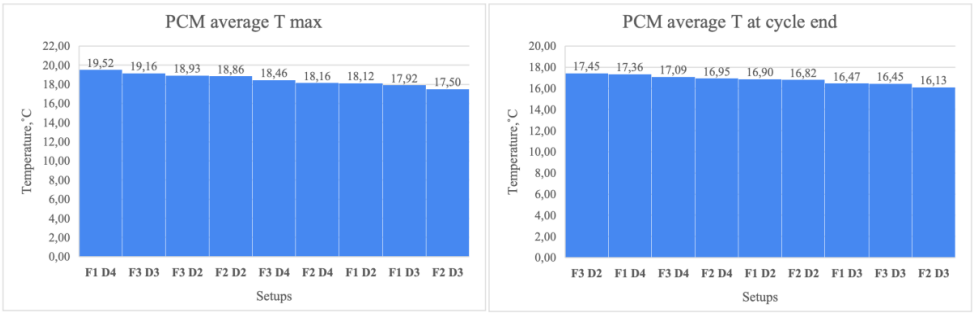

Fig. 4.30. Maximum (left) and end-of-cycle (right) average PCM temperatures.

Figure 4.30 shows that the highest maximum average PCM temperature is achieved in Setup F1 D4. However, by the end of the experimental cycle, this temperature drops below that of Setup F3 D2. In Setup F3 D3, the second-highest maximum PCM temperature is reached, yet by the end of the cycle the temperature decreases by almost 3 °C.

Figure 4.31 illustrates temperature development in different PCM layers measured by thermocouples. In Setup F1 D4, temperatures rise with similar gradients across all layers throughout the day. In contrast, in Setups F2 D3 and F3 D2, temperatures in different layers diverge more significantly. In all setups, the central layer (T_M) reaches the highest temperature at the end of the cycle. No consistent pattern is observed across other PCM layers: in some setups, a given layer reaches the highest temperature, while in others the same layer reaches the lowest during the daytime cycle.

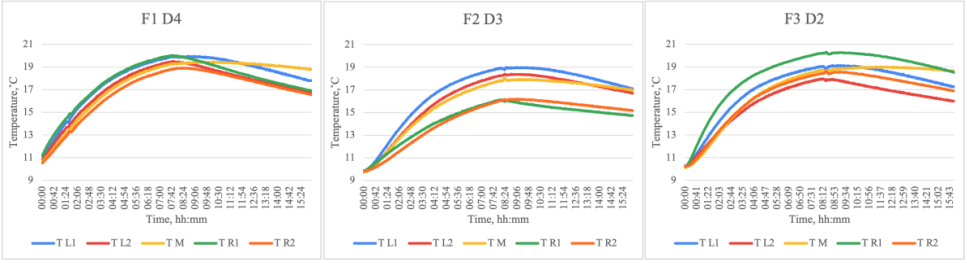

(a) (b) (c)

Fig. 4.31. Temperatures in PCM layers (L1, L2, M, R1, R2) in Setups (a) F1 D4, (b) F2 D3 and (c) F3 D2.

4.3.4. Conclusions and insights (E6 – FP-LAB 3/5/7)

The obtained PCM temperature results allow the following conclusions:

1. The highest daytime heat transfer is achieved in Setup F1 D4, where the maximum PCM temperature reaches 19.52 °C during the day-time cycle.

2. The highest end-of-cycle PCM temperature is observed in the setup with the narrowest cone diameter, differing by 7.5% from the lowest-performing setup. This indicates lowest night-time heat losses in Setup F3 D2.
3. By shifting the focal point deeper into the PCM container, effective heat transfer is achieved with narrower cone diameters. Comparing Setups F1 D4 and F3 D2, the difference in average PCM temperature is only about 3%.
4. Heat-transfer enhancement during the charging phase can be accomplished with a wide cone and a thin aerogel layer (F3); however, increased heat losses during the night-time cycle may reduce the overall benefit. For example, in Setup F3 D3, the second-highest daytime temperature (19.16 °C) drops to the second-lowest end-of-cycle value (16.45 °C).
5. Both focal point location and cone diameter significantly affect heat-transfer performance. Comparing Setups F1 D2 and F1 D4, the average PCM temperature increases by 7.2%. Similarly, comparing F3 D4 and F1 D4 yields a 5.4% increase.

The experiments indicate that Setup F1 D4 provides the best overall performance. However, when integrating the module into the dynamic solar envelope, the final focal point distance must also consider the aerogel insulation thickness, since this layer directly affects night-time heat losses. The obtained results show that wider cone diameters enhance heat transfer; therefore, for the developed solar facade, the most suitable configuration combines a 7 cm aerogel insulation layer with focal point location F1.

5. LARGE-SCALE OUTDOOR TESTING

In this chapter the evolution of the final methodological stage experimental testing have been presented and discussed. This stage of testing involves system-level outdoor comparative experiment of full-scale facade module in relevant climatic conditions. The main goal of this experiment is the evaluation of indoor thermal fluctuations and energy consumption across seasons to gain insights and conclusions about energy efficiency of proposed technological solution - dynamic solar envelope.

5.1. Development of a large-scale facade module

The concept for the large-scale solar facade module builds upon the configuration developed in the small-scale experiments by assembling nine small-scale units into a unified building-envelope component. For performance comparison, a triple-glazed window was selected as the reference technology. This choice aligns with the primary functional objectives of the proposed system such as light transmission and heat conservation.

Triple-glazed windows are widely implemented in contemporary building construction due to their high thermal-insulation performance and favourable solar-control characteristics. The additional glass pane significantly reduces conductive heat losses during cold periods and limits unwanted heat gains during summer conditions. The multilayer glazing structure also enhances solar-control performance by mitigating glare and limiting excessive solar penetration [181]. Furthermore, triple-glazed systems maintain excellent visible-light transmission, allowing substantial daylight to enter the indoor environment, thereby reducing reliance on artificial lighting and contributing to overall energy savings.

Thus, the selection of triple-glazing as the reference system ensures a fair, functionally aligned comparison, as both technologies aim to combine daylight utilisation with enhanced thermal performance. A conceptual drawing of the large-scale solar facade module integrated into the test stand, alongside the reference stand equipped with triple glazing, is presented in Figure 5.1.

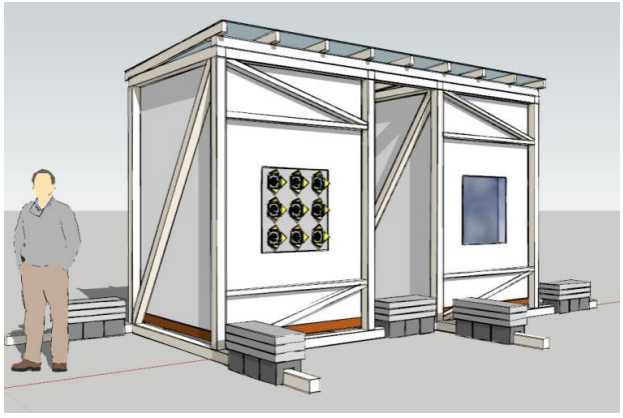

Fig. 5.1. Conceptual drawing of solar facade module (left) and reference (right) stands.

5.1.1. Development of the dynamic component

A key requirement for conducting a comprehensive and accurate assessment of both the proposed solar facade technology and the conventional reference system is the consideration of their physical dimensions. These include size, shape, thicknesses and spatial requirements, all of which directly influence system performance, integration potential and compatibility with building-envelope constraints. Evaluating the dimensional characteristics of the two systems allows for a more meaningful comparison, helps identify strengths and limitations and clarifies any potential trade-offs related to installation, operation and maintenance.

Because the small-scale module incorporates a dynamic component, its movement range must also be taken into account. Figure 5.2 shows the dimensions of the dynamic assembly in both fully closed and fully open positions, illustrating the spatial envelope required for blade rotation.

When nine small-scale components are arranged in a 3×3 matrix to form the concept for the large-scale solar facade module, the spacing between units becomes crucial. Sufficient distance must be maintained to prevent overlapping of the blades in their fully open position. An optimal centre-to-centre spacing of 306 mm was selected to avoid such interference.

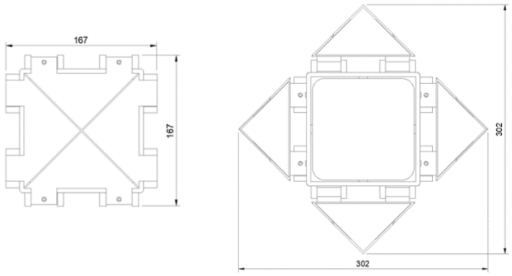

(a) (b)

Fig. 5.2. Drawings of dynamic component in (a) closed and (b) open positions with dimensions in mm.

All components were mounted onto a 6 mm glass shield. The glass shield performs several essential functions:

- it provides mechanical support and ensures precise alignment of the dynamic components;
- it enables high levels of light transmission;
- it accommodates an aerogel insulation layer.

By serving as both a structural and optical interface, the glass shield maintains system stability and ensures consistent blade operation during solar tracking - an important requirement for reliable performance. Its transparency facilitates daylight transmission into the interior space, thereby reducing the demand for artificial lighting. Moreover, enclosing the aerogel insulation layer within the glass shield offers durable protection from environmental exposure

while maintaining excellent thermal resistance. Aerogel, due to its low density and exceptionally low thermal conductivity [182], is particularly suitable for this application.

Figure 5.3 presents the drawings of the glass shield in three configurations: (a) without dynamic components, (b) with blades in the closed position and (c) with blades fully opened.

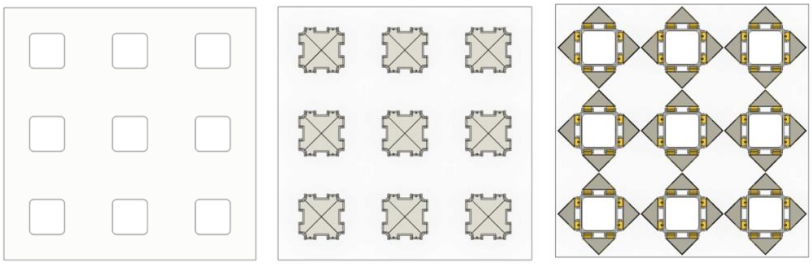

(a) (b) (c)

Fig. 5.3. Drawings of glass shield: (a) without dynamic components, (b) with dynamic components in closed position and (c) with dynamic components in open position.

5.1.2. Adjustment of the control algorithm for the system

In addition to the simplified control algorithm used for operating the dynamic component in the small-scale system, the large-scale system incorporates two additional operational modes designed to enhance both performance and maintenance capabilities. The automatic mode enables continuous system operation, ensuring precise and consistent movement of the dynamic component throughout all seasons. In contrast, the manual mode provides the flexibility required for system calibration and maintenance, allowing the operator to stop the system at any moment and adjust blade positions as necessary. This mode therefore offers a higher degree of control during testing, troubleshooting and fine-tuning.

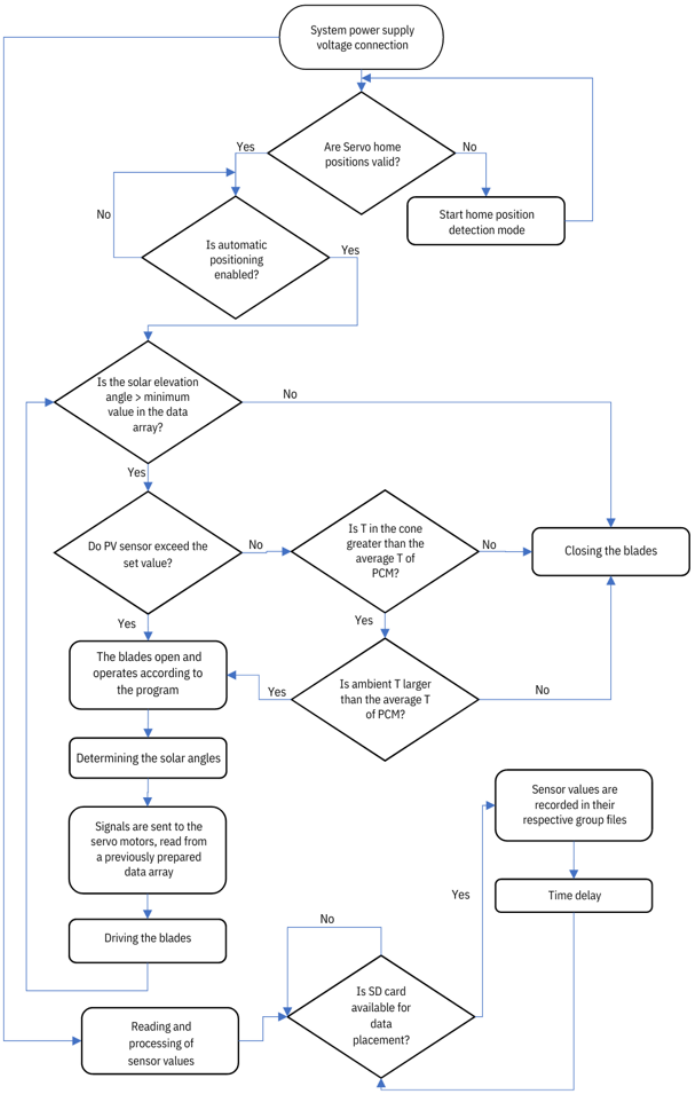

Fig. 5.4. Automatic mode of the control algorithm.

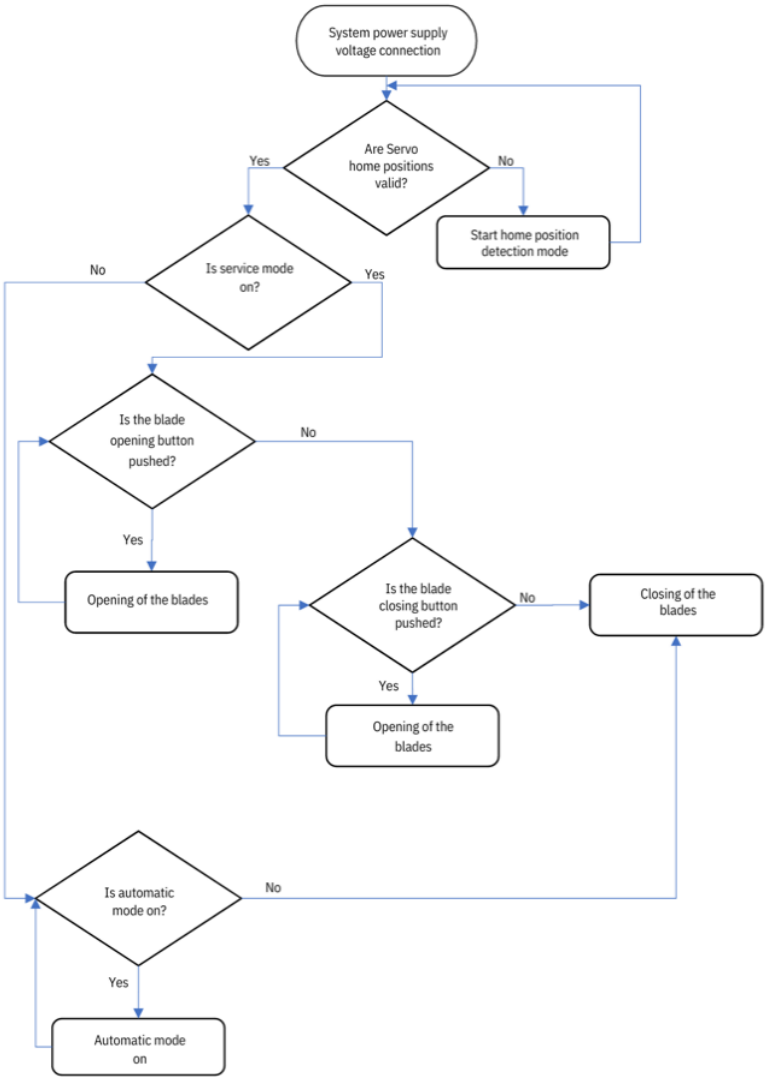

Fig. 5.5. Manual mode of the control algorithm.

While the fundamental principles governing the movement of the dynamic component remain unchanged, the large-scale control system integrates additional sensors and refined algorithms to improve accuracy and operational reliability. The system continuously monitors ambient temperature, solar irradiance, temperature inside the cone and temperature within the PCM. These data streams are processed by the control algorithm to determine the optimal blade orientation in real time, ensuring that sunlight is consistently focused on the centre of the Fresnel lens. As a result, the system achieves high solar-energy concentration efficiency while maintaining the safety of the components and ensuring reliable collection of measurement data. Both the automatic and manual control algorithms are presented in Figure 5.4 and 5.5.

5.2. Comparative outdoor testing setup (E7 – TEST A/P/H)

5.2.1. Experimental design (E7 – TEST A/P/H)

To evaluate the performance of the proposed technological solution, two PASLINK-type experimental stands were constructed and tested under real weather conditions (Fig. 5.6).

Fig. 5.6. Testing (left) and reference (right) stands (a); solar facade system containing 9 small-scale dynamic modules from outside (b) and inside (c) testing booth.

In this experimental study each test booth was designed with external dimensions of 1.8 × 1.8 × 2.4 m (width × length × height). The enclosure was constructed from 100 mm polyurethane sandwich panels forming the walls, roof and floor, ensuring stable thermal conditions and minimising external heat losses. Both booths were aligned with the cardinal directions and the solar facade dynamic system together with the reference element was installed in the south-facing wall to ensure maximum solar exposure. The performance assessment focuses on comparing the proposed technological solution with a conventional high-performance glazing solution commonly used in low-energy and passive buildings. For this purpose, a triple-glazed window with a U-value of 0.85 W/m²K is selected as the benchmark reference.

Two categories of measurement equipment are used in this study:

- instruments dedicated to performance monitoring (indicated in green in Fig. 5.7 and Fig. 5.8),
- instruments integrated directly into the control algorithm (indicated in blue in Fig. 5.7 and Fig. 5.8).

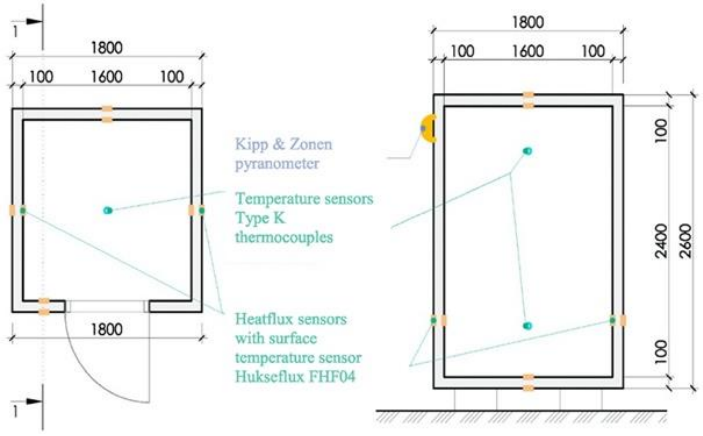

Fig. 5.7. Measuring equipment in PASLINK-type testing booths.

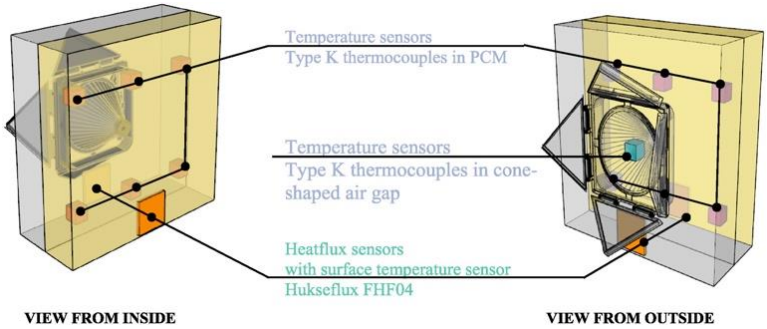

Fig. 5.8. Measuring equipment in dynamic solar facade module.

A total of twelve heat-flux sensors with built-in temperature probes are installed on each plane of the test booth - walls, roof and floor - both on the interior and exterior surfaces. In addition, a pyranometer is mounted on the vertical plane, supplying real-time solar irradiance data to the control algorithm. A second group of sensors is installed within the solar facade modules themselves. Each module contains six thermocouples positioned at characteristic locations, one thermocouple inside the cone and two heat-flux sensors with integrated temperature probes placed on the inner and outer surfaces of the PCM container (Fig. 5.8). A complete overview of the measurement equipment and their locations is provided in Table 5.1.

Table 5.1

Measurement equipment

Equipment purpose	Location	Heat-flux/temperature sensors	Thermocouples	Pyranometer
Monitoring	Solar facade booth	12 each surface in and out	2, in the centre of the booth	-
Monitoring	Reference booth	12 each surface in and out	2, in the centre of the booth	-
Monitoring	Solar faccade module	18 (9 × 2) each module in and out	–	-
Monitoring	Outside	-	1, ambient temperature	-
Monitoring/ Control	Solar facade module	-	54 (9 × 6), 6 sensors in each module embedded in PCM	-
Control	Solar facade module	-	9, 1 sensor in each cone	-
Control	Outside	-	-	1, placed vertically on the front wall of the facade

5.2.2. Experiment plan (E7 – TEST A/P/H)

The dynamic solar facade modules containing PCM RT21HC was operated in automatic mode using a previously described control algorithm as part of the experimental setup from January 2023 to July 2025. The main goal of the experiment was to maintain comfort indoor temperature (16 to 26 degrees) with lowest possible energy consumption in all the seasons of year by using on-site solar-thermal energy. To regulate indoor temperatures during seasonal conditions - cooling in summer and heating in winter - *DAIKIN* heat pumps were installed in both the test and reference booths. These heat pumps can be controlled online, allowing desired temperatures to be set according to specific needs. The heat pumps can be configured to operate in heating mode, cooling mode, or both simultaneously. Energy consumption of both heat pumps is collected to compare the performance between both stands. The system was tested under two operational regimes: active mode, with the heat pumps activated and passive mode, with the heat pumps deactivated. During both regimes, comprehensive data were collected, including air and surface temperatures inside the booths, temperatures within the PCMs, as well as heat fluxes on the inner and outer surfaces of the solar facade. In addition, solar irradiance and ambient temperature data were obtained from a nearby meteorological station. To monitor indoor thermal conditions, three temperature sensors were placed at different heights within each booth. The average of these three readings was used as a representative value for indoor air temperature, allowing for a consistent comparison between the test booth equipped with the dynamic solar facade and the reference booth with conventional triple glazing. All measurements are registered at interval of one minute.

The experiments have been executed in various regimes to observe the impact of each component on indoor climate and energy consumption. Throughout all the seasons of year both stands have been tested in 3 main regimes (listed in Table 5.2): 1) passive – when only dynamic component is operated; 2) active – when heat pumps are activated to maintain constant

temperature in both booths; 3) active and passive combined – in the daytime heat pumps deactivated, but in night activated (or vice versa).

Table 5.2

Time periods of different regimes tested in solar facade

	Passive	Active	Passive (Day)-Active (Night)	Passive (Night)-Active (Day)
Winter	2/01-10/02/2023 1/12/2023-26/01/2024	10-27/02/2023	27/02-04/03/2023. 2-06/01/2025 18-25/01/2025 27/01-25/02/2025	14-22/05/2024
Spring	13-31/03/2023 7-8/04/2023 18-20/04/2025	4-6/03/2023 21/04-31/05/2023 29/04-14/05/2024 17-18/05/2025	6-13/03/2023 31/03-7/04/2023 8-21/04/2023 2/03-18/04/2025 20/04-15/05/2025 19/05-31/05/2025	2/09-13/09/2024
Summer	19/07-31/08/2023 28/06-29/07/2024 2-5/07/2025 6-9/07/2025 12-29/07/2025	1/06-19/07/2023 29/07-29/08/2024	1/06-2/07/2025	
Autumn	1/09-31/11/2023 13-19/09/2024		19/09-18/10/2024	

5.3. Large-scale outdoor testing results (E7 – TEST A/P/H)

5.3.1. Evaluation of thermal and energy consumption performance

To comprehensively evaluate the experimental data and derive meaningful conclusions regarding the performance of the test stand, a set of comparison criteria was established to assess differences between the test and reference booths:

- Temporal comparison - experimental results were analysed over 24-hour periods to capture full day–night cycles.
- Thermal performance - evaluation was based on how effectively indoor temperatures were maintained within the comfort range of 15–25 °C.
- Energy efficiency - assessment was performed according to the electrical consumption of the heat pumps across all operating regimes.

Using these criteria, representative 24-hour periods were selected to ensure a robust and meaningful performance analysis. The chosen days cover all operational modes of the dynamic solar facade and span a wide range of climatic conditions, including both sunny and overcast days in all four seasons.

Day selection was based on data from the local meteorological station, particularly measured solar irradiance and outdoor temperature. A complete list of the selected days used for detailed evaluation is provided in Table 5.3.

Table 5.3

List of selected days for experimental data evaluation based on weather, season and regime

Winter	**Sunny weather**	**Cloudy weather**
Passive	X	X
Active	X	15/02/2023
Passive (Day)-Active (Night)	14/02/2023	22/02/2025
Spring	**Sunny weather**	**Cloudy weather**
Passive	19/04/2025	14/03/2023
Active	14/05/2023	16/05/2023
Passive (Day)-Active (Night)	5/05/2025	6/05/2025
Summer	**Sunny weather**	**Cloudy weather**
Passive	8/07/2024	5/07/2024
Active	22/08/2024	23/08/2024
Passive (Day)-Active (Night)	26/06/2025	24/06/2025
Autumn	**Sunny weather**	**Cloudy weather**
Passive	22/09/2023	23/09/2023
Passive (Day)-Active (Night)	16/10/2024	14/10/2024
Passive (Night)-Active (Day)	7/09/2024.	X

The results from the winter season, during which the solar facade operated in active mode, are presented in Figure 5.9. Throughout the 24-hour period, the indoor temperature in both the test and reference booths remained consistently around 20 °C, indicating effective thermal regulation. Due to low outdoor temperatures and minimal solar irradiance on this day, the dominant heat flow direction was outward from the interior to the exterior. The gradual decrease in PCM temperature further reflects the thermal load placed on the heat pump, which maintained indoor conditions within the comfort range despite the absence of solar gain. Both booths exhibited identical energy consumption, with each heat pump consuming 2 kWh of electricity over the 24-hour period.

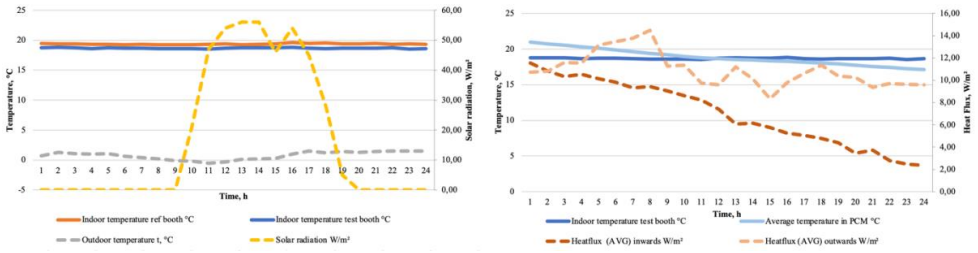

Fig. 5.9. Comparison of results. Cloudy day in Winter (15/02/2023); operational regime: Active.

A sunny winter day was observed on 14 February 2023 (Fig. 5.10), when the solar facade operated in the Passive (Day) – Active (Night) regime. During daytime, when the heat pump

was deactivated, solar energy alone was sufficient to maintain indoor temperatures within the comfort range.

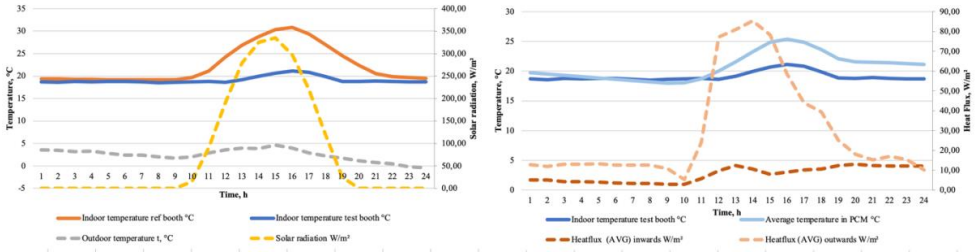

Fig. 5.10. Comparison of results. Sunny day in Winter (14/02/2023); operational regime: Passive (Day)-Active (Night).

However, in the reference booth, the excess solar heat resulted in overheating, exceeding the upper comfort limit. In contrast, the test booth maintained stable indoor conditions due to the heat storage capacity of the PCM, which absorbed and moderated the excess solar gains. The total energy consumption of the heat pumps in both booths during this 24-hour period was identical, amounting to 1.2 kWh.

Under cloudy weather conditions, as shown in Figure 5.11, the same Passive (Day) – Active (Night) regime reveals the critical role of solar energy in maintaining indoor comfort during the day. In the absence of sufficient solar radiation, the indoor temperature in both booths drops significantly, reaching approximately 5 °C - well below the comfort range. Due to the cold outdoor temperatures and lack of solar gain, even the phase change material (PCM) in the test booth is unable to buffer the temperature drop effectively. As a result, both systems rely heavily on nighttime heating to restore thermal comfort. The total energy consumption of the heat pumps reflects this increased heating demand. The reference booth consumed 2.4 kWh, while the test booth consumed slightly more at 2.5 kWh, indicating the marginal impact of the PCM under low solar irradiance conditions.

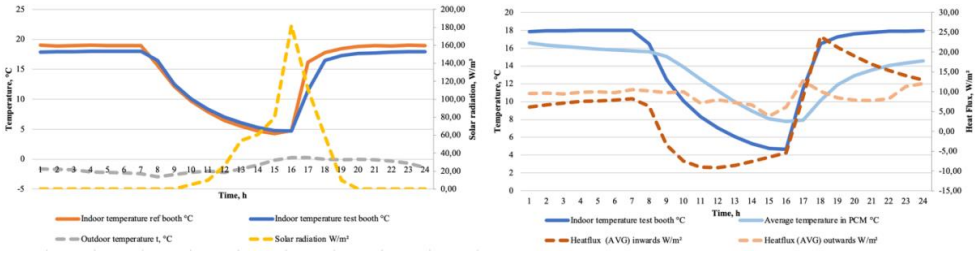

Fig. 5.11. Comparison of results. Cloudy day in Winter (22/02/2025); operational regime: Passive (Day)-Active (Night).

The passive regime was tested on a sunny and warm spring day, 19 March 2025 (see Fig. 5.12). Under these conditions, the test booth demonstrated a more balanced thermal response, maintaining indoor temperatures closer to the comfort range. This stability is attributed to the

thermal buffering properties of the PCM, which absorbs excess heat during peak solar exposure and releases it back into the room as the indoor temperature begins to drop. In contrast, the reference booth, lacking thermal storage capability, experienced a significant indoor temperature rise, reaching approximately 34 °C, leading to pronounced overheating.

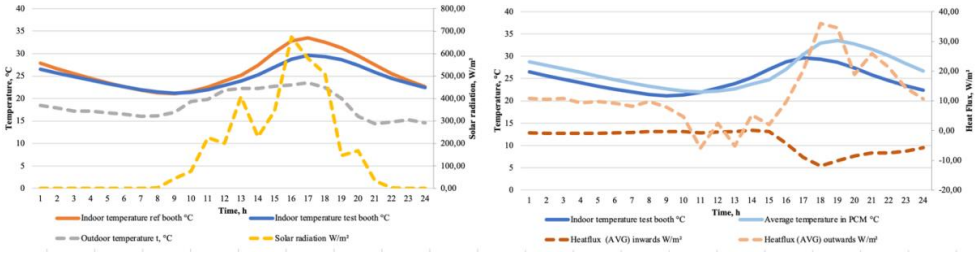

Fig. 5.12. Comparison of results. Sunny day in Spring (19/04/2025) operational regime: Passive.

A similar trend is observed on a cold yet sunny spring day (see Fig. 5.13). Although the test booth does not reach the full comfort temperature range due to the low outdoor temperatures, it exhibits a smoother and more stable indoor temperature profile throughout the 24-hour cycle. This is a result of the PCM's thermal regulation capability, which helps moderate temperature fluctuations even under suboptimal external conditions.

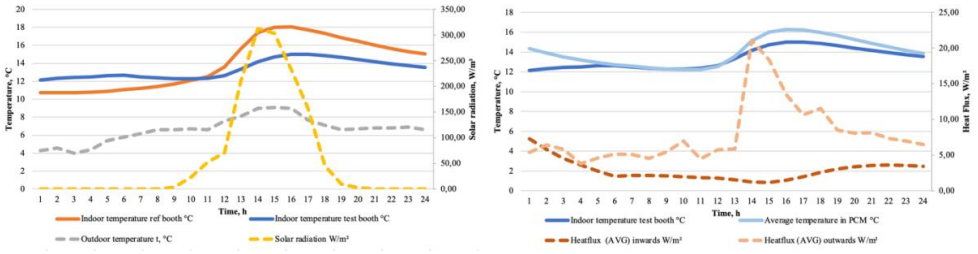

Fig. 5.13. Comparison of results. Cloudy day in Spring (14/03/2023) operational regime: Passive.

On a warm, sunny spring day, the active regime was tested (see Figure 5.14). During periods of high solar irradiance, the PCM in the test booth effectively absorbed excess heat from the environment. However, analysis of the heat flux direction indicates that the PCM was not only storing solar energy but also absorbing heat from the indoor space, including heat supplied by the heat pump. This behaviour is reflected in the energy consumption data: the test booth's heat pump consumed 0.1 kWh more than that of the reference booth over the 24-hour period. In this case, the PCM did not provide a performance benefit; instead, it acted as a heat sink, removing useful heat from the interior and dissipating it outward, resulting in reduced system efficiency.

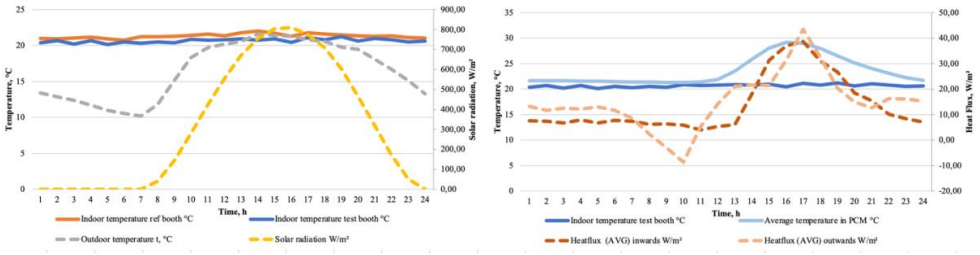

Fig. 5.14. Comparison of results. Sunny day in Spring (14/05/2023) operational regime: Active.

When the same active regime is applied on a cloudy spring day with a similar ambient temperature (see Fig. 5.15), the absence of solar irradiance shifts the entire thermal load onto the heat pumps, which are set to maintain a constant indoor temperature of 20 °C in both booths. Under these conditions, the PCM temperature remains stable, slightly above its melting point, indicating limited phase change activity. Minimal heat flux is observed, suggesting that no significant thermal exchange occurs between the PCM and its surroundings. Energy consumption data shows that the reference booth consumed 3.3 kWh, while the test booth consumed slightly more at 3.6 kWh. This difference suggests that, in the absence of solar input, the PCM in the test booth absorbs heat from the indoor environment, including from the heat pump, rather than contributing to energy savings - thereby slightly reducing system efficiency.

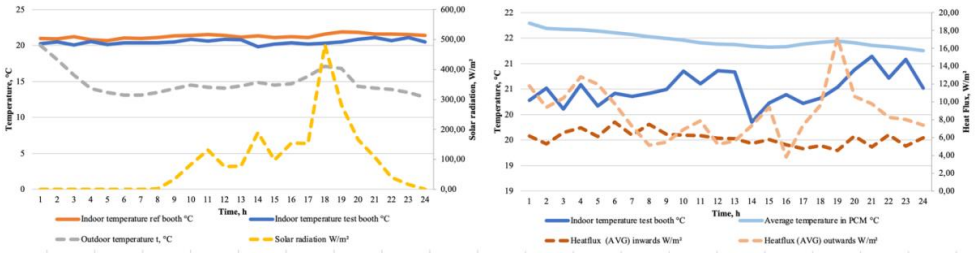

Fig. 5.15. Comparison of results. Cloudy day in Spring (16/05/2023) operational regime: Active.

When the Passive (Day) – Active (Night) regime was tested on a cold but sunny spring day (see Fig. 5.16), the heat pumps were set to maintain a constant indoor temperature of 16 °C. The test booth exhibited a more stable and linear temperature profile throughout the day, attributed to the PCM's ability to absorb excess solar heat during daylight hours and moderate temperature fluctuations. In contrast, the reference booth showed more pronounced temperature variations due to the lack of thermal buffering. Despite these differences in thermal behaviour, the energy consumption of both heat pumps was identical, with each consuming 0.9 kWh over the 24-hour period.

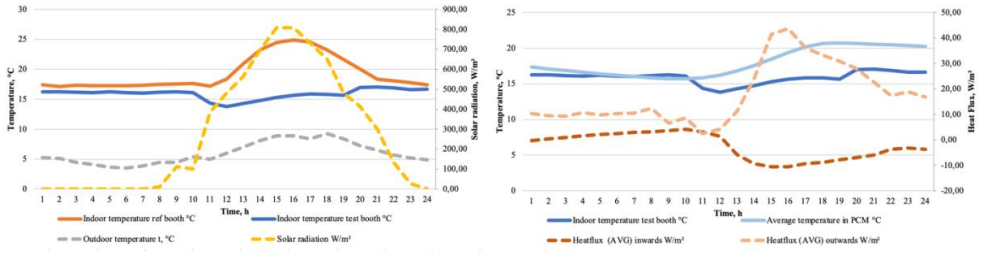

Fig. 5.16. Comparison of results. Sunny day in Spring (5/05/2025) operational regime: Passive (Day)-Active (Night).

A similar trend is observed when the Passive (Day) – Active (Night) regime is applied on a cloudy spring day (see Fig. 5.17). However, in this case, the absence of solar radiation during daytime leads to a noticeable drop in indoor temperature, particularly in the test booth. Without solar input, the PCM is unable to contribute thermal energy, resulting in reduced temperature stability during the day.

Figure 5.18 presents the results of testing the Passive regime on a sunny summer day. The reference booth experienced significant overheating during peak solar hours, with indoor temperatures exceeding 40 °C. In contrast, the test booth remained considerably cooler, with a maximum indoor temperature of only 31 °C, due to the excess heat absorption capacity of the PCM, which effectively mitigated overheating and moderated indoor thermal conditions.

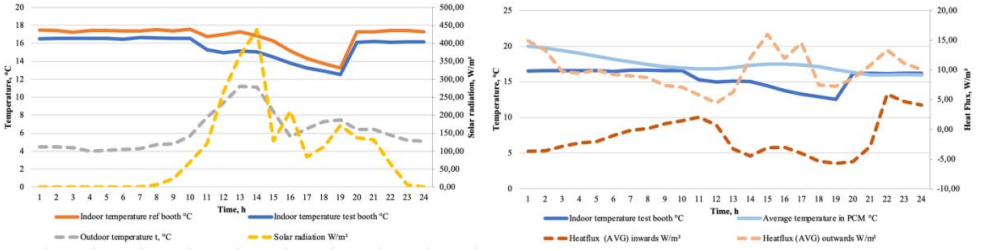

Fig. 5.17. Comparison of results. Cloudy day in Spring (6/05/2025) operational regime: Passive (Day)-Active (Night).

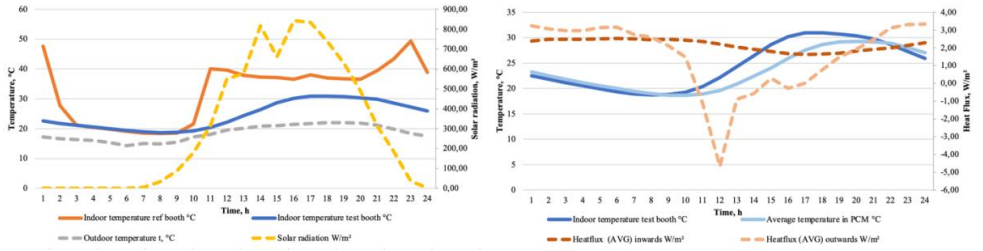

Fig. 5.18. Comparison of results. Sunny day in Summer (8/07/2024) operational regime: Passive.

When the same Passive regime is tested on a less sunny day, such as 5 July 2024 (see Fig. 5.19), the test booth again demonstrates a stable and linear indoor temperature profile over the 24-hour period, indicating effective thermal regulation. In this case, the reference booth also avoids overheating due to the limited solar irradiance throughout the day, resulting in more moderate indoor temperatures in both setups.

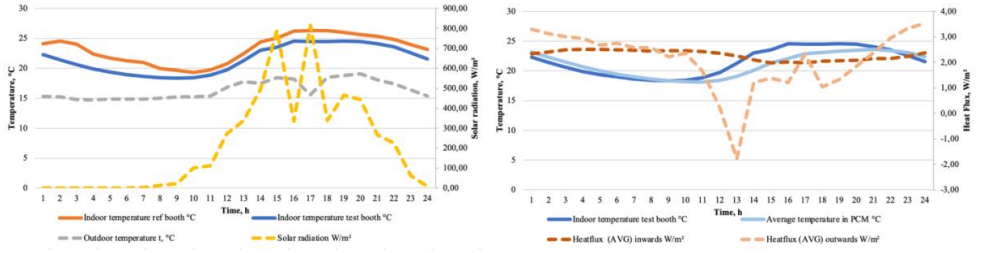

Fig. 5.19. Comparison of results. Cloudy day in Summer (5./07/2024) operational regime: Passive.

The Active regime was tested over two consecutive summer days under different weather conditions - sunny (see Fig. 5.20) and cloudy (see Fig. 5.21). In both cases, the performance of the test and reference booths closely mirrors the results observed during Active regime testing in spring. The indoor temperature profiles and energy consumption patterns remain comparable, indicating that in Active mode, the influence of the PCM is limited when the heat pump is the primary driver of indoor climate control.

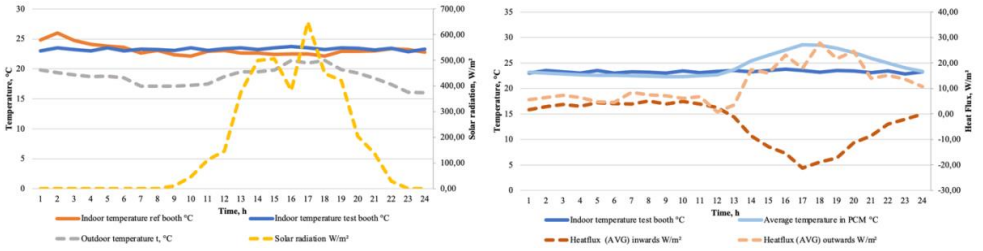

Fig. 5.20. Comparison of results. Sunny day in Summer (22/08/2024) operational regime: Active.

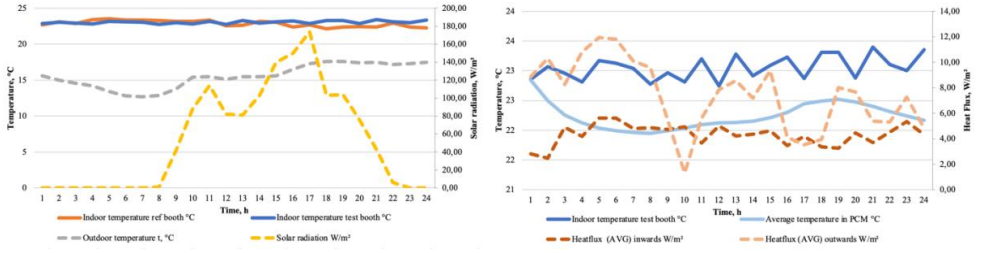

Fig. 5.21. Comparison of results. Cloudy day in Summer (23/08/2024) operational regime: Active.

The Passive (Day) – Active (Night) regime was tested on a sunny summer day, 26 June 2025 (see Fig. 5.22).

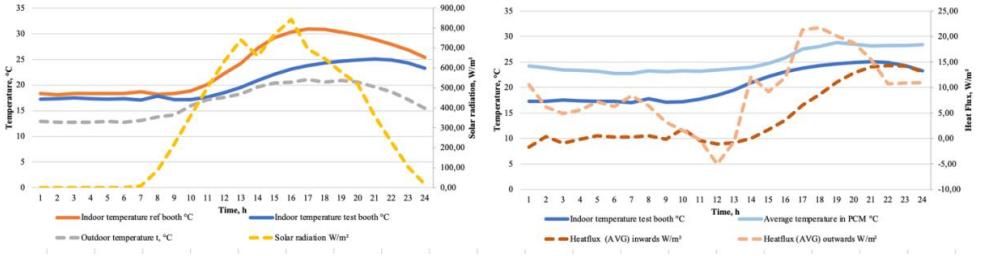

Fig. 5.22. Comparison of results. Sunny day in Summer (26/06/2025) operational regime: Passive (Day)-Active (Night).

The indoor temperature was set to 17 °C at night and under these conditions, the test booth demonstrated superior thermal performance compared to the reference booth, maintaining indoor temperatures within the comfort range. During daytime, the PCM effectively acted as a thermal barrier, preventing overheating despite high solar irradiance. However, throughout the 24-hour period, the PCM remained in the sensible heat zone, with temperatures consistently above its melting point. This indicates that while the PCM helped buffer heat, it did not undergo phase change and therefore did not store latent heat. Despite this, heat pump energy consumption was identical in both booths, measured at 0.3 kWh.

When the same regime was tested on a cloudy day (see Fig. 5.23), similar indoor temperature patterns were observed. In this case, however, the PCM temperature dropped, reaching the solidification stage, which indicates potential for latent heat release. Again, heat pump consumption remained identical in both booths, at 0.2 kWh.

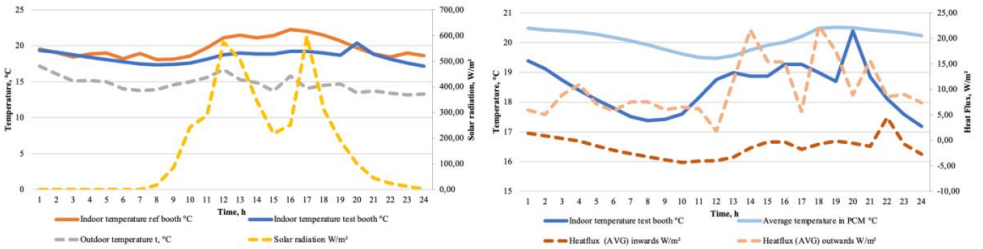

Fig. 5.23. Comparison of results. Cloudy day in Summer (24/06/2025) operational regime: Passive (Day)-Active (Night).

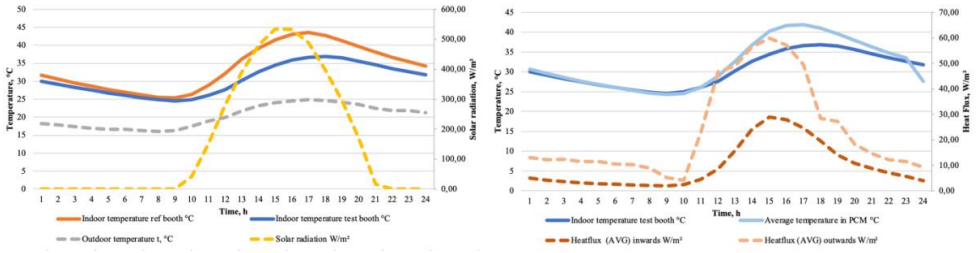

Fig. 5.24. Comparison of results. Sunny day in Autumn (22/09/2023) operational regime: Passive.

The Passive regime was tested over two consecutive autumn days under hot weather conditions - one sunny (see Fig. 5.24) and one cloudy (see Fig. 5.25).

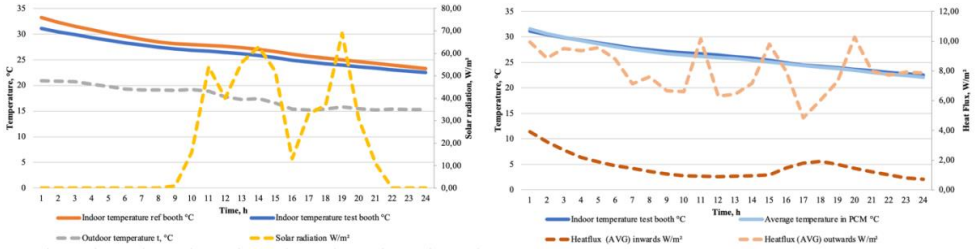

Fig. 5.25. Comparison of results. Cloudy day in Autumn (23/09/2023) operational regime: Passive.

In both cases, significant overheating occurred in both the test and reference booths due to intense solar radiation during the day and elevated ambient temperatures persisting into the night. However, the PCM in the test booth effectively limited the indoor temperature rise, preventing it from exceeding 36 °C, while the reference booth experienced even higher peak temperatures. This demonstrates the PCM's continued ability to moderate indoor conditions and mitigate extreme heat, even under sustained high-temperature scenarios.

The Passive (Day) – Active (Night) regime was also tested in autumn under two distinct conditions: a cold sunny day (see Fig. 5.26) and a cold cloudy day (see Fig. 5.27). The heat pumps were configured to maintain an indoor temperature of 20 °C. The observed thermal behaviour follows patterns similar to those seen in previous tests of this regime. However, a notable difference is observed in heat pump energy consumption: the test booth consumed 0.7 kWh, while the reference booth consumed 0.8 kWh. This slight reduction in energy use suggests that the PCM-enhanced system operated more efficiently under these specific autumn conditions, highlighting the effectiveness of this regime in colder weather.

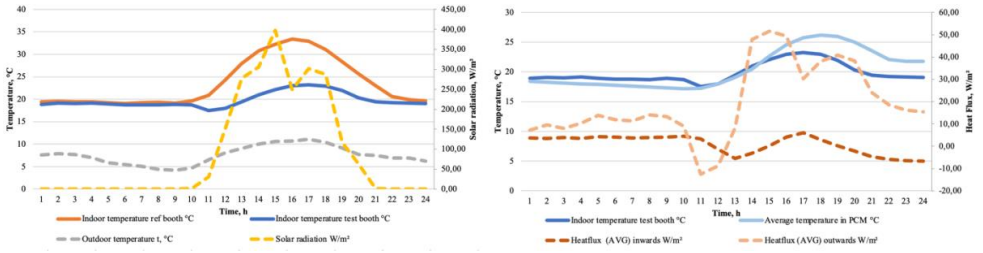

Fig. 5.26. Comparison of results. Sunny day in Autumn (16/10/2024) operational regime: Passive (Day)-Active (Night).

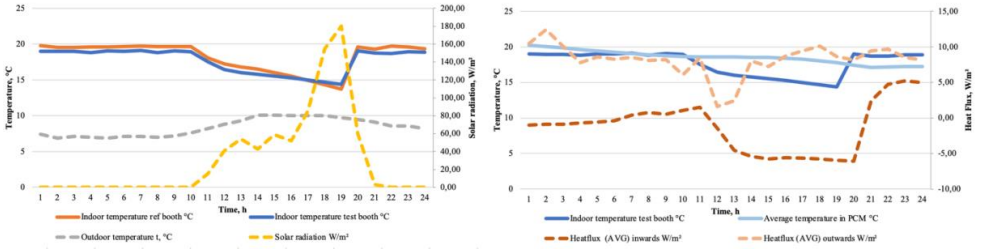

Fig. 5.27. Comparison of results. Cloudy day in Autumn (14/10/2024) operational regime: Passive (Day)-Active (Night).

The Passive (Night) – Active (Day) regime was tested on a sunny and hot autumn day (see Fig. 5.28), with the heat pumps set to maintain a daytime cooling temperature of 24 °C. The results show that the indoor temperature profiles of both the test and reference booths are nearly identical throughout the 24-hour period, indicating that the heat pumps effectively controlled the indoor environment. The PCM temperature profile closely follows the solar irradiance curve, suggesting that solar heat was absorbed by the PCM during daylight hours. However, since the indoor temperature in the test booth was actively maintained by the heat pump, the PCM did not contribute to passive cooling. Instead, the heat pump worked to dissipate the absorbed solar energy, effectively cooling the PCM while the sun was shining. This indicates an inefficient use of on-site solar energy, as the thermal storage capacity of the PCM was not utilized. Nevertheless, indoor thermal comfort was successfully maintained and the energy consumption of both heat pumps was identical, measured at 0.5 kWh.

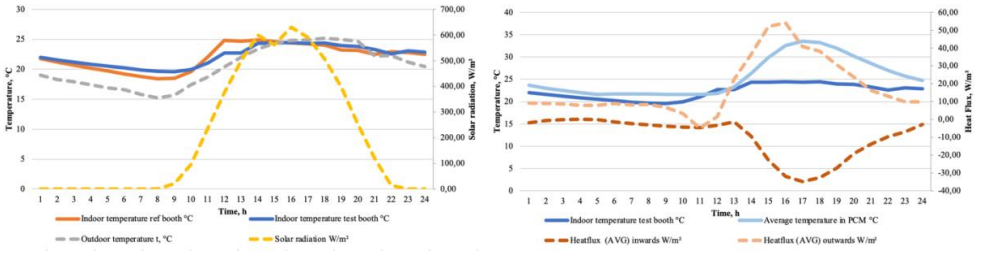

Fig. 5.28. Comparison of results. Sunny day in Autumn (7/09/2024) operational regime: Passive (Night)-Active (Day).

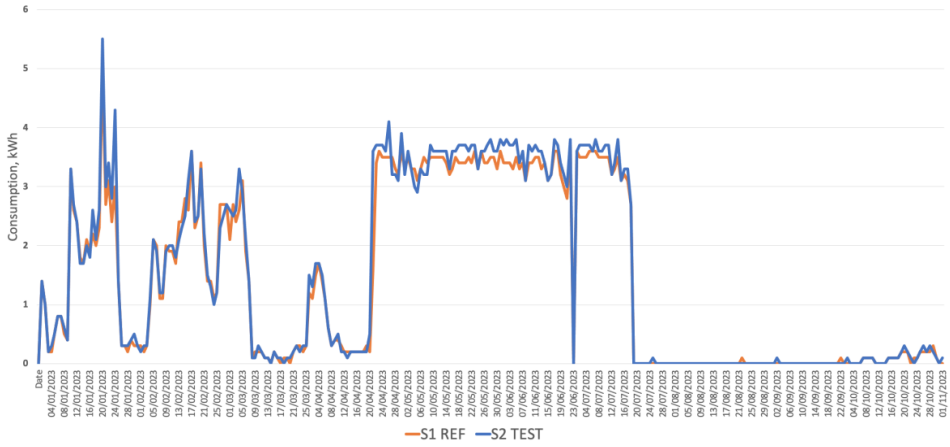

Fig. 5.29. Power consumption of heat pumps from January 4 to November 1 in 2023.

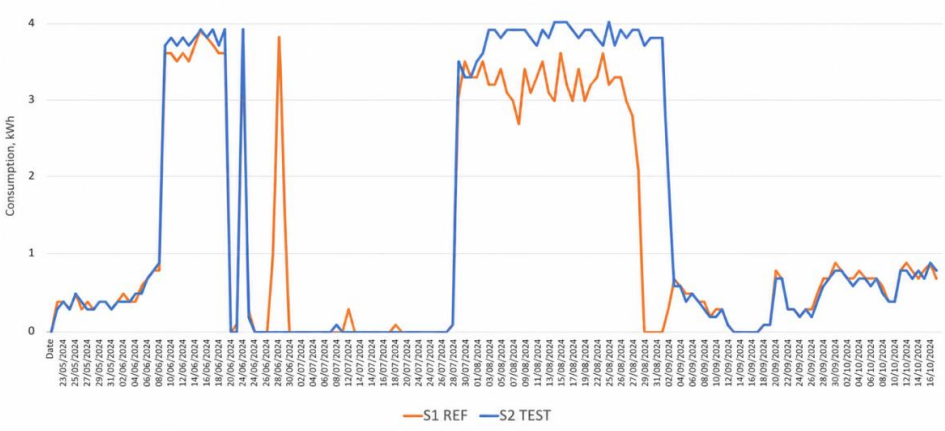

Fig. 5.30. Power consumption of heat pumps from May 23 to October 16 in 2024.

Power consumption data for the years 2023 and 2024 are graphically presented in Figures 5.29 and 5.30, respectively. In the graphs, the labels “S1 REF” and “S2 TEST” correspond to the heat pumps in the reference and test stands, respectively. As expected, seasonal variation strongly influences the energy consumption of both heat pumps. In 2023, the consumption curves for both stands generally follow a similar pattern; however, the test stand (S2) consistently consumes slightly more energy to maintain the desired indoor temperature. A notable peak consumption is observed during the winter period, particularly on January 23, when the test stand’s energy use exceeds 5 kWh. During the spring and summer months (April to July 2023), both systems display a relatively steady consumption trend, typically ranging between 3 to 4 kWh per day. Intervals with near-zero consumption indicate periods when the heat pumps were deactivated. In 2024, the heat pump energy consumption follows a similar seasonal pattern. However, during the period from August 1 to August 29, the test stand operates continuously and consumes approximately 1 kWh more energy per day than the

reference stand. From September 3 to October 16, the system was tested in various operational regimes, with the heat pumps running either only during the day or only at night. During this period, the trend reverses slightly, with the test stand consuming marginally less energy than the reference stand, suggesting improved efficiency under alternating operation modes.

5.3.2. Determination of the effective thermal transmittance (U-value)

The determination of the U-value of the PCM-integrated solar facade module required a methodology that differs fundamentally from standard approaches typically used for conventional, static building envelope components. Unlike mineral wool insulation or fixed glazing systems, PCM-based dynamic facades exhibit pronounced time-dependent thermal behaviour. Their effective thermal resistance varies with PCM phase state, internal heat redistribution and transient external conditions. For this reason, the steady-state U-value tests defined by ISO 6946, ISO 8301, ISO 8302, or the average method of ISO 9869 cannot be directly applied to such systems without careful filtering of the data to isolate periods in which the facade behaves as a purely conductive element. The objective of the present methodology was therefore to extract a "true" conductive U-value from long-term full-scale PASLINK-type outdoor test cell experiments under real climate exposure, while ensuring that the influence of PCM melting, solar charging and transient internal gains was excluded from the analysis. For the present analysis, only the following variables were required: the inner-surface heat fluxes of the solar facade module (measured in W/m²), the outdoor ambient temperature and the indoor air temperature of the testing booth.

The core of the U-value determination lies in the instantaneous relationship between conductive heat flux and temperature difference. Under purely conductive conditions, the heat flux through the facade satisfies the fundamental relation:

$$q(t) = U \cdot [T_{room}(t) - T_{out}(t)], \tag{5.1}$$

where q - conductive heat-flux, W/m²;

U - effective thermal transmittance, W/m²K;

T_{room} – air temperture inside the room, K;

T_{out} – outside ambient temperture, K;

which can be rearranged into the working form:

$$U_{inst}(t) = \frac{-q(t)}{T_{room}(t) - T_{out}(t)}, \tag{5.2}$$

where U_{inst} – instantaneous U-value, W/m²K.

In this formulation, heat flux is positive when heat flows from the interior towards the exterior, which is consistent with the sign convention used by the installed sensors. The denominator is simply the instantaneous thermal driving force:

$$\Delta T(t) = T_{out}(t) - T_{room}(t) \tag{5.3}$$

The heat flux q(t) was computed as the arithmetic mean of the nine module heat-flux sensors, which reduces local measurement noise and provides a facade-area-averaged conductive signal.

However, not every minute of data is suitable for computing a meaningful U-value. Near-neutral temperature gradients lead to inflated or undefined U-value estimates due to division by

values close to zero. For this reason, a filter was applied whereby only those time steps where $|\Delta T| > 0.5$ K, were retained for analysis. This threshold is consistent with recommendations in ISO 9869 for avoiding numerical instability in field U-value estimation and it proved effective for eliminating non-informative data. In the selected days used for the calculations, the indoor temperature of the test booth was consistently higher than the outdoor temperature and therefore almost the entire 24-hour cycle passed this filter. Also, the periods when solar irradiance is present were filtered out.

Although instantaneous U-values may be computed for each valid minute, single-point values are very sensitive to short-term fluctuations in heat flux and room temperature. To obtain a stable and physically meaningful estimate for each date, the nighttime U-value was determined using an integrated energy-balance approach analogous to the cumulative method of ISO 9869, adapted for dynamic test-cell environments. The U-value is therefore computed as:

$$U_{night} = -\frac{\sum_{t=1}^{N} q_{module}(t)}{\sum_{t=1}^{N} \Delta T(t)}, \tag{5.4}$$

where the summations extend over all 1-minute samples satisfying the temperature-difference filter. Conceptually, the numerator represents the total heat transferred through the facade over the night, while the denominator represents the integrated thermal driving force available to drive conduction. Their ratio yields the effective conductive transmittance averaged over the calculated period. This integrated method is significantly more stable than relying on instantaneous values and is widely used in in-situ U-value research [183], [184].

The correctness of the computed U-value depends critically on the assumption that the facade system is behaving as a purely conductive element during the analysed period. For PCM facades, this requires confirming that the PCM remains in the solid or liquid state and that no melting or solidification occurs that would complicate the heat flux signal with latent heat effects. This was verified independently using PCM container temperature measurements, which showed that in the winter, spring and autumn dates analysed all PCM temperatures remained well below the melting range and summer dates were well above it (19-21°C for RT21HC). In addition, no heating, cooling or ventilation systems were operating in the booths during these experiments, ensuring that the thermal environment was governed solely by the natural indoor-outdoor temperature difference and internal radiative equilibrium. The solar facade module was also inactive on these calculated periods (dynamic elements were in closed position) and solar irradiance was not present to introduce appreciable solar charging into the PCM. Calculated nighttime U-values are listed in Table 5.4.

Table 5.4

Calculated steady-state U-value at night

Date	U-value [W/m²K]	n (valid minutes)	PCM state	$\bar{q}$ [W/m²]	$\Delta\bar{T}$ [K]
07/02/2023	0.248	945	Solid	+1.64	-6.60
17/03/2023	0.593	780	Solid	+4.82	-8.11

Date	U-value [W/m²K]	n (valid minutes)	PCM state	$\bar{q}$ [W/m²]	$\Delta\bar{T}$ [K]
19/03/2023	0.498	869	Solid	+3.29	-6.61
27/08/2023	0.289	711	Liquid	+2.32	-8.01
23/10/2023	0.102	895	Solid	+0.56	-5.48
25/10/2023	0.233	935	Solid	+1.71	-7.32
29/10/2023	0.090	969	Solid	+0.53	-5.91
25/07/2025	0.342	507	Liquid	+1.37	-4.01
26/07/2025	0.534	544	Liquid	+2.70	-5.05

These values represent the intrinsic thermal transmittance of the facade module when the PCM is fully solidified and functioning purely as a passive insulator.

5.3.3. Calculation of Energy-Comfort Performance Index

The performance of the developed adaptive solar facade was evaluated using a combined approach that accounts for both indoor thermal conditions and the electricity demand required to maintain them. In the experimental setup, both test and reference booths operate without mechanical ventilation and without additional HVAC systems; thus, the only active energy input during the analysed periods is the electricity consumed by the air-to-air heat pumps. Under these conditions, a meaningful comparison between technologies cannot rely on a single criterion (e.g., energy consumption alone), because low electricity use may coincide with unacceptable indoor temperatures, while stable indoor temperatures may be achieved at the expense of high electrical consumption. For this reason, the assessment method is formulated as a joint energy–comfort indicator that enables transparent benchmarking of the developed facade against the reference system under identical outdoor boundary conditions. The metric for Energy–Comfort Performance Index (ECPI) is defined as a dimensionless performance score. This naming explicitly reflects what the indicator represents: a balanced performance score combining thermal comfort compliance and energy demand.

Thermal comfort is assessed using indoor air temperature. A comfort range of 15-25°C is applied. This range is consistent with the operational setpoints used in the experiments and provides a practical criterion for comparing day-to-day performance in the test and reference booths. For each analysed 24-hour period, the total time during which indoor temperature remains within the defined comfort zone is calculated. Let T_{eff} denote the cumulative duration (in minutes) when the indoor air temperature satisfies:

$$15°C \leq T_{in} \leq 25°C \tag{5.5}$$

The total evaluation duration is:

$$T_{max} = 1440\ min \tag{5.6}$$

A normalized comfort compliance ratio is then computed:

$$\frac{T_{eff}}{T_{max}} \tag{5.7}$$

This term ranges from 0 to 1, where 1 indicates that the indoor air temperature remained within the comfort band for the entire day, while values closer to 0 indicate frequent or long comfort violations.

The energy component is quantified as the daily electricity consumption of the heat pump: $Q_{HP}[kWh]$. To enable comparison across different days and regimes, Q_{HP} is normalized using a reference maximum value $Q_{HP,max}$. In this study, $Q_{HP,max}$ is selected as 5.5 kWh, representing the highest observed daily electricity consumption during the extended experimental period. This choice provides a realistic upper boundary for scaling within the context of the measured dataset. The normalized energy term is therefore:

$$\frac{Q_{HP}}{Q_{HP,max}} \tag{5.8}$$

In typical operating conditions, this ratio lies between 0 and 1.

To create a performance score that is intuitive and easy to interpret, the indicator is rescaled to a clean 0-1 range, where:

- ECPI = 1 corresponds to best-case performance (full comfort compliance with zero electricity consumption), and
- ECPI = 0 corresponds to worst-case performance (no comfort compliance and maximum electricity consumption).

The ECPI is defined as:

$$ECPI = \frac{1}{2}\left(\frac{T_{eff}}{T_{max}} + \left(1 - \frac{Q_{HP}}{Q_{HP,max}}\right)\right) \tag{5.9}$$

This formulation combines two normalized components:

1. The comfort compliance fraction $\frac{T_{eff}}{T_{max}}$, and
2. The energy saving fraction $\left(1 - \frac{Q_{HP}}{Q_{HP,max}}\right)$, which increases when electricity consumption decreases.

The factor $\frac{1}{2}$ ensures equal weighting between comfort and energy. The resulting ECPI is a balanced indicator that rewards both maintaining indoor temperature within the comfort band and reducing heat pump electricity demand.

The ECPI was calculated for representative days (see Table 5.3) across winter, spring, summer and autumn under different operational regimes (fully Passive, fully Active and hybrid day/night switching). By applying the same calculation procedure to both the developed facade system and the reference system, the results provide a consistent basis for ranking performance across weather conditions and identifying which regimes yield the most favourable balance between indoor comfort stability and energy demand.

In Figure 5.31, the calculated results are summarized and arranged in ascending order according to the ECPI values of the tested technology.

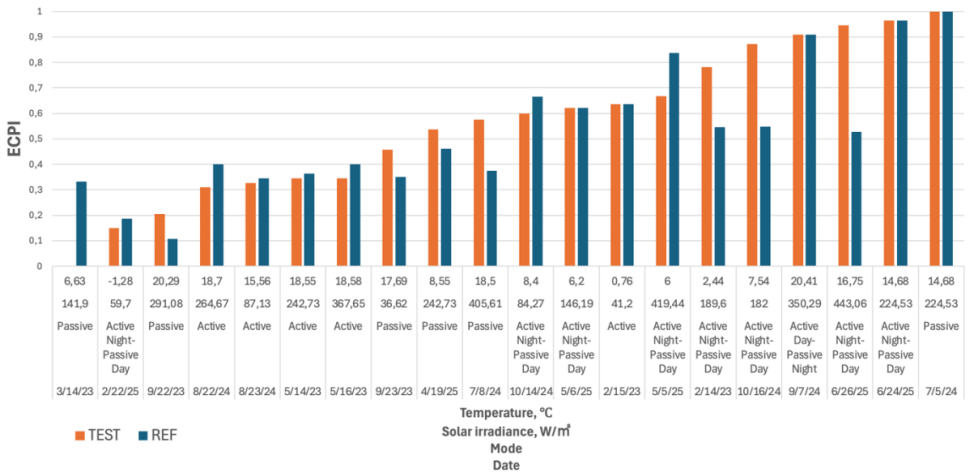

Fig. 5.31. Comparison of calculated ECPI values for solar facade and reference technologies.

Based on the calculated ECPI values, it can be observed that the developed adaptive facade generally demonstrates lower overall performance when operating continuously in either fully Passive or fully Active modes. Two notable exceptions to this trend are identified. First, under moderate outdoor temperatures combined with moderate solar irradiance, the Passive mode yields competitive ECPI values. These conditions typically correspond to temperate summer periods, where solar gains are sufficient to support indoor stability without causing overheating, and auxiliary energy demand remains limited. Second, under low outdoor temperatures (approximately 0°C) and reduced solar irradiance, the Active mode performs comparatively well, reflecting conditions characteristic of mild winter periods where controlled heat pump operation effectively stabilizes indoor temperature without excessive electricity consumption.

The ECPI analysis further indicates that the most consistently favourable performance of the developed technology occurs in the Active (Night) – Passive (Day) regime during transitional seasons. In these mid-season conditions, nocturnal activation supports thermal stabilization and pre-conditioning, while daytime passive operation enables effective utilization of solar gains and stored thermal energy. Conversely, during hot and sunny summer conditions, the highest ECPI values are achieved under the Active (Day) – Passive (Night) regime. In this case, daytime active control mitigates overheating risk, while passive night operation benefits from reduced cooling demand and natural temperature decline.

After identifying regime-dependent performance patterns from the single-day ECPI analysis, extended five-day periods representing the most characteristic and energetically relevant operating modes were examined in greater detail. The selected five-day periods corresponding to the identified optimal regimes are summarized in Table 5.5.

Table 5.5

5-day periods for detailed ECPI calculation

Mode	Season	Dates
Passive (Day)-Active (Night)	Spring/Autumn (cool)	6-10/03/2025
Passive (Day)-Active (Night)	Spring/Autumn (warm)	9-13/05/2025
Passive (Night)-Active (Day)	Summer (hot)	9-13/09/2024
Passive	Summer (warm)	3-7/07/2024
Active	Winter (medium)	15-19/02/2023

Figures 5.32 to 5.36 present the calculated ECPI values for the selected five-day periods representing the most characteristic operating regimes identified in the previous analysis.

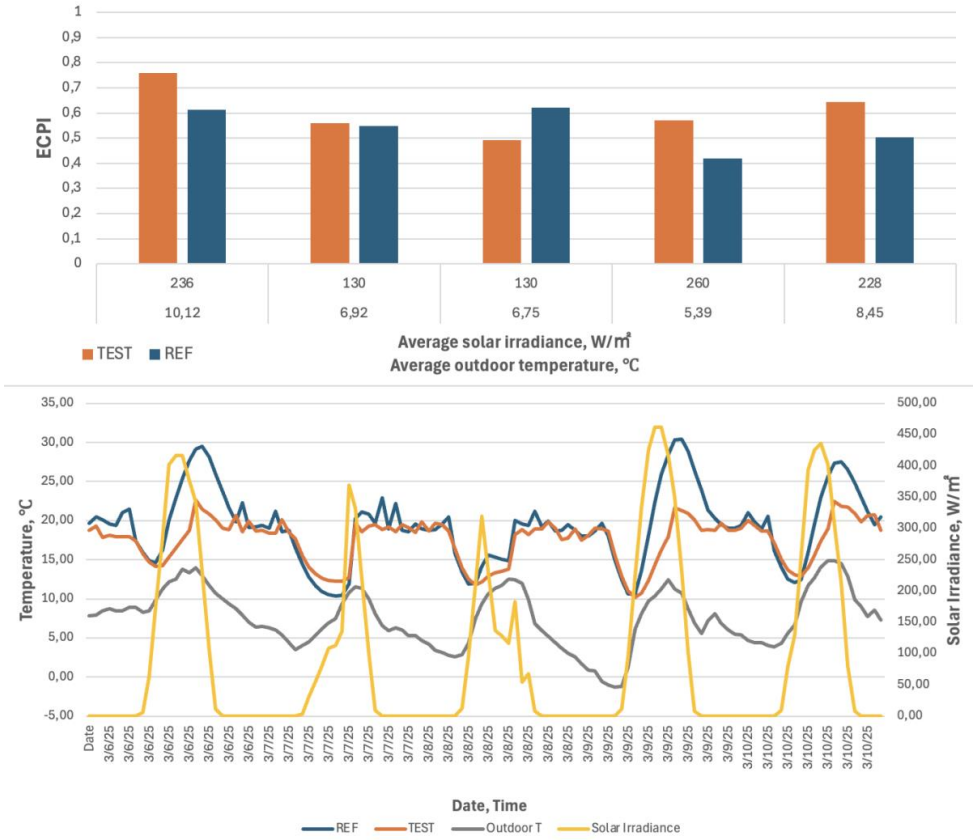

Fig. 5.32. Comparison of calculated ECPI values for 5-day period from 3-10/03/2025.

(6–10/03/2025). In the observed five-day period (cool mid-season), it is evident that only on the third day the developed technology's efficiency is lower compared to the reference (see Fig. 5.32). On this day, the lowest average outdoor temperature and solar irradiance are also

observed. The overall average efficiency across the whole period is 6% higher for the developed technology.

Fig. 5.33. Comparison of calculated ECPI values for 5-day period from 9-13/05/2025.

In warm mid-season five-day period (see Fig. 5.33), a similar trend emerges: at lower average outdoor temperature and solar irradiance the ECPI value of the developed technology is lower (day 1 and day 3). Comparing average ECPI across the whole period, it is 13% higher for the solar facade.

In the hot summer period with the Passive (Night) – Active (Day) regime (see Fig. 5.34), both technologies show high ECPI values (not lower than 0.8), while the solar facade performance is slightly higher or equal to the reference on all days. The average ECPI across the entire period is 6% higher for the solar facade.

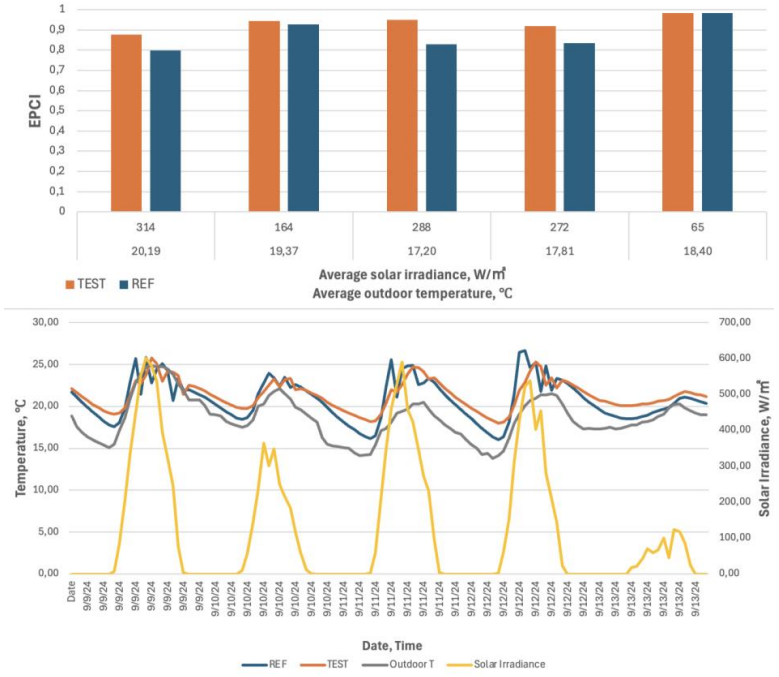

Fig. 5.34. Comparison of calculated ECPI values for 5-day period from 9-13/09/2024.

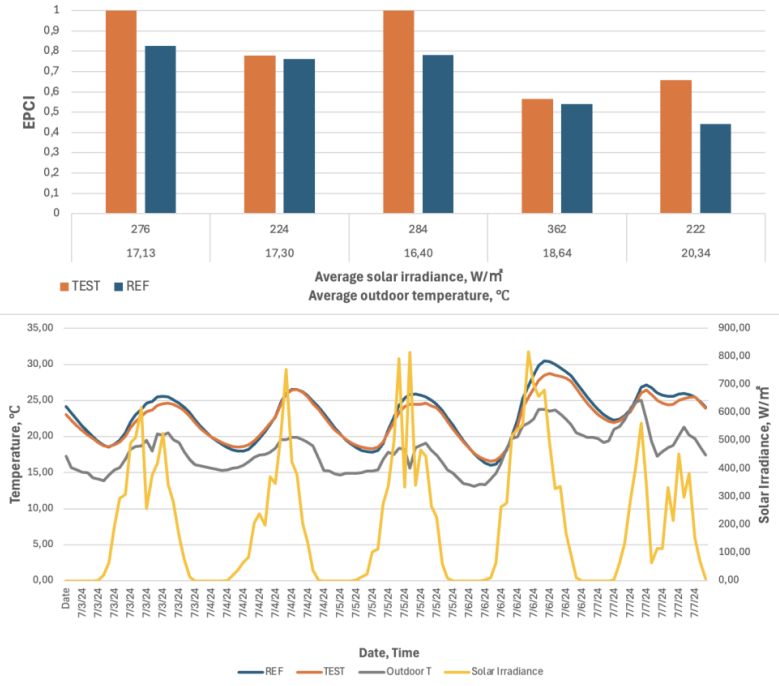

Fig. 5.35. Comparison of calculated ECPI values for 5-day period from 3-7/07/2024.

In warm summer conditions (Fig. 5.35), with the experimental stand operating fully in Passive mode, the solar facade shows higher EPCI than the reference stand on all days, reaching the maximum value on two days (day 1 and day 3). Overall, the value of EPCI in the period is 13% higher for the developed technology.

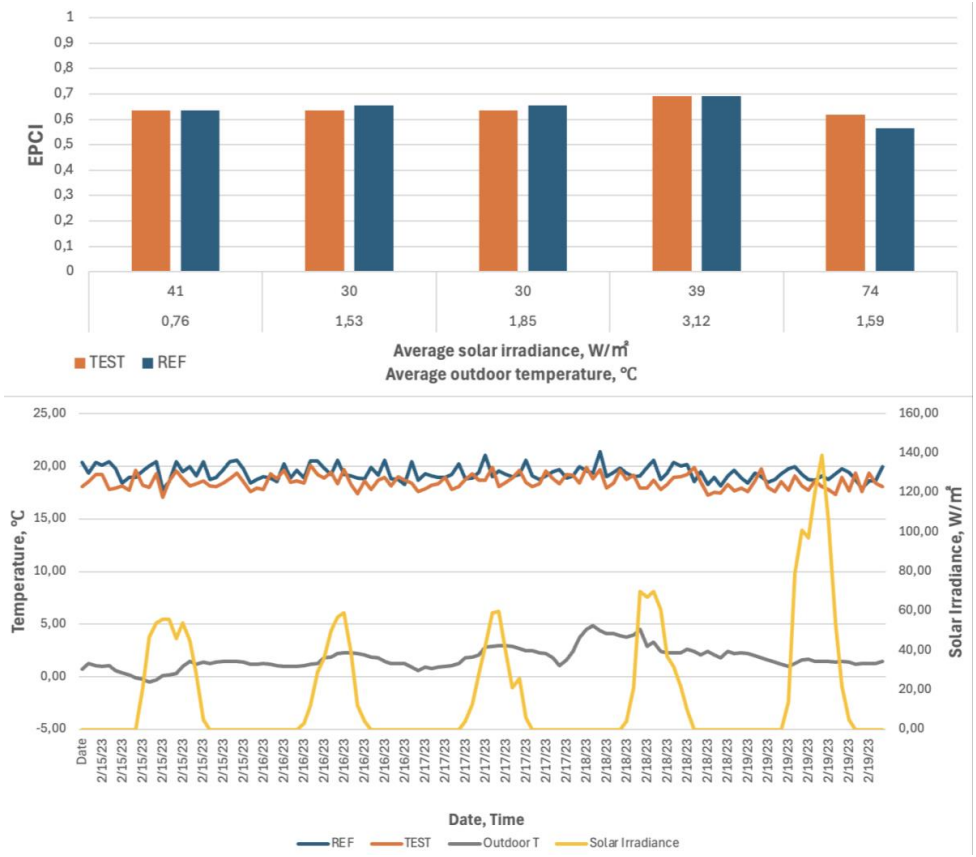

Fig. 5.36. Comparison of calculated ECPI values for 5-day period from 15-19/02/2023.

During the winter five-day period (15-19/02/2023) both stands were tested in Active mode (see Fig. 5.36). Both technologies show very similar EPCI values, leading to an equal overall balance. It can be observed how sensitive both technologies are to temperature fluctuations, which directly affect efficiency for both technologies across the period. On the final day, when slightly higher solar irradiance intensity is observed, the solar facade reflects this with a higher EPCI value.

5.3.4. Preliminary economic assessment

The adaptive PCM-integrated solar facade developed in this Thesis represents an experimental prototype intended to evaluate thermal performance and operational potential

rather than a fully commercialised building product. Therefore, a complete life-cycle cost analysis cannot yet be performed with high precision because several economic parameters - including industrial manufacturing costs, maintenance requirements and long-term operational durability - remain uncertain. Nevertheless, a preliminary quantitative economic assessment can provide important insight into the practical feasibility and future commercial potential of the developed technology. The economic assessment presented in this section therefore focuses on a comparative cost–benefit evaluation between the developed adaptive facade system and a conventional high-performance reference facade represented by a triple-glazed window system with a thermal transmittance value of approximately 0.85 W/m²K. The analysis is based on experimentally observed thermal-performance improvements, indicative market prices for comparable facade technologies and estimated operational energy savings.

The performed economic assessment evaluates the relationship between additional investment costs associated with the adaptive facade system and the potential operational energy savings achieved through improved thermal performance and thermal energy storage. The simplified payback period (SPP) [185] is calculated according to Equation 5.10.

$$SPP = \frac{C_{Adaptive} - C_{Reference}}{E_{Saved} \times P_{el}} \quad (5.10)$$

where SPP – simple payback period, years;

$C_{Adaptive}$ – investment cost of the adaptive facade system, €/m²;

$C_{Reference}$ – investment cost of the reference facade system, €/m²;

E_{Saved} – annual energy savings, kWh/m²·year;

P_{el} – electricity price, €/kWh.

The analysis is intentionally simplified because the developed facade system remains at prototype-development level and several economic parameters cannot yet be determined with full certainty. Therefore, three economic scenarios were established:

1) conservative scenario;
2) realistic scenario;
3) optimistic future-development scenario.

These scenarios allow evaluation of the sensitivity of the technology's economic feasibility to future reductions in manufacturing costs and improvements in operational efficiency.

The adaptive facade system consists of several integrated components: PCM containers, glass enclosure, aerogel insulation layer, Fresnel lens, dynamic reflective blades, control system, sensors and structural support elements. Because no directly comparable commercial product currently exists on the market, the cost estimation was based on available market prices for similar facade technologies and materials. Based on currently available market data for high-performance glazing and facade systems, triple-glazed facade technologies typically range between approximately 500 and 750 €/m² depending on glazing configuration, frame material, thermal performance requirements and installation complexity [186]. Aerogel-based insulation products remain significantly more expensive (18–46 €/m²) than conventional insulation materials [187], while PCM integration (69–212 €/m²) [188] and dynamic control systems (140-220 €/m²) introduce additional manufacturing and assembly costs (assumed to be 50% of all material costs: 227–478 €/m²). Based on the prototype configuration developed during this

research, the estimated adaptive facade investment cost was assumed to range between approximately 600 and 1000 €/m² depending on production scale and technological maturity. Table 5.6 summarises the assumed economic scenarios.

Table 5.6

Indicative economic scenarios for adaptive facade system

Scenario	Reference facade cost (€/m²)	Adaptive facade cost (€/m²)	Additional investment (€/m²)
Conservative	600	1000	400
Realistic	600	800	200
Optimistic	600	600	0

The optimistic scenario assumes future industrial-scale manufacturing, improved component integration and reduced PCM and aerogel material costs due to technological maturation and wider market adoption.

The experimental investigations demonstrated that the adaptive facade system improved thermal stability and reduced heating and cooling demand under multiple operational conditions. The Energy-Comfort Performance Index (ECPI) analysis indicated average performance improvements of approximately:

- 6% during cool transitional periods;
- 13% during warm transitional periods;
- 6–13% during summer operational periods depending on the selected regime.

The experimentally determined effective U-values of the adaptive facade were significantly lower than the reference facade during winter nighttime conditions, reaching values as low as approximately 0.09–0.25 W/m²K compared to the reference value of 0.85 W/m²K. Because the developed adaptive facade system was evaluated using experimental test stands rather than fully occupied buildings, exact annual whole-building energy savings could not be directly determined. Therefore, annual operational energy savings were estimated using simplified comparative assumptions derived from experimentally observed thermal-performance improvements and literature-reported energy-saving potentials of adaptive facade and PCM-integrated envelope systems. Previous studies indicate that PCM-enhanced and adaptive facade technologies may reduce annual heating and cooling demand by approximately 10–80 kWh/m²·year depending on climate, building type and operational strategy [189], [190], [191]. Based on these findings and the experimental results obtained in this Thesis, three simplified annual energy-saving scenarios were assumed:

1) conservative: 15 kWh/m²·year;
1) realistic: 35 kWh/m²·year;
2) optimistic: 60 kWh/m²·year.

For the calculations, an average electricity price of 0.24 €/kWh was used, corresponding approximately to Latvian household electricity prices during 2025 according to Eurostat statistics [192].

Using the simplified payback methodology, the estimated payback periods for the investigated scenarios are summarised in Table 5.7.

Table 5.7

Estimated simple payback periods for adaptive facade system

Scenario	Additional investment (€/m²)	Energy savings (kWh/m²×year)	Annual savings (€/m²×year)	Estimated SPP (years)
Conservative	400	15	3.6	111
Realistic	200	35	8.4	24
Optimistic future scenario	0	60	14.4	0

The results demonstrate that under current prototype-level cost conditions, the feasibility of the adaptive facade system is strongly dependent on manufacturing cost optimisation and operational performance. Under conservative assumptions, the developed facade system still exhibits relatively long payback periods compared to conventional facade technologies when only direct operational energy savings are considered. However, the realistic and optimistic scenarios indicate a substantial improvement in economic competitiveness compared to the initial prototype-level assessment. In particular, the realistic scenario suggests that the adaptive facade could achieve a payback period of approximately 24 years, while the optimistic scenario approaches cost parity with conventional high-performance facade systems.

Importantly, the presented calculation considers only direct heating and cooling energy savings. Several additional benefits were not monetarily quantified within the present analysis, including improved indoor thermal comfort, peak-load reduction, increased renewable-energy self-consumption, reduced greenhouse gas emissions, potential contribution to future smart-grid flexibility services and architectural and technological innovation value. The economic competitiveness of adaptive facade systems is expected to improve under future conditions characterised by increasing energy prices, stricter building-energy regulations, wider implementation of zero-emission-building requirements, industrial-scale production of PCM and aerogel materials and improved automated manufacturing technologies.

5.3.5. Conclusions and insights (E7 – TEST A/P/H)

Over the course of two years, a wide range of experiments were carried out under varying seasonal and weather conditions to evaluate the effectiveness of different operational regimes and the impact of PCM integration on thermal performance and energy efficiency. One of the central findings of the study is that the effectiveness of the dynamic facade system is highly dependent on the selected control regime and the prevailing weather conditions. Three main regimes were evaluated: Passive (Day) – Active (Night), Active (24/7) and fully Passive. Each of these regimes displayed specific strengths and limitations depending on the season.

The Passive (Day) – Active (Night) regime emerged as the most balanced and energy-efficient approach, particularly during the spring and autumn months. These transitional

seasons offer moderate solar irradiance during the day and cooler temperatures at night - conditions under which the PCM could successfully undergo phase transitions. On sunny days, the PCM absorbed excess solar heat, preventing overheating in the test booth and released the stored heat during colder nighttime hours when the heat pump was reactivated. This led to improved indoor temperature stability and reduced energy consumption in many cases. On cloudy days in spring and autumn, the benefits of this regime were still apparent, although less pronounced. The PCM was occasionally able to reach its solidification point and release heat, offering limited thermal support. Notably, during such conditions, the energy consumption of the test stand was often slightly lower than that of the reference stand, suggesting that even under reduced solar input, the PCM contributed to thermal buffering.

In contrast, the Active regime, where heat pumps operated continuously to maintain target indoor temperatures, showed less distinction between the test and reference stands. In many instances, both booths maintained similar indoor temperatures with nearly identical energy consumption. However, during hot, sunny days in summer, the PCM in the test booth absorbed not only solar gains but also indoor heat from the heat pump, especially when it remained in a fully melted state. This led to a situation where the heat pump was effectively dissipating the very heat that the PCM was absorbing, creating an energy loop that reduced system efficiency. These findings highlight the importance of optimizing the control algorithm to recognize when the PCM should be allowed to absorb heat and when it should be insulated to prevent unnecessary charging during active cooling phases.

The fully Passive regime was most beneficial during sunny summer days, particularly in avoiding indoor overheating. In several test cases, the reference booth experienced indoor temperatures exceeding 40 °C, while the test booth, protected by the PCM, remained significantly cooler - often not exceeding 36 °C. The PCM acted as an effective thermal barrier, absorbing excess heat and moderating the indoor environment. However, it is important to note that the PCM often remained above its melting point throughout the day and night, functioning primarily in its sensible heat range rather than undergoing a full phase transition. As a result, the system's energy storage potential was limited, even though comfort was improved.

During winter, the benefits of PCM integration were more constrained. Due to consistently low solar irradiance and low ambient temperatures, the PCM often failed to reach its melting point. Both the test and reference booths required active heating to maintain comfort and in some cases, the test booth consumed slightly more energy due to the additional thermal mass and delayed temperature response associated with the PCM. However, on rare sunny winter days, the PCM was able to contribute marginally to thermal stability by capturing limited solar gains during the day and releasing some heat at night, although the overall impact on energy savings was modest.

The seasonal energy consumption data collected over 2023 and 2024 supports these observations. In both years, consumption patterns of the test and reference booths varied by weather and regime, but in several key periods, particularly during the Passive (Day) – Active (Night) mode in spring and autumn, the test stand demonstrated either equal or slightly lower energy demand. In contrast, during fully active operation in summer, the test stand occasionally

consumed more energy, especially when the PCM acted as a competing thermal sink during cooling.

The calculated U-values derived exclusively from periods without solar radiation provide a clear and consistent picture of the true conductive performance of the PCM-integrated solar facade module. When the PCM remained fully solid and no solar charging occurred, the module exhibited very low thermal transmittance values- 0.09-0.25 W/m²K during the late-autumn and mid-winter days (23/10, 25/10, 29/10 and 07/02) - demonstrating insulation performance that significantly surpasses that of the reference triple-glazed window (U = 0.85 W/m²K) installed in the comparison booth. Even during the early spring days (17/03 and 19/03), where the module's U-value increased to 0.50-0.60 W/m²K, the facade still consistently outperformed the reference window by providing 30-50% lower thermal transmittance. These seasonal differences reflect the temperature sensitivity of the PCM layer: the October and February values correspond to a fully solid PCM with maximal thermal resistance, while the higher March values arise from elevated ambient conditions and early pre-melting behaviour, which reduce effective resistance even though the PCM does not undergo full phase transition.

Further insight is provided by the three analysed summer cases – 27/08/2023, 25/07/2025 and 26/07/2025 - during which the PCM remained fully liquid throughout the day and night. Under no-sun conditions, the module exhibited moderate conductive transmittance on 27/08/2023 (U ≈ 0.29 W/m²K), consistent with the higher thermal conductivity of liquid PCM. The two late-July 2025 cases produced conductive transmittance values of U ≈ 0.34-0.54 W/m²K, which align closely with the expected behaviour of the facade in the fully liquid regime. These summer results confirm that the PCM facade continues to provide better insulation performance than the reference window even when the PCM is liquid, although its effective resistance decreases compared to the solid-state winter conditions as conductive pathways become more active within the melted material.

While regime-based and thermal transmittance analyses provide essential physical understanding, the introduction of the ECPI adds an important multi-criteria dimension to the evaluation. The ECPI integrates two equally weighted components: thermal comfort compliance (time within the 15–25 °C indoor temperature band) and normalized electricity consumption of the heat pump. The ECPI results quantitatively confirm the regime-dependent behaviour observed in the experimental analysis. Continuous fully Passive or fully Active operation generally yields lower overall performance scores. The most favourable and consistent ECPI values occur in hybrid regimes aligned with seasonal characteristics. During transitional seasons, the Active (Night) – Passive (Day) strategy produces the highest performance scores, confirming that daytime passive solar harvesting combined with controlled nighttime stabilization optimally activates the PCM's thermal storage potential. In hot summer conditions, the optimal regime shifts toward Active (Day) – Passive (Night), where active daytime cooling mitigates overheating while passive night operation benefits from natural temperature reduction. This seasonal inversion of optimal control strategy represents one of the key scientific insights of the study.

Extended five-day ECPI evaluations reinforce these conclusions. In cool mid-season conditions, the developed solar facade achieved on average 6% higher ECPI values than the

reference system. In warm mid-season conditions, the advantage increased to 13%. During hot summer operation under the hybrid regime, both systems performed strongly (ECPI > 0.8), yet the solar facade maintained a consistent 6% advantage. Under fully Passive warm summer conditions, the solar facade achieved a 13% higher overall ECPI. In winter Active mode, both systems demonstrated nearly identical performance, reflecting the limited contribution of PCM under low solar availability.

Taken together, these findings demonstrate that the developed adaptive solar facade does not simply reduce energy demand or improve comfort in isolation. Rather, it enhances the balance between energy consumption and thermal stability when operated under seasonally optimised control strategies. The solar facade system performs as a highly effective passive insulator during cold conditions, provides adaptive solar buffering during transitional periods, and significantly mitigates overheating in summer. Its full performance potential, however, is unlocked only when the operational regime is dynamically adjusted in accordance with climatic conditions.

Although the developed adaptive facade system remains at prototype-development level, the performed economic assessment demonstrates promising long-term technological potential. Similar development trajectories have historically been observed for photovoltaic systems, high-performance glazing and advanced insulation technologies, which initially exhibited high investment costs before becoming economically competitive through industrialisation and technological optimisation.

The adaptive facade system developed in this Thesis should therefore be viewed as an emerging next-generation building-envelope technology rather than a fully commercially optimised product. The experimental investigations confirm that the system possesses clear technical potential for improving building thermal performance and renewable-energy utilisation. Future optimisation of PCM materials, control systems, manufacturing processes and facade integration strategies may substantially improve both thermal performance and economic competitiveness.

5.3.6. Optimisation proposal (E7 – TEST A/P/H)

The results of the comparative experimental study clearly demonstrate the potential of the PCM-integrated dynamic solar facade in improving indoor thermal comfort and reducing energy demand. However, several limitations were identified in certain operational regimes - particularly in high solar gain conditions or during full operation of the heat pump - where system efficiency was compromised. To address these challenges and enhance the overall performance and adaptability of the system, several optimization strategies are proposed:

- Integration of a heat exchanger for excess heat utilization. One of the most significant inefficiencies observed during summer testing in Active regimes was the unintended overheating of the PCM, which not only limited its storage capability but also led to increased energy consumption by the cooling system. To counter this, it is proposed to integrate a small-scale heat exchanger inside the glass container that houses the PCM. During periods of high solar gains, the excess thermal energy absorbed by the PCM

could be actively extracted via a fluid loop and diverted for domestic hot water preheating or low-temperature energy storage. This would allow the system to function as both a solar heat concentrator and thermal energy distributor, significantly increasing the system's exergy efficiency. Moreover, such a system could help avoid oversaturation of the PCM in peak summer conditions, allowing it to return to its solid phase overnight and resume effective functioning the next day.

- Enhancement of thermal properties using nanoparticles. To improve the thermal conductivity and heat absorption/release rates of the PCM, the incorporation of nanoparticles is proposed. Among various options, zinc oxide (ZnO) nanoparticles are particularly promising due to their favourable optical transparency, which is crucial in systems relying on concentrated sunlight. Additionally, carbon-based nanoparticles, such as multi-walled carbon nanotubes (MWCNTs), offer high thermal conductivity and could be used in hybrid combinations with metal oxides to achieve synergistic performance improvements. Literature shows that even small additions of nanoparticles can significantly enhance both thermal conductivity and energy storage/release rates, leading to faster system response times and improved performance in dynamic conditions [193–195].
- Insulation mechanism for PCM during heat pump operation. Another observed inefficiency arises when the PCM unintentionally absorbs heat from the heat pump during its operation, particularly in Active cooling mode. To mitigate this, it is recommended to implement an insulation mechanism, such as a thermal barrier or shutter system, that can isolate the PCM container from the booth environment when the heat pump is active. This would prevent the PCM from acting as a thermal sink during cooling periods and ensure that stored solar energy is preserved for passive heating when needed. The insulation could be controlled by the same algorithm governing the blades, based on real-time indoor and PCM temperatures.
- Upgrade of the control algorithm. The control algorithm plays a critical role in managing the dynamic interactions between solar input, PCM behaviour and mechanical systems. A series of enhancements are proposed:
    1) Separation of heat pump modes (heating and cooling) and their operational times. Instead of restricting operation to "day" or "night," the system should respond dynamically based on real-time ambient conditions, solar irradiance and indoor temperature trends.
    2) Introduction of temperature buffer zones to avoid short cycling of the heat pump. For example, heating would start when the temperature drops below 16 °C and stop once it reaches 18 °C, while cooling would begin above 26 °C and stop at 24 °C. This would reduce wear on the heat pump, improve energy efficiency and create a more stable indoor environment.
    3) Incorporation of weather forecasts into the control logic to pre-emptively adjust operation modes, such as activating night cooling in anticipation of a hot, sunny day.

6. DISCUSSION

The present Doctoral Thesis investigated the development and performance of an adaptive solar facade system integrating PCMs for thermal energy storage under both controlled laboratory and real outdoor climatic conditions. The research combined material-level thermal analysis, small-scale optimisation, large-scale experimental validation and numerical simulation to evaluate the potential of PCM-enhanced adaptive facades to improve building energy performance and support the transition toward climate-neutral buildings.

The results obtained throughout the experimental and numerical investigations demonstrate that the proposed facade concept possesses significant potential for reducing indoor temperature fluctuations, improving thermal stability and decreasing heating and cooling demand under varying climatic conditions. At the same time, the findings also reveal that the effectiveness of PCM-integrated adaptive facades strongly depends on climatic conditions, operational regimes, solar availability and the interaction between thermal storage capacity and dynamic control strategies.

The discussion presented in this chapter critically evaluates the thermal behaviour of the investigated PCM systems, the effectiveness of different operational strategies, the role of dynamic facade components and the applicability of the developed technology under different climatic conditions. In addition, the limitations of the experimental and numerical methodologies are discussed together with the broader implications of the research findings for future adaptive facade development and building decarbonisation strategies.

6.1. Thermal performance and PCM behaviour

The experimental and numerical investigations performed in this Thesis demonstrate that the thermal performance of PCM-integrated adaptive facade systems is strongly influenced by the thermophysical properties of the selected PCM, the operating boundary conditions and the interaction between solar gains, heat transfer mechanisms and environmental dynamics. The obtained results confirm that PCMs can significantly contribute to thermal energy storage within building envelopes; however, their effectiveness depends not only on latent heat capacity but also on the ability of the material to consistently undergo complete phase transitions under realistic climatic conditions.

The first stage of the research focused on determining the thermal behaviour and effective thermal conductivity of two paraffin-based PCMs with different melting temperatures - RT21HC and RT28HC. The steady-state hot-plate experiments demonstrated that both materials exhibit relatively low effective thermal conductivity, characteristic of paraffin-based PCMs, with measured values of approximately 0.255 W/(m·K) for RT21HC and 0.30 W/(m·K) for RT28HC. These results are consistent with values reported in the scientific literature for paraffin-type latent heat storage materials and confirm the suitability of both PCMs for building-envelope applications where low conductive heat transfer and thermal storage are desired simultaneously.

At the same time, the dynamic experiments revealed important differences between the two materials. Although RT28HC frequently reached higher peak temperatures during charging periods due to its higher melting range, RT21HC generally demonstrated superior overall thermal performance under Northern European climatic conditions. This behaviour is primarily related to the ability of RT21HC to more consistently enter and complete the phase transition cycle during typical spring, autumn and moderate winter conditions. In contrast, RT28HC often remained partially within the sensible heat region because the available thermal energy was insufficient to fully activate the latent heat storage process. Consequently, a significant portion of the theoretical storage potential of RT28HC could not be utilised during many experimental cycles.

These findings highlight a critical aspect of PCM integration into building envelopes: the melting temperature must be carefully selected according to the climatic conditions and operational objectives of the building system. While higher melting-temperature PCMs may provide advantages in warmer climates or under intense solar exposure by suppressing overheating, they may underperform in colder climates where solar radiation and ambient temperatures are insufficient to complete the melting process. The present study therefore confirms that PCM selection cannot be based solely on latent heat capacity or nominal material properties; instead, the entire climatic and operational context must be considered.

The seasonal laboratory experiments further demonstrated that dynamic boundary conditions substantially influence PCM behaviour compared to idealised steady-state conditions. Under uninterrupted steady-state heating, both PCMs achieved higher temperatures and more stable charging behaviour. However, under dynamic conditions simulating realistic outdoor fluctuations, the charging and discharging processes became considerably more complex due to varying irradiance intensity, intermittent heating and transient thermal losses. This confirms that steady-state testing alone is insufficient for evaluating adaptive envelope technologies intended for real climatic operation. The findings therefore support the importance of PASLINK-type dynamic testing methodologies for assessing building-envelope systems incorporating latent heat storage.

An additional important observation concerns the interaction between latent and sensible heat storage within the PCM containers. Although latent heat storage is typically considered the primary advantage of PCM systems, the experiments indicate that sensible heat effects remain highly relevant, particularly during incomplete phase transitions. In several experimental cases, especially for RT28HC, the thermal response of the system was dominated by sensible heat accumulation rather than latent heat storage. This suggests that practical facade performance may differ significantly from idealised theoretical assumptions frequently presented in PCM-related literature.

The numerical simulations performed in ANSYS Fluent provided further insight into the thermal behaviour of the PCM systems and the associated heat-transfer mechanisms. The validated hot-plate simulation model successfully reproduced the general thermal trends observed experimentally, particularly under moderate boundary conditions. Good agreement between experimental and numerical results confirms that the enthalpy-porosity approach can adequately describe the phase transition process for building-scale PCM applications.

However, the simulations also revealed several limitations. Under extreme boundary conditions, particularly during rapid cooling or high-temperature charging cycles, discrepancies between experimental and numerical results became more pronounced. These deviations are primarily associated with unavoidable simplifications within the numerical model, including idealised boundary conditions, assumptions regarding uniform material properties and limitations in accurately reproducing real transient environmental fluctuations. Furthermore, the complexity of natural convection inside liquid PCM regions remains difficult to fully capture numerically, especially within geometrically constrained facade elements.

Despite these limitations, the numerical models provided valuable conceptual understanding of PCM behaviour across different climatic regions. The simulations demonstrated that RT21HC is generally more suitable for colder Northern European climates, whereas RT28HC may provide greater overheating protection under warmer and high-irradiance conditions. This climate-dependent behaviour reinforces the importance of tailoring PCM selection and facade operation strategies to specific environmental contexts rather than pursuing universally applicable configurations.

The combined experimental and numerical results demonstrate that PCM-integrated adaptive facades can effectively contribute to building thermal regulation and energy-efficiency improvement. However, the results also indicate that the practical effectiveness of such systems depends on achieving a balanced interaction between PCM properties, climatic conditions, dynamic control strategies and facade design parameters. Successful implementation of PCM-enhanced adaptive facades requires a highly integrated design methodology combining material selection, dynamic testing, numerical simulation and climate-specific optimisation.

6.2. Adaptive facade operational regimes

One of the most significant findings of this Thesis is that the thermal and energy performance of PCM-integrated adaptive facades depends strongly on the selected operational regime and the interaction between facade control strategies and outdoor climatic conditions. The large-scale outdoor experiments demonstrated that the adaptive facade cannot be evaluated as a static technology with uniform behaviour throughout the year. Instead, its effectiveness is dynamic and highly dependent on seasonal solar availability, outdoor temperature fluctuations and the timing of charging and discharging processes within the PCM layer.

The investigated operational regimes - including fully passive operation, fully active operation and hybrid active–passive control strategies - produced substantially different thermal responses and energy-efficiency outcomes under varying climatic conditions. Among these approaches, the Passive (Day) – Active (Night) regime consistently demonstrated the most balanced and effective overall performance, particularly during spring and autumn conditions characteristic of Northern European climates.

The superior performance of this regime is primarily associated with its ability to utilise daytime solar energy for passive thermal charging while simultaneously reducing nighttime heat losses through controlled active insulation and heat-pump operation. During sunny daytime periods, the facade system absorbed excess solar energy, which was stored within the

PCM through latent heat accumulation. This process reduced indoor overheating by buffering temperature peaks and delaying heat transfer into the indoor environment. Subsequently, during colder nighttime periods, the stored thermal energy was gradually released, thereby reducing the duration and intensity of auxiliary heating demand.

This operational principle effectively addresses one of the central challenges associated with renewable energy utilisation in buildings - the temporal mismatch between energy generation and energy demand. Solar energy availability typically peaks during daytime periods, whereas heating demand often increases during nighttime conditions. By integrating thermal storage directly into the facade envelope, the proposed adaptive system partially compensates for this mismatch and improves utilisation of on-site renewable energy.

The experiments also demonstrated that the effectiveness of the Passive (Day) – Active (Night) strategy is strongly influenced by weather conditions. Under moderate outdoor temperatures and sufficiently high solar irradiance, the PCM successfully underwent complete charging and discharging cycles, enabling stable indoor temperature regulation and reduced HVAC energy consumption. However, during periods characterised by low solar irradiance, prolonged cloud cover, or extremely low outdoor temperatures, the available solar energy was insufficient to fully activate the latent heat storage potential of the PCM. Under such conditions, the thermal benefits of the facade became less pronounced and the system behaviour approached that of a conventional insulated envelope.

The fully passive operational regime demonstrated several important advantages but also notable limitations. During temperate summer conditions, passive operation effectively reduced overheating by absorbing excess solar heat within the PCM layer and limiting rapid indoor temperature increases. In these cases, the facade functioned as a thermal buffer capable of stabilising indoor conditions without requiring additional energy input for active control systems.

However, prolonged passive operation also revealed limitations associated with incomplete discharge cycles. When the PCM was unable to fully release stored heat during nighttime periods, residual thermal accumulation reduced the storage capacity available for subsequent daytime charging. This effect became particularly evident during consecutive warm days and reduced the long-term effectiveness of passive thermal regulation. The findings therefore suggest that passive PCM operation alone may not be sufficient for maintaining optimal thermal performance over extended periods without supplementary discharge mechanisms or adaptive control strategies.

In contrast, the fully active operational regime provided greater controllability but often reduced the overall energy-efficiency advantages of the facade system. Continuous activation of heat pumps and dynamic components improved short-term thermal stability; however, it also increased operational energy consumption and partially diminished the passive energy-saving benefits associated with PCM-based thermal storage. The experiments indicate that excessive reliance on active systems may compromise the broader objective of reducing building energy demand, particularly when auxiliary systems operate during periods where passive solar charging would otherwise provide sufficient thermal regulation.

An important contribution of the developed adaptive facade system is the integration of dynamic reflective components and adjustable insulation strategies. The laboratory and outdoor investigations demonstrated that the rotating reflective blades significantly improved solar concentration during charging phases while simultaneously reducing thermal losses during discharging periods due to the aerogel-filled blade structure. This dual functionality transformed the facade from a passive thermal-storage element into an actively managed solar-energy system capable of adapting its thermal behaviour according to environmental conditions.

The interaction between the dynamic component, Fresnel lens geometry, focal point positioning and PCM behaviour further demonstrated the complexity of adaptive facade optimisation. The results show that facade performance cannot be evaluated solely through isolated component analysis because the effectiveness of each subsystem depends strongly on the behaviour of the surrounding elements. For example, increased solar concentration improved charging efficiency during cold and moderate conditions but could also increase overheating risks during high-irradiance summer periods if discharge mechanisms were insufficient.

The outdoor testing additionally revealed that adaptive facade technologies require intelligent and climate-responsive control algorithms. The current rule-based control approach demonstrated clear performance improvements; however, the experiments suggest that future adaptive facade systems could benefit substantially from predictive control methodologies incorporating weather forecasts, occupancy patterns and dynamic optimisation strategies. Such approaches would allow the system to anticipate future charging and discharging requirements rather than reacting only to instantaneous environmental conditions.

The results demonstrate that the operational strategy is equally as important as the physical facade configuration itself. The adaptive facade system achieved the highest effectiveness when thermal storage, solar utilisation and dynamic control were balanced according to climatic conditions and building energy demand. The findings confirm that PCM-integrated adaptive facades should not be considered as static envelope technologies but rather as dynamic energy-management systems whose performance depends on the successful coordination of material behaviour, environmental conditions and intelligent operational control.

6.3. Comparison with conventional facade technologies

One of the clearest differences observed during the large-scale outdoor testing was the ability of the adaptive facade system to moderate indoor temperature fluctuations compared to the reference triple-glazed facade system. The PCM-enhanced facade consistently demonstrated a more stable indoor thermal response during periods of rapidly changing outdoor conditions. In spring and autumn conditions, the adaptive facade absorbed excess daytime solar heat and released it gradually during colder nighttime periods, thereby reducing both overheating risk and nighttime temperature decline. In contrast, the reference facade responded more directly to instantaneous outdoor climatic variations due to the absence of thermal storage capacity.

The comparative experiments also revealed that the adaptive facade system can outperform conventional technologies in terms of effective thermal insulation under specific operational conditions. During winter and nighttime no-solar periods, the measured effective U-values of the PCM facade were substantially lower than the reference triple-glazed window system. In several experimental cases, the facade achieved apparent thermal transmittance values as low as approximately 0.09–0.25 W/m²K when the PCM remained in a solid phase, whereas the reference glazing system maintained a conventional U-value of approximately 0.85 W/m²K. These findings indicate that PCM-enhanced adaptive facades can provide not only dynamic thermal storage but also highly effective insulation performance under appropriate climatic conditions.

However, unlike conventional facade systems, the thermal performance of adaptive PCM facades cannot be fully described using traditional steady-state U-value methodology alone. The experiments demonstrated that latent heat storage processes introduce time-dependent thermal behaviour that may significantly alter instantaneous heat-flow characteristics. In some summer conditions, apparent negative U-values were observed due to delayed heat release and transient energy-flow reversals associated with liquid-phase PCM behaviour. These results highlight a fundamental limitation of conventional envelope performance metrics when applied to adaptive or energy-storage-integrated facade technologies.

The adaptive facade system additionally demonstrated clear advantages in managing solar energy utilisation compared to traditional glazing systems. Conventional high-glazing facades often experience significant overheating problems during periods of intense solar radiation, particularly during summer conditions. The developed PCM facade reduced these overheating effects by absorbing a portion of incoming solar energy into latent heat storage rather than immediately transferring it indoors. This thermal buffering capability improved indoor thermal stability and reduced cooling demand during high-irradiance periods.

At the same time, the comparison also revealed several important challenges associated with adaptive facade technologies. Conventional facade systems are generally simpler, more predictable and easier to implement due to their passive and static nature. In contrast, PCM-integrated adaptive facades require significantly more complex system integration involving dynamic components, control algorithms, thermal storage management and climate-responsive operation strategies. The performance of the adaptive system also depends strongly on proper PCM selection, climatic compatibility and operational control, whereas conventional facade systems tend to exhibit more stable and predictable behaviour across broader environmental conditions.

Another important distinction concerns long-term operational reliability and technological maturity. Conventional insulation and glazing technologies are highly standardised and supported by extensive long-term performance data. In contrast, adaptive PCM facades remain relatively novel technologies with limited large-scale implementation experience, particularly under Northern European climatic conditions. Several practical challenges identified during this research - including incomplete PCM cycling, dependence on solar availability and sensitivity to operational regimes - demonstrate that adaptive facades still require further optimisation before widespread commercial deployment becomes feasible.

The findings of this Thesis clearly indicate that adaptive PCM-integrated facades provide functionalities that conventional static envelopes fundamentally cannot achieve. Traditional facades primarily aim to resist heat transfer, whereas adaptive facades actively manage and redistribute thermal energy according to environmental conditions and building demands. This transition represents a broader paradigm shift in building-envelope design - from passive thermal separation toward active participation in building energy management.

The comparison with conventional facade technologies therefore confirms that adaptive PCM-based systems hold considerable potential for supporting future zero-emission and energy-flexible buildings. While conventional facade systems remain highly effective for reducing steady-state heat losses, the proposed adaptive facade demonstrates additional capabilities related to renewable energy utilisation, thermal energy storage, peak-load reduction and dynamic indoor climate regulation. The research suggests that future high-performance building envelopes will increasingly combine conventional insulation principles with adaptive thermal-storage technologies capable of responding intelligently to changing environmental and operational conditions.

6.4. Numerical modelling and experimental limitations

The combined experimental and numerical methodology applied in this Thesis enabled a comprehensive investigation of PCM-integrated adaptive facade systems across multiple scales and climatic conditions. Nevertheless, several limitations associated with both the experimental setup and the numerical modelling approach must be critically acknowledged, as they influence the interpretation, precision and broader applicability of the obtained results.

One of the primary challenges encountered throughout the research was the inherently complex thermal behaviour of phase change materials under dynamic environmental conditions. Compared to conventional solid building materials with relatively stable thermophysical properties, PCMs exhibit nonlinear thermal behaviour due to latent heat storage, temperature-dependent material properties and transient solid–liquid phase transitions. These processes become particularly difficult to analyse under fluctuating solar irradiance and varying outdoor climatic conditions, where charging and discharging cycles are continuously affected by short-term environmental variations.

The experimental investigations were designed to minimise uncertainty through controlled laboratory conditions, calibrated instrumentation and long-term monitoring. However, several unavoidable limitations remained. In the hot-plate experiments, maintaining perfectly stable boundary conditions over extended testing periods proved challenging, particularly during extreme cooling conditions approaching 2 °C and high-temperature charging phases above 45 °C. Minor fluctuations in plate temperature and heat-flux stability introduced uncertainties into the measured thermal conductivity and phase-transition behaviour of the investigated PCMs. Additionally, asymmetrical thermal conditions between the hot and cold plates occasionally influenced the temporal progression of the melting and solidification processes.

Another important limitation concerns the scale dependency of the experimental setups. The small-scale laboratory modules enabled highly controlled comparative investigations and

rapid optimisation of facade parameters; however, they cannot fully replicate the thermal complexity of real building-envelope systems operating under long-term outdoor conditions. Heat transfer mechanisms within the reduced-scale prototypes differ from those occurring in full-scale facade assemblies due to differences in thermal mass, airflow patterns, geometric proportions and environmental exposure. Although the large-scale outdoor experiments partially addressed this limitation, practical constraints related to experimental duration, climatic variability and system controllability remained unavoidable.

The outdoor testing itself introduced additional sources of uncertainty. Real climatic conditions inherently contain uncontrollable fluctuations in solar irradiance, wind speed, cloud cover, humidity and ambient temperature, all of which influence facade behaviour. While such variability represents a major advantage of outdoor testing compared to purely laboratory-based studies, it simultaneously complicates direct comparison between experimental periods and operational regimes. Even when experiments were performed under similar seasonal conditions, no two measurement periods were completely identical in terms of climatic boundary conditions. Consequently, certain observed performance differences may partially reflect environmental variability rather than purely technological effects.

The determination of effective thermal transmittance (U-value) for the adaptive PCM facade also revealed methodological limitations associated with applying conventional steady-state evaluation techniques to dynamic thermal-storage systems. Traditional U-value calculations assume stable conductive heat transfer through stationary materials, whereas PCM-enhanced facades exhibit transient energy storage and delayed heat-release phenomena. The presence of latent heat storage complicated the interpretation of instantaneous heat-flux measurements, particularly during transitional phase states. For this reason, the evaluation was restricted primarily to nighttime periods without solar radiation and under conditions where the PCM was assumed to be fully solidified or fully liquid. Despite these precautions, certain calculated results - including apparent negative U-values - indicate that conventional thermal transmittance methodologies may not be fully suitable for adaptive energy-storage envelopes.

The numerical simulations performed in ANSYS Fluent similarly involved several simplifying assumptions that limit model precision. The enthalpy-porosity method applied for modelling PCM phase transitions represents a widely accepted approach for latent heat simulations; however, it still simplifies several physical phenomena associated with real PCM behaviour. For example, the simulations assumed homogeneous material properties and idealised phase-transition ranges, whereas actual PCM behaviour may involve local temperature gradients, incomplete melting regions and small-scale material inhomogeneities.

Furthermore, accurately modelling natural convection inside liquid PCM regions remains particularly challenging. During melting, density differences within the liquid PCM generate complex buoyancy-driven flow patterns that strongly influence heat transfer and phase-transition dynamics. Capturing these transient convection effects with high precision requires extremely fine spatial and temporal discretisation, which significantly increases computational demand. As a result, certain simplifications related to mesh resolution, turbulence modelling and numerical stability were necessary in order to maintain feasible computational times.

The numerical models also relied on idealised boundary conditions that could not fully reproduce the variability observed during experimental investigations. In reality, laboratory and outdoor experiments were affected by short-term environmental fluctuations, measurement noise and thermal disturbances that are difficult to incorporate into numerical simulations. Although the models reproduced general thermal trends and phase-transition behaviour reasonably well, discrepancies became more pronounced during extreme charging and cooling conditions. The limitations were particularly evident during rapid transient events and long-duration simulations involving complex environmental interactions.

An additional limitation concerns the climate specificity of the performed investigations. The experimental work was conducted primarily under climatic conditions representative of Northern Europe, particularly Latvia. While this provides valuable insight into PCM facade performance in cold and temperate climates, the obtained results cannot be universally generalised to all climatic regions without further investigation. The simulations partially addressed this issue by comparing facade behaviour under different climatic scenarios; however, additional long-term experimental validation in warmer climates would be necessary to fully evaluate the global applicability of the proposed technology.

Despite these limitations, the combined methodology employed in this Thesis provides a framework for analysing adaptive PCM-integrated facade systems. The experimental investigations generated valuable long-term datasets under both controlled and real outdoor conditions, while the numerical simulations enabled interpretation of complex heat-transfer processes that are difficult to observe experimentally. Importantly, the limitations identified throughout the study also highlight key directions for future research, including improved PCM characterisation methods, advanced dynamic performance metrics, predictive control algorithms and higher-fidelity numerical modelling approaches capable of more accurately representing transient environmental interactions and phase-transition phenomena.

The research demonstrates that while PCM-integrated adaptive facades remain complex systems with significant modelling and experimental challenges, the applied methodology provides a sufficiently reliable basis for evaluating their thermal behaviour, operational potential and contribution to building energy-efficiency improvement under realistic climatic conditions.

6.5. Hypothesis evaluation

The central hypothesis of this Doctoral Thesis stated that the integration of phase change materials into an adaptive facade system would improve building energy efficiency by enabling controlled thermal energy storage and release, thereby reducing indoor temperature fluctuations and lowering heating and cooling demand across varying climatic conditions. Based on the combined results of the laboratory experiments, outdoor testing and numerical simulations, the hypothesis can be considered largely confirmed.

The performed investigations consistently demonstrated that PCM integration significantly alters the thermal behaviour of the building envelope compared to conventional static facade systems. The PCM-enhanced facade was capable of absorbing excess thermal energy during

periods of elevated solar irradiance and subsequently releasing the stored heat during colder periods. This thermal buffering effect reduced rapid indoor temperature fluctuations and improved overall thermal stability within the experimental test stands.

One of the clearest confirmations of the hypothesis was observed during the large-scale outdoor experiments under spring and autumn climatic conditions. During these transitional seasons, the developed adaptive facade system effectively reduced daytime overheating while simultaneously improving nighttime thermal stability through delayed heat release from the PCM layer. Compared to the reference facade system, the adaptive facade consistently maintained indoor temperatures within a narrower and more stable comfort range. These results directly confirm that PCM-based thermal storage can improve indoor thermal regulation under dynamic climatic conditions.

The experimental results additionally demonstrated that PCM integration can contribute to reducing heating and cooling energy demand, particularly when combined with appropriate operational regimes. The Passive (Day) – Active (Night) strategy proved especially effective because it enabled passive solar charging during daytime conditions while reducing auxiliary heating demand during nighttime periods. The developed facade therefore functioned not only as a thermal barrier but also as an intermediate thermal storage system capable of partially shifting thermal energy availability over time.

At the same time, the investigations revealed that the degree of hypothesis confirmation depends strongly on climatic conditions, PCM properties and operational control strategies. Although the facade system demonstrated clear thermal and energy-efficiency advantages in many scenarios, the performance improvements were not uniform throughout all seasons and environmental conditions. Under periods of low solar irradiance, prolonged cloud cover, or extremely low outdoor temperatures, the available solar energy was occasionally insufficient to fully activate the PCM phase transition process. In such cases, the latent heat storage potential was only partially utilised and the thermal performance improvements became less pronounced.

The comparison between the two investigated PCMs further emphasised this climate dependency. RT21HC generally demonstrated superior performance under Northern European climatic conditions because its melting range more closely matched the typical operational temperatures encountered during spring, autumn and moderate winter periods. In contrast, RT28HC often remained outside its optimal phase-transition range, limiting its ability to fully exploit latent heat storage under colder climatic conditions. These findings indicate that successful implementation of PCM-integrated adaptive facades requires careful matching between PCM properties and local climatic characteristics.

The hypothesis is also supported by the measured thermal transmittance behaviour of the adaptive facade. During no-solar winter conditions, the facade achieved significantly lower effective U-values than the reference triple-glazed facade system, demonstrating improved insulation performance combined with thermal storage functionality. Furthermore, the facade reduced overheating during summer conditions by absorbing and delaying solar heat transfer through latent heat accumulation. These findings confirm that PCM integration can simultaneously support both heating-demand reduction and cooling-load mitigation depending on seasonal operation.

The research additionally demonstrates that PCM integration alone is insufficient to guarantee optimal energy performance under all conditions. The effectiveness of the system depended heavily on the interaction between PCM behaviour, solar availability, dynamic facade components and operational control algorithms. The adaptive reflective blades, adjustable insulation strategies and hybrid operational regimes played an essential role in maximising thermal-storage utilisation and reducing heat losses. The results suggest that future adaptive facades should be understood as integrated energy-management systems rather than isolated material-based technologies.

The numerical simulations further reinforced the hypothesis by demonstrating that PCM-enhanced adaptive facades can provide different performance benefits across varying climatic regions. The simulations confirmed that lower melting-temperature PCMs are generally more suitable for colder climates, whereas higher melting-temperature materials may offer better overheating protection under warmer environmental conditions. This supports the broader hypothesis that adaptive PCM facades can contribute to building energy-efficiency improvement across different climatic scenarios when appropriately optimised.

The research confirms that integrating PCMs into adaptive facade systems can significantly improve thermal regulation and contribute to reducing building energy demand. At the same time, the findings reveal that the effectiveness of such systems is highly dependent on climate-responsive design, operational optimisation and intelligent control strategies. Therefore, the hypothesis is not only validated in terms of general thermal performance improvement but also expanded through the recognition that adaptive PCM facades must be carefully tailored to specific environmental and operational contexts in order to achieve their full energy-efficiency potential.

6.6. Practical applicability and future development potential

The performed experiments demonstrate that the technology is particularly suitable for climates characterised by significant seasonal variation and prolonged heating periods, such as those found in Northern and Eastern Europe. Under these climatic conditions, the facade effectively reduced indoor temperature fluctuations, improved thermal stability and contributed to lowering heating demand during transitional seasons. The findings therefore indicate strong potential for implementation in both newly constructed high-performance buildings and deep-renovation projects targeting energy-efficiency improvement of the existing building stock.

The developed facade concept is especially relevant within the context of current European Union energy and climate policy. The transition from nearly zero-energy buildings toward zero-emission buildings requires not only improved insulation performance but also greater integration of renewable energy systems and energy-storage technologies. By embedding thermal storage directly into the building envelope, the proposed system contributes to increasing on-site renewable energy utilisation while reducing dependence on fossil-based heating and cooling systems. In this regard, the technology aligns closely with the objectives of the European Green Deal, the Energy Performance of Buildings Directive and the Renovation Wave Strategy.

An additional practical benefit concerns the potential role of adaptive facades within future energy-flexible buildings and smart energy networks. Buildings equipped with facade-integrated thermal storage systems may contribute to reducing peak heating and cooling loads by shifting thermal energy demand over time. Such load-shifting capability could become increasingly important in future electricity systems with high penetration of intermittent renewable energy sources. In this context, adaptive PCM facades may function not only as passive building components but also as active participants within broader district-level energy-management systems.

The research additionally demonstrates that the proposed technology can be adapted according to different climatic conditions and operational objectives through optimisation of PCM properties, control strategies and facade geometry. This flexibility increases the broader applicability of the concept and allows future development of climate-specific adaptive facade configurations. For example, lower melting-temperature PCMs may be prioritised in colder climates dominated by heating demand, whereas higher melting-temperature materials may be more suitable for warmer regions where overheating prevention becomes more critical.

Despite the demonstrated potential, several challenges currently limit immediate large-scale commercial implementation of PCM-integrated adaptive facades. One of the most important barriers remains system complexity. Compared to conventional static facade systems, adaptive facades require significantly more sophisticated integration of materials, dynamic components, sensors, control systems and operational algorithms. This increases both design complexity and potential maintenance requirements.

Economic feasibility also remains an important consideration. Although the present research focused primarily on thermal and energy performance evaluation, practical implementation will ultimately depend on balancing performance benefits against investment and operational costs. The integration of PCM containers, dynamic reflective elements, aerogel insulation and control systems inevitably increases initial system costs compared to traditional facade technologies. However, the experiments indicate that long-term energy savings and improved thermal comfort may partially offset these higher investments, particularly in buildings with high energy demand or stringent decarbonisation requirements.

Another important practical consideration concerns long-term durability and operational reliability. While paraffin-based PCMs generally demonstrate good thermal stability over repeated phase-transition cycles, additional long-duration investigations are necessary to evaluate ageing effects, material degradation and long-term performance stability under real outdoor exposure conditions. Similarly, the long-term mechanical reliability of dynamic facade components and automated control systems requires further investigation prior to widespread commercial deployment.

The results of this Thesis also identify several important directions for future research and technological development. One major area concerns the advancement of intelligent control algorithms. The current rule-based operational strategies demonstrated clear performance benefits; however, future adaptive facade systems could significantly benefit from predictive and self-optimising control approaches integrating weather forecasting, occupancy prediction and real-time energy management. Artificial intelligence and machine-learning-based control

methodologies may further improve facade responsiveness and energy efficiency under highly dynamic environmental conditions.

Further research is additionally required regarding advanced PCM materials and composite thermal-storage systems. Although the investigated paraffin-based PCMs demonstrated favourable thermal behaviour, future studies could explore nano-enhanced PCMs, composite PCM structures and cascaded phase-transition materials capable of extending operational temperature ranges and improving thermal conductivity. Such developments may significantly increase the practical efficiency and adaptability of future facade-integrated thermal-storage systems.

The numerical modelling approaches developed in this Thesis also provide a strong basis for future simulation-driven optimisation of adaptive facade technologies. Higher-fidelity numerical models incorporating more advanced convection modelling, dynamic environmental coupling and whole-building energy simulation could support more precise optimisation of facade geometry, PCM selection and operational strategies prior to experimental implementation.

Generally, the research demonstrates that PCM-integrated adaptive facades represent a promising technological pathway toward next-generation energy-efficient buildings capable of dynamically responding to environmental conditions while improving renewable energy utilisation. Although further optimisation and technological maturation are still required, the developed system demonstrates clear potential to contribute to future low-carbon building design and to support the ongoing transformation of the built environment toward climate neutrality and energy flexibility.

CONCLUSIONS

The main goal of this Thesis was to develop an innovative adaptive facade system integrating thermal energy storage through PCMs and to evaluate its effectiveness in enhancing building energy performance under both controlled laboratory and real outdoor conditions.

The research was motivated by the urgent need to improve the energy performance of the European building stock in alignment with the European Green Deal, the EPBD and the Renovation Wave Strategy. Buildings remain one of the largest consumers of final energy and sources of CO_2 emissions within the European Union. Consequently, innovation at the building-envelope level represents a critical pathway toward achieving long-term climate neutrality objectives. The present work addresses this challenge by combining material-level analysis, small- and large-scale experimentation and numerical modelling within a structured methodological framework.

The literature review established the scientific, technological and policy foundations of the research. It confirmed that LHTES, particularly through solid-liquid PCMs, offers significantly higher storage density than sensible heat systems and enables energy exchange at nearly constant temperatures. This characteristic makes PCMs especially suitable for integration into building envelopes, where they can moderate indoor temperature fluctuations, reduce peak loads and enhance solar energy utilisation. The review also highlighted that, despite extensive laboratory investigations, long-term full-scale validation of PCM-integrated adaptive facades remains limited. Furthermore, it emphasised that steady-state U-value measurements alone are insufficient to characterise dynamic solar facades; instead, real-climate experimental evaluation combined with transient simulation is required. These identified gaps directly shaped the experimental and modelling strategy adopted in this Thesis.

The testing of properties for RT21HC and RT28HC PCMs provided essential thermophysical input parameters for facade development. Repeated guarded hot-plate experiments across twelve rounds confirmed stable and repeatable thermal conductivity values of 0.255 W/(m·K) for RT21HC and 0.30 W/(m·K) for RT28HC. Although certain rounds were influenced by imperfect boundary control, particularly limited cooling performance, the overall dataset demonstrated sufficient consistency to support numerical modelling. RT21HC exhibited more stable thermal behaviour during heating and cooling cycles, while RT28HC showed slightly greater sensitivity to boundary conditions. Comparative steady-state and dynamic testing further revealed that, under Northern European climatic conditions, RT21HC provided more favourable thermal contributions to indoor air temperature despite RT28HC occasionally reaching higher peak PCM temperatures. This indicates that RT21HC more effectively utilised latent heat storage in transitional climates, whereas RT28HC displayed a stronger sensible heat response when complete melting was not achieved.

The validated S1 numerical model successfully reproduced the dominant phase-change dynamics observed experimentally, particularly under moderate boundary conditions. Good agreement between simulated and measured temperatures confirmed the physical reliability of the adopted material parameters and modelling approach. Deviations under extreme heating or cooling conditions were primarily attributed to experimental boundary inconsistencies rather

than modelling deficiencies. This validated framework enabled the further development of the small-scale simulation model (S2) under realistic climatic boundary conditions, demonstrating that RT21HC is a more suitable option for the development of an adaptive solar facade in colder climates.

Small-scale laboratory and outdoor experiments demonstrated that facade performance is highly sensitive to insulation configuration and optical–thermal interaction. The introduction of adjustable insulation layers increased both PCM and indoor temperatures across all setups, with the most pronounced improvements observed in configurations including an air-gap layer. These modules exhibited slower heat dissipation during the discharge phase, indicating improved thermal retention. When evaluating the complete charging–discharging cycle, air-gap configurations gained and released more energy overall, whereas more heavily insulated setups demonstrated greater stability during latent heat plateaus.

The integration of dynamic components - reflective blades combined with aerogel insulation and a Fresnel lens - produced measurable performance enhancements. Under laboratory conditions, the dynamic configuration improved PCM charging rates and extended effective discharge periods. Outdoor validation confirmed that dynamic blade actuation enhanced late-day solar capture, particularly as solar azimuth angles shifted. Systematic focal-point optimisation revealed that both cone diameter and focal position significantly influence heat-transfer efficiency. Setup F1 D4 achieved the highest balanced performance, reaching maximum daytime PCM temperatures of 19.52 °C while maintaining favourable end-of-cycle retention. These findings demonstrate that geometric precision and component synergy are critical to overall facade efficiency.

The two-year large-scale PASLINK-type experimental testing provided comprehensive insight into seasonal and regime-dependent behaviour. The results clearly show that facade performance is strongly influenced by the selected operational regime and prevailing climatic conditions. During spring and autumn, the Passive (Day) – Active (Night) regime delivered the most balanced and energy-efficient performance. Under these conditions, daytime solar gains enabled partial or full PCM charging, while nighttime discharge supported indoor thermal stability and often reduced heat pump demand. Even during partially cloudy transitional periods, modest buffering effects were observed.

In summer, fully Passive operation proved particularly beneficial for overheating mitigation. The reference booth frequently exceeded indoor temperatures of 40 °C, whereas the PCM-integrated test booth typically remained below 36 °C. Although the PCM often operated within its sensible heat range rather than completing full phase transitions, it nonetheless acted as an effective thermal buffer. Conversely, under fully Active summer operation, inefficiencies emerged when the PCM absorbed heat that was simultaneously being removed by the cooling system, creating counterproductive thermal loops.

Winter results demonstrated limited PCM activation due to low solar irradiance and ambient temperatures. However, the facade exhibited excellent insulation performance. Under no-solar conditions with fully solid PCM, the module achieved U-values between 0.09 and 0.25 W/m²K during late autumn and mid-winter periods, substantially outperforming the reference triple-glazed window (U = 0.85 W/m²K). Even in early spring, when U-values increased to 0.50–0.60

W/m²K due to partial pre-melting, the facade still maintained 30–50% lower thermal transmittance than the reference. In fully liquid summer states, U-values ranged from approximately 0.29 to 0.54 W/m²K, remaining superior to the reference system. These findings confirm that the facade provides year-round insulation advantages independent of phase-change activation.

The ECPI, combining thermal comfort compliance and normalised heat pump electricity consumption, provided an integrated performance metric. ECPI results quantitatively confirmed the regime-dependent behaviour observed experimentally. Hybrid seasonal strategies consistently produced the highest performance scores. In cool mid-season periods, the adaptive facade achieved approximately 6% higher ECPI values than the reference system, while in warm mid-season conditions the advantage increased to 13%. During hot summer hybrid operation, both systems achieved high ECPI values (above 0.8), yet the adaptive facade maintained a 6% advantage. Under fully Passive warm summer conditions, the advantage reached 13%. In winter Active mode, both systems performed nearly identically, reflecting limited PCM contribution under low solar availability.

Taken together, these results demonstrate that the adaptive PCM-integrated solar facade does not universally reduce energy demand under all conditions. Rather, it enhances the balance between energy consumption and thermal stability when operated under seasonally optimised regimes. The hypothesis of the Thesis is therefore partially confirmed. PCM integration demonstrably improves thermal performance, overheating mitigation and energy efficiency under suitable climatic and operational conditions. However, its effectiveness depends strongly on solar availability, control strategy and coordination of heat-pumps.

The research makes several key contributions. It provides long-term, full-scale validation of a PCM-integrated adaptive solar facade under Northern European conditions. It establishes a multi-scale methodological framework linking material characterisation, small-scale optimisation, dynamic outdoor testing and performance-index evaluation. It demonstrates the insulation superiority of PCM-enhanced facades and identifies regime-specific optimisation strategies. Finally, it proposes practical improvements including heat-exchanger integration, nanoparticle-enhanced PCM formulations and advanced predictive control algorithms.

In conclusion, this Thesis demonstrates that adaptive solar facades integrating PCMs represent a technically viable and scientifically validated approach to improving building-envelope performance. Their effectiveness is maximised through seasonally adaptive control strategies and integrated system design. By combining thermal storage, optical concentration, high-performance insulation and dynamic operation, the developed facade concept contributes meaningfully to advancing energy-efficient and climate-responsive building technologies aligned with European decarbonisation goals.

REFERENCES

[1] European Commission, The European Green Deal, European Commission - Press Re 53 (2019) 24. https://doi.org/10.1017/CBO9781107415324.004.

[2] European Commission, Clean energy for all Europeans, Euroheat and Power 14 (2019) 3. https://doi.org/10.2833/9937.

[3] E. Union, Directive (EU) 2018/844 of the European Parliament and of the Council amending Directive 2010/31/EU on the energy performance of buildings and Directive 2012/27/EU on energy efficiency, 2018.

[4] EU, Directive (EU) 2018/2001 of the European Parliament and of the Council on the promotion of the use of energy from renewable sources, Official Journal of the European Union 2018 (2018) 82–209.

[5] M. Lazzaroni, G. Bianchi Porro, Preparation, premedication and surveillance, Endoscopy 35 (2003) 103–111. https://doi.org/10.1055/s-2003-37012.

[6] M. Economidou, V. Todeschi, P. Bertoldi, D. D'Agostino, P. Zangheri, L. Castellazzi, Review of 50 years of EU energy efficiency policies for buildings, Energy Build. 225 (2020) 110322. https://doi.org/10.1016/j.enbuild.2020.110322.

[7] D. Kumar, M. Alam, P.X.W. Zou, J.G. Sanjayan, R.A. Memon, Comparative analysis of building insulation material properties and performance, Renewable and Sustainable Energy Reviews 131 (2020) 110038. https://doi.org/10.1016/j.rser.2020.110038.

[8] B. Nashaat, A. Waseef, Responsive Kinetic Facades : An Effective Solution for Enhancing Indoor Environmental Quality in Buildings RESPONSIVE KINETIC FACADES : AN EFFECTIVE SOLUTION, (2017) 0–13.

[9] Directive (EU) 2018/844 of the European Parliament and of the Council, Official Journal of the European Union L156 (2018).

[10] T. Physical, S. Basis, Climate Change 2021—The Physical Science Basis, 2021. https://doi.org/10.1515/ci-2021-0407.

[11] I. Pakere, T. Prodanuks, A. Kamenders, I. Veidenbergs, S. Holler, A. Villere, D. Blumberga, Ranking EU climate and energy policies, Environmental and Climate Technologies 25 (2021) 367–381. https://doi.org/10.2478/rtuect-2021-0027.

[12] M. Miezis, K. Zvaigznitis, N. Stancioff, L. Soeftestad, Climate change and buildings energy efficiency - The key role of residents, Environmental and Climate Technologies 17 (2016) 30–43. https://doi.org/10.1515/rtuect-2016-0004.

[13] United Nations, Global Status report for Buildings and Construction 2021, United Nations Environment Programme (2021).

[14] BPIE, TOWARDS A DECARBONISED EU BUILDING STOCK: EXPERT VIEWS ON THE ISSUES AND CHALLENGES FACING THE TRANSITION Factsheet, (2018).

[15] D. Shuja, S.S.S. Gardezi, M.R. Idrees, Prospects of Transforming Conventional Commercial Buildings to Net Zero Energy Building-Balancing the Economic Aspects with Energy Patterns, Environmental and Climate Technologies 25 (2021) 990–1002. https://doi.org/10.2478/rtuect-2021-0075.

[16] S.J. HAYTER, A. KANDT, Renewable Energy Applications for Existing Buildings Preprint Renewable Energy Applications for Existing Buildings Applicazioni dell'energia rinnovabile su edifici esistenti, Pix 16560 (2011).

[17] A. Ruse, J. Pubule, The Boundaries of Scientific Innovation in the EU Green Deal Context, Environmental and Climate Technologies 26 (2022) 115–128. https://doi.org/10.2478/rtuect-2022-0010.

[18] M. Ibrahim, P.H. Biwole, P. Achard, E. Wurtz, Aerogel-Based Materials for Improving the Building Envelope's Thermal Behavior: A Brief Review with a Focus on a New

Aerogel-Based Rendering, in: A. Sharma, S.K. Kar (Eds.), ENERGY SUSTAINABILITY THROUGH GREEN ENERGY, PSL Res Univ, MINES ParisTech, PERSEE Ctr Proc Renewable Energies & Energy Syst, F-06904 Sophia Antipolis, France, 2015: pp. 163–188. https://doi.org/10.1007/978-81-322-2337-5_7.

[19] S. Attia, S. Bilir, T. Safy, C. Struck, R. Loonen, F. Goia, Current trends and future challenges in the performance assessment of adaptive façade systems, Energy Build. 179 (2018) 165–182. https://doi.org/10.1016/j.enbuild.2018.09.017.

[20] M. Juaristi, T. Gómez-Acebo, A. Monge-Barrio, Qualitative analysis of promising materials and technologies for the design and evaluation of Climate Adaptive Opaque Façades, Build. Environ. 144 (2018) 482–501. https://doi.org/10.1016/j.buildenv.2018.08.028.

[21] A.G. Hestnes, Building Integration Of Solar Energy Systems, Solar Energy 67 (1999) 181–187. https://doi.org/https://doi.org/10.1016/S0038-092X(00)00065-7.

[22] I. Pakere, D. Blumberga, Solar Energy in Low Temperature District Heating, Environmental and Climate Technologies 23 (2019) 147–158. https://doi.org/10.2478/rtuect-2019-0085.

[23] N. Abdou, Y. El Mghouchi, S. Hamdaoui, M. Mhamed, Optimal Building Envelope Design and Renewable Energy Systems Size for Net-zero Energy Building in Tetouan (Morocco), in: 2021 9th International Renewable and Sustainable Energy Conference (IRSEC), 2021: pp. 1–6. https://doi.org/10.1109/IRSEC53969.2021.9741188.

[24] G. Zsembinszki, A.G. Fernandez, L.E. Cabeza, Selection of the Appropriate Phase Change Material for Two Innovative Compact Energy Storage Systems in Residential Buildings, APPLIED SCIENCES-BASEL 10 (2020). https://doi.org/10.3390/app10062116 WE - Science Citation Index Expanded (SCI-EXPANDED).

[25] U. Batra, S. Singhal, Optimum level of insulation for energy efficient envelope of office buildings, International Journal of Environmental Science and Technology 14 (2017) 2389–2398. https://doi.org/10.1007/s13762-017-1322-2.

[26] A.K. Ansu, R.K. Sharma, V. V Tyagi, A. Sarı, P. Ganesan, D. Tripathi, A cycling study for reliability, chemical stability and thermal durability of polyethylene glycols of molecular weight 2000 and 10000 as organic latent heat thermal energy storage materials, Int. J. Energy Res. 44 (2020) 2183–2195. https://doi.org/https://doi.org/10.1002/er.5079.

[27] G. Duttaluru, P. Singh, A. Kumar, Materials Today : Proceedings Methods to enhance the thermal properties of organic phase change materials : A review, Mater. Today Proc. (2022). https://doi.org/10.1016/j.matpr.2022.04.911.

[28] W.R. Sutterlin, Phase Change Materials, A Brief Comparison of Ice Packs, Salts, Paraffins, and Vegetable-derived Phase Change Materials, (2011).

[29] J. Paul, K. Kadirgama, M. Samykano, A.K. Pandey, V. V Tyagi, A comprehensive review on thermophysical properties and solar thermal applications of organic nano composite phase change materials, J. Energy Storage 45 (2022) 103415. https://doi.org/https://doi.org/10.1016/j.est.2021.103415.

[30] J. Heier, C. Bales, V. Martin, Combining thermal energy storage with buildings - A review, Renewable and Sustainable Energy Reviews 42 (2015) 1305–1325. https://doi.org/10.1016/j.rser.2014.11.031.

[31] N. Ahmed, K.E. Elfeky, L. Lu, Q.W. Wang, Thermal and economic evaluation of thermocline combined sensible-latent heat thermal energy storage system for medium temperature applications, Energy Convers. Manag. 189 (2019) 14–23. https://doi.org/10.1016/J.ENCONMAN.2019.03.040.

[32] S. Kossambe, G. Phaldessai, S. Jain, Fabrication and Analysis of Cooling Jacket Incorporated With Phase Change Material, International Journal of Latest Trends in Engineering and Technology 17 (2020) 19–26. https://doi.org/10.21172/1.173.03.
[33] J. Soibam, Numerical Investigation of a heat exchanger using phase change materials (PCMs), NTNU, 2017.
[34] S. Ben Romdhane, A. Amamou, R. Ben Khalifa, N.M. Saïd, Z. Younsi, A. Jemni, A review on thermal energy storage using phase change materials in passive building applications, Journal of Building Engineering 32 (2020) 101563. https://doi.org/10.1016/j.jobe.2020.101563.
[35] C.M. Lai, S. Hokoi, Thermal performance of an aluminum honeycomb wallboard incorporating microencapsulated PCM, Energy Build. 73 (2014) 37–47. https://doi.org/10.1016/j.enbuild.2014.01.017.
[36] T. Silva, R. Vicente, N. Soares, V. Ferreira, Experimental testing and numerical modelling of masonry wall solution with PCM incorporation: A passive construction solution, Energy Build. 49 (2012) 235–245. https://doi.org/10.1016/j.enbuild.2012.02.010.
[37] A. de Gracia, L. Navarro, A. Castell, Á. Ruiz-Pardo, S. Alvárez, L.F. Cabeza, Experimental study of a ventilated facade with PCM during winter period, Energy Build. 58 (2013) 324–332. https://doi.org/10.1016/j.enbuild.2012.10.026.
[38] I. van der Winden, Phase Change Materials: Technology and Applications, Nova, New York, 2020.
[39] H. Hussein, A.H. Abed, A.R. Abdulmunem, An experimental investigation of using aluminum foam matrix integrated with paraffin wax as a thermal storage material in a solar heater, (2018).
[40] G. Bumanis, D. Bajare, PCM Modified Gypsum Hempcrete with Increased Heat Capacity for Nearly Zero Energy Buildings, Environmental and Climate Technologies 26 (2022) 524–534. https://doi.org/10.2478/rtuect-2022-0040.
[41] S. Rucevskis, P. Akishin, A. Korjakins, Performance Evaluation of an Active PCM Thermal Energy Storage System for Space Cooling in Residential Buildings, Environmental and Climate Technologies 23 (2019) 74–89. https://doi.org/10.2478/rtuect-2019-0056.
[42] D. Wu, M. Rahim, M. El Ganaoui, R. Bennacer, R. Djedjig, B. Liu, Dynamic hygrothermal behavior and energy performance analysis of a novel multilayer building envelope based on PCM and hemp concrete, Constr. Build. Mater. 341 (2022) 127739. https://doi.org/10.1016/j.conbuildmat.2022.127739.
[43] G.T. Nguyen, H.S. Hwang, J. Lee, D.A. Cha, I. Park, N-octadecane/fumed silica phase change composite as building envelope for high energy efficiency, Nanomaterials 11 (2021) 1–15. https://doi.org/10.3390/nano11030566.
[44] Y. Yang, W. Wu, S. Fu, H. Zhang, Study of a novel ceramsite-based shape-stabilized composite phase change material (PCM) for energy conservation in buildings, Constr. Build. Mater. 246 (2020) 118479. https://doi.org/10.1016/j.conbuildmat.2020.118479.
[45] C. Buratti, Translucent Silica Aerogel: Properties, Preparation and Applications, Nova, New York, 2019.
[46] C. Buratti, E. Moretti, E. Belloni, Nanogel Windows for Energy Building Efficiency BT - Nano and Biotech Based Materials for Energy Building Efficiency, in: F. Pacheco Torgal, C. Buratti, S. Kalaiselvam, C.-G. Granqvist, V. Ivanov (Eds.), Springer International Publishing, Cham, 2016: pp. 41–69. https://doi.org/10.1007/978-3-319-27505-5_3.

[47] N. Lolli, I. Andresen, Aerogel vs. argon insulation in windows: A greenhouse gas emissions analysis, Build. Environ. 101 (2016) 64–76. https://doi.org/https://doi.org/10.1016/j.buildenv.2016.03.001.
[48] B.P. Jelle, R. Baetens, A. Gustavsen, Aerogel Insulation for Building Applications, The Sol-Gel Handbook 3–3 (2015) 1385–1412. https://doi.org/10.1002/9783527670819.ch45.
[49] N.R.M. Sakiyama, J. Frick, M. Stipetic, T. Oertel, H. Garrecht, Hygrothermal performance of a new aerogel-based insulating render through weathering: Impact on building energy efficiency, Build. Environ. 202 (2021) 108004. https://doi.org/10.1016/j.buildenv.2021.108004.
[50] A.N. Karim, P. Johansson, A. Sasic Kalagasidis, Knowledge gaps regarding the hygrothermal and long-term performance of aerogel-based coating mortars, Constr. Build. Mater. 314 (2022). https://doi.org/10.1016/j.conbuildmat.2021.125602.
[51] J. Paulos, U. Berardi, Optimizing the thermal performance of window frames through aerogel-enhancements, Appl. Energy 266 (2020) 114776. https://doi.org/10.1016/j.apenergy.2020.114776.
[52] X. Yue, H. Wu, T. Zhang, D. Yang, F. Qiu, Superhydrophobic waste paper-based aerogel as a thermal insulating cooler for building, Energy 245 (2022) 123287. https://doi.org/10.1016/j.energy.2022.123287.
[53] Y. Luo, L. Zhang, M. Bozlar, Z. Liu, H. Guo, F. Meggers, Active building envelope systems toward renewable and sustainable energy, Renewable and Sustainable Energy Reviews 104 (2019) 470–491. https://doi.org/10.1016/j.rser.2019.01.005.
[54] H.S.M. Shahin, Adaptive building envelopes of multistory buildings as an example of high performance building skins, Alexandria Engineering Journal 58 (2019) 345–352. https://doi.org/10.1016/j.aej.2018.11.013.
[55] Q. Lei, L. Wang, H. Xie, W. Yu, Active-passive dual-control smart window with thermochromic synergistic fluidic glass for building energy efficiency, Build. Environ. 222 (2022) 109407. https://doi.org/10.1016/j.buildenv.2022.109407.
[56] Q. Lin, Y. Zhang, A. Van Mieghem, Y.C. Chen, N. Yu, Y. Yang, H. Yin, Design and experiment of a sun-powered smart building envelope with automatic control, Energy Build. 223 (2020) 110173. https://doi.org/10.1016/j.enbuild.2020.110173.
[57] Y. Ke, Y. Tan, C. Feng, C. Chen, Q. Lu, Q. Xu, T. Wang, H. Liu, X. Liu, J. Peng, Y. Long, Tetra-Fish-Inspired aesthetic thermochromic windows toward Energy-Saving buildings, 315 (2022). https://doi.org/10.1016/j.apenergy.2022.119053.
[58] A. Tabadkani, A. Roetzel, H.X. Li, A. Tsangrassoulis, Design approaches and typologies of adaptive facades: A review, Autom. Constr. 121 (2021) 103450. https://doi.org/10.1016/j.autcon.2020.103450.
[59] M.P. Voigt, K. Chwalek, D. Roth, M. Kreimeyer, L. Blandini, The integrated design process of adaptive façades – A comprehensive perspective, Journal of Building Engineering 67 (2023) 106043. https://doi.org/10.1016/j.jobe.2023.106043.
[60] T. Mols, A. Blumberga, Inverse modelling of climate adaptive building shells. System dynamics approach, Environmental and Climate Technologies 24 (2020) 170–177. https://doi.org/10.2478/rtuect-2020-0064.
[61] R. Rotas, M. Fotopoulou, P. Drosatos, D. Rakopoulos, N. Nikolopoulos, Adaptive Dynamic Building Envelopes with Solar Power Components: Annual Performance Assessment for Two Pilot Sites, Energies (Basel). 16 (2023). https://doi.org/10.3390/en16052148.
[62] J. Čurpek, M. Čekon, Climate response of a BiPV façade system enhanced with latent PCM-based thermal energy storage, Renew. Energy 152 (2020) 368–384. https://doi.org/10.1016/j.renene.2020.01.070.

[63] C. Koukelli, A. Prieto, S. Asut, Kinetic solar envelope: Performance assessment of a shape memory alloy-based autoreactive façade system for urban heat island mitigation in athens, Greece, Applied Sciences (Switzerland) 12 (2022). https://doi.org/10.3390/app12010082.
[64] S.O. Sadegh, E. Gasparri, A. Brambilla, A. Globa, Kinetic facades: An evolutionary-based performance evaluation framework, Journal of Building Engineering 53 (2022) 104408. https://doi.org/10.1016/j.jobe.2022.104408.
[65] S. Wang, C. Yan, F. Xiao, Quantitative energy performance assessment methods for existing buildings, Energy Build. 55 (2012) 873–888. https://doi.org/10.1016/J.ENBUILD.2012.08.037.
[66] P.A. Strachan, L. Vandaele, Case studies of outdoor testing and analysis of building components, Build. Environ. 43 (2008) 129–142. https://doi.org/10.1016/j.buildenv.2006.10.043.
[67] M. Fletcher, A. Erkoreka, C. Gorse, K. Martin, J.M. Sala, Optimising test environment and test set up for characterizing actual thermal performance of building components and whole buildings, Energy Procedia 78 (2015) 3264–3269. https://doi.org/10.1016/j.egypro.2015.11.715.
[68] S. Hammarsten, D. van Hattem, H. Bloem, R. Colombo, Passive solar component testing with identification methods, Solar Energy 41 (1988) 5–13. https://doi.org/10.1016/0038-092X(88)90108-9.
[69] U. Norlén, Estimating thermal parameters of outdoor test cells, Build. Environ. 25 (1990) 17–24. https://doi.org/10.1016/0360-1323(90)90036-Q.
[70] H. Madsen, J. Holst, Estimation of continuous-time models for the heat dynamics of a building, Energy Build. 22 (1995) 67–79. https://doi.org/10.1016/0378-7788(94)00904-X.
[71] P. Wouters, L. Vandaele, P. Voit, N. Fisch, The use of outdoor test cells for thermal and solar building research within the PASSYS project, Build. Environ. 28 (1993) 107–113. https://doi.org/10.1016/0360-1323(93)90044-4.
[72] H.A.L. Van Dijk, G.P. Van der Linden, The PASSYS method for testing passive solar components, Build. Environ. 28 (1993) 115–126. https://doi.org/10.1016/0360-1323(93)90045-5.
[73] E. Hahne, R. Pfluger, Improvements on PASSYS test cells, Solar Energy 58 (1996) 239–246. https://doi.org/10.1016/S0038-092X(96)00080-1.
[74] P.H. Baker, H.A.L. van Dijk, PASLINK and dynamic outdoor testing of building components, Build. Environ. 43 (2008) 143–151. https://doi.org/10.1016/j.buildenv.2006.10.009.
[75] A. Erkoreka, J.J. Bloem, C. Escudero, K. Martin, J.M. Sala, Optimizing Full Scale Dynamic Testing of Building Components: Measurement Sensors and Monitoring Systems, Energy Procedia 78 (2015) 1738–1743. https://doi.org/10.1016/J.EGYPRO.2015.11.285.
[76] R.C.G.M. Loonen, S. Singaravel, M. Trčka, D. Cóstola, J.L.M. Hensen, Simulation-based support for product development of innovative building envelope components, Autom. Constr. 45 (2014) 86–95. https://doi.org/10.1016/j.autcon.2014.05.008.
[77] N. Gazo, Building Envelope Calculations, (n.d.). https://guides.co/g/building-code-interpretation-insulation-and-energy-efficiency-requirements/169232 (accessed January 21, 2022).
[78] V.C. Thomas, Energy Usage Analysis of Buildings, (n.d.). https://energy-models.com/energy-usage-analysis-buildings (accessed January 21, 2022).

[79] S.N. Al-Saadi, Z. Zhai, Modeling phase change materials embedded in building enclosure: A review, Renewable and Sustainable Energy Reviews 21 (2013) 659–673. https://doi.org/10.1016/J.RSER.2013.01.024.
[80] C. Li, X. Wen, W. Cai, H. Yu, D. Liu, Phase change material for passive cooling in building envelopes: A comprehensive review, Journal of Building Engineering 65 (2023) 105763. https://doi.org/10.1016/J.JOBE.2022.105763.
[81] van E. NJ, L. Waltman, Software survey: VOSviewer, a computer program for bibliometric mapping, Scientometrics 84 (2010) 523–538. https://doi.org/10.1007/S11192-009-0146-3.
[82] A.P. Selvaraju, A. Ranganathan, A.A.R. Vincent, P. Arumugam, V. Ramalingam, THERMAL MANAGEMENT ANALYSIS OF PCM INTEGRATION IN BUILDING USING A NOVEL PERFORMANCE PARAMETER PCM Effectiveness Index, THERMAL SCIENCE 26 (2022) 883–895. https://doi.org/10.2298/TSCI200830208S.
[83] M. Dastmalchi, B. FA, Exergy and economic analyses of nanoparticle-enriched phase change material in an air heat exchanger for cooling of residential buildings, J. Energy Storage 32 (2020) 101705. https://doi.org/10.1016/j.est.2020.101705.
[84] T. Zhou, Y. Xiao, H. Huang, J. Lin, Numerical study on the cooling performance of a novel passive system: Cylindrical phase change material-assisted earth-air heat exchanger, J. Clean. Prod. 245 (2020) 118907. https://doi.org/10.1016/j.jclepro.2019.118907.
[85] S. Rucevskis, P. Akishin, A. Korjakins, S. Ručevskis, P. Akishin, A. Korjakins, Parametric analysis and design optimisation of PCM thermal energy storage system for space cooling of buildings, Energy Build. 224 (2020) 110288. https://doi.org/10.1016/j.enbuild.2020.110288.
[86] N. Elawady, M. Bekheit, S. AA, A. Radwan, Energy assessment of a roof-integrated phase change materials, long-term numerical analysis with experimental validation, Appl. Therm. Eng. 202 (2022) 117773. https://doi.org/10.1016/j.applthermaleng.2021.117773.
[87] D.K. Bhamare, M.K. Rathod, J. Banerjee, Numerical model for evaluating thermal performance of residential building roof integrated with inclined phase change material (PCM) layer, Journal of Building Engineering 28 (2020) 101018. https://doi.org/10.1016/j.jobe.2019.101018.
[88] A.U. Rehman, S.R. Sheikh, Z. Kausar, S.J. McCormack, Numerical Simulation of a Novel Dual Layered Phase Change Material Brick Wall for Human Comfort in Hot and Cold Climatic Conditions, Energies (Basel). 14 (2021). https://doi.org/10.3390/en14134032.
[89] B. Pandey, R. Banerjee, A. Sharma, Coupled EnergyPlus and CFD analysis of PCM for thermal management of buildings, Energy Build. 231 (2021) 110598. https://doi.org/https://doi.org/10.1016/j.enbuild.2020.110598.
[90] W.G. Su, J. Darkwa, G. Kokogiannakis, Numerical thermal evaluation of laminated binary microencapsulated phase change material drywall systems, Build. Simul. 13 (2020) 89–98. https://doi.org/10.1007/s12273-019-0563-z.
[91] S. Lu, Q. Lin, Y. Liu, L. Yue, R. Wang, Study on thermal performance improvement technology of latent heat thermal energy storage for building heating, Appl. Energy 323 (2022) 119594. https://doi.org/10.1016/j.apenergy.2022.119594.
[92] E. Commission, R. AM, J. Radulovic, B. JM, S. Al-Hallaj, S. Wilke, B. Schweitzer, Comprehensive Review of Compressed Air Energy Storage (CAES) Technologies, in: S. Murad, E. Baydoun, N. Daghir (Eds.), Water, Energy & Food Sustainability in the Middle East, Springer, Cham, 2023: pp. 161–192. https://doi.org/10.1007/978-3-319-48920-9_8.

[93] S. Al-Hallaj, S. Wilke, B. Schweitzer, Energy storage systems for smart grid applications, in: S. Murad, E. Baydoun, N. Daghir (Eds.), Water, Energy & Food Sustainability in the Middle East, Springer, Cham, 2017: pp. 161–192. https://doi.org/10.1007/978-3-319-48920-9_8.
[94] M.E. Yassi, I.E. Abbassi, A. Pierre, Y. Melinge, Comparative Study of Two Materials Combining a Standard Building Material with a PCM, FDMP-FLUID DYNAMICS & MATERIALS PROCESSING 19 (2023) 1283–1290. https://doi.org/10.32604/fdmp.2022.023183.
[95] N. Soares, N. Rosa, J.J. Costa, A.G. Lopes, T. Matias, P.N. Simões, L. Durães, Validation of different numerical models with benchmark experiments for modelling microencapsulated-PCM-based applications for buildings, International Journal of Thermal Sciences 159 (2021) 106565. https://doi.org/https://doi.org/10.1016/j.ijthermalsci.2020.106565.
[96] R. AU, N. Ghafoor, S. SR, Z. Kausar, F. Rauf, F. Sher, et al., A Study of Hot Climate Low-Cost Low-Energy Eco-Friendly Building Envelope with Embedded Phase Change Material, Energies (Basel). 14 (2021) 3544. https://doi.org/10.3390/en14123544.
[97] P.N.S. Teja, S.K. Gugulothu, G.R. Sastry, B. Burra, S.S. Bhurat, Numerical analysis of nanomaterial-based sustainable latent heat thermal energy storage system by improving thermal characteristics of phase change material, ENVIRONMENTAL SCIENCE AND POLLUTION RESEARCH 29 (2022) 50937–50950. https://doi.org/10.1007/s11356-021-15485-y.
[98] A. Yadav, S. Samir, Experimental and numerical investigation of spatiotemporal characteristics of thermal energy storage system in a rectangular enclosure, J. Energy Storage 21 (2019) 405–417. https://doi.org/10.1016/j.est.2018.12.005.
[99] R. Zeinelabdein, S. Omer, E. Mohamed, Parametric study of a sustainable cooling system integrating phase change material energy storage for buildings, J. Energy Storage 32 (2020) 101972. https://doi.org/10.1016/j.est.2020.101972.
[100] N.P. T, D. JMPQ, G. AS, F.M. HL, G. Moreira, B.C. B, et al., Phase Change Material Melting Process in a Thermal Energy Storage System for Applications in Buildings, Energies (Basel). 13 (2020) 3254. https://doi.org/10.3390/en13123254.
[101] K. BE, A. AM, Y. BN, Design and Optimization of Air to PCM Heat Exchanger Using CFD, Arab. J. Sci. Eng. 48 (2022) 12609–12623. https://doi.org/10.1007/s13369-022-07360-w.
[102] I. Baskar, M. Chellapandian, Experimental and finite element analysis on the developed real-time form stable PCM based roof system for thermal energy storage applications, Energy Build. 276 (2022) 112514. https://doi.org/10.1016/j.enbuild.2022.112514.
[103] D.M. Liang, M. Ibrahim, T. Saeed, A.M. El-Refaey, Z.X. Li, M.A. Fagiry, Simulation of a Trombe wall with a number of semicircular fins placed on the absorber plate for heating a room in the presence of nano-PCM, JOURNAL OF BUILDING ENGINEERING 50 (2022). https://doi.org/10.1016/j.jobe.2022.104173.
[104] A.H.N.N. Al-mudhafar, M.T. Hamzah, A.L. Tarish, Potential of integrating PCMs in residential building envelope to reduce cooling energy consumption, CASE STUDIES IN THERMAL ENGINEERING 27 (2021) 101360. https://doi.org/10.1016/j.csite.2021.101360.
[105] S. Srivastava, A. Srivastava, S. Jain, N. Kumar, M. CS, Performance analysis of PCM curtain for thermal comfort, Research Journal of Textile and Apparel 26 (2022) 439–451. https://doi.org/10.1108/RJTA-05-2021-0066.
[106] A.P. Selvaraju, A. Ranganathan, A.A.R. Vincent, P. Arumugam, V. Ramalingam, THERMAL MANAGEMENT ANALYSIS OF PCM INTEGRATION IN BUILDING

USING A NOVEL PERFORMANCE PARAMETER PCM Effectiveness Index, THERMAL SCIENCE 26 (2022) 883–895. https://doi.org/10.2298/TSCI200830208S.
[107] S. Ručevskis, P. Akishin, A. Korjakins, Parametric analysis and design optimisation of PCM thermal energy storage system for space cooling of buildings, Energy Build. 224 (2020) 110288. https://doi.org/10.1016/j.enbuild.2020.110288.
[108] S. Rucevskis, P. Akishin, A. Korjakins, Performance Evaluation of an Active PCM Thermal Energy Storage System for Space Cooling in Residential Buildings, Environmental and Climate Technologies 23 (2019) 74–89. https://doi.org/10.2478/rtuect-2019-0056.
[109] A.U. Rehman, S.R. Sheikh, Z. Kausar, S.J. McCormack, Numerical Simulation of a Novel Dual Layered Phase Change Material Brick Wall for Human Comfort in Hot and Cold Climatic Conditions, Energies (Basel). 14 (2021). https://doi.org/10.3390/en14134032.
[110] W.G. Su, J. Darkwa, G. Kokogiannakis, Numerical thermal evaluation of laminated binary microencapsulated phase change material drywall systems, Build. Simul. 13 (2020) 89–98. https://doi.org/10.1007/s12273-019-0563-z.
[111] E.Y. M, E.A. I, A. Pierre, Y. Melinge, Comparative Study of Two Materials Combining a Standard Building Material with a PCM, Fluid Dynamics & Materials Processing 19 (2023) 1283–1290. https://doi.org/10.32604/fdmp.2022.023183.
[112] N. Soares, N. Rosa, J.J. Costa, A.G. Lopes, T. Matias, P.N. Simões, L. Durães, Validation of different numerical models with benchmark experiments for modelling microencapsulated-PCM-based applications for buildings, International Journal of Thermal Sciences 159 (2021) 106565. https://doi.org/https://doi.org/10.1016/j.ijthermalsci.2020.106565.
[113] R. AU, N. Ghafoor, S. SR, Z. Kausar, F. Rauf, F. Sher, et al., A Study of Hot Climate Low-Cost Low-Energy Eco-Friendly Building Envelope with Embedded Phase Change Material, Energies (Basel). 14 (2021) 3544. https://doi.org/10.3390/en14123544.
[114] P.N.S. Teja, S.K. Gugulothu, G.R. Sastry, B. Burra, S.S. Bhurat, Numerical analysis of nanomaterial-based sustainable latent heat thermal energy storage system by improving thermal characteristics of phase change material, ENVIRONMENTAL SCIENCE AND POLLUTION RESEARCH 29 (2022) 50937–50950. https://doi.org/10.1007/s11356-021-15485-y.
[115] C. Kandilli, B. Mertoglu, An Experimental and Numerical Study on the Optimum Flow Rate of a Photovoltaic Thermal System Integrated with Phase Change Materials, Journal of Engineering Thermophysics 31 (2022) 458–476. https://doi.org/10.1134/S1810232822030080.
[116] D.M. Liang, M. Ibrahim, T. Saeed, A.M. El-Refaey, Z.X. Li, M.A. Fagiry, Simulation of a Trombe wall with a number of semicircular fins placed on the absorber plate for heating a room in the presence of nano-PCM, JOURNAL OF BUILDING ENGINEERING 50 (2022). https://doi.org/10.1016/j.jobe.2022.104173.
[117] A.H.N.N. Al-mudhafar, M.T. Hamzah, A.L. Tarish, Potential of integrating PCMs in residential building envelope to reduce cooling energy consumption, CASE STUDIES IN THERMAL ENGINEERING 27 (2021) 101360. https://doi.org/10.1016/j.csite.2021.101360.
[118] N. Kerroumi, B. Touati, J. Virgone, Thermal performance analysis of sensible and pcm-integrated thermal insulation layers to improve thermal comfort in building, Interfacial Phenom. Heat Transf. 8 (2020) 67–80. https://doi.org/10.1615/InterfacPhenomHeatTransfer.2020034117.
[119] N. Essid, A. Eddhahak-Ouni, J. Neji, Experimental and Numerical Thermal Properties Investigation of Cement-Based Materials Modified with PCM for Building Construction

Use, Journal of Architectural Engineering 26 (2020) 4020018. https://doi.org/10.1061/(ASCE)AE.1943-5568.0000399.
[120] N. Elawady, M. Bekheit, S. AA, A. Radwan, Energy assessment of a roof-integrated phase change materials, long-term numerical analysis with experimental validation, Appl. Therm. Eng. 202 (2022) 117773. https://doi.org/10.1016/j.applthermaleng.2021.117773.
[121] B. Pandey, R. Banerjee, A. Sharma, Coupled EnergyPlus and CFD analysis of PCM for thermal management of buildings, Energy Build. 231 (2021) 110598. https://doi.org/https://doi.org/10.1016/j.enbuild.2020.110598.
[122] I. Baskar, M. Chellapandian, Experimental and finite element analysis on the developed real-time form stable PCM based roof system for thermal energy storage applications, Energy Build. 276 (2022) 112514. https://doi.org/10.1016/j.enbuild.2022.112514.
[123] S. Srivastava, A. Srivastava, S. Jain, N. Kumar, M. CS, Performance analysis of PCM curtain for thermal comfort, Research Journal of Textile and Apparel 26 (2022) 439–451. https://doi.org/10.1108/RJTA-05-2021-0066.
[124] M. Dastmalchi, B. FA, Exergy and economic analyses of nanoparticle-enriched phase change material in an air heat exchanger for cooling of residential buildings, J. Energy Storage 32 (2020) 101705. https://doi.org/10.1016/j.est.2020.101705.
[125] T. Zhou, Y. Xiao, H. Huang, J. Lin, Numerical study on the cooling performance of a novel passive system: Cylindrical phase change material-assisted earth-air heat exchanger, J. Clean. Prod. 245 (2020) 118907. https://doi.org/10.1016/j.jclepro.2019.118907.
[126] R. Zeinelabdein, S. Omer, E. Mohamed, Parametric study of a sustainable cooling system integrating phase change material energy storage for buildings, J. Energy Storage 32 (2020) 101972. https://doi.org/10.1016/j.est.2020.101972.
[127] N.P. T, D. JMPQ, G. AS, F.M. HL, G. Moreira, B.C. B, et al., Phase Change Material Melting Process in a Thermal Energy Storage System for Applications in Buildings, Energies (Basel). 13 (2020) 3254. https://doi.org/10.3390/en13123254.
[128] K. BE, A. AM, Y. BN, Design and Optimization of Air to PCM Heat Exchanger Using CFD, Arab. J. Sci. Eng. 48 (2022) 12609–12623. https://doi.org/10.1007/s13369-022-07360-w.
[129] J. Cofré-Toledo, D. Roa-Cossio, V. DA, C. LF, F. Rouault, Numerical simulation of the melting and solidification processes of two organic phase change materials in spherical enclosures for cold thermal energy storage applications, J. Energy Storage 51 (2022) 104337. https://doi.org/10.1016/j.est.2022.104337.
[130] P. Talebizadehsardari, M. HI, M. JM, M. Gillott, W. GS, D. Grant, et al., Effect of airflow channel arrangement on the discharge of a composite metal foam-phase change material heat exchanger, Int. J. Energy Res. 45 (2021) 2593–2609. https://doi.org/10.1002/er.5949.
[131] T. Hai, S. SM, Z. JM, E.-S. AS, M. Sharifpur, The effect of using tubes filled with phase change materials in the air conditioning system of a residential building, Journal of Building Engineering 49 (2022) 104079. https://doi.org/10.1016/j.jobe.2022.104079.
[132] S. Lu, Q. Lin, Y. Liu, L. Yue, R. Wang, Study on thermal performance improvement technology of latent heat thermal energy storage for building heating, Appl. Energy 323 (2022) 119594. https://doi.org/10.1016/j.apenergy.2022.119594.
[133] A. Yadav, S. Samir, Experimental and numerical investigation of spatiotemporal characteristics of thermal energy storage system in a rectangular enclosure, J. Energy Storage 21 (2019) 405–417. https://doi.org/10.1016/j.est.2018.12.005.
[134] A. Sharma, D. SK, Performance analysis of melting behavior of phase change material encapsulated within differently shaped macro-capsule, International Journal of Energy

and Environmental Engineering 13 (2022) 377–394. https://doi.org/10.1007/s40095-021-00431-y.
[135] B. AK, S. PK, Constructal invasion of fins for melting time prediction of a phase change material in a triplex-tube heat exchanger, J. Energy Storage 54 (2022) 105281. https://doi.org/10.1016/j.est.2022.105281.
[136] J. MM, F. Haghighat, S. Seddegh, Y. Yuan, Simultaneous charging and discharging of phase change materials: Development of correlation for liquid fraction, Solar Energy 188 (2019) 788–798. https://doi.org/10.1016/j.solener.2019.06.051.
[137] Q. Luo, B. Li, Z. Wang, S. Su, H. Xiao, A study of unidirectional spiral tube for air evacuation in a solar heater with phase-change material, Journal of Building Engineering 46 (2022) 103659. https://doi.org/10.1016/j.jobe.2021.103659.
[138] R. Anish, J. MM, S. Seddegh, V. Mariappan, F. Haghighat, Y. Yuan, Sensitivity analysis of design parameters for erythritol melting in a horizontal shell and multi-finned tube system: Numerical investigation, Renew. Energy 163 (2021) 423–436. https://doi.org/10.1016/j.renene.2020.08.153.
[139] S. Lu, X. Zhai, J. Gao, R. Wang, Performance optimization and experimental analysis of a novel low-temperature latent heat thermal energy storage device, Energy 239 (2022) 122496. https://doi.org/10.1016/j.energy.2021.122496.
[140] D.K. Bhamare, M.K. Rathod, J. Banerjee, Numerical model for evaluating thermal performance of residential building roof integrated with inclined phase change material (PCM) layer, Journal of Building Engineering 28 (2020) 101018. https://doi.org/10.1016/j.jobe.2019.101018.
[141] J. Kośny, J. Thakkar, T. Kamidollayev, M.J. Sobkowicz, J.P. Trelles, C. Schmid, S. Phan, S. Annavajjala, P. Horwath, Dynamic Thermal Performance Analysis of PCM Products Used for Energy Efficiency and Internal Climate Control in Buildings, Buildings 13 (2023). https://doi.org/10.3390/buildings13061516.
[142] G. Baldinelli, F. Bianchi, S. Gendelis, A. Jakovics, G.L. Morini, S. Falcioni, S. Fantucci, V. Serra, M.A. Navacerrada, C. Díaz, A. Libbra, A. Muscio, F. Asdrubali, Thermal conductivity measurement of insulating innovative building materials by hot plate and heat flow meter devices: A Round Robin Test, International Journal of Thermal Sciences 139 (2019) 25–35. https://doi.org/10.1016/j.ijthermalsci.2019.01.037.
[143] N. Khalaf Alshammari, A. Trigui, R. Hassani, Thermal and mechanical performance assessment of composite (CPCM) for energy storage, Heliyon 10 (2024) e37212. https://doi.org/https://doi.org/10.1016/j.heliyon.2024.e37212.
[144] A. Kaboré, J.V. Simo Tala, Z. Younsi, D. Bougeard, Experimental characterization of the thermophysical properties of some selected phase change materials for building applications: Critical input data for numerical simulations, J. Energy Storage 111 (2025) 115463. https://doi.org/https://doi.org/10.1016/j.est.2025.115463.
[145] J. Guo, G. Zhang, Investigating the performance of the PCM-integrated building envelope on a seasonal basis, J. Taiwan Inst. Chem. Eng. 124 (2021) 91–97. https://doi.org/10.1016/j.jtice.2021.04.066.
[146] N.J. Wald, C. Rodeck, A.K. Hackshaw, J. Walters, L. Chitty, A.M. Mackinson, Solar Energy Perspectives: Executive summary, J. Med. Screen. 10 (2003) 56–57. https://doi.org/10.1258/096914103321824133.
[147] Y. Cho, J.J. Kim, Lifetime decrease of halogen lamps for automotive by duty cycle stress, IEEE Trans. Reliab. 60 (2011) 550–556. https://doi.org/10.1109/TR.2011.2135730.
[148] AnsysFluent, CFD EXPERTS Simulate the Future, (2021) 231–232.

[149] Y. Lin, G. Alva, G. Fang, Review on thermal performances and applications of thermal energy storage systems with inorganic phase change materials, Energy 165 (2018) 685–708. https://doi.org/10.1016/j.energy.2018.09.128.
[150] F. Kuznik, D. David, K. Johannes, J.J. Roux, A review on phase change materials integrated in building walls, Renewable and Sustainable Energy Reviews 15 (2011) 379–391. https://doi.org/10.1016/j.rser.2010.08.019.
[151] D. Zhou, C.Y. Zhao, Y. Tian, Review on thermal energy storage with phase change materials (PCMs) in building applications, Appl. Energy 92 (2012) 593–605. https://doi.org/10.1016/j.apenergy.2011.08.025.
[152] Y. Zhang, CFD modeling for phase change materials integrated in energy-efficient building envelopes, Energy Reports 9 (2023) 1583–1595. https://doi.org/10.1016/j.egyr.2022.12.187.
[153] R. Moradi, A. Kianifar, S. Wongwises, Optimization of a solar air heater with phase change materials: Experimental and numerical study, Exp. Therm. Fluid Sci. 89 (2017) 41–49. https://doi.org/10.1016/j.expthermflusci.2017.07.011.
[154] G.D. Shekata, G.S. Tibba, A.T. Baheta, CFD simulation of a solar collector integrated with PCM thermal storage, Energy Storage 6 (2024) 1–15. https://doi.org/10.1002/est2.592.
[155] S. Ranjbar, A. Khodadadi, Numerical study on melting process of phase change material in thermal energy storage, Numeri. Heat Transf. A Appl. 77 (2020) 148–165. https://doi.org/10.1080/10407782.2020.1736332.
[156] H. Mahdi, H. Naji, Numerical investigation on the phase change process of PCM in an energy-efficient wall, Energy Build. 183 (2019) 139–149. https://doi.org/10.1016/j.enbuild.2018.11.047.
[157] M. Naghdbishi, M.S. Sefid, Numerical study on the performance of a glazed photovoltaic thermal system integrated with PCM (GPVT/PCM), ArXiv (2021).
[158] A. Basem, A.M. Al-Tajer, I. Omar, H. A. Dhahad, W.H. Alawee, Improvement of heat transfer within phase change materials using V-shaped rods, Heliyon 10 (2024) e28146. https://doi.org/10.1016/j.heliyon.2024.e28146.
[159] C. Amaral, F. Gomez, M. Moreira, T. Silva, R. Vicente, Thermal Performance of Multifunctional Facade Solution Containing Phase Change Materials: Experimental and Numerical Analysis, Polymers (Basel). 15 (2023). https://doi.org/10.3390/polym15132971.
[160] G. Zhang, Y. Min, D. Chen, M. Wang, B. Wang, Optimization study on thermal performance of a novel dynamic phase change material wall, Discover Chemical Engineering 4 (2024). https://doi.org/10.1007/s43938-024-00040-1.
[161] A.I. Brzezinski, Thermal Performance of Multifunctional Facade Solution Containing PCM, Materials 16 (2023) 5236. https://doi.org/10.3390/ma16135236.
[162] Y. Yu, W. Liu, Y. Su, Simulation Study on Dynamic Thermal Performance of a New Ventilated Roof with Form-Stable PCM, Sustainability 12 (2020) 9315. https://doi.org/10.3390/su12229315.
[163] R. Crosby, D. Das, M.C. Paul, Numerical study and experimental validation of a porous biochar supported form stable composite for thermal energy storage, J. Energy Storage 99 (2024) 113314. https://doi.org/10.1016/j.est.2024.113314.
[164] A. Saliby, B. Kovács, Enhancing thermal performance of phase change materials in building envelopes, Pollack Periodica 20 (2025) 87–94. https://doi.org/10.1556/606.2024.01153.
[165] K. El Omari, T. Kousksou, Y. Le Guer, Impact of shape of container on natural convection and melting inside enclosures used for passive cooling of electronic devices,

Appl. Therm. Eng. 31 (2011) 3022–3035. https://doi.org/10.1016/j.applthermaleng.2011.05.036.
[166] A. Ebrahimi, C.R. Kleijn, I.M. Richardson, Sensitivity of numerical predictions to the permeability coefficient in simulations of melting and solidification using the enthalpy-porosity method, Energies (Basel). 12 (2019) 1–22. https://doi.org/10.3390/en12224360.
[167] A. Amatriain, C. Gargiulo, G. Rubio, Numerical and experimental study of open-cell foams for the characterization of heat exchangers, Int. J. Heat Mass Transf. 217 (2023) 1–32. https://doi.org/10.1016/j.ijheatmasstransfer.2023.124701.
[168] N. Yehya, C. Maatouk, H. Charaf, Numerical Analysis of Phase-Change Material Integration in Building Envelopes: A Case Study in Lebanon, Buildings 15 (2025). https://doi.org/10.3390/buildings15081369.
[169] A. Castell, M. Medrano, F. Goia, Modelling envelope components integrating phase change materials (PCMs) with whole-building energy simulation tools: A state of the art, Journal of Facade Design and Engineering 6 (2018) 132–148. https://doi.org/10.7480/jfde.2018.3.2572.
[170] F.J. González Gallero, G.G. Siles, I.R. Maestre, J.L. Foncubierta Blázquez, M. Bottarelli, Experimental validation of a simplified CFD model for a PCM-water finned heat exchanger, International Journal of Low-Carbon Technologies 20 (2025) 234–248. https://doi.org/10.1093/ijlct/ctae293.
[171] R. Crosby, D. Das, M.C. Paul, A. Saliby, B. Kovács, K. El Omari, T. Kousksou, Y. Le Guer, A. Ebrahimi, C.R. Kleijn, I.M. Richardson, A. Amatriain, C. Gargiulo, G. Rubio, N. Yehya, C. Maatouk, H. Charaf, A. Castell, M. Medrano, F. Goia, F.J. González Gallero, G.G. Siles, I.R. Maestre, J.L. Foncubierta Blázquez, M. Bottarelli, T. Alam, D. Bacellar, J. Ling, V. Aute, Numerical Study and Validation of Melting and Solidification in PCM Embedded Heat Exchangers with Straight Tube, International Journal of Low-Carbon Technologies 20 (2025) 113314. https://doi.org/10.1016/j.est.2024.113314.
[172] D. Guarda, F. Wahli, D. Gwerder, J. Martinez-Garcia, A. Stamatiou, J. Worlitschek, S. Mancin, P. Schuetz, Phase Change Material numerical simulation: enthalpy-porosity model validation against liquid fraction data from an X-ray computed tomography measurement/system, Nondestructive Testing and Evaluation 37 (2022) 508–518. https://doi.org/10.1080/10589759.2022.2070164.
[173] J. Vogel, A. Thess, Validation of a numerical model with a benchmark experiment for melting governed by natural convection in latent thermal energy storage, Appl. Therm. Eng. 148 (2019) 147–159. https://doi.org/10.1016/j.applthermaleng.2018.11.032.
[174] B.L. Gowreesunker, S.A. Tassou, Effectiveness of CFD simulation for the performance prediction of phase change building boards in the thermal environment control of indoor spaces, Build. Environ. 59 (2013) 612–625. https://doi.org/10.1016/j.buildenv.2012.10.004.
[175] E. Zavrl, U. Tomc, M. El Mankibi, M. Dovjak, U. Stritih, Parametric study of an active-passive system for cooling application in buildings improved with free cooling for enhanced solidification, Sustain. Cities Soc. 99 (2023) 104960. https://doi.org/10.1016/j.scs.2023.104960.
[176] A. Kasaeian, CFD simulation of a solar collector integrated with PCM thermal storage, Renew. Energy 191 (2022) 297–309. https://doi.org/10.1016/j.renene.2022.04.005.
[177] A. Fluent, MAN - ANSYS Fluent User' s Guide Releasde 15.0, Knowledge Creation Diffusion Utilization 15317 (2013) 724–746.
[178] RUBITHERM, RT21HC, (2020) 2020. https://www.rubitherm.eu/media/products/datasheets/Techdata_-RT21HC_EN_09102020.PDF (accessed February 15, 2021).
[179] Global Monitoring Laboratory, Solar Calculation Details, (n.d.).

[180] BBC, Light and sound - reflection and refraction, (2021). https://www.bbc.co.uk/bitesize/guides/zchyj6f/revision/2 (accessed April 15, 2021).
[181] Norrsken, WHY USE TRIPLE GLAZED WINDOWS & DOORS?, (2020). https://www.norrsken.co.uk/sustainability/why-triple-glazing (accessed December 12, 2022).
[182] G.P. Thomas, What is Aerogel? Theory, Properties and Applications, (n.d.). https://www.azom.com/article.aspx?ArticleID=6499 (accessed May 3, 2021).
[183] L. Kosmina, Guide to In-situ U-value measurement of walls in existing dwellings In-situ measurement of U-value, Bre (2016) 1–13.
[184] Y.J. Lee, J.H. Moon, D.S. Choi, M.J. Ko, Influences of Average Temperature Difference and Measurement Period on Estimation of In Situ Thermal Transmittance of Building Exterior Walls Using the Average Method of ISO 9869-1, Energies (Basel). 17 (2024) 1–16. https://doi.org/10.3390/en17051177.
[185] C. Wu, R. Buyya, Cost Model Categories, Cloud Data Centers and Cost Modeling (2015) 611–647. https://doi.org/10.1016/B978-0-12-801413-4.00015-5.
[186] Horizon windows and doors, (n.d.). https://horizonwindows.ie/blog/triple-glazing-cost/ (accessed April 18, 2026).
[187] M. Ganobjak, W.J. Malfait, J. Just, M. Käppeli, F. Mancebo, S. Brunner, J. Wernery, Get the light & keep the warmth - A highly insulating, translucent aerogel glass brick for building envelopes, Journal of Building Engineering 64 (2023). https://doi.org/10.1016/j.jobe.2022.105600.
[188] Ł. Mika, E. Radomska, K. Sztekler, A. Gołdasz, W. Zima, Review of Selected PCMs and Their Applications in the Industry and Energy Sector, Energies (Basel). 18 (2025). https://doi.org/10.3390/en18051233.
[189] X. Zhang, H. Zhang, Y. Wang, X. Shi, Adaptive Façades: Review of Designs, Performance Evaluation, and Control Systems, Buildings 12 (2022). https://doi.org/10.3390/buildings12122112.
[190] P. Marin, M. Saffari, A. de Gracia, X. Zhu, M.M. Farid, L.F. Cabeza, S. Ushak, Energy savings due to the use of PCM for relocatable lightweight buildings passive heating and cooling in different weather conditions, Energy Build. 129 (2016) 274–283. https://doi.org/10.1016/J.ENBUILD.2016.08.007.
[191] H. Akeiber, P. Nejat, M.Z.A. Majid, M.A. Wahid, F. Jomehzadeh, I. Zeynali Famileh, J.K. Calautit, B.R. Hughes, S.A. Zaki, A review on phase change material (PCM) for sustainable passive cooling in building envelopes, Renewable and Sustainable Energy Reviews 60 (2016) 1470–1497. https://doi.org/10.1016/J.RSER.2016.03.036.
[192] European statistics on electricity prices for household and final non-household customers, (n.d.). https://doi.org/https://doi.org/10.2908/NRG_PC_204.
[193] F. Khlissa, M. Mhadhbi, W. Aich, A.K. Hussein, M. Alhadri, F. Selimefendigil, H.F. Oztop, L. Kolsi, Recent Advances in Nanoencapsulated and Nano-Enhanced Phase-Change Materials for Thermal Energy Storage: A Review, PROCESSES 11 (2023). https://doi.org/10.3390/pr11113219.
[194] J.M. Khodadadi, S.F. Hosseinizadeh, Nanoparticle-enhanced phase change materials (NEPCM) with great potential for improved thermal energy storage, International Communications in Heat and Mass Transfer 34 (2007) 534–543. https://doi.org/10.1016/j.icheatmasstransfer.2007.02.005.
[195] Z. Ma, W. Lin, M.I. Sohel, Nano-enhanced phase change materials for improved building performance, RENEWABLE & SUSTAINABLE ENERGY REVIEWS 58 (2016) 1256–1268. https://doi.org/10.1016/j.rser.2015.12.234.

DOCTORAL THESIS PUBLICATIONS

1. Narbuts, J., Vanaga, R., Freimanis, R., Blumberga, A. Laboratory and outdoor testing of small-scale active solar facade module. Environmental and Climate Technologies 2021, vol. 25, no. 1, pp. 455–466. Available: doi: https://doi.org/10.2478/rtuect-2021-0033
2. Vanaga, R., Narbuts, J., Freimanis, R., Blumberga, A. Laboratory testing of small-scale solar facade module with phase change material and adjustable insulation layer. *Energies.* 2022, 15, 1158. Available: https://doi.org/10.3390/en15031158
3. Narbuts, J., Blumberga, A., Zundāns, Z., Freimanis, R., Bāliņš, R., Vanaga, R. The Effect of Fresnel Lens Focal Point Location on Heat Transfer in Phase Change Material (PCM) Enhanced Dynamic Solar Facade. Environmental and Climate Technologies, 2022, vol. 26, no. 1, pp. 1268–1278. e-ISSN 2255-8837. Available: doi:10.2478/rtuect-2022-0096
4. Vanaga, R., Narbuts, J., Zundāns, Z., Blumberga, A. On-site Testing of Dynamic Facade System with the Solar Energy Storage, *Energy,* 2023, vol. 283, 128257, ISSN 0360-5442. Available: https://doi.org/10.1016/j.energy.2023.128257
5. Vanaga, R., Narbuts, J., Freimanis, R., Zundāns, Z., Blumberga, A. Performance Assessment of Two Different Phase Change Materials for Thermal Energy Storage in Building Envelopes, *Energies*, 2023, vol. 16, no. 13, 5236. Available: https://doi.org/10.3390/en16135236
6. Narbuts, J., Vanaga, R. Revolutionizing the Building Envelope: A Comprehensive Scientific Review of Innovative Technologies for Reduced Emissions. Environmental and Climate Technologies 2023, vol. 27, no. 1, pp. 724–737. Available: https://doi.org/10.2478/rtuect-2023-0053
7. Vanaga, R., Narbuts, J., Zundāns, Z., Gušča, J. Systematic literature review of software tools for modeling heat transfer in phase change materials for building applications. *IOP Conference Series: Earth and Environmental Science*. 2024, 1372 012017. Available: https://doi.org/10.1088/1755-1315/1372/1/012017

PAPER 1: LABORATORY TESTING OF SMALL-SCALE ACTIVE SOLAR FACADE MODULE

Environmental and Climate Technologies
2021, vol. 25, no. 1, pp. 455–466
https://doi.org/10.2478/rtuect-2021-0033
https://content.sciendo.com

Laboratory Testing of Small-Scale Active Solar Façade Module

Janis NARBUTS[1*], Ruta VANAGA[2], Ritvars FREIMANIS[3], Andra BLUMBERGA[4]

[1–4]*Institute of Energy Systems and Environment, Riga Technical University, Riga, Latvia*

***Abstract* – Buildings are linked to a significant untapped energy saving potential, accounting for 40 % of European Union's (EU) final energy and 36 % of CO_2 emissions. Energy efficient building envelopes plays the key role to achieve decarbonization of the EU's building stock by 2050. Active building envelopes are emerging and novel trend offering the paradigm shift in perception of building enclosures. Paper presents study of active solar façade containing phase change material for energy storage. Study seeks for optimisation of solar façade module by introducing dynamic component and variating in the composition of module itself to ensure faster energy harvesting and minimise the heat losses at discharging phase. Comparative tests were carried out in laboratory, in controlled heating and cooling conditions to evaluate impact of dynamic component. The dynamic component has reflective inner coating that focuses solar radiation on the element in heating phase and aerogel insulation filling in the blades that decreases heat loss in the cooling phase. Varying components in the design were used– thickness of aerogel insulation, Fresnel lens and width of concentrating cone diameter. Wide range of phase change material average temperature was observed 24 °C in setups with full aerogel filling to 50 °C in setup Fresnel lens. Average temperature in phase change material was reached higher in all setups with dynamic component compared to identical setups without dynamic component. Temperature differences were in the range from 1 °C in aerogel filled setups till 6 °C in setups with Fresnel lens.**

***Keywords* – Building envelope; energy efficiency; policy for buildings; renewable technology; solar energy; thermal storage**

1. INTRODUCTION

Many Intergovernmental Panel on Climate Change (IPCC) Assessment Reports, United Nations Framework Convention on Climate Change (UNFCCC) papers, protocols, and international agreements highlight energy saving and energy demand reduction as primary mitigation options [1]. Buildings are linked to a significant untapped energy saving potential, accounting for 40 % of EU final energy and 36 % of CO_2 emissions [2]. EU Energy Performance of Buildings Directive sets the goal of building decarbonization by 2050. Following the traditional path of energy efficiency strategies, it will be difficult to achieve ambitious goal. There is an urge for innovative technologies for building energy efficiency. Due to the demographic growth and changes in human lifestyles brought on by technological advancements and urbanization, it is expected that the energy consumption can increase by 53 % in the next decade, potentially increasing GHG pollution from this field [3]. A lot of the energy presently used in buildings is wasted due to out-of-date construction practices. There is a high demand of innovative technological solutions for the significant reduction of heating

* Corresponding author.
E-mail address: j.narbuts@gmail.com

and cooling in buildings. Most of the building technologies today are based on static principle and conventional building insulation materials. To provide the necessary comfort for the inhabitants living inside the building and at the same time ensure high energy efficiency performance, building envelopes has to adapt to environmental conditions. New design trends of active building envelopes as dynamic and kinetic façades have appeared that are responding to surrounding environmental conditions such as sound, light, wind, heat and humidity [4].

1.1. Active building envelopes (ABEs)

Thanks to a growing demand to satisfy more progressive environmental, social and economic performance requirements, successful building style is changing into a more and more advanced task. The appliance of climate adaptive building envelopes has lately been suggested as a hopeful option among this try for increased rate of sustainability within the designed setting. Compared to traditional façades, ABEs provide possibilities that can occur for energy economy in addition improvement of indoor climate conditions [5]. These envelopes should be ready to adapt to the current condition and even return to their normal state if necessary in order to produce the intended outcome [6]. ABEs fulfil a number of requirements that are either incompatible or contradictory, such as finding a balance between sunlight and shadow, fresh air and draft, airflow and moisture, shutters and reflectors, heat gains and overheating [7]. There are various ways to achieve the dynamism of the envelope for example the moving components can be introduced by airflows or a chemical change of the material, but make it sufficient, adaptive features must be integrated into a whole system [8]. They can be categorized by several independent characteristics such as climatic factors (heat, light, air, water or other types of energy), the time frame scale, the scale of change [9], the control type (intrinsic or extrinsic regulators), the spatial scale (size of a system), the inspirational scale (biomimetic adaptive building skins), the development stage, the number of functions and the performance task [10]. ABEs are building element systems that:

- effectively manages the cooling and heating capacity of itself, reducing the load on central heating, ventilation, and air conditioning (HVAC) systems and often replacing their work by mechanical, electrical, or chemical actions;
- performs as energy converter by transforming renewable energy (solar, wind) into mechanical or chemical energy to improve the performance of the building [11].

Solar responsive systems work by converting solar energy into various forms. More detailed review on these systems can be found in studies [12]–[14]. They are usually based on 5 types of solar control devices: external, integrated, internal, double skin and ventilated cavity [6]. Heat too is a form of solar energy. Solar heat systems are designed and work to gain the maximum heat during wintertime and minimalize it during the summer months. The solar barrel wall, rooftop water tanks, dynamic adaptable insulation, and colour-changing (thermos-chromic) materials on walls or windows are some examples of this technology [8].

Light is another form of solar energy that can be controlled by indoor illuminance levels, distributions, window views, and glare in systems that use this energy source. Classic mechanical systems such as venetian blinds, advanced mechanical systems that can rotate, slide and self-adjust, and smart glass or transparent thermos-chromic or photo-chromic materials are the three major approaches to achieve these functions. Systems used in windows, usually adapt their optical characteristics such as lighting angle and direction, visual aspects, and already mentioned thermo-chromic properties. Electrical façade glazing for buildings, for example, has evolved to be able to work in market condition and is by far the likely choice for smart building materials.

Luo *et al.* have highlighted in the review of active building envelopes that the studies in this field is insufficient [11]. There are available in decent amount of studies on photovoltaic systems and building integrated PV systems are even recognised by Faunhofer institute as the only mass-produced system [15]. More attention have been paid to passive strategies and there is a lack of studies devoted to active systems. Study on presented in paper solar façade module will enrich the knowledge base in the field of active building envelopes, solar thermal façades and building components containing phase change materials.

1.2. Phase change materials (PCMs)

Through temperature differences in controlled conditions, phase change materials (PCM) allow energy to be stored and released according to heating and cooling demands [16]. A wide range of phase change materials are available depending on the temperature range needed. Solid-liquid PCMs are the most common to use in the building sector and they are divided into three main categories: organic, inorganic, and eutectics [17]. The most commonly used organic PCMs are based on paraffin, fatty acid and sugar alcohols with the temperature range of 0 °C to 150 °C. Paraffin is usually used because of its low temperature performance from −10 °C to 100 °C [18]. Hydrated salts are the mainly used inorganic PCMs due to their medium-low temperature heat storage properties. These materials are available and inexpensive, however they suffer from such problems as sub-cooling and phase separation [19]. Eutectics are mixtures of multiple solids in different ratios to reach the lowest melting temperature. The density of their storage volume is slightly higher than in organic compounds [20]. They can be divided in three main groups: organic-organic, inorganic-inorganic and inorganic-organic.

PCMs are used for wide range of applications in the latest decades such as thermal storage materials, air-conditioning systems, electronics, medicine and building envelopes [18]. In most cases temperature range for the building applications varies from −10 °C to +70 °C. PCMs such as salt hydrates, sugar alcohols, fatty acids, polyethylene glycols and paraffins are suitable for applications in building sector due to their melting point properties. Three fundamental considerations influence the choice of PCMs in any application: melting temperature, latent heat of fusion, and PCM thermo-physical concerns. Two key conditions in the selection method are a high heat of fusion and a specific melting/solidification temperature [21].

PCMs can be applied in passive storage systems such as walls, windows, ceilings, floor and roof where no mechanical interference is used to initiate charge and discharge cycles whereas in the active systems energy is added to make the storage system operate as necessary [22].

Research has been launched to develop an innovative dynamic façade system with solar energy storage and to evaluate the energy performance of the proposed technology. The technology is based on several previous studies of the solar façade module containing phase change material as energy storage media, silica aerogel as insulation layer and Fresnel lens for concentration of solar energy. Vanaga *et al.* [23] described comparative study – façade system containing phase change material was compared to the performance of traditional wall containing thermal insulation layer in small scale PASLINK type test cell that imitates building thermal envelope. In one cell solar façade module was built, in another test cell traditional lightweight wall construction was imitated. It was measured in 24h outdoor testing that in autumn façade system containing phase change material ensured higher indoor temperature than traditional wall. Širmelis *et al.* [25] performed laboratory testing seeking for optimisation of solar façade module. Six alternative module compositions were developed – with air gap, full aerogel filling, cone shaped insulation layer and these three were

multiplied in two variations: with and without the Fresnel lens. Results were compared with reference wall results. Small scale PASLINK test cell was used for indoor testing in climate chamber that ensured defined 'outdoor' temperatures and solar radiation simulation. Under these conditions laboratory testing results highlighted that 1) all modules containing phase change material ensured higher indoor temperature, thus demonstrating the advantages of energy storage thermal envelope and 2) all modules containing Fresnel lens ensured higher indoor temperature. In extended 48h testing period Mols *et al.* [24] revealed in detail charging end discharging processes in proposed façade modules. Gained results showed that despite wide range of peak temperatures at charging phase (22 °C to 35 °C) after 24h temperature in both indoor space in phase change material are close in all setups. In second 24h period devoted for discharging, less insulated modules lagged behind temperature wise. It was concluded that the combination between faster charging and slower discharging would provide better performance.

2. METHODOLOGY

Study presented in this paper seeks for optimisation of solar façade module developed in previous studies by introducing dynamic component and variating in the composition of module itself to ensure faster energy harvesting and minimise the heat losses at discharging phase. Basic structure is similar to the one in previous studies – it consists of phase change material that stores collected thermal energy and insulation layer. Introducing dynamic component in the next research steps will provide solar tracking function to absorb solar energy, respond to changing outdoor conditions (temperature and solar radiation) and diminish heat loos to the outdoor in discharging phase.

Launched research within upcoming years will follow the route reflected in Fig. 1. It consists of 4 stages – starts with conceptual design, followed by indoor and outdoor testing and ends with large scale testing where knowledge gained in first stages will be aggregated. The scope of this paper lies in first two stages of research – developing concept and indoor testing.

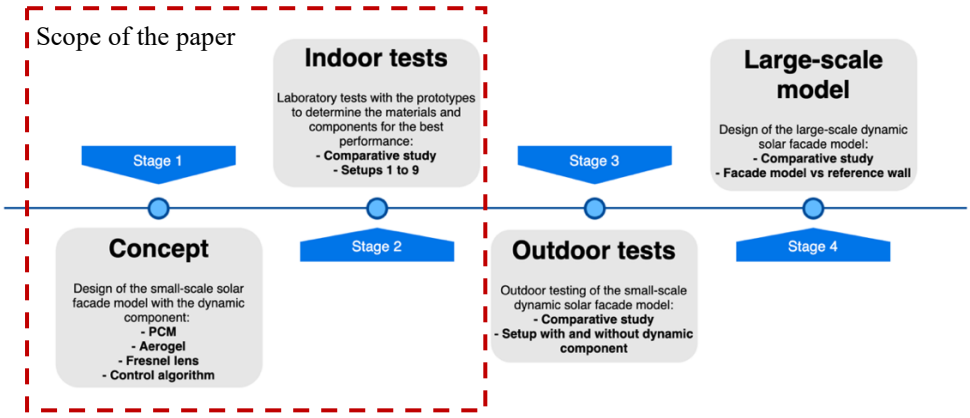

Fig. 1. Methodology of the research and the scope of the paper.

It is suggested to advance solar façade module by introducing dynamic element at the outer surface. Element consists of rotatable blades that opens and closes depending on the availability of solar radiation. Blades are covered with reflective coating and performs solar

tracking, thus harvesting more solar energy. When solar energy is available at a necessary intensity, blades opens and concentrates energy in the centre of the solar façade module where it is accumulated in phase change material. When solar radiation is at low intensity or at night rotating blades are closed to diminish the heat loss to surrounding environment thus allowing energy accumulated in phase change material to dissipate at a slower rate. The structure of the element is described in next chapters. The experiments in second stage are performed in controlled laboratory conditions as described later in the paper. Aim of indoor testing is to evaluate the impact of dynamic element on performance of solar façade composition variations.

2.1. Setups of solar façade module for the test

The design of the system with solar energy storage was based on the previous study [24], using the components and materials that showed the best performance results. The components included in the design is listed in Table 1.

TABLE 1. COMPONENTS OF THE WALL FAÇADE MODULE

Component	**Characteristics**
Phase-change material (PCM)	RUBITHERM RT21HC Melting area: 20–23 °C Congealing area: 21–19 °C
PCM glass container	Dimensions: 127×127×60 mm
Plastic box	Material: Polyethylene terephthalate glycol (PETG)
Cone	Material: Acrylonitrile styrene acrylate (ASA) white
Glass	Dimensions: 129×129×4 mm
Poly (methyl methacrylate) (PMMA) glass	Dimensions: 127×127×2 mm
Fresnel lens	Dimensions: 127×127×1.5 mm Focal length: 71.12 mm
Aerogel 1 Aerogel 2 Aerogel 3	LUMIRA translucent aerogel LA1000 ENERSENS Kwark GS Thermal Wrap 8 mm blanket

RUBITHERM RT21HC is paraffin wax PCM with high thermal energy storage capacity of 190 kJ/kg. It is chemically inert and has no super-cooling effect. It is described by manufacturers as a long-life product, with stable performance through the phase change cycles. For the better solar energy concentration on the PCM, Edmund Optics Fresnel lens was used. It has a series of concentric grooves etched into plastic. The processing of solar light, which is nearly parallel, is one of the most popular uses for a Fresnel lens.

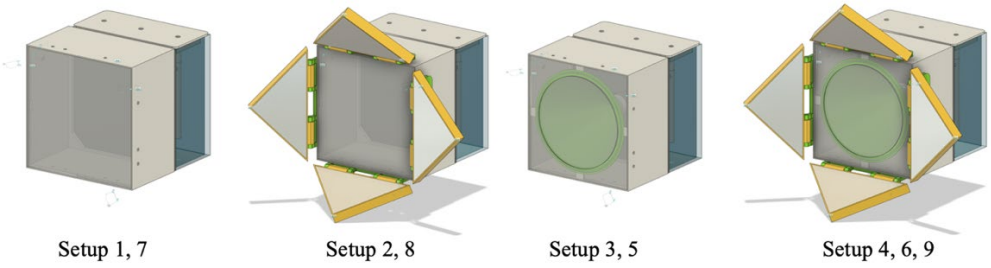

Fig. 2. Drawings of module in different setups.

Three kinds of aerogel were used for insulation. Aerogel 1 is LUMIRA Translucent Aerogel LA1000. It is a high-performance thermal insulator made from a modified, synthetic amorphous silica gel. The particle size ranges from 0.7 to 4 mm and the light transmission is more than 90 % per cm. Aerogel 2 is ENERSENS Kwark GS. This aerogel was chosen because of its high thermal conductivity performance (0.018–0.022 $Wm^{-1}K^{-1}$) and its small particle size (10 to 1250 micrometres). Thermal Wrap 8 mm blanket or Aerogel 3 was used as filling for the blades due to its flexibility. The main difference comparing to the previous study is the implementation of dynamic component – rotating blades. This component has two main functions – concentrating light to the element to gain solar energy intensity and aerogel inner filling to protect module from heat loss. To determine the best combination of elements and materials in module, tests were performed in several setups. All setups had PCM, PCM glass container, glass and plastic box components unchanged during the whole first phase. Depending on the results of each setup some corrections and upgrades were made to reach better performance of the solar façade module such as change in the volume of aerogel filling and cone diameter. The components of all the setups are listed in the Table 2 and the drawings of different setups are illustrated in Fig. 2. The aerogel filament for setups 1 and 2 was chosen accordingly to the focal length in setups 3 to 6, but in setup 7 and 8 it was equated to the volume of filament in setups 3 and 4. Cone diameter from 1.5 to 2.4 cm in setups 5 and 6 was changed to improve the heat transmission to PCM.

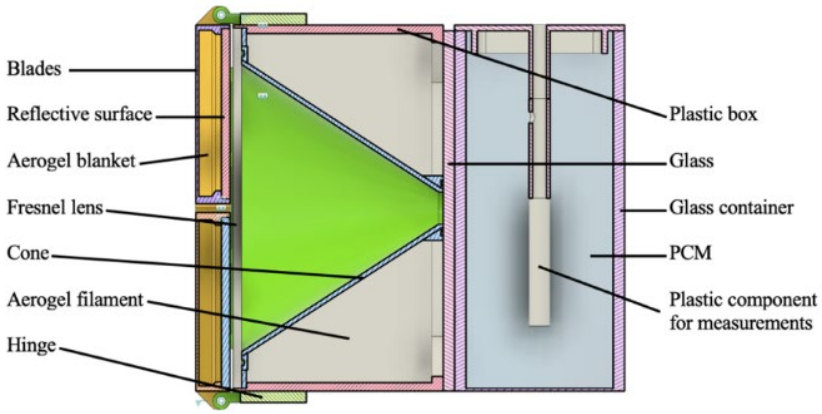

Fig. 3. Cross-section of a solar façade module with dynamic component.

Fig. 3 represents the cross-section of the solar façade module with dynamic component. Module consists of 3 main elements – dynamic component (blades with hinges), heat transmission element (Fresnel lens, cone and plastic box) and energy storage (PCM). Plastic component for measurements is necessary to determine the temperature in different spots of PCM during the test. Glass container was made out of 5 sheets of 4 mm glass glued together with silicon paste. The glass component seals the aerogel in heat transmission element so that it can be easily moved between setups. Plastic box, hinges and the blades were printed out using 3D printer. Settings for the printer was chosen accordingly to printing filament. For the hinges and plastic boxes, the printing material was chosen PETG which is durable and tough with high impact strength with maximum service temperature from 51 °C to 64 °C. As the

plastic box nor hinges gets to exposed to intensive solar radiation, the material is completely compatible for its purpose.

TABLE 2. COMPONENTS IN ALL OF THE SETUPS

Setup	1	2	3	4	5	6	7	8	9
Phase-change material (PCM)	+	+	+	+	+	+	+	+	+
PCM glass container	+	+	+	+	+	+	+	+	+
Glass	+	+	+	+	+	+	+	+	+
Plastic box	+	+	+	+	+	+	+	+	+
Hinges		+		+		+		+	+
Aerogel 1 (1006.69 cm^3)	+	+							
Aerogel 1 (768.47 cm^3)					+	+	+	+	
Aerogel 1 (763.62 cm^3)			+	+					
Aerogel 2 (683.80 cm^3)									+
Aerogel 3		+		+		+		+	+
Cone (diameter 1.5 cm)			+	+					
Cone (diameter 2.4 cm)					+	+			
Cone (diameter 4 cm)									+
Fresnel lens			+	+	+	+			+
Blades with reflector and aerogel filling		+		+		+		+	+

The blades and cones were printed out using ASA material because of its resistance in high temperatures (up to 105 °C). Cone, glass and lens were fixed together using transparent glue. The inner part of the blade has a shelf design so it can hold in the aerogel blanket from one side and provide the space for reflective component to lay down and seal from the other side. PMMA mirror was used as the reflective element of the blade.

This decision was made based on the characteristics of the component. PMMA is tough, durable and lightweight thermoplastic and its density is a half less than that of glass. It was cut into a triangle shape so that it can fit into the design of blade. Aerogel Thermal Wrap blanket was used as filling because of its superior thermal and insulation performance. Its operating temperature range is −200 °C up to 125 °C and thermal conductivity at room temperature is around 23 $mWm^{-1}K^{-1}$. To reduce the heat loss while the ambient temperature is lower than the temperature in PCM, rubber sealing was introduced to the air gaps of dynamic component.

2.2. Experiment planning

The main goal of the second stage laboratory test is to find out the most efficient and the most appropriate solar façade module for the outdoor testing, considering the temperature and heat flow performance of the PCM energy storage. Tests are carried out as a comparative study between different setups and taking place in a controlled indoor environment. The conditions including heating and cooling are provided equal for all of the setups. Conditions of experiment is summarised in Table 3.

TABLE 3. CONDITIONS OF THE EXPERIMENT

Condition	Value
Heating	7 hours
Cooling	17 hours
Irradiance	1000 W/m^2
Temperature of PCM	16 °C
Cooling temperature	2 °C
Cooling humidity	30 %

The length of the test is 24 hours. The heating phase of 7 hours is chosen based on spring and autumn whether conditions in temperate climate zone with an average daily solar irradiance of 1000 W/m^2. The temperature of PCM at the beginning of the test is set 16 °C to ensure the PCM is still in solid form as the melting starts from 20 °C. Cooling temperature is lowered to 2 °C to imitate the conditions in the night time. The necessary irradiance in the heating phase is provided by Litecraft PAR 64 light. The value of irradiance is set manually using the dimmer. In the cooling stage the test module is placed in environmental test chamber where the required temperature and humidity is set (see Fig. 4).

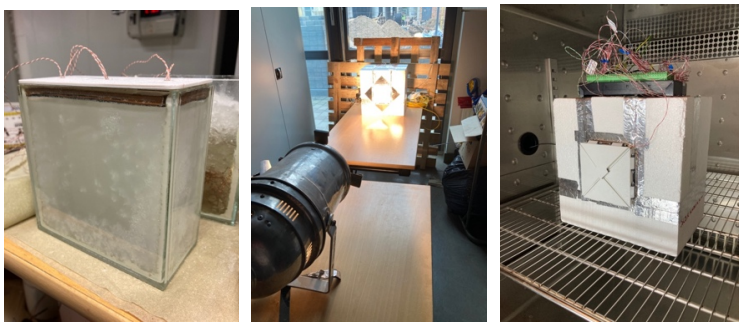

Fig. 4. PCM in solid state (left), heating phase (in the middle) and cooling phase (right).

PCM component is cooled to solid state (16 °C) before the insertion in the testing setup module. In the setups with dynamic component (setups 2, 4, 6, 8 and 9) the reflective blades have been set that they focus the light from the source to the centre of tested module in heating phase but during the cooling phase blades have been closed and fixed with the screws in hinges.

2.3. Selection of measuring equipment

During the test measurements are registered via Multipurpose data logger CR1000 Campbell Scientific combined with multiplexer AM16/32 Campbell Scientific. The period of data reading is one minute. Pyranometer CMP3, Kipp & Zonen is used to measure solar radiation and the usage for Type K thermocouples is to measure temperature in PCM. To capture heat flow and temperature measurements, Flux Tecq PHFS-01e sensors are used.

Temperatures inside the PCM is measured in 6 spots. Ambient room and outdoor temperature as well as temperature measures inside the cones in different setups has been taken. Heat flow and temperature measurements were taken by adding a heat flux sensor on the lens or PMMA (depending on the setup) in the cooling cycle.

3. RESULTS AND DISCUSSION

3.1. Laboratory testing results

Fig. 6 shows the graph of average temperature comparison between all setups. The first tests were done with Setups 1 and 2, where the thickness of aerogel filling was equalled to the length of the focal point of Fresnel lens. Temperature measurements in PCM showed that the phase change happens only in the upper layer of PCM. The lower layer does not reach the temperatures as high to completely melt. In the Setup 2 blades were added to concentrate more light on the test module. However, the temperature performance was similar to the Setup 1 and the phase change was not registered in all of the layers. In the comparison between average temperatures in PCM, Setup 2 reaches 1 °C higher at a peak. To provide faster energy transfer to PCM in the charging phase, the cone and Fresnel lens were added in the Setup 3 and Setup 4. Thermocouple sensor was added inside the cone to observe the temperature in the air gap between the lens and the PCM container. The temperature registered inside the cone was 75.6 °C in Setup 4 and the highest temperature inside the PCM was approximately 1.5 °C higher than in Setup 3. Based on temperatures in measurement points it is concluded that the phase change in all of the layers in PCM has happened in both of these setups (Setups 3 and 4). Due to higher temperatures inside the PCM reached in Setup 4, the time it takes to release heat is longer. Compared to first three setups, Setup 4 shows the best temperature performance in both, charging and discharging cycles of the PCM – temperatures are higher, and the solidification cycle takes longer time.

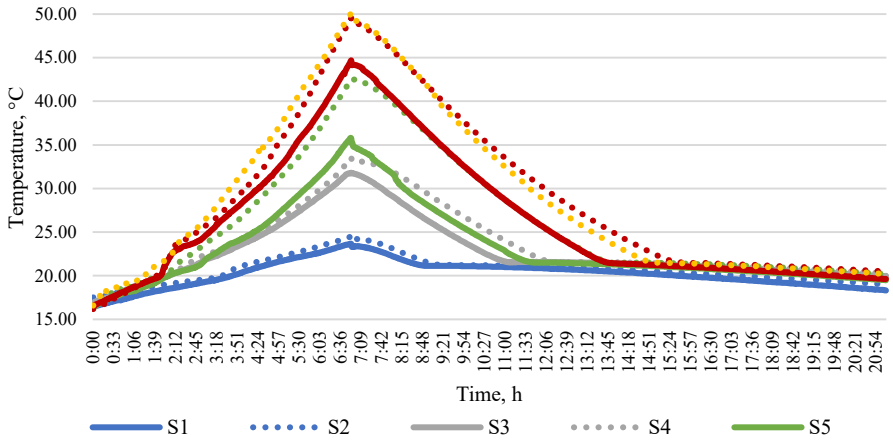

Fig. 6. Average temperature comparison in PCM between setups. Dotted lines for setups with blades.

Despite the fact that all the layers of PCM has reached the phase change in Setup 3 and 4, the maximum temperature in the lower layers does not exceed 28.5 °C. However, the temperatures in cone are high in both setups (69 °C and 75.6 °C) that points to a potential of using this heat to gain higher temperatures in PCM. For this reason, cone diameter (from 1.5 cm to 2.4 cm) at the PCM glass container was introduced in Setups 5 and 6. Temperature graphs shows that the phase change in lower layers has happened faster (approximately after 5:30 h) in Setup 6 compared to previous setups and the temperatures inside the PCM are higher as well, peaking at 40.6 °C and 46.4 °C in Setups 5 and 6 accordingly.

PCM in Setup 1 and 2 did not reach the phase change in lower layers possibly because of the thick aerogel coating. In Setups 7 and 8 the aerogel layer was reduced by the volume of cone in Setups 5 and 6. It is visible that the change of the aerogel coating layer dramatically effects the performance of the test module. Average PCM temperature peaks from 23.7 °C in Setup 1 to 49.5 °C in Setup 8. In Setup 8 phase change in the lower layers of PCM starts already at 4:40 h and the solidification period is the longest compared to all previous setups. These differences are significant between Setups 7 and 8 as well that highlights the positive effect of added blades. Comparing Setups 6 and 8, it is visible that the setup with cone (Setup 6) is lacking performance in average maximum temperature (42.57 °C in Setup 6 and 49.53 °C in Setup 8) and the length of the solidification of PCM (7 hours in Setup 6 and 8:30 hrs). Besides that, the high temperature inside the cone (the highest peak of 79 °C) indicates a possibility to transfer more heat energy to the PCM. Considering all of the factors mentioned above the test module for Setup 9 was designed. The cone diameter was increased from 2.4 cm to 4 cm and different kind of aerogel (Aerogel 3) with better thermal performance properties was introduced.

It is clearly seen that all of the setups with the dynamic component presents better thermal performance in heating and cooling cycles (see Fig. 8). In spite the slight lack of temperature performance in Setup 9 in solidification phase of the PCM comparing to Setup 8, it gathers significantly more heat in the charging phase. Due to the usage of cone and lens, heat energy is transferred to the PCM much faster. The aerogel used in Setups 1, 2, 7 and 8 is translucent and transfers solar radiation well, however, it takes some time and higher temperatures to deliver heat energy to the PCM. The solution in Setup 9 is more adaptive to changing environmental conditions and responds more dynamically by rising temperature in PCM and initiating melting and latent energy storing faster.

3.2. Further study

Setup 9 with cone diameter 4 cm and rotating blades demonstrated the highest performance – it had the fastest charging rate and due to the gained sensible heat, it entered solidification phase later in time compared to other setups – and is suggested for outdoor testing in the next steps of the research. Comparative testing is suggested for outdoor testing as well to evaluate the impact of dynamic component on overall performance of solar façade under real climatic conditions. Laboratory testing was performed in static circumstances – blades opened in optimal position in charging phase and closed in discharging phase. For outdoor testing, control mechanism will be applied to ensure the solar tracking function for blades and faster energy harvesting.

Results gained in laboratory and presented in paper are suitable for verification mathematical modelling. Mathematical modelling compared to laboratory testing allows exploring wider range of climatic conditions and dynamics. Verification of mathematical modelling results with laboratory testing raises the liability of modelling results. Verified model would allow to explore further optimisation strategies of solar façade model design to find optimal balance between charging and discharging of various climatic conditions.

4. CONCLUSION AND RECOMMENDATIONS

A new technology of dynamic façade with solar energy storage has been developed and tested in laboratory under controlled conditions. 9 designs of a small-scale façade modules were tested in laboratory with and without dynamic component – rotating blades that functions as solar energy concentrator during the availability of sun and as additional insulator

(blades with reflective surface and aerogel filling) when it is unavailable. Laboratory tests show the potential of dynamic component in proposed technology in both – thermal energy absorption in the PCM charging phase and storage in discharging phase. Wide range of phase change material average temperature was observed in laboratory testing under defined solar simulation and temperatures 24 °C in setups 1 and 2 with 7 cm aerogel filling to 50 °C in setup 9 with wider cone diameter (4 cm). Average temperature in phase change material was reached higher in all setups with dynamic component compared to identical setups without dynamic component. Temperature differences were in the range from 1 °C in aerogel filled (7 cm) setups 1 and 2 till 6 °C in setups 5 and 6.

Introduced Fresnel lens ensures more dynamic thermal behaviour of the module. Under real climatic loads it is crucial to enhance heat transfer when certain level of solar radiation is achieved especially in the conditions when sun shines periodically during the day.

Developed façade module demonstrates a potential to become on-site renewable energy storage media ensuring conversion of solar energy to thermal energy. Some further improvements are necessary to make for proposed façade module's dynamic component to increase the energy efficiency such as reflective component`s performance should be controlled more dynamically according to changing environmental conditions and the air movements should be reduced by optimising air tightness.

ACKNOWLEDGEMENT

This study has been supported by Fundamental and Applied Research project "Smart building EnVElope with solaR Energy STorage (EVEREST)", project No. lzp-2019/1-0363, funded by the Latvian Council of Science.

REFERENCES

[1] Lazzaroni M., Bianchi Porro G. Preparation, premedication and surveillance. *Endoscopy* 2003:35:(2):103–111. https://doi.org/10.1055/s-2003-37012

[2] Economidou M., Todeschi V., Bertoldi P., D'Agostino D., Zangheri P., Castellazzi L. Review of 50 years of EU energy efficiency policies for buildings. *Energy and Buildings* 2020:225:110322. https://doi.org/10.1016/j.enbuild.2020.110322

[3] Kumar D., Alam M., Zou P. X. W., Sanjayan J. G., Memon R. A. Comparative analysis of building insulation material properties and performance. *Renewable and Sustainable Energy Reviews* 2020:131:110038. https://doi.org/10.1016/j.rser.2020.110038

[4] Nashaat B., Waseef A. Responsive Kinetic Façades: An Effective Solution for Enhancing Indoor Environmental Quality in Buildings. *The First Memaryat International Conference (MIC 2017) Architecture of the Future: Challenges and Visions*. Saudi Arabia, 2017.

[5] Loonen R. C. G. M., Trčka M., Cóstola D., Hensen J. L. M. Climate adaptive building shells: State-of-the-art and future challenges. *Renewable and Sustainable Energy Reviews* 2013:25:483–493. https://doi.org/10.1016/j.rser.2013.04.016

[6] Hasselaar B. L. H. Climate adaptive skins: Towards the new energy-efficient façade. *WIT Transactions on Ecology and the Environment* 2006:99:351–360. https://doi.org/10.2495/RAV060351

[7] Mols T., Blumberga A., Karklina I. Evaluation of climate adaptive building shells: Multi-criteria analysis. *Energy Procedia* 2017:128:292–296. https://doi.org/10.1016/j.egypro.2017.09.077

[8] Wang J., Beltrán L. O., Kim J. From static to kinetic: A review of acclimated kinetic building envelopes. World Renewable Energy Forum, WREF 2012, Including World Renewable Energy Congress XII and Colorado Renewable Energy Society (CRES) Annual Conference, 2012.

[9] Shahin H. S. M. Adaptive building envelopes of multistory buildings as an example of high performance building skins. *Alexandria Engineering Journal* 2019:58(1):345–352. https://doi.org/10.1016/j.aej.2018.11.013

[10] Kuru A., Oldfield P., Bonser S., Fiorito F. Biomimetic adaptive building skins: Energy and environmental regulation in buildings. *Energy and Buildings* 2019:205:109544. https://doi.org/10.1016/j.enbuild.2019.109544

[11] Luo Y., Zhang L., Bozlar M., Liu Z., Guo H., Meggers F. Active building envelope systems toward renewable and sustainable energy. *Renewable and Sustainable Energy Reviews* 2019:104:470–491. https://doi.org/10.1016/j.rser.2019.01.005

[12] Jouhara H., Milko J., Danielewicz J., Sayegh M. A., Szulgowska-Zgrzywa M., Ramos J. B., Lester S. P. The performance of a novel flat heat pipe based thermal and PV/T (photovoltaic and thermal systems) solar collector that can be used as an energy-active building envelope material. *Energy* 2016:108:148–154. https://doi.org/10.1016/j.energy.2015.07.063

[13] Yu G., Yu J., Hu Y., Cheng X., Liu H., Liu W. Moisture transport analysis for integrated structures of flat plate solar collector and building envelope. *Solar Energy* 2021:217:145–154. https://doi.org/10.1016/j.solener.2021.01.068

[14] Elghamry R., Hassan H., Hawwash A. A. A parametric study on the impact of integrating solar cell panel at building envelope on its power, energy consumption, comfort conditions, and CO_2 emissions. *Journal of Cleaner Production* 2020:249:119374. https://doi.org/10.1016/j.jclepro.2019.119374

[15] Schneider A., Karin M., Kuhn T. E. Building-Integrated Photovoltaics Moves from the Niche to the Mass Market Industrial manufacture of solar building components and their integration into the building planning process Photovoltaic Building Components: Multiple Advantages for Building Owners Press release. [Online]. [Accessed 14 June 2021]. Available: www.ise.fraunhofer.de

[16] Sari A. Thermal Energy Storage and Applications Using Phase Change Materials. *3rd International Turkic World Conference on Chemical Sciences and Technologies*, 2017.

[17] Soibam J. Numerical Investigation of a heat exchanger using phase change materials (PCMs). NTNU, 2017.

[18] Romdhane S. B., Amamou A., Ben Khalifa, Rim, SAÏD, Nejla Mahjoub, Younsi, Zohir and Jemni, Abdelmajid. A review on thermal energy storage using phase change materials in passive building applications. *Journal of Building Engineering* 2020:32:101563. https://doi.org/10.1016/j.jobe.2020.101563

[19] Lin Y., Alva G., Fang G. Review on thermal performances and applications of thermal energy storage systems with inorganic phase change materials. *Energy* 2018:165(PA):685–708. https://doi.org/10.1016/j.energy.2018.09.128

[20] Baetens R., Jelle B. P., Gustavsen A. phase change materials for building applications: A state-of-the-art review. *Energy and Buildings* 2010:42(9):1361–1368. https://doi.org/10.1016/j.enbuild.2010.03.026

[21] Sarbu I., Sebarchievici C. A comprehensive review of thermal energy storage. *Sustainability (Switzerland)* 2018:10:(1):10010191. https://doi.org/10.3390/su10010191

[22] Heier J., Bales C., Martin V. Combining thermal energy storage with buildings – A review. *Renewable and Sustainable Energy Reviews* 2015:42:1305–1325. https://doi.org/10.1016/j.rser.2014.11.031

[23] Vanaga R., Blumberga A., Freimanis R., Mols T., Blumberga D. Solar façade module for nearly zero energy building. *Energy* 2018:157:1025–1034. https://doi.org/10.1016/j.energy.2018.04.167

[24] Mols T., Vanaga R., Blumberga A. Solar Façade Module for Nearly Zero Energy Building. Extended Test Period. *Environmental and Climate Technologies*. 2020:24(1):442–453. https://doi.org/10.2478/rtuect-2020-0027

[25] Sirmelis R., Vanaga R., Freimanis R., Blumberga A. Solar Façade Module for Nearly Zero Energy Building. Optimization Strategies. *Environmental and Climate Technologies* 2019:23(3):170–181. https://doi.org/10.2478/rtuect-2019-0087

PAPER 2: LABORATORY TESTING OF SMALL-SCALE SOLAR FACADE MODULE WITH PHASE CHANGE MATERIAL AND ADJUSTABLE INSULATION LAYER

energies

MDPI

Article

Laboratory Testing of Small Scale Solar Facade Module with Phase Change Material and Adjustable Insulation Layer

Ruta Vanaga *, Jānis Narbuts, Ritvars Freimanis and Andra Blumberga

Institute of Energy Systems and Environment, Riga Technical University, LV-1048 Riga, Latvia; janis.narbuts_1@edu.rtu.lv (J.N.); ritvars.freimanis@rtu.lv (R.F.); andra.blumberga@rtu.lv (A.B.)
* Correspondence: ruta.vanaga@rtu.lv

Abstract: Active building envelopes that act as energy converters—gathering on-site available renewable energy and converting it to thermal energy or electricity—is a promising technological design niche to reduce energy consumption in the building sector, cut greenhouse gas emissions, and thus tackle climate change challenges. This research adds scientific knowledge in the field of composite building envelope structures containing phase-change materials for thermal energy storage. In this study, the focus lies on the cooling phase of the diurnal gain and release of solar energy. The experimental setup imitates day and night environment. Six alterations of small-scale solar facade modules are tested in two different configurations—with and without the adjustable insulation layer on their outer surface during the discharging phase. Modules explore combinations of aerogel, air gap, and Fresnel lenses for solar energy concentration. The results allow us to compare the impact of the application of an additional insulation layer at "night" for different designs of solar facade modules. The results show that modules with an air gap provide higher heat gains but do not take full advantage of the latent heat capacity of phase-change materials.

Keywords: active building envelope; building energy efficiency; Fresnel lens; nearly zero-energy buildings; solar concentrator; solar thermal energy storage

Citation: Vanaga, R.; Narbuts, J.; Freimanis, R.; Blumberga, A. Laboratory Testing of Small Scale Solar Facade Module with Phase Change Material and Adjustable Insulation Layer. *Energies* **2022**, *15*, 1158. https://doi.org/10.3390/en15031158

Academic Editors: Matthias Haase and Petter Wallentén

Received: 11 November 2021
Accepted: 29 January 2022
Published: 4 February 2022

1. Introduction

The EU goal to reach carbon neutrality in 2050 defined in the European Green Deal [1] calls to accelerate the transition to more efficient technologies, consumes less energy, and create less CO_2 emissions. Since the building sector consumes 40% of the overall energy and creates 36% of the CO_2 emissions in the EU [2], unhesitant measures are needed in this sector, and amendments in directive 2010/31/EU on the energy performance of buildings and Directive 2012/27/EU on energy efficiency [3] call for smarter buildings that can provide better overall energy performance.

To make the shift towards a greener economy, the share of renewable energy shall be increased as well [4]. The on-site use of renewable energy for buildings is one of the decarbonization steps. Traditional building envelopes provide shelter to inhabitants and help to reduce undesirable heat losses or heat gains from the surrounding environment. The better the thermal properties of an envelope, the lower the energy bill for heating and cooling.

However, what if instead of being a passive component of the building energy balance, the building envelope could take an active part in the energy balance, providing the energy necessary for maintaining a comfortable indoor climate? One of the former trends of recent decades is improving the heat capacity of building envelopes, for instance, developing Trombe walls [5], [6], where solar energy is gathered and heat is accumulated in the building envelope itself.

Other similar trends providing thermal energy storage can be structures supplemented with phase-change materials (PCM) since those have higher heat capacity [7,8], compared

to conventional materials—concrete, lightweight concrete, and wood. A more recent and equally important direction is the active/adaptive building envelopes that act as energy converters [9,10]; thus, energy that is available on–site is transformed into electrical or thermal energy. Such an approach combines the need for advanced building components and promotes the transition to the use of renewable energy instead of fossil.

Among active systems, there are building-integrated photovoltaic or photovoltaic and thermal systems [11,12], ventilated active thermoelectric envelopes [13], active systems with phase-change materials [14–16], transpired solar collectors [10], active glazed facades [17,18]; glazing with phase-change materials [19,20], and others. In 2019, the Fraunhofer Institute For Solar Energy Systems ISE stated that only the building-integrated photovoltaic systems are recognized as mass-produced products [21]. Therefore, in the field of active building envelope systems, the knowledge base on the performance of different types of building components has to be strengthened for these systems to become widely applicable.

The incorporation of phase-change materials (PCM) into building envelopes has great potential to raise the energy efficiency for new and retrofitted buildings and support on-site renewable energy use. Since none of the recently developed PCM enhanced materials have gained mass production status, adding scientific knowledge to the field helps to fill this knowledge gap.

Phase-change materials can serve as the energy storage medium in building thermal envelopes allowing them to store and release energy according to the heating and cooling demands of the building. In passive storage systems, PMCs can be embodied in building envelopes initiating energy charging and discharging cycles with no auxiliary energy used; however, in active storage systems, auxiliary energy is used for the operation of the system [22]. In passive PCM enhanced solar heating systems, thermal energy from daytime solar radiation is gathered inside the building envelope element (wall, roof, or floor).

Gained heat is released when solar energy decreases and the ambient temperature drops. However, an active heating system can provide the necessary room temperature by heating the PCM with a solar collector system, heat pump, or using cheap nighttime electricity. In the study of the optimization of PCM wallboard for building use [23], the 10 mm thick PCM layer was compared to other building materials to determine the maximum storable energy. The simulation results showed that the wallboard with only 10 mm of PCM had the highest energy storage capacity.

Different approaches and technologies have been proposed in recent years regarding how the PCMs can be incorporated into the building envelopes. In one of the studies [24], an aluminium honeycomb containing a micro-encapsulated PCM wallboard was investigated. The experimental results showed sufficient heat conduction enhancement. In another study [25], PCM macro-capsules were incorporated in masonry wall clay bricks that led to an indoor temperature swing reduction from 10 to 5 °C and a time delay of around 3 h. A study of a numerical model of a residential building roof with a PCM layer was developed to evaluate thermal performance using the data of climatic conditions in Chennai for the month of January [26].

The findings indicate that a PCM-embedded rooftop maintains a ceiling temperature that is approximately stable in the region of 25.5–27.5 °C and decreases the highest recorded heat levels as a contrast to a rooftop without PCM. The study is expanded to account for the PCM plane's various inclinations within the layout of the roof. In comparison to a non-PCM room, a PCM slab inclined at 2 °C offers a maximum ceiling temperature reduction of 2.38 °C and daily heat gain savings of 0.106 kWh/m^2 or 16% for the same thickness and material properties.

The energetic demand for active heating, ventilation, air conditioning (HVAC) systems can be reduced by implanting PCMs in these systems. An experimental study by de Gracia, Navarro, and Castell [27] of ventilated double-skin facades with PCM during the winter period in Spain showed that the use of PCMs significantly improved the thermal behaviour

of the whole building by reducing the electrical consumption and serving as heat supplier in the periods when it is necessary.

A comparison between active and passive PCM systems was developed by Gholamibozanjani and Farid [28]. The potential of passive and active systems for energy savings and peak load shifting was investigated using two identical test booths, each fitted with a control system. One of the booths was outfitted with PCM-integrated wallboards, while the other one was designed with active PCM heat storage units based on air. When both systems had the same amount of heat storage capacity, the energy used in the booth for an active system was 22 percent less over ten days in winter. When peak load shifting was investigated, it was discovered that using an active system resulted in a 32 percent reduction in energy costs.

Depending on the temperature range required, a variety of phase-change materials (PCM) are available; however, solid–liquid PCMs are the most suitable for the building sector due to their characteristics. They are divided into three main categories: organic, inorganic, and eutectics [29]. Fatty acids, sugar alcohols, and paraffin-based organic materials are the most often used solid–liquid PMCs due to their wide range of temperature performance. For temperatures beneath 0 °C, paraffin is the best option for building materials [30].

Phase separation and subcooling are the main obstacles for the broad usage of inorganic hydrated salts despite their excellent medium-low temperature heat storage properties, availability, and price [31]. Eutectics are the materials combined with several solids in various ratios to lower the melting temperature of the substance. A slightly higher density is one of the key disadvantages compared to organic PCMs [32].

The use of PCM's in an active or passive building envelope is one of the most promising alternative ways to reduce energy demand in buildings and to improve the energy efficiency at the same time providing thermal comfort for the inhabitants.

The research presented in the paper aims to create a composite solar facade that harvests solar energy, stores it in phase-change material, and releases it to the indoor space on demand. The study is a continuation of a series of experiments on composite facade structures containing phase-change material, an insulation layer, and heat transfer enhancers—copper plate and rods (Figure 1). The proposed system is intended to function as a thermal energy storage system (TES)—to absorb on-site available solar energy in the charging phase and release stored energy to the spaces in need for heating at the discharging phase.

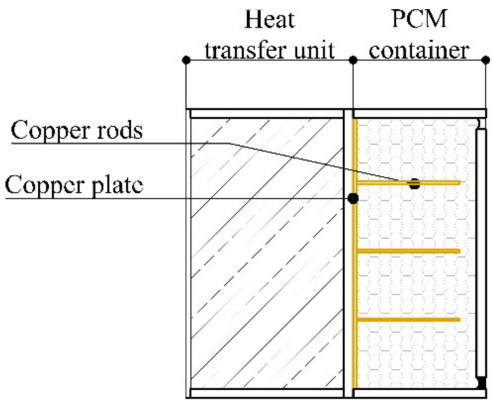

Figure 1. Conceptual design of a solar facade module consisting of a PCM container and heat transfer unit.

Six alterations of the solar wall module have been tested in previous studies [33,34]. The energy storage unit (PCM container) is one element that does not change. What changes is the heat transfer unit—there are three basic forms: unventilated air gap, aerogel filling, and cone-shaped air gap (air gap inside and aerogel outside), and those are repeated in two versions—with a Fresnel lens for the concentration of solar radiation and with PMMA glass (described in more detail later in the text). It was concluded that solar wall module variations with less insulation, on the one hand, heat up much faster and the temperature in PCM was found to be up to 25 degrees higher than in those with higher thermal resistance at the outer layer; however, on the other hand, heat is lost as fast as it was gained in the given experimental setup. It was concluded that a balance between optimal charging speed and reduced heat losses must be found.

The proposal for optimization of the solar facade module by application of an adjustable insulation layer as well as the experimental setup to evaluate the impact of the proposed solution is presented in the next section. The gained results are analysed in Section 3.

2. Materials and Methods

As a possible solution to reduce heat losses at the discharging phase while not compromising the charging speed, we suggest the use of an adjustable insulation layer—to add to the external surface of the solar facade module an additional 5 cm of insulation during the discharging phase (Figure 2a,b).

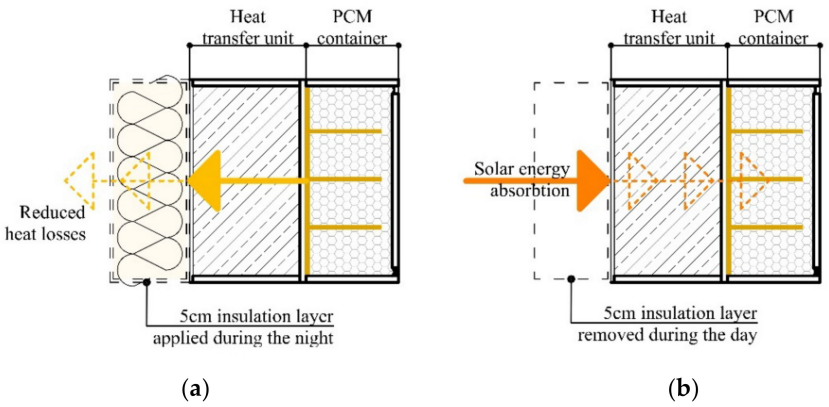

Figure 2. Charging phase with no insulation layer (**a**) and discharging phase with an insulation layer (**b**).

The impact of adjustable insulation is evaluated in this study on all six previously developed variations of the solar facade (Figure 3).

2.1. Experimental Setup

The experimental setup is a small-scale replica of the PASLINK test. The PASLINK test is a method to determine the performance of developed building components under real climatic loads that has been developed from the PASSYS Project (Passive Solar Components and Systems Testing) [35]. The PASLINK test stand consists of a building envelope (in one facade tested material is built-in) and a room under observation surrounded by the envelope.

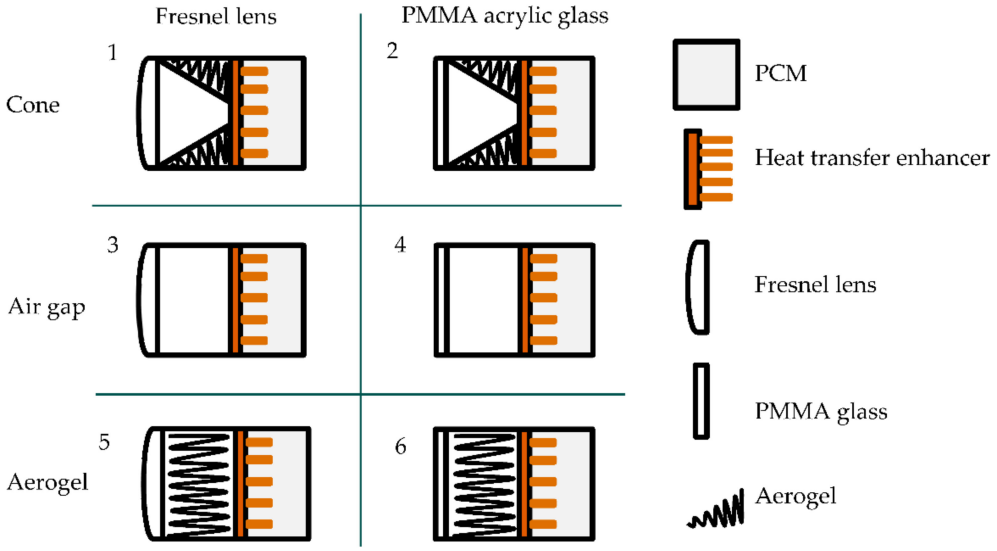

Figure 3. Schematic representation of six solar facade variations.

In the experiment presented in the paper, a small-scale replica is created, and a test is performed in controlled circumstances in a climate camera. The experiment is based on the comparative testing of six small-scale solar facade modules each with a different design. The test aims to compare the performance of different design modules with and without an external insulation layer to define the best performing setup in a controlled environment and to give an insight into which combination of components could potentially be used for the development of a large-scale solar facade module.

The testing box (0.6 × 0.6 × 0.55 m) imitates the building thermal envelope—walls, floor and roof and small inside an unconditioned space. It is made from 18 mm plywood and is lined with 200 mm thermal insulation (λ = 0.037 W/mK). The thickness of the thermal insulation layer is chosen accordingly to reach the U-value determined in Latvian construction standards. In one of the walls, the developed facade module is built in (Figure 4).

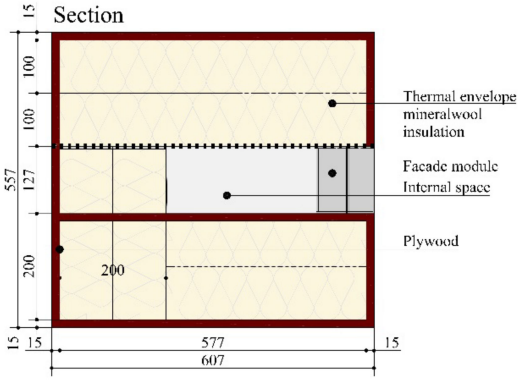

Figure 4. Small-scale PASLINK type test box.

For monitoring purposes, a set of thermocouples and heat flux sensors are placed in the experimental setup (Figure 5). There are five thermocouples (T1, T2, T3)—three are placed in PCM container at different heights to observe temperature changes in different layers of phase-change materials, one thermocouple (T4) registers the temperature in the climate chamber, and one thermocouple (T5) is placed in the "indoor space" of the test box. T4 is not reflected in the paper since its main purpose is to notice technical issues in ensuring equal temperatures in all test rounds.

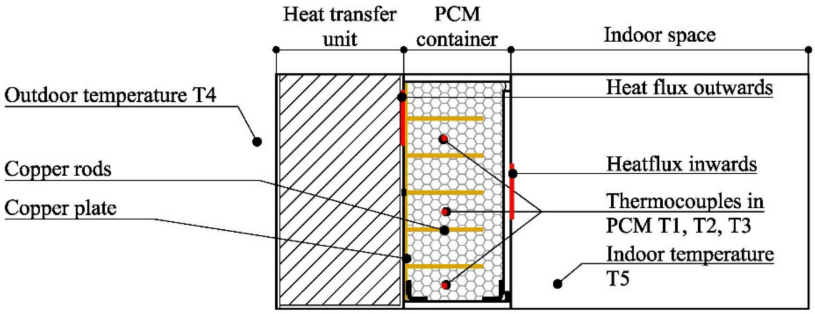

Figure 5. Measuring equipment.

The provided set of thermocouples will allow to compare changes in PCM temperature and "indoor space" temperature among different setups under defined conditions. Two heat flux sensors are placed at inside (facing "indoor space") and outside (facing heat transfer unit) surfaces of the PCM container. The first sensor provides data on the heat exchange between phase-change material and indoor space, and the second sensor illustrates heat exchange with surroundings via heat transfer unit.

The test box is placed in the climate chamber (Figure 6). The heating/cooling unit ensures the desired temperature in the climate chamber.

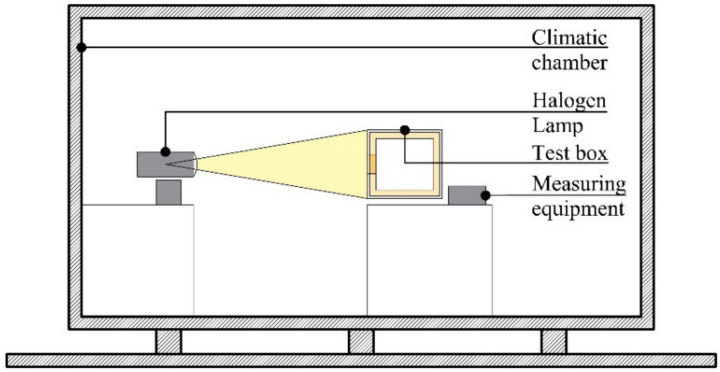

Figure 6. The experimental setup in the climate chamber (scheme).

The experimental stand is located in the laboratory at Riga Technical University (Figure 7).

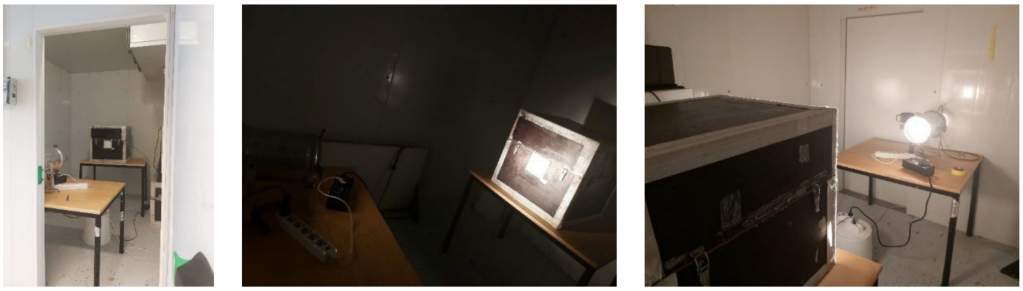

Figure 7. The experimental setup in the climate chamber (Riga Technical University laboratory).

2.2. Experiment Plan

Six variations of designed solar wall modules are tested in the laboratory as presented in Figure 3. As mentioned before, the PCM container is the core of the solar wall module and is not changed during the experiment. The phase-change material used is Rubitherm paraffin RT21HC. All differences are made in the heat transfer unit varying with an unventilated air gap, aerogel filling, and cone-shaped unventilated air gap embedded in the aerogel layer.

To gain insights into the whole energy charging and discharging cycle, conditions are set to provide heating and cooling phases in laboratory testing conditions:

(1) Initial state 10 °C. All solar wall module setups and the climate chamber itself is cooled to 10 °C before the start of the experiment. This temperature was determined considering the average outdoor temperature throughout the spring and autumn seasons in northern Europe. As these periods of the year demand space heating, there is a great potential to partly or fully cover them by using on-site solar energy in a particular climate zone.

(2) In the heating phase, the temperature in the climate chamber is raised to 15 °C and a halogen lamp GE SUPER CP60 EXC VNS 230 V | 1000 W G16d 3200 K | General Electric combined with dimmer UNI BAR Elation professional imitates solar radiation. The solar irradiance is set to 1000 W/m^2 as this is considered a global standard in test conditions. The charging phase takes place for 7 h 39 min.

(3) In the cooling phase, the lamp is switched off, and the temperature in the climate chamber is lowered to 10 °C. This phase is 40 h 21 min long.

All together, testing takes 48 h.

For each setup, two rounds of tests are performed—with and without an additional 5 cm insulation layer at the outer surface of the solar wall module; thus, altogether, there are 12 setups (S-setup; 1, 2, 3 . . . number of setups) (Table 1). For graphical visualization of the setups, see Figure 3.

Table 1. Experiment plan. Twelve setup variations.

Heat Transfer Unit Variations	Cone + Aerogel	Unventilated Air Gap	Aerogel Filling
Fresnel Lens	S1—W/O	S3—W/O	S5—W/O
Polymethyl methacrylate (PMMA)	S2—W/O	S4—W/O	S6—W/O
Fresnel Lens + adjustable insulation	S1—W	S3—W	S5—W
PMMA + adjustable insulation	S2—W	S4—W	S6—W

W—with, W/O without an adjustable insulation.

The characteristics of the materials used in the modules and PASLINK test cell are summarized in Tables 2 and 3.

Table 2. Components of the solar facade model.

Component	Characteristics
Phase-change material (PCM)	RUBITHERM RT21HC Melting area: 20–23 °C Congealing area: 21–19 °C
PCM glass container	Dimensions: 127 × 127 × 60 mm
Plastic box	Material: Polyethylene terephthalate glycol (PETG)
Cone	Material: Polyethylene terephthalate glycol (PETG)
Glass	Dimensions: 129 × 129 × 4 mm
Poly (methyl methacrylate) PMMA glass	Dimensions: 127 × 127 × 1.5 mm
Fresnel lens	Dimensions: 127 × 127 × 1.5 mm Focal length: 71.12 mm
Aerogel	LUMIRA translucent aerogel LA1000

Table 3. Components of the small scale PASLINK test cell.

Component	Characteristics
Plywood	15 mm λ = 0.13 W/mK
Mineral wool	200 mm λ = 0.037 W/mK
Adjustable layer XPS insulation	50 mm λ = 0.037 W/mK

2.3. Measuring Equipment

During the test, measurements are registered via multipurpose data logger CR1000 Campbell Scientific. Data are logged once in a minute. Solar radiation is measured by pyranometer CMP3, Kipp & Zonen. Type K thermocouples are used to measure the temperature in PCM. To capture the heat flow, a Sequoia SHF series (40 × 40 mm, 12.6 μV) sensor is used. The specifications of the measuring equipment are listed in Tables 4 and 5.

Table 4. Specifications of the CMP and Kipp & Zonen pyranometer (based on the datasheet).

Characteristics	Value
Spectral range (50% points)	300 to 2800 nm
Sensitivity	10 to 32 μV/W/m^2
Response time	20 s
Zero offset A	<15 W/m^2
Zero offset B	<5 W/m^2
Directional response (up to 80° with 1000 W/m^2 beam)	<20 W/m^2
Temperature dependence of sensitivity (−10 °C to +40 °C)	<4%
Operational temperature range	−40 °C to +80 °C
Maximum solar irradiance	2000 W/m^2
Field of view	180°

Table 5. Specifications of the Type K thermocouples.

Characteristics	Value
Temperature range	−270 °C to 1260 °C
Accuracy	±2.2 °C or ±0.75%

3. Results

In this section, the results of testing are presented and organized as follows:

- Temperature and heat flux graphs (average temperature in PCM, "indoor space", heat flux inwards and outwards) are compared for each of six basic setups—the performance of one particular setup with and without an adjustable insulation layer is compared.
- Temperature graphs (average temperature in PCM and "indoor space") are compared for six basic setups compiled—the performance of all setups with and without an adjustable insulation layer are compared.
- Heat flux graphs (inwards and outwards) are compared for six basic setups compiled—the performance of all setups with and without an adjustable insulation layer is compared.

3.1. Temperature and Heat Fluxes in Setups

The physical processes and transitions in detail are displayed in Figure 8. In the charging phase of the cycle, the temperature in PCM is raised from 10 °C to 18 °C in a linear manner gaining sensible heat. Then, the phase-change material starts to melt—the measured temperatures at different depths of PCM container start to differ due to melting proceeding faster in the upper part compared with in the lower part of the PCM. The increase of average temperature slows down after reaching 18 °C since, in some parts of the PCM, it has already melted and turned into liquid, and latent heat is being stored.

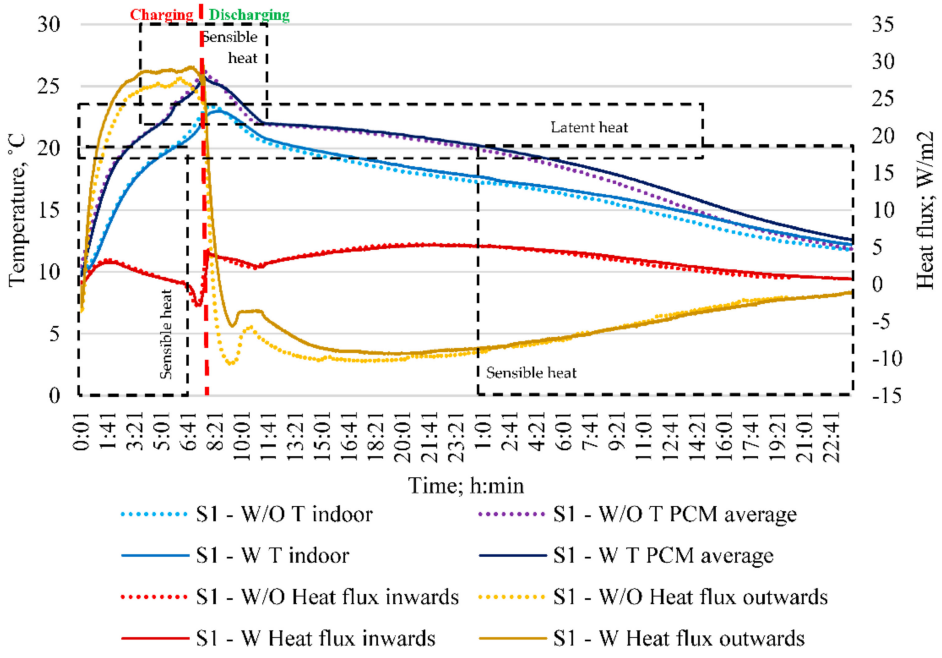

Figure 8. The "indoor space" and average PCM temperatures, inwards and outwards heat fluxes in Setup S1 (Fresnel lens + Cone + Aerogel) variations with (W) and without (W/O) an adjustable insulation layer.

When the average temperature is above 23–24 °C, the phase change in the whole volume of PCM has ended, and sensible heat is gained. In discharging phase of the cycle, the average temperature drops after the lamp is switched off. The sensible heat gained above the melting state is lost (if any was gained), and at reaching the point of 22 °C, the solidification process starts releasing the latent heat.

The gradient of temperature drop at this stage decreases. In the next ~20 h, the temperature in phase-change material tends to reach the surrounding temperature of 10 °C. The "indoor space" temperature follows the same tendency as described for the average temperature in PCM. The only difference is that the temperature change gradient in the charging phase is steeper for the PCM average temperature curve; however, in the solidification phase, it is steeper for the "indoor space" temperature curve.

Figures 8–13 illustrates a comparison of changes in average PCM(Tavg) and "indoor space" (Tin) temperatures as well as heat fluxes inwards and outwards with (W) and without (W/O) adjustable insulation layer applied during the discharging phase for all of the setups. The time of the charging phase is equal in both configurations (W and W/O) for all of the setups further on. After 7 h and 39 min, the discharging phase begins and differences between Setups with equal basic design can be observed.

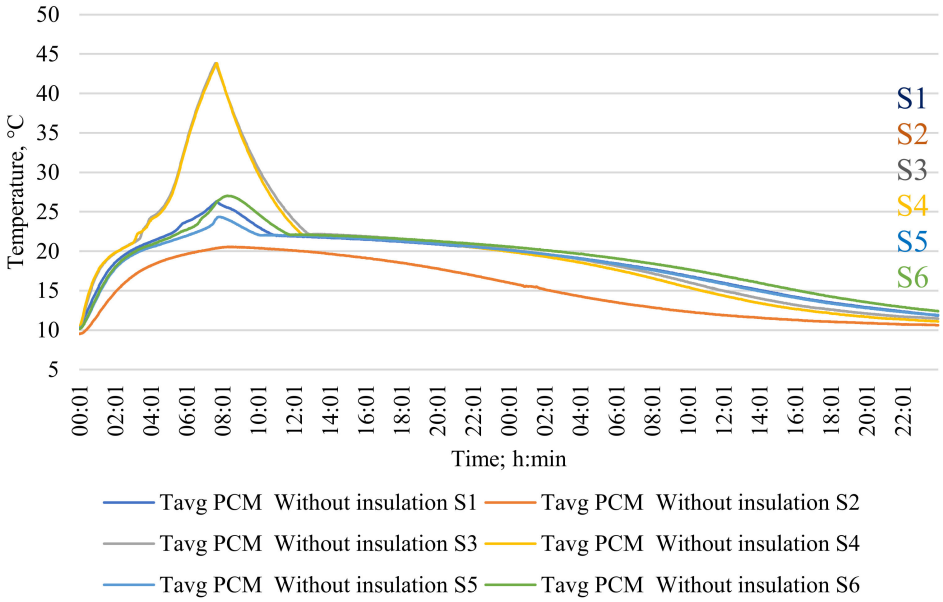

Figure 9. The average temperature in phase-change material in six setups without insulation applied at night.

Here, after losing the sensible heat, PCM enters the phase of discharging latent heat. At this point, it is noticeable that, with the adjusted layer of insulation, the cooling of PCM and indoor space is taking place at a slower rate, and PCM enters the solidification phase at a later point in time (see annex for close-ups). In the whole discharging phase, the temperature drop in the configuration with adjusted insulation is delayed.

At the end of the charging–discharging cycle in S1 (Fresnel lens + Cone + Aerogel), the average PCM temperature, as well as the "indoor space" temperature, is, respectively, 0.8 and 0.5 °C higher in configuration with the adjustable insulation layer (see Appendix A for close-up Figure A1). The solidification phase of PCM starts 30 min later in this configuration (Figure 8). The maximum temperature difference in PCM is 1.0 and 0.8 °C in the "indoor space". Comparison of heat fluxes in configurations with and without an adjustable insulation layer shows that the inwards heat flow is higher, yet the outwards flux is lower in the case when the insulation layer is used. This tendency is observed in all of the setups.

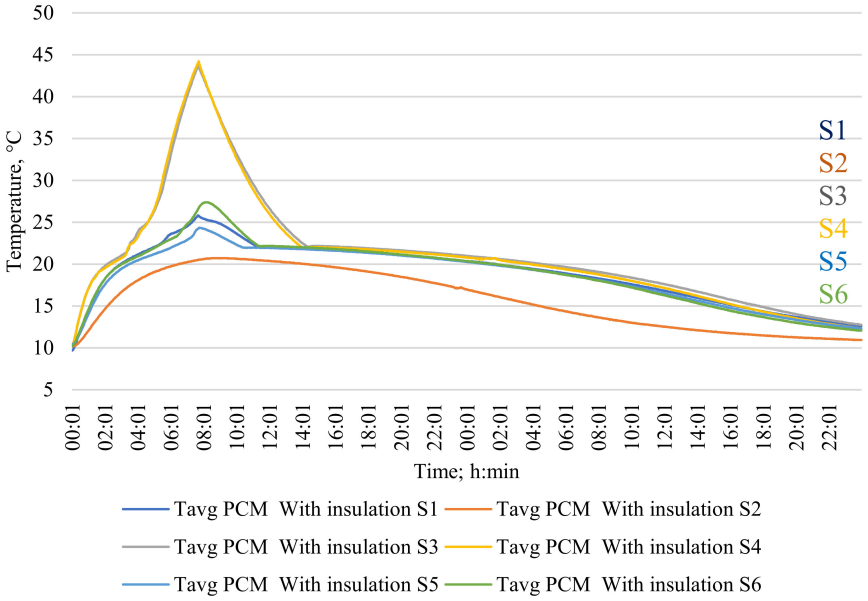

Figure 10. The average temperature in phase-change material in six setups with insulation applied at night.

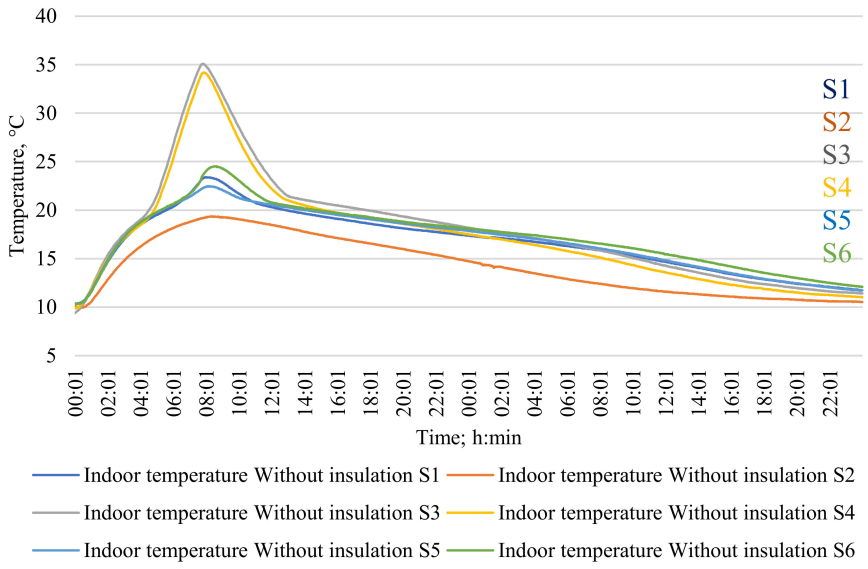

Figure 11. "Indoor" temperature in six setups without insulation applied "at night".

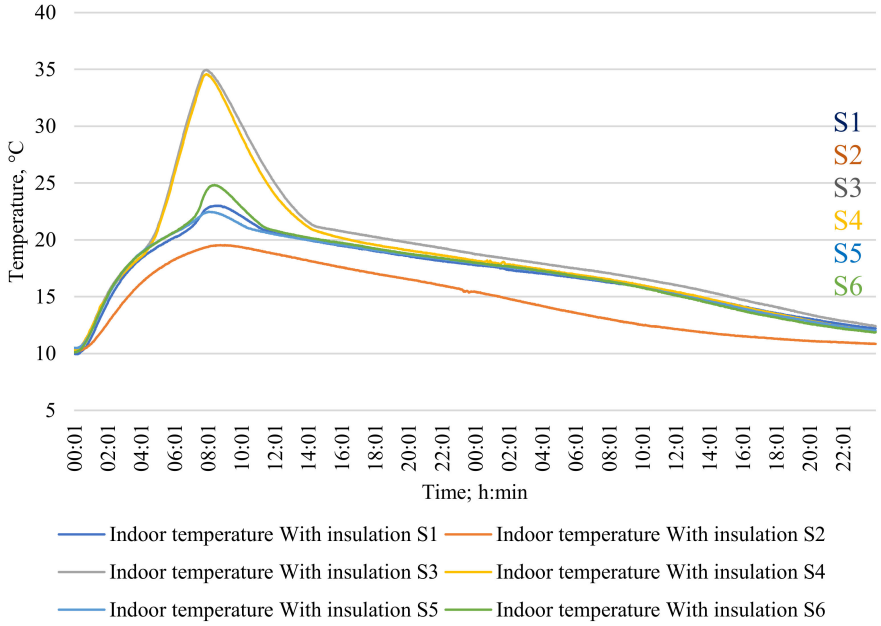

Figure 12. "Indoor" temperature in six setups with insulation applied "at night".

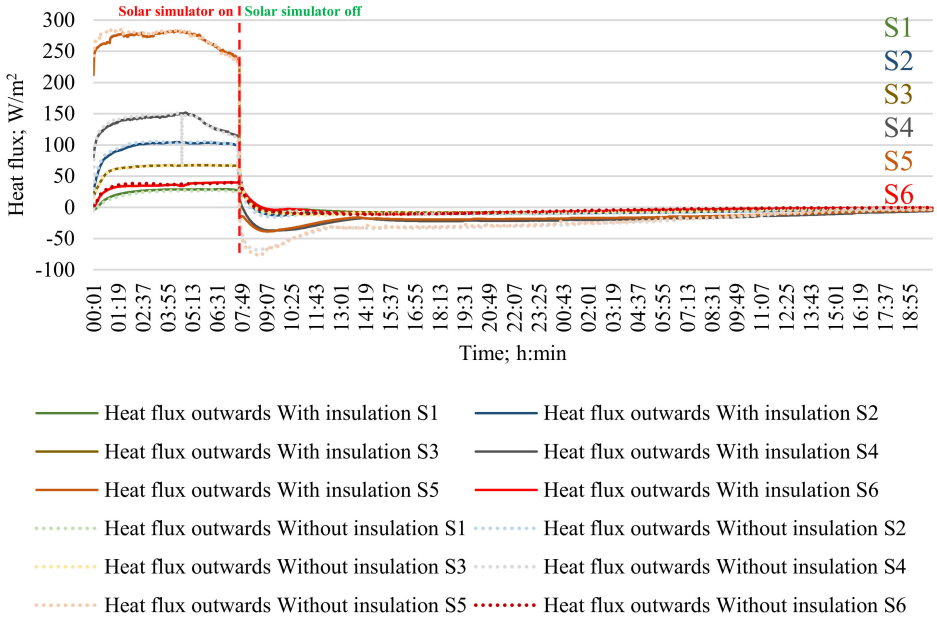

Figure 13. Outward heat flux comparison in all of the Setups with (W) and without (W/O) an adjustable insulation layer.

Figures 9–12 show the average PCM and "indoor space" temperature comparison, and Figures 13 and 14 illustrate inward and outward heat flux comparison in all of the setups with (W) and without (W/O) adjustable insulation layer.

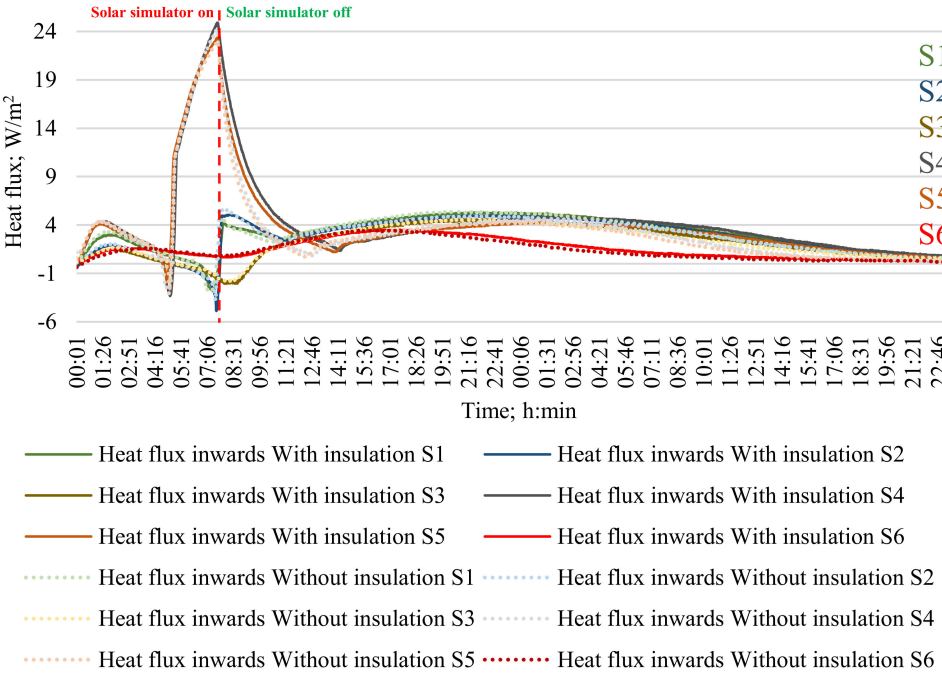

Figure 14. Inward heat flux comparison in all of the Setups with (W) and without (W/O) an adjustable insulation layer.

In S2 (PMMA + Cone + Aerogel) at the end of the charging–discharging cycle in the configuration with the adjusted layer of insulation, both the average temperature in PCM and the temperature in "indoor space" is 0.3 °C higher compared to the layout without an adjustable insulation layer. Sensible heat above melting temperature is not gained in S2, PCM has not entirely melted, and the solidification process starts right after the solar simulator is switched off. The maximum temperature difference in PCM and "indoor space" is 1.1 and 1.0 °C, respectively.

At the end of the charging–discharging cycle in S3 (Fresnel lens + Air gap), the average PCM temperature is 1.2 °C higher but the "indoor space" temperature is 0.9 °C higher in configuration with the adjustable insulation layer. The PCM enters the solidification phase approximately 1 h and 30 min minutes later in this configuration. The maximum temperature difference in PCM is 3.0 and 2.1 °C in the "indoor space".

In S4 (PMAA + Air gap) at the end of the charging–discharging cycle in the configuration with the adjusted layer of insulation average temperature in PCM is 1.3 °C higher, and the "indoor space" temperature is 1.0 °C higher. The solidification phase is delayed by 1 h and 35 min compared to the configuration with no insulation layer. The maximum temperature variation in PCM is 2.8 but 2.0 °C in "indoor space".

The average temperature in PCM is 0.4 °C higher and the "indoor space" temperature is 0.3 °C higher in configuration with the adjustable insulation layer at the end of the charging–discharging cycle in S5 (Fresnel lens + Aerogel). In this setup, the time difference

between both configurations for PCM to reach the solidification phase is insignificant—only 15 min. The maximum temperature variation in PCM is 0.7 and 0.5 °C in "indoor space".

At the end of the charging–discharging cycle in S6 (PMMA + Aerogel), the average PCM temperature is 0.3 °C higher but the "indoor space" temperature is 0.2 °C higher in configuration with the adjustable insulation layer. The PCM enters the solidification phase approximately 30 min later in this configuration. The maximum temperature difference in PCM is 0.6 and 0.4 °C in the "indoor space".

The measured outward heat fluxes show similar tendencies in all of the setups (Figure 13). Values above 0 indicate that the heat flows from outside into phase-change material, and values below 0 indicate the direction of heat flow is from PCM to the surrounding environment. At first, the heat flux rises and reaches its maximum capacity, and when PCM has changed its state from solid to liquid, the value of heat flux decreases. After the solar simulator is switched off, the heat flux changes its direction and values drop negative. When sensible heat is lost, the heat flux outward accelerates. However, when the solidification of PCM starts, the heat flux slows down (see Figure 8).

The tendency of the inward heat flux is similar in setups 1, 3, 4, and 6—there is a distinctive sensible heat phase observed after PCM has changed its state to liquid (see Figure 14). In setups 2 and 5, the inward heat flux values indicate heat flow from PCM to "indoor space". Generally, at the beginning of the charging phase, the heat flow increases in the direction to indoor space but decreases when the phase change takes place. Heat flow to "indoor space" rapidly increases at the moment when PCM is melted and the sensible heat is gained. After switching off the solar simulator, the heat flux decreases until the sensible heat is lost; however, at the beginning of the solidification process, it starts to increase again. Heat flux continues to rise for 10–12 h and then gradually decreases until the end of the experiment.

In the following sections, a comparison of temperatures in PCM and "indoor space" as well as inward and outward heat fluxes are presented to inspect the impact of adjustable insulation layer usage on the outer surface of the solar wall module.

3.2. Comparison of Setups

Table 6 provides a summary of fixed average PCM (Tavg) and "indoor space" (Tin) temperatures after 24 and 48 h in setups with and without an adjustable insulation layer (parameters compared are assigned with the same colour). It can be seen that, after 24 h, PCM is in the phase of partial solidification. The value of Tavg in setups 1, 3, 4, 5, and 6 stays in a very narrow range of 0.4 °C without and 0.7 °C with the usage of the adjustable insulation layer. After 48 h, the range of average temperature in PCM is 1.0 °C in the configuration without the insulation layer; however, the range has become narrower in the case with the usage of the additional insulation layer, suggesting that the less insulated setups have benefited in "night-time" as their performance has improved.

Table 6. Highest and lowest average phase-change material temperature in solar facade module.

	Without Adjustable Insulation Layer T_{avg}		**With Adjustable Insulation Layer T_{avg}**		**Without Adjustable Insulation Layer T_{indoor}**		**With Adjustable Insulation Layer T_{indoor}**		**T_{avg}**	**T_{in}**	**T_{avg}**	**T_{in}**	
Type	t, °C 24 h	t, °C 48 h	t, °C 24 h	t, °C 48 h	t, °C 24 h	t, °C 48 h	t, °C 24 h	t, °C 48 h	Max Δt, °C 24 h	Max Δt, °C 24 h	Max Δt, °C 48 h	Max Δt, °C 48 h	Time Delay, min
Setup 1 Fresnel lens, cone, aerogel	20.1	11.8	20.4	12.6	17.4	11.7	17.8	12.2	0.98	0.78	0.77	0.49	30
Setup 2 PMMA, cone, aerogel	16.0	10.6	17.0	10.9	14.7	10.5	15.5	10.9	1.07	0.93	0.32	0.32	-
Setup 3 Fresnel lens and air gap	20.0	11.1	20.8	12.3	17.5	11.0	18.2	12.2	3.02	2.13	1.20	0.91	90
Setup 4 PMMA and air gap	20.2	11.5	21.0	12.7	18.2	11.4	18.8	12.2	2.82	1.98	1.29	1.00	95
Setup 5 Fresnel lens and aerogel	20.2	11.9	20.3	12.3	17.9	11.7	18.0	12.2	0.73	0.51	0.41	0.28	15
Setup 6 PMMA and aerogel	20.4	12.1	20.6	12.4	18.0	11.9	18.1	12.1	0.58	0.44	0.33	0.21	30

Analysing the "indoor" temperature, a similar trend is seen—after 24 h, the temperature range without insulation layer is narrower compared to the temperature range with additional insulation used. After 48 h, the temperature range has become wider in configurations without the insulation layer, yet in setups with additional insulation, it has become insignificant. This emphasizes the impact of the adjustable insulation layer.

Cells coloured in grey summarize the temperature and time differences in each module in two configurations—with and without the adjustable insulation layer. Maximum delta T is determined by comparing the difference in average PCM and "indoor" temperature values in 24 and 48 h periods. The highest delta T is in S3 and S4—the setups with the air-gap layer in front of the PCM container. In addition, the time delay of PCM entering the solidification phase is the highest as well. This indicates that the impact of the adjustable insulation layer on modules with the air-gap layer is the highest. Heat loss is prevented during the discharging phase.

As setups 3 and 4 have the highest maximal temperature difference, the time delay in these setups is the highest as well in both of the configurations—with and without the adjustable insulation layer.

Table 7 presents rankings of the setups in every point of reference. The rank for every position differs. The least performing is Setup 2 in all of the points of reference. When ranking performance after 48 h with adjustable insulation, four setups share first place. Thus, adjustable insulation has served as an equalizer with a smaller impact on well-insulated setups and a higher impact on less insulated ones—this is confirmed with temperature differences in setups 3 and 4 as they rank the highest. Solar facades might be installed in different climates, different cardinal directions and their main function might differ as well.

Thus, for different applications, different setups might be the preferable choice. For example, setups 3 and 4 in tested conditions exhibit the fastest melting rate and highest temperatures, and this would be appropriate for surfaces where the time duration of solar radiation is shorter so the phase change can take place faster. On surfaces more exposed to the sun, other applications might serve better (or in combination with other setups) to avoid gaining sensible heat that raise the temperature above comfortable levels.

Table 7. Ranking of setups in defined points of reference.

	Without Adjustable Insulation Layer		**With Adjustable Insulation Layer**		**Without Adjustable Insulation Layer**		**With Adjustable Insulation Layer**		**T_{avg}**	**T_{in}**	**T_{avg}**	**T_{in}**	
	T_{avg}		**T_{avg}**		**T_{indoor}**		**T_{indoor}**						
	t, °C	t, °C	t, °C	t, °C	t, °C	t, °C	t, °C	t, °C	Max Δt, °C	Max Δt, °C	Max Δt, °C	Max Δt, °C	Time Delay, min
	24 h	48 h	24 h	48 h	24 h	48 h	24 h	48 h	24 h	24 h	48 h	48 h	
Setup 1 Fresnel lens, cone, aerogel	3	3	4	2	5	2	5	1	4	4	3	3	3
Setup 2 PMMA, cone, aerogel	5	6	6	5	6	5	6	3	3	3	5	4	-
Setup 3 Fresnel lens and air gap	2	4	1	1	1	3	1	1	2	2	1	1	1
Setup 4 PMMA and air gap	4	5	2	4	4	4	2	1	1	1	2	2	2
Setup 5 Fresnel lens and aerogel	2	2	5	4	2	2	4	1	5	5	4	5	4
Setup 6 PMMA and aerogel	1	1	3	3	3	1	3	2	6	6	5	6	3

Ranking of the performance: 1—best (green); 2—good (light green); 3—medium high (yellow); 4—medium low (light orange); 5—bad (orange); 6—worst (red).

4. Conclusions and Discussion

To ensure a faster transition to decarbonised building stock, there is an urge for new building thermal envelope concepts ensuring both high energy efficiency and the use of on-site available energy. Constructions enriched with phase-change materials are a recent development thread with great potential that can allow the building envelope to become an active part of the building's energy balance.

The research presented in the paper adds scientific knowledge in the field of composite thermal energy storage wall structures containing phase-change materials. In this study, the focus lies on the cooling phase of the diurnal energy gain and release. The experiment was prolonged to 48 h to observe the cooling phase in-depth. Six alterations of solar facade modules in two different configurations were tested. Modules explored combinations of aerogel, air gap, and Fresnel lenses for solar energy concentration. In the first configuration, the composition of modules remained the same throughout the experiment; however, in the second one, there was an adjustable insulation layer applied to the outer surface of the solar facade modules.

The following insights were gained:

- As expected, the average temperature in the phase-change material and "indoor space" was higher when the adjustable insulation layer was applied in all of the alterations; however, the most significant impact on the average PCM and indoor temperature was in modules with an air gap layer compared with more insulated modules.
- Modules with an air gap were more competitive among others (cone + aerogel and aerogel filling) as, after the solidification in the cooling phase, temperature splines in the graph lay closer together compared to modules without the adjustable insulation layer.
- Thus, we concluded that, when looking at the whole cycle (charging and discharging), more energy was gained and released in modules with the air gap; however, modules with different insulation layers took advantage of the latent heat storage.

In the defined setup, the average PCM and indoor temperatures reached were high due to the small size of the modules and relatively low volume of PCM that set the limit of the total available stored energy capacity. Thus, in the next steps, we plan to enhance the model to a larger scale and perform the experiment in a relevant environment under real climatic conditions, thus, gaining insights on the impact of the proposed solar facade on the energy demand of the building.

Modules were compared in several points of reference—indoor temperature and the average temperature in PCM after 24 and 48 h and with and without an adjustable insulation layer. Furthermore, the highest temperature differences were analysed in setups to evaluate the impact of adjustable insulation. Combinations of different setups might be preferred depending on the purpose of the solar facade.

Author Contributions: The contributions of authors are as follows—conceptualization: R.V., R.F. and A.B.; methodology: R.V., R.F. and A.B.; experimental setup, experiment: R.V. and R.F.; formal analysis: R.V. and J.N.; investigation: R.V. and J.N.; data curation: R.V.; writing—original draft preparation: R.V. and J.N.; writing—review and editing: A.B. and J.N; visualization: R.V.; supervision A.B.; project administration: R.V.; funding acquisition: R.V. and A.B. All authors have read and agreed to the published version of the manuscript.

Funding: This study has been supported by Fundamental and Applied Research project "Smart building EnVElope with solaR Energy STorage (EVEREST)", project No. lzp-2019/1-0363, funded by the Latvian Council of Science.

Institutional Review Board Statement: Not applicable.

Informed Consent Statement: Not applicable.

Data Availability Statement: The data presented in this study are openly available in Zenodo repository (10.5281/zenodo.5969896).

Conflicts of Interest: The authors declare no conflict of interest. The funders had no role in the design of the study; in the collection, analyses, or interpretation of data; in the writing of the manuscript, or in the decision to publish the results.

Appendix A

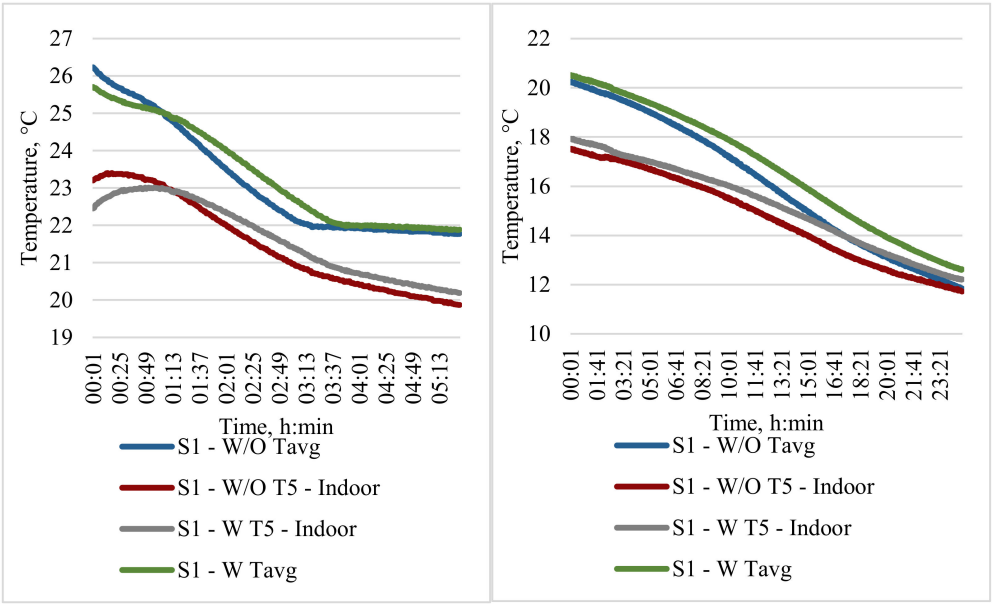

Figure A1. (**Left**) Close-up of average PCM temperature and "indoor" temperature at the beginning of the discharging phase where, after losing sensible heat, PCM entered a phase of discharging latent heat. With an adjusted layer of insulation, cooling is at a slower rate, and PCM enters the solidification phase at a later point in time. (**Right**) Close-up of the average PCM temperature and indoor temperature at the end of the charging—discharging cycle. With an adjusted layer of insulation, the average temperature in PCM is 0.5 °C higher and the temperature in the "indoor space" is 0.9 °C higher than in the sample without an adjustable insulation layer.

References

1. European Commission. *The European Green Deal*; European Commission: Brussels, Belgium, 2019.
2. European Commission. Clean energy for all Europeans. *Euroheat Power* **2019**, *14*, 3. [CrossRef]
3. EU. Directive (EU) 2018/844 of the European Parliament and of the Council amending Directive 2010/31/EU on the energy performance of buildings and Directive 2012/27/EU on energy efficiency. *Off. J. Eur. Union* **2018**, *L 156*, 75–91.
4. EU. Directive (EU) 2018/2001 of the European Parliament and of the Council on the promotion of the use of energy from renewable sources. *Off. J. Eur. Union* **2018**, *2018*, 82–209.
5. Sergei, K.; Shen, C.; Jiang, Y. A review of the current work potential of a trombe wall. *Renew. Sustain. Energy Rev.* **2020**, *130*, 109947. [CrossRef]
6. Hu, Z.; He, W.; Ji, J.; Zhang, S. A review on the application of Trombe wall system in buildings. *Renew. Sustain. Energy Rev.* **2016**, *70*, 976–987. [CrossRef]
7. Heidenthaler, D.; Leeb, M.; Schnabel, T.; Huber, H. Comparative analysis of thermally activated building systems in wooden and concrete structures regarding functionality and energy storage on a simulation-based approach. *Energy* **2021**, *233*, 121138. [CrossRef]
8. Ručevskis, S.; Akishin, P.; Korjakins, A. Parametric analysis and design optimisation of PCM thermal energy storage system for space cooling of buildings. *Energy Build.* **2020**, *224*, 110288. [CrossRef]
9. Luo, Y.; Zhang, L.; Bozlar, M.; Liu, Z.; Guo, H.; Meggers, F. Active building envelope systems toward renewable and sustainable energy. *Renew. Sustain. Energy Rev.* **2019**, *104*, 470–491. [CrossRef]

10. Wang, Y.; Shukla, A.; Liu, S. A state of art review on methodologies for heat transfer and energy flow characteristics of the active building envelopes. *Renew. Sustain. Energy Rev.* **2017**, *78*, 1102–1116. [CrossRef]
11. Jouhara, H.; Milko, J.; Danielewicz, J.; Sayegh, M.; Szulgowska-Zgrzywa, M.; Ramos, J.; Lester, S. The performance of a novel flat heat pipe based thermal and PV/T (photovoltaic and thermal systems) solar collector that can be used as an energy-active building envelope material. *Energy* **2016**, *108*, 148–154. [CrossRef]
12. Wang, M.; Peng, J.; Li, N.; Yang, H.; Wang, C.; Li, X.; Lu, T. Comparison of energy performance between PV double skin facades and PV insulating glass units. *Appl. Energy* **2017**, *194*, 148–160. [CrossRef]
13. Ibañez-Puy, M.; Martín-Gómez, C.; Bermejo-Busto, J.; Sacristán, J.A.; Ibañez-Puy, E. Ventilated Active Thermoelectric Envelope (VATE): Analysis of its energy performance when integrated in a building. *Energy Build.* **2018**, *158*, 1586–1592. [CrossRef]
14. Diarce, G.; Urresti, A.; García-Romero, A.; Delgado, A.; Erkoreka, A.; Escudero, C.; Campos-Celador, A. Ventilated active façades with PCM. *Appl. Energy* **2013**, *109*, 530–537. [CrossRef]
15. Laaouatni, A.; Martaj, N.; Bennacer, R.; Lachi, M.; El Omari, M.; El Ganaoui, M. Thermal building control using active ventilated block integrating phase change material. *Energy Build.* **2019**, *187*, 50–63. [CrossRef]
16. Guo, J.; Dong, J.; Wang, H.; Jiang, Y.; Tao, J. On-site measurement of the thermal performance of a novel ventilated thermal storage heating floor in a nearly zero energy building. *Build. Environ.* **2021**, *201*, 107993. [CrossRef]
17. Ghosh, A.; Norton, B. Advances in switchable and highly insulating autonomous (self-powered) glazing systems for adaptive low energy buildings. *Renew. Energy* **2018**, *126*, 1003–1031. [CrossRef]
18. Sheikh, W.T.; Asghar, Q. Adaptive biomimetic facades: Enhancing energy efficiency of highly glazed buildings. *Front. Arch. Res.* **2019**, *8*, 319–331. [CrossRef]
19. Arranz, B.; Ruiz-Valero, L.; González, M.P.; Sánchez, S.V. Comprehensive experimental assessment of an industrialized modular innovative active glazing and heat recovery system. *Energy* **2020**, *212*, 118748. [CrossRef]
20. Zhang, S.; Hu, W.; Li, D.; Zhang, C.; Arıcı, M.; Yıldız, Ç.; Zhang, X.; Ma, Y. Energy efficiency optimization of PCM and aerogel-filled multiple glazing windows. *Energy* **2021**, *222*, 119916. [CrossRef]
21. Schneider, A.K.M.; Kuhn, T.E. Building-Integrated Photovoltaics Moves from the Niche to the Mass Market Industrial Manufacture of Solar Building Components and Their Integration into the Building Planning Process Photovoltaic Building Components: Multiple Advantages for Building Owners PRESS RELEASE. Available online: https://www.ise.fraunhofer.de/content/dam/ise/en/documents/press-releases/2019/0719_ISE_e_PR_BIPV_final.pdf (accessed on 10 November 2021).
22. Heier, J.; Bales, C.; Martin, V. Combining thermal energy storage with buildings—A review. *Renew. Sustain. Energy Rev.* **2015**, *42*, 1305–1325. [CrossRef]
23. Kuznik, F.; Virgone, J.; Noel, J. Optimization of a phase change material wallboard for building use. *Appl. Therm. Eng.* **2008**, *28*, 1291–1298. [CrossRef]
24. Lai, C.-M.; Hokoi, S. Thermal performance of an aluminum honeycomb wallboard incorporating microencapsulated PCM. *Energy Build.* **2014**, *73*, 37–47. [CrossRef]
25. Silva, T.; Vicente, R.; Soares, N.; Ferreira, V. Experimental testing and numerical modelling of masonry wall solution with PCM incorporation: A passive construction solution. *Energy Build.* **2012**, *49*, 235–245. [CrossRef]
26. Bhamare, D.K.; Rathod, M.K.; Banerjee, J. Numerical model for evaluating thermal performance of residential building roof integrated with inclined phase change material (PCM) layer. *J. Build. Eng.* **2019**, *28*, 101018. [CrossRef]
27. De Gracia, A.; Navarro, L.; Castell, A.; Ruiz-Pardo, Á.; Alvárez, S.; Cabeza, L.F. Experimental study of a ventilated facade with PCM during winter period. *Energy Build.* **2013**, *58*, 324–332. [CrossRef]
28. Gholamibozanjani, G.; Farid, M. A comparison between passive and active PCM systems applied to buildings. *Renew. Energy* **2020**, *162*, 112–123. [CrossRef]
29. Soibam, J. *Numerical Investigation of a Heat Exchanger Using Phase Change Materials (PCMs)*; NTNU: Trondheim, Norway, 2017.
30. Ben Romdhane, S.; Amamou, A.; Ben Khalifa, R.; Saïd, N.M.; Younsi, Z.; Jemni, A. A review on thermal energy storage using phase change materials in passive building applications. *J. Build. Eng.* **2020**, *32*, 101563. [CrossRef]
31. Lin, Y.; Alva, G.; Fang, G. Review on thermal performances and applications of thermal energy storage systems with inorganic phase change materials. *Energy* **2018**, *165*, 685–708. [CrossRef]
32. Baetens, R.; Jelle, B.P.; Gustavsen, A. Phase change materials for building applications: A state-of-the-art review. *Energy Build.* **2010**, *42*, 1361–1368. [CrossRef]
33. Sirmelis, R.; Vanaga, R.; Freimanis, R.; Blumberga, A. Solar Facade Module for Nearly Zero Energy Building. Optimization Strategies. *Environ. Clim. Technol.* **2019**, *23*, 170–181. [CrossRef]
34. Mols, T.; Vanaga, R.; Blumberga, A. Solar Facade Module for Nearly Zero Energy Building. Extended Test Period. *Environ. Clim. Technol.* **2020**, *24*, 442–453. [CrossRef]
35. Martínez, S.; Erkoreka, A.; Eguía, P.; Granada, E.; Febrero, L. Energy characterization of a PASLINK test cell with a gravel covered roof using a novel methodology: Sensitivity analysis and Bayesian calibration. *J. Build. Eng.* **2018**, *22*, 1–11. [CrossRef]

PAPER 3: THE EFFECT OF FRESNEL LENS FOCAL POINT LOCATION ON HEAT TRANSFER IN PHASE CHANGE MATERIAL (PCM) ENHANCED DYNAMIC SOLAR FACADE

Environmental and Climate Technologies
2022, vol. 26, no. 1, pp. 1268–1278
https://doi.org/10.2478/rtuect-2022-0096
https://content.sciendo.com

The Effect of Fresnel Lens Focal Point Location on Heat Transfer in Phase Change Material (PCM) Enhanced Dynamic Solar Facade

Jānis NARBUTS[1*], Andra BLUMBERGA[2], Zigmārs ZUNDĀNS[3], Ritvars FREIMANIS[4], Roberts BĀLIŅŠ[5], Ruta VANAGA[6]

[1–6]*Institute of Energy Systems and Environment, Riga Technical University, Riga, Latvia*

***Abstract* – In recent years, the demand for energy-efficient technological solutions in the building sector has risen significantly worldwide. The exploitation of phase change material as a medium for thermal energy storage in building envelopes has increased due to its superior properties. There is still a knowledge gap to cover in the way to the effective solar thermal energy storage in the building envelope – to enhance the heat transfer, to reduce the heat loss, etc. This paper deals with the optimisation of heat transfer using a solar concentrator (Fresnel lens). This study examines the effect of Fresnel lens focal point location on heat transfer in a dynamic solar facade prototype that stores thermal energy in phase change material. Nine different setups (solar façade compositions) were tested in the laboratory – two parameters with three alternatives each. Testing conditions simulate the relevant Northern Europe climate. By changing the air gap configuration and location of the Fresnel lens focal point, the heat transfer to phase change material was observed by measuring temperatures in the phase change material container using five thermocouples. The results show the improved thermal performance in test modules with larger cone diameter by 7.2 % and Fresnel lens focal point positioning closer to the back of the phase change material container by 5.4 %.**

***Keywords* – Building envelope; melting temperature; solar thermal energy storage; latent heat; small-scale dynamic solar module**

1. INTRODUCTION

The demand for energy-efficient technological solutions in the building sector is significantly rising. The concern about air pollution caused by CO_2 and other GHG emissions has been growing worldwide in recent years. The latest data mark the recovery of the building sector after the COVID-19 crisis, as the industry output is 2.5 % higher than in 2019 [1]. The renovation of old buildings and construction of new buildings must be based on green and carbon-neutral technology involvement to reach the EU's climate targets [2]. Hybrid energy systems can be used to reduce the dependency on conventional fuel-based heating and cooling systems. Here, on-site renewable energy utilization is critical in providing clean and green energy for buildings [3].

The building envelope can serve as the energy transformation media - energy available on site is captured and transmitted to the end user directly [4]. The most common in buildings is

* Corresponding author.
E-mail address: janis.narbuts_1@rtu.lv

solar energy transformed into electricity or heat. Systems can be free-standing photovoltaic (PV) panels or solar thermal systems, or building-integrated both – photovoltaic panels (BiPV – building integrated photovoltaic panels) and solar thermal systems (BiST Building integrated solar thermal systems). Based on the number of examples gathered in a thorough literature review conducted by Vassiliades *et al*., it can be concluded that there is significantly more research on BiPV than BiST [5]. There are technological advancements offered to couple BiPV and BiST systems with latent energy storage using phase change materials. However, there are scarce examples of PCM embedded in the thermal envelope itself to store solar energy.

Solar power is used for this purpose because of its wide availability in almost any climate zone. For instance, when solar radiation is available in the daytime, it can be collected in thermal storage appliances and used later in the nighttime for heating purposes while the outside temperature is low. However, a challenge is the collected thermal energy storage systems, as solar radiation is not available at all times [6]. While solar energy can be transferred into electrical energy by using photovoltaic panels and stored in batteries [5], the long-term storage of solar thermal energy is more complex. It requires more financial investments. In climate zones where solar radiation is available for most of the daytime throughout the year, solar thermal power concentrating systems are used for medium heating and generation of electricity [7]. These systems are based on focusing solar heat on one area by using a reflective surface and can be efficiently used in desert areas. Yet, for the northern climate zone with the longer heating season, solar thermal energy must be collected in insulated storage to provide the system's efficiency. Developing innovative solutions for on-site renewable energy, such as solar thermal power conservation, is an absolute necessity to reach the goals of building sector decarbonization by 2050. According to data [8], solar thermal power capacity grew by 3 % in 2021 compared to 2020. Thermal energy storage systems can be exploited to collect energy for later use by stocking energy in a storage medium. These systems can be sorted into two main types - thermal and chemical. While chemical systems collect thermal energy with chemical reactions, thermal systems are based on storing energy in sensible and latent heat. Thermal systems are the most common energy storage systems that are used for heating and cooling purposes in buildings. Some of the conventual sensible heat storages are water tank storage, underground storage (that makes use of the heat or cold from the ground), aquifer storage, and packed-bed storage. Latent heat storage is based on the phase change properties of the medium and has the advantage of storing heat at an almost constant temperature [9]. In recent years phase change materials (PCM) have drawn their attention as a medium for thermal energy storage in building envelopes due to their superior properties [10]. PCM has been incorporated in building envelopes (walls, roof, windows, and floor) to minimize the need for additional heating and cooling systems [11]. In the study [12], a PCM-enhanced gypsum board is installed on the building envelope (retrofitting) to reach higher energy flexibility and power efficiency than the regular building envelope. Another study examined the PCM-enriched hempcrete and concluded that by adding 20 wt% microencapsulated PCM to the concrete/hemp mixture, heat capacity was raised by 70 % [19]. Kalbasi and Kassani, in the study of the effect of PCM presence on comfort, conclude that the building with the addition of PCM can reach a comfortable temperature range (18 °C to 27 °C) up to 82 % of the year without an additional heating system [13]. In many other recent papers [14]–[19], PCM incorporation in building envelopes has been studied and proven successful in reducing additional heating and cooling demand in buildings. Active PCM systems can save up to one-third of the additional energy consumed in heating and cooling systems than passive solutions [20]. Despite the advantageous PCM properties of energy storage capacity, when used in building envelopes,

it has to be coupled with insulation material to preserve stored heat for longer periods of time. The insulation is crucial for building envelopes that are used in northern climate zones on account of cold winter and medium spring and autumn seasons, as well as only partial solar radiation availability. To intensify the energy accumulation of the available solar energy in northern Europe climate zones, the application of active building envelopes (ABE) is one of the most reasonable solutions [21] as they interact with the changing environment. By using ABE, which utilizes on-site solar radiation, thermal energy can be stored and released from the building, taking off the load from heating [22] and cooling [23] systems. Conventional building insulation materials do not always meet the needs of ABE applications due to their properties (weight, size, volume, etc.). Here innovative insulation materials such as aerogel can be useful. It is an ultra-light, transparent, ecological material with excellent heat insulation properties [24]. Solar energy is available only partially due to different seasons and dynamic weather changes in the northern Europe climate zone. Such conditions indicate the need to capture available solar heat as much as possible. Additional dynamic elements in ABE, such as reflective blades and light-concentrating lenses, can enhance heat transfer into thermal storage. This study aims to utilize PCM in combination with high thermal performance insulation – aerogel into the dynamic solar facade module; it is possible to accumulate solar thermal energy that can be used for water and space heating. The application in buildings of such facade modules in the northern European climate zone has a great potential to noticeably reduce the dependence on conventional fuel-based energy usage for heating [13].

2. METHOD

Our research team is working on developing a dynamic solar facade with solar energy storage in PCM for the northern Europe climate zone. The methodology steps for elaborating the dynamic solar facade are presented in Fig. 1. The overarching research is divided into four large stages to advance through technological readiness levels from TRL2 – evaluating the potential of suitable components; to TRL6 – demonstration in the relevant environment. In this paper Stage 2 of the research is presented – variations of components of solar façade are compared. Particularly, the effect of the Fresnel lens focal point location and cone dimensions on heat transfer in small-scale solar facade modules is tested in laboratory conditions.

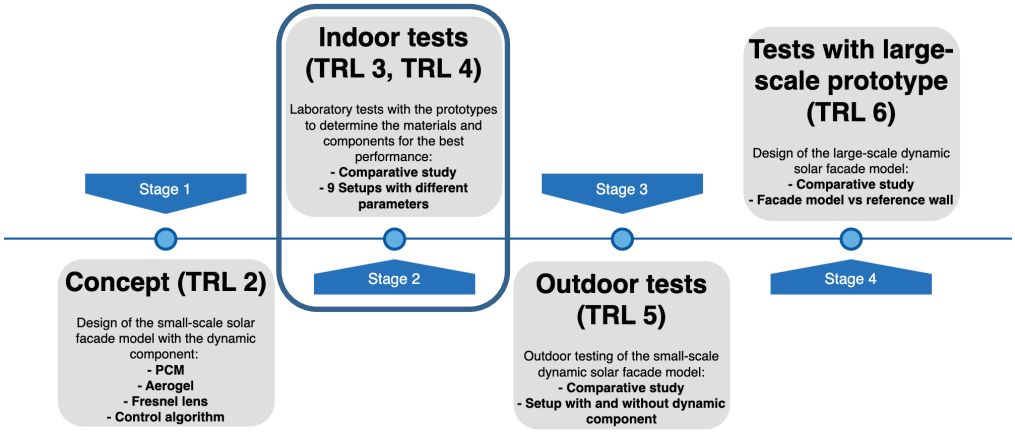

Fig. 1. Scope of the research (Stage 2) within the framework of the whole study [25].

The terminology used in this paper is illustrated below in Fig. 2. The setup is a tested composition of a solar façade module (left). Nine different composition variations are compared and described here in the paper. The test stand is an arrangement and equipment of the experiment (middle). Large-scale solar façade module will be tested in the relevant environment and composed of several small-scale solar façade modules (right).

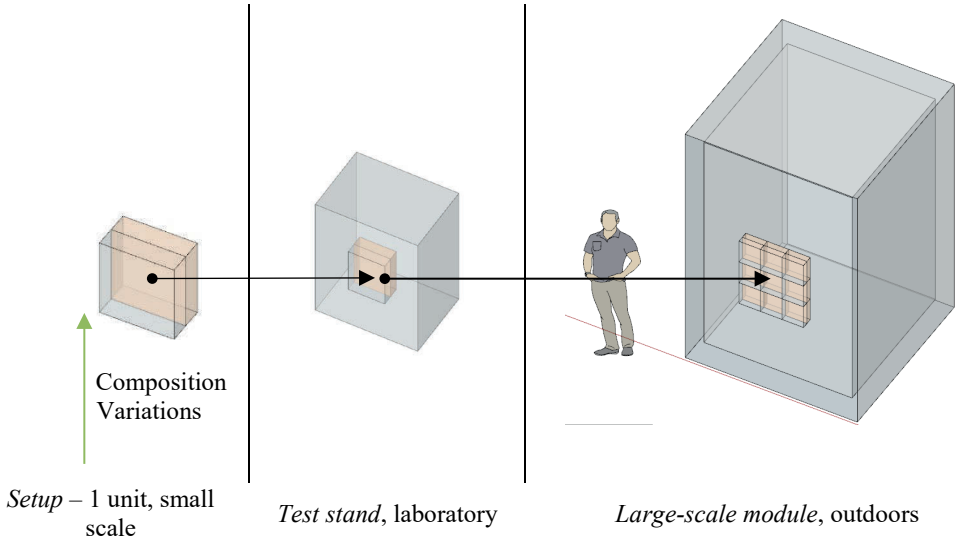

Fig. 2. The terminology used in paper.

2.1. Small-scale solar facade module

The proposed solar façade is a complex system; it consists of different components that provide the system's operation. To ensure optimal operation and heat transfer into the energy storage (phase change material), it is necessary to configure the components and their combinations for relevant border conditions. Small-scale solar facade module consists of several components (see Fig. 3): dynamic component, which includes moving reflective blades filled with aerogel insulation; Fresnel lens; cone-shaped air gap; aerogel (semi-transparent) insulation layer; PCM container and transparent glass shell that encloses the aerogel layer. The size of the small-scale module is 250 mm in width and 250 mm in height. The depth is dependent on the composition. The dynamic component supports the energy transfer from solar radiation to phase change material and reduces heat losses. Fresnel lens operates as an energy transfer enhancer into the PCM storage unit. A previous study [25] concluded that the aerogel layer thickness and cone diameter directly affect the temperature changes in PCM. These two variables are directly responsible for heat transfer between indoor and outdoor environments as the cone diameter determines the air gap volume between the Fresnel lens and PCM container. However, the aerogel insulation layer sets the focal point location of the Fresnel lens and insulates the heat storage around the cone. It was observed that the location of the focal point on the surface of the PCM container in some compositions was not beneficial. Therefore, as the next, the question of the impact of the focal point location in the phase change material on heat transfer in the proposed solar façade was raised. The experiment plan was designed to test the advanced versions of the solar façade module and evaluate the effect of focal point location and the size of cone diameter on heat transfer.

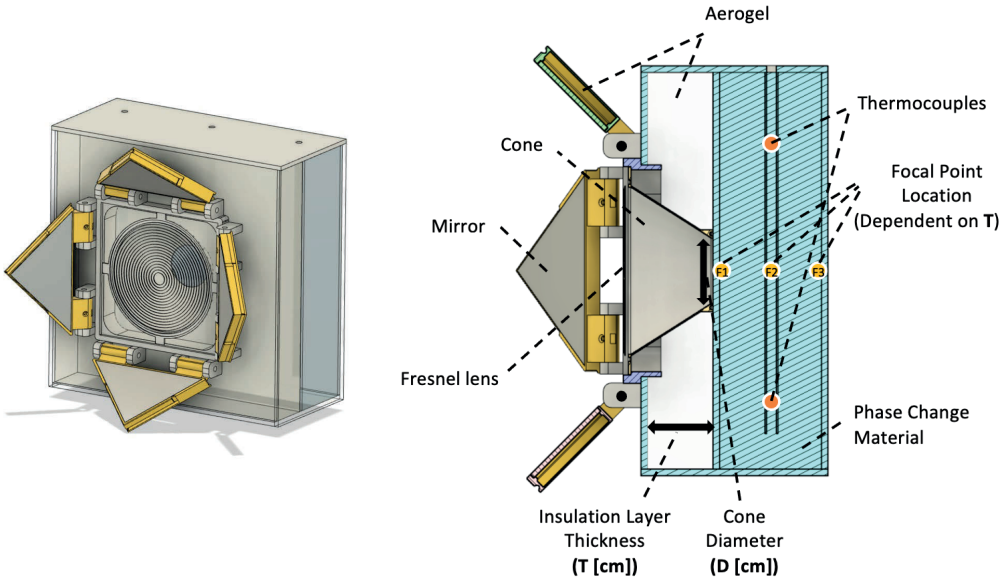

Fig. 3. Design of the small-scale solar facade module and its cross-section (TRL4).

2.2. Experimental testing stands and measurements

Nine different setups (solar façade compositions) of solar façade module were elaborated based on three variations of two parameters – the location of the Fresnel lens focal point (defined as the insulation layer thickness) and the size of the cone diameter. The focal point has been described with three different values that reflect its location on the inner and outer surfaces and in the middle of the PCM container. The values for cone diameter are selected from two to four centimeters. The variations of the setups are listed in Table 1.

TABLE 1. VARIATIONS OF THE EXPERIMENTAL SETTINGS IN TEST SETUPS

Insulation layer thickness T, cm			
	3	**5**	**7**
Cone diameter D, cm			
2	Setup F1 D2	Setup F2 D2	Setup F3 D2
3	Setup F1 D3	Setup F2 D3	Setup F3 D3
4	Setup F1 D4	Setup F2 D4	Setup F3 D4

For the testing rounds, a test stand was created. Small-scale solar facade module setups were enclosed into the extruded polystyrene (XPS) layer and plywood case (350×350×250 mm) to limit the impact of the surrounding environment on the heat transfer processes in the setup (see Fig. 4). The thickness of the insulation layer all around the tested module is 100 mm.

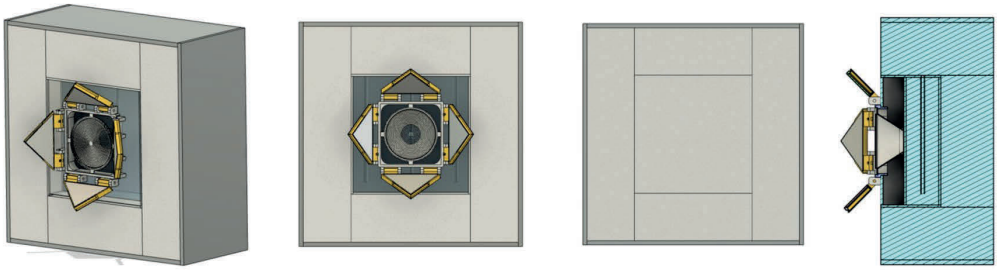

Fig. 4. Experimental stand of small-scale solar facade module.

The material characteristics of the components used in the small-scale solar facade module setups and test stand are listed in Table 2.

TABLE 2. COMPONENTS OF THE SMALL-SCALE SOLAR FACADE MODULE

Component	
PCM	RUBITHERM RT21HC Melting area: 20–23 °C Congealing area: 21–19 °C Density 15 °C: 0.88 kg/l Density 40 °C: 0.77 kg/l Heat storage capacity ± 7.5 % 190 kJ/kg
PCM glass container	Dimensions: 242 × 242 × 62 mm Thickness: 4 mm
Plywood	Thickness: 9 mm λ = 0.13 W/mK
XPS	100 mm λ = 0.037 W/mK

Experiments were conducted in the climate chamber under the same conditions. Two setups were tested simultaneously using two halogen lamps to simulate solar irradiance. The application of halogen lamps for solar radiation simulation was based on studies [26] and [27] that describe lamps' characteristics and properties and indicate their similarities to the sun's light. Comparison of setups is based on the analysis of temperature changes in phase change material. Temperature is registered in the PCM container with five thermocouples labeled according to their location in the PCM container (see Fig. 5(b)): the letters L, M, and R stand for their place on the x-axis (L – left, M – in the middle, R – right) and the numbers represent the location on the y-axis (1 – lower, 2 – upper). The measurements were registered once a minute using multipurpose data logger CR1000 Campbell Scientific. Solar irradiance was measured with the pyranometer CMP3, Kipp & Zonen. Type T thermocouples were used to measure the temperature in the PCM. Fig. 5(a) shows the layout of the test stand in the climate chamber and the spots of temperature measurements in the PCM container.

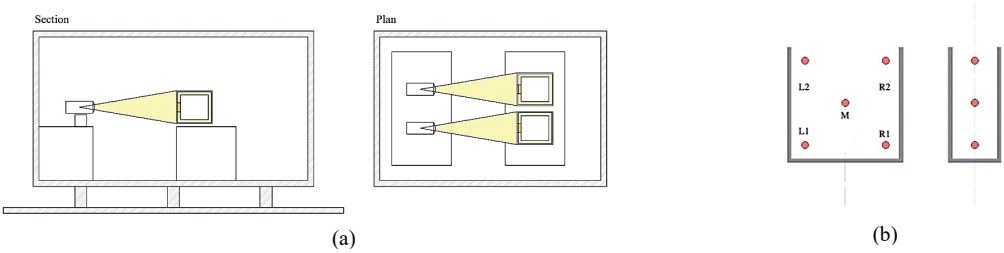

Fig. 5(a) Layout of the test stand in the climate chamber and (b) temperature measurement spots inside the PCM container.

The conditions for all the setups are listed in Table 3. The climate conditions in the autumn and spring seasons provide the most significant potential for the proposed solar facade system to reduce energy consumption for heating. These two seasons in northern Europe's climate are similar in average temperature and amount of available solar radiation. Parameters such as solar irradiance, ambient temperature, and the duration of daylight were set for experimental conditions according to a typical autumn/spring day in Riga (Latvia). They were identified by data analysis from the local metrological station (see Fig. 6). Average solar radiation and average ambient temperature was calculated based on measured data. In the period of observation, it is 300 W/m^2 and 10 °C, respectively.

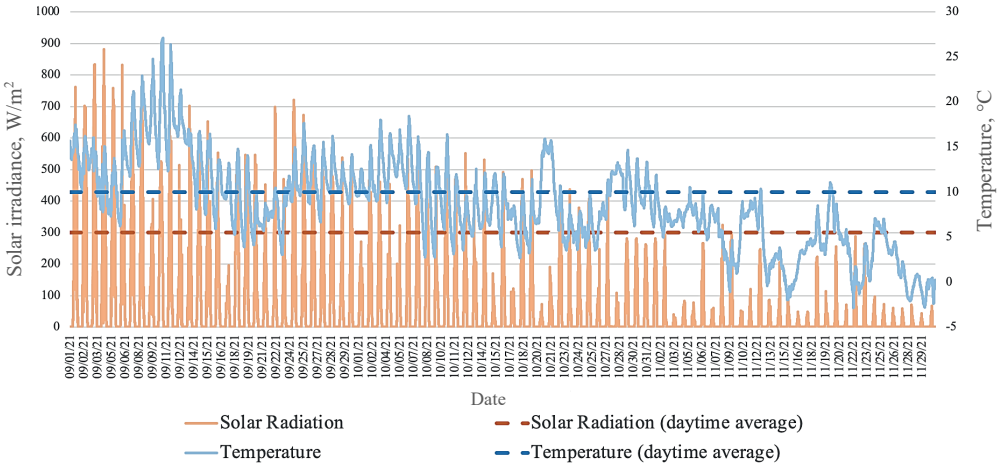

Fig. 6. Data from the Riga Technical University metrological station from September to December 2021.

The experiments were conducted in the climate chamber where the ambient temperature was set to 10 °C. The experiment takes place for 16 hours – 8 h with solar radiation simulation (‘daytime’ phase) and 8 h without solar radiation (‘nighttime’ phase). The blades of the dynamic component were static in this experiment. Two positions were set – during the ‘daytime’ blades were open and concentrated the light from the lamps to the center of Fresnel lens, but in the nighttime, blades were in a closed position, to reduce heat losses from PCM to the surroundings. Test conditions are summarised in the Table 3.

TABLE 3. CONDITIONS OF THE TEST SETUPS

Condition	Value
'Daylight' duration (solar simulation is switched on)	8 h
'Night-time' period (solar simulation is switched off)	8 h
Irradiance (solar simulator) intensity	300 W/m^2
Outdoor (ambient) temperature	10 °C

3. RESULTS

Nine test rounds were performed (one for each setup). The obtained results of the average temperatures in PCM containers in all setups are presented in Fig. 6 and Fig. 7, and sorted by focal point location and cone diameter.

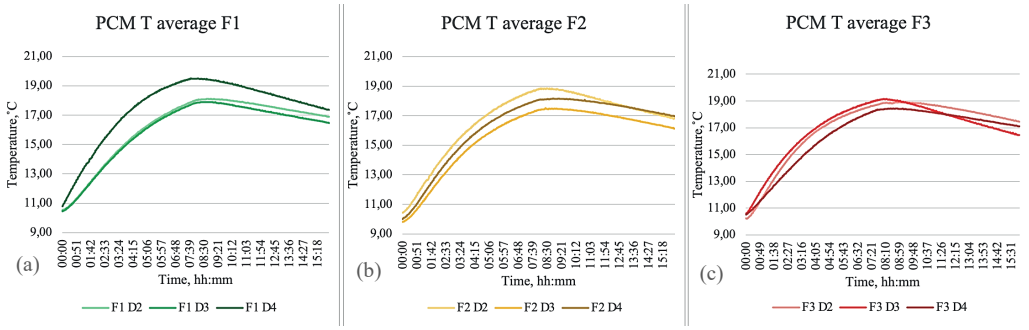

Fig. 6. Average temperatures in PCM container in all the Setups by focal point location: (a) – F1, (b) – F2 and (c) – F3.

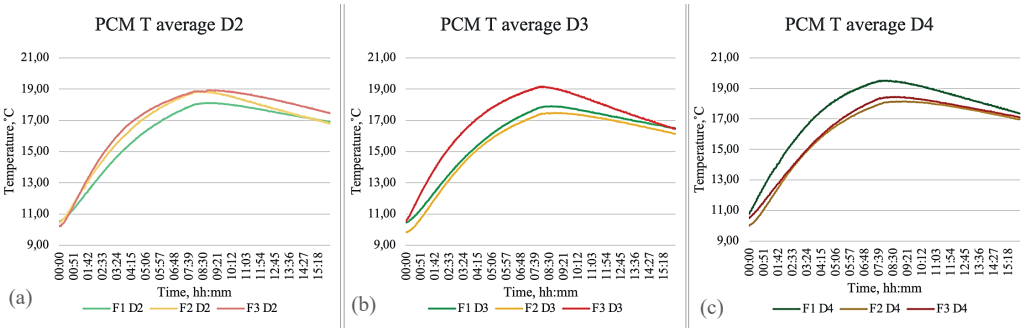

Fig. 7. Average temperatures in PCM container in all the Setups by cone diameter: (a) – D2, (b) – D3 and (c) – D4.

In the Setups with focal point location F1, the highest average temperature in PCM is reached with the widest cone diameter – D4. However, moving the focal point closer to the center of the PCM container gains higher average PCM temperatures with cone diameters D3 and D2. The graphs of setups F2 D2 and F3 D3 indicate a steeper temperature drop during the 'nighttime' period compared to other setups with the same focal point location. A similar tendency can be observed in Fig. 7 diagrams, where steeper 'nighttime' period curves (i.e., temperature drop) appear by enlarging the cone diameter.

Fig. 8 represents the maximum average PCM temperature during the test cycle and average PCM temperature at the end of the test cycle. The maximum temperature is reached in setup F1 D4; however, at the end of the experimental cycle, it drops lower than in setup F3 D2. The highest average PCM temperature at the end of the test cycle is in The most significant temperature drop during the test cycle is observed in setup F3 D3 – it has the second highest maximum average PCM temperature, and at the end of the experimental cycle, temperature decreases almost by 3 °C.

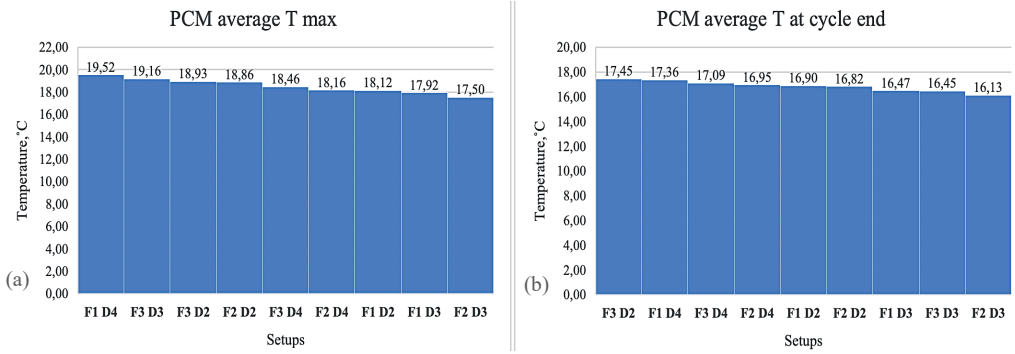

Fig. 8. Maximum average PCM temperature (a) and average PCM temperature at the end of the test cycle (b).

Fig. 9 illustrates the temperatures in PCM different layers measured by thermocouples. The temperature in Setup F1 D4 gradually rises in similar inclination in all the layers of PCM during the daytime cycle; on the contrary, the same temperature curves in Setups F2 D3 and F3 D2 are in broader amplitude. The central layer T M of PCM in all the Setups reaches the highest temperature at the end of the experimental cycle.

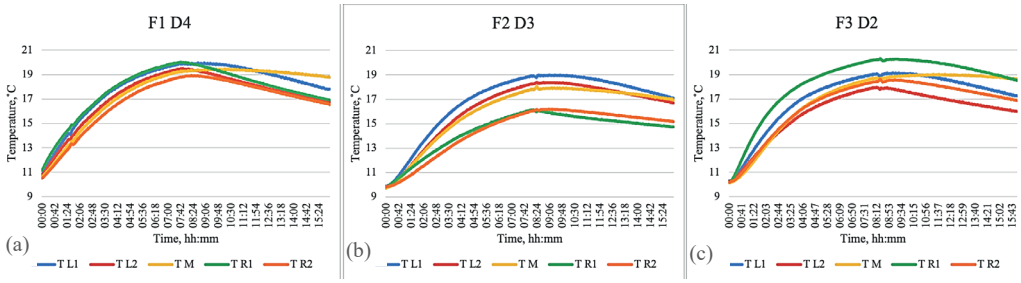

Fig. 9. Temperatures in PCM different layers (L1, L2, M, R1, R2) in Setups F1 D4 (a), F2 D3 (b) and F3 D2 (c).

4. CONCLUSIONS

The obtained results of temperatures in PCM indicate several conclusions:

1. The most significant amount of heat transferred into the phase change material is reached with setup F1 D4; during the 'daytime' cycle, the highest maximum temperature of 19.52 °C is gained in this setup.
2. The highest average temperature in PCM at the end of the test cycle is observed in the setup with the smallest cone diameter, which differs by 7.5 % compared to the setup with the lowest average PCM temperature. The lowest amount of heat was lost in setup F3 D2.
3. Moving the focal point location from the place on the PCM container's surface closer to

the PCM container's center means faster heat transfer with smaller cone diameters. Comparing setups F1 D4 and F3 D2, the results show that the average PCM temperature is 3 % higher in setup F1 D4.

4. Heat transfer enhancement can be achieved with a large cone diameter and thin aerogel layer (F3) in the 'daytime' cycle, yet the heat loss in 'nighttime' cycle reduces the total benefit. In setups F3 D3, the average PCM temperature is the second highest – 19.16 °C, however at the end of the cycle temperature drops to the second lowest 16.45 °C.
5. Both – focal point location and cone diameter significantly affect heat transfer enhancement in PCM. Comparing setups F1 D2 and F1 D4, the average PMC temperature increase is observed by 7.2 %. Similarly, comparing setups F3 D4 and F1 D4, the temperature increase is 5.4 %.

The experiments show that the best-performing test setup is Setup F1 D4. However, by implanting the module into the dynamic solar envelope, the focal point distance should be selected considering the aerogel insulation layer thickness. The aerogel insulation layer prevents the system from heat losses when ambient temperatures are low, and solar radiation is not enough. Obtained results show that by selecting a wider cone diameter, the heat transfer can be enhanced; therefore, for the studied solar facade, the most suitable setup is with an aerogel insulation layer of 7 cm and focal point location F1.

This paper reviews the laboratory testing stage of the complete dynamic solar facade development research. The effect of Fresnel lens focal point location and cone diameter on heat transfer enhancement in PCM has been evaluated. In a further study, it is planned to incorporate small-scale modules presented here into a large-scale façade and test it in relevant conditions. A PASLINK-type experimental setup will be used to conduct a comparative analysis – the proposed solar energy storage technology will be compared to the performance of a conventional facade such as a triple-glazed window.

ACKNOWLEDGEMENT

This study has been supported by Fundamental and Applied Research project 'Smart building EnVElope with solaR Energy STorage (EVEREST)', project No. lzp-2019/1-0363, funded by the Latvian Council of Science.

REFERENCES

[1] Global Data. Global construction industry set to grow by 5.2% in 2021, according to GlobalData. [Online]. [Accessed: 10.10.2022]. Available: https://www.globaldata.com/media/construction/global-construction-industry-set-grow-5-2-2021 according-globaldata/#:~:text=Following%20the%20historic%20collapse%20in,leading%20data%20and%20analytics%20company

[2] European Commission. Delivering the European. 2021.

[3] Felseghi R.-A., Bolboacă A. R., Raboaca M.-S., Aşchilean I. Hybrid Energy Systems for Power of Sustainable Buildings. Case Study: A Renewable Energy Based on-Site Green Electricity Production. *Comprehensive Renewable Energy* 2022:4:420–436. https://doi.org/10.1016/B978-0-12-819727-1.00037-6

[4] Luo Y., Zhang L., Bozlar M., Liu Z., Guo H., Meggers F. Active building envelope systems toward renewable and sustainable energy. *Renewable and Sustainable Energy Reviews* 2019:104:470–491. https://doi.org/10.1016/j.rser.2019.01.005

[5] Vassiliades C., Agathokleous R., Barone G., Forzano C., Giuzio G. F., Palombo A., Buonomano A., Kalogirou S. Building integration of active solar energy systems: A review of geometrical and architectural characteristics. *Renewable and Sustainable Energy Reviews* 2022:164:112482. https://doi.org/10.1016/j.rser.2022.112482

[6] Lyden A., Brown C. S., Kolo I., Falcone G., Friedrich D. Seasonal thermal energy storage in smart energy systems: District-level applications and modelling approaches. *Renewable and Sustainable Energy Reviews* 2022:167:112760. https://doi.org/10.1016/j.rser.2022.112760

[7] Santos José J. C. S., Palacio José C. E., Reyes Arnaldo M. M., Carvalho M., Freire A. J. R., Barone M. A. Concentrating Solar Power. *Advances in Renewable Energies and Power Technologies* 2018:1:373–402. https://doi.org/10.1016/B978-0-12-812959-3.00012-5

[8] Weiss W., Spörk-Dür M. Solar Heat World 2022. Global Market Development and Trends 2021. Detailed Market Figures 2020. https://doi.org/10.18777/ieashc-shw-2021-0001

[9] Sarbu I., Sebarchievici C. A comprehensive review of thermal energy storage. *Sustainability (Switzerland)*. 2018:10(1). https://doi.org/10.3390/su10010191

[10] Sari A.. Thermal Energy Storage and Applications Using Phase Change Materials. 3rd International Turkic World Conference on Chemical Sciences and Technologies. 2017.

[11] De Gracia A., Cabeza L. F. Phase change materials and thermal energy storage for buildings. *Energy and Buildings* 2015:103:414–419. https://doi.org/10.1016/j.enbuild.2015.06.007

[12] Saffari M., Roe C., Finn D. P. Improving the building energy flexibility using PCM-enhanced envelopes. *Applied Thermal Engineering* 2022:217:119092. https://doi.org/10.1016/j.applthermaleng.2022.119092

[13] Kalbasi R., Hassani P. Buildings with less HVAC power demand by incorporating PCM into envelopes taking into account ASHRAE climate classification. *Journal of Building Engineering* 2022:51:104303. https://doi.org/10.1016/j.jobe.2022.104303

[14] Alshuraiaan B. Efficient Utilization of Pcm in Building Envelope in a Hot Environment Condition. *International Journal of Thermofluids* 2022:16:100205. https://doi.org/10.1016/j.ijft.2022.100205

[15] Ajour M. N., Abduaal M. J., Hariri F. A., Abu-Hamdeh N. H., Karimipour A. Reducing electricity demand by integrating a sustainable pack into HVAC- adding PCM in sustainable pack as well as building envelopes. *Journal of Building Engineering* 2022:57:104915. https://doi.org/10.1016/j.jobe.2022.104915

[16] Piselli C., Prabhakar M., De Gracia A., Saffari M., Pisello A. L., Cabeza L. F. Optimal control of natural ventilation as passive cooling strategy for improving the energy performance of building envelope with PCM integration. *Renewable Energy* 2020:162:171–181. https://doi.org/10.1016/j.renene.2020.07.043

[17] Al-mudhafar A. H. N., Hamzah M. T., Tarish A. L. Potential of integrating PCMs in residential building envelope to reduce cooling energy consumption. *Case Studies in Thermal Engineering* 2021:27:101360. https://doi.org/10.1016/j.csite.2021.101360

[18] Abu-Hamdeh N. H., Melaibari A. A., Alquthami T. S., Khoshaim A., Oztop H. F., Karimipour A. Efficacy of incorporating PCM into the building envelope on the energy saving and AHU power usage in winter. *Sustainable Energy Technologies and Assessments* 2021:43:100969. https://doi.org/10.1016/j.seta.2020.100969

[19] Bumanis G., Bajare D. PCM Modified Gypsum Hempcrete with Increased Heat Capacity for Nearly Zero Energy Buildings. *Environmental and Climate Technologies* 2022:26(1):524–534. https://doi.org/10.2478/rtuect-2022-0040

[20] Gholamibozanjani G., Farid M. A comparison between passive and active PCM systems applied to buildings. *Renewable Energy* 2020:162:112–123. https://doi.org/10.1016/j.renene.2020.08.007

[21] Arumugam P., Ramalingam V., Vellaichamy P. Effective PCM, insulation, natural and/or night ventilation techniques to enhance the thermal performance of buildings located in various climates – A review. *Energy and Buildings* 2022:258:111840. https://doi.org/10.1016/j.enbuild.2022.111840

[22] Shen J., Wang Z., Luo Y., Xu J., Zhao H., De'en Cui., Tian Z. Performance evaluation of an active pipe-embedded building envelope system to transfer solar heat gain from the south to the north external wall. *Journal of Building Engineering* 2022:59:105123. https://doi.org/10.1016/j.jobe.2022.105123

[23] Luo Y., De'en Cui, Cheng N., Zhang S., Su X., Chen X., Tian Z., Deng J., Fan J. A novel active building envelope with reversed heat flow control through coupled solar photovoltaic-thermoelectric-battery systems. *Building and Environment* 2022:222:109401. https://doi.org/10.1016/j.buildenv.2022.109401

[24] Balaji D., Sivalingam S., Bhuvaneswari V., Amarnath V., Adithya J., Balavignesh V., Ganesh Surya R. Aerogels as alternatives for thermal insulation in buildings – A comparative teeny review. *Materials Today: Proceedings* 2022:62(P8):5371–5377. https://doi.org/10.1016/j.matpr.2022.03.541

[25] Narbuts J., Vanaga R., Freimanis R., Blumberga A. Laboratory Testing of Small-Scale Active Solar Façade Module. *Environmental and Climate Technologies* 2021:25(1):455–466. https://doi.org/10.2478/rtuect-2021-0033

[26] Cho Y., Kim J.-J. Lifetime decrease of halogen lamps for automotive by duty cycle stress. *IEEE Transactions on Reliability* 2011:60(3):550–556. https://doi.org/10.1109/TR.2011.2135730

[27] Hume R. A. Tungsten halogen lamps. *Lamps and Lighting* 2012:177–193.

PAPER 4: ON-SITE TESTING OF DYNAMIC FACADE SYSTEM WITH THE SOLAR ENERGY STORAGE

Energy 283 (2023) 128257

Contents lists available at ScienceDirect

Energy

journal homepage: www.elsevier.com/locate/energy

On-site testing of dynamic facade system with the solar energy storage

Ruta Vanaga *, Jānis Narbuts, Zigmārs Zundāns, Andra Blumberga **

Institute of Energy Systems and Environment, Riga Technical University, Riga, Latvia

ARTICLE INFO

Handling Editor: Dr. Henrik Lund

Keywords:
Phase change material
Active building envelope
PASLINK
Buildings for on-site energy storage
Renewable energy in building envelope

ABSTRACT

Decarbonistation goals for building stock calls for innovative solutions on both supply and demand side. Thermal envelopes with in-build energy storage could gather on-site solar energy and reduce cooling or heating loads of the buildings. Results of on-site testing of dynamic facade system with the solar energy storage are presented in the paper. Proposed solar façade consists of phase change material to rise the heat capacity of the building envelope, aerogel for insulation, Fresnel lens for solar energy concentration accompanied by moving reflective blades for heat transfer enhancement. Comparative study was conducted in PASLINK type test booths– the performance of proposed solar façade was compared to the reference element – the highest performance triple glazed window suitable for low energy buildings. The detailed measuring setup provide information on the thermal performance of phase-change material enhanced building envelope under different outdoor conditions (summer, autumn, winter) in Northern European climate. The gained results indicate that proposed solar façade module provides lower energy demand during the cooling season compared to the window, in mid-season it performs similarly, however in heating season proposed solar façade in its current composition is outperformed by high performance triple glased window.

1. Introduction

European Union's largest energy sector is heating and cooling as it is responsible for round about 50% of EU's total energy consumption [1]. The European Green Deal sets the climate targets including zero net emissions of greenhouse gases (GHG) by 2050 [2] and the building sector is one of the main sections where these emissions can be considerably reduced. Scientific innovations are needed to ensure the energy transition and reaching the Green Deal goals [3]. Renewable energy integration in cooling and heating systems is the key aspect to attain building decarbonization goals [4]. Energy performance of buildings directive requires all new buildings from 2021 to be nearly zero-energy buildings (NZEB) and the energy required should be covered from renewable sources [5]. Building envelope can serve as the media that diverts the on-site available renewable energy to cover the energy demand of the building including the energy storage thus providing the energy flexibility capacities to the building [6,7]. There are several approaches used for energy storage in buildings and one of these is the use of phase change materials (PCM) to enhance the heat capacity of building thermal envelope [8].

Bibliometric analysis using Web of Science database was performed to analyse the availability of scientific literature sources in the field of phase change material enriched building materials (Fig. 1).

Three searches were run in search engine defined as follows:

1) ALL = (Building energy efficiency); years 2011–2020, Document type – Articles and Review articles;
2) Within results of 1) building envelope related articles were searched: (ALL = (energy efficiency)) AND (ALL = (Building envelope*) OR ALL = (roof*) OR ALL = (floor*) or ALL = (window*) OR ALL = (wall*) or ALL = (glazing*) OR ALL = (glasing*));
3) Within results of 1), PCM applications in building envelope were searched: (ALL = (energy efficiency)) AND (ALL = (Building envelope*) OR ALL = (roof*) OR ALL = (floor*) or ALL = (window*) OR ALL = (wall*) or ALL = (glazing*) OR ALL = (glasing*) AND (Phase change material*)).

Obtained data shows that during the last decade the number of building energy efficiency related articles has increased almost six-fold. Bigger half of more than 30 k (2011–2020) articles are related to building envelope, but only 5% of envelope related articles are devoted to the use of phase change materials (Fig. 1).

* Corresponding author.
** Corresponding author.
E-mail addresses: ruta.vanaga@rtu.lv (R. Vanaga), andra.blumberga@rtu.lv (A. Blumberga).

https://doi.org/10.1016/j.energy.2023.128257
Received 20 December 2022; Received in revised form 17 June 2023; Accepted 23 June 2023
Available online 26 June 2023

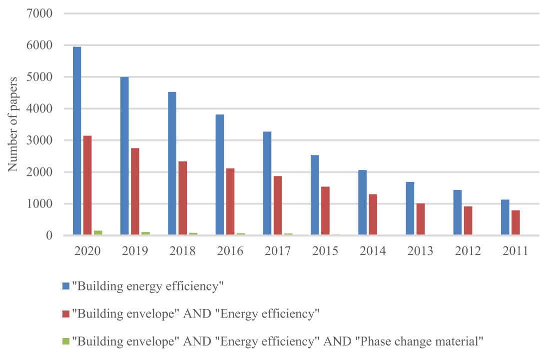

Fig. 1. Proportion of PCM related articles within articles focusing on building energy efficiency and building envelope.

Vosviewer software was used to visualise the keyword interactions in the selection of articles (first search – building energy efficiency). Five main groups are visualized in building energy efficiency related article set – energy consumption and building energy renovation, thermal comfort and occupant behaviour, renewables (including PCMs) and thermal properties. Numerical simulation is a key word related to several fields and the size of the bubble indicates the frequency level of reoccurrence (Fig. 2).

Analysing PCM related articles within articles focusing on building energy efficiency and building envelope (review articles excluded) significant increase can be observed within the last decade (Fig. 3). Comparing the number of numerical and experimental studies, first ones slightly outnumber the second ones. In even less articles both numerical and experimental studies are combine. The paper adds scientific knowledge on the performance of PCM-enhanced building envelope under real climatic conditions.

The described in paper solar facade contribute to this less studied

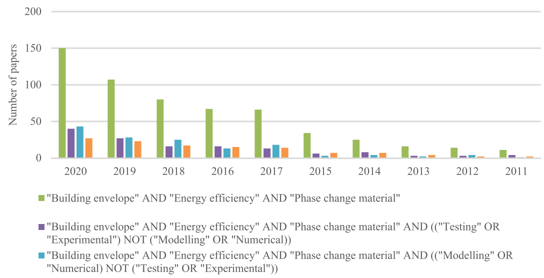

Fig. 3. Proportion of PCM related articles within articles focusing on building energy efficiency and building envelope.

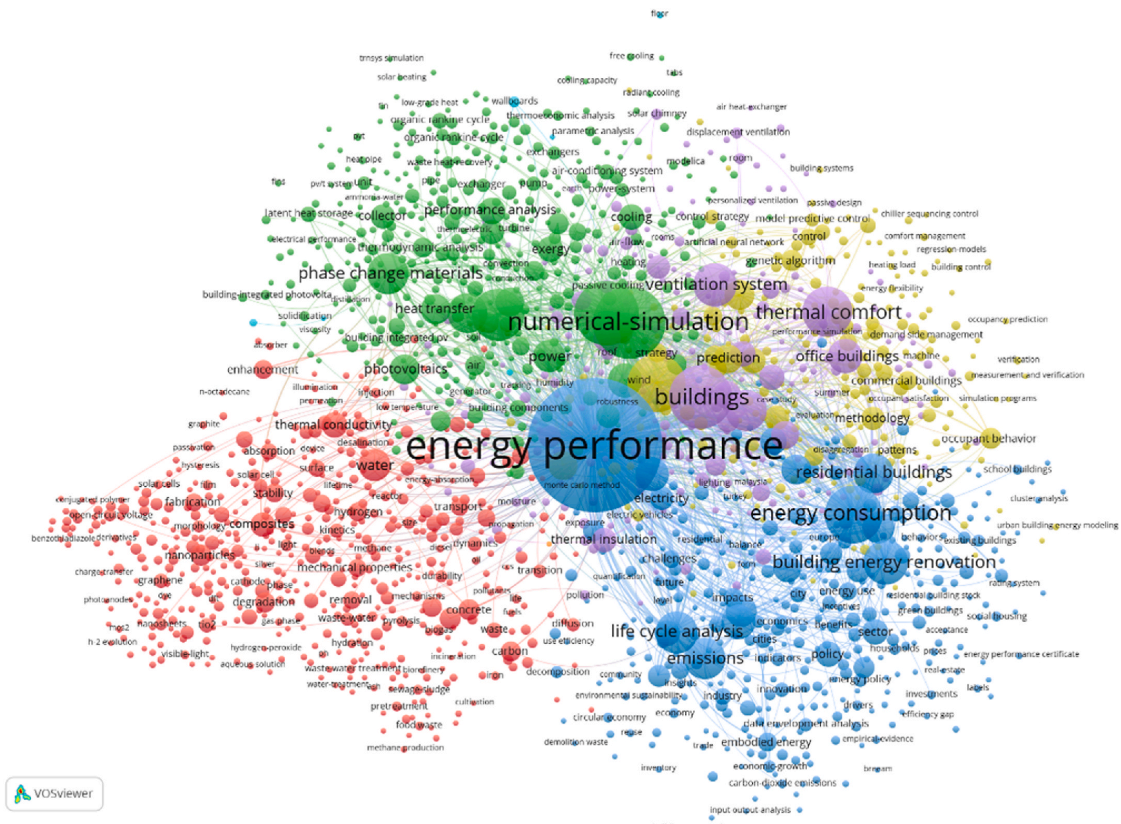

Fig. 2. Reoccurrences of keywords in selection of articles on building energy efficiency.

field but also combine two emerging trends – PCM containing building envelopes and adaptive building envelopes, thus promoting the innovation in the field.

This paper focuses on the development of innovative technological solution for buildings that is based on renewable on-site solar energy utilization and thermal storage to reduce total energy consumption and to balance the load on heating and cooling systems and builds on previous studies [9–12]. This technology is developed to be suitable for buildings located in Northern Europe climate zone, where the space heating is required for three seasons and cooling demand increases due to the increase in summer outdoor temperature. In spring and autumn seasons, the sun is not present as often as in the summertime; even so, there are enough sunny days to use solar-thermal energy for heating purposes. While the ambient temperature outside in sunny day can reach up to 20 °C, in the night it can go down below 0 °C and the necessity for space heating can occur. To prevent cooling down of the room, solar-thermal energy can be collected at the daytime, when it was available, and stored for later use in the night. Phase-change materials can be used to provide energy storage as they have sensible and latent heat characteristics. There are multiple studies on the PCM enriched building components, exploring their advantages and disadvantages [13–17]. To ensure maximum energy conservation into the PCM, aerogel insulation layer is used. Compared to conventional insulation materials, aerogels have superior insulation properties and the lowest density of any known solid [18]. Silica aerogels are translucent which makes them perfect insulation material in cases, where solar radiation has to be captured [19]. For the heat transfer enhancement into the PCM Fresnel lens is used. Fresnel lenses have been used in many novel technological solutions and prove to be effective in concentrating the sunlight. Kumar has integrated Fresnel lens into the segmented mirror reflector with parabolic concentrator to capture the sunlight for indoor daylight illumination [20]. Highly efficient daylight factor of 35% was reached in the experiments conducted in this study. In another study Karimi was investigating Photovoltaic/thermal solar system by using Fresnel lens for energy concentration [21]. Observations show that the output power increased by 28% under metrological weather conditions in Shanghai. In Northern Europe climate zone more precisely in Latvia the sun shines 1790 h on average per year [22], furthermore it is crucial to capture sunlight as much as possible when it is present. Dynamic component is the main feature of proposed technology that is responsible for capturing solar radiation and lead it inside the envelope. Solar tracking technology has been used efficiently in many applications, for instance, Zhou has analysed compact solar concentrator tracking through reflection of the rotating prism, where this technology showed 41,1% efficiency by land area, which is 17,6 points higher that flat plate collectors exhibited [23]. In case of suggested technology dynamic component is tracking the sunlight throughout the daytime and with mirror blades reflects it on the surface of Fresnel lens. In the night, when outside temperature drops low, or during the time, when sunlight is not present, these blades close up, in such way insulating the collected thermal energy into the envelope.

To fasten the energy transition several innovative building thermal envelope concepts have appeared. Converting facade systems from passive elements of building energy balance to active ones, the share of utilization of available on-site would rise and in combination with energy storage, it could offer energy demand flexibilities.

1.1. Use of renewable energy in building envelope

The technologies that are used in building envelopes are adapted to the climate zone and requirements of the inhabitants. Improving the quality of building envelope is one of the key aspects to achieve better energy efficiency. As the global construction market is keep growing [24], it is crucial to provide sustainable energy efficient and low-carbon emission buildings to overcome challenges of the climate change. Introducing new and innovative technologies such as responsive or intelligent building envelopes can provide new pathway in reaching goals. Such technologies use renewable sources to balance the energy consumption of the building and adapt to changing meteorological conditions on-site to provide comfortable indoor conditions.

Xingxing Zhang have carried out extensive review on renewable-energy-source envelope solutions and made a classification of the recent development traits. There are three groups in Zhang's et al. proposed classification: 1) solar power; 2) solar/air thermal and 3) energy efficiency focused solutions how renewable energy technologies can be integrated in building envelope. The proposed solar façade explores several of the emerging trends – it combines elements of solar/air thermal - solar thermal façade that absorbs the solar energy into its structure and energy efficiency – phase change material to rise the capacity for energy storage in building envelope combined with the dynamic and adaptive capabilities (see Fig. 4).

1.2. Innovative concepts for building envelope

There are several terms describing the concept of adaptive and active concepts emerging. New typologies of building constructions are being researched and developed in last decades. Next chapters provide description of some of emerging conceptual frameworks.

1.2.1. Climate adaptive building shell

Increasing requirements for environmental, social and economic performance calls for more sophisticated solutions for building and its components design. Climate adaptive building shells (CABS) have been recently been suggested as a promising alternative to traditional building envelope. CABS provide potential opportunities for energy savings for heating, cooling, ventilation or lighting in addition to improvement of indoor microclimate [26].

CABS is defined by Loonen: "Due to new performance requirements and variable boundary conditions, a climate sensitive building shell may modify any of its functions, characteristics, or behaviour continuously and reversibly over time, with the goal of enhancing total building quality" [26]. These shells should be ready to adapt to the current condition and even return to their normal state if necessary in order to produce the intended outcome [27]. The key goal is to make the building more adaptive to its surrounding environment in order to improve the indoor climate conditions and users experiences while reducing energy consumption. CABS fulfil a number of requirements that are either incompatible or contradictory, such as finding a balance between sunlight and shadow, fresh air and draft, airflow and moisture, shutters and reflectors, heat gains and overheating [28]. There are various ways to achieve the dynamics of the envelope for example the moving components can be introduced by airflows or a chemical change of the material, but make it sufficient, adaptive features must be integrated into a whole system [29].

CABS can be described by the range of different terms. Variations of term "adaptive" can be used for example active, advanced, dynamic, interactive, kinetic, responsive intelligent or switchable. They can be categorized by several independent characteristics envelopes are based on such as climatic factors (heat, light, air, water or other types of energy), the time frame scale, the scale of change (macro-scale or micro-scale changes) [30], the control type (intrinsic or extrinsic regulators), the spatial scale (size of a system), the inspirational scale (biomimetic adaptive building skins), the development stage, the number of functions and the performance task [31].

1.2.2. Solar responsive building envelopes

Solar responsive systems work by converting solar energy into various forms. They typically employ one of the five types of solar control devices: external, integrated, internal, double skin, and ventilated cavity [27].

Heat is one of the forms of solar energy. Solar heat systems are designed to maximize heat gain in the winter and reduce it in summer.

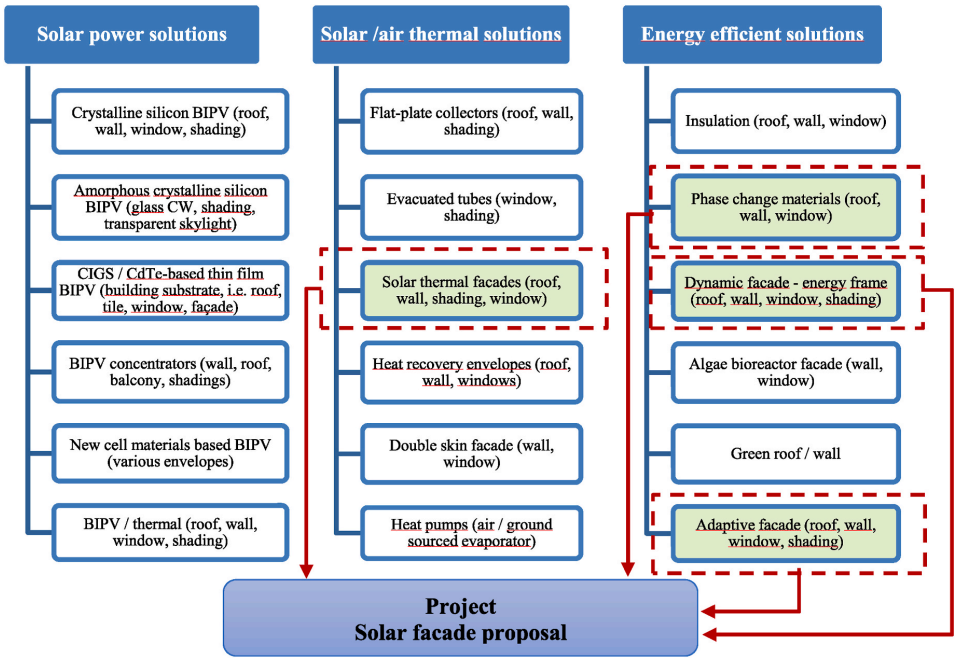

Fig. 4. Classification of renewable-energy-source envelope solutions by Ref. [25] and the project scope in the structure of the proposed classification.

The solar barrel wall, water bags on the roof, dynamic insulation, and thermochromic (colour changes due to temperature) materials on walls or windows are some examples of this technology [29].

Light is another form of solar energy that can be controlled by indoor illuminance levels, distributions, window locations, and glare in systems that use this energy source. Classic mechanical systems such as venetian blinds, advanced mechanical systems that can rotate, slide and self-adjust, and smart glass or transparent thermochromic or photochromic materials are the three major approaches to achieve these functions. Systems that are used in windows, usually change optical properties, lighting direction, visual appearance, and thermal properties. Electrically activated glazing for building facades has achieved market feasibility and is covers smart building material niche in glazing systems.

Electricity is the third kind of solar energy, and it is based on the installation of advanced photovoltaic systems. CABS must be kinetic rather than independently movable panels in order to be called CABS. This is usually accomplished by using heliotropic sun-tracking systems to optimize solar energy capture [29].

There are many terms describing similar concepts. No stringent typology is introduced yet to define difference between dynamic or kinetic, smart or intelligent facades. In this literature review these are assumed to be synonyms and façade examples are reflected under the terms as met in literature sources.

1.2.3. *Dynamic facades*

Inspired by Mashrabiya Arab traditional shading system built by Jean Nouvel for the Arab World Institute's south facade in Paris is one of the most famous designs of dynamic facades designed and built in 1981–1987. Façade consists of composition of apertures, that regulate the light transmittance [32]. Because of the movement of the white aluminum perforated plate, this facade changes every day, every hour, revealing a new face. The architects have also created a choreography that allows the structure to transform into desired pattern. Not only is it a sun-shading device, but it is also a way to express contributes to the aesthetics of the building.

Another example was created by Adaptive Building Initiative, a joint venture between Hobermann Associates of New York and Buro Happold - dynamic facade system that consists of overlapping layers that flow over one another. It is a self-contained, framed screen with a constantly shifting perforated pattern. As a result, a dynamic architectural feature that controls light and solar gain, ventilation and airflow, privacy, and views is developed. The device is made up of a series of stacked panels made of different metals or plastics. The effect is a visual display of patterns aligning and then diverging into a light-diffusing mesh as the layers overlap [33].

Adaptive Fritting is the name of the other system developed in the framework of adaptive building initiative. It is an integrated glass device with a custom moveable graphic pattern that can alter transmitted light, solar gain, privacy, and views by modulating its pattern composition. Opacity changing effect is created by spinning a series of fritted glass layers in a way that the visual pattern alternates between aligning and diverging [34].

Often dynamic facades fulfil several requirements. Thus, sunscreen in Ginza Pola Building in Tokyo, which was constructed in 2009 [35], fulfils three functions – it is a visual attraction (LED (light-emitting diode) lights are integrated in the structure), controls daylighting and takes part in passive night cooling [36].

A dynamic facade in a variety of shapes and materials can be used to build a dynamic exterior. Perforated metal panels, typically of a basic design, such as rectangular, are widely used. They shape the building's outer skin by being positioned in front of the glass surfaces. Electro-mechanical systems embedded in the facade's support framework ensure their movement. The Kiefer Technic Showroom in Bad Gleichenberg Austria is an example of this kind of façade [37].

1.2.4. *Kinetic building envelopes*

A kinetic facade allows movement on a building's surface by changing dynamically rather than being static or fixed. This helps to

create a skin-like articulation effect, as described by architect Buckminster Fuller, and is an extension of the concept that a building's envelope is an active system rather than just a container [38].

A kinetic facade can control light, air, energy, and character. They can help to maintain the quality of indoor environment by reducing solar gain while also bringing fresh air into the room. The moving elements of the facade may be designed to respond to climatic or other environmental conditions, time, levels and type of occupancy, and other factors to increase efficiency and productivity. Designers are increasingly able to accept kinetic components as develop solutions, thanks to advancements in sensor, material, and building management technology.

As an example of such systems serves Aedas and Arup's dynamic envelope for the Abu Dhabi Investment Council's headquarters is made up of specially engineered fabric sunscreen components that are moved by robotic arms [39]. The design of the shading elements is based on the Mashrabiya Arab tradition similar concept to the one used in Arab institute. Other examples can be mentioned - FLARE facade created by WHITEvoid and The Theme Pavilion EXPO in South Korea [40].

1.2.5. Active building envelopes

Luo et al. propose a term "Active building envelopes (ABE)" and define them to be building element systems that:

1) "actively utilizes energy input to manage the cooling/heating load of envelope or indoor artificial daylighting load, directly reducing the demand on central HVAC systems, and often supplanting their function with the ABE through mechanical, electrical or chemical actions;
2) acts as an energy convertor that transforms renewable energy (solar energy, wind energy, etc) into conventional energy (specifically electrical, mechanical or chemical energy) for a certain means of improving building performance" [6].

If the building envelope system satisfies at least one of these conditions, it is considered as ABE. There are ABEs that also have some passive technologies applied in system. The most critical aspect of ABE, however, is its reliance on additional energy input to improve building performance. An efficient and high-performing ABE architecture must ensure that the energy saving amount is greater than the energy input during service [6]. Several researchers [41,42], for instance, propose hybrid photovoltaic/thermal modules (ventilated façade) for active building envelopes. Dehwah summarises that movable photovoltaic-integrated shading devices and switchable insulation systems are among the most used active building integrated systems [43].

1.3. Phase change material for energy storage

Availability of renewable technologies (in contrast to conventional fossil energy) exhibit inconsistencies compared the energy demand – at peaks it may exceed the demand and at lows it may not cover the energy needed. It has diurnal and seasonal or meteorological swings depending on the type of renewable energy technology. The performance of solar technologies is directly dependant on the availability of solar radiation. The solar radiation is not always available when there is the greatest demand for the heat or electricity. Thus, energy storage has become a critical component of renewable energy systems. Thermal energy storage (TES) is a technique for storing thermal energy by heating or cooling a storage medium, which can then be used for heating and cooling applications at a later time. TES systems are used in a variety of applications, including buildings and manufacturing processes. The use of TES in an energy system has many advantages, including increased overall performance and reliability, as well as improved economics, lower maintenance and operating costs, and less contamination of the atmosphere, such as less carbon dioxide emissions [44].

PCMs can be applied in passive storage systems such as walls, windows, ceilings, floor and roof where no mechanical interference is used to initiate charge and discharge cycles whereas in the active systems energy is added to make the storage system operate as intended [45]. In passive solar heating using PCMs heat is collected inside the element (wall, roof or floor) absorbing solar radiation. This heat is released when the solar energy decreases and the ambient temperature drops. Active heating system provides the necessary room temperature by heating up the PCM with solar collector system, heat pump or using cheaper night-time electricity.

Different approaches and technologies have been proposed in recent years of how the PCMs can be implanted into the building envelopes. In one of the studies [46] an aluminium honeycomb containing a micro-encapsulated PCM wallboard was researched. Experimental results showed sufficient heat conduction enhancement. In other study [47] PCM macro-capsules were incorporated in masonry wall clay bricks that lead to indoor temperature swing reduction from 10 °C to 5 °C and the time delay of around 3 h.

A study of a numerical model of residential building roof with PCM layer has been developed to evaluate thermal performance using the data of climatic conditions in Chennai for the month of January [48]. The findings indicate that a PCM embedded rooftop maintains the ceiling temperature in the region of 25,5 °C–27,5 °C and decreases highest recorded heat levels as contrast to a rooftop without PCM. In comparison to a non-PCM room, a PCM slab inclined at 2 °C offers a maximum ceiling temperature reduction of 2,38 °C and daily heat gain savings of 0,106 kW h/m^2 or 16% for the same thickness and material properties.

Garcia et al. introduced phase change material for ventilated double skin façade for Mediterranean climate [49]. In comparative experimental study during winter period in Spain two test buildings were observed – one reference building and in other PCM enriched double skin façade was incorporated. Results show that the use of PCMs significantly improves the thermal behaviour of all building by reducing the electrical consumption and serving as heat supplier in the periods when it is necessary.

A comparison between active and passive PCM systems was carried out by Gholamibozanjani and Farid [50]. The potential of passive and active systems for energy savings and peak load shifting were investigated using two identical test booths, each fitted with a control system. One of the booths was outfitted with PCM-integrated wallboards, while the other one was designed with active air-PCM heat storage units. When both systems have the same amount of heat storage capacity, the energy used in the booth for an active system was 22% fewer over ten-day period in winter. When peak load shifting was investigated, it was discovered that using an active system resulted in a 32% reduction in energy costs.

In recent studies phase change materials are used to advance the concept of Trombe wall. Ke et al. proposed to combine Trombe wall with photovoltaic panels and studied the impact of the phase change material placement in such system [51]. Researchers concluded that out that the placement (closer to inner or outer surface) of PCM layer benefits either electrical performance or passive heating, but not both and that in cold climates PCM layer shal be placed closer to the room.

Number of prosumers is growing worldwide and buildings become more active part of a wider and smart energy system [52]. Smart energy system can be defined as a strategy, where different energy grids are combined in order to find the best solution to each of them and as a whole system together by the result of their interaction [53]. By combining renewable energy utilization and the storage advantages of smart energy systems, it is possible to ensure flexibility of the power grid while providing carbon neutral energy to consumers [54]. Smart energy systems can be implanted in different scales. For instance, Yang [55] has researched community-level smart thermal grid, which was integrated with distributed and centralized seasonal thermal energy storages. Two systems, where the short-term thermal storage was supported by individual solar collectors and used for space heating while demand for

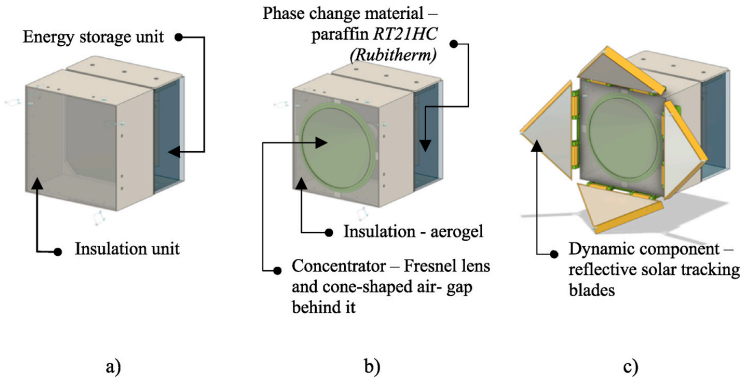

Fig. 5. The conceptual design of proposed solar façade – insulation unit + energy storage unit + dynamic component.

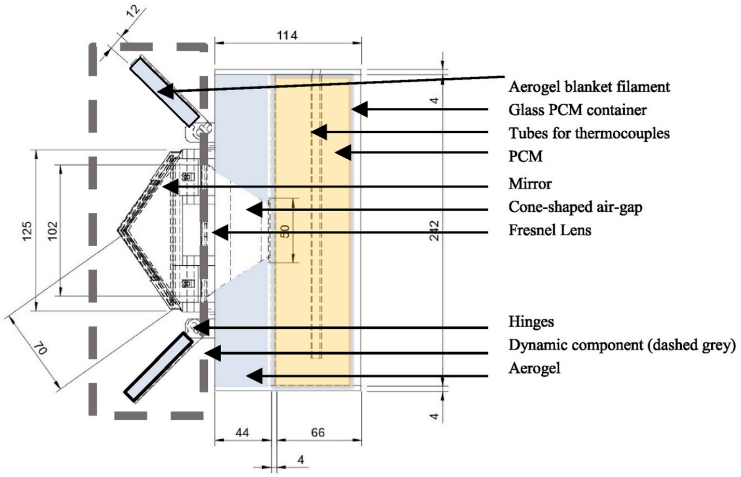

Fig. 6. The composition of proposed solar façade in closer detail.

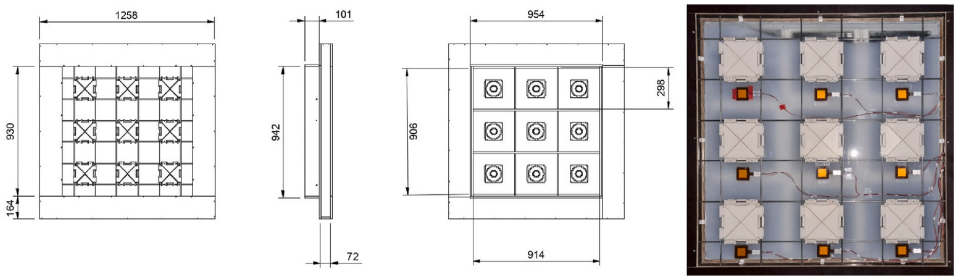

Fig. 7. Tested solar facade sample consisting of nine modules.

district heating is low, with various settings were simulated for a group of 50 houses. Simulations showed 11%–12% reduction of heat losses in district heating system and 20% to 58% reduction of heat losses in distributed solar systems as well as improved overall system efficiency and reduced primarily energy consumption and GHG emissions. Recent studies have shown the great potential of PCM integration in buildings by leading to reasonable energy savings and GHG emission reduction.

Described on paper soar façade module is in line with the latest research trends. From several proposed descriptions of non-static façade systems “active building envelope” describes the closest presented in

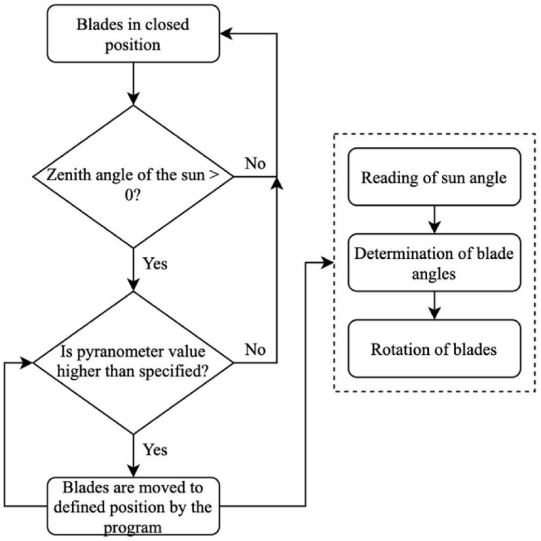

Fig. 8. The control algorithm principle for the dynamic component.

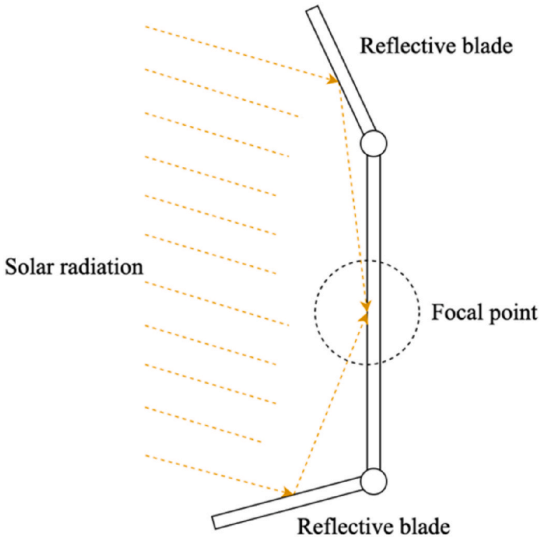

Fig. 10. Principle of the solar radiation reflection into facade model.

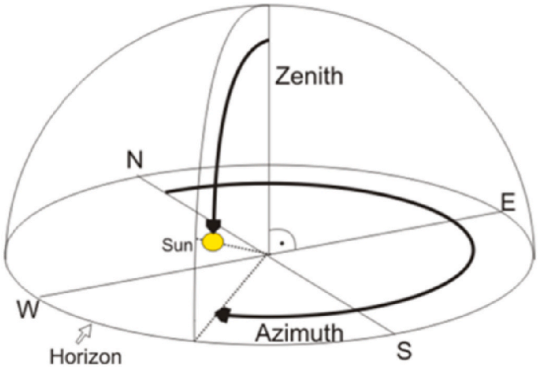

Fig. 9. Zenith and azimuth angles [56].

paper solar façade module – auxiliary energy is used to operate the system and proposed façade system converts solar energy to thermal and stores it. The core of the concept of the innovative solar façade module described in this paper lies in the advanced combination of dynamics and adaptivity for most advantageous use of phase change material for energy storage in building envelope. In terms of coupling with smart energy systems, building envelope itself might provide the energy buffering and flexibility capacities thus entering the era where building envelope takes active part in energy balance.

2. Materials and methods

2.1. Conceptual design of solar facade

Proposed solar façade consists of three main parts (see Fig. 5) – insulation unit and energy storage unit (Fig. 5a); and dynamic unit (Fig. 5c). Insulation unit faces outdoors, and energy storage unit faces indoors. Energy storage unit is filled with Phase change material – paraffin RT21HC (*Rubitherm*) (Fig. 5b). For faster heat transfer at the outer surface Fresnel lens is built in, and behind Fresnel lens there is a cone-shaped air-gap in insulation layer so that there are no obstacles for concentration of solar energy. Dynamic unit consists of four solar tracking blades that opens and closes under defined circumstances described later in text.

Fig. 6 depicts the composition of one solar façade module and the dimensions are given. Dynamic component of system 1) using the mirror on the blades assists to the solar energy concentration; and 2) prevents from the heat losses when solar radiation is not available due to the aerogel blanket filling. Blades and the cone construction are 3D printed using PLA (polylactide) material. Blades are hollow and are filled with aerogel blanket. Fig. 7 illustrates the whole testing sample cinsisting of nine modules.

In charging phase, direct and reflected solar rays travel through the transparent aerogel or Fresnel lens and are projected directly on the Phase change material (PCM) component where the energy from the sunlight is stored. Laboratory testing showed that in fixed position rotating blades enhance the performance of solar façade module. In temperate climate in spring and autumn there are days when during the day solar radiation is available and there is no need for heating the rooms, but at night time temperature drops and heating is needed to cover the heat losses of building thermal envelope and ventilation. Energy stored in solar façade system could be used to gather solar energy at daytime and release it to the room at night time.

Dynamic component would allow façade system to react to changing conditions – temperature, solar radiation and thus gain and store more energy. When solar radiation is available blades should open and should be placed in the position to reflect solar rays to the system depending on the location of the sun. When solar radiation is not available blades closes and prevent solar façade module from heat losses.

The tested sample consists of nine such modules that are built in plywood frame. Overall size of the tested sample is 0,95 × 0,95 m and the width is 0,11 m–0,066 m PCM container and 0,044 m aerogel layer (Fig. 4).

Adaptive properties of the proposed solar façade ensures the mechanics and the control algorithm. The algorithm system should follow is shown in Fig. 8. The main principle of the dynamic component is simple – four blades with reflective surface are tracking sunlight throughout the day and focusing it on the center of lens. When the sun

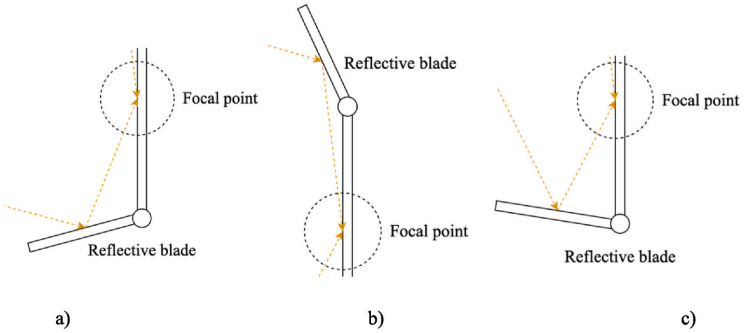

Fig. 11. Three different situations of blade position.

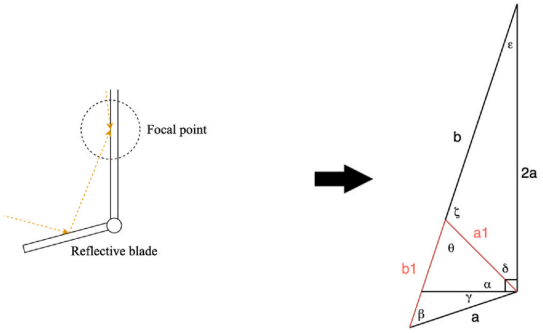

Fig. 12. Trigonometric visualisation of the angles in situation (a).

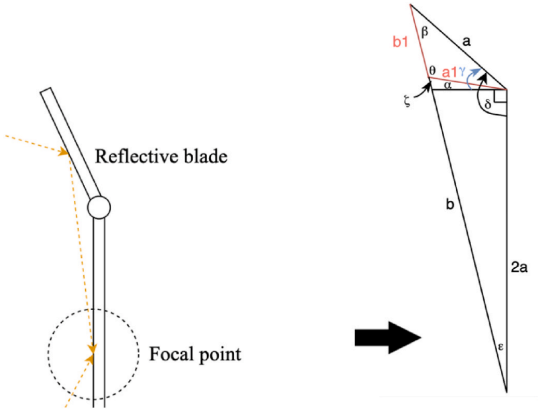

Fig. 13. Trigonometric visualisation of the angles in situation (b).

sets, blades are moved to initial closed position to insulate the model and to keep the heat inside PCM. Blades are opening again when the sun starts to shine. In addition:

1) blades should not be opened when the irradiance of the sun is less than defined, so that it would not open if presumably at lower intensity of solar radiation there would be more losses than gains;
2) blades should not be opened if the Sun is not in the angle to light the façade of the building where solar façade module is placed.

According to the objectives set, the control algorithm principle for the dynamic component was designed (see Fig. 8).

The angles for the blades to rotate can be calculated according to the angles of the sun – zenith and azimuth (see Fig. 9).

The position of these angles can be defined throughout the year based on the geographical location (longitude and latitude) [57]. If the angles of the sun are determined, it is possible to use basic principles of trigonometry to calculate the angle of each blade at a time of the day needed. Fig. 10 visually presents the principle of blades guiding the sun rays to the centre of the facade model considering the law of reflection which states that "an incident ray of light hits a plane mirror at an angle and is reflected back off it" [58].

The angle of the blade is dependant of blade's placement in module – vertical or horizontal axis. Upper and lower blades (horizontal axe) are responsible for capturing the sun's movement in zenith plane, but the eastern and western blades (vertical axe) should respond to the location of the sun in azimuth plane. Zenith or the altitude angle of the sun will always be in the range from 0 to 90° and will change according to geographical location. The azimuth angle will be obtained from 90 to 270° to capture the solar radiation while sun is in the range of the façade's southern direction. Every day there is a different Sun path. In winter equinox in Latvia solar path azimuth angle is only 90° - Sun rises in South-east and sets in South-west; but in summer solstice it is 270° - Sun Rises in North-east and sets in North-west. Solar path is dependant on geographical latitude and longitude of particular location building would be located. All calculations at this point in project are based on geographical location Riga, Latvia.

As the initial state it is defined that all of the blades in fully closed position is at 0° and fully open – 180°. According to these principles, it is possible to transfer the movement of the blades in geometrical triangles. The whole cycle can be divided in 3 different steps:

a) When the angle of lower and eastern blade is in the range from 90 to 180°
b) When the angle of upper and western blade is in the range from 90 to 180°
c) When all of the blades are in the range from 0 to 90°.

There are four blades and the angles are defined for each according to the position – left, right, lower, upper.

Fig. 11 depicts three positions of the blades.

If a triangle is used to visualise the situation (a) where angle γ determines the blade position and $\alpha + \delta = 90°$, then it is possible to assume that two of the triangle sides are a and 2a, but the angle α determines the sun position (see Fig. 12). In triangle a1-b1-a the length of the side a1 is equal to side b1 because of the law of reflection. That leads to:

$$\beta = \alpha + \gamma \text{ and } \theta = 180° - \alpha - \gamma \quad (1)$$

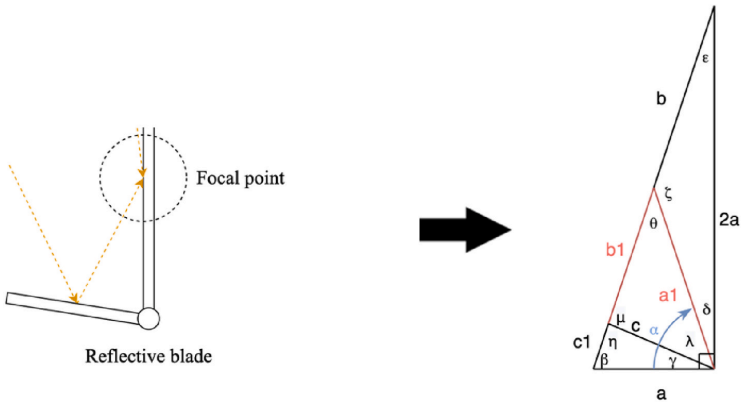

Fig. 14. Trigonometric visualisation of the angles in situation (c).

Table 1
Mechanical components for the dynamic control.

Component	Characteristics
Servo motor SG90 × 4	Voltage: 4,8–6 V
Arduino Mega microcontroller	Operating voltage: 5 V Flash memory: 128 KB
Operational amplifier	
3D printed protection box × 4	Material: PETG
Rotational axes × 12	Material: Steel

Table 2
Components of the solar facade module.

Component	
PCM	RUBITHERM RT21HC Melting area: 20–23 °C Congealing area: 21–19 °C Density 15 °C: 0,88 kg/l Density 40 °C: 0,77 kg/l Heat storage capacity ±7,5% 190 kJ/kg
PCM glass container (x9)	Dimensions: 242 × 242 × 44 mm Glass thickness: 4 mm
Plywood	Thickness: 9 mm λ = 0,13 W/mK
Aerogel	LUMIRA translucent aerogel LA1000 100 mm λ = 0,017 W/mK
Fresnel lens	127 × 127 × 1.5 mm Focal length: 71.12 mm
Inner/Outer cover	Poly (methyl methacrylate) PMMA glass 127 × 127 × 1.5 mm
Cone construction	PLA 3D printed
Movable blades	PLA 3D printed filled with aerogel blanket 50 mm, covered with mirror 2 mm

In triangle b–b1–2a:

$$\delta = 90 - \alpha, \zeta = 180 - (180 - \alpha - \gamma) = \alpha + \gamma \text{ and } \varepsilon = 180 - (90 - \alpha + \alpha + \gamma) = 90 - \gamma \quad (2)$$

In the triangle b–b1–2a using the sine law:

$$b1/\sin(90 - \gamma) = 2a/\sin(\alpha + \gamma) | \sin(90\text{-}\gamma) = \cos(\gamma)$$

$$b1 = 2a \times \cos(\gamma)/\sin(\alpha + \gamma) \quad (3)$$

And using the sine law in triangle a–a1–b1

$$b1/\sin(\alpha + \gamma) = a/\sin(180 - 2\alpha - 2\gamma) | \sin(180 - 2(\alpha + \gamma)) = -\sin2(\alpha + \gamma)$$

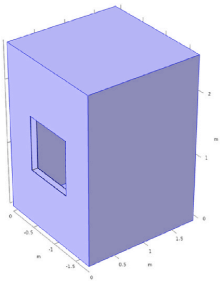

Fig. 15. PASLINK type testing booth.

Fig. 16. Testing booths on the roof. Location – Riga, Latvia. Left solar façade module built in, right – reference booth with triple glazed window.

$$b1 = a \times \sin(\alpha + \gamma)/\sin2(\alpha + \gamma) = a \times \sin(\alpha + \gamma)/2 \times \sin(\alpha + \gamma) \times \cos(\alpha + \gamma) = a/\cos(\alpha + \gamma) \quad (4)$$

Now it is possible to equate side b1:

$$2a \times \cos(\gamma)/\sin(\alpha + \gamma) = a/\cos(\alpha + \gamma) | /a$$

$$2\cos(\gamma) = \sin(\alpha + \gamma)/\cos(\alpha + \gamma)$$

$$2\cos(\gamma) = \tan(\alpha + \gamma) \quad (5)$$

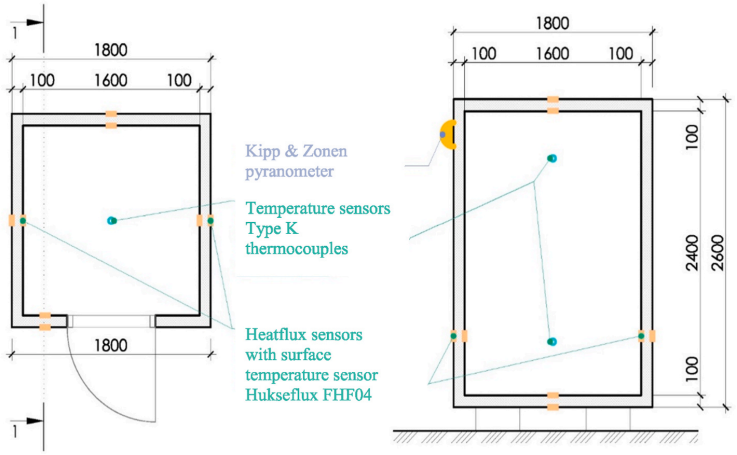

Fig. 17. Plan and section of PASLINK type testing booth with measuring equipment.

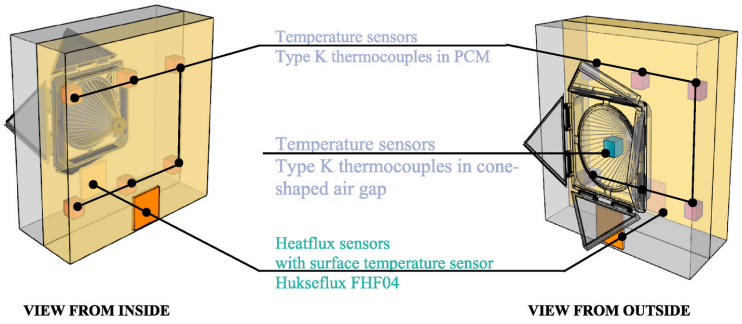

Fig. 18. Measuring and control equipment in solar façade module.

Table 3
Monitoring equipment.

Location/Monitoring equipment	Heat flux/temperature FHF04	Type K thermocouples
Façade booth	12 each surface in and out	2 in the centre of the booth
Reference booth	12 each surface in and out	2 in the centre of the booth
Solar façade module	18 (9 × 2) each module in and out	–
Outside	–	1 Ambient temperature

Table 4
Control equipment.

Control equipment	Façade booth
Type K thermocouples	54 (9 × 6) 6 sensors in each module embedded in PCM
Type K thermocouples	1 sensor in each cone
Pyranometer Kipp & Zonen	1

$$\gamma = \arccos(\tan(\alpha + \gamma)/2)$$

At the end the equation is derived to two variables – γ and α. This function can be used to determine blade angle according to defined angle of sun. In the case of lower blade, the angle of sun is equal to α, but the angle of the blade is calculated as γ + 90 o. For the western blade angle of the sun is α – 180 o and angle of the blade is γ + 90o.

For the situation (b) conditions are similar only the angles are different (see Fig. 13).

In triangle a–a1–b1:

$$\beta = \gamma - \alpha \text{ and } \theta = 180^\circ + 2\alpha - 2\gamma \quad (6)$$

And in triangle a–2a–b–b1 the angles can be calculated as follows:

$$\delta = 90^\circ + \gamma \text{ and } \varepsilon = 180^\circ - (\gamma - \alpha) - (90^\circ + \gamma) = 90^\circ - \gamma + \alpha - \gamma = 90^\circ - 2\gamma + \alpha \quad (7)$$

And using the sine law in triangle a–2a–b–b1:

$$a/\sin(90^\circ - 2\gamma + \alpha) = 2a/\sin(\gamma - \alpha) | :a$$

$$\sin(\gamma - \alpha) = 2 \times \sin(90^\circ - 2\gamma + \alpha) | \sin(90^\circ - x) = \cos x \quad (8)$$

$$\sin(\gamma - \alpha) = 2 \times \cos(2\gamma - \alpha)$$

$$\gamma = \arcsin(2 \times \cos(2\gamma - \alpha)) + \alpha$$

Table 5
Specifications of the Type K thermocouples.

Characteristics	Value
Temperature range	−270 °C–1260 °C
Accuracy	±2.2 °C or ±0.75%

Table 6
Specifications of the heat flux/temperature sensor FHF04.

Characteristics	Value
Measurement range	(−10 to +10) × 10^3 W/m^2
Uncertainty of calibration	±5% (k = 2)
Temperature range	−70 to +120 °C
Temperature measurement uncertainty	2% of value in °C

Table 7
Specifications of the Kipp & Zonen pyranometer (based on the datasheet).

Characteristics	Value
Spectral range (50% points)	300–2800 nm
Sensitivity	10–32 μV/W/m^2
Temperature dependence of sensitivity (−10 °C to +40 °C)	<4%
Operational temperature range	−40 °C to +80 °C
Maximum solar irradiance	2000 W/m^2
Field of view	180°

The equation for situation (b) has been derived to two variables as well. The angles of western and upper blade can be calculated in the same manner as for the situation (a). The trigonometric visualisation of the angles in situation (c) is shown Fig. 14. In the triangle b1–a1–c the angles are:

$$\lambda = \mu = \alpha - \gamma \text{ and } \theta = 180^\circ - (2\alpha - 2\gamma) = 180^\circ - 2\alpha + 2\gamma \quad (9)$$

In triangle a1–b–2a:

$$\zeta = 180^\circ - (180^\circ - 2\alpha + 2\gamma) = 2\alpha - 2\gamma;\ \delta = 90^\circ - \alpha$$

$$\text{and } \varepsilon = 180^\circ - (90^\circ - \alpha) - (2\alpha - 2\gamma) = 90^\circ - \alpha + 2\gamma \quad (10)$$

And the angles in triangle a-c-c1 are:

$$\eta = 180^\circ - (\alpha - \gamma) = 180^\circ - \alpha + \gamma \text{ and } \beta = 180^\circ - (180^\circ - \alpha + \gamma) - \gamma = \alpha - 2\gamma \quad (11)$$

Using the sine law in triangle 2a–b–b1–c:

$$a/\sin(90^\circ - \alpha + 2\gamma) = 2a/\sin(\alpha - \gamma) \mid :a$$

$$\sin(\alpha - \gamma) = 2 \times \sin(90^\circ - \alpha + 2\gamma) \mid \sin(90^\circ - x) = \cos x \quad (12)$$

$$\sin(\alpha - \gamma) = 2 \times \cos(\alpha - 2\gamma)$$

$$\gamma = \alpha - \arcsin(2 \times \cos(\alpha - 2\gamma))$$

In this case for the lower blade sun's angle is equal to α and angle of the blade is 90° − γ. The upper blade's angle is 90° − γ and sun's angle is equal to 90° − α. The eastern blade's angle is 90° − γ and sun's angle α − 180°. And the western blade's angle is α − 180°.

All the angles, accordingly to the date, time and the location of the place where tests were carried out (Riga, Latvia).

For the outdoor tests dynamic component with the control system that drives the blades in right place accordingly to the angle of sun was introduced. To provide this movement, 4 motors that turns the blades were used. Program code was created to fulfil the needs of the algorithm. The necessary mechanical components for the dynamic control system are listed in Table 1.

The system code consists of 4 arrays, where the information about the blade angles in defined period (6-min interval between) is stored as well as data about the solar radiation from pyranometer. As the pyranometer gives out voltage values, an algorithm that converts them to actual W/m^2 is applied. After that, an "IF" function is used so that, if the solar radiation is higher than defined, signal is sent to motors to open the blades accordingly to the defined position, if the solar radiation is not higher than defined all blades take the initial closed position. To avoid interference between the blades, the closing time for upper and lower blade is delayed. At the end the solar radiation data is saved into the defined array.

For provide mechanic movement of blades two types of motors will be considered – servo and stepper motors. At the first stage Servo SG90 motors were used due to their simple control mechanism and feedback. Wedges were used to strengthen the axes inside the hinges of the blades. To avoid voltage peaks that could interfere with the microcontroller, noise filter with two condensers were used on the power supply.

Mechanics of the dynamic component is organised as follows. Each blade is fixed on its own axis, which in turn is coupled to the motor using a gear system for movement transmission. Two axes are arranged vertically, two – horizontally for each line of modules. (there are three lines with three modules in each line). To ensure the solar tracking function of the facade system, each of the blades is connected to a separate axis of rotation, respectively, and each of the axes is connected to one motor. To ensure the precise fixed position of the blades, a worm-type drive (worm thread and gear) with a speed transmission ratio of 1:20 is used. The motor is coupled using clutch together with the power rod, on which a worm-type thread is attached, which transmits the rotational movement through the gear to the axes, which, in turn, are attached to the hinges of the vanes.

The list of the materials used in tested solar façade module are summarised in Table 2.

2.2. Experimental setup

To conduct a comparative study, two identical PASLINK type test booths were assembled (Fig. 16). The PASLINK test is a method to investigate the performance of developed building components under real climatic loads. Initially PASLINK test was developed from the PASSYS Project (Passive Solar Components and Systems Testing) [35]. The composition of the PASLINK test stand is: 1) a building envelope with one façade used for embedding the tested material and a room inside the envelope for observations.

In study presented in paper test booth outer dimensions are 1,8 × 1,8 × 2,4 m (width, length, height). Walls, roof and floor are of polyurethane sandwich panels 100 mm. Booths are oriented according to the cordial points and the tested sample and the reference sample are embedded in the southern wall of the test booths. In the scope of this study the performance of the proposed solar façade module is compared to the performance of triple glazed window since it would be the choice for low energy and passive buildings. U value for triple glazed window (SmartWin) is 0,85 W/m^2 K. In comparison U value for the same size window of an average thermal quality would be 0,92 W/m^2 K and glazed area would be ~15% due to the width of the window frame.

Both booths are equipped with heatpumps. Thus, the design of the experiment allows to test two regimes – 1) to compare indoor temperature changes with no energy source; and 2) compare the energy consumption with heat-pumps switched-on. Data on the energy consumed by heatpumps are registered in the monitoring system.

The test takes place in Riga, Latvia (56° 56′46″N/24° 6′21″E). Testing booths are placed on the roof (20 m above ground). There are no significant shading objects closer than 200 m to the site. Figure below depicts the testing setup – two testing booths next to each other (Fig. 15).

2.3. Measuring equipment

There are two types of measuring equipment: 1) monitoring the

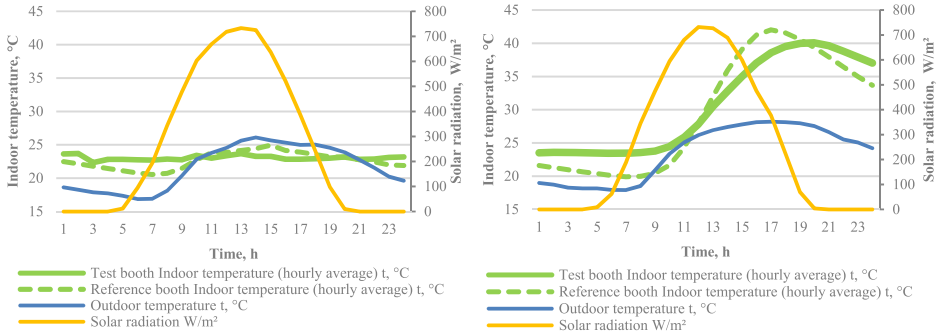

Fig. 19. Indoor temperature in august in active mode (with heap-pump on (left)) and passive mode (heat-pump off (right)).

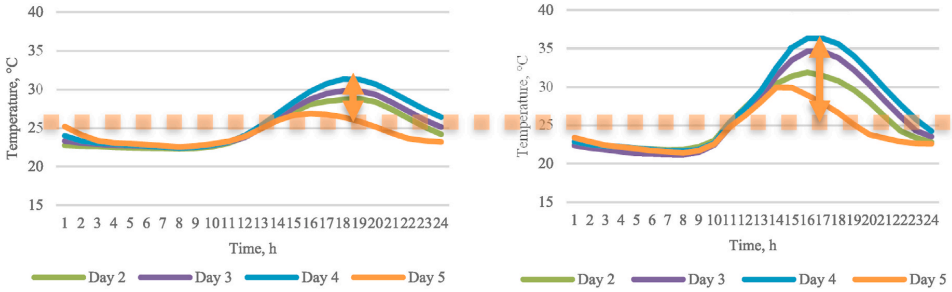

Fig. 20. Indoor temperature in solar facade booth (left) and reference booth (right).

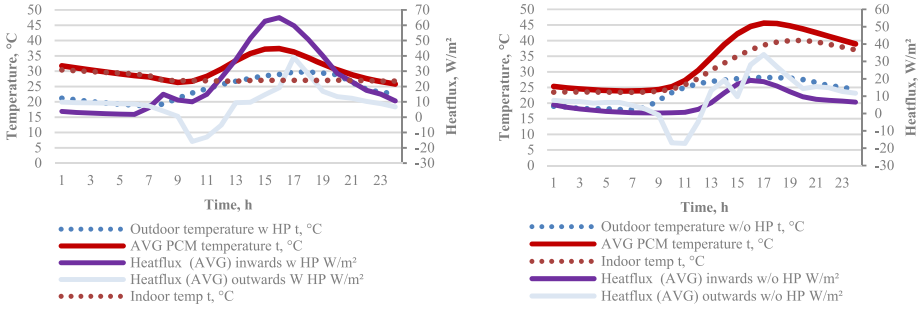

Fig. 21. Heatflux in solar façade modules (inwards and outwards). August. (heat-pump switched-on (left), heat-pump switched-on (right)).

results (green in Fig. 17) and 2) taking part in the control algorithm (blue in Fig. 17). There are placed 12 heatflux sensors with in-built temperature sensor to each plane of the test booth – walls, roof and floor – inside and outside. On the vertical plane pyranometer is placed and providing the input data to the control algorithm.

Other set of measuring equipment is placed in solar façade modules – six thermocouples in each module, 1 in the cone and two heatflux sensors with in-built temperature sensor on inner and outer surfaces (Fig. 18).

Measuring equipment sets and specifications are summarised in Tables 3–7. For heatflux sensors voltage value is converted into heatflux using the data provided by manufacturer for each sensor.

3. Results

3.1. Experiment takes place in August–January

In Fig. 19 on the left results from hot sunny day with heatpump switched on are presented. It can be observed that indoor temperature is more smooth in solar facade booth compared to reference booth. The graph on the right side depicts indoor temperature changes on sunny day and heatpump switched-off. In the morning temperature drop in reference booth can be observed. Then steeper temperature climb is seen in reference booth compared to the test booth an at the end of the day indoor temperature in test booth is higher.

In Fig. 20 results in a passive mode – with no cooling from four sunny

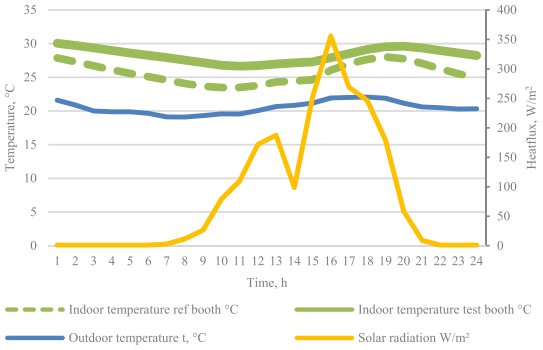

Fig. 22. August 22nd indoor temperature in test booth, reference booth, outdoors and solar radiation passive mode - heat-pump off.

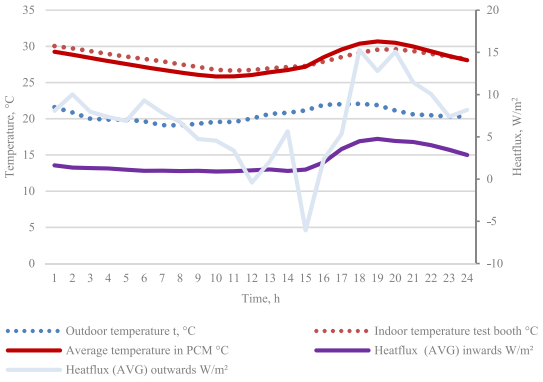

Fig. 23. August 22nd. Heatflux from solar façade inwards and outwards, average temperature in PCM, indoor and outdoor temperature (passive mode – heat pump is switched-off).

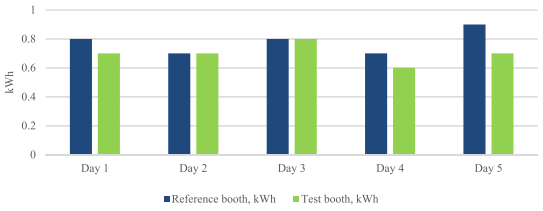

Fig. 24. Energy consumption in solar façade booth (solid green) and reference booth (blue).

days are compiled. In all days temperature was higher in reference booth compared to the solar façade booth. Dotted line indicates the optimal comfort temperature for indoor comfort, i.e. 25 °C. In the tested circumstances in all five days temperature was above optimal comfort temperature. It is the effect of the intensive solar radiation and the size of the tested booths - those are smaller in size compared to the average room (15–20 m^2), test booth envelope has low thermal inertia and no shading devices are installed.

In hot and sunny august day heatflux inwards and outwards was measured in solar facade module (Fig. 21). Outdoor temperature on both days was similar. In hot sunny summer days, when heatpump is swiched on, heatflux inwards (purple line) is much higher compared to conditions where heatpump is swiched off 60 W/m^2 *vs* 20 W/m^2. Heatflux outwards is similar in both conditions – ~10 W/m^2 when solar radiation is not present and down to −20 W/m^2 when the Sun starts to shine and up to 30 W/m^2 at the second part of the day. Negative values of the outward heatflux indicates that the heat is absorbed by the surface. Positive values indicate the heat from the PCM is being transferred to the surroundings. Temperature in the PCM with the heat-pump switched-on raises and returns to the initial temperature. When heat-pump was swithed-off and the booth was not cooled temperature in the PCM at the end o the day was 15 °C higher than the initial temperature.

Results from the day where solar radiation was in less intensity (Aug 22nd partially cloudy) are depicted in Figs. 22 and 23. Outdoor temperature is from 19 to 22 °C. Solar radiation follows disrupted parabolic curve that indicates that the solar radio was interrupted by cloudiness. At the peak solar radiation reached ~350 W/m^2. Indoor temperatures in test booth and reference booth are similar – splines follow similar trend and are 2–3 °C apart – at first temperature drops in both booths, when solar radiation raises indoor temperature raises as well, in test booth with a delay. Temperature in test booth is higher. However, during the day overall increase and decrease is similar.

Indoor heatflux on the Aug 22nd exhibits a bit different trend compared to the sunny day on Aug 14th (Fig. 21). Similarly, the inwards heatflux at the beginning of the day is close to zero and stays low all first part of the day, but the difference is, that in partially cloudy day heat transfer room PCM to the indoor space takes place not in the middle of the day, but in afternoon and evening. Solar radiation till 2 p.m. does not exceed 200 W/m^2; at 6 p.m. it reaches 350 W/m^2 and this is followed by an increase in the inwards heatflux. Heatflux outwards follows similar trend as in sunny day, however the heatflux peaks are different; both the heatflux's negative values is −6 W/m^2 compared to −17 W/m^2 in sunny day and positive value is 15 W/m^2 compared to 34 W/m^2 in sunny day. Temperature in PCM in cloudy days are within a range of 26–30 °C, in sunny day 25–40 °C.

Comparing the energy demand for cooling in Fig. 24 for five days it can be seen, that in three out of five days energy consumption was slightly higher in reference booth in the tested period.

It was observed in September that daily indoor temperature fluctuations were between 13 and 22 °C in reference booth and 15–20 °C in the test booth. To compare energy consumption to ensure desired indoor temperature, it was decided to switch on the heat pump in heating mode. Fig. 25 depicts indoor temperatures in test booth and reference booth, outdoor temperature and solar radiation when heat pumps are set to heating to 22 °C September 8–14th. Outdoor temperature peaks in selected days are from 8 to 15 °C and lows during the night are from 6 to 10 °C. Solar radiation peaks are from 120 W/m^2 to 600 W/m^2. It can be observed in Fig. 25, that during the availability of solar radiation in high intensity, temperature in both booths rises above the set temperature – in reference booth it is more significant. In cloudy days, there are no such peaks.

Despite mentioned indoor temperature peaks in reference booth, energy consumption for heating was higher in the reference booth compared to the test booth in selected period (Fig. 26). The energy consumption was significantly higher in cloudy days with the solar radiation not exceeding 200 W/m^2.

Fig. 27 depicts the indoor temperatures in test booth and reference booth, outdoor temperature and solar radiation when dynamic system is switched-off October 17–23rd. Outdoor temperature peaks in selected days are from 3 to 13 °C and lows during the night are from 4 to 10 °C. Solar radiation peaks are from 50 W/m^2 to 400 W/m^2. It can be observed in Fig. 27 that despite indoor temperature reaches much higher peaks 20–25 °C in reference booth compared to the test booth, at the end of the day temperatures in booths are similar. In cloudy day indoor temperatures are similar throughout the day.

Looking in closer detail in Fig. 28 results from three days – sunny, partially sunny and cloudy (November 19th to 21st) are showed. In the

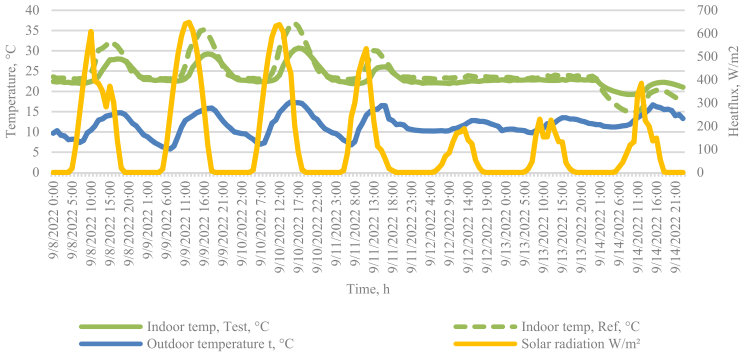

Fig. 25. Indoor temperature in test booth and in reference booth, outdoor temperature and solar radiation September 8th–14th.

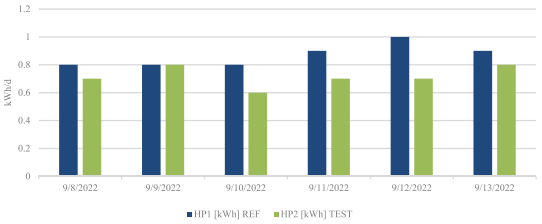

Fig. 26. Energy consumption comparison in six days in September.

first of the selected days, temperature difference between reference booth and test booth was 7 °C (higher in reference booth), in partially cloudy day, temperature difference was less than 2 °C, and in cloudy day temperature splines in both booths are almost overlaying. Temperature drop in reference booth was significantly steeper compared to the test booth 14 °C, 6 °C and 1,5 °C vs 5 °C, 3 °C, and 1,5 °C.

Fig. 29 depicts testing results in November. Outdoor temperature range on selected day is from 8 to 12 °C. Solar radiation follows reaches only 100 W/m^2 – typical average solar radiation intensity in November in Latvia (Fig. 29). It can be observed that during the daytime indoor temperature at the peak of solar radiation was reached ~2 °C higher in reference booth. However, at the end and beginning of the day indoor temperature is equal in both booths, which indicates that the gained solar heat is lost in reference booth.

In Fig. 30 heatfluxes on solar façade module (inwards and outwards), indoor, outdoor and average temperature in PCM are depicts (November). Indoor temperature spline in the graph overlays with the PCM average temperature spline and those follow similar tendency as the outdoor temperature spline. Heatflux inwards is close to zero at the beginning and at the end of the day, in the middle of the day heatflux increases in the direction from the indoor space to PCM (with a minus sign). Heatflux outwards is positive all the day, indicating that heat losses are higher than gains whole day through and there is no negative heatflux like it was observed in the August graphs (Fig. 21).

The next day November 9th heat pump was switched-on (Fig. 31). Outdoor temperature is similar - from 9 to 12 °C. Solar radiation follows distorted spline reaching only 180 W/m^2 – above the typical average solar radiation intensity (100 W/m^2) in November in Latvia, however solar radiation spline deviates from a typical parabolic shape indicating, that the solar radiation was impacted by clouds. Heat pump is switched-on in a heating mode (it does not provide cooling to ensure the set temperature). It can be observed that during the daytime indoor temperature in reference booth raises ~3 °C higher than the indoor temperature in test booth due to the solar heat gains.

In Fig. 32 heatfluxes on solar façade module (inwards and outwards), indoor, outdoor and average temperature in PCM is depicted in November 9th in active mode (heat pump is switched-on). Indoor temperature spline rapidly raises after heat pump is switched-on, Average temperature in PCM raises at a much slower rate and does not follow the character of outdoor temperature changes. Heatflux inwards from close to zero at the beginning of the day rapidly decreases to <−15 W/m^2

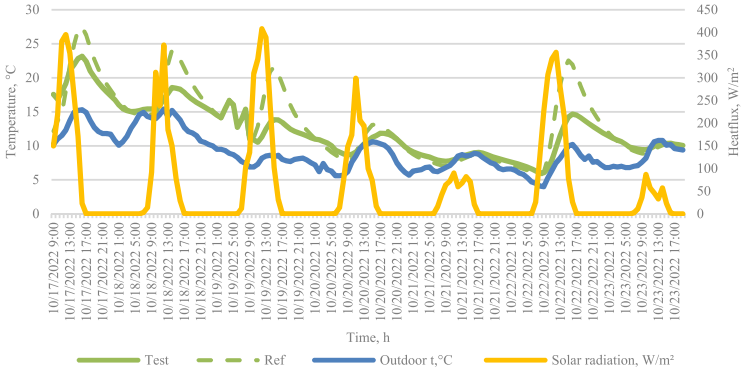

Fig. 27. Indoor temperature in test booth and in reference booth, outdoor temperature and solar radiation November 17th – 23rd.

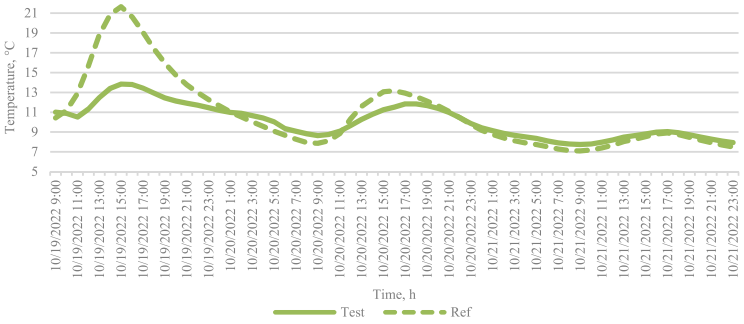

Fig. 28. October 19th-21st indoor temperatures in test booth and reference booth.

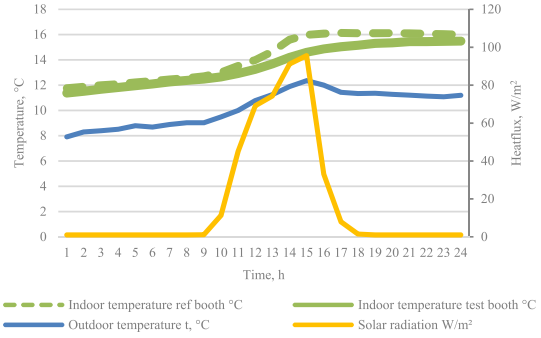

Fig. 29. November 8th. Indoor temperature in test booth, reference booth, outdoors and solar radiation (passive mode with heat-pump off).

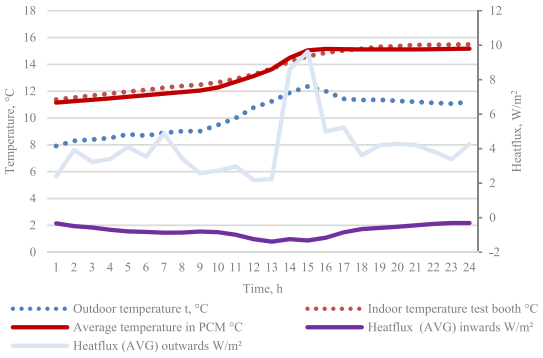

Fig. 30. November 8th. Heatflux from solar façade inwards and outwards, average temperature in PCM, indoor and outdoor temperature (passive mode – heat pump is switched-off).

indicting that the heat is transferred from the indoor space to the PCM at the beginning faster and then slowly gradually decreasing to ~ -5 W/m^2 at the end of the day. Heatflux outwards is positive all the day, indicating that heat losses are higher than gains whole day through and there is no negative heatflux like it was observed in the August graphs. Heatflux outwards is higher compared to the day before ~10 W/m^2 *vs* 5 W/m^2 respectively. The heatflux outwards higher due to both – temperature difference between average temperature in PCM is higher (heat-pump is switched-on and it heats the PCM) and solar radiation on

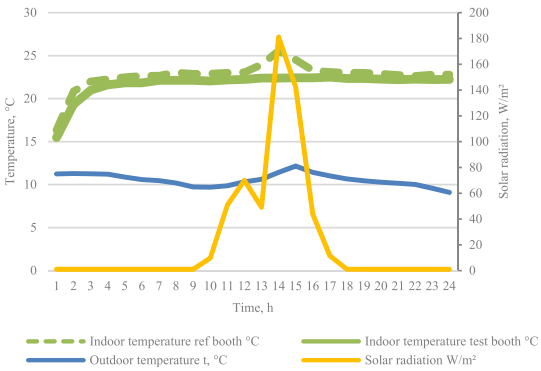

Fig. 31. November 9th. Indoor temperature in test booth, reference booth, outdoors and solar radiation (active mode with heat-pump on).

selected day is higher as well and it raises the temperature of PCM ae well.

Fig. 33 depicts temperature in phase change material in one of nine modules in November 9th, when the heat pump was switched-on. In other modules situation is alike. Temperature in all the layers follow the same tendency – at the beginning there is a steeper increase in temperature for approximately 5 h (heat-pump warms the PCM), then again steeper increase follows due to the increase in solar radiation intensity

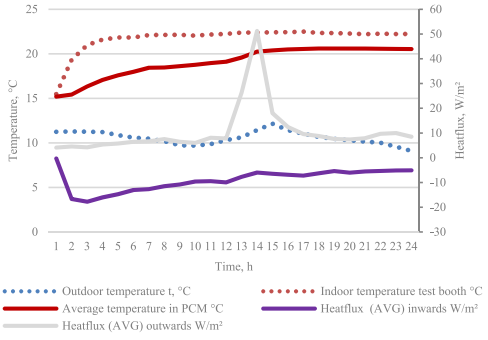

Fig. 32. November 9th. Heatflux from solar façade inwards and outwards, average temperature in PCM, indoor and outdoor temperature (active mode – heat pump is switched-on).

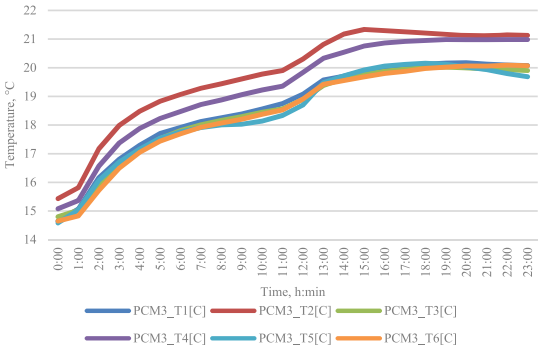

Fig. 33. Temperature in phase change material. November 9th – active mode (heat pump is switched-on).

(~12.00–13.00) and then temperature has reached the melting temperature of phase change material stabilizes. Temperature in the spot PCM3_T2 has reached the highest and that is the only spot, where temperature slightly decreases following the decrease in solar radiation intensity. Other spot with the temperature decrease is PCM3_T5, in this spot it is related to the decrease in outdoor temperature. PCM melts gradually – some parts of PCM is liquid and some are solid. Temperature drop in one spot after the solar radiation decreases might indicate that in that particular point PCM has overgone the phase change as has begun to gain sensible heat.

Fig. 34 presents the visualisation from the site – partial melting of phase change material when heat pump is switched-on, there are liquid PCM at the perimeter of the test cell.

Fig. 35 depicts three days in a row (Nov 8th, 9th, 10th). Heatfluxes inwards and outwards from the solar façade module and the PCM average temperature are illustrated. Increase in outward heatflux, decrease of inwards heatflux (negative values) and increase in the average PCM temperature are visualized in three days – transition from passive to active mode. Heatflux inwards after the first two days described before (Figs. 29–32), continues to be slightly negative – PCM is warmed by the heat pump. Temperature in PCM has reached the ~20 °C and does not raise – it is now approximately the same as the indoor temperature.

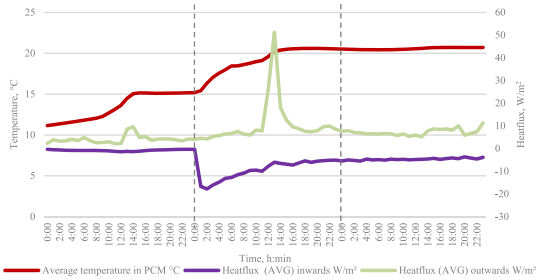

Fig. 35. November 8th, 9th, 10th. Heatflux from solar façade inwards and outwards, average temperature in PCM, indoor and outdoor temperature (transition from passive (heat pump is switched-off) to active mode (heat pump is switched-on).

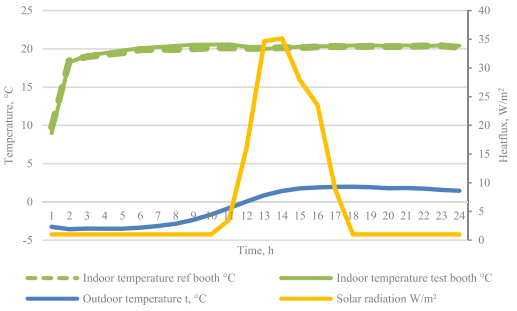

Fig. 36. January 10th. Indoor temperature in test booth, reference booth, outdoors and solar radiation (active mode with heat-pump on).

The experiment with switched-off and switched-on heat pump to observe dynamics in temperatures and heatfluxes was repeated in January. Prior to the experiment heat pump was switched-off. Fig. 36

Fig. 34. November. Partial melting of PCM.

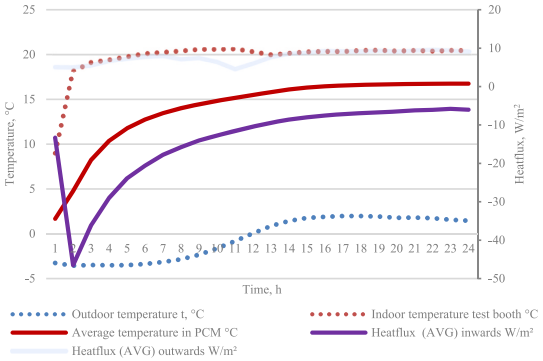

Fig. 37. January 10th. Heatflux from solar façade inwards and outwards, average temperature in PCM, indoor and outdoor temperature (active mode – heat pump is switched-on).

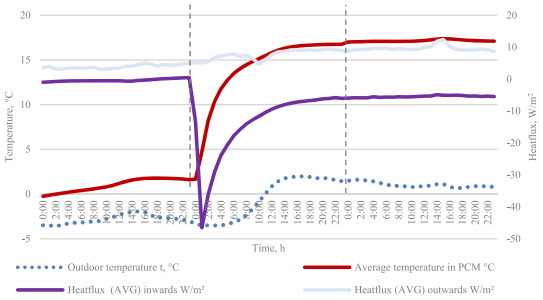

Fig. 38. January 9th, 10th, 11th. Heatflux from solar façade inwards and outwards, average temperature in PCM, indoor and outdoor temperature (transition from passive (heatpump is switched-off) to active mode (heatpump is switched-on).

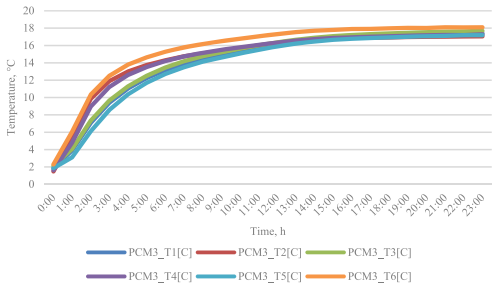

Fig. 39. Temperature in phase change material. January 10th – active mode (heat pump is switched-on).

depicts results from the January 10th. At the beginning of the day heat pumps are switched-on. The outside temperature was from −3 °C to +2 °C and a scarce solar radiation peaking at 35 W/m^2. Indoor temperatures at the beginning of the day are similar ~9 °C, and it raises identically during 2 h–18 °C and the gradually reaches 20 °C in both booths.

Fig. 37 depicts inwards and outwards heatfluxes from solar façade module in selected day on January. Heatflux peak in negative values is significantly lower compared to autumn heatflux – the lowest value is ~ -45 W/m^2 compared to autumn −17 W/m^2. The average temperature in PCM is much lower compared to the Autumn test and thus is the temperature difference between PCM and indoor temperature larger. However, at the end of the day heatflux reaches −6 W/m^2 *vs* −3 W/m^2 in autumn. Outwards heatflux during the day varies in small range - from 5 W/m^2 to 9 W/m^2.

Fig. 38 depicts three days in a row (Jan 9th, 10th, 11th). In first day, heat pump is switched-off, in the second and third days heatpump is switched-on. Heatfluxes inwards and outwards from the solar façade module and the PCM average temperature are illustrated. Increase in outward heatflux from 4 W/m^2 to 12 W/m^2, decrease of inwards heatflux from close to zero to −5 W/m^2, with peak negative values of – 45 W/m^2, and increase in the average PCM temperature from zero to +17 °C are visualized in three days – transition from passive to active mode in January. PCM average temperature stabilizes at 17 °C. In the third day, both heatfluxes inwards and outwards have stabilized.

Temperature dynamics in different spots in the phase change material has similar trend as in Autumn – at the beginning it increases steeper and then stabilizes (Fig. 39).

In Figs. 40–44 energy consumption of heatpumps is illustrated from September to January. It can be seen that in September energy consumption is higher in reference booth, in October when heatpumps were switched-on energy consumption is identical, but in winter months, energy consumption was higher in the test booth. Even in winter days there are some days where heat pump energy consumption in reference booth is slightly higher compared to test booth.

Overall energy consumption is summarised in Table 8. In September energy in was consumed 11% less in the test booth, in December and January more energy was consumed for test booth heatpumps 4% and 6% respectively.

Gained results in large scale testing in real climatic conditions provided valuable insights in the thermodynamic processes in the developed solar façade module. Onsite monitoring was carried out in all typical seasons in cold European climate – summer, midseason and winter.

4. Conclusions

The described in paper comparative study layout allowed to compare performance of the proposed solar façade with the performance of triple glazed window suitable for low energy buildings in two modes: 1) passive mode with no internal cooling energy source (changes in indoor temperature were compared; and 2) active mode with internal energy source for cooling, i.e. air-to-air heat-pump. The monitoring of the façade was carried out from the August 2022 to January 2023.

The gained results provide the insights in the thermal performance of the proposed solar façade module under real climatic conditions:

1) Results indicate the potential of developed solar facade module to reduce peak indoor temperature in passive mode (heatpump swithed off) in the hot summer days;
2) In cloudy summer days solar facade in testing conditions ensured smoother temperature swings and slightly higher indoor temperature compared to the reference booth;
3) In active mode when the heat-pump is switched-on heat transfer to indoor is much faster due to the convection and thus the energy consumption is higher. Accumulation tank can be considered in addition to remove (store) excess heat;
4) Heatflux outwards is similar in both passive and active modes.

Summarised by months it was concluded, that energy consumption for heatpumps in September was higher in reference booth, October – the same, but in December and January energy consumption was higher in the test booth as it was hypothesized, that winter time is passive mode

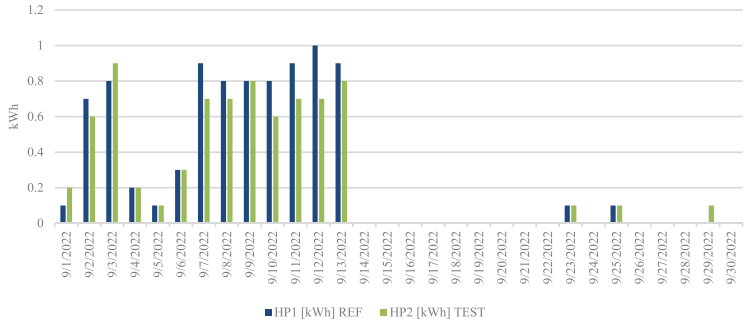

Fig. 40. Energy consumption for heatpumps in September in test booth and in reference booth.

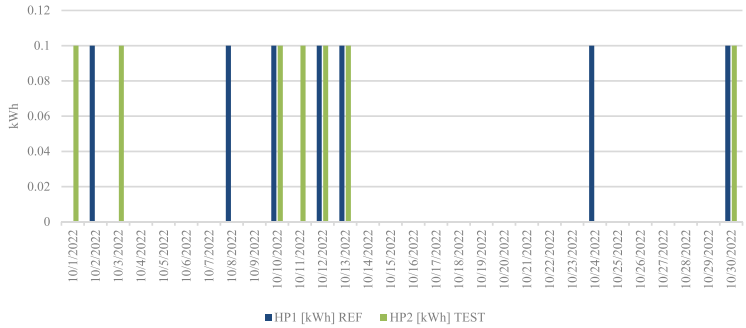

Fig. 41. Energy consumption for heatpumps in October in test booth and in reference booth.

and mid-season and summer is where benefits of phase change material are explored. In some winter days heatpump energy consumption in reference booth was observed to be slightly higher compared to test booth.

Solar heat gains are crucial component in the design of the low energy buildings in cold heating season, however in cooling season solar heat gains are to be reduced. The first results indicate that the proposed solar façade module during the coldest heating season is outperformed by the highest performance triple glased window, in midseason performs similarly, and in summer reduces the cooling demand compared to the conventional high performance glased system. Based on the findings during the testing, the potential for the advancement of the design is revealed. To improve the performance of the proposed solar façade, additional internal insulation layer could be added to avoid unnecessary heating of the phase change material in the absence of storable solar energy, thus reducing the amount of energy used during the heating season.

Data gained in this comparative study will be used to validate mathematical simulation. Validated mathematical model will be used to simulate the use of the developed facade under different boundary conditions and in different climates.

In the next phases of further development of proposed façade possibility to use additional accumulation tank could be studied. In summer time surplus heat could be diverted to accumulation tank and used for

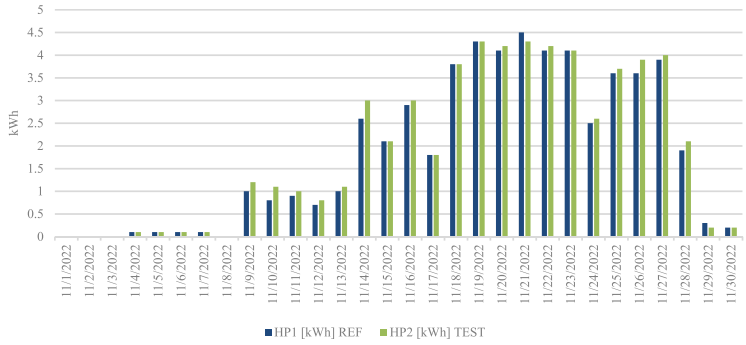

Fig. 42. Energy consumption for heatpumps in November in test booth and in reference booth.

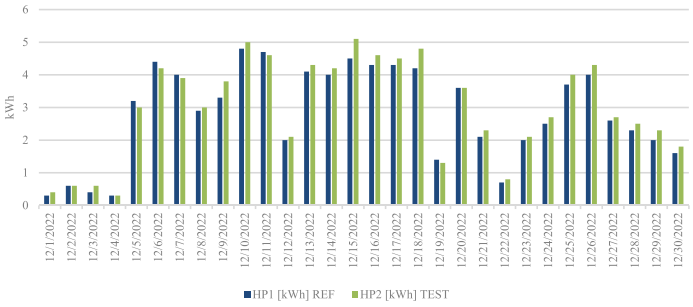

Fig. 43. Energy consumption for heatpumps in December in test booth and in reference booth.

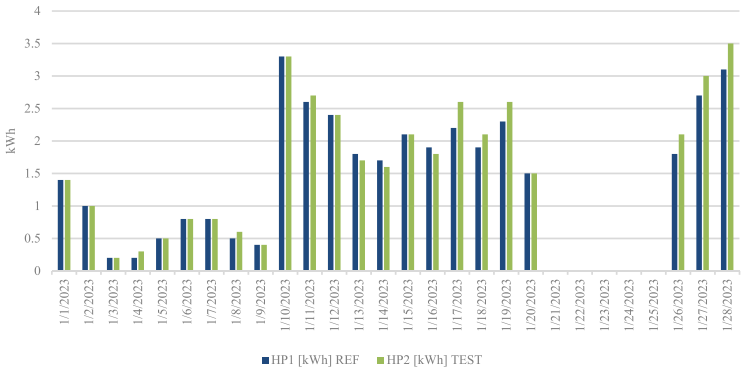

Fig. 44. Energy consumption for heatpumps in January in test booth and in reference booth.

Table 8
Energy consumption for heatpumps in test booth and in reference booth.

	Energy consumption for heatpump REF	Energy consumption for heatpump TEST	Difference
September	8,5	7,6	−11%
October	0,7	0,7	0%
November	55,1	57,1	4%
December	86,4	91,3	6%

preheating the domestic hot water or seasonal storage. In discharging phases it is vital that gained heat is not lost to the surroundings, instead usefully consumed in short distances.

In addition, innovative solutions for building thermal envelope provide alternatives for both – architects when choosing building materials based on functional characteristics and aesthetics of the material; and engineers for optimizing the building energy balance. In low energy building design there are several principles to follow in order to achieve energy efficient result. One of such is the extensive glazing facing South. However, in real life, specially in densely built environments, it is not always possible due to the special characteristics of the building site. The results indicate that the proposed façade could serve as an alternative.

Author contributions

Saba Aslani: Conceptualization; Formal analysis; Investigation; Methodology; Project administration; Validation; Visualization; Writing - original draft; Writing - review & editing; Daniel W. Armstrong: Conceptualization; Funding acquisition; Investigation; Project administration; Resources; Supervision; Writing - review & editing.

Funding

This study has been supported by Fundamental and Applied Research project “Smart building EnVElope with solaR Energy STorage (EVEREST)”, project No. lzp-2019/1–0363, funded by the Latvian Council of Science.

Declaration of competing interest

The authors declare that they have no known competing financial interests or personal relationships that could have appeared to influence the work reported in this paper.

Data availability

Data will be made available on request.

Acknowledgement

This study has been supported by Fundamental and Applied Research project “Smart building EnVElope with solaR Energy STorage (EVEREST)”, project No. lzp-2019/1–0363, funded by the Latvian Council of Science.

References

[1] EC, "Delivering the European. Eur Commision 2021. no. July, p. 2021.
[2] European Commission. The European green deal [Online]. Available: https://sustainabledevelopment.un.org/post2015/transformingourworld; 2019.
[3] Ruse A, Pubule J. The boundaries of scientific innovation in the EU green deal context. Environ. Clim. Technol. 2022;26(1):115–28. https://doi.org/10.2478/RTUECT-2022-0010.
[4] Rikkas R, Lahdelma R. Energy supply and storage optimization for mixed-type buildings. Energy 2021;231:120839. https://doi.org/10.1016/j.energy.2021.120839.
[5] European Commission, "DIRECTIVE 2010/31/EU OF THE EUROPEAN PARLIAMENT AND OF THE COUNCIL of 19 May 2010 on the energy performance of buildings." .
[6] Luo Y, Zhang L, Bozlar M, Liu Z, Guo H, Meggers F. Active building envelope systems toward renewable and sustainable energy. Renew Sustain Energy Rev 2019;104:470–91. https://doi.org/10.1016/J.RSER.2019.01.005.
[7] Krumins A, Lebedeva K, Tamane A, Millers R. Possibilities of balancing buildings energy demand for increasing energy efficiency in Latvia. Environ Clim Technol 2022;26(1):98–114. https://doi.org/10.2478/RTUECT-2022-0009.
[8] Kant K, Shukla A, Sharma A. Advancement in phase change materials for thermal energy storage applications. Sol Energy Mater Sol Cells 2017;172:82–92. https://doi.org/10.1016/j.solmat.2017.07.023.
[9] Vanaga R, Blumberga A, Freimanis R, Mols T, Blumberga D. Solar facade module for nearly zero energy building. Energy 2018;157. https://doi.org/10.1016/j.energy.2018.04.167.
[10] Sirmelis R, Vanaga R, Freimanis R, Blumberga A. Solar facade module for nearly zero energy building. Optimization strategies. Environ Clim Technol 2019;23(3). https://doi.org/10.2478/rtuect-2019-0087.
[11] Mols T, Vanaga R, Blumberga A. Solar facade module for nearly zero energy building. Extended test period. Environ Clim Technol 2020;24(1):442–53. https://doi.org/10.2478/rtuect-2020-0027.
[12] Vanaga R, Purvins R, Blumberga A, Veidenbergs I, Blumberga D. Heat transfer analysis by use of lense integrated in building wall. Energy Proc 2017;128. https://doi.org/10.1016/j.egypro.2017.09.030.
[13] Ručevskis S, Akishin P, Korjakins A. Parametric analysis and design optimisation of PCM thermal energy storage system for space cooling of buildings. Energy Build 2020;224:110288. https://doi.org/10.1016/j.enbuild.2020.110288.
[14] Soares N, Gaspar AR, Santos P, Costa JJ. Experimental study of the heat transfer through a vertical stack of rectangular cavities filled with phase change materials. Appl Energy 2015;142:192–205. https://doi.org/10.1016/j.apenergy.2014.12.034.
[15] Kenisarin M, Mahkamov K. Solar energy storage using phase change materials. Renew Sustain Energy Rev 2007;11(9):1913–65. https://doi.org/10.1016/J.RSER.2006.05.005.
[16] John Z, Zhai ML, Abarr L, Al-Saadi SNJ, Yate P. Energy storage technologies for residential buildings. J Architect Eng 2014;20(4):B4014004. https://doi.org/10.1061/(ASCE)AE.1943-5568.0000159.
[17] Rucevskis S, Akishin P, Korjakins A. Performance evaluation of an active PCM thermal energy storage system for space cooling in residential buildings. Environ Clim Technol 2019;23(2):74–89. https://doi.org/10.2478/RTUECT-2019-0056.
[18] Thapliyal PC, Singh K. Aerogels as promising thermal insulating materials: an overview. J Mater 2014;2014:1–10. https://doi.org/10.1155/2014/127049.
[19] Jelonek Z, Drobniak A, Mastalerz M, Jelonek I. Get the light & keep the warmth - a highly insulating, translucent aerogel glass brick for building envelopes. Sci Total Environ 2020:141267. https://doi.org/10.1016/j.energy.2022.125507.
[20] Ballabh K, Gupta M, Singh D. Efficient sunlight harvesting with combined system of large Fresnel lens segmented mirror reflectors and compound parabolic concentrator without tracking sun for indoor daylight illumination. October 2022 Renew Energy 2023;202:1198–214. https://doi.org/10.1016/j.renene.2022.11.117.
[21] Karimi F, Xu H, Wang Z, Chen J, Yang M. Experimental study of a concentrated PV/T system using linear Fresnel lens. Energy 2017;123:402–12. https://doi.org/10.1016/j.energy.2017.02.028.
[22] Meteo, "Climate of Latvia." .
[23] Zhou R, et al. Design and analysis of a compact solar concentrator tracking via the refraction of the rotating prism. Energy 2022;251:123800. https://doi.org/10.1016/j.energy.2022.123800.
[24] Global Data, "Global construction industry set to grow by 5.2% in 2021, according to GlobalData.".
[25] Zhang X, et al. A review of urban energy systems at building cluster level incorporating renewable-energy-source (RES) envelope solutions. Appl Energy 2018;230:1034–1056, Nov. https://doi.org/10.1016/J.APENERGY.2018.09.041.
[26] Loonen RCGM, Trčka M, Cóstola D, Hensen JLM. Climate adaptive building shells: state-of-the-art and future challenges. Renew Sustain Energy Rev 2013;25:483–93. https://doi.org/10.1016/j.rser.2013.04.016.
[27] Hasselaar BLH. Climate adaptive skins: towards the new energy-efficient façade. no. August WIT Trans Ecol Environ 2006;99:351–60. https://doi.org/10.2495/RAV060351.
[28] Mols T, Blumberga A, Karklina I. Evaluation of climate adaptive building shells: multi-criteria analysis. Energy Proc 2017;128:292–6. https://doi.org/10.1016/j.egypro.2017.09.077.
[29] Wang J, Beltrán LO, Kim J. From static to kinetic: a review of acclimated kinetic building envelopes. In: World Renew. Energy Forum, WREF 2012, Incl. World renew. Energy Congr. XII color. Renew. Energy Soc. Annu. Conf., vol. 5; 2012. p. 4022–9.
[30] Shahin HSM. Adaptive building envelopes of multistory buildings as an example of high performance building skins. Alex Eng J 2019;58(1):345–52. https://doi.org/10.1016/j.aej.2018.11.013.
[31] Kuru A, Oldfield P, Bonser S, Fiorito F. Biomimetic adaptive building skins: energy and environmental regulation in buildings. Energy Build 2019;205:109544. https://doi.org/10.1016/j.enbuild.2019.109544.
[32] C. Traub, "Complete guide to the Institut du Monde Arabe in Paris.".
[33] Parametrichouse, "KAFD Spas Facade". .
[34] Drozdowski Z, Gupta S. Adaptive fritting as case exploration for adaptivity in architecture. In: ACADIA 09 reForm( ) Build. a Better Tomorrow - Proc. 29th Annu. Conf. Assoc. Comput. Aided Des. Archit.; 2009. p. 105–9.
[35] Premier A. Dynamic façades and smart technologies for building envelope requalification. no. 1. In: Gasparini K, editor. Media Environ. New Technol. tools built Environ. Comun. valorization; 2012. p. 66–9.
[36] Bedon C. Key structural aspects for adaptive facades - activity progress from the EU-COST action TU1403 'structural' task group. Int J Struct Glas Adv Mater Res 2018;2(1):135–54. https://doi.org/10.3844/SGAMRSP.2018.135.154. Jun.
[37] Kiefer Technic Showroom in Bad Gleichenberg Austria." .
[38] Ibrahim JA, Alibaba HZ. Kinetic façade as a tool for. Int J Eng Res Rev 2019;7(4):1–7.
[39] B. Meinhold, "Solar-powered crystalline towers Unveiled for Abu Dhabi." .
[40] L. Soma, "One Ocean, thematic Pavilion EXPO 2012/soma." .
[41] Liang R, Wang P, Zhou C, Pan Q, Riaz A, Zhang J. Thermal performance study of an active solar building façade with specific PV/T hybrid modules. Energy 2020;191:116532. https://doi.org/10.1016/J.ENERGY.2019.116532.
[42] Jouhara H, et al. The performance of a novel flat heat pipe based thermal and PV/T (photovoltaic and thermal systems) solar collector that can be used as an energy-active building envelope material. Energy 2016;108:148–54. https://doi.org/10.1016/j.energy.2015.07.063.
[43] Dehwah AHA, Krarti M. Energy performance of integrated adaptive envelope systems for residential buildings. Energy 2021;233:121165. https://doi.org/10.1016/J.ENERGY.2021.121165.
[44] Sarbu I, Sebarchievici C. A comprehensive review of thermal energy storage. Sustain Times 2018;10(1). https://doi.org/10.3390/su10010191.
[45] Heier J, Bales C, Martin V. Combining thermal energy storage with buildings - a review. Renew Sustain Energy Rev 2015;42:1305–25. https://doi.org/10.1016/j.rser.2014.11.031.
[46] Lai CM, Hokoi S. Thermal performance of an aluminum honeycomb wallboard incorporating microencapsulated PCM. Energy Build 2014;73:37–47. https://doi.org/10.1016/j.enbuild.2014.01.017.
[47] Silva T, Vicente R, Soares N, Ferreira V. Experimental testing and numerical modelling of masonry wall solution with PCM incorporation: a passive construction solution. Energy Build 2012;49:235–45. https://doi.org/10.1016/j.enbuild.2012.02.010.
[48] Bhamare DK, Rathod MK, Banerjee J. Numerical model for evaluating thermal performance of residential building roof integrated with inclined phase change material (PCM) layer. J Build Eng 2020;28:101018. https://doi.org/10.1016/j.jobe.2019.101018. October 2019.
[49] de Gracia A, Navarro L, Castell A, Ruiz-Pardo Á, Alvárez S, Cabeza LF. Experimental study of a ventilated facade with PCM during winter period. Energy Build 2013;58:324–32. https://doi.org/10.1016/j.enbuild.2012.10.026.
[50] Gholamibozanjani G, Farid M. A comparison between passive and active PCM systems applied to buildings. Renew Energy 2020;162:112–23. https://doi.org/10.1016/j.renene.2020.08.007.
[51] Ke W, Ji J, Zhang C, Xie H, Tang Y, Wang C. Effects of the PCM layer position on the comprehensive performance of a built-middle PV-Trombe wall system for building application in the heating season. Energy 2023;267:126562. https://doi.org/10.1016/J.ENERGY.2022.126562.
[52] Ajanovic A, Hiesl A, Haas R. On the role of storage for electricity in smart energy systems. Energy 2020;200:117473. https://doi.org/10.1016/j.energy.2020.117473.
[53] Lund H, Østergaard PA, Connolly D, Mathiesen BV. Smart energy and smart energy systems. Energy 2017;137:556–65. https://doi.org/10.1016/J.ENERGY.2017.05.123.
[54] Herc L, Pfeifer A, Duić N, Wang F. Economic viability of flexibility options for smart energy systems with high penetration of renewable energy. Energy 2022;252. https://doi.org/10.1016/j.energy.2022.123739.
[55] Yang L, Entchev E, Rosato A, Sibilio S. Smart thermal grid with integration of distributed and centralized solar energy systems. Energy 2017;122:471–81. https://doi.org/10.1016/j.energy.2017.01.114.
[56] Beckhoff. Solar position algorithm. 2011.
[57] Global Monitoring Laboratory, "Solar calculation details.".
[58] BBC. Light and sound - reflection and refraction. 2021.

PAPER 5: PERFORMANCE ASSESSMENT OF TWO DIFFERENT PHASE CHANGE MATERIALS FOR THERMAL ENERGY STORAGE IN BUILDING ENVELOPES

energies

MDPI

Article

Performance Assessment of Two Different Phase Change Materials for Thermal Energy Storage in Building Envelopes

Ruta Vanaga *, Jānis Narbuts, Ritvars Freimanis, Zigmārs Zundāns and Andra Blumberga

Institute of Energy Systems and Environment, Riga Technical University, 1048 Riga, Latvia; janis.narbuts_1@rtu.lv (J.N.)
* Correspondence: ruta.vanaga@rtu.lv

Abstract: To meet the 2050 EU decarbonization goals, there is a need for new and innovative ideas to increase energy efficiency, which includes reducing the energy consumption of buildings and increasing the use of on-site renewable energy sources. One possible solution for achieving efficient thermal energy transition in the building sector is to assign new functionalities to the building envelope. The building envelope can function as a thermal energy storage system, which can help compensate for irregularities in solar energy availability. This can be accomplished by utilizing phase change materials as the energy storage medium in the building envelope. In this paper, two phase change materials with different melting temperatures of 21 °C and 28 °C are compared for their application in a dynamic solar building envelope. Both experimental and numerical studies were conducted within the scope of this study. The laboratory testing involved simulating the conditions of the four seasons through steady-state and dynamic experiments. The performance of the phase change materials was evaluated using a small-scale PASLINK test stand that imitates indoor and outdoor conditions. A numerical model of a small-scale building envelope was created using data from laboratory tests. The purpose of this model was to investigate how the tested phase change materials perform under different climate conditions. The experimental findings show that RT21HC is better at storing thermal energy in the PCM and releasing it into the indoor area than RT28HC. On the other hand, the numerical simulation results demonstrate that RT28HC has an advantage in terms of thermal storage capacity in climates found in Southern Europe, as it prevents overheating of the room.

Keywords: building envelope; solar thermal energy storage; melting temperature; latent heat; small-scale PASLINK test; ANSYS Fluent

Citation: Vanaga, R.; Narbuts, J.; Freimanis, R.; Zundāns, Z.; Blumberga, A. Performance Assessment of Two Different Phase Change Materials for Thermal Energy Storage in Building Envelopes. *Energies* **2023**, *16*, 5236. https://doi.org/10.3390/en16135236

Academic Editor: Francesco Minichiello

Received: 31 March 2023
Revised: 24 April 2023
Accepted: 16 May 2023
Published: 7 July 2023

1. Introduction

The EU Green Deal aims to achieve a decarbonized building stock by 2050 and advocates for the utilization of renewable energy sources (RES) and intelligent technologies in buildings to attain this goal [1–3]. The definition of nearly zero-energy buildings is proposed as one of the approaches towards decarbonizing building stock, which recommends the usage of on-site available renewable energy sources to meet the energy requirements. However, there are inconsistencies between the availability of renewable technologies and the energy demand, unlike the case of conventional fossil energy. Renewable energy technologies may exceed the demand during peak periods or may not be sufficient to meet the energy needs during low periods, and they exhibit diurnal and seasonal fluctuations depending on the type of renewable energy technology employed. Each member state in the EU defines the benchmark for cost-effective nearly zero-energy buildings. Lowering the benchmark for heating energy demand in the northern climate is more challenging. Innovative concepts for building thermal envelopes might provide a breakthrough in the energy transition. Converting the thermal envelope of a building into a solar thermal energy storage unit is one promising path that would increase the share of on-site renewables

in covering the heating and cooling energy demand. In recent years, the acceptance of phase change materials (PCM) in building envelopes has increased due to their thermal energy transition characteristics. Ahangari and Maerefat performed a numerical study comparing the performance of a facade system consisting of concrete, insulation, and soil/plaster layers with the same façade system enhanced by two layers of PCM with different melting temperatures. The simulation results indicated that applying a double PCM layer reduced energy consumption for heating in dry and semi-arid climates in the amounts of 17.5% and 10.4%, respectively [4]. In another study, Saffari researched the improvement of energy flexibility in buildings by using PCM-enhanced envelopes. The results show that the maximum energy flexibility efficiencies range from 250% for the LW Gypsum Board envelope to 356% for the LW PCM-2 envelope [5]. PCM building envelopes can also be used to reduce the load from cooling systems in hot environmental conditions. Referring to Alshuraiaan, the thermal energy flow to indoor space can be reduced by 50% by using a PCM with a suitable melting temperature in the building envelope [6]. A detailed literature review of PCM building envelopes used in various climates has been conducted by Arumugam [7], with the conclusion that buildings with integrated PCM elements have significantly reduced energy demands. Moreover, it is stated that to improve building energy performance in warmer climate zones, PCM elements should be integrated into the outer surface of the wall, while, on the contrary, for colder climate zones they should be built into the innermost layer of the building envelope. Most of the techniques where PCM elements are used in building envelopes are passive and they perform most successfully only in steady climate zones where temperature changes are gradual. To achieve better energy performance and improve the energy efficiency of the whole building throughout the whole year in climate zones with different seasons and constantly changing weather, it is necessary to equip homes with building envelopes that can interact with irregular ambient environment changes and available on-site renewable energy sources, such as solar power.

1.1. Goal and Scope of the Study

The authors of this study are working on developing an innovative and adaptive dynamic solar building envelope that can be utilized in various locations worldwide, regardless of the climate zone. In this paper, comparative research is performed with PCMs that have two different melting point temperatures. The aim of this study was to identify the most appropriate PCM melting temperature for use in a dynamic solar facade module with thermal energy storage, which will be integrated into a large-scale adaptive dynamic solar facade system. The selected PCM should be suitable for application in various climate zones. Choosing the most appropriate PCM, and knowledge of the PCM behavior under different climatic loads is vital in the scope of this study as well as for other scientific or industrial research projects using PCM-enhanced building envelopes. Laboratory experiments were conducted under controlled temperature and solar radiation conditions to determine the PCM that is most appropriate for a specific application. Additionally, a numerical model was created to investigate the viability of this technology in varying climate zones. The main indicator is the exhibition of latent heat energy storage and its impact on indoor temperature dynamics. A testing setup to compare the thermodynamic processes in the selected PCMs was created in the laboratory at Riga Technical University Institute of Energy Systems and Environment.

1.2. Literature Review of PCM Numerical Modeling

The primary objective of numerical modeling is to replicate laboratory conditions that mimic real-life scenarios in various climate zones, where there are changes in temperature and solar irradiation. This can aid in assessing the performance of a PCM under different environmental conditions. ANSYS Fluent is among the most used software to model PCM-enhanced building envelopes [8]. A more in-depth investigation of ANSYS-based modeling of PCM-enhanced building envelopes was conducted. To perform a bibliometric

analysis, the researchers utilized the Web of Science (WOS) online database and selected publications based on keywords such as "building", "PCM", "phase change material", "paraffin", "simulation", "numerical analysis", "model", "software", and "ANSYS". To refine the scope of the search, the publications were filtered based on their document types, which included articles, early access, and review articles. The search was limited to the years 2019–2023. The analysis yielded 42 publications, of which seven were irrelevant to the search scope and thus excluded from further examination. Out of all the studies chosen, only nine met the two main requirements: utilizing ANSYS Fluent simulation software and focusing on walls as the object of research. The publications meeting these criteria are detailed in Table 1.

Table 1. WOS selection of publications on ANSYS modeling of PCM-enhanced building components.

Publication	Time Scale	Scale (Element, Room, or Building)	Building Envelope
Performance Evaluation of an Active PCM Thermal Energy Storage System for Space Cooling in Residential Buildings [9]	Month	Room	Wall
Comparative Study of Two Materials Combining a Standard Building Material with a PCM [10]	Hour	Element	Wall
Numerical Simulation of a Novel Dual Layered Phase Change Material Brick Wall for Human Comfort in Hot and Cold Climatic Conditions [11]	Month	Element	Wall
Parametric analysis and design optimisation of PCM thermal energy storage system for space cooling of buildings [12]	Day	Room	Wall
Thermal management analysis of PCM integration in building using a novel performance parameter—PCM effectiveness index [13]	Year	Room	Wall, roof
Numerical analysis of nanomaterial-based sustainable latent heat thermal energy storage system by improving thermal characteristics of phase change material [14]	Seconds	Element	Wall, floor
Simulation of a Trombe wall with a number of semicircular fins placed on the absorber plate for heating a room in the presence of nano-PCM [15]	Hour	Room	Wall
Numerical thermal evaluation of laminated binary microencapsulated phase change material drywall systems [16]	Month	Room	Wall
Potential of integrating PCMs in residential building envelope to reduce cooling energy consumption [17]	Hour	Room	Wall

1.3. Thermal Energy Storage

The ability to store thermal energy is crucial in renewable energy systems as it allows for better management of energy demand and increases flexibility. Thermal energy storage can be divided into two main categories: thermal storage (which includes sensible and latent storage) and thermochemical energy storage (as shown in Figure 1). Currently, sensible heat storage is widely available commercially (accumulation tanks in heating systems), while others are still under development [18,19]. Sensible heat storage depends on the mass and heat capacity of the material, while latent energy storage is calculated in two states, before phase change and after the phase change (as a sensible heat), and, in addition, the enthalpy of fusion (J/g) is taken into account. There are three types of thermal energy storage systems, based on sensible, latent, and thermochemical heat storage, but the first two are more applicable in buildings. Sensible heat storage systems are simpler and already available on the market, whereas latent heat thermal energy storage systems

(LHTES) have a higher storage capacity per unit volume [20]. Such systems are applicable and convenient for passive and net-zero energy buildings as they can be directly implanted into building envelopes that use on-site renewable energy sources, namely solar thermal energy. The most important advantage of the application of correspondent technology is the reduction in heating season duration, especially in climate zones where the autumn and spring seasons are long.

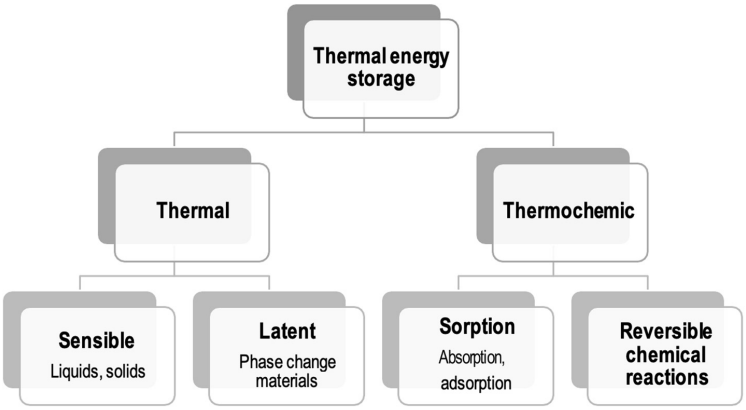

Figure 1. Classification of thermal energy storage methods.

Thermal energy storage techniques vary in terms of their operating temperature range, storage capacity, and duration of storage, which can range from hours to months for seasonal storage. These methods are used to balance energy demand between day and night, store summer heat for winter heating, and store winter cold air for summer air conditioning. Among the thermal energy storage methods, sensible heat storage is the most versatile, covering the widest range of operating temperatures (sub-zero to 500 °C) and can be utilized on both an hourly and seasonal scale [21]. Yet for application in building thermal envelopes the most suitable temperature range is 18–50 °C (given for different types of paraffin wax) [22]. Storing thermal energy for later use through heating or cooling an energy storage medium is known as thermal energy storage (TES). These systems can help balance the fluctuations in the availability of renewable energy sources (RES) on a daily or seasonal basis. In PCMs, energy can be stored as either sensible or latent heat [23]. Sensible heat is the measure of energy necessary to change a body's temperature, whereas latent heat occurs at a nearly linear temperature while changing the phase of the substance (solid to liquid, liquid to gaseous, solid to solid) [24] (see Figure 2).

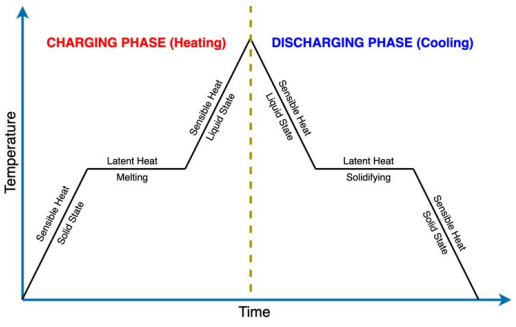

Figure 2. Theoretical latent heat curve for solid/liquid phase transition.

In the charging phase, the heat is applied to the PCM and the energy is stored, while in the discharging phase, the stored heat is released. Incorporating TES into an energy system provides several benefits, such as improved performance and reliability, better economics, reduced maintenance and operating costs, and decreased environmental pollution. This includes lower carbon dioxide emissions as the energy demand for heating decreases [18]. Both passive and active techniques are utilized for TES in a range of settings, including HVAC systems, building structures, and systems located near buildings [25].

1.4. Phase Change Materials

PCM is utilized as the energy storage medium in LHTES systems (see Figure 3).

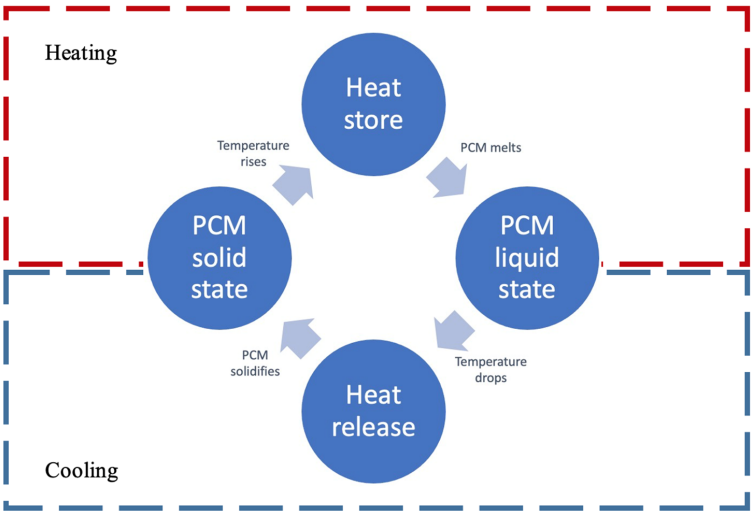

Figure 3. The working cycle of phase change material.

In building applications, solid–liquid PCMs are commonly used and are classified into three main categories: organic, inorganic, and eutectics [26]. Paraffin, fatty acid, and sugar alcohols are the most commonly used organic PCMs, with paraffin having the advantage of a phase change temperature range from 10 °C to 100 °C [27]. Various studies have been conducted on incorporating phase change materials into building components such as boards, bricks, and shading devices [28–30]. Despite this, PCM-enhanced building components have not yet reached the mass production level, leaving room for potential optimization and innovation. Scientific understanding of PCM behavior and characteristics can pave the way for technological advancements. The melting temperature of a PCM is one of the parameters that determine its suitability for specific building applications with defined performance objectives, such as reducing heating or cooling loads, and the environment in which the PCM-enhanced building component is placed, including daily and seasonal temperature ranges.

2. Materials and Methods

2.1. Materials

The design of the test stands incorporates various materials, including extruded polystyrene (XPS) from Finfoam (Salo, Finland) for insulation, plywood from Ergos (Riga, Latvia) for external construction, glass from Glass (Riga, Latvia) for containers, polyethylene terephthalate glycol (PETG) from Prusa Research (Prague, Czech Republic) for container covers, and PCMs from Rubitherm Technologies GmbH (Berlin, Germany) for experimental study. These RTHC PCMs are composed of organic materials, such as paraffin wax, which

undergo a solid-to-liquid (and vice versa) melting process to efficiently store and release substantial amounts of heat within a relatively constant temperature range [31]. These versatile PCMs can be used in a wide range of applications at various temperatures, depending on their melting point. One notable advantage of RTHC PCMs is their significantly higher latent heat capacity of 25–30% compared to traditional PCMs, and they melt within a narrower temperature range. This makes them well-suited for situations where space is limited, as they are ideal for efficient thermal energy storage in confined spaces. The properties and characteristics of the materials used in the design of the test stands are summarized in Table 2.

Table 2. Material properties and characteristics.

Material	Properties	Characteristics
RUBITHERM RT21HC	Dimensions: 127 × 127 × 60 mm^3	Melting area: 20–23 °C Congealing area: 21–19 °C Density at 15 °C: 0.88 kg/L Density at 40 °C: 0.77 kg/L Heat storage capacity ±7.5% 190 kJ/kg
RUBITHERM RT28HC	Dimensions: 127 × 127 × 60 mm^3	Melting area: 27–29 °C Congealing area: 29–27 °C Density at 15 °C: 0.88 kg/L Density at 40 °C: 0.77 kg/L Heat storage capacity ±7.5% 250 kJ/kg
Plywood	Thickness: 15 mm	λ = 0.13 W/mK SHGC = 0.28
XPS	Thickness: 50 mm	λ = 0.037 W/mK
Glass	Thickness: 4 mm	λ = 1.2 W/mK SHGC = 0.8
PETG	Thickness: 2 mm	λ = 0.2 W/mK

2.2. PASLINK-Type Testing

To evaluate the performance of each of the PCMs, comparative testing was performed based on the PASLINK testing method. This method is one of the most commonly used methods for testing passive solar-thermal-energy-based building components and envelopes. PASLINK evolved from the European project PASSYS (Testing Passive Solar Energy Components and Systems), which began in 1985 with the aim of increasing confidence in both the use of energy-efficient and passive solar buildings and their assessment methods [32]. The PASSYS project focused on a test cell bench as a means of determining the energy performance of passive solar building components and providing more information on building design and simulation tools [33]. The advantage of test cells is that they provide a well-controlled environment [34].

2.3. Experimental Setup

The thermal energy transmission rate of the dynamic solar building envelope is largely influenced by the various components that make up its overall design. Figure 4 shows an innovative design of a building envelope developed by the research team. The design incorporates a PCM container, an aerogel layer to minimize heat loss, and a heat transfer enhancer (Fresnel lens), which concentrates solar energy onto the surface of the PCM container. This study focuses on the use of latent heat thermal energy storage, where a PCM is the main component responsible for thermal energy transfer through the building envelope. Choosing the optimal PCM can significantly reduce heating and cooling loads, particularly during periods when solar radiation is available. Various factors must be

considered when selecting the PCM for specific applications, including the optimal volume, layer thickness, and melting temperature range, as outlined by Guo and Zhang [35].

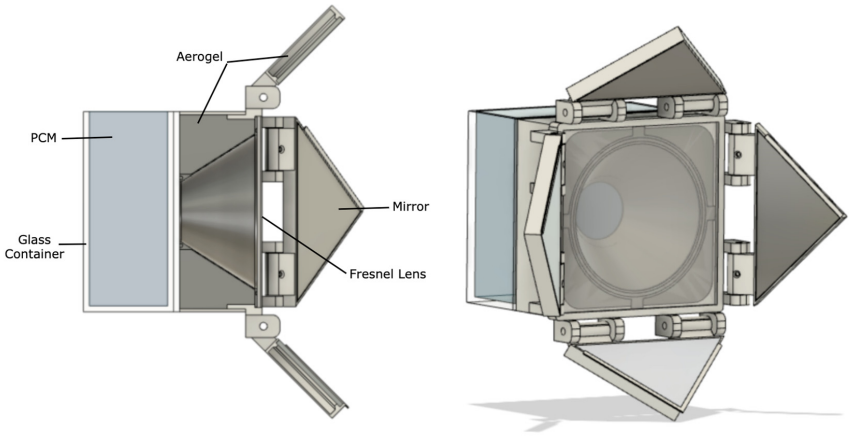

Figure 4. The design of a solar building envelope module.

The optimal PCM volume and layer thickness must be selected to ensure geometric compatibility with other components of the system, including the Fresnel lens focal length and point location, aerogel insulation layer, and dimensions of the large-scale system (an upscaled version of the small-scale module). The system aims to provide an efficient energy balance for the entire building while maintaining a comfortable indoor environment for occupants, with room temperatures ranging from 18 °C to 27 °C throughout all seasons.

To compare the thermal behavior of two different PCMs under different climatic conditions simulating different seasons of the year, two comparative experiments—steady-state and dynamic—were conducted in laboratory testing. While Rubitherm RT21HC has a lower melting temperature closer to the average indoor temperature, Rubitherm RT28HC has a higher latent heat storage capacity. The experimental setup was designed to replicate a small-scale PASLINK-type test cell, with two test stands prepared for the comparative study—one for RT21HC and the other for RT28HC. The plywood box was lined with 50 mm insulation (XPS) to simulate the "indoor" space, and the PCM container was built into one of the walls of each test box (see Figure 5).

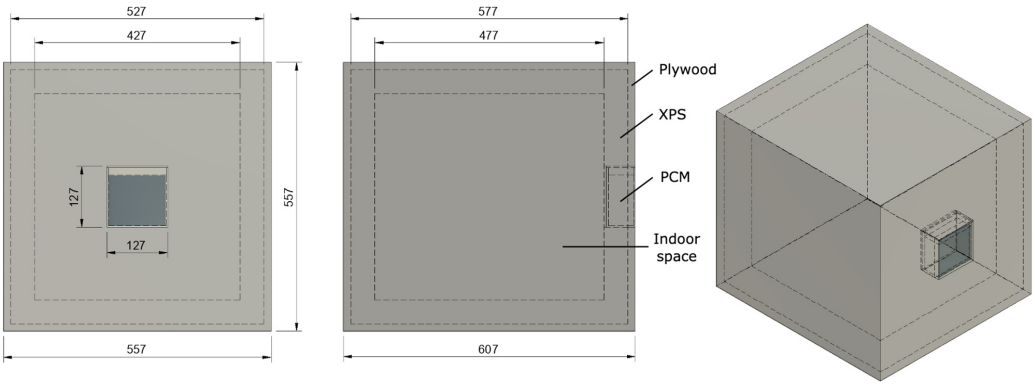

Figure 5. Test box. Small-scale PASSLINK-type test cell.

To monitor the experimental setup, a set of thermocouples was placed as shown in Figure 6. A total of eleven thermocouples were installed for each test box—six placed in the PCM container at different heights to observe temperature changes in different layers of the phase change materials and five thermocouples located in the indoor space of the test box at different heights. The thermocouples are labeled based on their location inside the PCM container, with letters L, M, and R indicating their location on the x-axis (L—left, M—middle, and R—right), and numbers indicating their location on the y-axis (1—lower and 2—upper). This set of thermocouples allows for a comparison of changes in PCM temperature and indoor space temperature between the two setups under defined conditions. The test stands were positioned adjacent to each other inside the climatic test chamber Tera Science TEMI 2500 (Changwon, Republic of Korea), as illustrated in Figure 7.

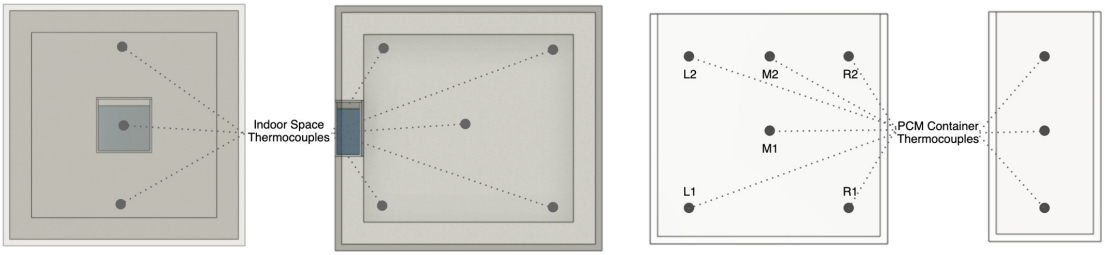

Figure 6. Thermocouples in small-scale PASLINK-type testing boxes (**left**) and PCM container (**right**).

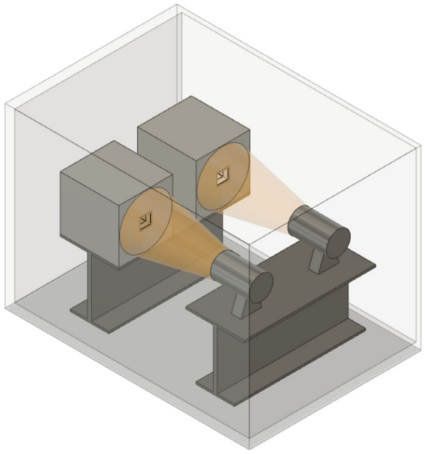

Figure 7. Experimental setup in the climate chamber.

Solar energy consists of radiant light and heat from the Sun [36]. To simulate solar radiation for the test setups, halogen lamps were used since they emit both heat and light with color characteristics similar to that of the Sun [37]. Specifically, two halogen lamps (GE SUPER CP60 EXC VNS 230V | 1000W G16d 3200K | General Electric (Schenectady, NY, USA) combined with dimmer UNI BAR Elation professional) were positioned along the longitudinal axes of each test box. A heating/cooling unit was utilized to maintain the desired temperature within the climatic chamber. The experimental setup is designed as a miniature version of a "structure", comprising a test box with a thermal enclosure and indoor area. This setup is exposed to climate-induced stresses such as heating and cooling, which are created by the predetermined conditions in the climate chamber. Temperature changes in both the indoor space and the phase change material of the thermal enclosure are recorded using measuring equipment.

2.4. Planning of the Experiment

The test conditions were designed to simulate the four seasons: spring, summer, autumn, and winter. For the steady-state experiment, three identical 24 h cycles were repeated for each season. The conditions for each season are determined by the following factors:

- The experiment begins with the outdoor temperature as the initial state. Both the solar wall module setups and the climate chamber are cooled to the same initial state before the start of the experiment.
- During both the heating and cooling phases, the outdoor temperature is kept constant, set to the average temperature of a typical day in that season.
- The duration of daylight and the intensity of solar radiation are also taken into consideration.

To obtain the average values of parameters such as daylight duration, solar irradiance, and outdoor temperature for a typical day in each season, data from the local meteorological station were analyzed.

The complete testing cycle lasts for 72 h, and all the experimental conditions are summarized in Table 3.

Table 3. Conditions for the steady-state experiment.

Season	Condition	Value
Spring	Daylight (solar simulation) duration	12 h
	Irradiance intensity	690 W/m^2
	Outdoor temperature	7 °C
Summer	Daylight (solar simulation) duration	12 h
	Irradiance intensity	750 W/m^2
	Outdoor temperature	19 °C
Autumn	Daylight (solar simulation) duration	10 h
	Irradiance intensity	440 W/m^2
	Outdoor temperature	10 °C
Winter	Daylight (solar simulation) duration	9 h
	Irradiance intensity	230 W/m^2
	Outdoor temperature	0 °C

In the second experiment, all test conditions were kept the same as in the first experiment, except for the solar irradiance intensity. To simulate dynamic environmental conditions, the solar simulator was turned on and off every 30 min during all the season test rounds that occurred during daylight hours.

Throughout the test, measurements were recorded every minute using the CR1000 Campbell Scientific multipurpose data logger. Solar radiation was measured using a Kipp & Zonen CMP3 pyranometer, while Type T thermocouples were used to measure temperature in both the indoor space and the phase change material (PCM). The specifications for the measuring equipment are listed in Table 4.

Table 4. Specifications of CMP, Kipp & Zonen pyranometer [38] and Type K thermocouples [39].

Equipment	Characteristics	Value
CMP, Kipp & Zonen pyranometer	Response time	20 s
	Directional response (up to 80° with 1000 W/m^2 beam)	<20 W/m^2
	Temperature dependence of sensitivity (−10 °C to +40 °C)	<4%
	Operational temperature range	−40 °C to +80 °C
	Maximum solar irradiance	2000 W/m^2
	Field of view	180°
Type K thermocouples	Temperature range	−270 °C to 1260 °C
	Accuracy	±2.2 °C or ±0.75%

2.5. Numerical Modeling of the System

The ANSYS Fluent software (2023 R1 version) was utilized for numerical modeling purposes, whereby the governing equations for fluid flow simulations were employed to conduct the simulations. One such fundamental principle of fluid dynamics is the continuity equation, which can be expressed as follows [40]:

$$\mathrm{div}(\rho V) + \partial\rho/\partial t = 0, \quad (1)$$

where div represents the divergence operator, ρ is the density of the fluid, V is the velocity vector of the fluid, and t is time.

The following assumptions were considered in the numerical modeling:

- Melting is a two-dimensional transient phenomenon.
- The movement of the PCM in its liquid state is turbulent, non-Newtonian, and incompressible.
- Viscosity, density, and thermal conductivity are constant.
- Heat generation, volume expansion, and viscous heating are not considered.

The total enthalpy of the PCM is calculated by adding the sensible enthalpy, represented by h, to the latent heat, denoted as ΔH [41]:

$$H = h + \Delta H, \quad (2)$$

and

$$h = h_{ref} + \int_{T_{ref}}^{T} C_p dT, \quad (3)$$

where h_{ref} is reference enthalpy, T_{ref} is reference temperature, and C_p is specific heat. The latent heat content is determined by taking into consideration both the latent heat of the material, denoted as L, and the liquid fraction, represented by β:

$$\Delta H = \beta L, \quad (4)$$

$$\beta = \frac{T - T_{solidus}}{T_{liquidus} - T_{solidus}}. \quad (5)$$

The amount of latent heat contained in a substance can change in direct proportion to the temperature shift between zero (for a solid) and L (for a liquid). This assumption is based on β = 0 when the material temperature is below the solidification (solidus) temperature, β = 1 when the material temperature is above the melting (liquidus) temperature, and a linear variation for temperatures between the solid and liquid states [9].

The Fusion 360 CAD tool is utilized to design a two-dimensional system drawing, which is then imported into the Design Modeler module of Ansys. This allows the drawing to be prepared for simulation in Fluent. Figure 8 displays the fluids utilized in the simulation as well as the boundary conditions that were applied.

In order to accurately replicate the conditions and dimensions of the real system, the simulation model includes an air gap (which allows space for the PCM to expand during laboratory experiments) and a plastic cover for the glass container. To determine the value of solar heat gain on each of the outer surfaces (plywood and glass), the solar heat gain coefficient (SHGC) has to be considered. Solar heat gain (SHG) can be calculated as follows:

$$SHG = SHGC \times SI, \quad (6)$$

where SI is the value of direct solar irradiation.

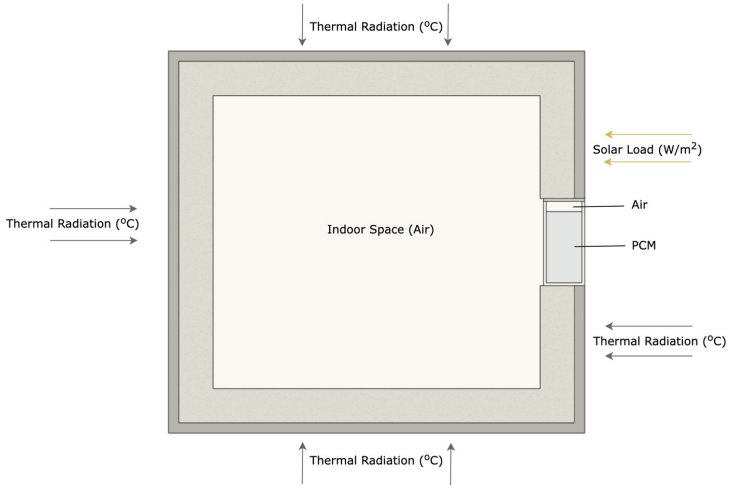

Figure 8. Design of the 2D simulation model.

To simulate isotropic turbulent flow, the k-epsilon model is utilized. The momentum equation's convective terms are discretized with a second-order upwind interpolation scheme, while the energy equation's convective terms are discretized using a first-order upwind interpolation scheme. To couple pressure and velocity, the Coupled algorithm is used, and for pressure interpolation, the PRESTO model is adopted.

3. Results

3.1. Steady-State Experiment

Figure 9 illustrates the results of a steady-state experiment conducted in a previous study [42] by our team of researchers. A series of experiments were performed to compare the behavior of two distinct PCMs during four different seasons, using the testing conditions outlined in Section 2.3.

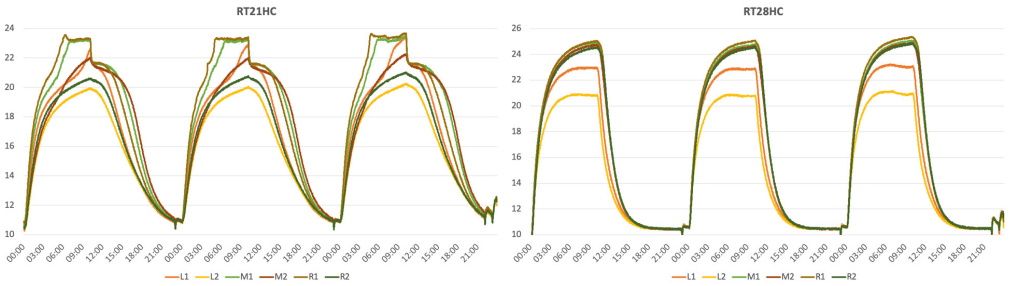

Figure 9. PCM temperatures in different layers of (**a**) RT21HC and (**b**) RT28HC in the autumn conditions.

Figure 9a shows that the upper layers of RT21HC have achieved the melting temperature, resulting in the storage of latent heat, while the lower sections have yet to reach the melting point. By contrast, Figure 9b displays temperature fluctuations across various layers of RT28HC under autumn conditions, with neither layer reaching the melting temperature. Previous study findings revealed that in the autumn setup, RT28HC PCM exhibits a higher peak temperature compared to RT21HC PCM during the charging phase, but RT21HC PCM achieves a higher indoor peak temperature due to latent heat storage. Both

PCMs return to their initial outdoor temperature at the end of each daily cycle. In the spring setup, both PCMs partially melt, but RT28HC PCM reaches a higher peak temperature than RT21HC PCM. RT21HC PCM has a lower temperature during the charging phase but higher during the discharging phase. In the winter setup, neither PCM reaches its melting temperature, resulting in smaller temperature differences between the indoor space and the PCM. RT21HC PCM experiences higher average temperatures and achieves a higher room temperature compared to RT28HC PCM. In the summer setup, RT28HC PCM has a longer plateau period during the solidification phase compared to other seasons, and RT21HC PCM exhibits higher temperatures during the charging phase, but RT28HC PCM has higher temperatures during the discharging phase.

The steady-state experiments show that the behavior of the two PCMs varies depending on the season and the specific conditions of the experiment. While RT28HC reaches higher peak temperatures during the charging phase, RT21HC achieves a higher indoor peak temperature due to latent heat storage.

3.2. Dynamic Experiment

The dynamic experiment involved the implementation of the experiment plan conditions with alternating on and off solar simulation cycles.

Although each seasonal setup was tested for 72 h, no substantial variations were observed in the temperature curves when comparing them day to day. Therefore, the dynamic experimental outcomes will be evaluated based on the 24 h cycle. Figure 10a illustrates the average temperature curves of both PCMs under spring testing conditions.

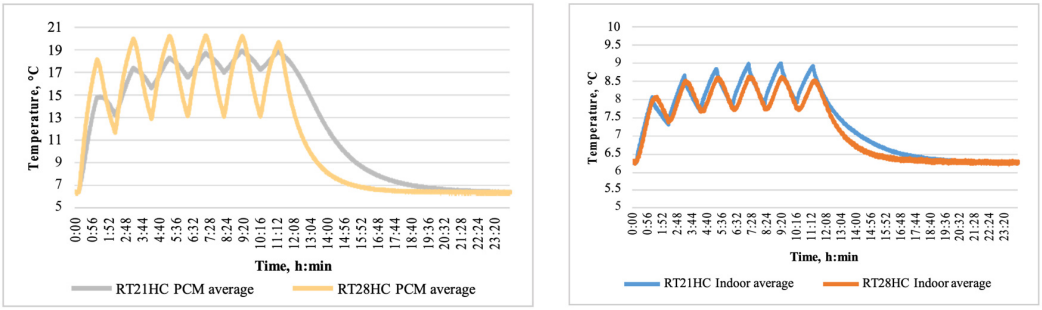

(**a**) (**b**)

Figure 10. Average temperatures in (**a**) PCMs and (**b**) indoor space; 72 h cycle. Dynamic test: Spring.

By contrast, RT28HC reaches higher temperature peaks during the daylight cycle but experiences a more significant temperature drop while the solar simulator is off, with thermal energy not being stored in the PCM due to sensible heat transition. The average indoor temperature in the RT21HC test box is higher than that in RT28HC, with a less steep slope of the temperature curve during the discharging phase (refer to Figure 10b).

Figure 11 displays temperature graphs for different layers of both PCMs. It is evident that all layers of RT21HC are in the melting phase, resulting in the storage of latent heat energy. By contrast, none of the layers of RT28HC have reached the melting point, with temperature oscillating between the highest and lowest values during the charging phase.

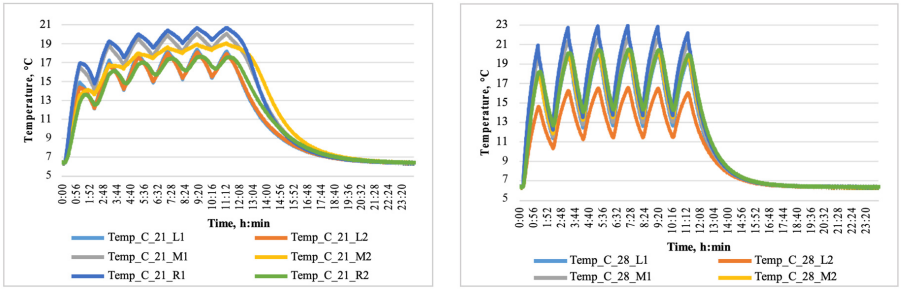

(**a**) (**b**)

Figure 11. PCM temperatures in different layers of (**a**) RT21HC and (**b**) RT28HC; 72 h cycle.

Similar temperature trends can be observed in both test stands during the autumn setup. In the summer setup, the average temperatures in both PCMs reach the melting point, with a gradual increase in temperature values (refer to Figure 12a). Although the RT21HC test box has the highest indoor temperature values, the temperature peaks do not exceed 21 °C (refer to Figure 12b). Upon observing temperatures in different locations of RT21HC (refer to Figure 13a), it is evident that all layers of the PCM have exceeded the melting temperature, and the PCM is completely melted starting from around 2:00, resulting in sensible heat energy storage. In the case of RT28HC (refer to Figure 13b), only one spot in the upper layer (L2) has not reached the melting point, indicating partial liquefaction of the PCM and partial latent heat energy storage. However, at the end of the 24 h cycle, the temperature in RT21HC PCM is 2–3 °C higher than in RT28HC, depending on the location of the layer measurement.

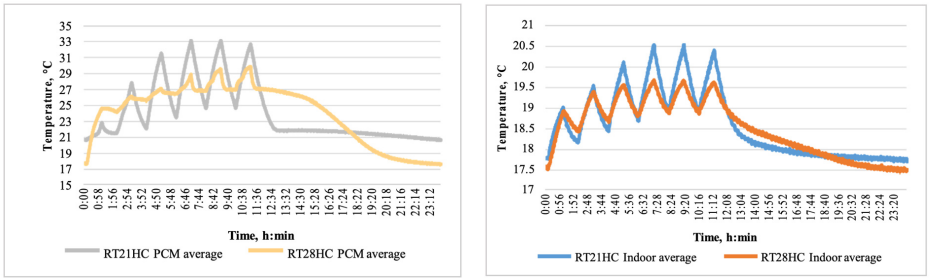

(**a**) (**b**)

Figure 12. Average temperatures in (**a**) PCMs and (**b**) indoor space; 72 h cycle. Dynamic test: summer.

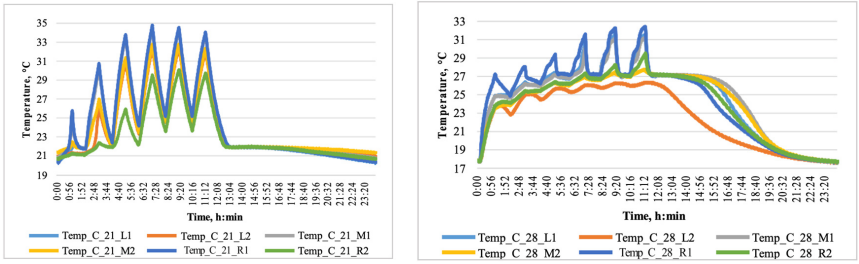

(**a**) (**b**)

Figure 13. PCM temperatures in different layers of (**a**) RT21HC and (**b**) RT28HC; 72 h cycle. Dynamic test: summer.

Figure 14 presents a comparison of the highest average temperatures in both PCMs and indoor spaces between the steady-state and dynamic experiments. Although there are similar temperature trends in both types of experiments, the overall temperature values are higher in the steady-state tests due to the absence of solar irradiance dropouts. While RT28HC reaches higher PCM peak temperatures in autumn, winter, and spring, RT21HC exhibits the highest indoor space temperatures in all seasons. This suggests that RT21HC is more effective in storing thermal energy in the PCM and releasing it into the indoor compartment.

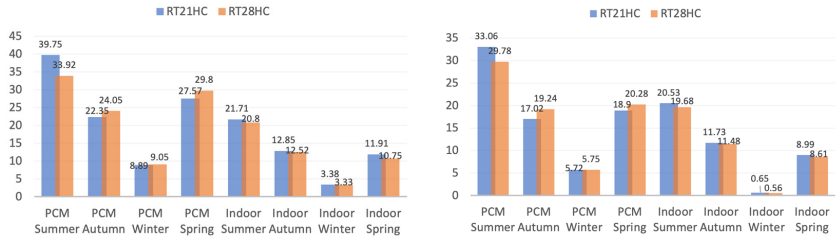

(**a**) (**b**)

Figure 14. Comparison between the highest temperatures reached by RT21HC and RT28HC in (**a**) steady-state test and (**b**) dynamic test.

3.3. Numerical Simulation

To assess how the system would perform under varying climate conditions such as changes in solar irradiance and outside temperature, it is essential to verify the accuracy of the model against experimental data. To accomplish this, a laboratory test was carried out where both experimental setups were heated until the PCM completely melted, and subsequently cooled to the ambient temperature. The results of the experimental test, as well as simulated temperature curves, are represented in Figure 15. Since the laboratory test was conducted inside a climate chamber that maintains a consistent temperature through its cooling system, the numerical calculations must consider the airflow velocity to match the dynamics of the actual system, which was recorded at approximately 0.5 m/s.

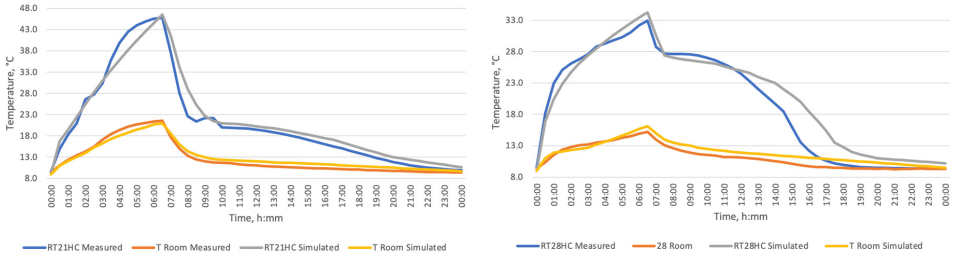

(**a**) (**b**)

Figure 15. Comparison between simulated and experimentally collected data of (**a**) RT21HC and (**b**) RT28HC PCMs.

To conduct the numerical simulation, information on the outside temperature and solar irradiance was gathered from two cities located in different regions of Europe. Helsinki, Finland, in the north, and Seville, Spain, in the south, were chosen for this purpose. The National Solar Radiation Database was used to collect data from the past three years. Hourly averages of the direct solar radiation and outside temperature were calculated for each of the four seasons—spring, summer, autumn, and winter.

The numerical model relies on various conditions and assumptions, including the use of global horizontal solar irradiance for solar load calculations, an assumption of clear skies, and the consideration that only the front-facing side of the box is impacted by the solar load; the wind direction and speed are ignored in these calculations. Ten simulations were conducted using the developed model, with six of them simulating the environmental conditions of spring, summer, and autumn in Helsinki, while the remaining four simulations imitated spring and winter conditions in Seville. The decision not to perform simulations for wintertime in Helsinki and summertime in Seville was based on previous laboratory experiments which indicated that neither of the PCMs provided any advantages in extremely hot or cold conditions.

The climate in Helsinki during spring and autumn is comparable and mild, with the exception of slightly higher outdoor temperatures in autumn. Figure 16 represents simulation results from the spring test in Helsinki.

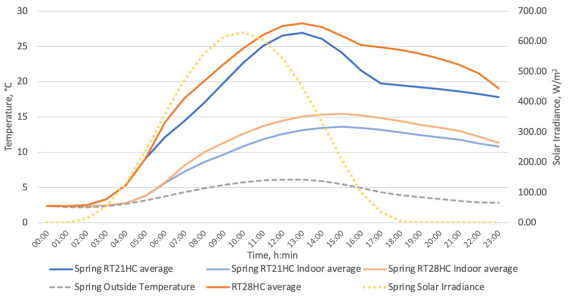

Figure 16. Average temperature in the PCMs and indoor room. Simulation results: Helsinki—spring.

From the Helsinki—spring graphs, it is evident that both PCMs underwent a partial melting process and absorbed thermal energy. Further analysis revealed that the RT28HC PCM experienced a slightly higher average temperature compared to the RT21HC examined. However, at the end of the 24 h cycle, both PCMs attained almost identical temperature values. The ambient temperature outside did not exceed 6 °C during the testing period. This implies that all of the thermal energy absorbed by the PCMs was from solar radiation.

Figure 17 displays the outcomes of the Helsinki autumn simulation. It reveals that the maximum average temperature of RT28HC was approximately 6 °C higher than that of RT21HC. However, by the end of the 24 h cycle, the temperature of RT28HC dropped 6 °C below that of RT21HC. This result can be attributed to the fact that although RT28HC attained a higher temperature while solar radiation was present, it was unable to reach its melting point. Therefore, it lost the absorbed heat by the end of the cycle. By contrast, RT21HC was able to store enough thermal energy to maintain a higher temperature in the room by the end of the cycle.

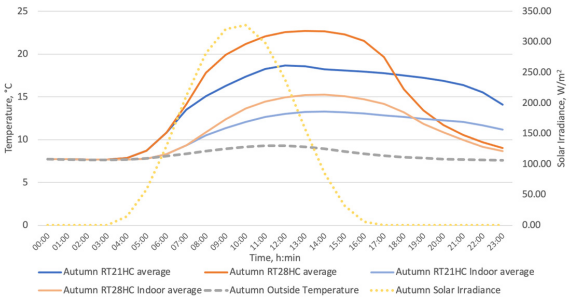

Figure 17. Average temperature in the PCMs and indoor room. Simulation results: Helsinki—autumn.

Compared to other European cities, especially those in Southern Europe, Helsinki experiences cooler and more moderate summers. Throughout the months of June, July, and August, the average high temperature in Helsinki typically falls between 18 °C to 22 °C, while the average low temperature ranges from 10 °C to 14 °C. Figure 18 illustrates the temperature graphs of the summer season in Helsinki. As solar radiation reaches high levels, both PCMs melted. However, it is evident that RT28HC had the advantage of a higher melting point temperature, preventing the room from overheating. In these conditions, RT28HC exhibited smoother temperature fluctuations throughout the entire cycle, which resulted in a more comfortable environment in the room.

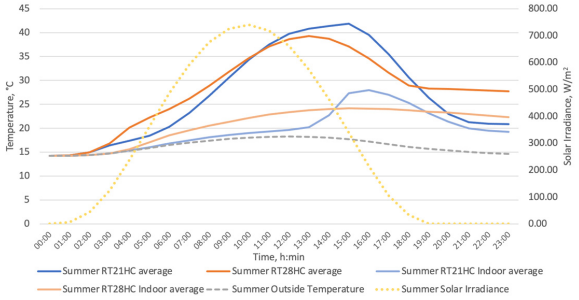

Figure 18. Average temperature in the PCMs and indoor room. Simulation results: Helsinki—summer.

Compared to Northern Europe, Southern Europe, exemplified by Seville, receives a higher amount of sunlight throughout the year in all seasons. Seville experiences an average of 129 sunny days annually, and the solar intensity is higher than in other European cities. In spring, the solar irradiance value can surpass 900 W/m^2, which raises concerns about the possibility of overheating. However, the nighttime temperatures are still relatively low, not exceeding 12 °C, which may require additional heating. The simulation results of Seville in spring are depicted in Figure 19. It is evident that RT21HC overheats in such a climate, causing the room temperature to rise to nearly 35 °C. Conversely, RT28HC has a great potential to prevent the room from overheating during the daytime while ensuring comfortable temperatures at night, without requiring additional heating. This case underscores the advantage of RT28HC's higher heat storage capacity, allowing it to absorb more thermal energy than RT21HC.

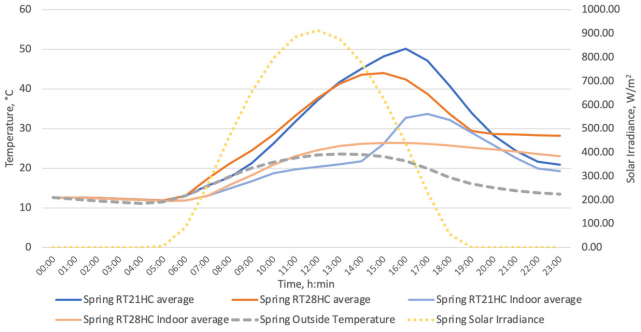

Figure 19. Average temperature in the PCMs and indoor room. Simulation results: Seville—spring.

Seville has a milder winter compared to many other European cities due to its southern location and Mediterranean climate. The average temperature in Seville during the winter months (December to February) ranges from 8 °C to 18 °C, which is considerably warmer than many other European cities during the same period. Yet, additional heating

is necessary for most of the time. The average PCM temperatures in the Seville—winter numerical simulation are illustrated in Figure 20.

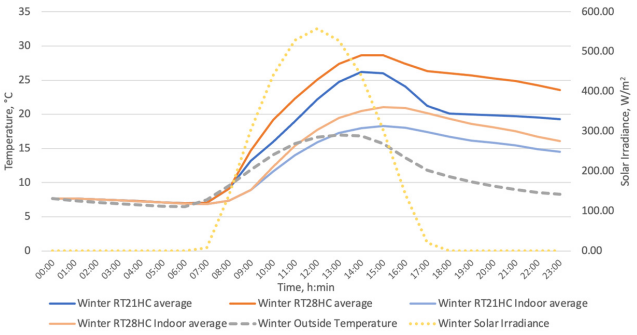

Figure 20. Average temperature in the PCMs and indoor room. Simulation results: Seville—winter.

Both PCMs exhibit comparable behavior in this scenario, as they have both achieved the melting point temperature and stored thermal energy through latent heat. The indoor temperature profiles follow a similar pattern, but the RT28HC performs slightly better, as it is able to attain a higher maximum room temperature of approximately 21 °C. Figure 21 represents the comparison of the highest liquid fraction reached in the PCMs in every simulation. It is clearly seen that RT21HC has melted fully in two cases, Helsinki—summer and Seville—spring, which highlights the potential for overheating. In all of the cases, RT21HC has reached liquid fraction values due to its lower heat storage capacity compared to RT28HC.

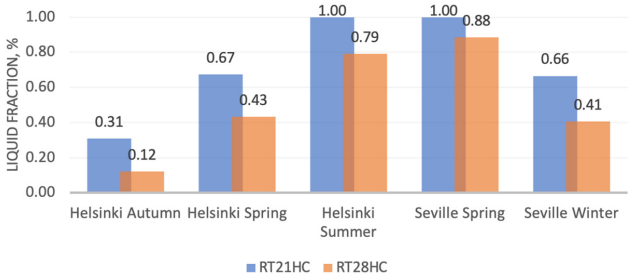

Figure 21. Comparison of the highest reached melted fraction of the PCMs in all simulations.

4. Discussion and Conclusions

Experimental and numerical research was conducted to compare two different phase change materials (PCMs) with melting temperatures of 21 °C and 28 °C, respectively, under specific climatic conditions that mimic the four seasons of the year. A small-scale model of a building was utilized for the experiment, comprising a test box with a thermal envelope and an indoor area subjected to heating and cooling loads within a climate chamber. Two types of experiments, steady-state and dynamic, were performed, and two parameters were compared: the average temperature of the PCM and the average temperature of the indoor space in the test box. The results showed that RT21HC PCM had a higher average indoor temperature than RT28HC, with a less steep slope of the temperature curve during the discharging phase. By contrast, RT28HC had higher temperature peaks during the daylight cycle but experienced a more significant temperature drop while the solar simulator was off, with thermal energy not being stored in the PCM due to sensible heat transition. The results also showed that all layers of RT21HC were in the melting phase, resulting in the storage of latent heat energy, while none of the layers of RT28HC reached the melting point,

with temperature oscillating between the highest and lowest values during the charging phase. In the summer setup, both PCMs reached the melting point, with a gradual increase in temperature values. The experimental results suggest that RT21HC is more effective in storing thermal energy in the PCM and releasing it into the indoor compartment compared to RT28HC in particular climate conditions.

The numerical modeling gives an insight into the effectiveness of each of the tested phase change materials applied in different climate zones. The laboratory test was carried out to verify the accuracy of the model against experimental data. The numerical simulations were conducted using the information on outside temperature and solar irradiance gathered from two cities in different regions of Europe—Helsinki, Finland, and Seville, Spain. The simulation results showed that the PCMs underwent a partial melting process and absorbed thermal energy during the spring, autumn, and summer seasons in Helsinki. The RT28HC PCM experienced a slightly higher average temperature compared to RT21HC examined in Helsinki. However, at the end of the 24 h cycle, both PCMs attained almost identical temperature values. By contrast, during the autumn season in Helsinki, the maximum average temperature of RT28HC was approximately 6 °C higher than that of RT21HC. However, by the end of the 24 h cycle, the temperature of RT28HC dropped 6 °C below that of RT21HC. The summer season simulations in Helsinki showed that both PCMs melted, but RT28HC had the advantage of a higher melting point temperature, preventing the room from overheating. In Seville, the RT28HC PCM had the potential to prevent the room from overheating during the daytime, while ensuring comfortable temperatures at night, without requiring additional heating. In the winter season in Seville, both PCMs achieved the melting point temperature and stored thermal energy through latent heat, but RT28HC performed slightly better.

This study provides data on thermodynamic processes under various outdoor temperatures and solar simulation intensities, which can be used to validate mathematical models and explore different design scenarios for PCM-enriched building components at various scales, from small-scale models to real-size buildings. This research is part of a larger effort to develop PCM-enriched adaptive solar facade systems that can actively contribute to building energy balance and represent a novel solution in the field of building components.

Author Contributions: Conceptualization, A.B.; Methodology, J.N.; Software, J.N.; Data curation, R.F. and Z.Z.; Writing—original draft, R.V.; Writing—review & editing, R.V. and J.N.; Visualization, J.N.; Supervision, R.V. All authors have read and agreed to the published version of the manuscript.

Funding: This work was supported by the European Social Fund within Project No. 8.2.2.0/20/I/008 «Strengthening of Ph.D. students and academic personnel of Riga Technical University and BA School of Business and Finance in the strategic fields of specialization» of the Specific Objective 8.2.2 «To Strengthen Academic Staff of Higher Education Institutions in Strategic Specialization Areas» of the Operational Program «Growth and Employment».

Data Availability Statement: Not applicable.

Conflicts of Interest: The authors declare no conflict of interest.

References

1. European Commission. *The European Green Deal*; European Commission: Brussels, Belgium, 2019.
2. European Union. Directive (EU) 2018/844 of the European Parliament and of the Council of 30 May 2018 amending Directive 2010/31/EU on the energy performance of buildings and Directive 2012/27/EU on energy efficiency. *Off. J. Eur. Union* **2018**, *L156*, 75.
3. EU. Directive (EU) 2018/2001 of the European Parliament and of the Council on the promotion of the use of energy from renewable sources. *Off. J. Eur. Union* **2018**, *L328*, 82–209.
4. Ahangari, M.; Maerefat, M. An innovative PCM system for thermal comfort improvement and energy demand reduction in building under different climate conditions. *Sustain. Cities Soc.* **2019**, *44*, 120–129. [CrossRef]
5. Saffari, M.; Roe, C.; Finn, D.P. Improving the building energy flexibility using PCM-enhanced envelopes. *Appl. Therm. Eng.* **2022**, *217*, 119092. [CrossRef]
6. Alshuraiaan, B. Efficient Utilization of Pcm in Building Envelope in a Hot Environment Condition. *SSRN Electron. J.* **2022**, *16*, 100205. [CrossRef]

7. Arumugam, P.; Ramalingam, V.; Vellaichamy, P. Effective PCM, insulation, natural and/or night ventilation techniques to enhance the thermal performance of buildings located in various climates—A review. *Energy Build.* **2022**, *258*, 111840. [CrossRef]
8. Al-Saadi, S.N.; Zhai, Z. Modeling phase change materials embedded in building enclosure: A review. *Renew. Sustain. Energy Rev.* **2013**, *21*, 659–673. [CrossRef]
9. Ručevskis, S.; Akishin, P.; Korjakins, A. Performance Evaluation of an Active PCM Thermal Energy Storage System for Space Cooling in Residential Buildings. *Environ. Clim. Technol.* **2019**, *23*, 74–89. [CrossRef]
10. Yassi, M.E.; Abbassi, I.E.; Pierre, A.; Melinge, Y. Comparative Study of Two Materials Combining a Standard Building Material with a PCM. *Fluid Dyn. Mater. Process.* **2023**, *19*, 1283–1290. [CrossRef]
11. Rehman, A.U.; Sheikh, S.R.; Kausar, Z.; Mccormack, S.J. Numerical Simulation of a Novel Dual Layered Phase Change Material Brick Wall for Human Comfort in Hot and Cold Climatic Conditions. *Energies* **2021**, *14*, 4032. [CrossRef]
12. Rucevskis, S.; Akishin, P.; Korjakins, A. Parametric analysis and design optimisation of PCM thermal energy storage system for space cooling of buildings. *Energy Build.* **2020**, *224*, 110288. [CrossRef]
13. Selvaraju, A.P.; Ranganathan, A.; Vincent, A.A.R.; Arumugam, P.; Ramalingam, V. Thermal management analysis of PCM integration in building using a novel performance parameter PCM effectiveness Index. *Therm. Sci.* **2022**, *26*, 883–895. [CrossRef]
14. Teja, P.N.S.; Gugulothu, S.K.; Sastry, G.R.; Burra, B.; Bhurat, S.S. Numerical analysis of nanomaterial-based sustainable latent heat thermal energy storage system by improving thermal characteristics of phase change material. *Environ. Sci. Pollut. Res.* **2022**, *29*, 50937–50950. [CrossRef] [PubMed]
15. Liang, D.M.; Ibrahim, M.; Saeed, T.; El-Refaey, A.M.; Li, Z.X.; Fagiry, M.A. Simulation of a Trombe wall with a number of semicircular fins placed on the absorber plate for heating a room in the presence of nano-PCM. *J. Build. Eng.* **2022**, *50*, 104173. [CrossRef]
16. Su, W.G.; Darkwa, J.; Kokogiannakis, G. Numerical thermal evaluation of laminated binary microencapsulated phase change material drywall systems. *Build. Simul.* **2020**, *13*, 89–98. [CrossRef]
17. Al-Mudhafar, A.H.N.; Hamzah, M.T.; Tarish, A.L. Potential of integrating PCMs in residential building envelope to reduce cooling energy consumption. *Case Stud. Therm. Eng.* **2021**, *27*, 101360. [CrossRef]
18. Sarbu, I.; Sebarchievici, C. A comprehensive review of thermal energy storage. *Sustainability* **2018**, *10*, 191. [CrossRef]
19. Allison, T.; Smith, N.R.; Ma, Z. Chapter 1—Introduction to energy storage. In *Thermal, Mechanical, and Hybrid Chemical Energy Storage Systems*; Brun, K., Allison, T., Dennis, R.B.T., Eds.; Academic Press: Cambridge, MA, USA, 2021; pp. 1–25. ISBN 978-0-12-819892-6. Available online: https://www.sciencedirect.com/science/article/pii/B9780128198926000010 (accessed on 12 February 2023).
20. Ahmed, N.; Elfeky, K.E.; Lu, L.; Wang, Q.W. Thermal and economic evaluation of thermocline combined sensible-latent heat thermal energy storage system for medium temperature applications. *Energy Convers. Manag.* **2019**, *189*, 14–23. [CrossRef]
21. IRENA. *Innovation Outlook Thermal Energy Storage*; IRENA: Masdar City, United Arab Emirates, 2020.
22. Al-Yasiri, Q.; Szabó, M. Paraffin as a Phase Change Material to Improve Building Performance: An Overview of Applications and Thermal Conductivity Enhancement Techniques. *Renew. Energy Environ. Sustain.* **2021**, *6*, 38. [CrossRef]
23. Ansu, A.K.; Sharma, R.K.; Tyagi, V.V.; Sari, A.; Ganesan, P.; Tripathi, D. A cycling study for reliability, chemical stability and thermal durability of polyethylene glycols of molecular weight 2000 and 10,000 as organic latent heat thermal energy storage materials. *Int. J. Energy Res.* **2020**, *44*, 2183–2195. [CrossRef]
24. Duttaluru, G.; Singh, P.; Kumar, A. Methods to enhance the thermal properties of organic phase change materials: A review. *Mater. Today Proc.* **2022**, *63*, 685–691. [CrossRef]
25. Heier, J.; Bales, C.; Martin, V. Combining thermal energy storage with buildings—A review. *Renew. Sustain. Energy Rev.* **2015**, *42*, 1305–1325. [CrossRef]
26. Soibam, J. Numerical Investigation of a Heat Exchanger Using Phase Change Materials (PCMs). Master's Thesis, Mälardalen University, Västerås, Sweden, 2017.
27. Ben Romdhane, S.; Amamou, A.; Ben Khalifa, R.; Saïd, N.M.; Younsi, Z.; Jemni, A. A review on thermal energy storage using phase change materials in passive building applications. *J. Build. Eng.* **2020**, *32*, 101563. [CrossRef]
28. Lai, C.M.; Hokoi, S. Thermal performance of an aluminum honeycomb wallboard incorporating microencapsulated PCM. *Energy Build.* **2014**, *73*, 37–47. [CrossRef]
29. Silva, T.; Vicente, R.; Soares, N.; Ferreira, V. Experimental testing and numerical modelling of masonry wall solution with PCM incorporation: A passive construction solution. *Energy Build.* **2012**, *49*, 235–245. [CrossRef]
30. De Gracia, A.; Navarro, L.; Castell, A.; Ruiz-Pardo, Á.; Alvárez, S.; Cabeza, L.F. Experimental study of a ventilated facade with PCM during winter period. *Energy Build.* **2013**, *58*, 324–332. [CrossRef]
31. Rubitherm. PCM RT-LINE. Available online: https://www.rubitherm.eu/en/productcategory/organische-pcm-rt (accessed on 20 April 2023).
32. Norlén, U. Estimating thermal parameters of outdoor test cells. *Build. Environ.* **1990**, *25*, 17–24. [CrossRef]
33. Madsen, H.; Holst, J. Estimation of continuous-time models for the heat dynamics of a building. *Energy Build.* **1995**, *22*, 67–79. [CrossRef]
34. Wouters, P.; Vandaele, L.; Voit, P.; Fisch, N. The use of outdoor test cells for thermal and solar building research within the PASSYS project. *Build. Environ.* **1993**, *28*, 107–113. [CrossRef]

35. Guo, J.; Zhang, G. Investigating the performance of the PCM-integrated building envelope on a seasonal basis. *J. Taiwan Inst. Chem. Eng.* **2021**, *124*, 91–97. [CrossRef]
36. Wald, N.J.; Rodeck, C.; Hackshaw, A.K.; Walters, J.; Chitty, L.; Mackinson, A.M. Solar Energy Perspectives: Executive summary. *J. Med. Screen.* **2003**, *10*, 56–57. [CrossRef]
37. Cho, Y.; Kim, J.J. Lifetime decrease of halogen lamps for automotive by duty cycle stress. *IEEE Trans. Reliab.* **2011**, *60*, 550–556. [CrossRef]
38. OTT Hydromet GMBH. Pyranometer CMP3 | SMP3. Available online: https://www.otthydromet.com/en/p-kippzonen-smp3-pyranometer/0374900 (accessed on 12 February 2023).
39. Thermocouple. Type K Thermocouple. Available online: https://www.thermocoupleinfo.com/type-k-thermocouple.htm (accessed on 12 February 2023).
40. ANSYS. Knowledge Creation Diffusion Utilization. In *ANSYS Fluent User' s Guide*; Release 13.0.; ANSYS, Inc.: Canonsburg, PA, USA, 2013; Volume 15317, pp. 724–746.
41. Hassab, M.A.; Sorour, M.M.; Mansour, M.K.; Zaytoun, M.M. Effect of volume expansion on the melting process's thermal behavior. *Appl. Therm. Eng.* **2017**, *115*, 350–362. [CrossRef]
42. Vanaga, R.; Narbuts, J.; Freimanis, R.; Blumberga, A. Laboratory Testing of Different Melting Temperature Phase Change Materials Under Four Season Conditions for Thermal Energy Storage in Building Envelope. In Proceedings of the International Conference on Applied Energy, Virtual, 29 November–5 December 2021.

PAPER 6: REVOLUTIONIZING THE BUILDING ENVELOPE: A COMPREHENSIVE SCIENTIFIC REVIEW OF INNOVATIVE TECHNOLOGIES FOR REDUCED EMISSIONS

Environmental and Climate Technologies
2023, vol. 27, no. 1, pp. 724–737
https://doi.org/10.2478/rtuect-2023-0053
https://content.sciendo.com

Revolutionizing the Building Envelope: A Comprehensive Scientific Review of Innovative Technologies for Reduced Emissions

Jānis NARBUTS[1*], Ruta VANAGA[2]

[1,2]*Institute of Energy Systems and Environment, Riga Technical University, Āzenes street 12/1, Riga, LV-1048, Latvia*

Received 12.04.2023; accepted 11.10.2023

***Abstract* – This paper reviews innovative building envelope technologies that can improve total building energy efficiency and reduce greenhouse gas emissions. The building envelope has a significant impact on energy and thermal performance, making various technologies like phase change materials, aerogel, and active and adaptive systems essential for enhancing the building envelope's energy efficiency. Phase change materials reduce energy consumption by lowering peak heating and cooling loads, improving thermal comfort. Paraffin wax is considered the most dependable phase change material for building envelopes, as it can decrease energy consumption for heating and cooling. Study shows that active PCM thermal energy storage system can reduce room temperature by 6.8 °C in summer. Aerogel, in comparison, is recognized for its exceptional insulation capabilities and low density that minimize heat transfer and boost thermal insulation in buildings. Silica aerogel's outstanding feature is its capacity to offer thermal performance that surpasses traditional insulation materials by 2–4 times, thereby delivering substantial energy savings of up to 35 %. Active and adaptive systems, such as smart windows and kinetic facades, enable real-time control of building envelope performance, improving energy efficiency and indoor comfort. Smart windows can lead to annual energy savings up to 35.9 kWh/m^2 compared to traditional windows, and kinetic facades can reduce cooling loads for buildings up to 21 %. The review assesses various adaptive facade solutions for their suitability in diverse climate zones, versatility in application and energy efficiency. Despite the existence of some limitations and challenges, such as high costs and insufficient understanding of their long-term performance, the continuous development and deployment of these technologies can still yield a significant contribution to improving building energy efficiency and mitigating greenhouse gas emissions.**

***Keywords* – Aerogel; building envelopes; energy efficiency; phase-change materials.**

1. INTRODUCTION

The emissions of carbon dioxide (CO_2) and other greenhouse gases (GHG) by humans is the primary contributor to climate change, making it one of the most pressing challenges facing the world today [1]. The European Green Deal is a fresh growth strategy proposed by European Commission to combat the existential threat posed by climate change and environmental degradation. This strategy has been developed to transform the EU into a modern, competitive, and resource-efficient economy that ensures no net emissions of

* Corresponding author.
E-mail address: janis.narbuts_1@rtu.lv

greenhouse gases by 2050 [2]. The data analyses show that there is a strong relationship between CO_2 and other GHG emissions and GDP per capita [3]. However, there is an unequal contribution to the overall EU green policy among the member states.

The Buildings Global Status Report reveals that in 2021, the building industry contributed to 36 % of global final energy usage and 37 % of energy-related CO_2 emissions [4]. This marks the significant influence of building sector on climate change and contribution in CO_2 emissions, necessitating their reduction to achieve the objectives of the EU's Green Deal. Yet, according to the report by the Buildings Performance Institute Europe (BPIE) [5], experts in the field believe that the decarbonization of the EU's building stock is not progressing as rapidly as it should. The current rates of renovation are inadequate to achieve the necessary reduction in energy use. Currently, Eastern Europe is facing an inevitable issue where the quality of multifamily apartment buildings is declining, however, apartment owners lack adequate resources, such as organizational, financial, technical, or legal support [6]. Conventional building methods create obstacles for sustainable energy consumption. Converting these structures into Net Zero Energy Buildings (NZEB) presents an opportunity to manage energy loads, but the cost of this transformation is a crucial factor [7]. An important factor in creating energy-efficient and sustainable buildings is to accurately predict the building's performance under various weather conditions and to use proper insulation materials in building envelopes [8]. Many conventional materials are not efficient in serving a wide range of changing climate conditions, which can result in significant energy loss during peak load periods. This study will examine three main approaches to address these challenges: utilizing on-site renewable energy, implementing high-quality novel insulation materials, and applying innovative technological solutions in building envelopes.

There are two synergistic approaches to decrease the energy consumption of existing buildings: reducing the energy demand by implementing energy-efficient measures and using renewable energy systems to compensate for the remaining energy requirements [9]. Solar, wind and geothermal are examples of renewable energy resources that are frequently utilized in building applications. Solar power is a very convenient option for energy systems and building envelopes, compared to wind power, which requires significant upfront costs, and geothermal energy, which is heavily reliant on location [10]. Solar technologies offer versatility and can serve for both centralized and decentralized energy production purposes [11]. Studies show, that application of solar energy systems are highly efficient and can result in over 30 % energy savings and immediate coverage of 50 % of the building's energy load [12].

Despite the advantages, solar power is dependent on sunlight, which is not constant and can be affected by weather conditions. This points out the necessity of energy storage system for periods while sunlight is not present. While energy from Photovoltaic (PV) panels can be store in batteries, solar thermal energy needs a thermal storage system (TES). The utilization of phase change materials (PCM) in thermal energy storage systems is a crucial factor in facilitating the integration of renewable energies, allowing for increased self-consumption and system efficiency that ultimately results in lower energy consumption in buildings [13].

A well-designed building envelope plays a critical role in boosting the energy efficiency of buildings. It can reduce the demand for heating, ventilation, and air conditioning (HVAC) and lighting load, and the integration of insulation into the building envelope can further heighten energy efficiency [14]. Presently, there is an increasing fascination with highly insulating materials, including aerogels, which have emerged as a highly promising option for building insulation owing to their exceptional insulating properties [15]. While the cost of using aerogel-based materials remains high, particularly for cost-sensitive industries like the building sector, there are expected to be cost reductions in the coming years due to

advancements in aerogel production technology and larger scale material production that can lead to lower unit costs.

As the Green Deal policy highlights the pivotal role of research and innovation in driving environmental changes to combat climate change [16], novel technological solutions constitute a crucial element in achieving energy-efficient building envelopes. Achieving energy savings and minimizing environmental impact can be significantly facilitated by the building facade, which is a crucial element of construction [17]. With the curtain wall being the primary facade system over the last few decades, its performance is now considered outdated. It is evident that facilities and facade technologies must progress to comply with the energy conservation agenda, incorporating inventive energy technologies and low-carbon solutions [18].

2. METHODOLOGY

The methodology of this paper is based on a literature review, which was conducted to identify and assess innovative technologies for building envelopes that can improve total building energy efficiency. Based on study [19], the literature search was conducted by using 'Web of Science' (WOS) data base due to its advantages in citation analysis tools, making it the best choice to explore impact and influence of recent trends in building technological solutions. The filtering process of scientific papers consisted of publication period, which is year 2020 to 2023, as well as on keywords – 'phase change material', 'aerogel insulation', 'smart windows' and 'active/adaptive systems'. By using keywords in various forms and combinations (Table 1 in annex), 214 papers have been found in total from which 53 were open access articles. From the search results, 19 papers have been selected for scientific review based on their access, popularity, and relevance to the scope of this study (Table 2 in annex).

3. PHASE CHANGE MATERIALS

3.1. Characteristics of phase change materials

There are three methods for achieving thermal energy storage (TES): sensible energy storage, latent energy storage, and thermochemical energy. Of these, phase change materials (PCM) utilizing latent energy storage are the most effective energy systems due to their high storage density under isothermal conditions [39]. These substances possess the capacity to absorb substantial quantities of energy without experiencing any alteration in their own temperature. Instead, the state of matter of the PCM material present in the storage system changes while absorbing (melting) and/or releasing (solidifying) energy [40]. This occurrence facilitates the creation of an energy storage mechanism for buildings in a simple manner that aids in the stabilization of room temperature by storing any surplus energy.

PCMs can be categorized into three types based on their material nature: organic, inorganic, and eutectic PCMs. Inorganic PCMs have high thermal storage capacity and good thermal conductivity, but they can undergo phase segregation with repeated cycles, subcooling, and may corrode metallic containers. On the other hand, organic PCMs have relatively lower phase change enthalpy and thermal conductivity. However, they have the advantage of small to no subcooling issues, thermal stability, non-corrosive nature, and chemical stability. Inorganic PCMs mainly include hydrated salts, while organic PCMs include paraffins, fatty acids, polyhydric alcohols, and sugar alcohols. Eutectics, which are mixtures of two or more PCMs, can be of the inorganic or organic type. Although these eutectics are stable from phase

separation and offer good phase change enthalpy, extensive research is necessary to discover eutectics with phase stability and suitable transition temperatures [41]. Solid-liquid PCMs, such as paraffin waxes, are commonly used due to their unique characteristics such as minimal supercooling, lack of toxicity, non-corrosiveness, chemical stability, and high latent heat energy [42].

3.2. Phase change material applications in buildings

Many applications are currently being evaluated for phase change polymers, and several of them have already been introduced for commercial use as heating/cooling systems and solar energy storages. Several studies in recent years have been conducted to evaluate the performance of paraffin wax PCMs in solar facades meant for nearly zero energy buildings (NZEB). Extensive research has been carried out to assess the temperature performance of PCMs when applied to building envelopes in these papers [20]–[22]. Studies aimed to optimize the solar facade module by introducing a dynamic component and varying the composition of the module itself to ensure faster energy harvesting and minimize heat losses during the discharging phase. The laboratory tests showed that the introduction of dynamic component has a significant impact on the performance of the test module, with higher average temperatures in the phase change material in all setups with the dynamic component compared to identical setups without it. The developed facade module demonstrates a potential to become an on-site renewable energy storage medium that converts solar energy to thermal energy.

In another paper [23] the use of hempcrete, a binder-aggregate material that utilizes hemp shive as a filler, in combination with gypsum binder and PCM to create an advanced bio-composite material has been researched. The addition of PCM increases the thermal mass of the hempcrete, allowing for better thermal stability and comfort in buildings. The results of the study show that the addition of up to 20 wt.% of microencapsulated PCM to the hempcrete composition increases its heat capacity by 70.4 %, which correlates well with theoretical thermal mass calculation. The physical and mechanical properties of the bio-composite were also evaluated, with compressive strength ranging from 387–552 kPa and a density of 366–392 kg/m^3. The addition of PCM did not significantly affect the density or thermal conductivity of the bio-composite but did result in a 25–30 % reduction in compressive strength. The increased heat capacity of the bio-composite has promising implications for reducing energy consumption and improving thermal comfort in buildings.

Rucevskis, Akishin and Korjakins [24] in their research evaluates the potential of an active thermal energy storage system using phase change material for cooling residential buildings. Stand-alone PCM storage units are installed between the concrete ceiling slab and ceiling finishing layer and are actively controlled by night cooling of a phase change material. Results show that the active system reduces indoor air temperature by 6.8 °C, and the stand-alone units can be easily incorporated into building interiors. The study suggests that further optimization of system design is necessary to achieve maximum performance with minimal energy consumption and operational costs.

Wu and Rahim [25] have investigated a multilayer building envelope integrated with both PCM and bio-based hygroscopic material (hemp concrete) to utilize their advantages. Four envelope configurations were experimentally studied based on the presence and location of the PCM to evaluate their effect on the hygrothermal behaviour and energy performance of the envelope. The results showed that compared to the configuration without PCM, the temperature and relative humidity amplitude was reduced by 50 %/60 %, the peak temperature was delayed by 70.4 %, and the energy consumption was reduced by 15.3 %. The

PCM placed on the outdoor side had the highest energy participation (64.2 %/71.0 %) and storage/release efficiency (21.5 %/18.8 %) during the energy storage/release process.

Phase change composite (PCC) has been evaluated for application as building envelope in recent scientific study [26]. The PCC made from n-octadecane, and fumed silica demonstrated a high latent heat storage capacity of 155.8 J/g, which is superior to previously reported PCCs. The PCC also exhibited a high crystallization fraction of 96.5 % and a melting temperature of 26.76 °C, which is close to that of pure n-octadecane (28.21 °C). The thermal conductivity of the PCC was reduced by 34 % after impregnation in fumed silica, with a thermal conductivity of only 0.184 W/m·K. In a comparison test, the PCC panel was found to retard heat transfer and delay the increase in indoor temperature than a commercial polystyrene foam panel, resulting in indoor temperatures of 19.8 and 22.9 °C for the PCC panel and 29.9 °C and 31.9 °C for the polystyrene panel at 2200 and 9000 s after lamp illumination more efficiently. These results suggest that the n-octadecane/fumed silica PCC has potential applications as a building envelope for energy conservation.

Another recent study [27] has been conducted about the composite PCM (CPCM) for energy conservation in buildings. The main conclusion of the paper was that the proposed shape-stabilized composite PCM LA-SA/Al_2O_3/C has encouraging thermal performances and effective encapsulation, making it suitable for application in building envelopes. The optimal proportion for the new binary PCM (LA-SA/Al_2O_3/C) is 82 wt% LA + 18 wt% SA with 0.5 wt% Al_2O_3 nanoparticle, with a melting temperature of 21.3 °C, a large latent heat of 205.9 kJ/kg, and an acceptable thermal conductivity of 0.2843 W/(m^2K). The prepared LA-SA/Al_2O_3/C PCM effectively prevents PCM leakage, with a melting temperature of 22.5 °C and a latent heat of 133.4 kJ/kg. The maximum mass fraction of LA-SA/Al_2O_3/C is 15 % for satisfactory stress-bearing capacity in concrete-based CPCM. The concrete panel with LA-SA/Al_2O_3/C inserted has a good thermal storage performance, reducing temperature fluctuations and delaying heat transfer. The new shape stabilized CPCM is convenient, economical, and has great potential to regulate indoor temperature and decrease energy consumption of heating and cooling devices in buildings.

4. AEROGEL INSULATION

4.1. Characteristics of aerogels

Nanostructured solid materials composed of amorphous silicon dioxide (SiO_2) are known as Silica Aerogels. These materials consist of around 96 % air and 4 % open-pored solid particle-network structure of silica. They are obtained by drying a gel using one of several process options. Due to their low density (ranging from 80–200 kg/m^3) and nanoporous structure, they are classified as superinsulation materials with a thermal conductivity lower than 0.020 W/m·K [43].

A type of aerogel known as opaque aerogels or aerogel blankets is utilized to enhance the thermal efficiency of buildings by reducing heat transfer in their opaque envelopes. The thermal conductivity of these materials is 0.013 W/m·K. However, when compared to other materials with comparable thermal properties, the cost of opaque aerogels is over 10 times higher [44]. Yet, Lolli and Andresen in their research [45] demonstrated that aerogel glazing has a favourable impact on reducing greenhouse gas (GHG) emissions when considering a cradle-to-grave life cycle assessment (LCA) for energy retrofitting of an apartment building. Although the production of aerogel generates higher GHG emissions per kilogram compared to argon, the overall life cycle assessment indicates a potential GHG reduction of 5–9 %.

The integration of various aerogel technologies, such as the creation of a novel aerogel glass material that is lightweight and has better thermal insulation, the use of aerogel granules in translucent windows, glazing, and solar walls, along with other materials and technologies such as controllable and adaptive coatings like electrochromic, thermochromic, and photochromic coatings, as well as phase change materials, provides the possibility of incorporating these materials into advanced and multifunctional building envelopes [43].

4.2. Aerogel insulation application in buildings

Aerogels are currently considered to be among the most promising high-performance thermal insulation materials for building applications due to their superior thermal properties. Additionally, the potential for high transmittance in the solar spectrum is highly desirable in the construction sector [46]. There has been an increase in research papers in recent years focused on the use of aerogel in building envelopes.

Recent article discusses the development and testing of a novel aerogel-based insulating external render for building envelopes [28], which was subjected to a large-scale weathering test to assess its durability. Despite high water absorption during weathering, the low thermal conductivity of the aerogel-based system was not significantly altered, and the insulation product performance was not drastically compromised over its lifetime. The impact of a degradation in hygrothermal properties on monthly heating loads was found to be almost negligible, highlighting the effectiveness of aerogel-based insulating systems in reducing thermal losses and promoting building energy efficiency.

Knowledge gaps regarding the hygrothermal and long-term performance of aerogel-based coating mortars have been evaluated in study [29] by Naman, Pär and Angela. In summary, aerogel-based coating mortars are an emerging class of multifunctional wall finishes that provide thermal insulation comparable to conventional insulation materials. However, the knowledge about their hygrothermal and mechanical properties has not been fully explored, which is necessary to assess moisture risks and long-term durability in different applications. There is a need for more information on the hygrothermal and mechanical compatibility of aerogel-based coating mortars with other materials in multilayer wall systems. Future research should focus more on moisture risk assessments, especially in areas with humid climates and freeze-thawing. In addition, the compatibility of aerogel-based mortars with other new and existing materials in different multilayer wall systems and climatic conditions need to be further evaluated. The hygrothermal performance of aerogel-based coating mortars at early-stage of application and when exposed to severe conditions should also be considered in future works. Overall, aerogel-based coating mortars are promising materials to increase energy efficiency in buildings and potentially create slimmer building envelopes.

Paulos and Berardi [30] have investigated the thermal transmittance of 48 commercially available high-performance aluminium, fibreglass, polyvinylchloride (PVC), and wood-composite window frames. The research concluded that filling existing empty cavities of window frames with aerogel granules could reduce the frame thermal transmittance by 4–29 %, depending on the frame type. The complete filling of the cavities with aerogel can further reduce the thermal transmittance by 35 %. For each investigated material, window frames with a thermal transmittance as low as 0.5 $W/m^2 \cdot K$ are proposed. The study found that replacing the existing insulation with aerogel can reduce the Uf-value for aluminium, fibreglass, PVC, and wood-composite frames by a maximum of 22 %, 17 %, 12 %, and 29 %, respectively. On average, this represented an 8 % thermal transmittance improvement compared to traditional insulation materials such as rigid polyurethane foam. Additional iterations of aerogel were performed, involving completely filling each cavity and being inserted in small, irregular voids such as thermal breaks. This resulted in significant

enhancements of frames, which could further reduce the Uf-value by 13 %. Amongst all cases studied, aluminium frames resulted in the greatest improvement, with frames achieving Uf-values as low as 0.46 W/m^{2}K. Such measures are typically difficult to achieve without increasing the frame width and heights, adding more cavity divisions, or changing the frame emissivity. The study suggests that using aerogel as an insulation material in window frames is a promising approach to enhance the energy efficiency of buildings, especially in those with high window-to-wall ratios.

Superhydrophobic wastepaper-based aerogel has been developed and evaluated as a thermal insulating cooler for buildings in China [31]. Researchers concluded that the superhydrophobic cellulose aerogel cooler (SHB-CAC) has high solar reflectance and long-wave infrared emittance and can achieve a temperature drop of 8.5 °C lower than ambient temperature under sunlight of 800 W/m^2. The SHB-CAC also possesses low thermal conductivity, which reduces parasitic heat gain and energy consumption. The self-cleaning property resulting from superhydrophobicity protects the SHB-CAC from water wetting and dust contamination, while maintaining its good surface radiation capacities under different humidity environments. The study recommends further exploration into the construction of cooling systems based on SHB-CAC, theoretical models to optimize radiant cooling performance, exploration of alternative IR-transparent materials, and implementation of modular SHB-CAC into existing cooling systems.

5. Active And Adaptive Systems

A building envelope that incorporates active components, such as mechanical systems, to regulate various parameters in the indoor environment, such as temperature, humidity, and ventilation is known as an active building envelope [47]. Adaptive building envelopes refer to building skins that have the ability to modify their properties and control various parameters in response to changes in climatic loads or indoor environment [48]. Active and adaptive systems used in building envelopes can include various types of systems such as mechanical shading, automated ventilation, smart glass, dynamic insulation, and others. The primary objective of these systems is to create a comfortable indoor environment for occupants while also ensuring energy efficiency of the building, thereby reducing the building's CO_2 and other GHG emissions footprint.

5.1. Smart windows

Windows are the least energy-efficient part of a building envelope. To address this issue, smart windows have been developed. However, traditional smart windows cannot adjust their transparency intelligently according to the complex outdoor climate, leading to an increase in indoor temperature caused by heat entering the room through convection.

The study [32] proposes embedding poly (N-isopropylacrylamide) hydrogel, which exhibits an ultrahigh luminous transmittance and solar modulation, into the double glass before the polyacrylamide matrix formation to develop an active and passive dual-control (APDC) smart window. The window is able to reduce indoor air temperatures by up to 16 °C compared to normal glass. By combining it with fluid glass, the APDC smart window achieves optimal energy-saving performance and has high potential to reduce carbon emissions. However, the possible problem of water evaporation from the hydrogel needs to be addressed. Overall, the study suggests that the APDC smart window has the potential to be a part of a new generation of energy-efficient buildings and greenhouses.

A novel sun-powered smart window blind (SPSWB) system has been designed [33], that uses self-powered sensing, controlling, and actuation to achieve optimal internal comfort with minimum energy expenditure. The energy is harvested by thin-film photovoltaic cells, voltage-regulated, and stored in a rechargeable battery with 55 % energy efficiency. The excessive heat absorbed by the solar cells is dissipated by a PVdF-HFP porous coating with more than 9 % temperature reduction. The smart control of the energy harvesting, and cooling is achieved based on the blinds' surface temperature by an Arduino-based sensing, controlling, and actuating system, whose energy consumption is closely monitored. Comprehensive tests have been conducted to quantify the system's performance, including the flexible PV cell's efficiency, the cooling performance of the PVdF-HFP passive cooling coating, and the energy delivery process. The energy equilibrium analysis is proposed for the self-powered design in any locations, and the optimal solar energy harvesting can be achieved by adjusting the window blinds angle. The energy harvesting capability of the smart window blinds far outweighs the power needed for the controller and motor, making it a feasible and robust system for an extensive range of sensors and applications. Further improvements could be achieved in energy conversion efficiency, optimal temperature thresholds, and reduction factors of non-south facing conditions. The SPSWB system's outlook may face potential resistance from building architects and owners due to the PV-integration, but the study suggests that it is a viable and effective solution for smart building envelope systems.

An innovative approach to developing adaptive solar modulation windows that meet both energy-saving and aesthetic demands has been developed [34]. This approach suggests that the windows are based on PCM and coated with photonic co-doped vanadium dioxides that exhibit angle-dependent vivid colours similar to the skin of tetra fishes. The glasses have high transmittance, a practical transition temperature, and an acceptable solar modulation property, surpassing the best-reported VO_2-windows in several aspects. The energy-saving performance of the windows is investigated, and it is demonstrated that they can result in annual energy savings of up to around 35.9 kWh/m^2 for a typical office building in representative cities in the Asia Pacific region. This significant reduction in energy consumption can help in the development of net-zero energy buildings. The study highlights the potential for the future development of novel materials in building envelopes that can meet both energy-saving and aesthetic demands. Overall, the development of the novel aesthetic thermochromic window represents a promising step towards the development of sustainable buildings that meet the energy demands of the present while minimizing the impact on the environment.

5.2. Adaptive facade solutions

Incorporating advanced technological systems that do not rely on complex electronics, adaptive facades can automatically adjust to internal and external conditions, resulting in improved energy efficiency without the need for user intervention [49]. By reducing energy consumption (and the emissions associated with it), adaptive facades help to advance the objectives of decarbonization of building stock and achieving climate neutrality [50]. There are three main design scenarios for non-conventional adaptive facades: using basic movements to create three-dimensional motion, taking advantage of foldable structures, and mimicking biological behaviour in technological practices [49]. Modelling tools also play an important role in the design phase of the building facade to assess the energy balance and cost of energy for different potential scenarios [51].

The study of annual performance assessment discusses the use of Adaptive Dynamic Building Envelopes (ADBEs) for building retrofitting to reduce energy consumption and improve thermal quality [35]. The research assessed the performance of two pilot sites in

Cardiff, Wales, and Grevena, Greece, with the installation of ADBEs consisting of Building Integrated Photovoltaics (BIPVs), additional thermal insulation, mechanical ventilation system with heat recovery, and solar air heaters (SAHs). The results showed that the ADBE system implemented in the Cardiff pilot site could potentially contribute up to 60 % and 21.8 % to the annual electricity and heating load of the space, respectively. The SAH unit was estimated to contribute to the annual space heating load by 22 %, leading to a 12 % decrease in fuel consumption. In the Grevena pilot site, the BIPV panels were able to provide an almost 43 % share of the annual electrical load.

In another recent study [36] climate response of a BiPV facade system was researched. The paper evaluates the use of PCM applied to the rear side of photovoltaic (PV) modules to increase energy production and decrease the operating temperature of the PV panels. The study investigates the integration of a latent thermal energy storage system using PCM in a ventilated BiPV facade system, and its influence on a building's thermal and energy performance. The experimental results indicate that the use of PCM on the rear side of PV panels significantly decreases their operating temperature, particularly during midday when high solar radiation is present. It is suggested that the optimal climate response of the facade system occurs under outside boundary conditions with a maximum global solar radiation of 600 W/m^2 and an outside air temperature of up to 26 °C. Above these limits, the overall latent heat capacity of the PCM starts to be overused, and the freezing process cannot be completed before the next diurnal cycle begins.

Authors conclude that the direct control of the velocity and direction of air flow from the facade cavity according to the building's interior requirements could reveal that the BiPV/PCM system has greater potential as an auxiliary source for HVAC systems. The economic feasibility of BiPV/PCM systems is still questionable due to investment costs, though their combination with HVAC systems could enhance their potential in overall thermal and energy management.

Kinetic solar envelope has been researched by Koukelli, Prieto and Asut [37] in Athens, Greece. The research presents the potential of shape memory alloys (SMAs) in autoreactive facade systems without using external energy. The study aims to optimize the geometry and movement of the shading component to improve both the indoor and outdoor environment, particularly in reducing the building's direct and indirect impact on the urban heat island (UHI) effect. The results showed that the proposed facade design with optimized geometry and movement could potentially reduce the building's direct UHI impact by 40 % of the reflected portion of total solar radiation, while reducing cooling loads by 21 % and having a negligible effect on overall UHI reduction. The study concludes that there is potential to enhance the use of SMAs in facade applications to increase building performance, but challenges lie in feasibility, user control, and operation cycles. The integrated systematic design approach through a computational workflow is an important contribution to the field and can be further explored for possible applications.

Multi-functional kinetic facades have great potential to improve building energy consumption, regulate shading and natural ventilation, and enhance human thermal and visual comfort. However, the complexity of kinetic facades makes their design and fabrication time-consuming, limiting their market uptake. In the case study [38] performance evolution framework for kinetic facades has been proposed that uses Multi-objective Evolutionary Algorithms (MOEA) to support decision making in performance evaluation and design optimization. The framework's structure allows designers to define the design goals based on parametric and simulation models. The framework's novelty lies in combining the Ranking method and the Pareto front for the selection of optimal solutions. The case study demonstrated the framework's applicability in optimizing the daylighting performance of a

kinetic facade. Future research can focus on improving the framework's applicability to other design problems, such as cost evaluation, form-finding, energy consumption, daylighting, or acoustics. One of the limitations in designing kinetic facades is understanding how to convert occupant feelings to adaptable design parameters. Soft computing methods, such as Fuzzy Logic, could be integrated to create a smart and intelligent performance evaluation framework.

6. Discussion And Conclusions

The study explores recent technological advancements in the building envelope industry, assessing greenhouse gas reduction potential through energy efficiency while identifying constraints and knowledge gaps.

Research on hempcrete combined with PCM shows that adding up to 20 wt.% microencapsulated PCM increases heat capacity by 70.4 %. PCM systems can reduce indoor air temperature by up to 6.8 °C. A phase change composite with n-octadecane and fumed silica has a high latent heat storage of 155.8 J/g.

Aerogels offer high-performance thermal insulation, reducing thermal losses and improving energy efficiency. Filling window frame cavities with aerogel granules reduces transmittance by 4–29 %, while complete filling can further reduce it by 35 %. Superhydrophobic wastepaper-based aerogel offers low thermal conductivity and self-cleaning properties. Research is needed to explore hygrothermal and long-term performance.

Smart windows with hydrogel tech reduce indoor temperatures by 16 °C. Sun-powered smart window blinds achieve optimal comfort with minimal energy use. Phase change materials and photonic co-doped vanadium dioxides can save 35.9 kWh/m^2 annually. Challenges include water evaporation, energy efficiency, and industry adoption.

Adaptive facades enhance energy efficiency without user intervention, contributing to decarbonization goals. Non-conventional designs, BiPV, and PCM systems improve energy management. Kinetic solar envelopes reduce urban heat island effects. Multi-functional kinetic facades have potential but face market limitations. A performance evolution framework using Multi-objective Evolutionary Algorithms supports decision-making. Future research areas include economic feasibility, BiPV/PCM systems, and occupant feedback for kinetic facades.

Acknowledgement

This work has been supported by the European Social Fund within the Project No 8.2.2.0/20/I/008 “Strengthening of PhD students and academic personnel of Riga Technical University and BA School of Business and Finance in the strategic fields of specialization” of the Specific Objective 8.2.2 “To Strengthen Academic Staff of Higher Education Institutions in Strategic Specialization Areas” of the Operational Programme “Growth and Employment”.

References

[1] IPCC. Climate Change 2021: The Physical Science Basis. 2021. [Online]. [Accessed: 10.03.2023]. Available: https://www.ipcc.ch/report/ar6/wg1/

[2] European commission. The European Green Deal. 2019. [Online]. [Accessed: 15.03.2023]. Available: https://eur-lex.europa.eu/legal-content/EN/TXT/PDF/?uri=CELEX:52019DC0640&from=EN

[3] Pakere I., Prodanuks T., Kamenders A., Veidenbergs I., Holler S., Villere A., Blumberga D. Ranking EU climate and energy policies. *Env. Climate Technologies* 2021:25(1):367–381. https://doi.org/10.2478/rtuect-2021-0027

[4] United nations. Global Status report for Buildings and Construction 2021. UN [Online]. [Accessed: 15.02.2023]. Available: https://globalabc.org/resources/publications/2021-global-status-report-buildings-and-construction

[5] BPIE. Towards a decarbonised eu building stock: expert views on the issues and challenges facing the transition Factsheet. 2018. [Online]. [Accessed: 15.03.2023]. Available: https://bpie.eu/wp-content/uploads/2018/10/NZE2050-factsheet_03.pdf
[6] Miezis M., Zvaigznitis K., Stancioff N., Soeftestad L. Climate change and buildings energy efficiency – the key role of residents. *Environmental and Climate Technologies* 2016:17(1):30–43. https://doi.org/10.1515/rtuect-2016-0004
[7] Shuja D., Gardezi S. S. S., Idrees M. R. Prospects of Transforming Conventional Commercial Buildings to Net Zero Energy Building-Balancing the Economic Aspects with Energy Patterns. *Environmental and Climate Technologies* 2021:25(1):990–1002. https://doi.org/10.2478/rtuect-2021-0075.
[8] Albatayneh A., Alterman D., Page A., Moghtaderi B. The Significance of Building Design for the Climate. *Environmental and Climate Technologies* 2018:22(1):165–178. https://doi.org/10.2478/rtuect-2018-0011
[9] Hayter S. J., Kandt A. Renewable Energy Applications for Existing Buildings Preprint Renewable Energy Applications for Existing Buildings. 2011. [Online]. Accessed: 15.03.2023]. Available: https://www.nrel.gov/docs/fy11osti/52172.pdf
[10] Hestnes A. G. Building Integration Of Solar Energy Systems. *Solar Energy* 1999:67(4–6):181–187. https://doi.org/10.1016/S0038-092X(00)00065-7
[11] Pakere I., Blumberga D. Solar Energy in Low Temperature District Heating. *Environmental and Climate Technologies* 2019:23(3):147–158. https://doi.org/10.2478/rtuect-2019-0085
[12] Abdou N., Mghouchi Y. El., Hamdaoui S., Mhamed M. Optimal Building Envelope Design and Renewable Energy Systems Size for Net-zero Energy Building in Tetouan (Morocco). Presented at 9th International Renewable and Sustainable Energy Conference (IRSEC). 2021. https://doi.org/10.1109/IRSEC53969.2021.9741188
[13] Zsembinszki G., Fernandez A. g., Cabeza L. E. Selection of the appropriate phase change material for two innovative compact energy storage systems in residential buildings. *Applied Sciences* 2020:10(6):2116. https://doi.org/10.3390/app10062116
[14] Batra U., Singhal S. Optimum level of insulation for energy efficient envelope of office buildings. *International Journal of Env. Science and Technology* 2017:14(11):2389–2398. https://doi.org/10.1007/s13762-017-1322-2
[15] Ibrahim M., Biwole P. H., Achard P., Wurtz E. Aerogel-Based Materials for Improving the Building Envelope's Thermal Behavior: A Brief Review with a Focus on a New Aerogel-Based Rendering. In Sharma A., Kar S. K. (eds.), *Energy Sustainability Through Green Energy* 2015:163–188. https://doi.org/10.1007/978-81-322-2337-5_7
[16] Ruse A., Pubule J. The Boundaries of Scientific Innovation in the EU Green Deal Context. *Environmental and Climate Technologies* 2022:26(1):115–128. https://doi.org/10.2478/rtuect-2022-0010
[17] Attia S., Bilir S., Safy T., Struck C., Loonen R., Goia F. Current trends and future challenges in the performance assessment of adaptive façade systems. *Energy and Buildings* 2018:179:165–182. https://doi.org/10.1016/j.enbuild.2018.09.017
[18] Juaristi M., Gómez-Acebo T., Monge-Barrio A. Qualitative analysis of promising materials and technologies for the design and evaluation of Climate Adaptive Opaque Façades. *Building and Environment* 2018:144:482–501. https://doi.org/10.1016/j.buildenv.2018.08.028
[19] Pranckutė R. Web of Science (WoS) and Scopus: the titans of bibliographic information in today's academic world. *Publications* 2021:9(1):12. https://doi.org/10.3390/publications9010012
[20] Vanaga R., Narbuts J., Freimanis R., Blumberga A. Laboratory Testing of Small Scale Solar Facade Module with Phase Change Material and Adjustable Insulation Layer. *Energies* 2022:15(3):1158. https://doi.org/10.3390/en15031158
[21] Narbuts J., Vanaga R., Freimanis R., Blumberga A. Laboratory Testing of Small-Scale Active Solar Façade Module. *Environmental and Climate Technologies* 2021:25(1):455–466. https://doi.org/10.2478/rtuect-2021-0033
[22] Vanaga R., Narbuts J., Freimanis R., Blumberga A. Laboratory Testing of Different Melting Temperature Phase Change Materials Under Four Season Conditions for Thermal Energy Storage in Building Envelope. *Energy Proceedings* 2021:22. https://doi.org/10.46855/energy-proceedings-9391
[23] Bumanis G., Bajare D. PCM Modified Gypsum Hempcrete with Increased Heat Capacity for Nearly Zero Energy Buildings. *Environmental and Climate Technologies* 2022:26(1):524–534. https://doi.org/10.2478/rtuect-2022-0040
[24] Rucevskis S., Akishin P., Korjakins A. Performance Evaluation of an Active PCM Thermal Energy Storage System for Space Cooling in Residential Buildings. *Environmental and Climate Technologies* 2019:23(2):74–89. https://doi.org/10.2478/rtuect-2019-0056
[25] Wu D., Rahim M., El Ganaoui M., Bennacer R., Djedjig R., Liu B. Dynamic hygrothermal behavior and energy performance analysis of a novel multilayer building envelope based on PCM and hemp concrete. *Construction and Building Materials* 2022:341:127739. https://doi.org/10.1016/j.conbuildmat.2022.127739
[26] Nguyen G. T., Hwang H. S., Lee J., Cha D. A., Park I. N-octadecane/fumed silica phase change composite as building envelope for high energy efficiency. *Nanomaterials* 2021:11(3):1–15. https://doi.org/10.3390/nano11030566
[27] Yang Y., Wu W., Fu S., Zhang H. Study of a novel ceramsite-based shape-stabilized composite phase change material (PCM) for energy conservation in buildings. *Construction and Building Materials* 2020:246:118479. https://doi.org/10.1016/j.conbuildmat.2020.118479

[28] Sakiyama N. R. M., Frick J., Stipetic M., Oertel T., Garrecht H. Hygrothermal performance of a new aerogel-based insulating render through weathering: Impact on building energy efficiency. *Building and Environment* 2021:202:108004. https://doi.org/10.1016/j.buildenv.2021.108004
[29] Karim A. N., Johansson P., Kalagasidis A. S. Knowledge gaps regarding the hygrothermal and long-term performance of aerogel-based coating mortars. *Construction and Building Materials* 2022:314:125602. https://doi.org/10.1016/j.conbuildmat.2021.125602
[30] Paulos J., Berardi U. Optimizing the thermal performance of window frames through aerogel-enhancements. *Applied Energy* 2020:266:114776. https://doi.org/10.1016/j.apenergy.2020.114776
[31] Yue X., Wu H., Zhang T., Yang D., Qiu F. Superhydrophobic waste paper-based aerogel as a thermal insulating cooler for building. *Energy* 2022:245:123287. https://doi.org/10.1016/j.energy.2022.123287
[32] Lei Q., Wang L., Xie H., Yu W. Active-passive dual-control smart window with thermochromic synergistic fluidic glass for building energy efficiency. *Building and Environment* 2022:222:109407. https://doi.org/10.1016/j.buildenv.2022.109407
[33] Lin Q., Zhang Y., Van Mieghem A., Chen Y. C., Yu N., Yang Y., Yin H. Design and experiment of a sun-powered smart building envelope with automatic control. *Energy and Buildings* 2020:223:110173. https://doi.org/10.1016/j.enbuild.2020.110173
[34] Ke Y., Tan Y., Feng C., Chen C., Lu Q., Xu Q., Wang T., Liu H., Liu X., Peng J., Long Y. Tetra-Fish-Inspired aesthetic thermochromic windows toward Energy-Saving buildings. *Applied Energy* 2022:315:119053. https://doi.org/10.1016/j.apenergy.2022.119053
[35] Rotas R., Fotopoulou M., Drosatos P., Rakopoulos D., Nikolopoulos N. Adaptive Dynamic Building Envelopes with Solar Power Components: Annual Performance Assessment for Two Pilot Sites. *Energies* 2023:16(5):2148. https://doi.org/10.3390/en16052148
[36] Čurpek J., Čekon M. Climate response of a BiPV façade system enhanced with latent PCM-based thermal energy storage. *Renewable Energy* 2020:152:368–384. https://doi.org/10.1016/j.renene.2020.01.070
[37] Koukelli C., Prieto A., Asut S. Kinetic solar envelope: Performance assessment of a shape memory alloy-based autoreactive façade system for urban heat island mitigation in Athens, Greece. *Applied Sciences (Switzerland)* 2022:12(1):82. https://doi.org/10.3390/app12010082
[38] Sadegh S. O., Gasparri E., Brambilla A., Globa A. Kinetic facades: An evolutionary-based performance evaluation framework. *Journal of Building Engineering* 2022:53:104408. https://doi.org/10.1016/j.jobe.2022.104408
[39] Pielichowska K., Pielichowski K. Phase change materials for thermal energy storage. *Progress in Materials Science* 2014:65:67–123. https://doi.org/10.1016/j.pmatsci.2014.03.005
[40] Lawag R. A., Ali H. M. Phase change materials for thermal management and energy storage: A review. *Journal of Energy Storage* 2022:55:105602. https://doi.org/10.1016/j.est.2022.105602
[41] van der Winden I. Phase Change Materials: Technology and Applications. New York: Nova, 2020.
[42] Hussein H., Abed A. H., Abdulmunem R. An experimental investigation of using aluminum foam matrix integrated with paraffin wax as a thermal storage material in a solar heater. Presented at the 2nd Sustainable & Renewable Energy Conference, Baghdad, Iraq. 2018.
[43] Buratti C. Translucent Silica Aerogel: Properties, Preparation and Applications. New York: Nova, 2019.
[44] Buratti C., Moretti E., Belloni E. Nanogel Windows for Energy Building Efficiency BT – Nano and Biotech Based Materials for Energy Building Efficiency. In: Pacheco Torgal F., Buratti C., Kalaiselvam S., Granqvist C. G., Ivanov V. (eds). Nano and Biotech Based Materials for Energy Building Efficiency. Springer, Cham. https://doi.org/10.1007/978-3-319-27505-5_3
[45] Lolli N., Andresen I. Aerogel vs. argon insulation in windows: A greenhouse gas emissions analysis. *Building and Environment* 2016:101:64–76. https://doi.org/10.1016/j.buildenv.2016.03.001
[46] Jelle B. P., Baetens R., Gustavsen A. Chapter 45 - Aerogel Insulation for Building Applications. In: Levy D., Zayat M. The Sol-Gel Handbook. Wiley-VCH Verlag GmbH & Co. KGaA, 2015. https://doi.org/10.1002/9783527670819.ch45
[47] Luo Y., Zhang L., Bozlar M., Liu Z., Guo H., Meggers F. Active building envelope systems toward renewable and sustainable energy. *Renewable and Sustainable Energy Reviews* 2019:104:470–491. https://doi.org/10.1016/j.rser.2019.01.005
[48] Shahin H. S. M. Adaptive building envelopes of multistory buildings as an example of high performance building skins. *Alexandria Engineering Journal* 2019:58(1):345–352. https://doi.org/10.1016/j.aej.2018.11.013
[49] Tabadkani A., Roetzel A., Li H. X., Tsangrassoulis A. Design approaches and typologies of adaptive facades: A review. *Automation in Construction* 2021:121:103450. https://doi.org/10.1016/j.autcon.2020.103450
[50] Voigt M. P., Chwalek K., Roth D., Kreimeyer M., Blandini L. The integrated design process of adaptive façades – A comprehensive perspective. *Journal of Building Engineering* 2023:67:106043. https://doi.org/10.1016/j.jobe.2023.106043
[51] Mols T., Blumberga A. Inverse modelling of climate adaptive building shells. System dynamics approach. *Environmental and Climate Technologies* 2020:24(2):170–177. https://doi.org/10.2478/rtuect-2020-0064

ANNEX

TABLE 1. LIST OF SEARCHED KEYWORDS AND CATEGORIES IN WOS

Category	Field	Keywords	Number of results
Phase change materials	Title	phase change material* OR phase-change material*	
	All	AND building envelope* OR wall* OR roof* OR floor* OR window*	100 articles 25 open access articles
		AND novel OR innovative OR state-of-art OR advanced	
		AND energy efficiency OR emission*	
	Topic	NOT review OR numerical OR simulation	
	Year published	AND 2020-2023	
Aerogel insulation	Title	aerogel* OR aerogel-based	
	All	AND building envelope* OR wall* OR roof* OR floor* OR window*	34 articles 12 open access articles
		AND novel OR innovative OR state-of-art OR advanced	
		AND energy efficiency OR emission*	
	Topic	NOT review OR numerical OR simulation	
	Year published	AND 2020-2023	
Smart windows	Title	Smart window*	
	All	AND novel OR innovative OR state-of-art OR advanced	54 articles 7 open access articles
		AND energy efficiency OR emission*	
	Topic	NOT review OR numerical OR simulation	
	Year published	AND 2020-2023	
Active and adaptive systems	Title	(active OR adaptive OR responsive OR kinetic OR movable) AND (facade* OR façade* OR system* OR building envelope*) AND building*	
	All	AND novel OR innovative OR state-of-art OR advanced	29 articles 9 open access articles
	Topic	NOT review	
	Year published	AND 2020-2023	

TABLE 2. LIST OF SELECTED PAPERS AND THEIR FIELDS

Category	Paper	Object of research	Field of research
Phase change materials	[20]–[22]	Small-scale facade module	Temperature characteristics
	[23]	Hempcrete	Energy consumption
	[24]	Energy storage system	Temperature characteristics
	[25]	Multilayer building envelope	Energy consumption
	[26]	Composite phase change material	Temperature characteristics
	[27]	Composite phase change material	Energy consumption
Aerogel insulation	[28]	External render for building envelopes	Energy efficiency
	[29]	Aerogel-based coating mortars	Knowledge gaps
	[30]	Aerogel granules filled window frames	Energy efficiency
	[31]	Wastepaper-based aerogel insulation	Temperature characteristics
Smart windows	[32]	Poly (N-isopropylacrylamide) hydrogel	Energy efficiency
	[33]	Sun-powered smart window blind	Energy storage
	[34]	Adaptive solar modulation windows	Energy efficiency
Active and adaptive systems	[35]	Adaptive Dynamic Building Envelopes	Energy efficiency
	[36]	PCM cooling BiPV facade system	Energy saving
	[37]	Shape-memory alley kinetic solar envelope	Energy saving
	[38]	Multi-functional kinetic facades	Energy efficiency

PAPER 7: SYSTEMATIC LITERATURE REVIEW OF SOFTWARE TOOLS FOR MODELING HEAT TRANSFER IN PHASE CHANGE MATERIALS FOR BUILDING APPLICATIONS

IOP Conference Series:
Earth and
Environmental Science

PAPER • **OPEN ACCESS**

Systematic literature review of software tools for modeling heat transfer in phase change materials for building applications

To cite this article: R Vanaga *et al* 2024 *IOP Conf. Ser.: Earth Environ. Sci.* **1372** 012017

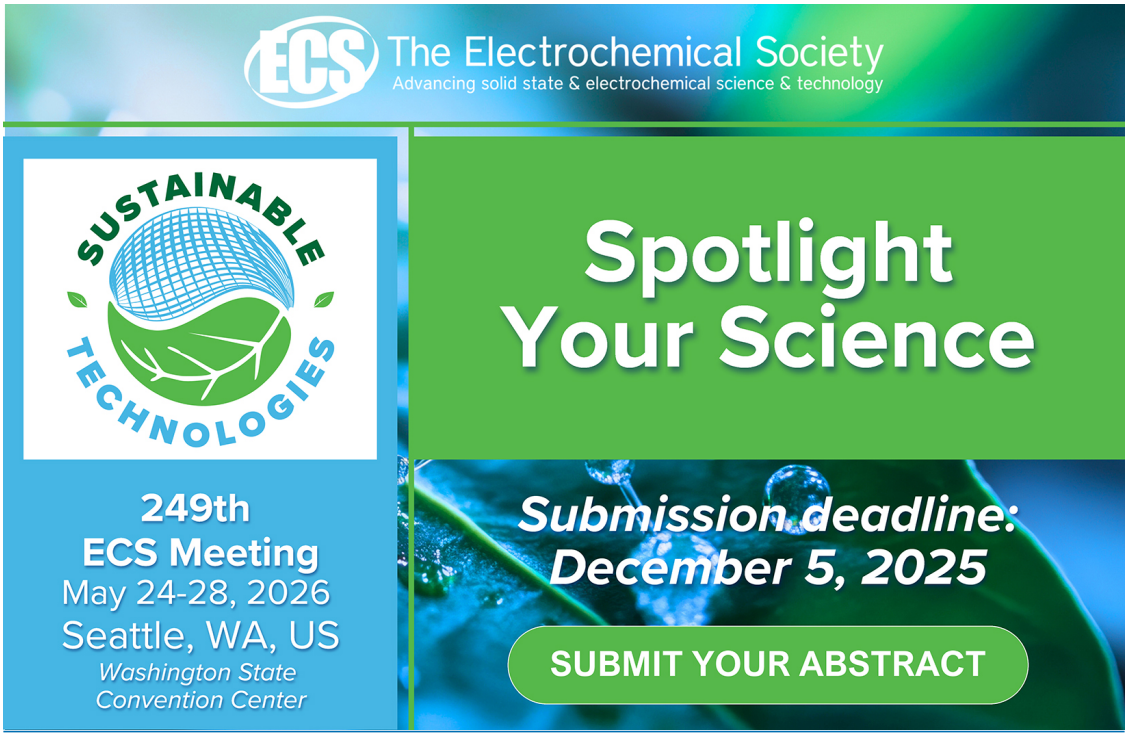

Systematic literature review of software tools for modeling heat transfer in phase change materials for building applications

R Vanaga[1]*, J Narbuts[1], Z Zundāns[1] and J Gušča[1]

[1] Riga Technical University, Institute of Energy Systems and Environment, 12 – K1 Āzene Street, Riga, Latvia, LV-1048

*E-mail: ruta.vanaga@rtu.lv

Abstract. New buildings in the European Union must attain nearly zero-energy status, emphasizing minimal energy consumption, partly met by on-site or nearby renewable sources. However, the fluctuating nature of on-site renewables poses a challenge, necessitating effective energy storage solutions. Addressing this, the use of phase change materials (PCMs) in building envelopes emerges as a promising trend. PCMs efficiently store excess thermal energy during abundance and release it when renewable generation falls short, ensuring a consistent energy supply. Introducing novel building components is time-intensive, with on-site testing demanding substantial resources. Numerical studies offer an efficient alternative, making modeling tools crucial. These tools facilitate exploration of design concepts under diverse conditions, allowing iterative refinement and optimization. This paper conducts a systematic literature review evaluating five prominent software programs—COMSOL, ANSYS, MATLAB, EnergyPlus, and TRNSYS—designed for modeling heat transfer within PCMs for building applications. In closer detail paper explores the use of ANSYS for heat transfer analysis for phase change materials.

Keywords: Phase change materials, numerical modeling, ANSYS, TRNSYS, COMSOL, MATLAB, ENERGYPLUS, VosViewer

1. Introduction

All new buildings in the European Union are mandated to achieve nearly zero-energy status - exceptionally low energy consumption, partially met through renewable sources on-site or in close proximity [1] . However, reliance on on-site renewables introduces a challenge— the fluctuations in energy availability. Thus, the effective utilization of energy storage becomes increasingly significant. One promising trend addressing energy storage challenge is the use of phase change materials (PCMs) PCMs play a pivotal role in capturing and storing excess thermal energy during periods of abundance and subsequently releasing it when renewable energy generation falls short, strengthening the consistency in energy supply. Energy storage and usage of PCMs in energy storage systems vary in scale it can be used in grid level system [2], [3], building heating and domestic hot water systems [4], and in building thermal envelope, serving as efficient energy storage buffers [5]. Storing energy in building thermal envelope aligns with the innovative concept of active building envelopes, that serves

as an energy convertor – energy that is available outside of the building, through the building envelope is converted to be used to cover building needs [6]. Building integrated photovoltaic systems, active shading systems are one such type of building envelope systems that can be assumed at a mass production level. However other types of active building envelopes still are at the early innovation phases.

The introduction of novel building components into the market is a time-intensive process, with on-site testing requiring considerable resources and time investments. In contrast, numerical studies offer a more efficient and expedited approach, making modeling tools an indispensable asset in the innovation process. A reliable modeling tool not only permits exploration of design concepts under diverse conditions but also enables iterative refinement and optimization of developed solutions.

Computer simulation allows to model various systems by determining their behaviour over time, which in turn provides insight into the creation of a real system that accurately performs its intended functions. In order to accurately model the system, the computer simulation must include several stages:

1) Problem identification;
2) Modelling process planning, goal setting and elaborating the model concept;
3) Data collection methods and modelling approaches;
4) Model validation;
5) Experiment planning and analysis;
6) Interpretation and analysis of results.

Creating a simulation model requires a detailed study, documentation and description of the thermodynamic processes in the system under study. Complex thermodynamic calculations are used in the simulation process, which take into account constant changes in weather and internal conditions of the building, as well as the dynamic response of the system. The reliability of simulation results mainly depends on the availability of input data, while the output data are used to calibrate the computer model.

Among the most popular software used to model thermodynamic processes in building thermal envelope are – ANSYS, TRNSYS, COMSOL Multiphysics, MATLAB, EnergyPlus. These programms, as described in a review [7] are used to model phase change materials enhanced building envelopes. In a review are number of programs are overviewed and divided in: simplified, intermediate and sophisticated simulation tools. ANSYS and COMSOL are categorised in sophisticated models the allow to model complex structures and provide more accurate result. All mentioned programs and others are reported to be used to analyse the impact of phase change materials in thermal envelope [8].

This paper offers a systematic literature review that analyses the bibliometric data using VOSviewer (COMSOL, ANSYS, TRNSYS, MATLAB and EnergyPlus) and conducts an in-depths analysis of ANSYS usage for modeling heat transfer within PCMs in the context of building applications.

2. Bibliometric analysis VosViewer

The initial bibliometric analysis involved a search in Web of Science that combined terms related to “phase change material” and “numerical simulation” to identify the actual fields, where PCMs are used and its behaviour studied. Search algorithm: “*"Phase change material"* OR "phase-change material*" (All Fields) AND "numerical simulation" OR "mathematical modeling" OR "mathematical modelling" OR "simulation*" OR "computational model" OR software* (All Fields) NOT "peak current mode" (All Fields) NOT "Power controlled multiple access" (All Fields) NOT "phase-change memor*" OR "phase change memor*" OR "phase-change memory (pcm)*" OR "phase change memory (pcm)*" (All Fields) NOT "Parallel Climate Model" (All Fields) NOT tropical* (All Fields)”*. A total of 6207 articles met the search criteria. In the figure below VOSviewer network (keywords phase change material and numerical simulation excluded form network) of authors` keywords is presented (470 co-occurring keywords (co-occurrence 5)). Four main research areas besides thermal and latent energy storage can be identified – buildings and solar energy technologies (PV, PVT, T), lithium-ion batteries, heat transfer enhancement (and significant part of that – nano-enhanced PCMs) and molecular dynamics. VOSviewer is a software tool for bibliometric analysis and based on authors keywords and their co-occurrence patterns [9].

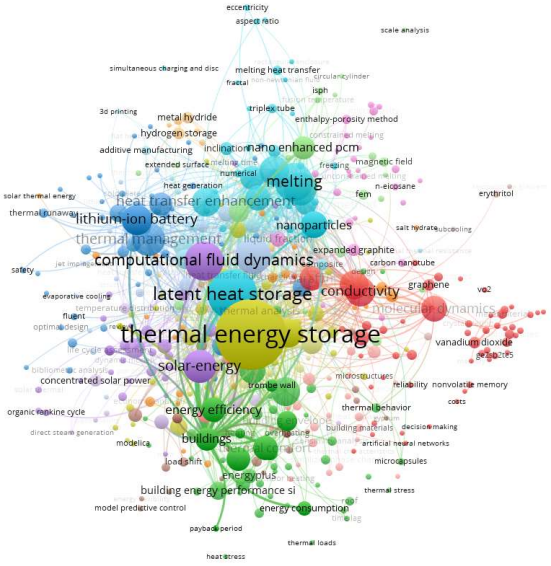

Figure 1. VOSviewer keyword network for PCMs and numerical simulation.

In the next step`s bibliometric analysis five heat transfer simulation softwares were explored - COMSOL, ANSYS, TRNSYS, MATLAB and EnergyPlus. The Web of Science online database was used, and a selection of publications based on keywords: “building” and “PCM” or “phase change material” or “paraffin” and “simulation” or “numerical analysis” or “model” or “software” and “[title of the simulation software]”. Search algorithm: *“PCM* OR "Phase change material"* OR "phase-change material*" OR "phase change" OR "phase-change" (All Fields) AND COMSOL (All Fields)”*. Results for each software tool will be described separately.

The most results gave the search on software ANSYS - 613 documents matched the search criteria. The Network visualizations (figures 2a, b, c, d) are based on 88 co-occurring keywords (co-occurrence 3) (excluding phase change materials, numerical simulation, ansys). Figure 2a illustrates the whole network. The main clusters besides thermal energy storage and computational fluid dynamics here are – heat transfer enhancement, buildings and li-ion batteries. In figure 2b heat transfer enhancement is highlighted and it can be seen, that ANSYS and heat transfer enhancement is co-occurring with such terms as – nanoparticles, fins, foam, heat exchangers and triplex tubes; in figure 2c buildings network co-occurs with passive cooling (through thermal comfort) and hvac (heating, ventilation, air-conditioning), heat exchangers and nanoparticles; in figure 2d li-ion batteries co-occurs with the electric vehicles and battery thermal management systems.

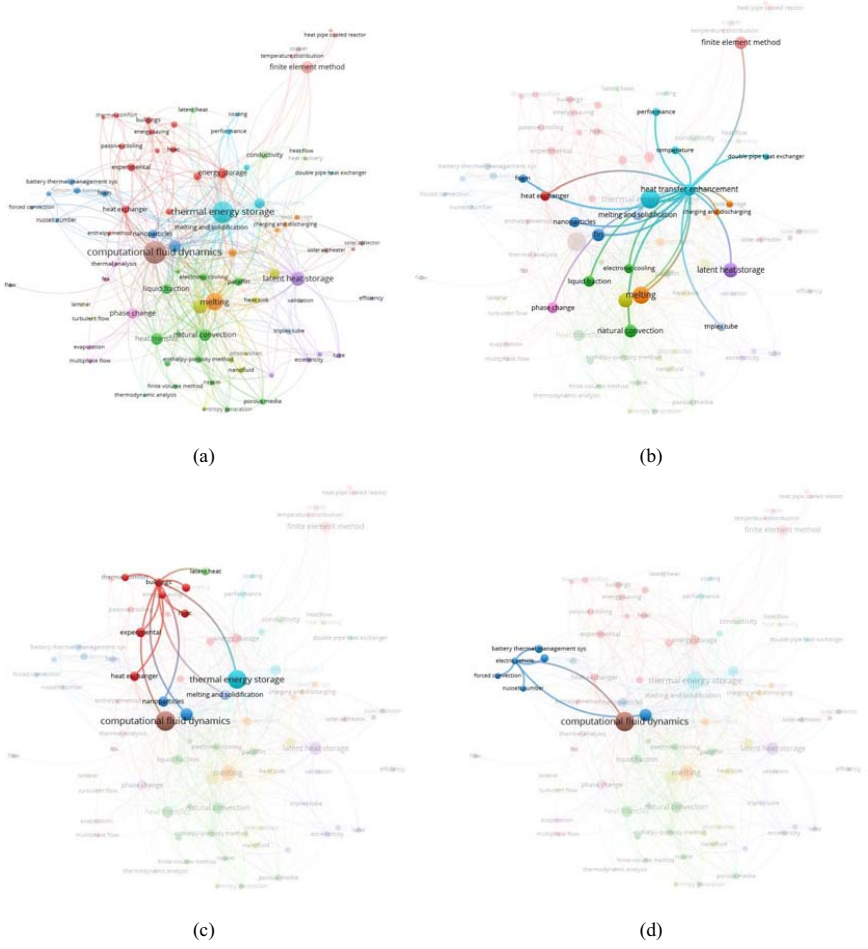

Figure 2. (a) VOSviewer keyword network for PCMs and ANSYS and significant clusters (b) heat transfer enhancement, (c) buildings and (d) batteries.

Search on software COMSOL provided 365 articles and 67 co-occurring authors` keywords (co-occurance 3) network (figures 3a, b, c, d). Figure 3.a. illustrates the whole network. The main clusters besides thermal management here are – lithium – ion batteries, finite element method and buildings. Compared to ANSYS software, in COMSOL keyword network heat transfer enhancement co-occurs less (figure 3c) and among other heat transfer enhancement methods, only term foam co-occurs. Term buildings in COMSOL network co-occurs with the terms solar systems, Trombe wall and cooling more closely and with nanoparticles more distantly. What was not observed in ANSYS network, in COMSOL network buildings co-occur with li-ion batteries. Lithium-ion batteries (figure 3d) co-occur with the cooling, finite element method and buildings.

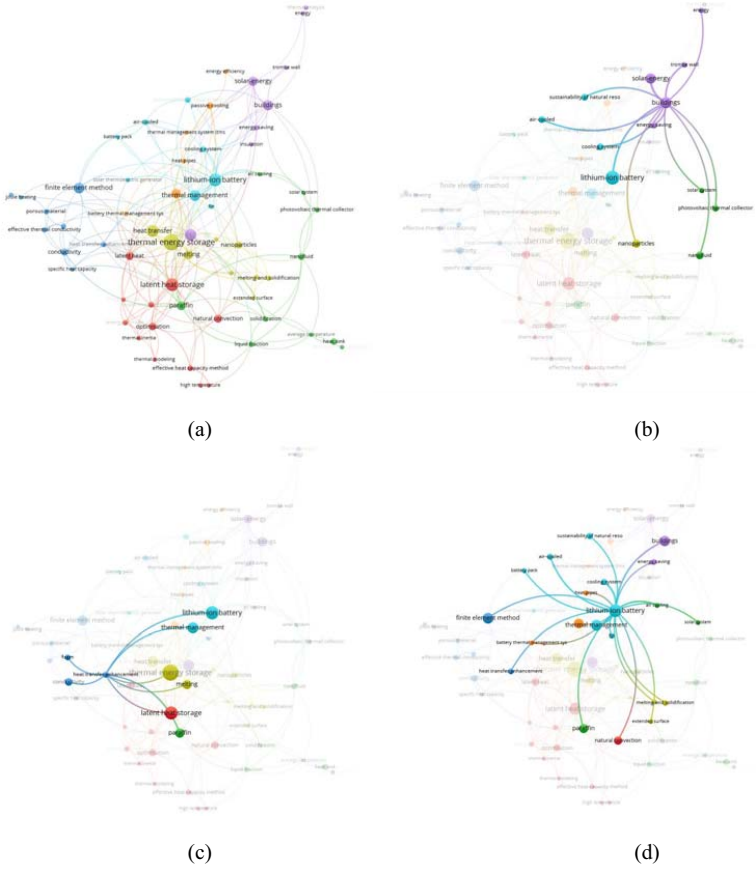

Figure 3. (a) VOSviewer keyword network for PCMs and COMSOL and significant clusters – (b) buildings, (c) heat transfer enhancement and (d) lithium – on batteries.

Search on software TRNSYS provided 212 articles and 46 co-occurring authors` keywords (co-occurance 3) network (figures 4a, b, c, d). This network differs more from previous two. Here main clusters are – buildings, thermal comfort, renewable energy sources + heat pumps and solar energy. Term buildings co-occurs with passive cooling and hvac (figure 4b). Solar energy thread combines – solar heating and cooling, hvac, heat pumps and storage tanks (figures 4c, 4d).

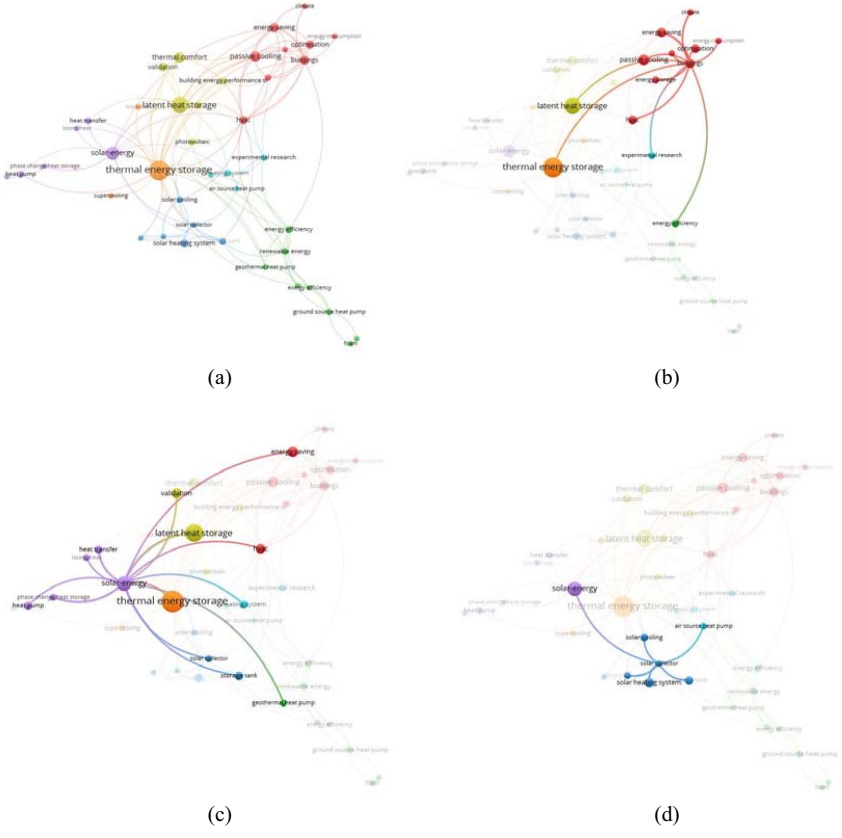

Figure 4. (a) VOSviewer keyword network for PCMs and TRNSYS and significant clasters – (b) buildings, (c) solar – energy and (d) more specifically hvac (heating and cooling).

Search on software MATLAB provided 363 articles and 28 co-occurring authors` keywords (co-occurance 3) network (figures 5a, b, c, d). Here main clusters are – buildings and building envelope, solar energy and concentrated solar power. Term buildings co-occurs with economic analysis and cold thermal energy storage (figure 5b); photovoltaics are in building cluster as well and co-occurs with hvac; solar energy thread combines – photovoltaic thermal collectors and heat pumps (figure 5c), lithium-ion batteries here are in co-occurrence with electric vehicles (figure 5d).

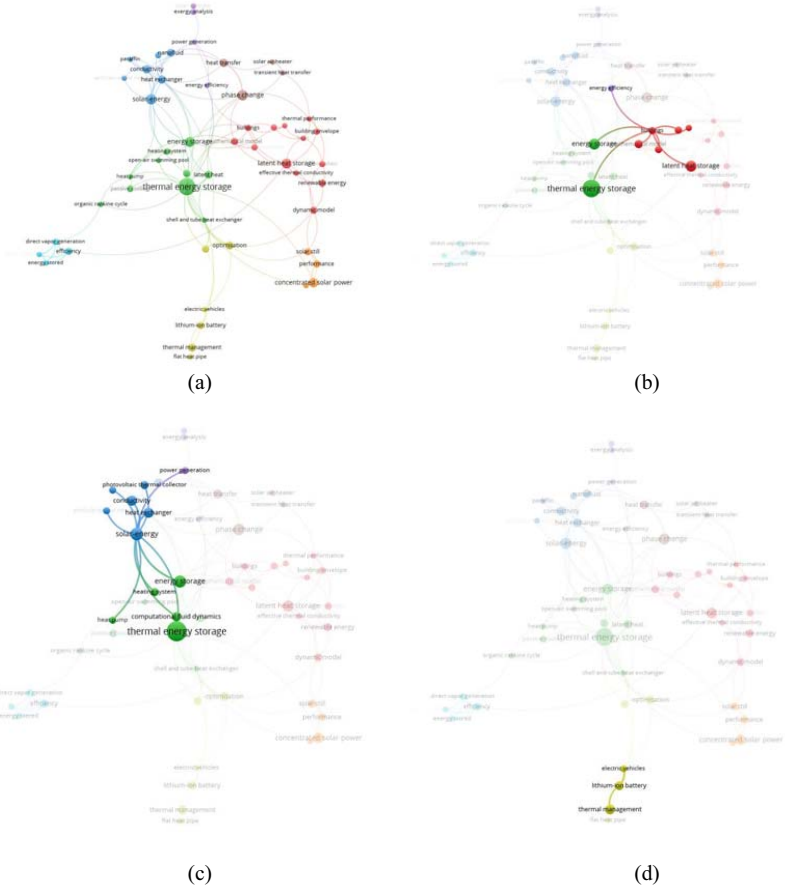

Figure 5. (a) VOSviewer keyword network for PCMs and MATLAB and significant clusters – (b) buildings, (c) solar energy and less distinctive (d) li-ion batteries.

Search on software EnergyPlus provided 173 articles and 61 co-occurring authors` keywords (co-occurrence 3) network (figure 6). EnergyPlus related keyword network is rather scarce – there are no distinct clusters and main co-occurring terms are more specifically oriented to building energy performance, thermal comfort and energy saving.

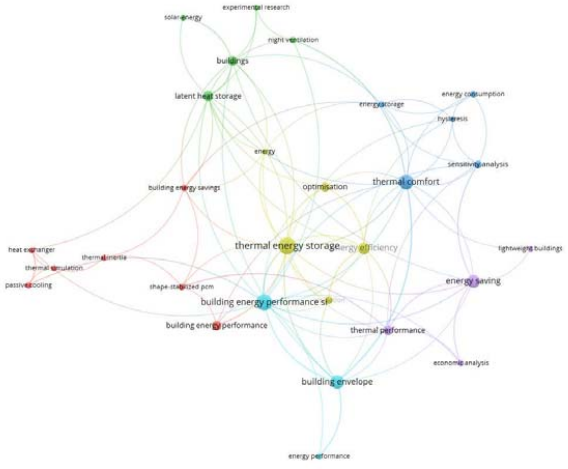

Figure 6. VOSviewer keyword network for PCMs and EnergyPlus.

3. ANSYS usage for modeling heat transfer in phase change material enhanced building envelopes

More detailed analysis of studies on modelling of PCM enhanced building envelopes in ANSYS was carried out. In the bibliometric analysis, the Web of Science online database was used, and a selection of publications based on keywords: “building” and “PCM” or “phase change material” or “paraffin” and “simulation” or “numerical analysis” or “model” or “software” and “ansys”. To define more precisely the scope of the search publications were filtered based on the Web of Science document types: Article or early access or review article. Years of the search were defined from 2019 – 2023. According to the relevant keywords and categories, 42 publications were obtained and further analysed (see ANNEX). Seven publications were excluded as not relevant to the search scope.

In appendix A details of selected publications are summarised. For analysis five parameters of interest were defined – 1) “ANSYS module” - which ANSYS software module was used for modelling; 2) “Time scale” -what was the time scale of modelling; 3) “Scale of model” – was it a small laboratory size test sample, a building thermal envelope component, or a room / building; 4) “Element type” – thermal envelope (wall, roof, floor, window) or HVAC; and 5) “Validation” – how was the model validated. These parameters offer a comprehensive framework for dissecting and categorizing the nuanced facets of each study and enables researchers to gain insights into the different research scopes across the spectrum of publications.

Among selected studies most used ANSYS Fluent module, only two reported using ANSYS CFX. Regarding the time scale of modelling only one publication described simulation over one year period [10], most of others used smaller time scale – a day [11]–[13], a week [14], a month [15]–[20]. Other 15 publication used a time scale less than a day. In 7 publications time scale used was not clearly specified. This indicates a research gap – there are little whole year or seasonal studies using ANSYS.

In terms of model scale – most (23) of the selected studies analysed PCM enriched systems in small scale [2], [3], [8], [12]–[29], followed by room size models (10) [10], [13]–[16], [18], [19], [39]–[41]. The various model scales, from small-scale laboratory settings to room-sized simulations, correspond to the complexity of building envelopes. Prevailing amount of element scale studies indicate to the early TRL studies.

8 of studies explored PCM in HVAC systems – ventilation systems [11], [12], [26]–[28], [34], [35], [42], heat exchangers [20], [25], [30]–[33], [36], [38] and other elements [20]; other 31 publications focused on walls [10], [13], [15], [17], [19], [21]–[24], [37], [39], [40], [43], [44], roofs [14], [18], [29], [37], floors [24], windows ([41]). In 20 studies models were validated using experimental data [10]–[12], [14], [16], [17], [20], [22], [25]–[27], [29], [31], [32], [34]–[38], [40], 1 used analytical validation [45], 4 based validation on findings in other studies in scientific literature [46]–[49].

4. Conclusions

Bibliometric analysis, conducted through VOSviewer, unveils four primary research areas related to PCMs and numerical simulations: buildings and solar energy technologies, lithium-ion batteries, heat transfer enhancement (including nano-enhanced PCMs), and molecular dynamics. Further analysis of five simulation tools reveals specific keyword networks associated with each software.

The study focus narrows to ANSYS for a detailed analysis of PCM-enhanced building envelope modeling. The study identifies key parameters: predominant use of ANSYS Fluent over CFX, a bias towards shorter time scales in simulations, a prevalence of small-scale models, and a common emphasis on experimental data for validation. In summary, the findings highlight ANSYS dominance, suggest research gaps in long-term studies, and showcase PCM versatility in various building elements and HVAC systems. The study offers valuable insights for future research, emphasizing opportunities for advancing sustainable building technologies through enhanced PCM modeling in building envelopes.

Acknowledgement

This study has been supported by Fundamental and Applied Research project “Smart building EnVElope with solaR Energy STorage (EVEREST - II)”, project No. Nr. lzp-2023/1-0164, funded by the Latvian Council of Science.

Appendix A

Table A.1. WOS selection of publications on ANSYS modelling PCM enhanced building components.

Publication	Ansys submodel	Time: hour, day, year, etc.	Scale - element, room or building	Where fitted: walls, floors, floor, windows, etc.	Is it validated and how
"Performance Evaluation of an Active PCM Thermal Energy Storage System for Space Cooling in Residential Buildings" [50]	Ansys fluent	Month	Room	Wall	No
"Numerical model for evaluating thermal performance of residential building roof integrated with inclined phase change material" (PCM) layer [16]	ANSYS Fluent using PISO algorithm	Month	Room	Roof	Experimental
"Comparative Study of Two Materials Combining a Standard Building Material with a PCM" [21]	ANSYS Fluent	Hour	Element	Wall	Analytical
"Validation of different numerical models with benchmark experiments for modelling microencapsulated-PCM-based applications for buildings" [22]	ANSYS CFX /ANSYS FLUENT	minute	Element	Wall	Experimental
"Thermal performance analysis of sensible and pcm-integrated thermal insulation layers to improve thermal comfort in building" [43]	Ansys fluent			Wall	
"Numerical Simulation of a Novel Dual Layered Phase Change Material Brick Wall for Human Comfort in Hot and Cold Climatic Conditions" [17]	Ansys fluent	Month	Element	Wall	Experimental
"Parametric analysis and design optimisation of PCM thermal energy storage system for space cooling of buildings" [13]	Ansys fluent	Day	Room	Wall	No
"A Study of Hot Climate Low-Cost Low-Energy Eco-Friendly Building Envelope with Embedded Phase Change Material" [23]	ANSYS software	-	Element	Wall	Analytical
"Thermal management analysis of PCM integration in building using a novel performance parameter - PCM effectiveness index" [10]	Ansys fluent/ANSYS DESIGN MODELLER	Year	Room	Wall, roof	Experimental
"Energy assessment of a roof-integrated phase change materials, long-term numerical analysis with experimental validation" [14]	Ansys fluent	Week	Room	Roof	Literature and experimental
"The effect of using tubes filled with phase change materials in the air conditioning system of a residential building" [42]	ANSYS-FLUENT 19	Hour	Building	Ventilation	Literature
"Numerical analysis of nanomaterial-based sustainable latent heat thermal energy storage system by improving thermal characteristics of phase change material" [24]	ANSYS Fluent R18.1	Seconds	Element	Wall, floor	Literature
"Experimental and Numerical Thermal Properties Investigation of Cement-Based Materials Modified with PCM for Building Construction Use" [44]	Ansys CFX 15	Seconds	Element	Wall	No

"Parametric study of a sustainable cooling system integrating phase change material energy storage for buildings" [26]	Ansys fluent	No time period.	Element	Ventilation		Experimental
"Coupled EnergyPlus and CFD analysis of PCM for thermal management of buildings" [18]	Ansys FLUENT	Month	Room	Roof		Yes
"Phase Change Material Melting Process in a Thermal Energy Storage System for Applications in Buildings" [27]	Ansys FLUENT/ ANSYS DesignModeler	-	Element	Ventilation		Experimental
"Simulation of a Trombe wall with a number of semicircular fins placed on the absorber plate for heating a room in the presence of nano-PCM" [39]	Ansys FLUENT	Hour	Room	Wall		Literature
"Numerical thermal evaluation of laminated binary microencapsulated phase change material drywall systems" [19]	Ansys FLUENT	Month	Room	Wall		No
"Exergy and economic analyses of nanoparticle-enriched phase change material in an air heat exchanger for cooling of residential buildings" [11]	Ansys FLUENT	Day	Element	Ventilation		Experimental
"Potential of integrating PCMs in residential building envelope to reduce cooling energy consumption" [40]	Ansys FLUENT	Hour	Room	Wall		Experimental
"Design and Optimization of Air to PCM Heat Exchanger Using CFD" [28]	Ansys FLUENT 19.2	Hour	Element	Ventilation		
"Performance analysis of PCM curtain for thermal comfort" [41]	Ansys		Room	Window		
"Experimental and finite element analysis on the developed real-time form stable PCM based roof system for thermal energy storage applications" [29]	ANSYS FE	Hour	Element	Roof		Experimental
"Performance analysis of melting behavior of phase change material encapsulated within differently shaped macro-capsule" [30]	ANSYS Fluent CFD	Seconds	Element	Heat exchanger		
"Constructal invasion of fins for melting time prediction of a phase change material in a triplex-tube heat exchanger" [31]	Ansys FLUENT R16	Seconds	Element	Heat exchanger		Experimental
"Study on thermal performance improvement technology of latent heat thermal energy storage for building heating" [20]	ANSYS FLUENT V15	Month	Element	Boiler, heat exchanger		Experimental
"Simultaneous charging and discharging of phase change materials: Development of correlation for liquid fraction" [32]	ANSYS Fluent (version 17.2)	minute	Element	Heat exchanger		Experimental
"A study of unidirectional spiral tube for air evacuation in a solar heater with phase-change material" [33]	Ansys	Hour	Element	Heat exchanger		No
"Numerical simulation of the melting and solidification processes of two organic phase change materials in spherical enclosures for cold thermal energy storage applications" [34]	ANSYS Fluent	-	Element	Ventilation		Experimental
"Numerical study on the cooling performance of a novel passive system: Cylindrical phase change material-assisted earth-air heat exchanger" [12]	ANSYS Fluent 16.0	Day	Element	Ventilation		Experimental
"Effect of airflow channel arrangement on the discharge of a composite metal foam-phase change material heat exchanger" [35]	ANSYS Fluent	Hour	Element	Ventilation		Experimental

"Sensitivity analysis of design parameters for erythritol melting in a horizontal shell and multi-finned tube system: Numerical investigation" [36]	ANSYS Fluent v. 19.0	-	Element	Heat exchanger	Experimental
"An Experimental and Numerical Study on the Optimum Flow Rate of a Photovoltaic Thermal System Integrated with Phase Change Materials" [37]	ANSYS Fluent	-	Element	Wall and roof	Experimental
"Experimental and numerical investigation of spatiotemporal characteristics of thermal energy storage system in a rectangular enclosure" [25]	ANSYS Fluent	Minute	Element	Heat exchanger	Experimental
"Performance optimization and experimental analysis of a novel low-temperature latent heat thermal energy storage device" [38]	Ansys	Hour	Element	Heat exchanger	Experimental
Do not match the search criteria					
"Application of PCM-based Thermal Energy Storage System in Buildings: A State of the Art Review on the Mathematical Modelling Approaches and Experimental Investigations" [51]					
"Numerical modelling of the fire resistance of double sheared steel-to-timber connections" [52]					
"Multiphysics modelling and simulation of laser additive manufacturing process" [53]					
"Effects of ground heat exchangers with different connection configurations on the heating performance of GSHP systems" [54]					
"Variational nodal method for three-dimensional multigroup neutron diffusion equation based on arbitrary triangular prism" [55]					
"A Hybrid Methodology for Analyzing the Performance of Induction Motors with Efficiency Improvement by Specific Commercial Measures" [56]					
"Numerical Investigation of Methane Number and Wobbe Index Effects in Lean-Burn Natural Gas Spark-Ignition Combustion" [57]					

References

[1] European Commission. Directive 2012/27/EU of the European Parliament and of the Council of 25 October 2012 on energy efficiency 2012:1–56
[2] Rabi AM, Radulovic J and Buick JM. Comprehensive Review of Compressed Air Energy Storage (CAES) Technologies. *J. Thermo* 2023;**3**:104–26. https://doi.org/10.3390/THERMO3010008
[3] Al-Hallaj S, Wilke S and Schweitzer B. Energy storage systems for smart grid applications. In: Murad, S., Baydoun, E., Daghir, N. (eds) Water, Energy & Food Sustainability in the Middle East. Springer, Cham. 2017:161–92. https://doi.org/10.1007/978-3-319-48920-9_8
[4] Nair AM, Wilson C, Huang MJ, Griffiths P and Hewitt N. Phase change materials in building integrated space heating and domestic hot water applications: A review. *J. Energy Storage* 2022;**54**:105227. https://doi.org/10.1016/J.EST.2022.105227
[5] Sawadogo M, Duquesne M, Belarbi R, Hamami AEA and Godin A. Review on the Integration of Phase Change Materials in Building Envelopes for Passive Latent Heat Storage. *J. Applied Sciences* 2021,**11**:9305. https://doi.org/10.3390/APP11199305
[6] Luo Y, Zhang L, Bozlar M, Liu Z, Guo H and Meggers F. Active building envelope systems toward renewable and sustainable energy. *J. Renewable and Sustainable Energy Reviews* 2019;**104**:470–91. https://doi.org/10.1016/J.RSER.2019.01.005
[7] Al-Saadi SN and Zhai Z. Modeling phase change materials embedded in building enclosure: A review. *J. Renewable and Sustainable Energy Reviews* 2013;**21**:659–73. https://doi.org/10.1016/J.RSER.2013.01.024
[8] Li C, Wen X, Cai W, Yu H and Liu D. Phase change material for passive cooling in building envelopes: A comprehensive review. *Journal of Building Engineering* 2023;**65**:105763. https://doi.org/10.1016/J.JOBE.2022.105763
[9] van Eck NJ and Waltman L. Software survey: VOSviewer, a computer program for bibliometric mapping. *J. Scientometrics* 2010;Vol **84**:523–38. https://doi.org/10.1007/S11192-009-0146-3
[10] Selvaraju A, Ranganathan A, Vincent A, Arumugam P and Ramalingam V. Thermal management analysis of PCM integration in building using a novel performance parameter - PCM effectiveness index. *J. Thermal Science* 2022;**26**:883–95. https://doi.org/10.2298/TSCI200830208S
[11] Dastmalchi M and Boyaghchi FA. Exergy and economic analyses of nanoparticle-enriched phase change material in an air heat exchanger for cooling of residential buildings. *J. Energy Storage* 2020;32:101705. https://doi.org/10.1016/j.est.2020.101705
[12] Zhou T, Xiao Y, Huang H and Lin J. Numerical study on the cooling performance of a novel passive system: Cylindrical phase change material-assisted earth-air heat exchanger. *J. Clean Prod* 2020;Vol **245**:118907. https://doi.org/10.1016/j.jclepro.2019.118907
[13] Ručevskis S, Akishin P and Korjakins A. Parametric analysis and design optimisation of PCM thermal energy storage system for space cooling of buildings. *J. Energy Build* 2020;**224**:110288. https://doi.org/10.1016/j.enbuild.2020.110288
[14] Elawady N, Bekheit M, Sultan AA and Radwan A. Energy assessment of a roof-integrated phase change materials, long-term numerical analysis with experimental validation. *J. Appl Therm Eng* 2022;**202**:117773. https://doi.org/10.1016/j.applthermaleng.2021.117773
[15] Rucevskis S, Akishin P and Korjakins A. Performance Evaluation of an Active PCM Thermal Energy Storage System for Space Cooling in Residential Buildings. *J. Environmental and Climate Technologies* 2019;**23**:74–89. https://doi.org/10.2478/rtuect-2019-0056
[16] Bhamare DK, Rathod MK and Banerjee J. Numerical model for evaluating thermal performance of residential building roof integrated with inclined phase change material (PCM) layer. *Journal of Building Engineering* 2020;**28**:101018. https://doi.org/10.1016/j.jobe.2019.101018
[17] Rehman AU, Sheikh SR, Kausar Z and McCormack SJ. Numerical Simulation of a Novel Dual Layered Phase Change Material Brick Wall for Human Comfort in Hot and Cold Climatic Conditions. *J. Energies* (Basel) 2021;**14**:4032. https://doi.org/10.3390/en14134032

[18] Pandey B, Banerjee R and Sharma A. Coupled EnergyPlus and CFD analysis of PCM for thermal management of buildings. *J. Energy Build* 2021;**231**:110598. https://doi.org/10.1016/j.enbuild.2020.110598
[19] Su W, Darkwa J and Kokogiannakis G. Numerical thermal evaluation of laminated binary microencapsulated phase change material drywall systems. *J. Build Simul* 2020;**13**:89–98. https://doi.org/10.1007/s12273-019-0563-z
[20] Lu S, Lin Q, Liu Y, Yue L and Wang R. Study on thermal performance improvement technology of latent heat thermal energy storage for building heating. *J. Appl Energy* 2022;**323**:119594. https://doi.org/10.1016/j.apenergy.2022.119594
[21] El Yassi M, El Abbassi I, Pierre A and Melinge Y. Comparative Study of Two Materials Combining a Standard Building Material with a PCM. *J. Fluid Dynamics & Materials Processing* 2023;**19**:1283–90. https://doi.org/10.32604/fdmp.2022.023183
[22] Soares N, Rosa N, Costa JJ, Lopes AG, Matias T, Simões PN, et al. Validation of different numerical models with benchmark experiments for modelling microencapsulated-PCM-based applications for buildings. *J. International Journal of Thermal Sciences* 2021;**159**:106565. https://doi.org/10.1016/j.ijthermalsci.2020.106565
[23] Rehman AU, Ghafoor N, Sheikh SR, Kausar Z, Rauf F, Sher F, et al. A Study of Hot Climate Low-Cost Low-Energy Eco-Friendly Building Envelope with Embedded Phase Change Material. *J. Energies* (Basel) 2021;**14**:3544. https://doi.org/10.3390/en14123544
[24] Teja PNS, Gugulothu SK, Sastry GR, Burra B and Bhurat SS. Numerical analysis of nanomaterial-based sustainable latent heat thermal energy storage system by improving thermal characteristics of phase change material. *J. Environmental Science and Pollution Research* 2022;**29**:50937–950. https://doi.org/10.1007/s11356-021-15485-y
[25] Yadav A and Samir S. Experimental and numerical investigation of spatiotemporal characteristics of thermal energy storage system in a rectangular enclosure. *J. Energy Storage* 2019;**21**:405–17. https://doi.org/10.1016/j.est.2018.12.005
[26] Zeinelabdein R, Omer S and Mohamed E. Parametric study of a sustainable cooling system integrating phase change material energy storage for buildings. *J. Energy Storage* 2020;**32**:101972. https://doi.org/10.1016/j.est.2020.101972
[27] Nascimento Porto T, Delgado JMPQ, Guimarães AS, Fernandes Magalhães HL, Moreira G, Brito Correia B, et al. Phase Change Material Melting Process in a Thermal Energy Storage System for Applications in Buildings. *J. Energies* (Basel) 2020;**13**:3254. https://doi.org/10.3390/en13123254
[28] Kareem BE, Adham AM and Yaqob BN. Design and Optimization of Air to PCM Heat Exchanger Using CFD. Arab *J. Sci Eng* 2022.48, 12609–623. https://doi.org/10.1007/s13369-022-07360-w
[29] Baskar I and Chellapandian M. Experimental and finite element analysis on the developed real-time form stable PCM based roof system for thermal energy storage applications. *J. Energy Build* 2022;**276**:112514. https://doi.org/10.1016/j.enbuild.2022.112514
[30] Sharma A and Dewangan SK. Performance analysis of melting behavior of phase change material encapsulated within differently shaped macro-capsule. *International Journal of Energy and Environmental Engineering* 2022;Vol **13**:377–94. https://doi.org/10.1007/s40095-021-00431-y
[31] Barik AK and Swain PK. Constructal invasion of fins for melting time prediction of a phase change material in a triplex-tube heat exchanger. *J. Energy Storage* 2022;**54**:105281. https://doi.org/10.1016/j.est.2022.105281
[32] Joybari MM, Haghighat F, Seddegh S and Yuan Y. Simultaneous charging and discharging of phase change materials: Development of correlation for liquid fraction. *J. Solar Energy* 2019;**188**:788–98. https://doi.org/10.1016/j.solener.2019.06.051
[33] Luo Q, Li B, Wang Z, Su S and Xiao H. A study of unidirectional spiral tube for air evacuation in a solar heater with phase-change material. *Journal of Building Engineering*

2022;**46**:103659. https://doi.org/10.1016/j.jobe.2021.103659
[34] Cofré-Toledo J, Roa-Cossio D, Vasco DA, Cabeza LF and Rouault F. Numerical simulation of the melting and solidification processes of two organic phase change materials in spherical enclosures for cold thermal energy storage applications. *J. Energy Storage* 2022;**51**:104337. https://doi.org/10.1016/j.est.2022.104337
[35] Talebizadehsardari P, Mohammed HI, Mahdi JM, Gillott M, Walker GS, Grant D, et al. Effect of airflow channel arrangement on the discharge of a composite metal foam-phase change material heat exchanger. *Int J Energy Res* 2021;**45**:2593–609. https://doi.org/10.1002/er.5949
[36] Anish. R, Joybari MM, Seddegh S, Mariappan V, Haghighat F and Yuan Y. Sensitivity analysis of design parameters for erythritol melting in a horizontal shell and multi-finned tube system: Numerical investigation. *J. Renew Energy* 2021;Vol **163**:423–36. https://doi.org/10.1016/j.renene.2020.08.153
[37] Kandilli C and Mertoglu B. An Experimental and Numerical Study on the Optimum Flow Rate of a Photovoltaic Thermal System Integrated with Phase Change Materials. *Journal of Engineering Thermophysics* 2022;**31**:458–76. https://doi.org/10.1134/S1810232822030080
[38] Lu S, Zhai X, Gao J and Wang R. Performance optimization and experimental analysis of a novel low-temperature latent heat thermal energy storage device. *J. Energy* 2022;**239**:122496. https://doi.org/10.1016/j.energy.2021.122496
[39] Liang D, Ibrahim M, Saeed T, El-Refaey AM, Li Z and Fagiry MA. Simulation of a Trombe wall with a number of semicircular fins placed on the absorber plate for heating a room in the presence of nano-PCM. *Journal of Building Engineering* 2022;**50**:104173. https://doi.org/10.1016/j.jobe.2022.104173
[40] Al-mudhafar AhmedHN, Hamzah MT and Tarish AL. Potential of integrating PCMs in residential building envelope to reduce cooling energy consumption. *J. Case Studies in Thermal Engineering* 2021;**27**:101360. https://doi.org/10.1016/j.csite.2021.101360
[41] Srivastava S, Srivastava A, Jain S, Kumar N and Malvi CS. Performance analysis of PCM curtain for thermal comfort. *J. Research Journal of Textile and Apparel* 2022;Vol **26**:439–51. https://doi.org/10.1108/RJTA-05-2021-0066
[42] Hai T, Sajadi SM, Zain JM, El-Shafay AS and Sharifpur M. The effect of using tubes filled with phase change materials in the air conditioning system of a residential building. *Journal of Building Engineering* 2022;Vol **49**:104079. https://doi.org/10.1016/j.jobe.2022.104079
[43] Kerroumi N, Touati B and Virgone J. Thermal performance analysis of sensible and pcm-integrated thermal insulation layers to improve thermal comfort in building. *J. Interfacial Phenom Heat Transf* 2020;**8**:67–80. https://doi.org/10.1615/InterfacPhenomHeatTransfer.2020034117
[44] Essid N, Eddhahak-Ouni A and Neji J. Experimental and Numerical Thermal Properties Investigation of Cement-Based Materials Modified with PCM for Building Construction Use. *J. Archit. Eng*. 2020;**26**: 04020018. https://doi.org/10.1061/(ASCE)AE.1943-5568.0000399
[45] Rehman AU, Ghafoor N, Sheikh SR, Kausar Z, Rauf F, Sher F, et al. A Study of Hot Climate Low-Cost Low-Energy Eco-Friendly Building Envelope with Embedded Phase Change Material. *J. Energies* (Basel) 2021;**14**:3544. https://doi.org/10.3390/en14123544
[46] Elawady N, Bekheit M, Sultan AA and Radwan A. Energy assessment of a roof-integrated phase change materials, long-term numerical analysis with experimental validation. *J. Appl Therm Eng* 2022;**202**:117773. https://doi.org/10.1016/j.applthermaleng.2021.117773
[47] Hai T, Sajadi SM, Zain JM, El-Shafay AS and Sharifpur M. The effect of using tubes filled with phase change materials in the air conditioning system of a residential building. *Journal of Building Engineering* 2022;**49**:104079. https://doi.org/10.1016/j.jobe.2022.104079
[48] Teja PNS, Gugulothu SK, Sastry GR, Burra B and Bhurat SS. Numerical analysis of nanomaterial-based sustainable latent heat thermal energy storage system by improving thermal characteristics of phase change material. *J. Environmental Science and Pollution Research* 2022;**29**:50937–950. https://doi.org/10.1007/s11356-021-15485-y

[49] Liang D, Ibrahim M, Saeed T, El-Refaey AM, Li Z and Fagiry MA. Simulation of a Trombe wall with a number of semicircular fins placed on the absorber plate for heating a room in the presence of nano-PCM. *Journal of Building Engineering* 2022;**50**:104173. https://doi.org/10.1016/j.jobe.2022.104173

[50] Rucevskis S, Akishin P and Korjakins A. Performance Evaluation of an Active PCM Thermal Energy Storage System for Space Cooling in Residential Buildings. *J. Environmental and Climate Technologies* 2019;Vol **23**:74–89. https://doi.org/10.2478/rtuect-2019-0056

[51] Zeng C, Yuan Y, Haghighat F, Panchabikesan K, Joybari MM, Cao X, et al. Application of PCM-based Thermal Energy Storage System in Buildings: A State of the Art Review on the Mathematical Modeling Approaches and Experimental Investigations. *Journal of Thermal Science* 2022;**31**:1821–52. https://doi.org/10.1007/s11630-022-1650-5

[52] Szász A, Hlavička V, Lublóy É and Biró A. Numerical modelling of the fire resistance of double sheared steel-to-timber connections. *Journal of Building Engineering* 2021;**37**:102150. https://doi.org/10.1016/j.jobe.2021.102150

[53] Khanafer K, Al-Masri A, Aithal S and Deiab I. Multiphysics modeling and simulation of laser additive manufacturing process. International *Journal on Interactive Design and Manufacturing* 2019;**13**:537–44. https://doi.org/10.1007/s12008-018-0520-6

[54] Qi D, Pu L, Ma Z, Xia L and Li Y. Effects of ground heat exchangers with different connection configurations on the heating performance of GSHP systems. *J. Geothermics* 2019;**80**:20–30. https://doi.org/10.1016/j.geothermics.2019.02.002

[55] Zhuang K, Shang W, Li T, Yan J, Wang S, Tang X, et al. Variational nodal method for three-dimensional multigroup neutron diffusion equation based on arbitrary triangular prism. *J. Ann Nucl Energy* 2021;**158**:108285. https://doi.org/10.1016/j.anucene.2021.108285

[56] Ai C, Lee CHT, Kirtley JL, Huang Y, Wang H and Zhang Z. A Hybrid Methodology for Analyzing the Performance of Induction Motors with Efficiency Improvement by Specific Commercial Measures. *J. Energies* (Basel) 2019;**l12**:4497. https://doi.org/10.3390/en12234497

[57] Liu J and Dumitrescu CE. Numerical Investigation of Methane Number and Wobbe Index Effects in Lean-Burn Natural Gas Spark-Ignition Combustion. *J. Energy & Fuels* 2019;**33**:4564–74. https://doi.org/10.1021/acs.energyfuels.8b04463

Jānis Narbuts was born in 1987 in Riga. He obtained a Professional Bachelor's degree in Electrical Engineering (2010), a Professional Master's degree in Computerised Control of Electrical Technologies (2011), and a Master's degree in Environmental Science (2021) from Riga Technical University (RTU). Since 2022, he has been a Researcher at the RTU Institute of Energy Systems and Environment. During his studies, he participated in the Erasmus exchange programme at the Polytechnic University of Turin (Italy). He is the author of several scientific publications on adaptive facades, phase change materials and building energy efficiency. His scientific interests are related to adaptive building envelopes, thermal energy storage and sustainable energy technologies.